Cranfield University

A. G. ADEDIGBA

TWO-PHASE FLOW OF GAS-LIQUID MIXTURES IN HORIZONTAL HELICAL PIPES

SCHOOL OF ENGINEERING

PhD THESIS

Cranfield University

SCHOOL OF ENGINEERING

PhD THESIS

Academic Year 2006-2007

A. G. ADEDIGBA

TWO-PHASE FLOW OF GAS-LIQUID MIXTURES IN HORIZONTAL HELICAL PIPES

Supervisor: Dr. H. C. Yeung

May 2007

This thesis is submitted in partial fulfilment of the requirements for the degree of Doctor of Philosophy

ABSTRACT

The aim of this study was to investigate hydrodynamic two -phase (namely water and air) fluid flow characteristics in *helical pipe*s of low amplitude and straight pipes of the same internal-diameter and constructional material: the results for the two pipes have then been compared.

One of the objectives was to measure pressure, pressure drop and liquid holdup in the two pipes. These are universal dominant parameters in the oil-and-gas industry as they significantly impact on the exploitation and conveyance of crude oil from wells or reservoirs to the process plant, where the crude is refined. The second objective was to examine applications of the *helical pipe*.

Experiments were performed on three different *helical pipe*s of internal diameters 25.4 mm, 50 mm and 100 mm and their straight counterparts. The single-phase preliminary experimental results from the 25.4 mm internal-diameter for both pipes have shown that both pressure and pressure drop are higher in the *helical pipe* than in the straight pipe. The friction factors were also evaluated for both pipes and found to be higher in the *helical pipe* than in the straight pipe. The single-phase and two-phase experimental results for the 50 mm internal-diameter pipes confirmed the conclusions from the preliminary experimental results. The two-phase results showed that slug flow occurred in the straight pipe at certain superficial velocities of air and water, whereas at the same superficial velocities of air and water, slug flow did not ensue in the helical pipe - instead bubbly flow was observed. Stratified flow occurred in the straight pipe at very low superficial velocities of air and water but under these same conditions, bubbly flow ensued in the *helical pipe*.

A section of 100 mm internal-diameter *helical pipe* was installed at some distance from a catenary-shaped riser, with a view to investigating the effectiveness of the *helical pipe* in mitigating severe slugging. The results showed promise as the section of the *helical pipe* proved to be successful in reducing the menace of severe slugging. This novel finding is regarded as a breakthrough for the oil-and-gas industry in this respect. This is because hydrocarbon proven reserves in the off-shore (i.e. deep sea-water) environment have been estimated to be close to 60%. All previous research studies over the past decade to provide solution to the problem posed by severe slugging have not yielded any appreciable results. This discovery also has the advantages of reducing the demand on the topside (process) facility and the achievement of stability of liquid production is resulted from the consequent flow assurance in the pipeline and riser.

ACKNOWLEDGEMENTS

I would first of all thank my supervisor in person of Dr. Hoi Yeung who introduced me to the subject of multiphase flow. His guidance, patience and constructive criticism during the course of this research study have been appreciated. The financial support provided towards the end of this study by the department is gratefully acknowledged. I also thank my co-supervisor, Dr. Ossama Badr for all his suggestions and advice.

I gratefully acknowledge the financial support provided by Petroleum Technology Development Fund (PTDF) of the Nigerian Government's Ministry of Petroleum Resources. Likewise, I thank my employer, the Nigerian National Petroleum Corporation (NNPC) for granting me study leave to undertake these studies at Cranfield University.

My deepest gratitude goes to Prof. S. D. Probert for his inspiration, suggestions, continuous encouragement and valuable pieces of advice since my arrival at Cranfield some two decades ago. I appreciate his continual guidance, as do his many ex-students all over the world: Doug Probert is a man of great intellect and dedication to scientific and engineering advancement.

I also appreciate the encouragement given by Dr. A. J. Oyekan, former Director of Petroleum Resources in the Nigerian Ministry of Petroleum Resources.

The assistance received from Mr. Flemming Nielson who was never tired of making one form of modification or the other to my experimental rigs is gratefully appreciated. Without his support the experiments would not have been successful. I thank Mr. Alan Hutchinson in the design office and the staff of the test-area workshop for their help. The assistance received from Mr. John W. Knopp is gratefully appreciated. I thank Mrs. Linda Whitfield and all staff members of the department for one form of assistance or another. All the staff of Cranfield Computer Centre, especially Deborah Hiscock and the library, have been wonderful and their assistance is acknowledged.

The prayers received from my brothers (Ayotade and Adewale) and other friends for the successful completion of this course are appreciated. I thank Latifat for her prayers and for looking after our home during the course of these studies at Cranfield University. Now that the task is over, I will have much more time to spend with my family.

I thank everyone else (I cannot mention their names here because of shortage of space) who has assisted me in one way or another to complete my task at Cranfield University.

Above all, I finally thank God, the Almighty for seeing me through the difficult times on this course.

DEDICATION

I dedicate this study to the undying memory of my late parents who answered the call of God when they were about reaping the fruits of their labour

God is the Giver and the Taker,
the Alpha and the Omega,
the First and the Last,
the Beginning and the End.

He says:

Seest thou a man diligent in His work He will stand before Kings and not mean Men

NOMENCLATURE

Symbol	*Variable*	*Unit*
A	Area	m^2
A_P	Helical pipe amplitude	m
A_1	Inlet area	m^2
A_2	Outlet area	m^2
a	Pipe internal radius ($\frac{D}{2}$)	m
bbl	barrel	
C	Proportionality parameter	
C_{B-B}	Parameter defined in Table 2-2	
C_7	Velocity ratio defined in equations 2-99	
C_8	Velocity ratio defined in equations 2-102	
C_9	Velocity ratio defined in equations 2-103	
d	Pipe internal or inner diameter	m
D	Coil Diameter	m
D_{str}	Downstream	
D_e	Dean number	
F	Force	N
f	Fanning friction factor	
g	Acceleration due to gravity (9.81)	ms^{-2}
g	gas	
G	Mass flow rate	gs^{-1}
H	Enthalpy	$kjkg^{-1}$
ΔH	Head loss	m
h	Height	m
K_H	Parameter defined in equation 2-107	

Nomenclature

l	Length	m
M	Total mass	kg
N	Velocity number	
N_{GV}	Gas-velocity number defined in equation 2-112	
N_{LV}	Liquid-velocity number defined in equation 2-113	
$N_{L}\mu$	Liquid-viscosity number defined in equation 2-114	
P or p	Pressure	bar
ΔP_{acc}	Pressure drop due to acceleration	Pa
ΔP	Pressure drop	bar
ΔP_{f}	Frictional pressure drop	bar
P_{t}	Pitch	m
Q	Volume flow rate	m^3/s or l/s
r	Radius	m
R	Universal gas constant (8314)	$JKmol^{-1}K^{-1}$
Re	Reynolds number	
SS1	Severe slugging class 1	
SS	Severe slugging class 2	
S	Ordinary slug	
T	Temperature	^{o}C or K
t	Time	sec
U or u	Velocity	ms^{-1}
U_{L}	Liquid velocity	ms^{-1}
U_{SL} or U_{W}	Liquid superficial velocity	ms^{-1}
U_{SG}	Gas superficial velocity	ms^{-1}
U_{M}	Two-phase mixture velocity	ms^{-1}
U_{str}	Upstream	
V	Volume	m^3 or l
W	Water	
X	Lockhart – Martinelli parameter	

Nomenclature

X_2	Defined as equation 2-42	
x	Co-ordinate direction	m
(Y_{L-M})	Inclination-parameter defined in equation 2-105	
y	Co-ordinate direction	m
Z	Compressibility factor	
Z_H	Parameter defined in equation 2-108	
Z_E	Parameter defined in equation 2-111	
z	Co-ordinate direction	m

Greek Symbols

α	Angle of inclination	0
β	Angle of inclination	0
ε	Phase fraction or holdup	
μ	Dynamic viscosity	Nsm^{-2}
μ_l	Liquid phase viscosity	Nsm^{-2}
μ_g	Gas phase viscosity	Nsm^{-2}
ν	Kinematic viscosity	m^2s^{-1}
ϕ	Two-phase multiplier	
θ	Angle of inclination	0
ω	Angular velocity	
ρ	Density	kgm^{-3}
ρ_n	Two-phase density	$kg\ m^{-3}$
ρ_M	Mixture density	$kg\ m^{-3}$
ρ_L	Liquid phase density	$kg\ m^{-3}$
ρ_G	Gas phase density	$kg\ m^{-3}$
σ	Surface tension	Nm^{-1}
τ	Shear force	Nm^{-1}
τ_w	Wall shear stress	Nm^{-2}

Subscripts

B	Base
Bub	Bubble
c	Coil
FR	Friction
G	Gas
H	Homogeneous
HYD	Hydrostatic
I	Inlet
L	Liquid
$Loss$	Losses (due to acceleration and friction)
O	Outlet
R	Riser
REF	Reference Condition
S	Superficial
TP	Two-phase
w	Wall

TABLE OF CONTENTS

Table of Contents

Table of Contents

TABLE OF FIGURES

Table of Figures

Table of Figures

Table of Figures

TABLE OF TABLES

Table of Tables

Chapter 1

1 Introduction

1.1 Research background

This thesis describes a research study on hydrodynamics of two-phase (air and water) flow characteristics in straight and *helical pipes*. The focus of the research has been on such flows through *helical pipes*; however, such flows through straight pipes of the same internal-diameters as the *helical pipes* have also been investigated and the results for both pipes have been compared. The challenges of hydrocarbon extraction in an off-shore environment have encouraged research to be intensified in the area of multiphase flows.

Multiphase flows are defined as the simultaneous flows of gases, liquids and solids in systems such as pipes or vessels. In multiphase flow, a phase is characterized by homogeneous composition and properties and it has clearly defined boundaries. The flow of multiphase mixtures is a common phenomenon in industrial plants, such as chemical reactors and power generation units. In particular, it is considered to be an important phenomenon in the oil-and-gas industry from an energy point of view. For oil-and-gas wells and flow lines, it is often the flow of all materials produced from a reservoir, and may consist of hydrocarbon gases (with carbon dioxide – CO_2 and traces of hydrogen sulphide - H_2S), hydrocarbon liquid (oil and condensate), water and solids (sand and grit).

In order to successfully design and operate any process plant, knowledge of the chemical and physical properties of the materials being processed is fundamental. In many cases, the materials that are being processed do not flow as a single phase such as a gas, liquid or solid. Instead, combinations of two or

more of these phases may predominate; gas-liquid, gas-solid, liquid-solid, liquid-liquid and even gas-liquid-solid flows are commonly encountered. In particular, gas-liquid flows frequently ensue in all types of process equipment and they are also prevalent in many gas and oil pipeline systems. Beggs and Brill (1973) stated that more than half of the natural gas gathered in the United States in the early 1970s flowed within two-phase pipelines.

1.2 Multiphase Flow Assurance Issues

One of the main applications of multiphase flows in the present time is in the oil industry, where the recovery of hydrocarbon products both on-shore and off-shore has been a big challenge. Complex mixtures of up to four phases of natural gas, oil, water and solid particles are transported through horizontal and vertical pipeline (riser) systems from the hydrocarbon wells located in the deep sea-bed to the on-shore processing plant. The intended mass flow rates in these pipelines are substantial, and any improvements in the prediction and the operation of the multiphase systems can result in significant economic returns. When the length of the deepwater risers is considered, the problem of slugging is expected to be more severe than in production systems installed in shallower waters. Severe slugging is an unstable flow regime, in the sense that it is associated with large and abrupt fluctuations in the pipe pressure and in the gas and liquid flow rates at the outlet. It can cause damage to process plant facilities. Hence a prime aim is to reduce the severe slugging.

Multiphase technology has been seen as a vital means of exploiting marginal fields, maximising the rate of return and minimising total expenditure. The savings that can be made by using multiphase technology can be substantial. The key issues in successfully developing these fields have been stated by Hill (1997) as minimising both Capital Expenditure (CAPEX) and Operational Expenditure (OPEX). The focus on the development of off-shore marginal fields in deep-water has also been highlighted with statistics showing that over fifty percent of the world's proven reserves of oil and gas are located off-shore and

in water depths greater than one thousand and eight hundred metres. Marginal fields are regarded as those fields where the rate of return on investment is the main feature in deciding the development prospects. As marginal-field developments move further off-shore and into deeper waters, the per-barrel cost of recovering hydrocarbons increases. The reduction in field size reduces in further economic pressures on the development due to the reduced revenue available. With the current pace of technological advancements in exploration, drilling, production and transportation, the deep waters are seen as the new frontier.

Extraction of hydrocarbons from below deep waters also poses a host of new challenges ranging from reservoir management to flow assurance. Another major problem in the recovery of hydrocarbon fluids in sub-sea environments is that of the formation of solids such as scales and sand which can inhibit flows or in an extreme case results in total blockage of the flow lines between the well and the platform or on-shore installation. These solids also have the potential to cause hydrates, wax/paraffin, asphaltenes, corrosion/erosion, emulsions, slugging and combinations of any of these. Such problems inhibiting flow assurance have been discussed by Forsdyke (1997). He highlighted that process facilities, flowline operability and solid deposition will be significantly affected by multiphase flow regime, especially slugging over long distances, up large risers and in transient conditions. It is therefore important that even if solids are formed in the hydrocarbon pipelines, they should be carried along with the flowing fluid and not allowed to agglomerate so that their formation can be tolerated.

In a survey of operators, two principal types of solid formation, namely, hydrates and wax have been identified to be key issues to be addressed. Since late 1980s, some of the challenges such as wax deposition, hydrate formation, multiphase pumping and phase separation have been studied.

Introduction

Hydrates are crystalline forms of substance which contain water, light hydrocarbons, carbon dioxide and hydrogen sulphide. The dominant factor in hydrate formation is the presence of water and gases, which are absorbed to form hydrates in various amounts depending on the composition, temperature and pressure. The existence of solid hydrates for a given crude depends on pressure and temperature. At high temperatures, the hydrates are disassociated and do not form a solid phase. Below a certain temperature, hydrates are formed. The behaviour of hydrates formation is extremely complex but one way of preventing their formation (and possibility of pipeline blockage due to hydrate plugs) is to maintain a high enough temperature of the fluids, or the pressure at a low enough value. Hydrates can also be prevented by using inhibitors, such as methanol or glycol.

Waxes consist of a multitude of higher molecular weight paraffinic hydrocarbons, which are slightly soluble in the liquid phase of black oil and condensates. The amount of solid material present in the hydrocarbon liquid-phase increases as the temperature decreases and this can significantly affect the viscosity of the oil. If there are sufficient waxes present, for instance on the pipe wall, this causes reductions in the effective diameter of the pipe and more significantly an increase in the pipe wall internal roughness, giving an increase in flow resistance, and a decrease in the production rate.

Thermal management of pipeline systems to ensure that internal temperatures remain above the relevant wax and hydrate-deposition temperatures are broadly divided into two classes namely (i) thermally well insulated pipe-in-pipe systems and (ii) multi-tube systems (i.e. tube bundles).

- Insulated pipe-in-pipe systems have the production line surrounded by an insulating material contained in an outer pipe and

- A multi-tube system (tube bundles) is a method in which a number of lines are carried within the carrier pipe. Some of these lines may carry a

heating fluid (usually hot water) in order to maintain the temperature and compensate for heat losses from the system.

Adedigba (1988) investigated the steady-state rate of heat transfer across a cold horizontal rectangular trench, which was filled with insulating hollow plastic spheres to determine the optimal position of the cold pipe in order to achieve the least rate of heat losses from the supply pipe.

In the case of multi-tube systems where some lines carrying a heating fluid, the positioning of that pipe relative to the production line is important. A study by Babus'Haq et al. (1989) has revealed that the optimal configuration for such an arrangement is to install the hot pipe above the cold one.

As seen from the above, the basic issues in multiphase flow include energy, integrity and delivery. Energy dissipation is necessary to provide sufficient pressure to transport hydrocarbons at the required flow rates from the reservoir to process plant. Integrity is concerned with designing the pipeline system to ensure required flow rates are achieved. Delivery is to ensure that process plant can handle fluids that are delivered from flow lines.

Engineers encounter two-phase flow mostly in well tubing and in flow lines. The flow may be vertical, inclined or horizontal and methods must be available to satisfy the three basic issues (energy, integrity and delivery). These include proper understanding of the requirements of multiphase flows. For instance, pressure and temperature drops must be well predicted to maintain the required energy flow in the pipeline systems. Corrosion, wax and scale occurrence as well as hydrate formation need to be remedied. Slug prediction and catchers and effects of risers should be given adequate attention at the preliminary stage of designing the hydrocarbon pipeline system.

Several issues must be addressed throughout the lifetime of a multiphase system. As the fields mature, the pressure, temperature and chemical

Two-phase flow of gas-liquid mixtures in horizontal *helical pipes*; Adedigba (2007)

characteristics of the products from wells change and water cut increases. All of these will have significant impacts on the fluid recovery over the asset life.

1.3 Hydrocarbon production challenges in an off-shore environment

There are many challenges to be overcome in order to exploit hydrocarbon products from the off-shore environment. These challenges according to Hill, (1997) include increased depth of the pipeline which causes a greater hydrostatic stress on the pipe walls. Pressure gradients frequently induce vortex and vibrations of different intensity along the riser length. The nature of the water-current gradients dictate the type of rig infrastructure required to transport the hydrocarbon products from the off-shore to the process facilities on the platform. Montgomery (2002) shows some of the different flexible riser-shapes which were developed for different deep-water environmental conditions. These riser-shapes are shown in Figure 1-1

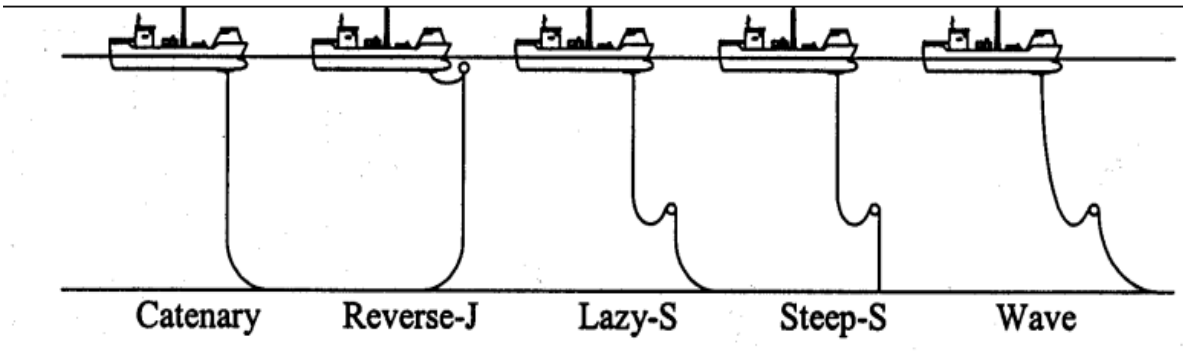

Figure 1-1: Riser shapes. Montgomery (2002)

Other related challenges that are likely to ensue in the deep-water environment include predicting the internal hydrodynamic behaviour which has an impact on the mechanical loads in the riser, the variations in hydrocarbon product delivery and corrosion or erosion of the internal surface of the pipeline. So the high-

pressure high-temperature like potential creep issues have to be critically considered as part of the deep-water challenges.

In order to solve these challenges, additional costs to the operational expenditure (OPEX) will be incurred. So in order to reduce the costs of oil fields, it is preferable to transport all the hydrocarbon products (gas, oil and water) coming from the wells to a process platform simultaneously, that is, through the same pipeline at the same time. It is then crucial to understand the multiphase phenomenon that then ensues in the pipeline in order to avoid unexpected crises and to increase productivity. Again, one of the most common problems to overcome in this area is severe slugging, which often occurs at a pipeline/riser junction. The process of severe slugging formation is described in section 5.2 of chapter 5 of this thesis.

1.4 Helical Pipes

Despite the great economic challenges of multiphase flows, particularly in the petroleum industry and the extensive study of multiphase flows over the last few decades, there has been little published work on *helical pipes* of more than 25.4 mm internal diameter. Most of the studies carried out on *helical pipes* have been on very narrow pipes of internal diameters of 12.7 mm or less and with high amplitudes. Therefore, the research study described in this thesis can be considered to be progressing the basic foundations of the subject of multiphase flows in *helical pipes*. In addition, it has opened up new avenues to be explored by future researchers particularly in multiphase flows in *helical pipes* of internal diameters exceeding 50 mm, low amplitude and their applications. The resulting knowledge will have many applications particularly in the petrochemical, process, and other industries where multiphase flows occur in low amplitude and much larger diameter pipes or tubes.

A *helical pipe*, because of its shape, can have significant changes on fluid flows in any pipeline systems and in heat transfer equipment. In particular, multiphase flow patterns in the *helical pipes* are different from those in the straight pipes of

Two-phase flow of gas-liquid mixtures in horizontal *helical pipes*; Adedigba (2007)

the same pipe dimensions and orientation. The flow regimes in *helical pipes* are also different from the flow regimes in equivalent straight pipes. Figure 1.2 shows a view of a *helical pipe* of internal-diameter **d**, helical diameter **D** and amplitude $\mathbf{A_P}$.

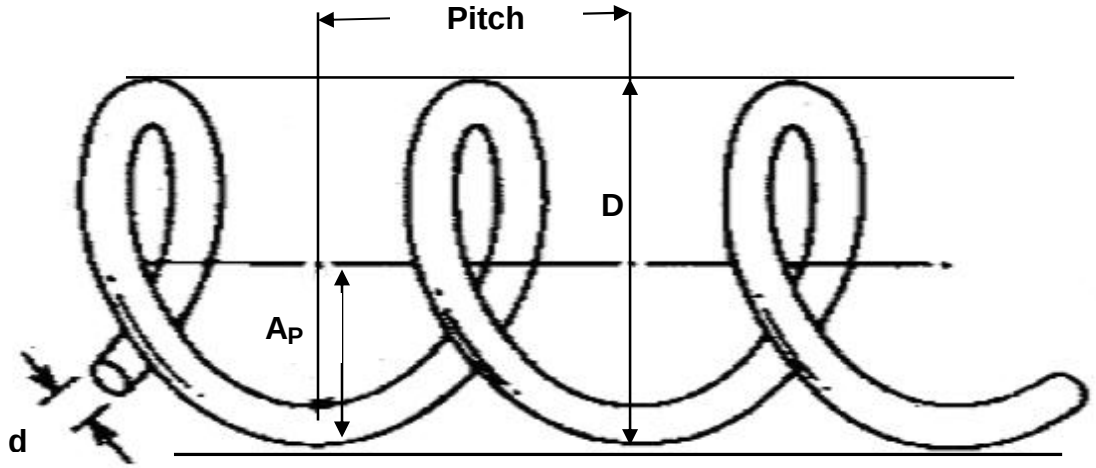

Figure 1-2: View of a helical pipe

Previous researchers, including Eustice (1910) and White (1929), found that coils have a higher pressure drop than straight pipes of the same diameter and length. Dean (1927) attributed the higher pressure drop to secondary circulations present due to centrifugal forces. White (1929) found the flow in a coil remains laminar at higher Reynolds numbers than in straight pipes. Due to the secondary circulation, the transition from laminar to turbulent flows is much less distinct than that for straight pipes.

Single-phase flow behaviour in coils has also been investigated by many authors and there are many equations to calculate the associated friction factor: these have been summarised by Srinivasan et al (1968) and Czop et al. (1994). Most of these studies are for coils with high amplitude and very little information exists on two-phase flow behaviour in *helical pipes* with low amplitude which is the focus of this investigation.

Slug flow is one of the regimes that ensue in multiphase flows. It is an intermittent flow pattern that commonly occurs in hydrocarbon transmission

pipelines. The slug flow is associated with an increase in pressure drop when compared with single-phase flow. The results of this research study have shown that the *helical pipe* by virtue of its geometry does not allow slug flow pattern to occur in multiphase flows in horizontal *helical pipes*. With this novel discovery, the flow assurance of hydrocarbon products is guaranteed in horizontal *helical pipes*. Also, from the flow visualizations observed during the course of this study, the occurrence of secondary flow in *helical pipe* imparts a swirling motion on the liquid-phase and the effect of that leads to a better mixing of the liquid-gas phase which again improves the flow assurance in multiphase flows.

1.5 Research Objectives

These have been to study experimentally two-phase hydrodynamic flow characteristics in horizontal *helical pipes* of low amplitude and compare the results with two-phase flow characteristics in straight pipes of the same internal-diameter. In particular, this objective was with a view to investigating the effectiveness of a *helical pipe* in destroying hydrodynamic slugs which occur in straight horizontal pipes which is a major problem in oil pipelines.

On the other hand, areas of applications for *helical pipes* have been found particularly in the petroleum industry. For this second reason considerable time has been spent using the three-phase facilities in the Department of Process and Systems Engineering laboratory of Cranfield University to investigate the hydrodynamic flow behaviour on a four-inch internal diameter *helical pipe* which was installed upstream of a catenary riser. The aim was to confirm if the *helical pipe* would reduce severe slugging in a pipeline riser system with a view to improving the production and transportation of hydrocarbon liquid. The result of this experiment has shown good promise for the use of a *helical pipe* to control severe slugging in the off-shore environment. The experimental result of this study will be added to the existing methods of controlling the menace of severe slugging in pipeline riser systems. Details of this result are discussed in chapter 6 of this thesis.

1.6 Thesis Structure

The structure of this thesis is given in chapter 1, which provides an introduction to the subject.

Chapter 2 reviews the pertinent literature concerning fluid flows through *helical pipes*. Empirical correlations for the calculation of frictional pressure drop in *helical coiled pipes* are also reviewed.

Chapter 3 describes preliminary experiments on 25.4 mm internal-diameter transparent PVC pipes (straight and helical). The chapter reports the experimental set-up and provides a discussion of the results.

Chapter 4 describes a series of experiments performed on 50 mm internal-diameter horizontal straight and *helical pipes*. This chapter also details the experimental set up, experimental data analysis and conclusions.

In chapter 5, applications of *helical pipes* are described. Criteria for the onset of severe slugging and the current methods of controlling severe slugging are reviewed in this chapter. The results of laboratory investigations on the effects of a *helical pipe* section installed upstream of a 10.5 m high catenary-shaped riser base are also discussed in this chapter.

Chapter 6 describes riser experiments which include details of the experimental facilities used, the data-acquisition system and results of analysis of severe slugging experiments.

Chapter 7 is the final chapter and it presents conclusions and recommendations for future work.

Chapter 2

2 Literature review

2.1 Introduction

Under various conditions encountered in the crude oil and natural gas industry, knowledge of the pressure drop and system liquid holdup is necessary for the safe, economic design and operation of pipeline systems. These properties will be determined by a variety of factors such as the inlet and outlet conditions, the physical properties of the fluids being transported and constraints such as pipe diameter and the terrain through which the pipeline passes. Consequently many studies (e.g. see McAdams et al., 1942; Lockhart & Martinelli, 1949; Baker, 1954; Baroczy, 1966; Eaton et al., 1967; Beggs & Brill, 1973; Friedel; 1979) have simply concentrated on providing generalised predictions of the flow characteristics. Of these generalised approaches, several researchers have developed their correlations by "best-fitting" a limited set of experimental runs.

A literature review of the industrially important parameters of pressure drop and liquid holdup have been undertaken during this study and presented in this chapter. Fluid flows in pipes are discussed in the first section of this chapter. A few generalised correlations for the two parameters (pressure drop and liquid holdup) are presented. Flow patterns in horizontal two-phase flow and steady-state flow pattern maps are described. Various methods for gas-liquid flow pattern detection are also reviewed. The second section reviews correlations for flows in helical coils.

2.2 Flow of fluids in pipes

Generally fluid flows in pipes can be characterized either as laminar or turbulent. Flows are said to be laminar when layers of fluid move relative to one another without any macroscopic intermixing. Laminar flow is also called streamline flow. It is associated with very viscous fluids or with low velocities and small dimensions. Laminar flow in pipes is said to occur if the Reynolds number is less than 2000.

Turbulent flow on the other hand has an irregular random movement of fluid in directions transverse to the main flow. The irregular fluctuating motion can be regarded as superimposed on the mean motion.

2.2.1 Single-phase flow in straight pipes

When a steady incompressible fluid flows through a straight pipe of constant circular cross-section, the velocity profile eventually attains a form which is independent of the axial co-ordinate. The flow is then said to be fully-developed.

Experimental evidence shows that the type of fully-developed flow that occurs in straight pipes of circular section is dependent on Reynolds number, Re (equation 2.1)

$$\mathrm{Re} = \frac{\rho u d}{\mu}$$ **Equation 2-1**

where

ρ is the density of the fluid

u is the velocity of the fluid

d is the pipe's internal diameter

μ is the dynamic viscosity of the fluid

For values of Reynolds number below 2000, the flow is said to be laminar, whereas values above 4000, the flow is said to be turbulent.

2.2.2 Laminar flow in circular-sectioned straight pipes

Fully-developed laminar flow in a straight pipe is often referred as Poiseuille or Hagen-Poiseuille flow. Miller (1978) recommended that for the purposes of analysis, it is convenient to use the Navier-Stokes equations expressed in cylindrical polar (r, θ) coordinates. The x-axis coincides with the axis of the duct and r denotes the radial coordinate measured outwards from the axis. Since the flow has axial symmetry about the x-axis, derivatives with respect to θ are zero. The system is governed by equations 2.2 and 2.3 after Miller (1978).

$$\frac{\partial u}{\partial x} + \frac{1}{r}\frac{\partial}{dr}(rv) = 0 \qquad \textbf{Equation 2-2}$$

$$\frac{\partial v}{\partial t} + u\frac{\partial v}{\partial x} + v\frac{\partial v}{\partial r} = -\frac{1}{\rho}\frac{\partial p}{\partial r} + v\left[\frac{1}{r}\frac{\partial}{\partial r}\left(r\frac{\partial v}{\partial r}\right) - \frac{v}{r^2} + \frac{\partial^2 v}{\partial x^2}\right] \qquad \textbf{Equation 2-3}$$

The axial velocity component is denoted by u and the radial component by v. For fully-developed flow, derivatives with respect to x vanish. Hence the continuity equation condition, (equation 2-2) shows that everywhere v appears is zero.

Evaluation of the momentum equation in the radial direction gives the result that pressure is constant at a cross-section, and the flow is fully specified by the momentum equation in the axial direction, which has the simplified form

$$\frac{dp}{dx} = \frac{\mu}{r}\frac{d}{dr}\left(r\frac{d\mu}{dr}\right) \qquad \textbf{Equation 2-4}$$

This equation may be integrated twice to obtain u in terms of r. The appropriate boundary conditions are:

i) $\frac{\partial u}{\partial r} = 0$ when r = 0

ii) $u = 0$ when r = 0

Poiseuille's equation for laminar flow is

$$\frac{-dp}{dx} = \frac{32\mu u}{d^2} = \frac{8\mu u}{a^2}$$ **Equation 2-5**

The friction factor, f is

$$f = \frac{\tau_W}{\frac{1}{2}\rho u^2}$$ **Equation 2-6**

where τ_W is the wall's shear-stress.

A force balance shows that for an incompressible flow,

$$\pi d\,\tau_W = -\frac{dp}{dx}\frac{\pi d^2}{4}$$ **Equation 2-7**

$$\tau_W = -\frac{dp}{dx}\frac{d}{4}$$ **Equation 2-8**

Hence

$$-\frac{dp}{dx} = \frac{4f}{d}\frac{1}{2}\rho u^2$$ **Equation 2-9**

Equations 2-6 to 2-9 are equally valid in both laminar and turbulent flows through circular pipes. Equation 2-9 is often referred to as Darcy or Darcy-Weisbach equation.

By eliminating $\frac{dp}{dx}$ between equations 2-5 and 2-9 gives equation 2-10

$$f = \frac{16\ \mu}{\rho\, ud} = \frac{16}{(\mathrm{Re})}$$ **Equation 2-10**

where (Re) = $\frac{\rho u d}{\mu}$ (equation 2-1)

Equation 2-10 shows the relationship between the friction factor and Reynolds number for laminar flow. The validity of this relationship has been confirmed experimentally by Stanton and Pannel (1914), Gunn and Darling (1963) and others over the range $10 \leq (Re) \leq 2000$ using air and thick oils.

2.2.3 Turbulent flow in circular-sectioned straight pipes

Turbulence is a complex phenomenon in fluid dynamics. Hence it is poorly understood. It is an area subject to considerable activities both on an experimental and analytical front. As a consequence of the increasing evidence that becomes available, old hypotheses are modified and new approaches are continually being introduced.

Research has shown that for attached flow close to the wall of pipes through which fluid flows, there is a region of flow where the proximity of the wall has a dominant influence on the velocity profile. This region is called the “inner or wall” region. Further away from this wall is the outer region in boundary-layer theory.

Investigations of the underlying motion within turbulent flows have shown that the turbulence is associated with the movement of rotating elements of fluid commonly known as eddies. The average diameter of these eddies in a given flow varies greatly. Unlike laminar flow, a problem with which the fluid dynamists sometimes confronted is to determine whether a turbulent flow is in fact fully-developed. The time-averaged velocity distribution, Reynolds stresses, wall shear stresses and axial pressure-gradient all become independent of axial distance, x within 70 times the pipe inner-diameter.

By varying the upstream conditions in a pipe, Patel (1974) and Lissenburg, Hinze and Leijdens (1975) have shown that variations in turbulence energy

spectra on the axis are much more persistent and can be measured up to 140 internal diameters downstream. This effect is explained by the fact that the larger eddies, which correspond with the low-frequency part of the spectrum, preserve their identity more readily than the smaller eddies. For fully turbulent flow v = 0 and w = 0. Also the velocity field is independent of x and derivatives with respect to angular coordinate (θ) are zero. Hence the momentum equations, in tensor-notation cylindrical polar coordinates, become

$$\frac{\partial p}{\partial x} = -\frac{\rho}{r}\frac{\partial}{\partial r}\left(\overline{ru^1v^1}\right) + \mu\left(\frac{\partial^2 u}{\partial r^2} + \frac{1}{r}\frac{\partial u}{\partial r}\right) \qquad \textbf{Equation 2-11}$$

$$\frac{\partial p}{\partial r} = \rho\left[-\frac{1}{r}\frac{\partial}{\partial r}\left(rv^{I2}\right) + \frac{\overline{w^{I2}}}{r}\right] \qquad \textbf{Equation 2-12}$$

and

$$0 = -\frac{\partial}{\partial r}\left(\overline{v^1w^1}\right) + 2\frac{\overline{v^1w}^1}{r} \qquad \textbf{Equation 2-13}$$

By integrating equations 2-11, 2-12 and 2-13 with respect to r and noting that at the wall of the pipe $\overline{v^1w^1} = 0,$ it follows that $\overline{v^1w^1}$ is zero for all values of r.

Thus the momentum equations for fully-developed turbulent incompressible flow reduce to

$$\frac{\partial p}{\partial x} = -\frac{\rho}{r}\frac{d}{dr}r\left(\overline{u^1v^1} - v\frac{du}{dr}\right) \qquad \textbf{Equation 2-14}$$

$$\frac{\partial p}{\partial r} = \rho\left[-\frac{1}{r}\frac{d}{dr}\left(\overline{rv^{I2}}\right) + \frac{\overline{w^{I2}}}{r}\right] \qquad \textbf{Equation 2-15}$$

Differentiating equation 2-15 with respect to x gives

$$\frac{\partial^2 p}{\partial r \partial x} = 0 \qquad \textbf{Equation 2-16}$$

Hence $\frac{\partial p}{\partial x}$ is independent of r and equations 2-14 and 2-15 may be integrated to give

$$\frac{r^2}{2}\frac{dp}{dx} = \rho\left[-r\left(\overline{u^1v^1} - v\frac{du}{dr}\right) + A(x)\right] \qquad \textbf{Equation 2-17}$$

$$\frac{p}{\rho} + \overline{v^{I2}} - \int_r^a \frac{\overline{w^{I2}} - \overline{v^{I2}}}{r} dr = B(x) \qquad \textbf{Equation 2-18}$$

where **a** is the pipe's internal radius. The boundary conditions at r = 0 are $\overline{u^1v^1}$ = 0, $\frac{du}{dr}$ = 0. Hence A(x) = O.

A force balance gives

$$\frac{dp}{dx} = -\frac{2}{a}\tau_W \qquad \textbf{Equation 2-19}$$

Introducing the friction velocity, u_W defined by $u_W = \left(\frac{\tau_W}{\rho}\right)^{\frac{1}{2}}$ it follows that

$$\frac{1}{\rho}\frac{\partial p}{\partial x} = -\frac{2}{a}{u_W}^2 \qquad \textbf{Equation 2-20}$$

which with p = p_w at x = 0, r = a, may be integrated again to obtain

$$\frac{p}{\rho} = -\frac{2}{a}{u_W}^2 x + C(r) + \frac{p_w}{\rho} \qquad \textbf{Equation 2-21}$$

Comparing equations 2-18 and 2-21 allows B(x) to be evaluated and hence equations 2-17 and 2-18 may be written in the form

$$\overline{u^1v^1} = v\frac{\partial u}{\partial r} + \frac{r}{a}{u_w}^2 \qquad \textbf{Equation 2-22}$$

$$\overline{v^{1^2}} + \int_r^a \frac{\overline{v^{I2}} - \overline{w^{I2}}}{r} dr = \frac{p_w}{\rho} + \frac{p}{\rho} - \frac{2}{a}{u_w}^2 x \qquad \textbf{Equation 2-23}$$

This is the final form of these two equations. Due to the presence of the turbulent terms, no further manipulation will reveal the relationships

$$u = u(r) \quad and \quad p = p(r) \qquad \textbf{Equation 2-24}$$

A further useful result concerns the shear-stress distribution in the flow. Equation 2-14 can be written in the alternative form

$$\frac{dp}{dx} = -\frac{1}{r}\frac{d}{dr}\left(r\tau_{XY}\right) = -\frac{1}{r}\frac{d}{dr}\left(r\tau\right) \qquad \textbf{Equation 2-25}$$

Integrating equation 2-25 with respect to r yields equation 2-26

$$\tau = -\frac{dp}{dx}\frac{r}{2} \qquad \textbf{Equation 2-26}$$

which can be written as:

$$\frac{\tau}{\tau_w} = \frac{r}{a} = \left(1 - \frac{y}{a}\right) \qquad \textbf{Equation 2-27}$$

This shows that the shear stress varies linearly over the cross-section.

On the other hand, the turbulent terms cause only a very small departure of the pressure from a constant value over the whole pipe's cross-section, and for all practical purposes in a straight pipe of constant cross-section it may be assumed that in turbulent flow, just as in laminar flow, the pressure is constant at a section. Turbulence measurements in pipe flow have been reported by Laufer (1949) and are further discussed by Townsend (1956), (1976) and Patel (1974).

Thus it has been demonstrated that the velocity profile cannot be calculated directly from the differential equations of turbulent flow. In order to proceed further with the consideration of fully-developed turbulent flow, it is necessary to have recourse to experimental data. In power-law relations for smooth and universal laws for the velocity distribution in smooth pipes, two widely-used approaches are examined to the consideration of velocity profiles, and other associated flow properties in incompressible turbulent-flow.

2.2.4 Single-phase flow pressure drop in a straight pipe

Generally, pressure drop in a straight pipe usually occurs due to frictional losses. For single-phase, non-compressible flow in a straight pipe, the frictional pressure drop can be calculated by applying equation 2-28.

$$\Delta P_f = 4 f \frac{l}{d} \frac{\rho u^2}{2}$$ **Equation 2-28**

where

ΔP_f is frictional pressure drop

f is Fanning friction factor

l is length of pipe considered

d is the internal diameter of the pipe

Friction factor is a function of Reynolds number. The Fanning friction factor for laminar flow is generally calculated by equation 2-29

$$f = \frac{16}{\mathrm{Re}}$$ **Equation 2-29**

For turbulent flows in smooth tubes, the Blasius equation, equation 2-30 is often used

$$f = 0.0079\,\mathrm{Re}^{-0.25}$$ **Equation 2-30**

Many other equations exist that can be used to calculate the turbulent friction factor. Other equations are shown in Bhatti and Shah (1987), Haaland (1983), Coulson and Richardson (1993), Perry (1984), Miller (1990), Ali and Seshadri (1971), Mori and Nakayama (1967b) and Lockin (1950). Alternatively, a friction factor versus Reynolds number chart can be used to determine the friction factor for different pipe roughnesses.

$\mathrm{Re} = \frac{\rho u d}{\mu}$ can be written as $\mathrm{Re} = \frac{Gd}{A\mu}$

where

Re is Reynolds number

G is mass flow rate

A is area

μ is dynamic viscosity

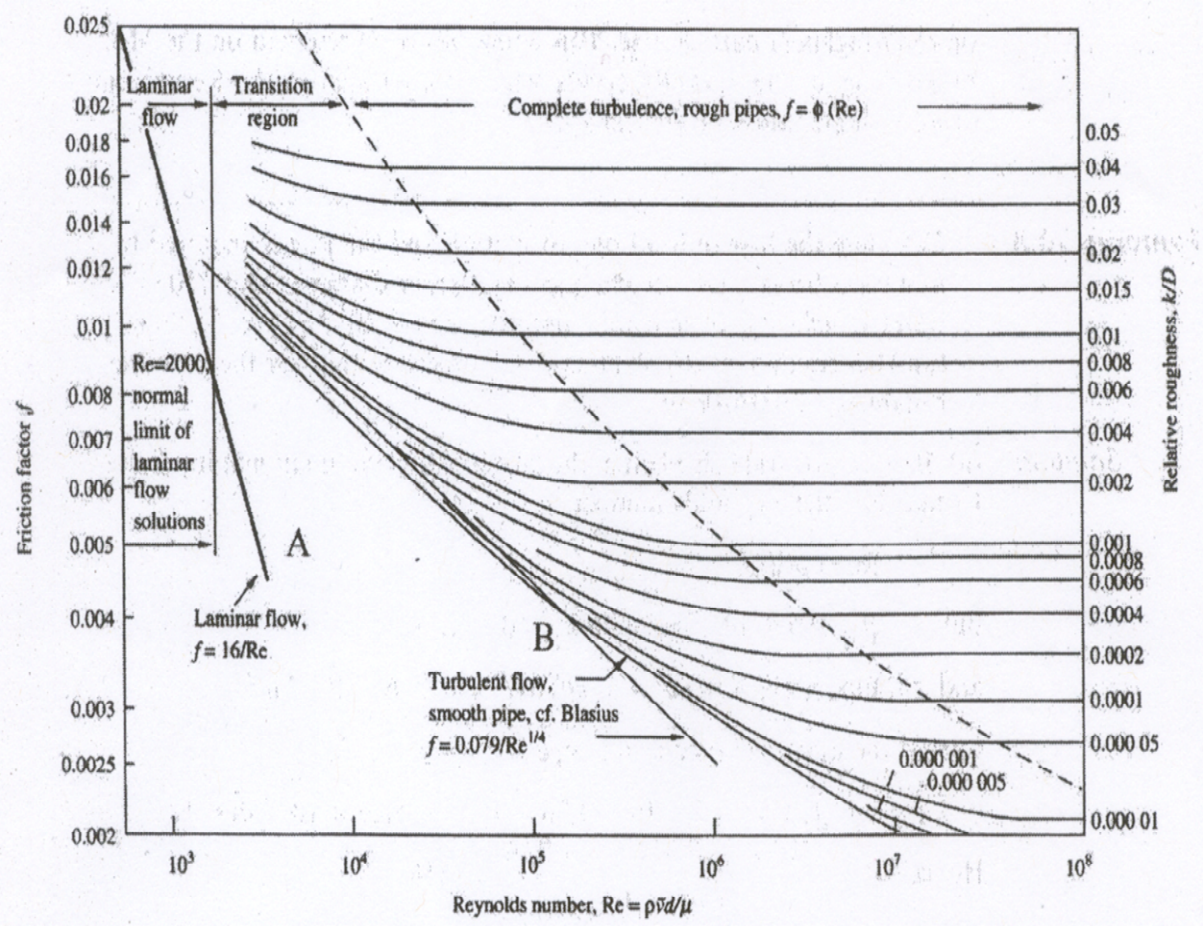

Figure 2-1: Friction factor chart after Douglas et al. (1998)

Figure 2-1 shows different regions corresponding to different flow types. The critical Reynolds number of 2000 represents the limit at which turbulent flow can be maintained once established. In the transition region between laminar and turbulent flows, the value of the friction factor is considerably higher than in streamline flow. In this region, it is difficult to reproduce pressure drop results

experimentally. Line B corresponds to turbulent flow through smooth tubes. At very high Reynolds numbers, the friction factor becomes independent of Reynolds number and depends only on the pipes relative roughness.

2.3 Two-phase flow in a straight pipe

The term ‘two-phase flow’ is used to describe any situation where a gas - liquid, gas - solid or liquid - solid mixture flows in a pipe. There are two types of two-phase flow: single component (e.g. steam - water) and two components (e.g. air - water, oil – water or oil -solid), and additional complications can be introduced when the former is present since then there is much more likelihood of mass transfer between the phases as the flow moves along the pipe, that is condensation or boiling may be taking place, with the result that conditions are not static. The case of two component flows of air and water is covered in this thesis with pipes in the horizontal position. Some studies on two-phase (oil–water, air-water, etc.) flows have been conducted: there still exists some uncertainties, and more data need to be added to the database of this kind of flow. Again, only gas - liquid mixtures have been considered in the research reported in this thesis since this is the most common type of two-phase flow.

Generally speaking, gas-liquid-liquid three-phase flows can be regarded as a special kind of gas-liquid two-phase flows. An ordinary gas-liquid two-phase flow is the two-phase flow of a gas and a uniform liquid, while gas-liquid-liquid, three-phase flow may be considered as the two-phase flow of a gas and a mixed liquid. Moreover, three-phase flows are always non-uniform spatially and temporarily in the pipe, which refers mainly to the non-uniformity of the liquid properties, such as viscosity, density and so on. On one hand, the non-uniformity makes the three-component flow considerably different from an ordinary gas-liquid two-phase flow. On the other hand, three-phase flow is strongly related to gas-liquid two-phase flow and therefore the methods, theories, correlations and conclusions developed for gas-liquid two-phase flow

can be used as the basis, reference or starting point in the investigation of three-phase flow.

Multiphase flows are far more complex than single-phase flows. The flow behaviour depends on component properties, their flow rates and system geometry. It is important in multiphase flow to understand the nature of the interactions among the phases and the influence on the phase distribution across the pipe's cross-section. The components often travel at different velocities giving rise to slip among the phases, which can influence a parameter like the liquid hold up. The residence times of each phase will often be different. The pressure drop in two-phase flows depends on the relative velocities of the phases and their flow patterns.

Compared with the numerous investigations of two-phase flow reported in the literature, there are only few publications on three-phase flow of gas-liquid-liquid mixtures. The review by Hewitt et al. (1995) states that the first paper on this subject was published six decades ago. Sobocinski (1953) conducted air-oil-water flow experiments and found that there is a maximum pressure gradient at an input water fraction in the liquid of approximately 0.77; this maximum value being even larger than that for an air-oil two-phase flow under the same conditions. Malinowsky (1975), Laflin and Oglesby (1976) and Hall (1992) confirmed the above result later but at different values of input water fractions and attributed it to phase inversion, i.e. an inversion in which the continuous phase changes from being oil to being water or vice versa. Sobocinski (1953) also noticed the effect of the oil and water configuration on flow patterns and tried to develop a three-dimensional flow- regime map for three-phase flow, but with limited success. Malinowsky (1975), Laflin and Oglesby (1976) and Stapelburg and Mewes (1994) extended existing two-phase flow regime maps to gas-liquid-liquid flow and claimed good agreement.

2.3.1 Two-phase flow pressure drop in straight pipes

Pressure drop is one of the most important parameters in the design of pipeline systems. Pipeline design requires a balance to be made among the cost of material thickness for pipeline fabrication, the driving pressure available at the pipeline inlet, the length of the pipeline and the required flowrate through the pipeline. The pressure gradient is strongly affected by the oil/water ratio: at constant total liquid volume flowrate, as the water fraction increases, the effective viscosity increases and therefore the frictional pressure gradient increases. At a time during the life span of any pipeline system, there is a dramatic drop in the effective viscosity (and hence the frictional pressure gradient) due to the change from the continuous phase being oil to it being water. There will be a further slight drop in viscosity if the water fraction increases from this point, due to decreasing oil content of the dispersion.

This phenomenon will occur in flows where the oil and water phases are well mixed. For example in slug flow, which is commonly observed in petroleum pipelines, the dominant component of the pressure gradient is from the motion of the liquid slugs, where the oil and water are likely to be well-mixed irrespective of the nature of the flow in the regions between slugs.

Many investigations have been carried out and many correlations and models have been proposed for prediction of the two-phase flow pressure drop. The total pressure loss gradient for a given steady state two-phase flow can be determined from the relation

$$\left(\frac{\Delta P}{L}\right)_T = \left(\frac{\Delta P}{L}\right)_{ACC} + \left(\frac{\Delta P}{L}\right)_{HH} + \left(\frac{\Delta P}{L}\right)_F \qquad \textbf{Equation 2-31}$$

where

$\left(\frac{\Delta P}{L}\right)_T$ is the total pressure loss gradient

$\left(\frac{\Delta P}{L}\right)_{ACC}$ is the pressure loss gradient due to acceleration (which is usually small)

$\left(\frac{\Delta P}{L}\right)_{HH}$ is the pressure loss gradient due to hydrostatic head (elevation)

$\left(\frac{\Delta P}{L}\right)_{F}$ is the pressure loss gradient due to fluid friction

In horizontal pipe flows, the head elevation and acceleration components can be neglected.

The most widely used graphical method for calculating a two-phase frictional pressure drop was produced by Lockhart and Martinelli (1949). Duckler et al. (1964) confirmed that the Lockhart and Martinelli method, although far from being perfect, was the best correlation they found. The Lockhart and Martinelli correlation is an extension of single-phase pressure drop calculations. The method considers two-phases separately and the combined effect is examined and this approach is called the 'separate-flow model'. Lockhart and Martinelli method is discussed in more detail in section 2.3.4.

There are generally two approaches to calculate two-phase pressure drop, namely the homogeneous model, where the gas and liquid are combined to form a mixture behaving as a homogeneous fluid and the separated model where the two fluids are considered separately and interact through the interfacial shear-stress.

2.3.2 Homogeneous flow model

In the two-phase homogeneous flow model, it is assumed that both phases are well mixed and flow at the same velocity. The homogeneous density and viscosity are used to calculate the pressure drop. The former can be calculated from equation 2-32, as shown in Whalley (1990).

$$\frac{1}{\rho_H} = \frac{x}{\rho_G} + \frac{1-x}{\rho_L}$$ **Equation 2-32**

where ρ_H is homogeneous density

Whalley presented three different equations for calculating the homogeneous viscosity. The simplest, is of the same form as the density equation and is

$$\frac{1}{\mu_H} = \frac{x}{\mu_G} + \frac{1-x}{\mu_L}$$ **Equation 2-33**

Dukler at al (1964) concluded that

$$\mu_H = \mu_G \frac{x\rho_H}{\rho_G} + \mu_L \frac{(1-x)\rho_H}{\rho_L}$$ **Equation 2-34**

Beattie and Whalley (1982) evolved equation 2-36 as a hybrid of other pertinent equations specific to certain flow patterns, to apply for flow patterns, using the void fraction, α. The equation was said to be suitable in conjunction with the Colebrook-White equation for the friction factor, shown as equation 2-35, even when the flow was laminar

$$\frac{1}{\sqrt{f}} = 3.48 - 4\log_{10}\left[2\frac{\varepsilon}{d} + \frac{9.35}{\mathrm{Re}\sqrt{f}}\right]$$ **Equation 2-35**

$$\mu_H = \mu_G\alpha + \mu_L(1-\alpha)(1+2.5\alpha)$$ **Equation 2-36**

where ε is the pipe's internal-surface roughness

Laskey (2002) reported that Whalley derived an equation for determining the total pressure drop for homogenous flow.

$$-\frac{\Delta \mathrm{P}}{\Delta Z} = \frac{2f_{L2}}{d\rho_H}\left(\frac{G}{A}\right)^2 + \rho_H g + \left(\frac{G}{A}\right)^2 \frac{d}{dz}\left(\frac{1}{\rho_H}\right)$$ **Equation 2-37**

This can be integrated for the total pressure change from an inlet of zero to an outlet of x_0.

$$-\frac{\Delta P}{\Delta Z}=\frac{2 f_{L2} l}{d}\left(\frac{G}{A}\right)^2\overline{\left[\frac{1}{\rho_H}\right]}+\overline{\rho_H} g l+\left(\frac{G}{A}\right)^2\left[\frac{1}{\rho_{H2}}-\frac{1}{\rho_L}\right] \qquad \textbf{Equation 2-38}$$

where

l is length

ρ_{H2} is the homogeneous density ρ_H when $x = x_2$. Equation 2-32 for the homogeneous density can be rearranged to produce equations 2-39 – 2-42.

$$\overline{\rho_H}=\rho_L\frac{In(1+X_2)}{X_2} \qquad \textbf{Equation 2-39}$$

$$\overline{\left[\frac{1}{\rho_H}\right]}=\frac{1}{\rho_L}\left(1+\frac{X_2}{2}\right) \qquad \textbf{Equation 2-40}$$

$$\frac{1}{\rho_{H2}}-\frac{1}{\rho_L}=\frac{X_2}{\rho_L} \qquad \textbf{Equation 2-41}$$

where

$$X_2=x_2\left[\frac{\rho_L-\rho_G}{\rho_G}\right] \qquad \textbf{Equation 2-42}$$

x_2 is gas mass fraction at the outlet

Hence, the total pressure change in a homogeneous flow can be written as

$$-\Delta P=\underset{A}{\left(\frac{2 f_{L2} l}{d}\left(\frac{G}{A}\right)^2\frac{1}{\rho_L}\right)}\underset{B}{\left(1+\frac{X_2}{2}\right)}+\underset{C}{\left(\rho_L g l\right)}\underset{D}{\left(\frac{In(1+X_2)}{X_2}\right)}+\underset{E}{\left(\frac{G}{A}\right)^2\frac{X_2}{\rho_L}} \qquad \textbf{Equation 2-43}$$

where

A is liquid-only frictional pressure change

B is additional term because of two-phase flow

C is liquid only gravitational pressure change

D is additional term because of two-phase flow

E is momentum pressure change.

In order to achieve a fully mixed, fluid in which the velocities of gas and liquid phase are equal, i.e. the homogeneous approach, a linear average equation can also be used as follows:

$$\rho_M = \frac{\rho_G \rho_L}{x\rho_L + (1-x)\rho_G} = (1-\varepsilon_{NL})\rho_G + \varepsilon_{NL}\rho_L \qquad \textbf{Equation 2-44}$$

where the liquid holdup ε_{NL} and the flow quality x are defined as:

$$\varepsilon_{NL} = \frac{u_{L,S}}{u_{L,S} + u_{G,S}} \qquad \textbf{Equation 2-45}$$

$$x = \frac{m_G}{m_G + m_L} \qquad \textbf{Equation 2-46}$$

where

m_G is gas mass flux

m_L is liquid mass flux

For viscosity, a linear form can also be used as follows:

$$\eta_M = (1-\varepsilon_{NL})\eta_G + \varepsilon_{NL}\eta_L \qquad \textbf{Equation 2-47}$$

There are many prediction models for measuring the pressure drop in two-phase flows using the homogeneous approach. They include the following.

McAdams et al. (1942)

They used the mass flux relationship to determine the pressure gradient using:

$$\left(\frac{d\mathrm{P}}{dz}\right)_M = \frac{2f\left(m_G - m_L\right)^2}{d\rho_M} \qquad \textbf{Equation 2-48}$$

where the frictional factor f is estimated by a Blasius-type formula:

$$f = 0.079\left(\mathrm{Re}_M\right)^{-0.25} \qquad \textbf{Equation 2-49}$$

in which the mixture's Reynolds number Re_M is

$$\mathrm{Re}_M = \frac{\left(m_L + m_G\right)d}{\eta_M} \qquad \textbf{Equation 2-50}$$

where η_M is the mixture's viscosity, which McAdams et al. calculated from the equation 2-51

$$\frac{1}{\eta_M} = \frac{x}{\eta_G} + \frac{\left(1-x\right)}{\eta_L} \qquad \textbf{Equation 2-51}$$

where η_G and η_L are the viscosities of the gas and the liquid phases respectively.

Beattie and Whalley (1982)

They developed a somewhat similar approach by incorporating different definitions for the friction factor f and the mixture viscosity η_M from those used by McAdams et al. (1942). This implicit model uses the frictional factor relationship developed by Colebrook (1939):

$$\frac{1}{\sqrt{f}} = 3.48 - 4\log_{10}\left[2\frac{\varepsilon}{d} + \frac{9.35}{\mathrm{Re}_M\sqrt{f}}\right] \qquad \textbf{Equation 2-52}$$

where ε is the equivalent internal surface roughness height and the mixture Reynolds number Re_M is determined using equation 2-50

Beattie and Whalley proposed the following mixture viscosity relationship, in an attempt to take into account the flow pattern.

$$\eta_M = \eta_L \varepsilon_{NL}\left[1 + 2.5\left(1 - \varepsilon_{NL}\right)\right] + \eta_G\left(1 - \varepsilon_{NL}\right) \quad \textbf{Equation 2-53}$$

The liquid holdup ε_{NL} is calculated using equation 2-45 and the pressure gradient is evaluated using equation 2-48.

2.3.3 Correlations arising for the homogeneous model for two-phase flow

Dukler et al. (1964)

They proposed the following two-phase pressure drop model:

$$\left(\frac{d\mathrm{P}}{dz}\right)_M = \frac{2\left(m_G - m_L\right)^2}{d\rho_M} f_{NS} \quad \textbf{Equation 2-54}$$

where friction factor f_{NS} is estimated as:

$$f_{NS} = \left[0.0014 + 0.125\left(\mathrm{Re}_M\right)^{-0.32}\right]\left[\varepsilon_{NL}\frac{\rho_L}{\rho_M} + \left(1 - \varepsilon_{NL}\right)\frac{\rho_G}{\rho_M}\right] \quad \textbf{Equation 2-55}$$

The mean gas-liquid mixture density (based on respective volumes) and viscosity are evaluated using equations 2-44 and 2-47 respectively. The mixture Reynolds number Re_M is defined by equation 2-50 with the holdup ε_{NL} given by equation 2-45

Beggs & Brill (1973)

A correlation for evaluating the pressure gradient for two-phase flow was introduced by Beggs & Brill (1973) as follows:

$$\left(\frac{d\mathrm{P}}{dz}\right)_M = \frac{2\left(m_G - m_L\right)^2}{d\rho_M} f_M \quad \textbf{Equation 2-56}$$

where the friction factor formula for the mixture is:

$$f_M = \left[2\log\left(\frac{\mathrm{Re}_M}{4.5223\log \mathrm{Re}_M - 3.8215} \right) \right]^{-2} \frac{\exp(C)}{4} \qquad \textbf{Equation 2-57}$$

where ρ_M and Re_M are given by equations 2-44 and 2-50 respectively, and C is determined by the parameter,

$$y_B = \frac{\varepsilon_{NL}}{\varepsilon^2_L} \qquad \textbf{Equation 2-58}$$

where ε_L is the actual in-situ liquid holdup: for y_B values in the range 1 < y_B < 1.2, the parameter C is given by

$$C = In(2.2y_B - 1.2) \qquad \textbf{Equation 2-59}$$

and for all other y_B values:

$$C = \frac{Iny_B}{-0.0523 + 3.182\,Iny_B - 0.8725\,(Iny_B)^2 + 0.01853\,(Iny_B)^4} \qquad \textbf{Equation 2-60}$$

The liquid holdup ε_{NL} is given by equation 2-45. It is somewhat inconsistent to use the value of ε_{NL} in a homogeneous type model since $\varepsilon_L \neq \varepsilon_{NL}$ implies a relationship between the phases. However, the whole correlation package should be regarded as an entity; the package being justified on its fit of the data on which it was based.

2.3.4 Separated flow model

This approach recognizes that the velocities of the gas and liquid phases are different. Combined equations are therefore written to take account of this. Empirical or semi-empirical correlations are developed in which the friction component of the pressure gradient is related to the pressure gradient of a single-phase flowing alone in the pipe. The pressure gradient multiplier ϕ^2_L is

applied to the single-phase (normally the liquid-phase) pressure gradient as follows:

$$\left(\frac{d\mathrm{P}_f}{dz}\right)_M = \phi^2{}_L\left(\frac{d\mathrm{P}_f}{dz}\right)_L \qquad \textbf{Equation 2-61}$$

The single-phase gradient is calculated assuming a uniform liquid-wall shear stress:

$$\left(\frac{d\mathrm{P}_f}{dz}\right)_L = \frac{4}{d}\tau_{WL} \qquad \textbf{Equation 2-62}$$

where the liquid-wall shear stress is evaluated using the liquid phase velocity:

$$\tau_{WL} = f_L \frac{\rho_L u^2{}_L}{2} \qquad \textbf{Equation 2-63}$$

The friction factor f_L is calculated from standard single-phase correlations.

As shown in equation 2-64, the single-phase liquid pressure gradient $\left(\frac{dP_f}{dz}\right)_L$ is given by:

$$\left(\frac{d\mathrm{P}_f}{dz}\right)_L = \frac{2 f_L m^2{}_L}{d\rho_L} \qquad \textbf{Equation 2-64}$$

The liquid's friction factor is calculated based on the nature of the flow, as determined by the Reynolds number. The latter is evaluated using the superficial liquid velocity:

$$\mathrm{Re}_{L,S} = \frac{\rho_L U_{L,S} d}{\eta_L} \qquad \textbf{Equation 2-65}$$

where the liquid's friction factor is determined using the following criteria:

$$f_L = \frac{16}{\mathrm{Re}_{L,s}} \quad (\textit{for}\ \mathrm{Re}_{L,S} < 2100) \qquad \textbf{Equation 2-66}$$

$$f_L = 0.042\,\mathrm{Re}^{-0.2}{}_{L,S} \quad (\textit{for}\ \mathrm{Re}_{L,S} \geq 2100) \qquad \textbf{Equation 2-67}$$

In the original literature, the multiplier ϕ_L was given in graphical form as a function of the ''Martinelli parameter'' X which was defined by:

$$X^2 = \frac{\left(dP_f / dz\right)_L}{\left(dP_f / dz\right)_G}$$ **Equation 2-68**

where the single-phase gas pressure gradient is:

$$\left(\frac{d\mathrm{P}_f}{dz}\right)_G = \frac{2 f_G m_G}{d\rho_G}$$ **Equation 2-69**

The friction factor of the gas is also dependent on the nature of the flow and is calculated in a similar manner to the liquid's friction factor:

$$f_G = \frac{16}{\mathrm{Re}_{G,s}} (\mathrm{Re}_{G,S} < 2100)$$ **Equation 2-70**

$$f_G = 0.042\,\mathrm{Re}^{-0.2}{}_{G,S}\,(\mathrm{Re}_{G,S} \geq 2100)$$ **Equation 2-71**

where the Reynolds number is based on the superficial gas velocity shown in equation 2-72

$$\mathrm{Re}_{G,S} = \frac{\rho_G U_{G,S} d}{\eta_G}$$ **Equation 2-72**

Lockhart & Martinelli (1949)

They proposed a graphical correlation in which the two-phase pressure gradient is calculated by applying a multiphase multiplier $\left(\phi^2{}_L\right)$ to the single-phase result. The two-phase pressure drop can be calculated from either equation 2-61 or equation 2-62 for gas or liquid separated flows respectively. The graphical correlation uses a parameter X calculated from the pressure drop for each phase if flowing alone. This is shown in equation 2-73.

$$\frac{-\Delta P_{TP}}{-\Delta P_G} = \phi_G{}^2$$ **Equation 2-73**

$$\frac{-\Delta P_{TP}}{-\Delta P_L} = \phi_L{}^2 \qquad \textbf{Equation 2-74}$$

$$X = \sqrt{\frac{-\Delta P_L}{-\Delta P_G}} \qquad \textbf{Equation 2-75}$$

where

$\phi_L{}^2$ and $\phi_G{}^2$ are the two-phase multipliers

$-\Delta P_{TP}$ is the two-phase flow pressure drop

$-\Delta P_L$ and $-\Delta P_L$ are the frictional pressure drops for the liquid and gas flows alone

X is the Lockhart and Martinelli parameter

The relationship, between X and the two-phase multipliers ($\phi_L{}^2$ and $\phi_G{}^2$) which was derived graphically is shown in Figure 2-2. It shows four separate curves depending on whether each phase was laminar or turbulent. The relationship was developed with tubes from 1.5 mm up to 25 mm in internal-diameter, with flows of water, oils and hydrocarbons, with air. Perry (1984) found that the correlation could be applied for pipes up to 100 mm in internal-diameter, with a similar degree of accuracy. Generally, the predictions were high for stratified, wavy and slug flows and low for annular flow. Many investigators therefore have studied flows in pipes and developed pressure drop correlations for their particular systems.

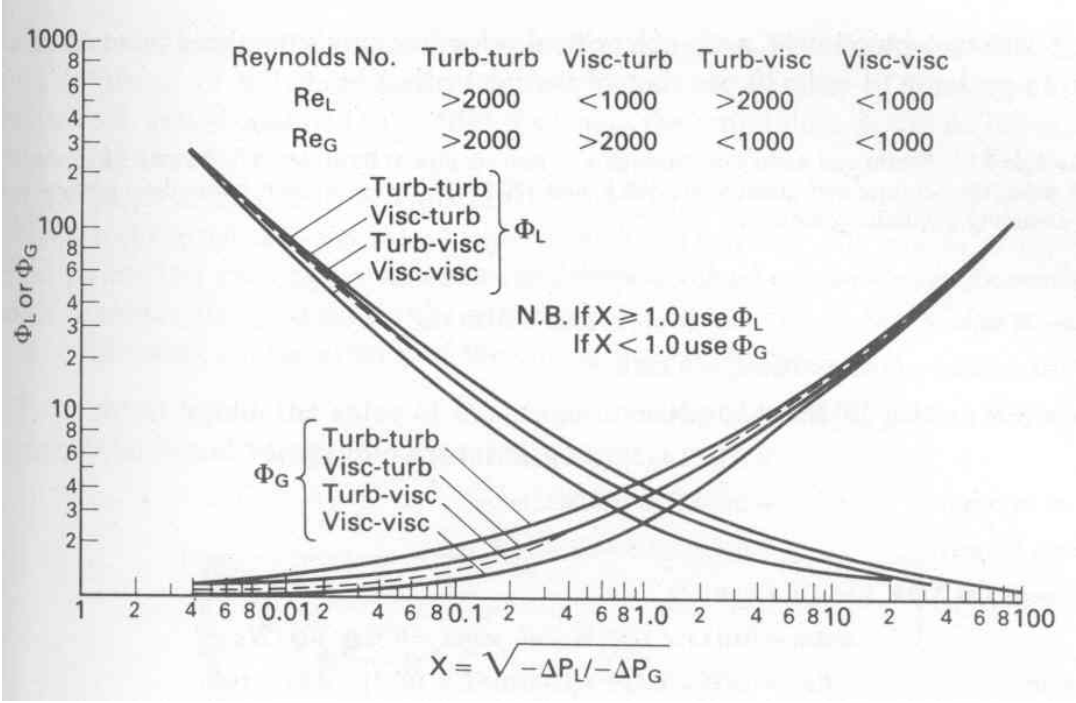

Figure 2-2: Lockhart and Martinelli correlation of X and ϕ

Coulson and Richardson (1993)

Chisholm (1967) developed the following formula that accurately fits the original graphical curve for the pressure gradient multiplier:

$$\phi^2_L = 1 + \frac{C_1}{X} + \frac{1}{X^2} \qquad \textbf{Equation 2-76}$$

where C_1, depends on the nature of the flow for the two phases.

Table 2-1 shows values of C_1 for the four possible turbulent/laminar permutations

Gas	Liquid	C_1
Laminar	Laminar	5
Laminar	Turbulent	10
Turbulent	Laminar	12
Turbulent	Turbulent	20

Table 2-1: Values of Constant C_1. Chisholm (1967)

Baroczy (1966) / Chisholm (1973)

Baroczy use the separated-flow analysis to develop a widely applied two-phase empirical correlation. The original graphical relationship for the pressure gradient multiplier (ϕ^2_{LO}) was curve-fitted to the following correlation by Chisholm (1973):

$$\phi^2_{LO} = \frac{\left(dP/dz\right)_M}{\left(dP_f/dz\right)_{LO}} = 1 + (C^2_2 - 1)\left[C_3 x^{(2-n)/2} + (1-x)^{(2-n)/2} + x^{2-n}\right] \quad \textbf{Equation 2-77}$$

where $\left(dP/dz\right)_{LO}$ is the friction pressure gradient for a fluid flowing along the pipe, n is the power in the friction factor - Reynolds number relationship (1 for laminar flows and 0.5 for turbulent flows in the Blasuis equation), x is the quality defined by equation 2-46 and C_3 is given by:

$$C_3 = \frac{55}{\left(m_G + m_L\right)^{0.5}} \; for \; 0 < C_2 < 9.5 \quad \textbf{Equation 2-78}$$

$$C_3 = \frac{520}{C_2\left(m_L + m_G\right)^{0.5}} \; for \; 9.5 < C_2 < 28 \quad \textbf{Equation 2-79}$$

$$C_3 = \frac{15000}{C^2_2\left(m_G + m_L\right)^{0.5}} \; for \; 28 < C_2 \quad \textbf{Equation 2-80}$$

with parameter C_2 defined as:

$$C^2_2 = \frac{\left(dP_f/dz\right)_{GO}}{\left(dP_f/dz\right)_{LO}} \quad \textbf{Equation 2-81}$$

where $\left(dP_f/dz\right)_{GO}$ is the frictional pressure gradient for a fluid flowing through the pipe having the physical properties of the gas,

$\left(dP_f/dz\right)_{LO}$ and $\left(dP_f/dz\right)_{GO}$ are calculated from:

$$\left(dP_f/dz\right)_{LO} = \frac{2 f_L (m_G + m_L)^2}{d\rho_L} \quad \textbf{Equation 2-82}$$

$$\left(dP_f \big/ dz\right)_{GO} = \frac{2 f_G (m_G + m_L)^2}{d\rho_G} \qquad \textbf{Equation 2-83}$$

The gas and liquid friction factors used in the above formulae are evaluated according to the nature of the flow, as determined by the values of the respective Reynolds numbers.

$$\mathrm{Re}_{LO} = \frac{(m_G + m_L)d}{\eta_L} \qquad \textbf{Equation 2-84}$$

$$\mathrm{Re}_{GO} = \frac{(m_G + m_L)d}{\eta_G} \qquad \textbf{Equation 2-85}$$

For laminar flow, the friction factors are given by:

$$f_{LO} = \frac{16}{\mathrm{Re}_{LO}} (\mathrm{Re}_{LO} < 2000) \qquad \textbf{Equation 2-86}$$

$$f_{GO} = \frac{16}{\mathrm{Re}_{GO}} (\mathrm{Re}_{GO} < 2000) \qquad \textbf{Equation 2-87}$$

where, as for turbulent flow, the following equations are used:

$$f_{LO} = 0.079\ \mathrm{Re}^{-0.25}{}_{LO}\ (\mathrm{Re}_{LO} \geq 2000) \qquad \textbf{Equation 2-88}$$

$$f_{GO} = 0.079\ \mathrm{Re}^{-0.25}{}_{GO}\ (\mathrm{Re}_{GO} \geq 2000) \qquad \textbf{Equation 2-89}$$

and:

$$\left(\frac{dp}{dx}\right)_{C_3} = \phi^2{}_{LO} \left(\frac{dp}{dx}\right)_{LO} \qquad \textbf{Equation 2-90}$$

Friedel (1980) concluded that this method was one of the best in his comparison of 14 pressure drop correlations using 12,868 data points. It was also recommended by Hewitt (1982) as the most widely used, advanced empirical correlation available at that time.

Friedel (1979)

Friedel proposed a pressure drop multiplier correlation based on 25,000 data points as follows:

$$\phi^2_{LO} = C_4 + \frac{3.24 C_5 C_6}{Fr_M^{0.045} We_M^{0.035}} \qquad \textbf{Equation 2-91}$$

where the parameters C_4, C_5 and C_6 are evaluated by:

$$C_4 = (1-x)^2 + x^2 \frac{\rho_L f_{GO}}{\rho_G f_{LO}} \qquad \textbf{Equation 2-92}$$

$$C_5 = x^{0.78}(1+x)^{0.24} \qquad \textbf{Equation 2-93}$$

$$C_6 = \left(\frac{\rho_L}{\rho_G}\right)^{0.91} \left(\frac{\eta_G}{\eta_L}\right)^{0.19} \left(1-\frac{\eta_G}{\eta_L}\right)^{0.7} \qquad \textbf{Equation 2-94}$$

The Weber number We_M, accounts for surface-tension effects.

$$\mathrm{We_M} = \frac{(m_G + m_L)^2 d}{\sigma \rho_M} \qquad \textbf{Equation 2-95}$$

The Froude number Fr_M is determined by:

$$\mathrm{Fr_M} = \frac{(u_{G,S} + u_{L,S})^2}{gd} \qquad \textbf{Equation 2-96}$$

The mixture density ρ_M in this correlation is evaluated using equation 2-44, that is, the homogeneous value. The friction factors f_{LO} and f_{GO} are calculated using equations 2-86 to 2-89.

2.3.4.1 Liquid holdup prediction

A wide range of correlations for in-situ holdup has been developed for use with the separated flow model and other models. Typical examples include: Lockhart

and Martinelli (1949), Guzhov et al. (1967), Premoli et al. (1971), Beggs and Brill (1973), Chen and Spedding (1981) and Kwaji et al. (1987). Brief descriptions of these correlations are given below.

Lockhart and Martinelli (1949)

Lockhart and Martinelli (1949) presented a graphical relationship between the liquid holdup ε_L and dimensionless parameters X. Pan (1996) accurately curve-fitted the original graphical form to the following formula for two-phase liquid holdup ε_{LT}:

$$\varepsilon_{LT} = 0.228 + 0.11(InX) + 0.0126[In(X)]^2 - 0.00109[(InX)]^3 \quad \textbf{Equation 2-97}$$

Guzhov et al. (1967)

Guzhov et al. (1967) presented a liquid holdup relationship based on the input liquid-fraction ε_{NL} and the mixture velocity via the mixture Froude number (Fr_M).

$$\varepsilon_{LT} = 1 - 0.81(1 - \varepsilon_{NL})\left[1 - \exp(-2.2 Fr_M{}^{0.5})\right] \quad \textbf{Equation 2-98}$$

where ε_{NL} and Fr_M are evaluated using equations 2-45 and 2-96 respectively.

Premoli et al. (1971)

A correlation was developed by Premoli et al. (1971) by making use of the velocity ratio C_7 to calculate the liquid holdup:

$$\varepsilon_{LT} = \frac{C_7 \rho_G (1 - x)}{C_7 \rho_G (1 - x) + \rho_L x} \quad \textbf{Equation 2-99}$$

The quality x has already been defined, while velocity ratio C_7 is defined by:

$$C_7 = 1 + C_8 \left(\frac{y_P}{1 + y_P C_9} - y_P C_9 \right)^{0.5} \quad \textbf{Equation 2-100}$$

and

$$y_p = \frac{1 - \varepsilon_{NL}}{\varepsilon_{NL}} \quad \textbf{Equation 2-101}$$

The non-slip liquid holdup ε_{NL} is defined in equation 2-45 and parameters C_8 and C_9 are defined as follows:

$$C_8 = 1.578\,\mathrm{Re}_p^{-0.19}\left(\frac{\rho_L}{\rho_G}\right)^{0.22} \qquad \textbf{Equation 2-102}$$

$$C_9 = 0.0273 We_p\,\mathrm{Re}_p^{-0.51}\left(\frac{\rho_L}{\rho_G}\right)^{-0.08} \qquad \textbf{Equation 2-103}$$

where the Reynolds number Re_p is based on equation 2-84

The Weber number We_p is defined in a similar manner to the Reynolds number as follows:

$$We_p = \frac{(m_L - m_G)^2 d}{\sigma \rho_L} \qquad \textbf{Equation 2-104}$$

Taitel & Dukler (1976)

Taitel & Dukler (1976) extended the work of Lockhart and Martinelli (1949) by solving steady-state one-dimensional gas-liquid momentum balances in dimensionless form to provide a plot of dimensionless liquid height $\left(h_L/D\right)$ against the Lockhart and Martinelli parameter $\left(X_{L-M}\right)$ at different pipe-inclinations. This was achieved by including an additional dimensionless inclination-parameter$\left(Y_{L\text{-}M}\right)$, where:

$$Y_{L-M} = .\left[\frac{(\rho_L - \rho_G) g \sin\beta}{\left(\frac{dp}{dx}\right)_{GS}}\right] \qquad \textbf{Equation 2-105}$$

Subsequently, by converting the dimensionless liquid-height $\left(h_L/D\right)$ into liquid holdup ε_{LT}, the following geometric relationship was used

$$\varepsilon_{LT} = \left(\frac{1}{\pi}\right)\left\{\pi - \cos^{-1}\left[2\left(h_L/d\right)-1\right] + \left[2\left(h_L/d\right)-1\right]\sqrt{\left(1-\left[2\left(h_L/d\right)-1\right]^2\right)}\right\}$$

Equation 2-106

and it is possible to obtain a plot of liquid holdup ε_{LT} against X_{L-M} for different values of Y_{L-M} as shown in Figure 2-3.

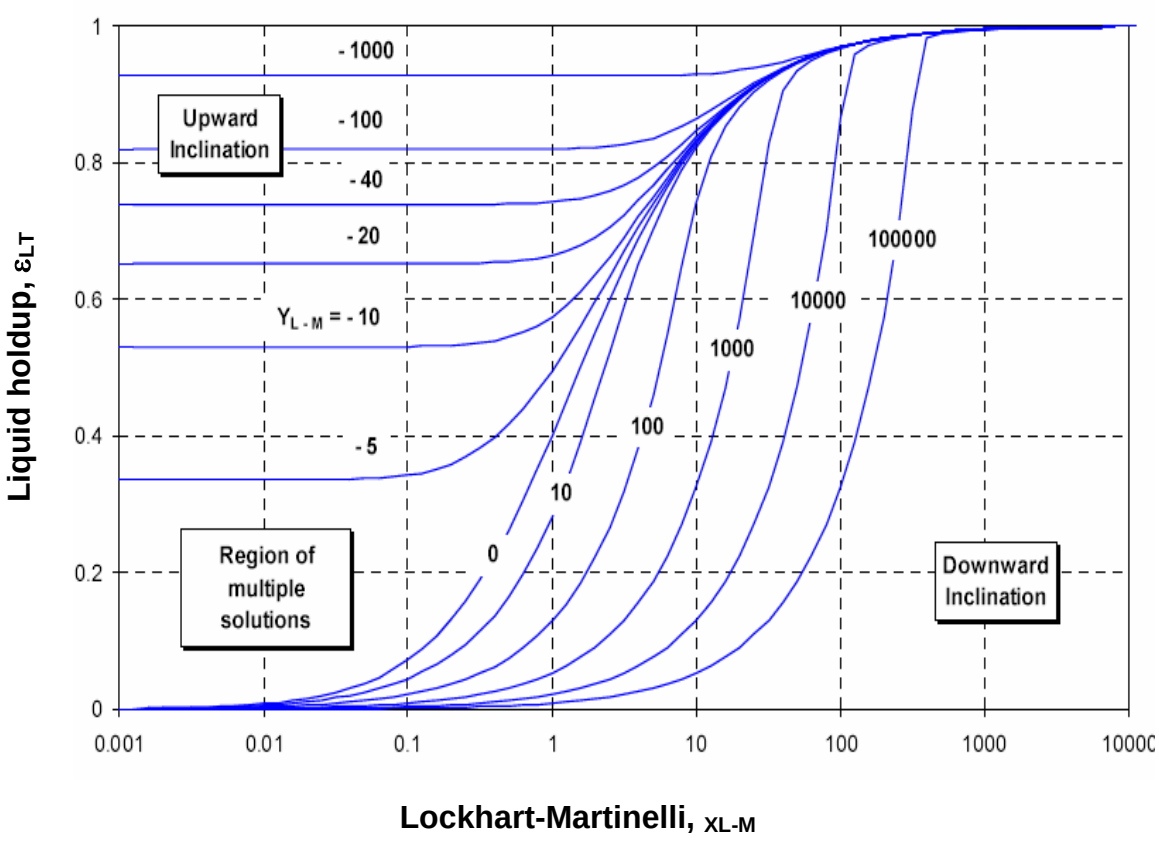

Figure 2-3: Liquid holdup (ε_{LT}) against Lockhart and Martinelli parameter (X_{L-M}) for different values of the Inclination parameter (Y_{L-M})

Turbulent gas and liquid flow is assumed in the plot of Liquid holdup (ε_{LT}) against Lockhart and Martinelli parameter (X_{L-M}) for different values of Inclination parameter (Y_{L-M}) shown in Figure 2-3.

Hughmark (1962)

Hughmark (1962) adopted a different approach to produce his liquid holdup correlation for vertical flow, but it was found that it also worked reasonably well for flows through horizontal pipes. This prediction was provided in the form of a graphical relationship between the parameters K_H and Z_H where

$$K_H = \frac{(1-\varepsilon_{LT})}{(1-\lambda)} \qquad \textbf{Equation 2-107}$$

$$Z_H = [\mathrm{Re}_H]^{\frac{1}{6}}[Fr_M]^{\frac{1}{8}}\lambda_L{}^{-\frac{1}{4}} \qquad \textbf{Equation 2-108}$$

$$\mathrm{Re}_H = \frac{(\rho_L u_{LS} + \rho_G u_{GS})d}{(1-\varepsilon_{LT})\mu_G + \varepsilon_{LT}\mu_L} \qquad \textbf{Equation 2-109}$$

Pan (1996)

For convenience, the above relationship was fitted by Pan (1996) with the following formula:

$$K_H = \exp\left[\begin{array}{l} -2.124 + 1.721(InZ_H) - 0.316(InZ_H)^2 - 0.124(InZ_H)^3 \\ +0.051(InZ_H)^4 - 0.005(InZ_H)^5 \end{array}\right]$$

Equation 2-110

However, since liquid holdup ε_{LT} appears in both Z_H and K_H, an iterative procedure will still be required to predict ε_{LT}. Inspite of these limitations, Mandhane et al. (1975) found that this correlation provided a very good overall agreement with a database of 2685 data points stored in the University of Calgary Multiphase Pipe Flow Data Bank, which represents a large number of independent studies.

Eaton et al. (1967)

Eaton et al. (1967) proposed an alternative graphical relationship between the liquid holdup ε_{LT} and a dimensionless group Z_E. His proposal was based on

tests in 518 m long horizontal pipelines of 50.8 mm and 101.6 mm internal diameters with water, distillate and crude oil used separately as the liquid phase and natural gas as the second phase.

$$Z_E = \frac{1.84 N_{LV}^{0.575} N_{L\mu}^{0.1}}{N_{GV} N_D^{0.028}} \left(\frac{P}{P_{bE}} \right)^{0.05}$$ **Equation 2-111**

where

gas-velocity number N_{GV} is given by:

$$N_{GV} = u_{GS} \left(\frac{\rho_L}{g\sigma} \right)^{0.25}$$ **Equation 2-112**

liquid-velocity number N_{LV} is given by:

$$N_{LV} = u_{LS} \left(\frac{\rho_L}{g\sigma} \right)^{0.25}$$ **Equation 2-113**

Liquid-viscosity number $N_{L\mu}$ is given by:

$$N_{L\mu} = \mu_L \left(\frac{g}{\rho_L \sigma^3} \right)^{0.25}$$ **Equation 2-114**

and the pipe's internal diameter number N_d is given by:

$$N_d = d \left(\frac{\rho_L g}{\sigma} \right)^{0.5}$$ **Equation 2-115**

where P is the system pressure and P_{bE} is the reference pressure for gas measurements.

Minami & Brill (1987)

Minami & Brill (1987) proposed a modified version of Eaton et al. (1967) correlation which gives an improved prediction. Their proposal was based on experiments using quick-closing valves in a 406.3 m long, 77.92 mm internal diameter horizontal pipeline at 5.5 barg with air-water, air-water (with surfactant)

and air-kerosene $\left(\mu_L = 2x10^3\, Ns/m^2\right)$. The liquid holdup ε_{LT} was then proposed as follows:

$$\varepsilon_{LT} = 1 - \exp\left[-\left(\frac{InZ_E + 9.21}{8.7115}\right)^{4.337}\right] \qquad \textbf{Equation 2-116}$$

where Z_E has been defined in Equation 2-111.

Beggs & Brill (1973)

Beggs & Brill (1973) performed 584 experiments using the quick-closing valves method and air and water as fluids at pressures between 2.4 bara and 6.5 bara in two 27.4 m long pipelines, which were 25.4 mm and 38.1 mm in internal diameters. The pipelines were also inclined at angles between -90^o and 90^o to the horizontal. Based on these tests, they suggested that a more accurate holdup prediction could be obtained by considering three distinct-flow types, namely separated, intermittent and dispersed, and provided different relations for each. As a result, they consequently proposed the following holdup correlation:

$$\varepsilon_{LT}(\beta) = \varepsilon_{LT}(0)\left\{1 + C_{B-B}\left[\sin(1.8\beta) - \sin^3\left(\frac{1.8\beta}{3}\right)\right]\right\} \qquad \textbf{Equation 2-117}$$

Beggs & Brill (1973) imposed some restrictions that $\varepsilon_{LT}(0) \geq \varepsilon_{LN}$ and $0 \leq \varepsilon_{LN}(\beta) \leq 1$ where $\varepsilon_{LT}(\beta)$ and $\varepsilon_{LT}(0)$ are the liquid holdup values at a pipe inclination of β to the horizontal and for a horizontal pipe. The formulae for $\varepsilon_{LT}(0)$ and C_{B-B} depend on flow patterns and are summarized in Table 2-2.

	Horizontal flow pattern		
	Separated	Intermittent	Distributed
Horizontal holdup, $\varepsilon_{LT}(0)$	$\frac{0.98\lambda_L^{0.4846}}{Fr_M^{0.0868}}$	$\frac{0.845\lambda_L^{0.5351}}{Fr_M^{0.0173}}$	$\frac{1.065\lambda_L^{0.5824}}{Fr_M^{0.0609}}$
C_{B-B} for upward flow	$(1-\lambda_L)\ln\left(\frac{0.011N_{LV}^{3.539}}{\lambda_L^{3.768}Fr_M^{1.614}}\right)$	$(1-\lambda_L)\ln\left(\frac{2.96\lambda_L^{0.305}Fr_M^{0.0978}}{N_{LV}^{0.4473}}\right)$	0
C_{B-B} for downward flow	$(1-\lambda_L)\ln\left(\frac{4.7N_{LV}^{0.1244}}{\lambda_L^{0.3692}Fr_M^{0.5056}}\right)$	(same as for separated flow)	(same as for separated flow)

Table 2-2: Correlations for calculating $\varepsilon_{LT}(0)$ and C_{B-B} [Beggs & Brill (1973]

2.3.5 Single-phase flow in helical pipes

Extensive studies have been made on fluid flows in *helical pipes* or tubes. The prediction of the pressure gradient of single-phase fluid flow through pipes, non-circular ducts, fittings and curved tubes is of importance for the design of equipment in the oil and gas (process) industry.

When a fluid flows through a *helical pipe* or tube, a secondary flow is induced due to the difference in the centrifugal force caused by fluid elements moving with different axial velocities. The resulting flow pattern may be described as a double-vortex circulation across the pipe cross-section, which is superimposed

on the axial velocity-profile. These counter-rotating flow patterns are maintained until dissipated downstream by viscous friction. Dean (1928) showed first, on a theoretical basis, that secondary flow is due to the centrifugal pressure gradient in the main flow. The perturbation analysis conducted by him predicted that, for laminar flow and small aspect ratio, d/D, the friction loss is a function of a single parameter, the so called Dean number De.

$$De = \mathrm{Re}\left(\frac{d}{D}\right)^{\frac{1}{2}} \qquad \textbf{Equation 2-118}$$

Equation 2-118 reveals that the Dean number is a measure of the ratio of geometric average of inertial and centrifugal forces to the viscous force. Since the secondary flow is induced by centrifugal forces and their interaction primarily with viscous forces, the Dean number is a measure of the magnitude of the secondary flow. Most subsequent papers were either based on the modification of Dean's theoretical flow analysis or they considered one of the following aspects:

- the pressure drop in curved tubes was calculated from experimental and theoretical velocity distributions;
- the experimental data for curved tubes have been expressed as friction factors or in the case of laminar flow as the ratio of the pressure gradients and they were interpreted against the Dean number.

However, most investigations have been restricted to the fully-developed flow regime. The theoretical studies have been limited almost entirely to flows in coils with zero pitch. From a practical point of view, a *helical pipe* with finite pitch is a more important configuration. In a *helically-coiled* tube and also in convoluted channels created in tubes with twisted tapes or by *helical* static - elements, the vortical motion is comparable with the basic axial flow in contrast to the assumption of Dean. Hence, the fluid elements have an approximately *helical* path and this results in a complex secondary flow.

Eustice (1910) found that in curved pipes, decreasing the coil diameter increased the flow resistance. Srinivasan et al. (1968) stated that the effect of coil curvature on the friction factor was substantially less in turbulent than laminar flow. Eustice (1911) used dyes to study the flow path through curved glass tubes. The flow was found to change position continuously within the pipe, whilst exerting a 'scouring' action on the pipe walls. When a single filament of dye was introduced into the central plane, it split into two, leaving the central plane in opposite directions, forming a loop through the tube. An increase in the flow velocity was found to increase the curvature of the filament. Unlike streamline flow in straight pipes, the dye eventually mixed throughout the tube diameter. Dean (1927) predicted the flow motion in coils to have two independent streamlines, in parallel planes going in opposite directions. Figure 2-7 shows that the secondary circulation Dean's theory agreed with Eustice's experiments, showing why the motion in one half of the pipe was different from the other. White (1929) suggested that, if complete slip existed at the boundary, the whole effect would cease. This secondary circulation in laminar flow causes a form of fluid mixing, which can be beneficial to heat transfer.

Taylor (1929) experimentally confirmed the presence of a secondary circulation in *helical pipes* by repeating Eustice's experiments. Coloured dye was slowly introduced through a small hole into the stream after one complete turn of the coil, so that the secondary circulation could be established. Eustice introduced the dye at the coil inlet so that the dye may mix with the flow whilst the secondary circulation was developing. Taylor found that the dye usually kept to one side of the tube. It first flowed inwards along the wall, until reaching the innermost point of the cross-section, when it left the wall and moved across the middle section and towards the wall again. It was said that, when the dye kept to one half of the cross-section, it was visually quite striking. It was observed that the dye occasionally crossed to the other side, but this was explained to be due to imperfections in the uniformity of the helix. It was also reported that, at a certain flowrate, the colour started to vibrate irregularly. Another important observation was that the colour retained its identity for at least one helix turn

until the unsteadiness gave rise to diffusion by eddies with a rapid rise in flow resistance. After a further increase in the flowrate, turbulence was achieved and the colour dispersed.

White (1929) investigated the flow in three different dimensions of coil and plotted the Dean number versus the ratio of resistance, C, of a curved pipe, $f_{c,}$ to that of a straight pipe $f_{s.}$ This produced a smooth curve as shown in figure 2-4. Points that departed from the main curve were found to be dependent on the coil's curvature and coincided with a change in motion from double helical streamline flow to turbulent flow. This point was also confirmed when Dean's theory was no longer applicable. The figure shows that the transitional Reynolds number increased with the coil curvature ratio, d/D, where d was the tube diameter and D the coil's diameter. A coil curvature ratio of 1/2050 was found to have a similar resistance to a straight pipe. A similar resistance to a straight pipe was also seen with a curvature ratio of 1/50, up to a Reynolds number of 80. The resistance then increased up to 2.9 times that of a straight pipe, when turbulence occurred at a Reynolds number of 6000. With a curvature ratio of 1/15, the transition from laminar to turbulent flow, occurred at a Reynolds number of 9000. White concluded that for large Reynolds numbers, the flow in small diameter coils was more stable than straight pipes. The additional resistance due to the pipe curvature was found to be less in turbulent flow than for streamline flow, as secondary circulation was not possible in conjunction with turbulent eddy-motion.

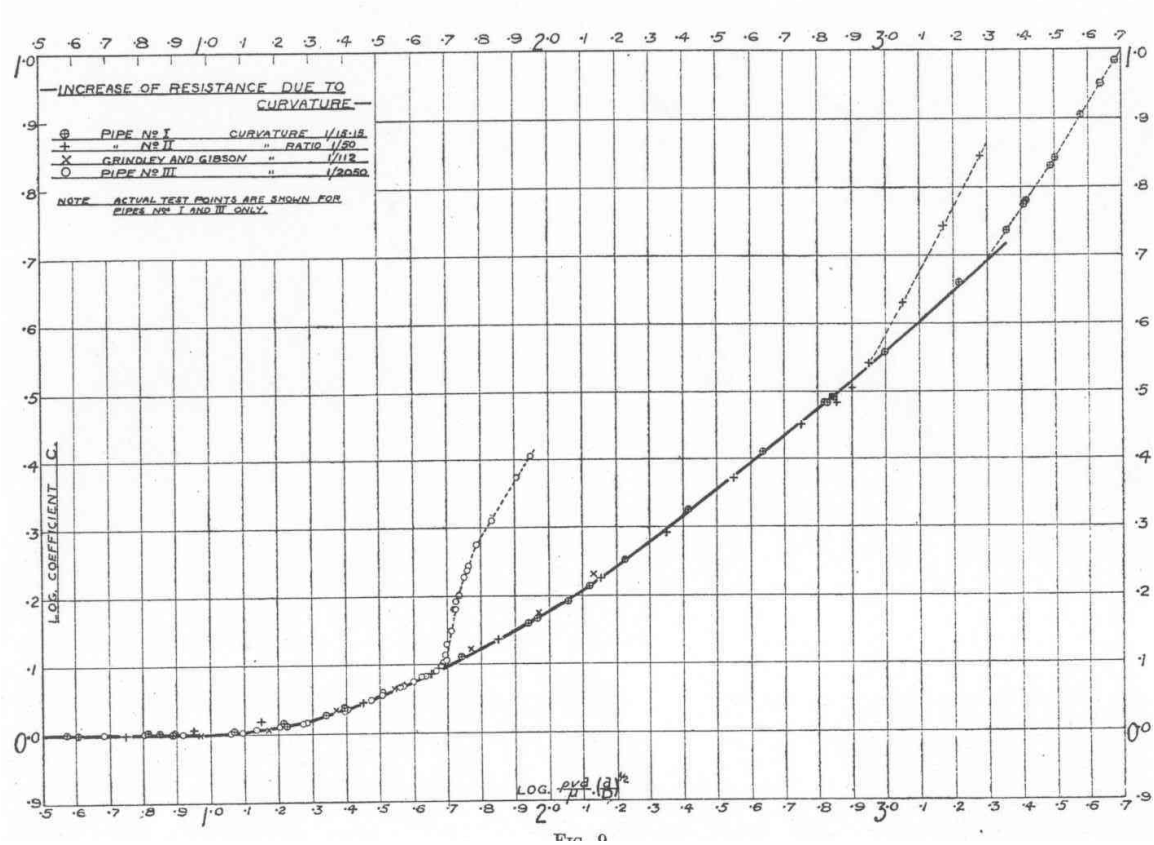

Figure 2-4: Increase of Resistance due to coil's curvature. White (1929)

The issue of the point at which transition from laminar flow to turbulent flow occurs has been controversial. Taylor (1929) found that there are two points that define the transition from laminar to turbulent flow in helical coils. The points are at the lowest Reynolds number at which the flow appeared completely turbulent and the highest Reynolds number at which the flow was steady. Many authors have produced equations to calculate the critical Reynolds number.

Turbulent flow in curved pipes was also studied by Ito (1959) and he found that the friction factor of larger diameter coils coincided with straight pipe correlations, but a considerable increase in resistance was observed with smaller curve diameters. Another method to determine the transition to turbulent flow was found by plotting the Dean number against $f_c\sqrt{D/d}$ as shown in Figure

2-5. This is a clearer proof than White's method shown in Figure 2-4. The numbered lines correspond to laminar flow equations from other authors. However, a slight discrepancy between the experimental data from different authors was found, depending on whether the flow was disturbed before the coil inlet.

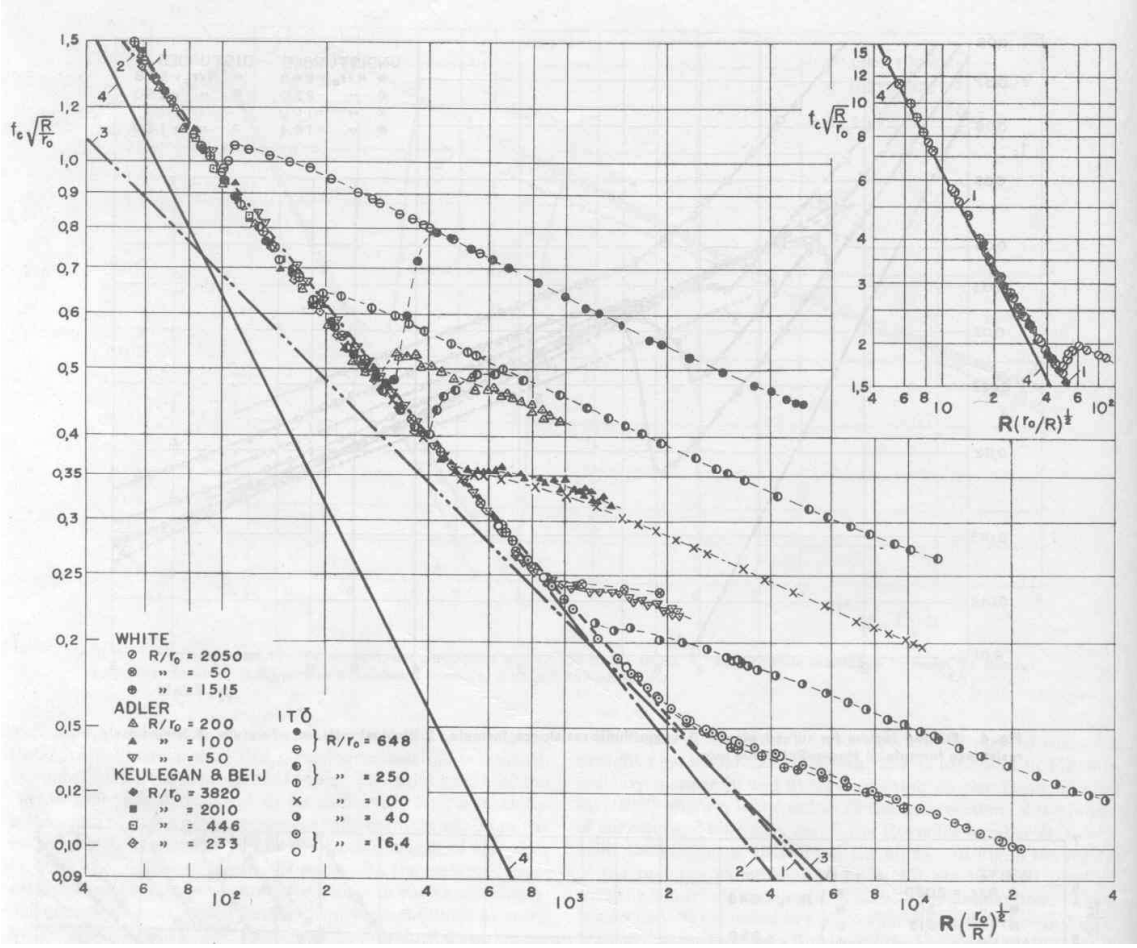

Figure 2-5: Transition from laminar to turbulent flow. Ito (1959)

Correlations to calculate friction factor in *helical* coils have been developed by many authors. An early summary of the correlations was provided by Srinivasan et al. (1968). Some of the equations are also compiled in section 2.5 of this thesis. The effect of coil pitch was investigated by Mishra and Gupta (1979) and Liu et al. (1994). Mishra found that the friction factor decreased with an increase in coil pitch, but the radius of curvature was the main factor responsible for an increased pressure drop. Kubair and Kuloor (1965) found the friction factor for

non–isothermal flow in coils was less than for isothermal flow. Hart et al. (1987) constructed a friction factor chart for a single-phase fluid flow through curved tubes. The value of the friction factor was plotted as a function of the Reynolds number with d/D as a parameter. In constructing the chart, equation 2-127 was used for the laminar domain $(0 < \mathrm{Re} < \mathrm{Re}_{crit})$: for the turbulent flow regime, equation 2-119 was used.

Equation 2-119

$$fc = f + 0.01\left(d/D\right)^{\frac{1}{2}}$$

The values of Re_{crit} was obtained from equation 2-120

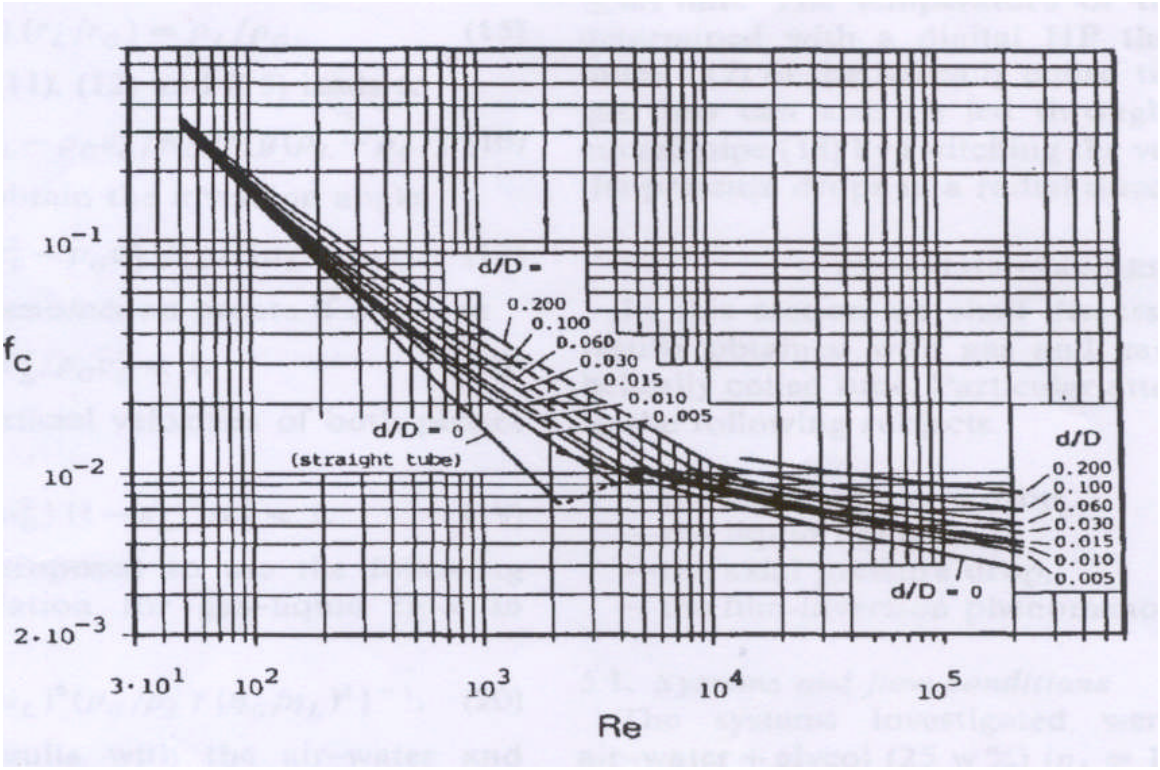

Figure 2-6: Straight and curved smooth tubes friction factor. Hart et al. (1987)

[The chart is valid for $0 \le d/D \le 0.2$ **and** $0 \le \mathrm{Re} \le 2 \times 10^{5}$**]**

2.3.6 Single-phase flow pressure drop in helical pipes

The frictional pressure loss of a single-phase fluid flow through a curved or *helical pipe* is larger than that for a flow through a straight tube under similar conditions of pressure, temperature, mass flow rates, pipe diameter, tube length, etc. In addition, the single-phase fluid flow through a coiled tube or bend becomes turbulent at a higher Reynolds number {White (1929); Taylor (1929); Adler (1934); Ito (1959)} than the fluid through a straight tube under otherwise identical flow conditions. The fluid in the *helical pipe* experiences a centrifugal force which causes the appearance of a secondary flow as shown in Figure 2-7.

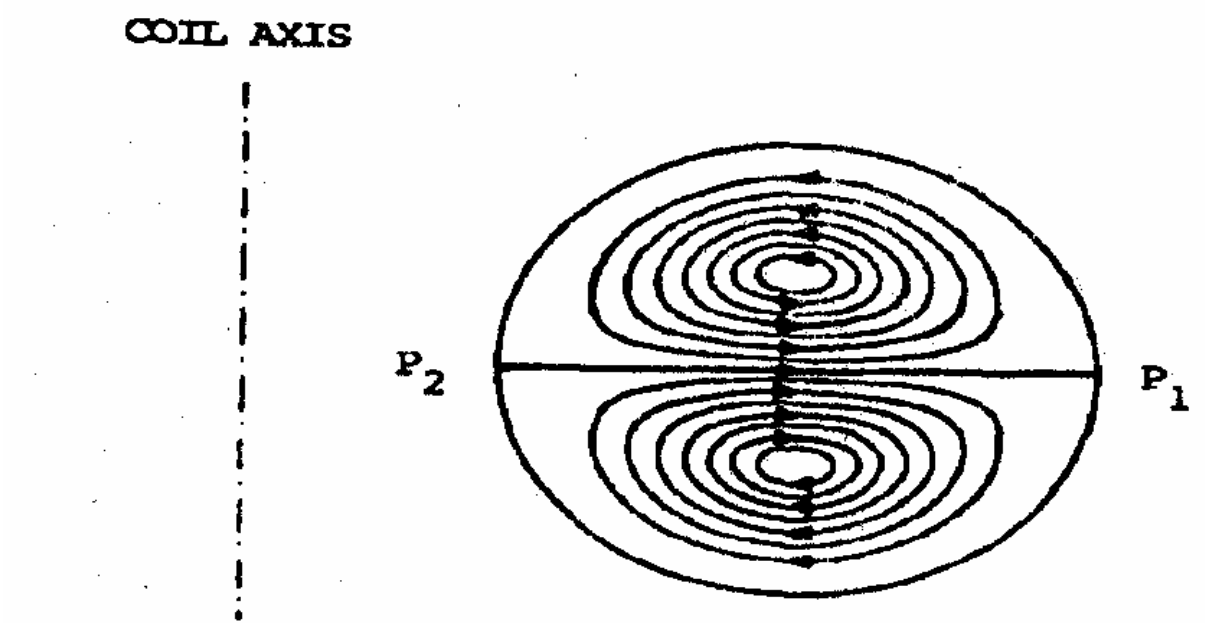

Figure 2-7 : Secondary flow in the cross section of a curved tube.
Dean (1928)

This secondary flow has a stabilising effect on the laminar fluid flow, resulting in a higher critical Reynolds number. The critical Reynolds number [Srinivasan et al. (1968)] increases with the ratio $\frac{d}{D}$ of the inner-tube diameter d and the coil diameter D and can be obtained from

$$\mathrm{Re}_{crit} = 2100\left[1+12\left(\frac{d}{D}\right)^{\frac{1}{2}}\right] \qquad \textbf{Equation 2-120}$$

Two-phase flow of gas-liquid mixtures in horizontal *helical pipes*; Adedigba (2007)

Dean (1927) showed that, for a given pressure gradient, the ratio of mass flow rate through pipes with different curvatures is governed by the Dean number (De). The Dean number can be calculated from equation 2-118. The secondary flow is sometimes called the Dean effect and it affects the transfer of heat, mass and momentum in bends and coils {Schmidt (1967); Mori and Nakayama (1965, 1967a, b)}.

A remarkable phenomenon in gas–liquid flow in coiled tubes has been reported by Banerjee et al. (1967). They found that, at high gas velocities, the liquid phase travels along the inside of the tube wall facing the coil axis. He called this phenomenon “film inversion”.

If a single-phase fluid flows through a coil or bend (see Figure 2-8), centrifugal forces act on the fluid. As a result of these forces, a pressure drop ΔP_{12} occurs in the radial direction.

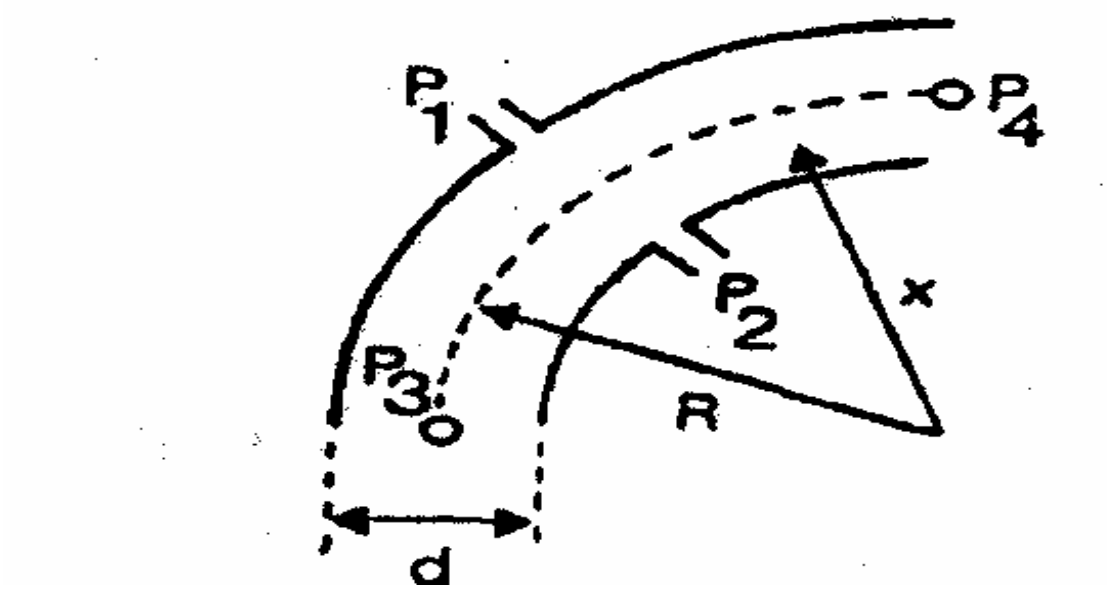

Figure 2-8 : Curved tube with four pressure taps (P_1-P_4)
Hart et al. (1987)

As shown in Figure 2-8, the difference in pressure between taps P_1 and P_2 is the radial pressure drop ΔP_{12} and between taps P_3 and P_4 is the axial pressure drop ΔP_{34}.

2.3.7 The radial pressure drop

In single-phase fluid flow in horizontal, curved pipes a positive pressure gradient arises from the centrifugal force acting on each fluid element. If the fluid phase is assumed to have a constant angular velocity ω in the cross-section of the bend, the pressure gradient in the radial direction in a horizontal plane at a distance x (as shown in Figure 2-8) from the axis of the bend can be obtained from Coulson and Richardson (1998);

$$\frac{dp}{dx} = \rho G \omega^2 X \qquad \textbf{Equation 2-121}$$

An appropriate value of the pressure drop in the radial direction for a fluid flow through a coiled tube or bend can be obtained by integrating equation 2-121 between $X = R - r$ and $X = R + r$.

The integration results in

$$\Delta P_{12} = \rho_G \omega^2 R d \qquad \textbf{Equation 2-122}$$

Introducing the average gas velocity $U_G = \omega R$ gives

$$\Delta P_{12} = \rho_G U^2{}_G \frac{d}{R} \qquad \textbf{Equation 2-123}$$

2.3.8 The axial pressure drop

A number of equations have been proposed for calculating the pressure drop in helical coils of constant curvature for both laminar and turbulent single-phase tube flow. White (1929) found laminar flow through coils of different curvature. All the points representing his experimental results lie on one curve if the ratio

f_C/f of the friction factors (where f_C for the coil and f for a straight tube) is plotted against the Dean number, $De = \mathrm{Re}\left(\frac{d}{D}\right)^{\frac{1}{2}}$. Although several authors have presented empirical correlations for predicting the friction factor f_c in a laminar or turbulent single-phase flow through helices, no model is available in the literature to describe this type of flow in the whole domain of Reynolds numbers. A good review of experimental and theoretical research work on coils is given by Srinivasan et al. (1968, 1970). The single-phase pressure drop in a coiled tube can be obtained from the equation for fluid flow through a straight tube after replacing the Fanning friction factor f by f_C. Then

$$\Delta p_{34} = 4 f_c \left(\frac{l}{D}\right)^{\frac{1}{2}} \rho U^2 \qquad \textbf{Equation 2-124}$$

Empirical correlations have been introduced in the literature to calculate the value of the friction factor f_C for both laminar and turbulent flows.

Two of these correlations, often used for laminar flows, are from White (1929) and Mishra et al. (1979).

White (1929):

$$f_C = f\left\{1-\left[1-\left(\frac{11.6}{De}\right)^{0.45}\right]^{2.2}\right\}^{-1} \qquad \textbf{Equation 2-125}$$

for $11.6 \le De \le 2000$

Mishra et al. (1979):

$$f_C = f\left[1+0.033(\log_{10} De)^{4.0}\right] \qquad \textbf{Equation 2-126}$$

for $De > 1$

However, the above two correlations and other formulae introduced in the literature have at least one of the following disadvantages:

- the formulae are only applicable for a limited range of Dean numbers, and
- they do not satisfy the boundary condition $f_c \rightarrow f$ if De $\rightarrow$ 0.

It was found that the friction factor of a curved tube could be better calculated with the following empirical correlation:

$$f_C = f\left\{1+\left[\frac{0.090\,De^{1.5}}{(70+De)}\right]\right\} \qquad \textbf{Equation 2-127}$$

Equation 2-127 satisfies the boundary condition $f_C = f$ for De $\rightarrow$ 0 and cover the whole domain 0 < Re < Re_{crit} in which Re_{crit} can be obtained from equation 2-120 where

$\mathrm{Re} > \mathrm{Re}_{crit}$ when turbulent flow occurs.

For single-phase turbulent flows in a *helical coil*, several prediction equations for friction factors are available, describing the empirically obtained values in a large range of Reynolds numbers. These include White (1932); Ito (1959); Schmidt (1967).

2.4 Two-phase flow in *helical pipes*

Relatively little research has been published for two-phase flow in *helical coils*. An observation was made by Rippel et al. (1966) that the presence of two phases significantly reduced the Dean effect shown in single-phase flow in *helical coils*. This was attributed to the Lockhart and Martinelli parameters being ratios and geometry not altering the ratio of two-phase to single-phase pressure drop. Banerjee et al. (1969) found that the flow patterns in coils were adequately predicted by Baker's flow map for straight pipes. Banerjee et al. (1969), Maddock et al. (1974) and Whalley (1980) studied the liquid film in annular flows in coils and observed a film inversion. The film was expected to

be thickest on the tube side furthest from the axis, due to centrifugal forces. However, in certain cases it was thickest closest to the coil axis.

2.4.1 Two-phase flow pressure drop in helical pipes

The literature review has shown that pressure drops in *helical coils* are higher than in straight pipes and the flow can remain laminar to higher Reynolds numbers than in straight pipes. A secondary circulation has been found to exist in laminar single-phase coil flow. The transition from laminar flow to turbulent flow has also been shown to be more gradual and far less marked.

Akagawa et al. (1971) found that the two-phase frictional pressure drop in coils was between 1.1 and 1.5 times that of straight pipes. Banerjee et al. (1969) found that, when both gas and liquid phases were turbulent in vertical coils, the pressure drop could be predicted reasonably well with the Lockhart and Martinelli correlation, using modified parameters. When both phases were laminar, the Lockhart and Martinelli relationship correlated the data well with the viscous liquid - turbulent gas correlation. It was assumed that irregular phase-boundaries would destroy the secondary flow patterns in laminar flow; therefore the same friction factor as straight pipes was used.

Rippel et al. (1996) found the Lockhart and Martinelli relationship for straight pipes accurately predicts the two-phase pressure drop in *helical coils*. Rippel et al. (1996) also correlated experimental data to produce different equations for different flow regimes. Boyce et al. (1969) found that calculating the two-phase friction factor in coils, using White's equation for laminar flow in coils and Ito's equation for turbulent flow, in conjunction with the Lockhart and Martinelli correlation, proved accurate at calculating the friction factor for two-phase flow in straight pipes.

Awwad et al. (1995a), (1995b) found that the Lockhart and Martinelli correlation was not valid for horizontal coils due to the water column accumulation in the

coil. It was therefore demonstrated that for horizontal coils, the frictional pressure drop was strongly related to the flowrate as well as the Lockhart and Martinelli parameter. Xin et al. (1996) showed that this was also true for vertical coils. Banerjee et al. (1969), and Awwad et al. (1995a), both concluded that the helix angle had little effect on the pressure drop and holdup. Awwad et al, (1995b) however, found that the effect of the coil diameter, D, decreased with an increase in Reynolds number. So it appeared that by increasing the tube diameter, d, the pressure drop multiplier, ϕ_L, became independent of the coil diameter, D.

2.4.2 Flow patterns in horizontal two-phase flow

A term used to describe the distribution of the different phases present in a multiphase system is called the flow pattern or flow regime. Flow patterns have long been used to study multiphase flows, as well as to present the regions of different flow regimes and the transitions between them. Visual observation can also be used to distinguish flow patterns. However, it should be noted that the concept of a flow pattern is not just useful to describe the physical appearance of a multiphase system. It is also useful when one wants to compare analysed multiphase experimental data with that for an existing flow regime. Also, the flow regime is useful because each flow pattern has its own physics which will determine the behaviour of flow parameters like pressure drop. Of the possible two-phase flows, gas-liquid flows are the most complex to study because of the boundary between the gas and the liquid, called the interface, is highly deformable. The flow patterns in a horizontal tube are different from those in a vertical tube. The present study is mainly about flows in horizontal pipes and flows in inclined or vertical pipes are therefore not addressed.

When a gas and a liquid (i.e. two-phase) flow concurrently in a pipe, both the gas and the liquid may be turbulent flow or they may both be in laminar flow. Alternatively, the gas may be in turbulent flow and the liquid in laminar flow or

vice versa. Flow patterns for gas-liquid systems have been extensively observed for both horizontal and vertical flows.

Horizontal flow patterns are more complex due to the gravitational force acting perpendicularly to the pipe's axis. This causes the denser phase to flow towards the bottom of the pipe. The pipe's internal diameter, properties of the fluids and flow rates all influence horizontal flow patterns. In horizontal pipes, as the flow rate is increased, the flow passes through the following stages: bubble flow, where the bubbles flow along the upper surface of the pipe, plug flow, where the gas bubbles coalesce into plugs, stratified flow, where the gas - liquid interface is smooth and well defined, wavy flow, where surface waves are formed, slug flow, where the waves touch the top of the pipe and form a frothy slug, annular flow, where the gas flows as a core surrounded by a wall of liquid and mist flow where the gas core entrains the liquid from the pipe wall.

Numerous studies have shown that no single theory or correlation can satisfactorily predict the pressure gradient or liquid holdup over all possible regimes encountered in multiphase flow in pipes. Although empirical correlation methods are still widely used, there is a growing trend towards the use and development of a mechanistic model. In either case, it is important from the designer's point-of- view to be able to predict accurately what pattern will occur for given input flow rates, pipe size, and fluid properties. Only then can the proper flow model be selected. Many methods have been presented in the literature for this purpose, usually in the form of two-dimensional maps in which the locations of the boundaries between flow pattern regions are based on empirical observations. Many of these maps result from data covering a rather limited range of fluid properties and pipe's internal diameters. Consequently, large discrepancies are often observed between a predicted flow regime and that actually observed in a subsequent test.

In general, classification and description of the flow distributions into flow patterns or regimes is still a very subjective process. However, there are some

accepted descriptions, such as those of Mandhane et al. (1974), Taitel & Dukler (1976) and Hewitt (1978). Considering gas-liquid flows in horizontal and near horizontal pipe positions, the flow patterns can be classified as follows:

Dispersed bubble flow: This flow pattern occurs at high liquid superficial velocities: for a wide range of gas superficial velocities, small bubbles are dispersed throughout a continuous liquid phase. Due to the effect of buoyancy, these bubbles tend to accumulate in the upper part of the pipe.

Plug flow: Plug flow pattern occurs at relatively low gas superficial velocities. As the liquid superficial velocities are reduced, the smaller bubbles coalesce to form larger bullet-shaped bubbles that move along the top of the pipe

Stratified smooth flow: At low liquid and gas or vapour superficial velocities, gravitational effects cause total separation of the two phases. This results in the liquid flowing along the bottom of the pipe and the gas or vapour flowing along the top.

Stratified wavy flow: Stratified wavy flow pattern occurs as a result of an increase in gas superficial velocity in stratified smooth flow pattern; this leads to the interfacial shear forces increasing, rippling the liquid surface and producing a wavy interface.

Slug flow: As the gas and liquid superficial velocities are increased further, the stratified liquid level grows and becomes progressively more wavy until eventually the whole cross-section of the pipe is blocked by a wave. The resultant "piston" of liquid is then accelerated by the gas flow surging along the pipe, and scooping up the liquid film in front as it progresses. This "piston" is followed by a region containing an elongated gas-bubble moving over a thin liquid-film. Hence an intermittent regime develops in which elongated gas-bubbles and liquid slugs alternately surge along the pipe.

Annular flow: At even higher gas superficial velocities, the gas pushes through the centre of the pipe leaving a ring or annulus of liquid around the inside of the pipe which, due to gravity, is thicker at the bottom. Some liquid may also be entrained in the gas core as small, dispersed droplets.

The described flow patterns in horizontal pipe are shown below in Figure 2-9.

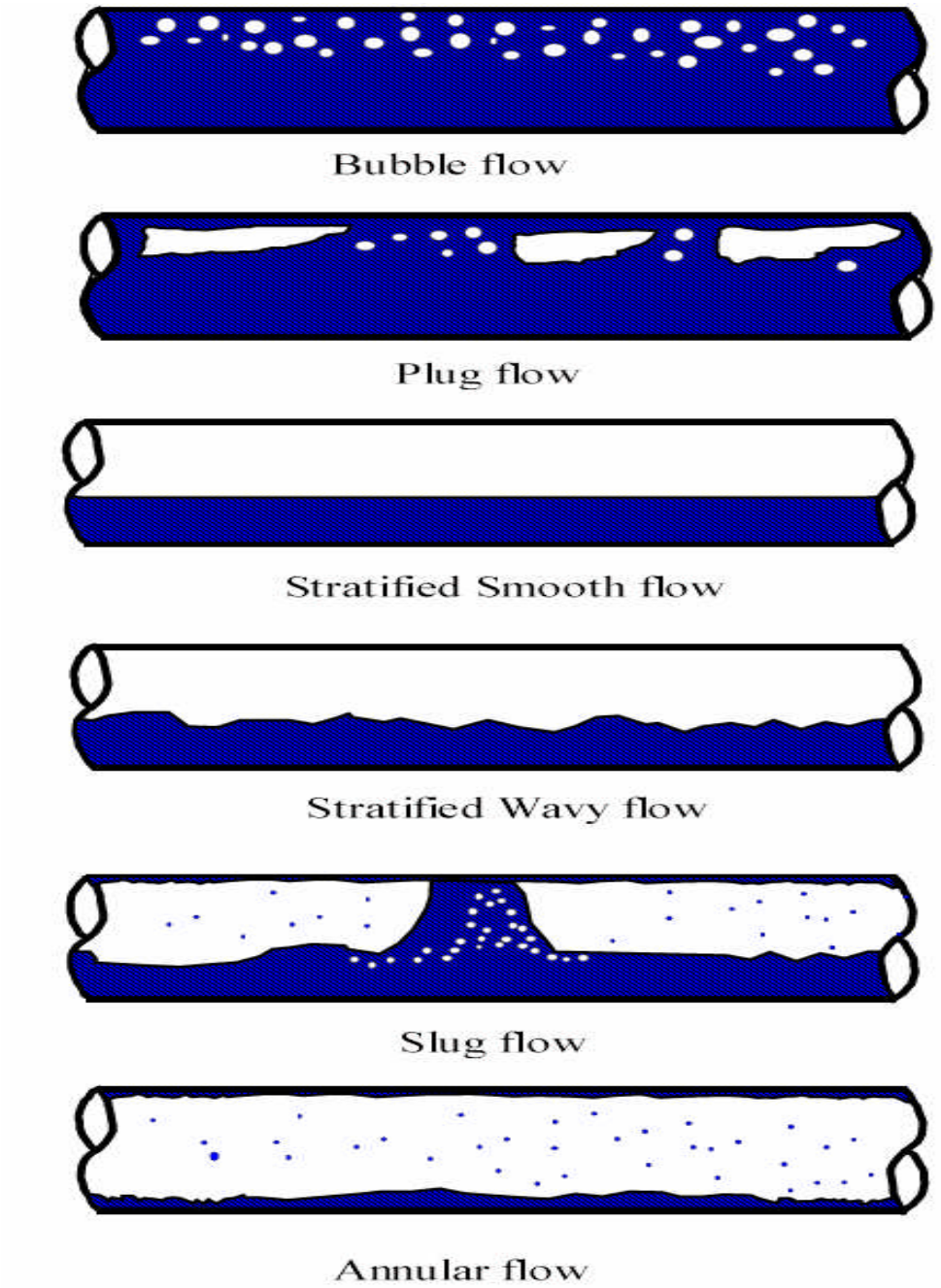

Figure 2-9: Horizontal flow patterns (Shoham, 1982)

It should be noted that transitions from one flow pattern to another have been widely investigated. Transition boundaries are often investigated from experiments but the resulting flow pattern map is then usually only valid for the system under consideration.

2.4.3 Flow pattern maps for horizontal two-phase flows

Flow pattern maps have long been used in the study of multiphase flows to present the regions of different flow regimes and the transitions among them. A thorough study was performed by Mandhane et al. (1974) using a large data-bank of flow pattern observations. This study resulted in the map shown in Figure 2-10 plotted in terms of gas and liquid superficial velocities. Mandhane et al. (1974) classified their flows into stratified, wavy, elongated bubble, slug, dispersed and annular regimes.

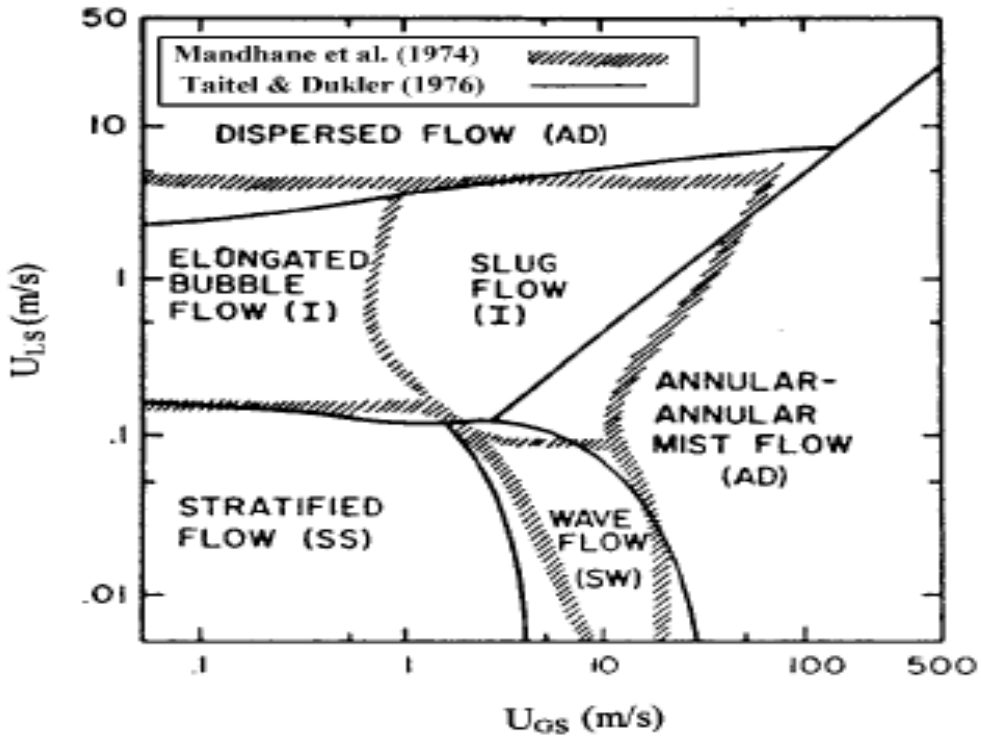

Figure 2-10: Flow pattern map due to Mandhane (1974)

But the most useful study, however, was that of Taitel & Duckler (1976). Their study comprises a series of semi-theoretical approaches. They presented a

model for the flow pattern transitions in horizontal gas-liquid flow and this has been widely used. They distinguished among stratified smooth, stratified wavy, intermittent, annular dispersed and dispersed bubble regimes in their flow pattern map. They also presented criteria for each of the flow pattern transitions in horizontal and near-horizontal flows. The basis of their models was a one-dimensional stratified flow model to give the equilibrium liquid height from which the flow pattern transitions were developed. The flow map was plotted in terms of dimensionless parameters. Using this approach, different physical properties, pipe inclination and pipe diameter can in principle be accommodated. It should however, be noted that the empirical correlation factors were largely determined from air-water flows at low pressures in small diameter pipes.

Considering their semi-theoretical models of each of the transitions from one flow pattern to another, they then suggested that the flow pattern changes are controlled by the combinations of some dimensionless groups. Figure 2-11 shows their map with the transition lines shown as a function of the dimensionless liquid height $\left({}^{h_L}\!/_{D} \right)$ for a general system.

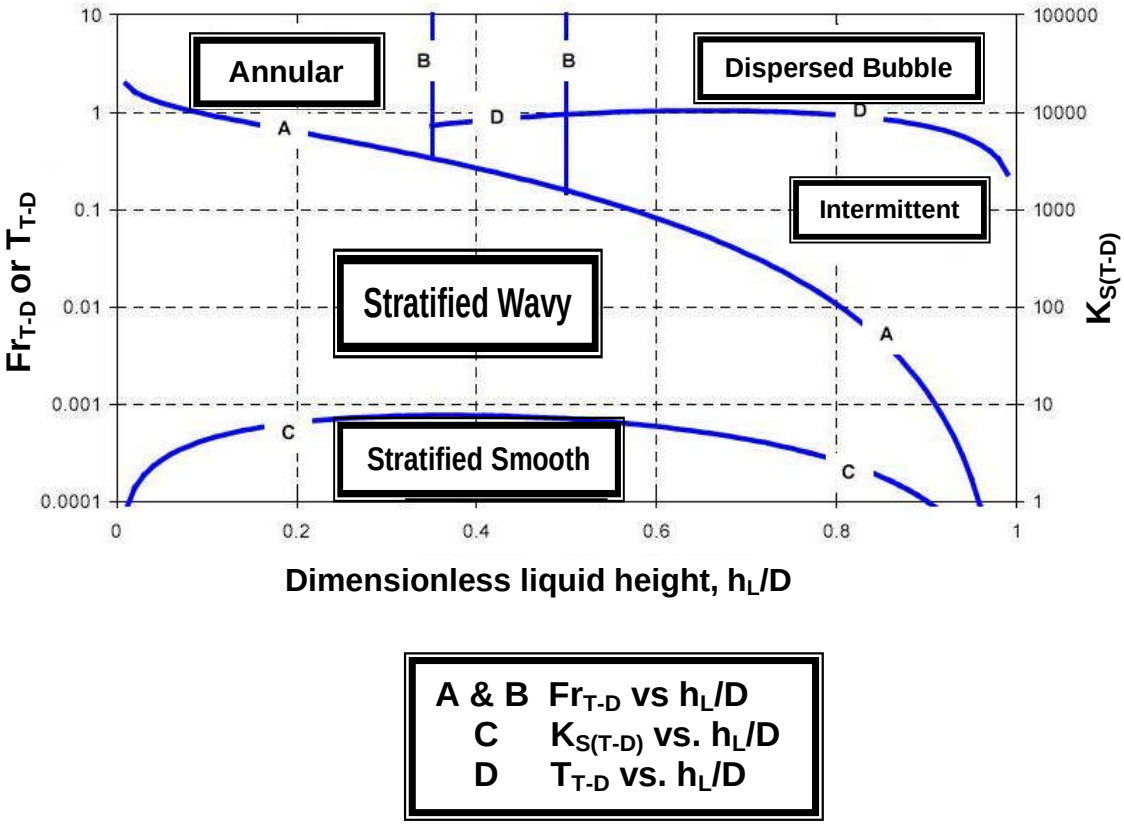

Figure 2-11: Flow pattern map in dimensionless form. Taitel & Duckler (1976).

As early as the 1950s, Baker (1954) divided his map into stratified, wavy, slug, plug, annular, dispersed and bubble (or froth) flow regions and produced transition lines on a plot of $\dot{m}_G / \lambda_B$ versus $m_L \lambda_B \Psi_B / m_B$ as shown in Figure 2-12

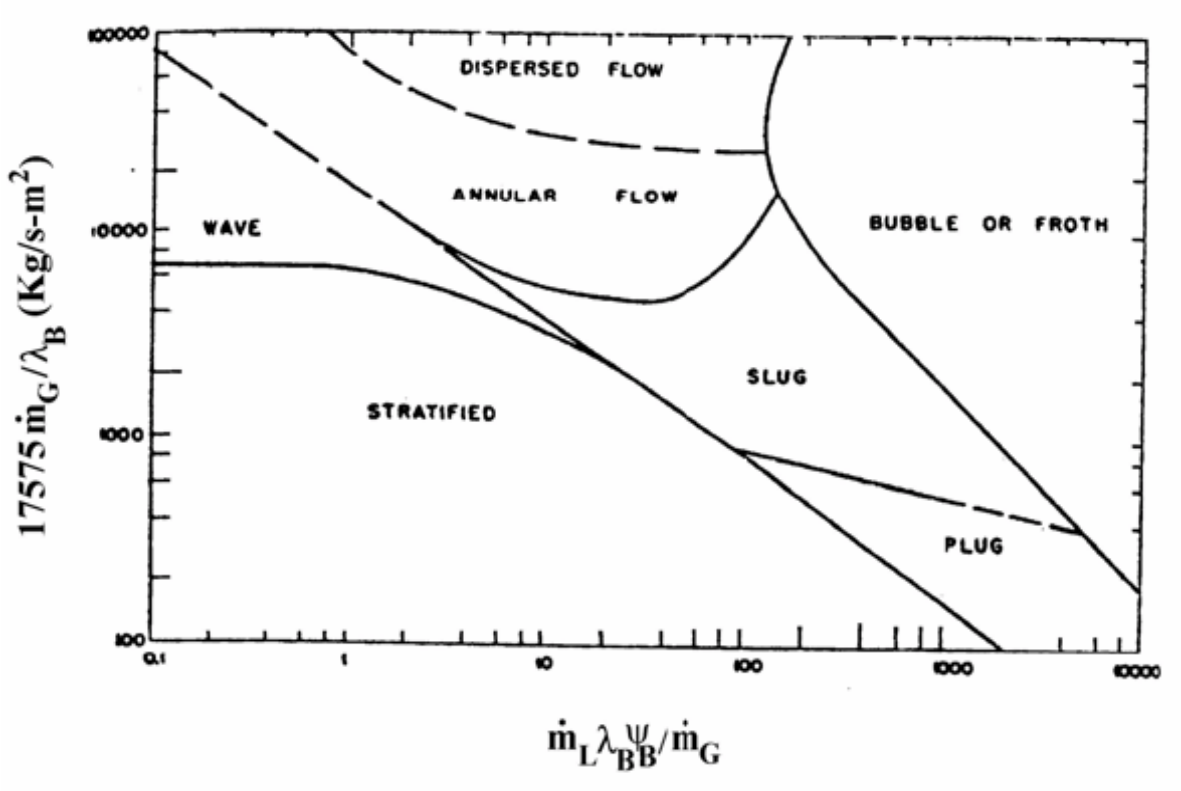

Figure 2-12: Flow pattern map of Baker (1954)
N. B. The constant 17575 is the conversion factor between Imperial and SI units]

Beggs & Brill (1976) tried to simplify their transition map by considering just three types of flow, viz: separated, intermittent and distributed flows. In their grouping, stratified wavy and annular flows were grouped as separated flows; plug and slug as intermittent and bubbly flow as dispersed. Using these classifications, they then proposed a completely dimensionless plot of Froude number (Fr_M) versus the input liquid content (λ_L), as shown in Figure 2-13.

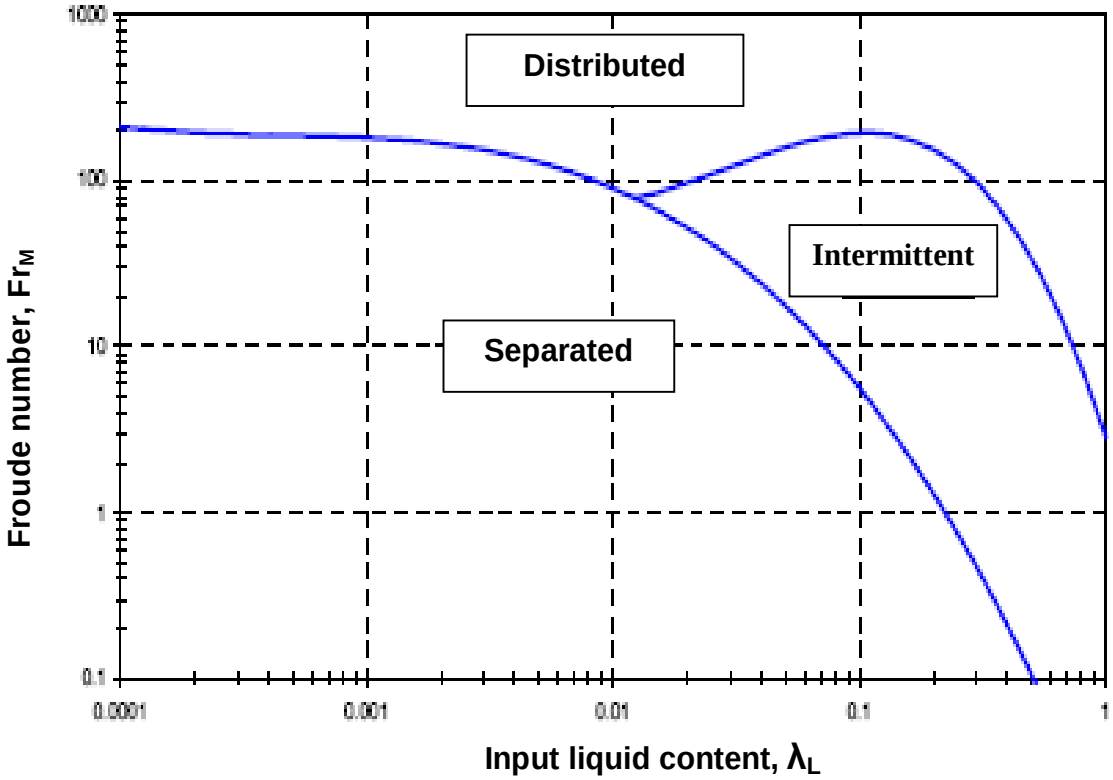

Figure 2-13: Beggs & Brill (1973) flow pattern map

Weisman et al. (1979) performed a series of experiments in 12 mm, 25 mm and 51 mm internal diameter horizontal test-sections to examine the effect of fluid properties and pipe diameter on flow pattern transitions. In their map, they considered the stratified smooth, stratified wavy, intermittent, annular and dispersed regimes with the intermittent region combining slug and plug flows and the dispersed one incorporating both dispersed bubble and mist flows. Consequently, the transitions they proposed were those for stratified smooth flow to stratified wavy flow, separated to intermittent flow, the change to dispersed flow and the onset of annular flow. Figure 2-14 shows Weisman et al. (1979) flow pattern map.

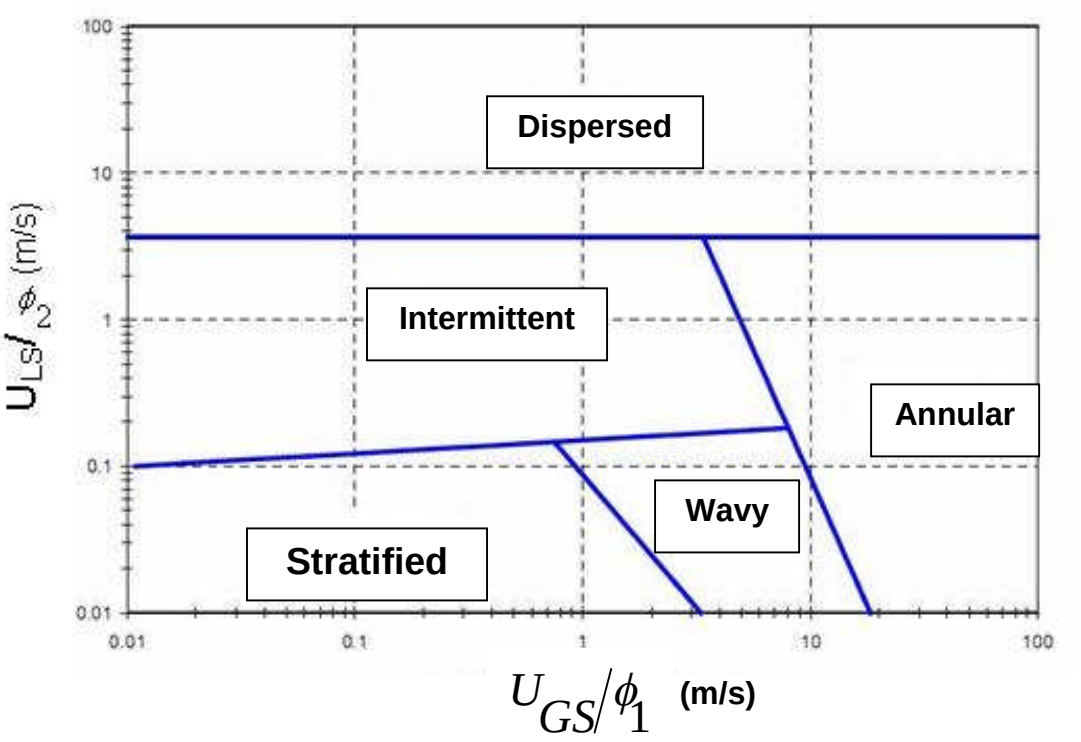

Figure 2-14: Flow pattern of Weisman et al. (1979)

Figure 2-15 shows a flow pattern map for a horizontal pipe. It was produced by Chhabra and Richardson and shown in Coulson and Richardson (1993). The divisions are approximate and based on subjective observations.

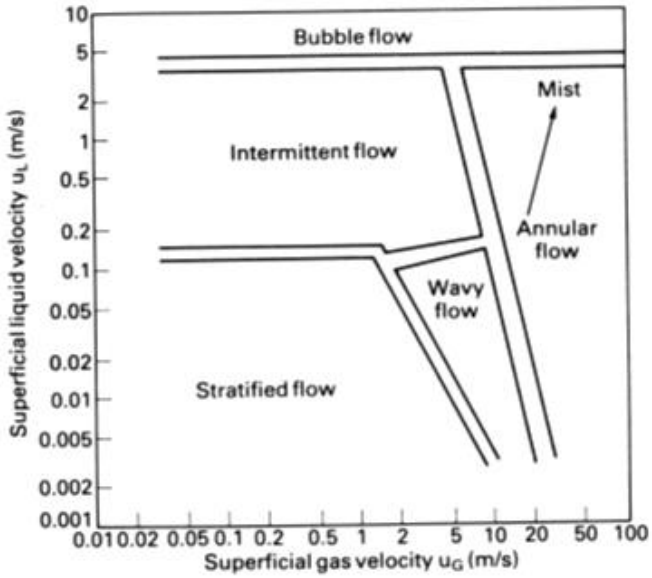

Figure 2-15: Flow pattern map of Coulson and Richardson (1993).

Two-phase flow of gas-liquid mixtures in horizontal *helical pipes*; Adedigba (2007)

2.4.4 Gas - Liquid flow pattern detection

Two problems exist in gas - liquid flow pattern detection, or determining which pattern actually exists:

(a) certain flow pattern descriptions contain arbitrary elements and
(b) transitions between some flow pattern pairs are gradual, and there is difficulty in defining the boundaries.

However, there exist some proven methods used to describe flow patterns, which are based in one way or another for observing the time, amplitude and positional variation of voids.

2.4.4.1 Visual observation

Flow pattern information in two-phase gas and liquid flows is usually obtained by visual observation. This seems to be the simplest method for detecting flow patterns through transparent test section walls. This is at flow rates where the velocities are low enough to make observation possible, and when dealing with transparent fluids. The eye simply detects the variation of voids. This is most successfully done by focusing on an element of liquid or gas allowing the line of sight to move with the velocity of the element and then scanning the whole length of the pipe.

At high flow rates, photographic methods are useful, as demonstrated by Raissan (1965), Hsu & Graham (1963), Bergles & Suo (1966) and Hewitt & Roberts (1969). Most photographic methods are limited by the size of the field-of-view, usually no more than several diameters long, so that only instantaneous local behaviour can be observed. This restricts the observation of the axial variation of the voids, which is important for the characterization.

Where the fluids are not transparent, X-ray photography has been used by Derbyshire et al. (1969) and Hewitt & Roberts (1969). Moving-picture

photography has proved to be less successful because the field-of-view is smaller than that necessary to get the resolution needed for observation.

The major difficulty of visual observation, even using high-speed photography, is that the picture is often confusing and difficult to interpret, especially when dealing with high velocity flows. In addition, there are systems which are opaque where flow visualization is impossible. A considerable number of experiments have been performed studying two-phase gas liquid flows, but not very much has been done in the development of an objective means for the flow pattern classification. Jones & Delhaye (1975) reviewed and summarized a variety of measuring techniques used in two-phase flow of which only few are used directly for flow pattern characterization. Hus et al. (1964) utilized a hot wire anemometry technique for measuring void distribution for vertical flow and used the signal output also for flow pattern characterization. Jones & Zuber (1975) developed an X-ray void measurement system for obtaining statistical measurements in vertical air-water flow in a rectangular channel. The probability density function of the void fraction fluctuations was used as a quantitative flow pattern discriminator for bubbly, slug and annular flows. Govier et al. (1975), Chaudhry et al. (1965) and Isbin et al. (1958) tried to relate the flow pattern to the pressure gradient variation. Their results, however, are not systematic. Furthermore, it needs mapping of the pressure gradient with flow conditions, which means that the flow pattern cannot be detected at one flow condition. Hubbard & Dukler (1966) suggested a method by which the flow pattern can be determined from the spectral distribution of the wall pressure fluctuations. They distinguish, however, only among separated, intermittent and distributed flows. They could not discriminate between stratified and annular flows, or between the dispersed liquid or dispersed gas flow regimes. Choe et al. (1976) detected the slug annular transition based on a direct trace of the pressure fluctuations on an oscilloscope.

2.4.4.2 Pressure measurement method

Early attempts to use pressure to characterise flow pattern were based on the observation that, as the flow pattern changed with a systematic change in gas or liquid flowrate, the slope of the time-averaged gradient curve changed as well Govier et al. (1957), Isbin et al. (1959) and Chaudry et al. (1965). While the result was descriptive, it was not particularly useful for detection since these slope changes could be related to flow pattern transitions.

Hubbard & Duckler (1966) suggested a method based on the spectral analysis of wall pressure fluctuations. The approach was based on the idea that the fluctuations in wall pressure were reflections of the manner in which the liquid and gas were distributed in the pipe and of their velocities, and this was precisely what characterised a flow pattern as well. For vertical flow systems, a method proposed by Tubu (1982) seems particularly useful. Two pressure transducers were located axially apart on the wall of the pipe, and the time variation of the pressure gradient is analysed for probability density distribution. In vertical flows, the pressure gradient is strongly dominated by hydrostatic gradients or void fractions, that is, for bubbly flow, the pressure gradient will fluctuate around $\rho_L(1-\varepsilon_G)g$, while for annular flow, it will centre on $\rho_G g$. If the two fluid densities are widely different, as they often are, this can be used as a diagnostic tool. Oscillations in pressure gradient during bubbly flow reflect the variation in voids with time between the two measuring stations and these results from a few bubbles entering or leaving this volume. Similarly, in annular flow, the fluctuations in ΔP result from variations in the concentration of droplets in the core, again a small number. However, in slug flow the pressure gradient will oscillate between a maximum of that for bubble flow, when the liquid slug occupies the space between the detectors and near zero when the Taylor bubble passes.

2.4.4.3 Electrical conductance probe method

For electricity-conducting liquids, such as water, conductance measurements can be used to discern flow patterns. This method was applied early by Solomon (1962), and Griffith (1964). They applied this technique using a single conductivity probe. Fiori & Bergles (1966) and Bergles *et al.* (1976) also used a conductivity probe for boiling flows in horizontal tubes. They used a single central probe and were able to detect differences among bubbly, slug and annular flows. In these early applications, needle probes were used in many instances and they were not specific for all the flow patterns. Barnea et al. (1980) have now suggested a multiple–probe modification that appears to be able to discriminate flow patterns in a more diagnostic way among the various patterns. They carried out some experiments in an air-water system using plexiglass pipe of 2.4 cm internal diameter. Electrical probes were installed at different locations in a short test-section of 30 cm long. Figure 2-16 shows their electrical diagram for a horizontal pipe flow.

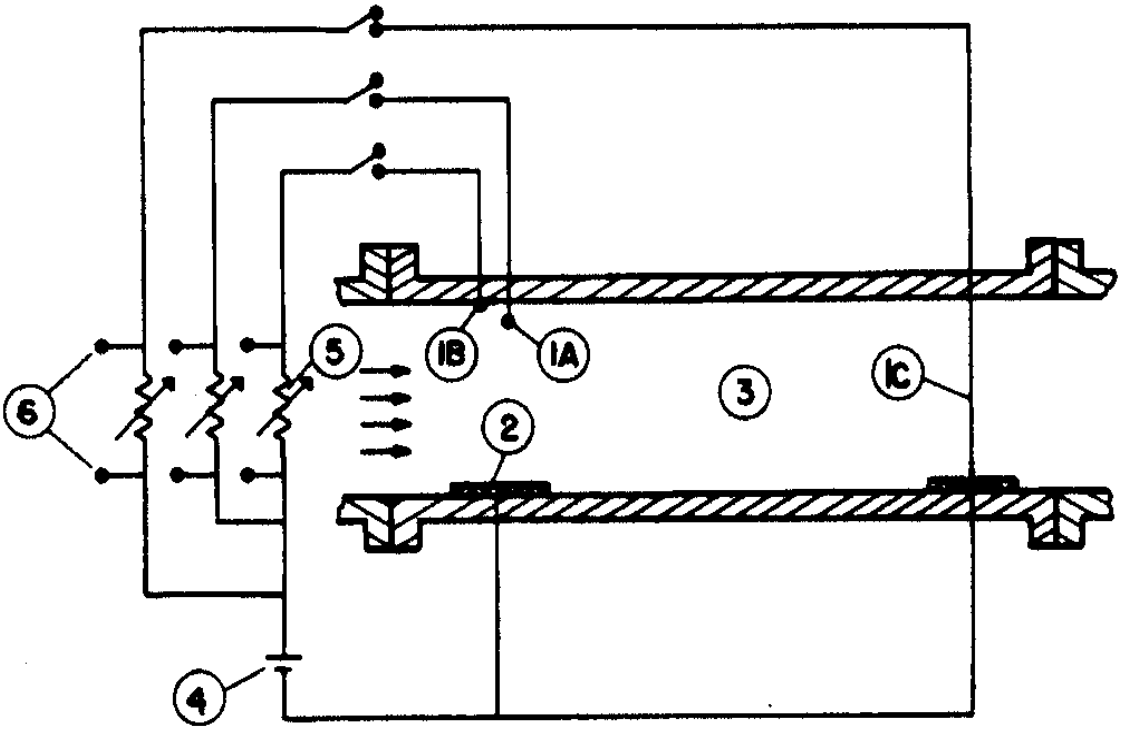

Figure 2-16 : Electrical conductance method. Barnea et al. (1980)

where

1A, 1B and 1C are probes

2 is copper electrode

3 is two-phase flow

4 is voltage supply

5 is variable resistors

6 is output signal

2.5 Correlations for *helical* coil pipes

2.5.1 Introduction

Many equations have been devised to calculate the friction factors dependence upon influential parameters for both single-phase and two-phase flows in *helical* coiled tubes. The equations were formulated to account for various flow-conditions and different internal diameters of pipes.

Many of the equations use the Dean number (Dn) which has been defined in equation 2-118 as:

$$De = \mathrm{Re}\left(\frac{d}{D}\right)^{\frac{1}{2}}$$

where

$$\mathrm{Re} = \frac{\rho U d}{\mu}$$

2.5.2 Single-phase flow

2.5.2.1 *Helical* coil friction factor equations for laminar flow

Dean (1928)

Dean's equation is suitable for $Dn \angle 20.45$:

$$\frac{f_c}{f_s} = 1 - 0.03058\left(\frac{Dn^2}{288}\right)^2 + 0.01195\left(\frac{Dn^2}{288}\right)^4 \qquad \textbf{Equation 2-128}$$

This equation has been recommended by Srinivasan et al. (1968), Larrain and Bonilla (1970), Van Dyke (1978), Manlapaz and Churchill (1980) and Berger et al. (1983).

White (1929)

This empirical equation is suitable for $11.6 < Dn < 2000$:

$$\frac{f_s}{f_c} = 1 - \left(1 - \left(\frac{11.6}{Dn}\right)^{0.45}\right)^{\frac{1}{0.45}} \qquad \textbf{Equation 2-129}$$

$$\frac{f_s}{f_c} = 1 \text{ for } Dn < 11.6$$

This equation has been recommended by Rogers and Mayhew (1964), Kubair and Kuloor (1966), Srinivasan et al. (1968), Boyce et al. (1969), Larrain and Bonilla (1970), Akagawa et al. (1971), Mishra and Gupta (1979), Manlapaz and Churchill (1980) and Liu et al. (1994).

Adler (1934)

This formula was derived theoretically, assuming a laminar boundary-layer adjacent to the wall:

$$\frac{f_c}{f_s} = 0.1064 Dn^{0.5} \qquad \textbf{Equation 2-130}$$

The equation has been recommended by Srinivasan et al. (1968), Larrain and Bonilla (1970), Van Dyke (1978), Manlapaz and Churchill (1980), Berger et al. (1983) and Liu et al. (1994).

Prandtl (1954)

This empirical equation is suitable for $20 < Dn < 1000$:

$$\frac{f_c}{f_s} = 0.037 Dn^{0.36} \qquad \textbf{Equation 2-131}$$

The equation has been also recommended by Kubair and Varrier (1961-62), Srinivasan et al. (1968) and Van Dyke (1978).

Ito (1959) - referenced in Mori and Nakayama (1976a), Srinivasan et al. (1968) and Oguri (1995)

This empirical equation is applicable for 13.5 < Dn < 2000 and d/D < 50:

$$\frac{f_c}{f_s} = \frac{21.5Dn}{(1.56 + \log_{10} Dn)^{5.73}} \qquad \textbf{Equation 2-132}$$

Kubair and Varrier (1961/1962)

This equation is suitable for 2000 < Re < 9000 and 0.037 < d/D 0.097:

$$f_c = 0.7716 e^{3.553\left(\frac{d}{D}\right)} \mathrm{Re}^{-0.5} \qquad \textbf{Equation 2-133}$$

The equation was recommended by Kubair and Kuloor (1965) and Srinivasan et al. (1968).

Barua (1963)

This formula was theoretically derived for large Dean numbers:

$$\frac{f_c}{f_s} = 0.0918 Dn^{\frac{1}{2}} + 0.509 \qquad \textbf{Equation 2-134}$$

It was recommended by Srinivasan et al. (1968), Van Dyke (1978) and Berger et al. (1983).

Hasson (1963) – referenced in Barua (1963), Srinivasan et al. (1968), Van Dyke (1978) and Liu et al. (1994)

This empirical equation is suitable for 30 < De < 2000:

$$\frac{f_c}{f_s} = 0.0969 Dn^{0.5} + 0.556 \qquad \textbf{Equation 2-135}$$

Kubair and Kuloor (1965)

This empirical equation was derived for non-isothermal fluids and is applicable for 170 < Re < $9000/\mathrm{Re}_{crit}$:

Two-phase flow of gas-liquid mixtures in horizontal *helical pipes*; Adedigba (2007)

$$f_c = I6\left[2.8 + 12\left(\frac{d}{D}\right)\right]\mathrm{Re}^{-1.15} \qquad \textbf{Equation 2-136}$$

The equation was also recommended by Srinivasan et al. (1968).

Mori and Nakayama (1965)

This equation was produced from experimental and theoretical studies. It is applicable for $13.5 < De < 2000$:

$$\frac{f_c}{f_s} = \frac{0.1080\,Dn^{0.5}}{\left[1 - 3.253/Dn^{-0.5}\right]} \qquad \textbf{Equation 2-137}$$

The equation was recommended by Srinivasan et al. (1968), Van Dyke (1978) and Berger et al. (1983).

Kubair and Kuloor (1966)

The formulae are suitable for Re ranging from 200 to 3000, and are based on the diameters of the first and last turns of the spiral:

$$f_c = 16.1\left[e^{\left(3.554\frac{d}{D_{\max}}\right)} - e^{\left(3.554\frac{d}{D_{\min}}\right)}\right]\mathrm{Re}^{-0.5} \qquad \textbf{Equation 2-138}$$

where max. and min. denote maximum and minimum respectively

and

$$f_c = 0.7716\left[e^{\left(16.1\frac{d}{D_{av}}\right)}\right]\mathrm{Re}^{-0.5} \qquad \textbf{Equation 2-139}$$

Kubair and Kuloor (1966) equations were recommended by Srinivasan et al. (1968).

Kubair and Kuloor (1966) – referenced in Srinivasan et al. (1968) and Ali and Seshadri (1971)

The equation uses the average of the first and last turns of the spiral. It fits their own data for $300 < \mathrm{Re} < 7000$:

$$f_c = 12.74\left[\frac{d^2}{lD_{av}}\right]^{0.3} \mathrm{Re}^{-0.5}$$ **Equation 2-140**

Schmidt (1967)

$$\frac{f_c}{f_s} = 1 + 0.14\left(\frac{d}{D}\right)^{0.97} \mathrm{Re}^{\left[1-0.644\left(\frac{d}{D}\right)^{0.312}\right]}$$ **Equation 2-141**

This equation was recommended by Manlapaz and Churchill (1980).

Ito (1969)

$$\frac{f_c}{f_s} = 0.1033 Dn^{\frac{1}{2}}\left[\left(1+\frac{1.729}{Dn}\right)^{\frac{1}{2}} - \left(\frac{1.729}{Dn}\right)^{\frac{1}{2}}\right]^{-3}$$ **Equation 2-142**

This equation was recommended by Van Dyke (1978), Manlapaz and Churchill (1980) and Berger et al. (1983).

Collins and Dennis (1975)

$$\frac{f_c}{f_s} = 0.1028 Dn^{0.5} + 0.38$$ **Equation 2-143**

The equation was recommended by Van Dyke (1978).

Van Dyke (1978)

This formula was theoretically derived and is suitable for 20 < Dn < 200:

$$\frac{f_c}{f_s} = 0.147136 Dn^{\frac{1}{4}}$$ **Equation 2-144**

The equation was recommended by Manlapaz and Churchill (1980), Berger et al. (1983) and Liu et al. (1994).

Manlapaz and Churchill (1980)

$$\frac{f_c}{f_s}=\left[\left(1-\frac{0.18}{\left[1+\left(\frac{35}{Dn}\right)^2\right]^{\frac{1}{2}}}\right)^m+\left(1+\frac{d}{3D}\right)^2\frac{Dn}{88.33}\right]^{\frac{1}{2}}$$ **Equation 2-145**

where

m =2 for $Dn < 20$

m =1 for $20 < Dn < 40$

m =0 for $Dn > 40$

This equation was recommended by Awwad et al. (1995b), and Xin et al. (1996).

2.5.2.2 *Helical* coil friction factor equations for turbulent flow

White (1932)

This equation is applicable for 15,000$< \mathrm{Re} <$ 100,000:

$$f = 0.08\,\mathrm{Re}^{-0.25}+0.012\left(\frac{d}{D}\right)^{0.5}$$ **Equation 2-146**

The equation was recommended by Kubair and Varrier (1961 / 62) and Srinivasan et al. (1968)

Ito (1959)

Ito derived his equations 2-147 and 2-148 from the 1/7th power velocity-distribution law for flows through a helical pipe.

$$f_c = 0.076\,\mathrm{Re}^{-0.25}+0.00725\left(\frac{d}{D}\right)^{0.5}$$ **Equation 2-147**

for $0.034 < \mathrm{Re}\left(\frac{d}{D}\right)^2 < 300$.

Below $\mathrm{Re}\left(\frac{d}{D}\right)^2 = 0.034$, the flow resembles that through a straight pipe.

The above equation was recommended by Rogers and Mayhew (1964), Mori and Nakayama (1965), Srinivasan et al. (1968), Boyce et al. (1969), Czop et al. (1964), Awwad et al. (1995b) and Xin et al. (1996).

$$\frac{f_c}{f_s} = 1.00\left[\mathrm{Re}\left(\frac{d}{D}\right)^2\right]^{\frac{1}{20}} \qquad \textbf{Equation 2-148}$$

for $\mathrm{Re}\left(\frac{d}{D}\right)^2 > 6$.

This equation was recommended by Seban and Mclaughlin (1963), Rogers and Mayhew (1964), Mori and Nakayama (1967), Srinivasan et al. (1968), Akagawa et al. (1971) and Oguri (1995).

Kubair and Varrier (1961/ 62)

This equation was obtained from experimental results and was suitable for $9{,}000 < \mathrm{Re} < 25{,}000$ and $10 < d/D < 27$:

$$f_c = 0.003538e^{1.887\left(\frac{d}{D}\right)}\mathrm{Re}^{0.09} \qquad \textbf{Equation 2-149}$$

The equation was recommended by Srinivasan et al. (1968).

Mori and Nakayama (1967a)

Mori and Nakayama produced two equations from experimental results and theoretical studies: The first equation is:

$$f_c = \frac{0.075}{\left[\mathrm{Re}\left(d/D\right)^2\right]^{\frac{1}{5}}}\left[1 + \frac{0.112}{\left[\mathrm{Re}\left(d/D\right)^2\right]^{\frac{1}{5}}}\right]\left(\frac{d}{D}\right)^{\frac{1}{2}} \qquad \textbf{Equation 2-150}$$

The second equation, which was theoretically verified, is:

$$f_c = \frac{0.048}{\left[\mathrm{Re}\left(d/D\right)^{2.5}\right]^{\frac{1}{6}}}\left[1+\frac{0.068}{\left[\mathrm{Re}\left(d/D\right)^{2.5}\right]^{\frac{1}{6}}}\right]\left(\frac{d}{D}\right)^{\frac{1}{2}} \qquad \textbf{Equation 2-151}$$

These equations were recommended by Srinivasan et al. (1968).

Kubair and Kuloor (1966) – referenced in Srinivasan et al. (1968) and Ali et al. (1971)

Equation 2-152 was verified by experimentation by Kubair and Kuloor:

$$f_c = 0.079\,\mathrm{Re}^{-0.25} + 0.1025\left(\frac{d}{D_{av}}\right)^{0.9} \qquad \textbf{Equation 2-152}$$

Mishra and Gupta (1979)

The equation is applicable for 4,500 $< \mathrm{Re} <$ 10^5 and 6.7 $< d/D <$ 346:

$$f_c = 0.079\,\mathrm{Re}^{-0.25} + 0.0075\left(\frac{d}{D}\right)^{0.5} \qquad \textbf{Equation 2-153}$$

The equation was also recommended by Das (1993).

Ruffel (1979) – referenced in Czop et al. (1994)

$$f_c = 0.015 + 2.53\left(\frac{d}{D}\right)^{0.275}\mathrm{Re}^{-0.4} \qquad \textbf{Equation 2-154}$$

This equation is suitable for rough pipes.

Czop et al. (1994)

$$f_c = 0.024\,Dn^{-0.1517} \qquad \textbf{Equation 2-155}$$

2.5.2.3 *Helical* coil critical Reynolds number equations

The critical Reynolds number for the transition from laminar to turbulent flow in a helical coil is commonly expressed as a function of d/D.

Ito (1959)

This empirical equation, according to Liu et al. (1994), is well accepted. Using it, enables one to calculate the critical Reynolds number for a curved pipe. Ito verified experimentally the equation and confirmed that the results show a good agreement for 15 < d/D < 860. He also confirmed that the critical Reynolds number coincides with that for a straight pipe

$$\mathrm{Re}_{crit} = 20000\left(\frac{d}{D}\right)^{0.32} \qquad \textbf{Equation 2-156}$$

The equation has been recommended by Rogers and Mayhew (1964), Mori and Nakayama (1967a), Srinivasan et al. (1968), Akagawa et al. (1971), Mishra and Gupta (1979), Das (1993), Czop et al. (1994) and Liu et al. (1994).

Kubair and Varrier (1961/ 62)

This equation was derived from experimental results for values of d/D ranging from 0.0005 to 0.103:

$$\mathrm{Re}_{crit} = 12730\left(\frac{d}{D}\right)^{0.2} \qquad \textbf{Equation 2-157}$$

This was recommended by Kubair and Kuloor (1965), Liu et al. (1994) and Srinivasan et al. (1968).

Kubair and Kuloor (1966) – referenced in Srinivasan et al. (1968) and Ali et al. (1971)

This formula was modified from Kubair and Varrier's (1961 / 62) equation for coils by replacing the coil diameter with the average spiral diameter (D_{av}):

$$\mathrm{Re}_{crit} = 12730\left(\frac{d}{D_{av}}\right)^{0.2}$$ **Equation 2-158**

Srinivasan et al. (1968)

This equation was modified from Srinivasan's equation for coils by using the coil's maximum internal diameter (D_{max}) as the independent variable.

$$\mathrm{Re}_{crit} = 2100\left[1+12\left(\frac{d}{D_{\max}}\right)^{0.5}\right]$$ **Equation 2-159**

This was also used in Ali and Seshadri (1971).

Kutateldze and Borishanskii (1966) – referenced in Srinivasan et al. (1968)

This equation is only valid for the limited range of d/D = 0.0417 to 0.1667:

$$\mathrm{Re}_{crit} = 2300 + 12930\left(\frac{d}{D}\right)^{0.3}$$ **Equation 2-160**

Srinivasan et al. (1968)

This equation is suitable for d/D in the range of 0.004 to 0.100:

$$\mathrm{Re}_{crit} = 2100\left[1+12\left(\frac{d}{D}\right)^{0.5}\right]$$ **Equation 2-161**

when d/D < 0.00116, Re_{crit} is the same as for a straight pipe (i.e. 2100).

This was also recommended by Czop et al. (1994), Liu et al. (1994), Perry (1984) and Awwad et al. (1995b).

Ali and Seshadri (1971)

Ali found two critical Reynolds numbers for a coil pipe.

$$\mathrm{Re}_{crit1} = 2100\left[1+4.9\left(\frac{d}{D_{\max}/2}\right)^{0.21}\left(\frac{P}{D_{\max}/2}\right)^{0.1}\right]$$ **Equation 2-162**

and

$$\mathrm{Re}_{crit11} = 2100\left[1+6.25\left(\frac{d}{D_{\min}/2}\right)^{0.17}\left(\frac{P}{D_{\min}/2}\right)^{0.1}\right] \qquad \textbf{Equation 2-163}$$

where

$D_{\max}$ is the maximum (external) diameter of coil

$D_{\min}$ is the minimum (internal) diameter of coil

P is pitch of coil

Re_{crit} is coil critical Reynolds number

Ward-Smith (1980) – referenced in Liu et al. (1994)

The formula is applicable for d/D < 0.1:

$$\mathrm{Re}_{crit} = 2300\left(1+10\left(\frac{d}{D}\right)^{0.5}\right) \qquad \textbf{Equation 2-164}$$

2.5.2.4 Annular coil friction factor equations

Xin et al. (1997)

This equation applies when Dn=35 $\rightarrow$ 20000, $D/(d_0 - d_i) = 21 \rightarrow 32$ and $d_0/d_i = 1.61 \rightarrow 1.67$:

$$f = 0.02985 + 75.89\frac{\left[0.5 - a\tan\left(\frac{Dn-39.88}{77.56}\right)/\pi\right]}{\left(\frac{D}{d_o - d_i}\right)^{1.45}} \qquad \textbf{Equation 2-165}$$

where

d_O is the outer diameter of outer tube

d_i is the inner diameter of inner tube

2.5.3 Two-phase flow

2.5.3.1 *Helical* coil friction factor equations

Rippel et al. (1966)

Rippel et al. (1966) used a two-phase drag coefficient to correlate the pressure drop in two-phase flow. In this study, they obtained correlations for various flow patterns (annular, bubbly or stratified flows) in a *helical tube*. The flow orientation of the coiled tube was in the downward direction. The equations apply for a coil with d = 1.27 cm and D = 20.32 cm.

For annular flow

$$\left(\frac{\Delta P}{\Delta l}\right)_{TP} = \left(\frac{\Delta P}{\Delta l}\right)_{G} + 4.44\lambda^{0.86}\,\frac{\rho_G U^2}{gd} \qquad \textbf{Equation 2-166}$$

For bubbly and slug flows

$$\left(\frac{\Delta P}{\Delta l}\right)_{TP} = \left(\frac{\Delta P}{\Delta l}\right)_{G} + 31.3\lambda^{1.25}\,\frac{\rho_G U^2}{gd} \qquad \textbf{Equation 2-167}$$

For stratified flow

$$\left(\frac{\Delta P}{\Delta l}\right)_{TP} = \left(\frac{\Delta P}{\Delta l}\right)_{G} + 3.20\lambda^{0.875}\,\frac{\rho_G U^2}{gd} \qquad \textbf{Equation 2-168}$$

where

λ is the liquid-fraction input flow = $Q_L \big/ (Q_L + Q_G)$

Q is the volumetric input flow rate, m^3/hr

U is the linear velocity of the liquid, m/s

Akagawa et al. (1971)

This empirical equation was obtained from experimental data for upward direction flows in coils of $d/D = \frac{1}{11}$ and $\frac{1}{22.7}$, with d = 9.92mm

$$\frac{\Delta P_{TP(coil)}}{\Delta P_{L(straight)}} = \frac{f_{L(coil)}}{f_{L(straight)}} + 9.63\left(1+1.7\frac{d}{D}\right)\left(\frac{\mathrm{Re}_G}{\mathrm{Re}_L}\right)^{0.747}\mathrm{Re}_L^{-0.019} \qquad \textbf{Equation 2-169}$$

Czop et al. (1994)

Czop et al. (1994) found a slightly better equation to fit their experimental result, namely:

$$X = \left(\frac{1-x}{x}\right)^{0.924}\left(\frac{\mu_G}{\mu_L}\right)^{-0.07585}\left(\frac{\rho_G}{\rho_L}\right)^{0.5} \qquad \textbf{Equation 2-170}$$

where X is described as the Martinelli parameter

Awwad et al. (1995a)

Awwad et al. (1995a) observed that the Lockhart and Martinelli correlation for a straight pipe is not suitable for calculating the frictional pressure-drop in two-phase flows in *helical pipes*. Based on his experimental data and by incorporating the Froude number, Fr, a new correlation was derived. The basic idea for creating the new correlation is to introduce an extra parameter to the Lockhart and Martinelli equation to account for the effect of liquid velocity. This was derived for horizontal coils and is expressed as:

$$\phi_L = \left(\frac{X}{9.63F_d^{0.61}}\right)\left(1+\frac{12}{X}+\frac{1}{X^2}\right)^{\frac{1}{2}} \qquad \textbf{Equation 2-171}$$

where F_d is defined as

$$F_d = Fr_L\left(\frac{d}{D}\right)^{0.1} \qquad \textbf{Equation 2-172}$$

Awwad et al. (1995b)

Awwad et al. (1995b) also used his experimental result to produce a slightly different version of equation 2-171:

$$\phi_L = \left(\frac{X}{C[F_d]^n}\right)\left(1+\frac{12}{X}+\frac{1}{X^2}\right)^{\frac{1}{2}} \qquad \textbf{Equation 2-173}$$

The values of C and n depend on the value of F_d :

$F_d \leq 0.3$, C = 7.79 and n = 0.576.

F_d > 0.3, C = 13.56 and n = 1.3.

Xin et al. (1996)

For vertical-coil flow:

- For $F_d \leq 0.1$

$$\frac{\phi_L}{\left(1+20/X+1/X^2\right)^{\frac{1}{2}}}=1+\frac{X}{65.45F_d^{0.6}} \qquad \textbf{Equation 2-174}$$

- For F_d > 0.1

$$\frac{\phi_L}{\left(1+20/X+1/X^2\right)^{\frac{1}{2}}}=1+\frac{X}{434.8F_d^{1.7}} \qquad \textbf{Equation 2-175}$$

F_d is defined as:

$$Fd = Fr_L\left(\frac{d}{D}\right)^{\frac{1}{2}}\left(1+\tan\beta\right)^{0.2} \qquad \textbf{Equation 2-176}$$

where β is the helix angle

2.5.3.2 Annular-coil friction factor equations

Xin et al. (1997)

For vertical coils:

When d_o/d_i values range between 1.61 and 1.67 and $\frac{D}{(d_o-d_i)}=21.32$.

$$\phi_L^{\,2}=1+\frac{10.646}{X}+\frac{1}{X^2} \qquad \textbf{Equation 2-177}$$

For horizontal flow:

Using the Froude number, Fr, when the values of d_o/d_i range between 1.61 and 1.67, the deduced d_o = 21.81 mm and $\frac{D}{(d_o - d_i)} = 21$, the single-phase friction factor has been deduced, as shown before for the annular coil, i.e.

$$\phi_L = \left(1 + \frac{0.0435 X^{1.5}}{F}\right)\left(1 + \frac{10.646}{X} + \frac{1}{X^2}\right)^{\frac{1}{2}} \qquad \textbf{Equation 2-178}$$

where F = Fr $^{0.9106}$ e$^{0.0458(\ln Fr)^2}$ and the Froude number is

$$Fr = \frac{U_L^{\,2}}{g(d_o - d_i)} \qquad \textbf{Equation 2-179}$$

2.6 Summary

As seen from the above, a wide variety of empirical and semi-empirical models have been developed for horizontal and near horizontal pipeline flows. However, none of these models is totally satisfactory.

Conclusively, it has been noted that most of the correlations have been developed for specific *helical pipe* geometries. They are limited either in terms of the range of Reynolds and Dean Numbers they cover and/or the ratio of the internal diameter of the *helical pipe* (d) to the *helical pipe* diameter (D). Hence more experimental work to cover a wider range of *helical pipe* geometries and an improved modelling approach are required.

Again, analytical solutions of two-phase flow parameters are also difficult if not impossible to achieve. Due to the fact that it is difficult to specify the flow patterns and define the interactions among the phases, analytical solutions for evaluating two-phase pressure drop in particular are impossible at present. Rapid fluctuations in the flow can occur and cannot easily be accounted for.

Hence design correlations are derived experimentally and care should be taken when applying them outside the experimental limits.

In view of the above, the emphasis of this present study on the one hand, has been on experimental work to compare hydrodynamic fluid flow characteristics in horizontal *helical pipes* with straight pipes of the same properties. On the other hand, areas of application of the *helical pipe* have been carefully studied.

Chapter 3

3 Preliminary Experiments

3.1 Introduction

The objective of the preliminary experiments was to investigate two-phase fluid flow characteristics in *helical* and straight pipes and compare the results for both pipes. In order to achieve the objective the parameters that were measured and analysed from the data collected from the preliminary experiments included pressure and pressure drop. Friction factor for single-phase (water) flow was also evaluated from the pressure drop. Pressure and pressure drop were considered important parameters due to the fact that sufficient pressure is required in the crude oil and gas industry to transport the required hydrocarbon flowrates from reservoir to process plant. Fluid flow pattern characteristics in two-phase (air and water) flow in both straight and *helical pipes* were observed and recorded. Both straight and *helical pipe*s used for the experiments were 25.4 mm in internal diameter. Figure 3 -1 shows a side view of the *helical pipe*. Experiments were performed on both straight and *helical pipes* in horizontal, inclined and vertical positions. However, pressure drop measurements were only possible in single-phase (water) experiments. This was due to excessive fluctuations of the manometer used for the pressure drop measurement. The test rig shown in Figure 3-2 was used for the preliminary experiments.

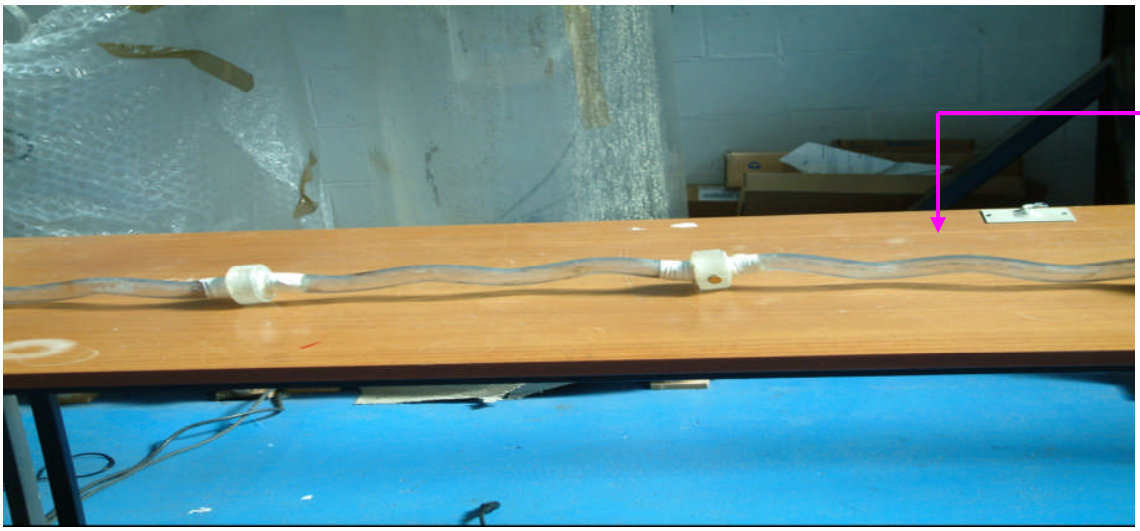

Figure 3-1: Side view of a low amplitude *helical pipe*

3.2 Experimental set-up

The preliminary experimental rig mainly consisted of an air/water flow loop and test section. A schematic representation of the air/water flow loop is shown in Figure 3.-2.

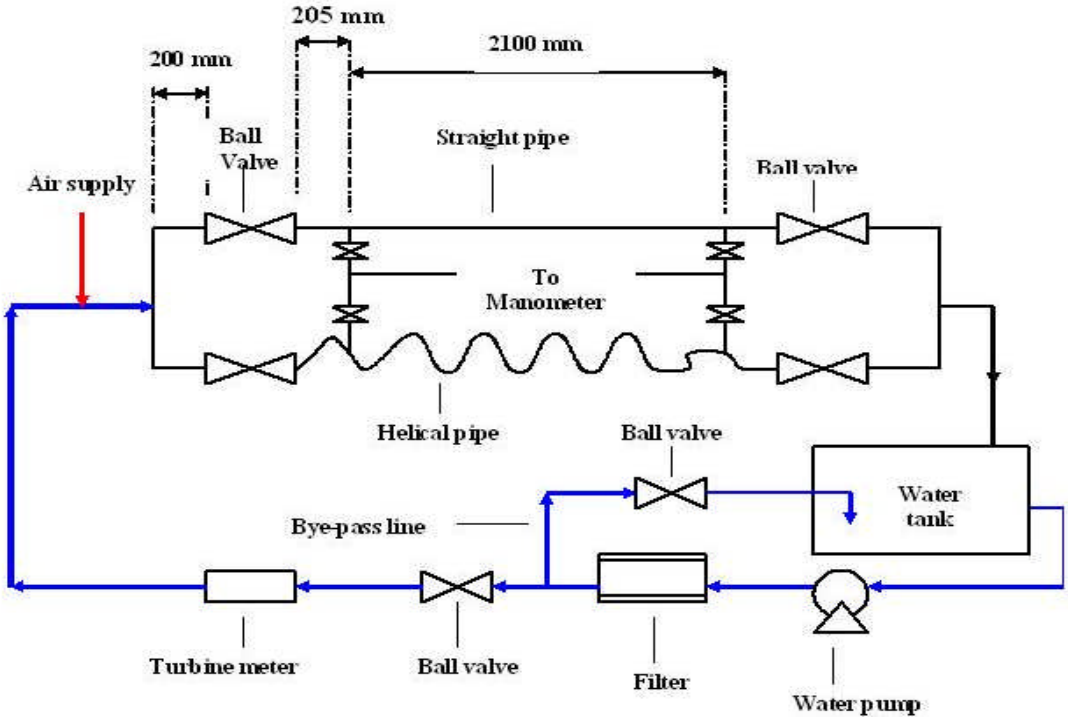

Figure 3-2: Schematic of preliminary test rig

The apparatus used consisted of a water tank, pump, filter, by-pass line, copper pipe of 25.4 mm internal diameter, valves, turbine flow-meter, frequency counter, air supply line, transparent straight and *helical pipes* of 25.4 mm internal diameter, each 387 cm long and a manometer. The manometer was connected to two points on the test section as shown in Figure 3-2. The head losses in mm of water were recorded for each experimental run. The distance between the pressure taps along the transparent straight and *helical pipes* was 210 cm. The distance between the ball valve after the air supply point and the first pressure tapping in the test section was 205 mm. This design was to allow fluid flow to be fully developed before entering the test-section.

Figure 3-3 shows the two pipes (straight and *helical*) securely fastened to a plywood board supported by a steel angle-iron structure in the test section of the experimental rig.

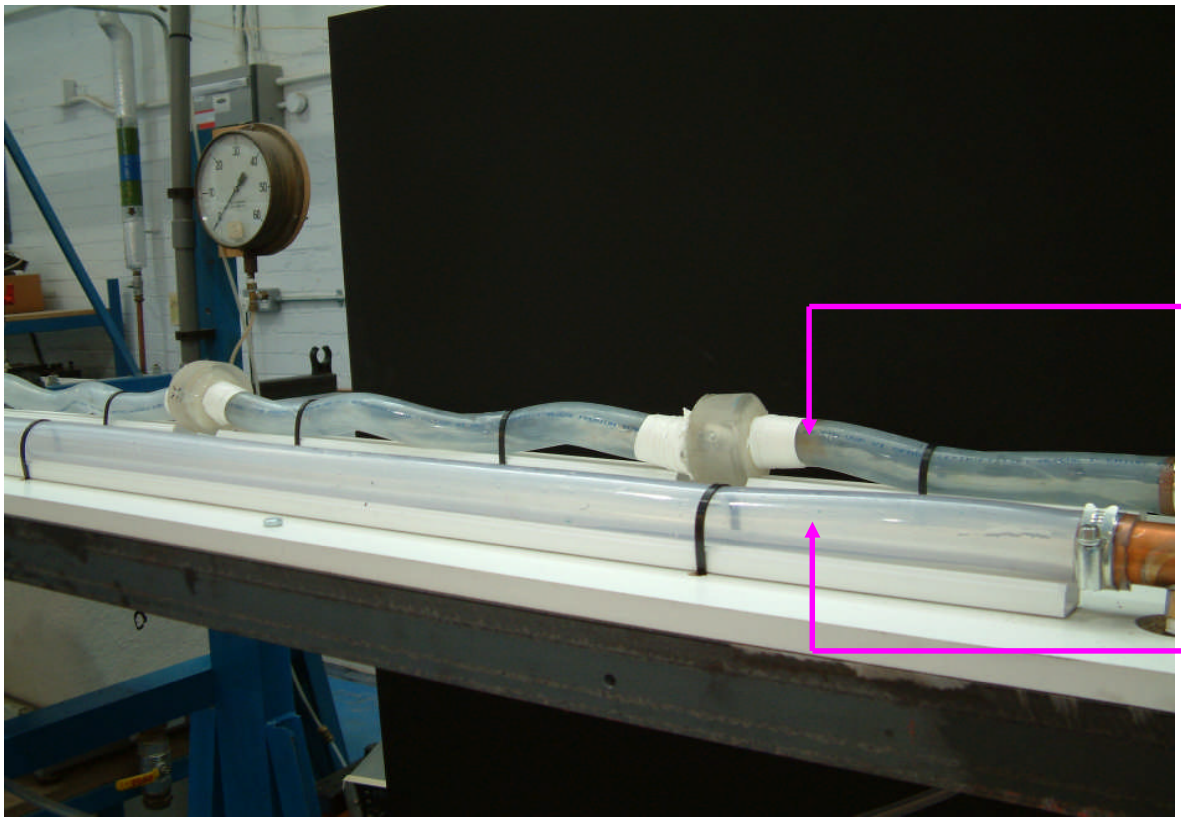

Figure 3-3: Straight and *helical pipes* in the test section of the experimental rig

3.3 Experimental procedure

Water was stored in a collection tank; from there, it flowed to the suction side of a 2 kW centrifugal pump. After exiting the pump, some of the water was forced through a water filter and the rest returned to the collection tank via a by-pass line. The water flow leaving the filter was conveyed to the turbine flow meter, where its flow rate was recorded. After the meter, the water passed directly to the transparent straight and *helical pipes* in the test section. Air from a laboratory compressor was supplied through an air regulator and then subsequently to the test section through a non-return check-valve, where it was mixed with the water before entering either the straight or *helical pipe*.

After the mixture exited the test section, it passed to the water-collection tank from where the air escaped to the ambient environment. The water line was part of a closed-circulation loop. In addition, the water flow rates were controlled by ball valves mounted in the flow loop. The ball valves also enabled one to direct the fluid flow from the straight pipe to *helical pipe* and vice versa.

The straight and *helical pipes* were made from transparent and flexible PVC material. They were securely fastened to a plywood board and a steel angle iron to inhibit vibration transmission to the pipes. The manner in which the pipes were fixed also made it possible to choose the pipe's inclination to the horizontal. Both the straight and *helical* transparent-pipes were of 30 mm outside diameter.

3.4 Experimental results and discussion

3.4.1 Single-phase flows

3.4.1.1 Pressure-drop measurements

The experiments were performed in order to compare single-phase (water) flow characteristics in both straight and *helical pipes*. The ambient environmental

atmospheric pressure and temperature in the laboratory were assumed to be approximately 1.013 bar and 18^0 C respectively. The following assumptions were also made for the experiments:

- Pipes with smooth internal surfaces
- Adiabatic pipes (i.e. no heat addition or losses through the walls of the pipes)

Pressure taps were located at the bottom of the test section of the rig. The pressure drop, expressed in terms of head loss, between the pressure taps, located upstream and down stream of each pipe was measured by the use of a manometer. The pressure drop was measured, in mm head of water, at various water-flow rates with an accuracy of ± 2% of full scale. Fifty-two readings were recorded for both straight and *helical pipes* on single-phase flow with the two pipes in horizontal and vertical positions. The readings are shown in Tables 3-1 to 3-4.

Test	Flow meter reading (Hz)	Flow rate (litre/s)	Flow velocity (m/s)	Pressure drop (mm H_20)	Friction factor (10^{-2})	Reynolds number of flow (10^3)
1	53	0.15	0.30	20	5.42	6.65
2	86	0.24	0.47	40	4.23	10.6
3	100	0.28	0.55	60	4.66	12.4
4	114	0.32	0.63	70	4.17	14.2
5	122	0.34	0.67	80	4.22	15.1
6	162	0.46	0.91	130	3.74	20.4
7	181	0.51	1.01	150	3.51	22.6
8	203	0.57	1.12	180	3.38	25.3
9	225	0.63	1.24	210	3.22	27.9
10	243	0.69	1.36	240	3.07	30.6
11	266	0.75	1.48	280	3.03	33.3
12	283	0.79	1.56	310	3.03	35.0
13	295	0.83	1.64	330	2.92	36.8

Table 3-1: Readings for the single-phase water flow through the horizontal straight pipe

Test	Flow meter reading (Hz)	Flow rate (litre/s)	Flow velocity (m/s)	Pressure drop (mm H_20)	Friction factor (10^{-2})	Reynolds number of flow (10^3)
1	53	0.15	0.30	25	6.77	6.65
2	86	0.24	0.47	50	5.29	10.6
3	100	0.28	0.55	70	5.44	12.4
4	114	0.32	0.63	80	4.76	14.2
5	122	0.34	0.67	90	4.74	15.1
6	162	0.46	0.91	150	4.32	20.4
7	181	0.51	1.01	180	4.22	22.6
8	203	0.57	1.12	220	4.13	25.3
9	225	0.63	1.24	290	4.45	27.9
10	243	0.69	1.36	310	3.97	30.6
11	266	0.75	1.48	360	3.90	33.3
12	283	0.79	1.56	400	3.91	35.0
13	295	0.83	1.64	430	3.80	36.8

Table 3-2: Readings for the single-phase water flow through the horizontal *helical pipe*

Test	Flow meter reading (Hz)	Flow rate (litre/s)	Flow velocity (m/s)	Pressure drop (mm H_20)	Friction factor (10^{-2})	Reynolds number of flow (10^3)
1	53	0.15	0.30	20	5.42	6.65
2	86	0.24	0.47	45	4.76	10.6
3	100	0.28	0.55	50	3.89	12.4
4	114	0.32	0.63	65	3.87	14.2
5	122	0.34	0.67	70	3.69	15.1
6	162	0.46	0.91	110	3.17	20.4
7	181	0.51	1.01	130	3.05	22.6
8	203	0.57	1.12	160	3.00	25.3
9	225	0.63	1.24	190	2.92	27.9
10	243	0.69	1.36	210	2.69	30.6
11	266	0.75	1.48	240	2.60	33.3
12	283	0.79	1.56	270	2.64	35.0
13	295	0.83	1.64	290	2.56	36.8

Table 3-3: Readings for the single-phase water flow through the vertical straight pipe

Test	Flow meter reading (Hz)	Flow rate (litre/s)	Flow velocity (m/s)	Pressure drop (mm H_20)	Friction factor (10^{-2})	Reynolds number of flow (10^3)
1	53	0.15	0.30	30	8.12	6.65
2	86	0.24	0.47	50	5.29	10.6
3	100	0.28	0.55	60	4.66	12.4
4	114	0.32	0.63	80	4.76	14.2
5	122	0.34	0.67	90	4.74	15.1
6	162	0.46	0.91	140	4.03	20.4
7	181	0.51	1.01	170	3.98	22.6
8	203	0.57	1.12	200	3.75	25.3
9	225	0.63	1.24	250	3.84	27.9
10	243	0.69	1.36	280	3.58	30.6
11	266	0.75	1.48	330	3.57	33.3
12	283	0.79	1.56	370	3.61	35.0
13	295	0.83	1.64	400	3.54	36.8

Table 3-4: Readings for the single-phase water flow through the vertical *helical pipe*

As shown in Tables 3-1 to 3-4, readings such as flow rates were measured with a turbine meter and indicated by a frequency (Hz) counter reading, which can

then be converted, by a provided calibration into litres per second (l/s). The head loss was measured in mm of water and velocity {in metres per second (ms^{-1})} was calculated by dividing flow rate (litres/s) by the internal cross section area (m^2) of the pipe. The Reynolds number (Re) was calculated using equation 2-1

$$\mathrm{Re} = \frac{\rho U d}{\mu}$$

where

ρ is the density of water

U is the velocity of water flow

μ is the dynamic viscosity of water

d is the internal diameter of the pipe.

The friction factor was calculated using equation 3-1

Equation 3-1

$$f = \frac{2gd\Delta H}{lU^2}$$

Figures 3-4 to 3-6 show the relationships between the pressure drop along the pipe against velocity of fluid flow. Figures 3-7 to 3-9 show relationships between friction factor and Reynolds number.

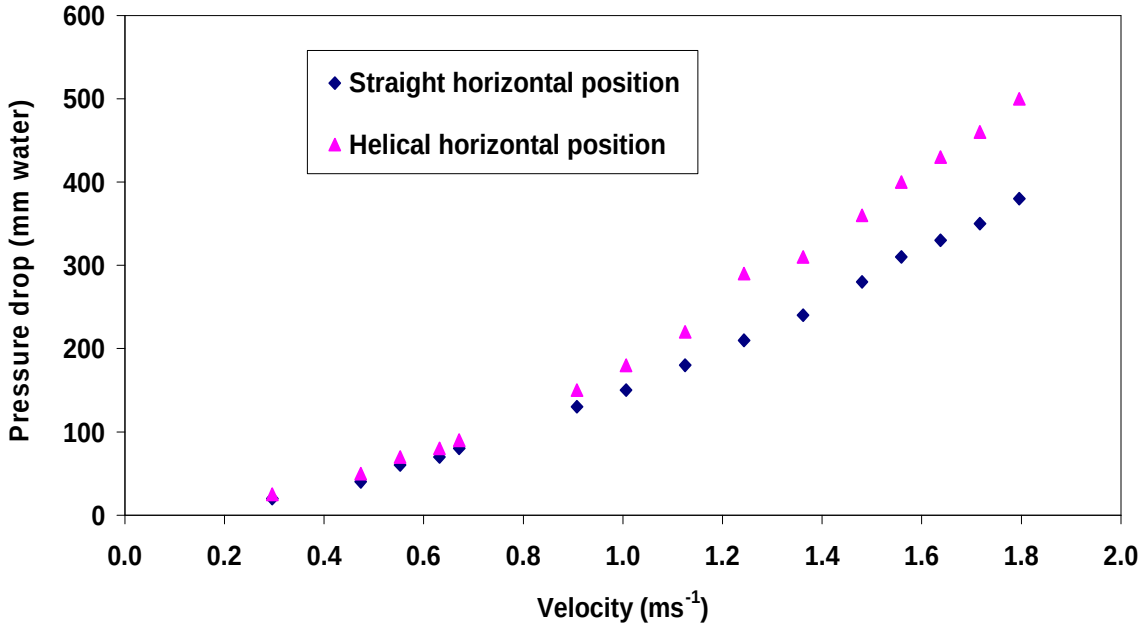

Figure 3-4: Pressure drop versus velocity for straight and *helical pipes* in the horizontal position

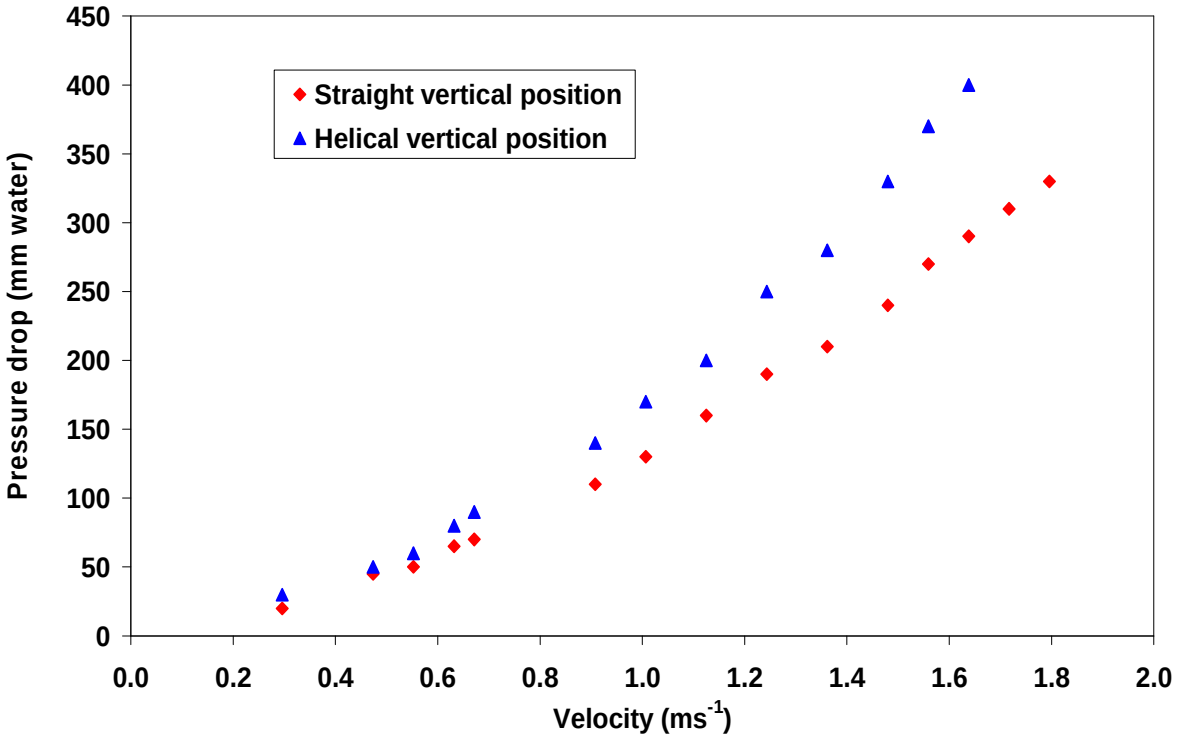

Figure 3-5: Pressure drop versus velocity for straight and *helical pipes* in the vertical position

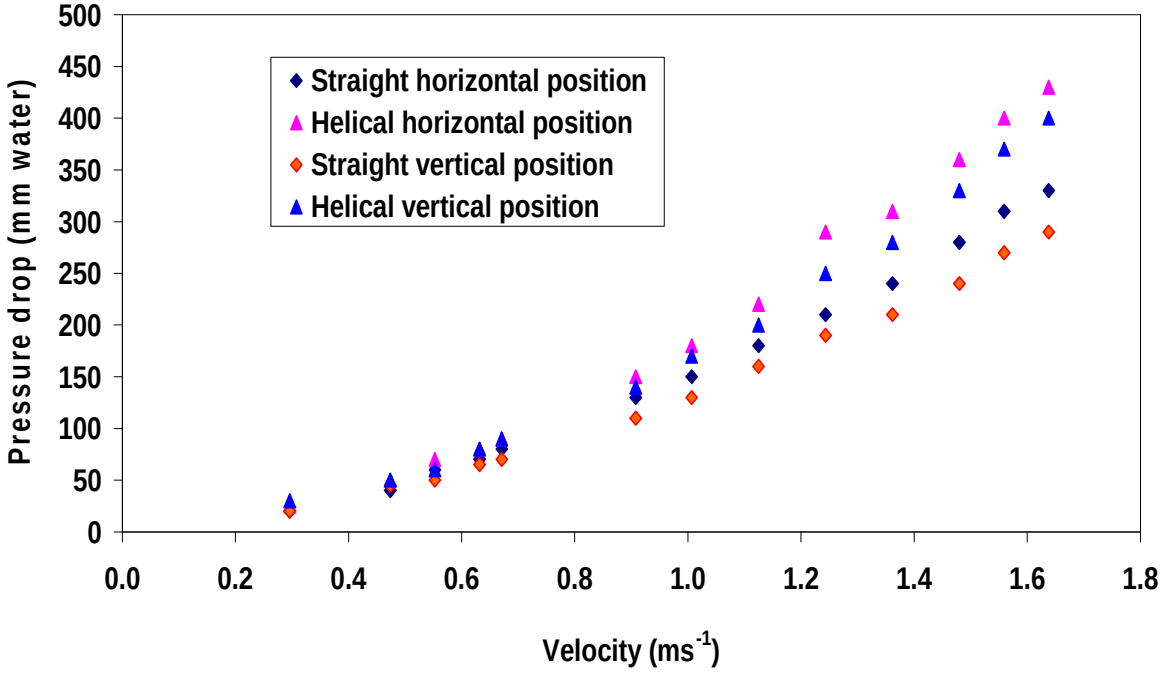

Figure 3-6: Pressure drop versus velocity for straight and *helical pipes* in the horizontal and vertical positions

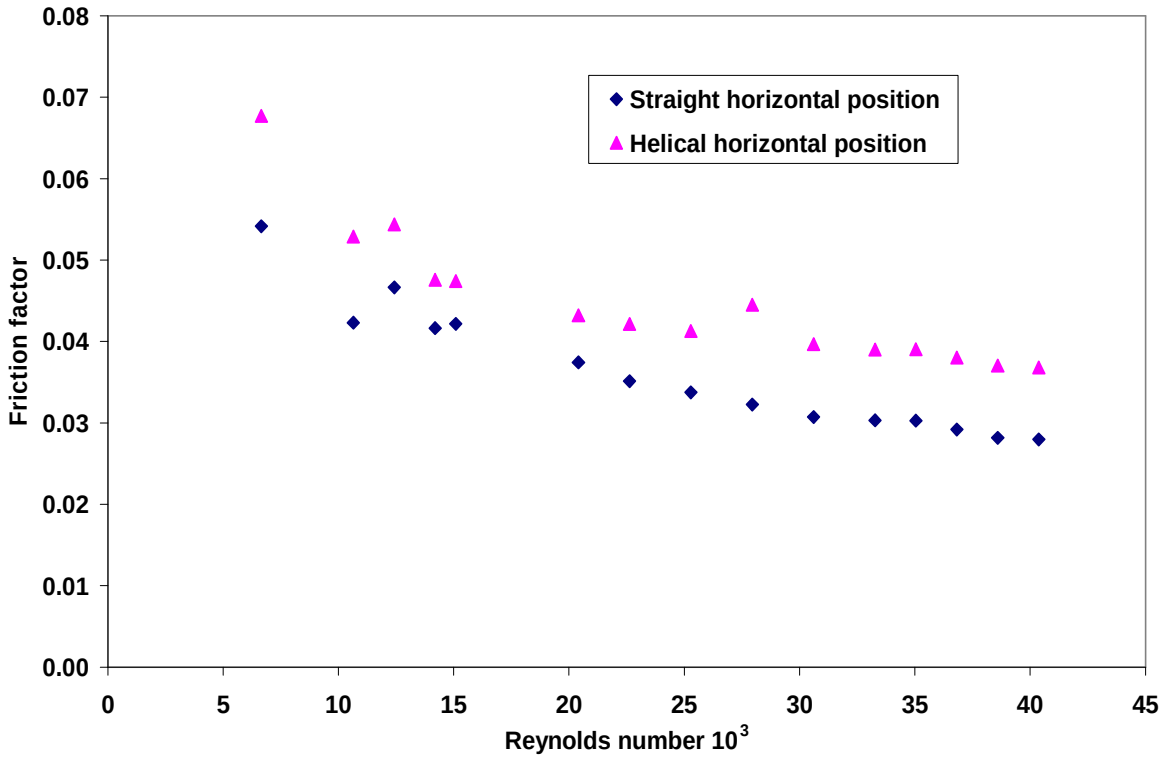

Figure 3-7: Friction factor versus Reynolds number for the straight and *helical pipes* in horizontal position

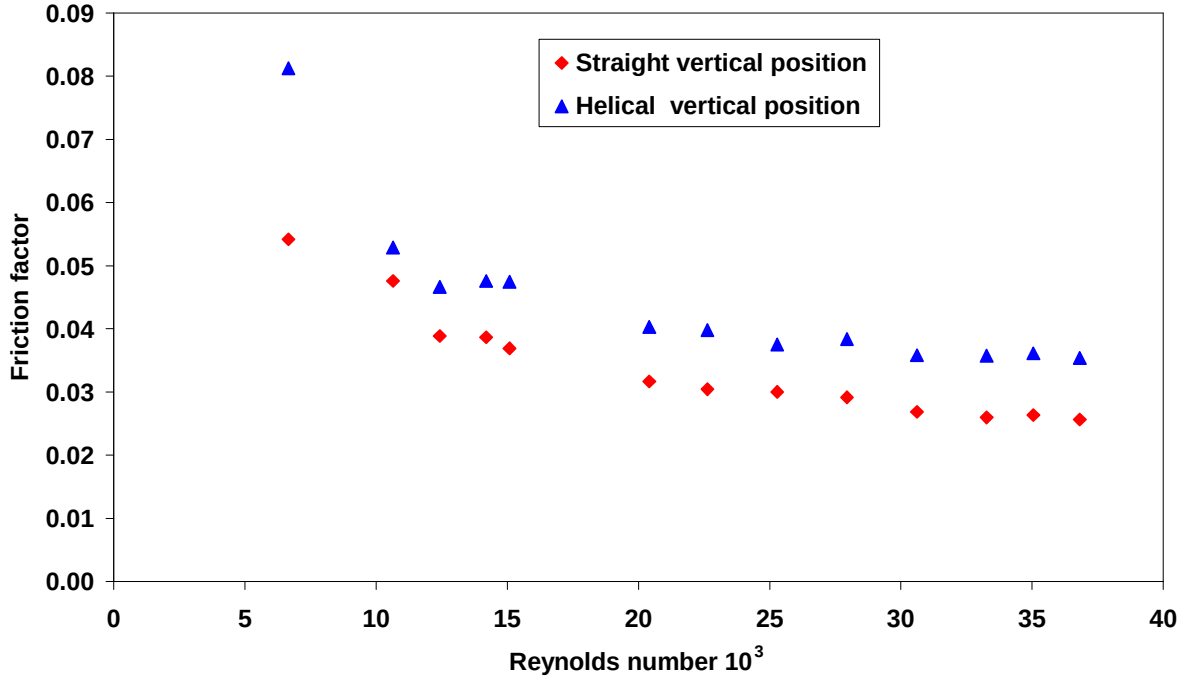

Figure 3-8: Friction factor versus Reynolds number for the straight and *helical pipes* in vertical position

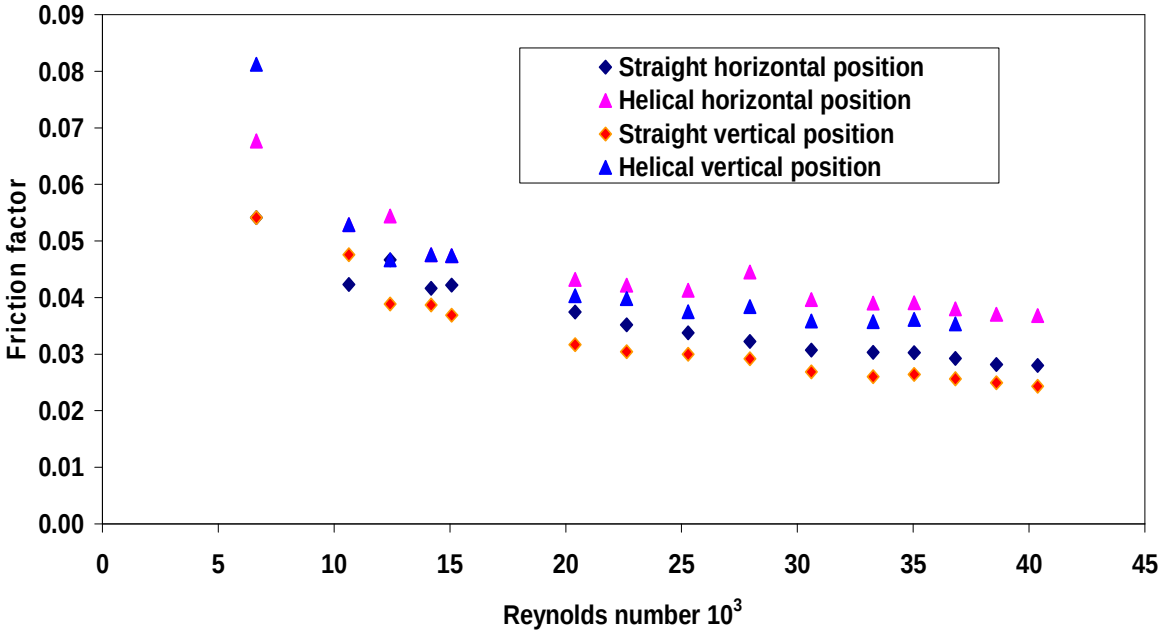

Figure 3-9: Friction factor versus Reynolds number for the straight and *helical pipes* in horizontal and vertical positions

As recorded in tables 3-1 to 3-4 and shown in Figures 3-4 to 3-6, the flow velocity ranged from 0.30 to 1.80 ms^{-1}. The *helical pipe* in the horizontal position incurred the highest head-losses, followed by the same *helical pipe* but in the vertical orientation. The straight pipe in the vertical position recorded the least head losses.

The measurements shown in Figure 3-9 corroborate the conclusions of the above paragraph, namely the *helical pipe* in horizontal position exhibits the highest friction factor, followed by *helical pipe* in vertical position. Also, the straight pipe in vertical position has the lowest friction factor.

In Figure 3-6, when the velocity is higher, the pressure loss is higher. But at low pressure-head values, there is no clear distinction in the flow behaviours between straight and *helical pipes* and between horizontal and vertical positions. Also in Figure 3-9, at low values of Reynolds number, there is no clear distinction between the flow behaviours for the straight and *helical pipes*

and between horizontal and vertical positions. But as the Reynolds number increases, the friction factor for each pipe, and in different positions, decreases.

The experimental data plotted in Figures 3-7 and 3-8 fit Moody's chart. The conflicting points may be due to some factors such as parallax error in taking the measurements of head losses and variations in the laboratory temperature.

3.4.2 Two-phase flows

3.4.2.1 Pressure-drop measurements

Due to fluctuations of the levels of the manometer liquid, it was difficult to provide truly representative pressure drops for two-phase (air and water) flows. However, this problem was overcome by improving the data acquisition and instrumentation on the two-phase (water and air) facility. Numerous data for the two-phase pressure drop were recorded in the 50 mm internal diameter pipe experiments and the data were subsequently interpreted.

3.4.3 Flow-pattern visualisation

This was accomplished by viewing through the transparent test-pipe walls. The flow pattern visualisation was successfully done by focusing on an element of liquid or gas and allowing the line of sight to move with it along the length of the pipe. The flow patterns were observed at four different water rates (0.34, 0.57, 0.79 and 0.91 litre/s). Air was also injected at four different flow rates (very small, small, medium and large) but there was no exact means of measuring the injection rates. This problem was overcome in subsequent experiments (50 mm internal diameter pipe in chapter 4) by providing appropriate instrumentation for two-phase experiments. The flow patterns were observed when the pipes were in horizontal and inclined (at 30^0 to the horizontal) positions. The fluid flow was uphill when the pipes were inclined at 30^0 to the horizontal.

Observations for straight and *helical pipes* in the horizontal position

Air–injection rate	Straight pipe	*Helical pipe*
Very small	Slug flow. The slugs were moving at slow speed.	Due to the swirling motion of the water the flow was bubbly.
Small	Elongated slug flow with the slugs moving at a higher velocity. The lengths of the slugs were larger than that in very small air-injection rate.	Slug flow initially, but later disappeared.
Medium	Slug flow. Slugs were moving at a relatively high velocity	Slug flow. Fast swirling motion was produced.
Large	Still slug flow with increased in velocity.	Slug flow. Slugs moved with high velocity and stronger swirling motion.

Table 3-5: Observations of flow patterns for a water-flow rate of 0.34 litres/s

Air–injection rate	Straight pipe	*Helical pipe*
Very small	Elongated slug flow moving at high velocity.	Slugs appeared and produced swirling motion.
Small	Slug flow with the slugs increased in length and moving at a higher velocity. Almost half of the pipe was filled with moving water.	Slugs moving with liquid in the direction of flow. Swirling motion was produced.
Medium	High velocity slug flow taking more liquid in the direction of flow.	Fast swirling motion.
Large	Still slug flow moving at a very high velocity.	Slug water swirls around the periphery of pipe.

Table 3-6: Observations of flow patterns for a water-flow rate of 0.57 litres/s

Air–injection rate	Straight pipe	*Helical pipe*
Very small	Wavy surface with irregular slugs moving fast on top of the liquid.	Small bubbles in clusters travelling in upper part of the pipe.
Small	Elongated slugs with wavier surface.	Fast swirling motion.
Medium	Annular flow with slugs moving at a high velocity. The whole periphery of pipe was filled with water.	Fast swirling motion.
Large	Further increase in velocity with the whole of periphery of pipe filled with water.	Very fast swirling motion.

Table 3-7: Observations of flow patterns for a water-flow rate of 0.79 litres/s

Air–injection rate	Straight pipe	*Helical pipe*
Very small	Bubbles coalesce in upper part of pipe and move at a relatively low velocity.	Small cluster of bubbles travelling through the upper part of the pipe.
Small	More gas moving in continuous fashion in the middle of pipe with thin liquid film adhering to the top of the pipe.	Turbulent swirling motion.
Medium	Elongated slug flow moving at a very high velocity. Wavy water surface as slugs moving along it.	More turbulent swirling motion.
Large	Noisy elongated slug flow moving at a very high velocity.	No experiment!

Table 3-8: Observations of flow patterns for a water-flow rate of 0.91 litres/s

3.4.3.1 Observations for straight and *helical pipes* at an inclination of 30 degrees to the horizontal

Air–injection rate	Straight pipe	*Helical pipe*
Very small	Slug flow.	Swirling motion with slug flow.
Small	Slug flow. Slugs were moving at a very high velocity	Swirling motion effect was interfacial. Water film was clearly seen going backwards.
Medium	Slug flow. Less water was being carried away by fast moving slugs. Slugs were moving at a higher velocity than previously.	Thick liquid-film was seen moving backwards while slugs were moving upwards.
Large	Very thin layer of water film at the bottom of pipe. A couple of water slugs moving at a very high velocity	Swirling motion occurring throughout the pipe.

Table 3-9: Observations of flow patterns for a water-flow rate of 0.34 litres/s

Air–injection rate	Straight pipe	*Helical pipe*
Very small	Pipe was full of water. No bubbles were seen!	As in straight pipe.
Small	Slugs of water moving at high speeds. Wavy water surface. Water film was moving backwards.	Swirling motion with thick water film moving backwards.
Medium	Water film was seen moving back-wards. A few slugs were seen moving at high speeds.	Slugs were seen initially but later disappeared. Swirling motion can be seen!
Large	Slugs were moving at high speeds in upward direction taking more water along with them.	Swirling motion with vibration, due to intermittent detachment of air bubbles.

Table 3-10: Observations of flow patterns for a water-flow rate of 0.57 litres/s

Air–injection rate	Straight pipe	*Helical pipe*
Very small	Pipe was full of water. No bubbles were seen!	As in straight pipe!
Small	Slugs moving while shedding bubbles from tails of slugs at the bottom of water film. Wavy water surface!	Slugs appeared as continuous swirling water moving upwards.
Medium	Slugs were moving fast at the beginning but later disappeared. Thick water film was moving backwards.	Slugs moving at high velocity. Swirling motion and vibration effects in the pipe.
Large	Slugs were moving very fast.	No visible flow! Slugs moved with swirling water. Pipe was vibrating.

Table 3-11: Observations of flow patterns for a water-flow rate of 0.79 litres/s

Air–injection rate	Straight pipe	*Helical pipe*
Very small	Pipe was full of water. No bubbles were seen!	As in straight pipe!
Small	Slugs moving at high velocities and producing wavy surface on the water in the pipe.	Swirling motion. Turbulent flow. Slugs moving at high velocities.
Medium	Slugs moving at very high velocities. Water film was also moving backwards at high velocity.	Slugs moving rapidly. Swirling motion and vibration effects.
Large	Slugs moving at higher velocities. Water film was all over the pipe's internal periphery.	High velocity slugs. Swirling motion and high vibration.

Table 3-12: Observations of flow patterns for a water-flow rate of 0.91 litres/s

3.4.4 Comparison of experimental friction- factors with published correlations

The friction factors obtained from these experimental results have been compared with published friction factor correlations. Table 3-13 shows five different correlations for friction factors obtained by five investigators and Figure 3-10 shows the comparison of these correlations with the experimental results. The correlations computed in Table 3-13 have been discussed in the literature review (chapter 2) and have been referenced again in Table 3-14.

		Correlations				
Test	**Reynolds Number (10^3)**	**Czop**	**Ito**	**Kubair & Varrier**	**Mishra & Gupta**	**White**
1	6.654	0.007	0.078	0.013	0.081	0.086
2	10.647	0.006	0.077	0.014	0.080	0.085
3	12.421	0.006	0.077	0.014	0.080	0.084
4	14.195	0.006	0.077	0.014	0.080	0.084
5	15.083	0.006	0.077	0.014	0.080	0.084
6	20.406	0.006	0.076	0.014	0.079	0.083
7	22.624	0.005	0.076	0.014	0.079	0.083
8	25.286	0.005	0.076	0.015	0.079	0.083
9	27.947	0.005	0.076	0.015	0.078	0.083
10	30.609	0.005	0.075	0.015	0.078	0.083
11	33.271	0.005	0.075	0.015	0.078	0.083
12	35.045	0.005	0.075	0.015	0.078	0.082
13	36.819	0.005	0.075	0.015	0.078	0.082
14	38.594	0.005	0.075	0.015	0.078	0.082
15	40.368	0.005	0.075	0.015	0.078	0.082

Table 3-13: Experimental friction factor comparison with correlations

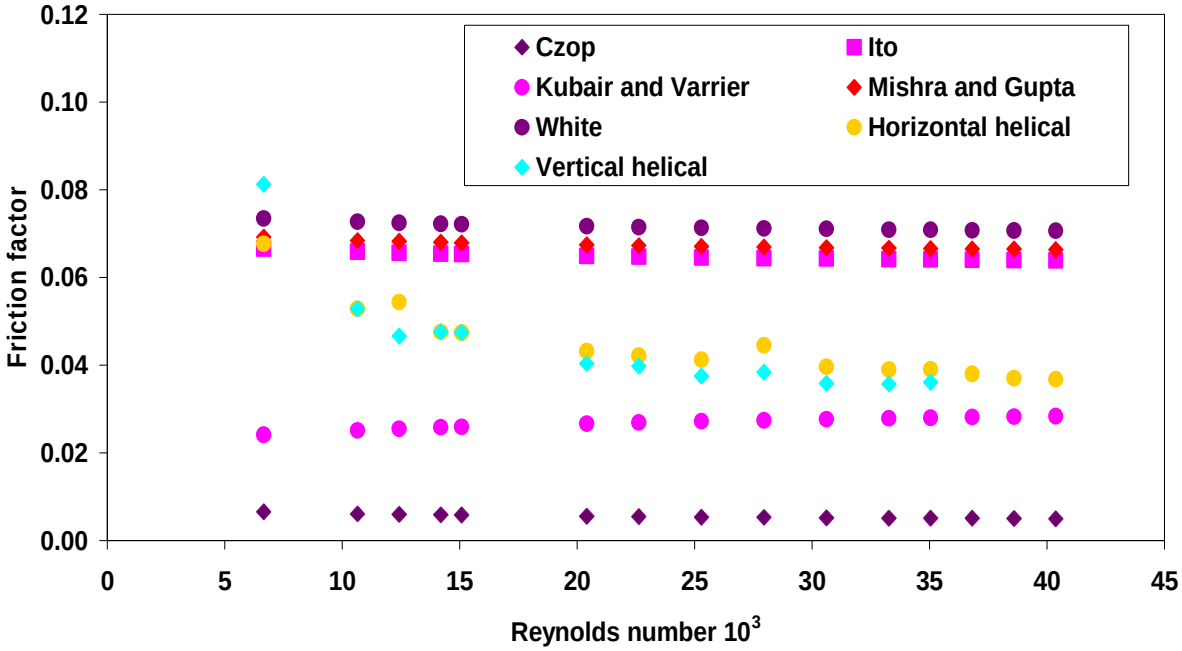

Figure 3-10: Experimental friction factor comparison with correlations

Figure 3-10 shows how the present experimental results compare with the correlations of White (1932), Mishra and Gupta (1979), Ito (1959), Kubair and Varrier (1961/1962), and Czop et al. (1994). As shown, the experimental data fall below the White, Mishra and Gupta and Ito correlations but higher than Kubair and Varrier and Czop correlations. The disparity between the present experimental results and the correlations may be due to the limited *helical pipe* geometries (in terms of the ratio d/D) for which the correlations were developed.

The Kubair and Varrier (1961/1962) correlation for example, was suitable for the small range d/D = 0.037 – 0.097 whereas this study involved a d/D = 0.5976.

Reference	Equation
White (1932)	$f = 0.08\,\mathrm{Re}^{-0.25} + 0.012\left(\frac{d}{D}\right)^{0.5}$ Equation 2-146
Ito (1959)	$f_C = 0.076\,\mathrm{Re}^{-0.25} + 0.00725\left(\frac{d}{D}\right)^{0.5}$ Equation 2-147
Kubair and Varrier (1961/1962),	$f_C = 0.003538e^{1.887\left(\frac{d}{D}\right)}\,\mathrm{Re}^{0.09}$ Equation 2-149
Mishra and Gupta (1979)	$f_C = 0.079\,\mathrm{Re}^{-0.25} + 0.0075\left(\frac{d}{D}\right)^{0.5}$ Equation 2-153
Czop et al. (1994)	$f_C = 0.024Dn^{-0.1517}$ Equation 2-155

Table 3-14: Referenced correlations compared with experimental results

3.5 Conclusions

The following conclusions can be drawn from these experiments:

- In single-phase (water) flows, the *helical pipe* has a higher head loss than the straight pipe. This is because the fluid flow in the *helical pipe* experiences a centrifugal force which causes a swirling motion of the fluid.

- Single-phase fluid flow in pipes in the horizontal position has a higher pressure loss than pipes in vertical position under similar conditions of pressure, temperature, flow rates, pipe's internal diameter and length. This is because of the elasticity of the material of the pipe, the higher pressure in the pipe leads to a slight expansion which will result in an increase in the cross-sectional area of the pipe. For the same flow rate, it results in a lower velocity than the calculated velocity based on the original cross-sectional area and hence a lower pressure drop and friction factor than for the pipe in the horizontal position.

- The experimental friction factors, within experimental error, corroborate the other correlations as shown in Figure 3-10.

Chapter 4

4 50 mm internal diameter pipe experiments

4.1 Introduction

This chapter describes a series of two-phase (air and water) experiments performed using 50 mm internal diameter horizontal straight and *helical pipes*. The *helical pipe* diameter (D) was 150 mm.

The aim of the experiment was to investigate hydrodynamic characteristics of two-phase (air and water) flows in straight and *helical pipes*. Both pipes were somewhat translucent which made fluid-flow visualization possible during the experiments.

The main objective of this experimental study was to investigate the effectiveness of a *helical pipe* in destroying hydrodynamic slugs which occur in flows through horizontal straight pipes. In order to achieve the set objective, liquid holdup was measured for both pipes and a comparison was made. Liquid holdup was measured because it has a major influence on the type of (i) flow pattern that will occur in a pipeline, and (ii) the slug-catcher facilities at the processing plant. Pressure and pressure drop were also measured and the results for both pipes were also compared. Fluid flow pattern characteristics were also observed in both straight and *helical pipes.*

The experimental data from both pipes have been analysed and discussed. Analysis of these experiments provides a basis for comparing hydrodynamic flow behaviours in straight and *helical pipes.*

Figure 4-1 shows a side view of the 50 mm internal-diameter *helical pipe* used for these experiments. The *helical pipe* was made by 'wrapping' a transparent reinforced flexible pipe round a 19 mm hollow pipe. Flange adaptors were provided at both ends of the *helical pipe* to connect it to the two-phase facility.

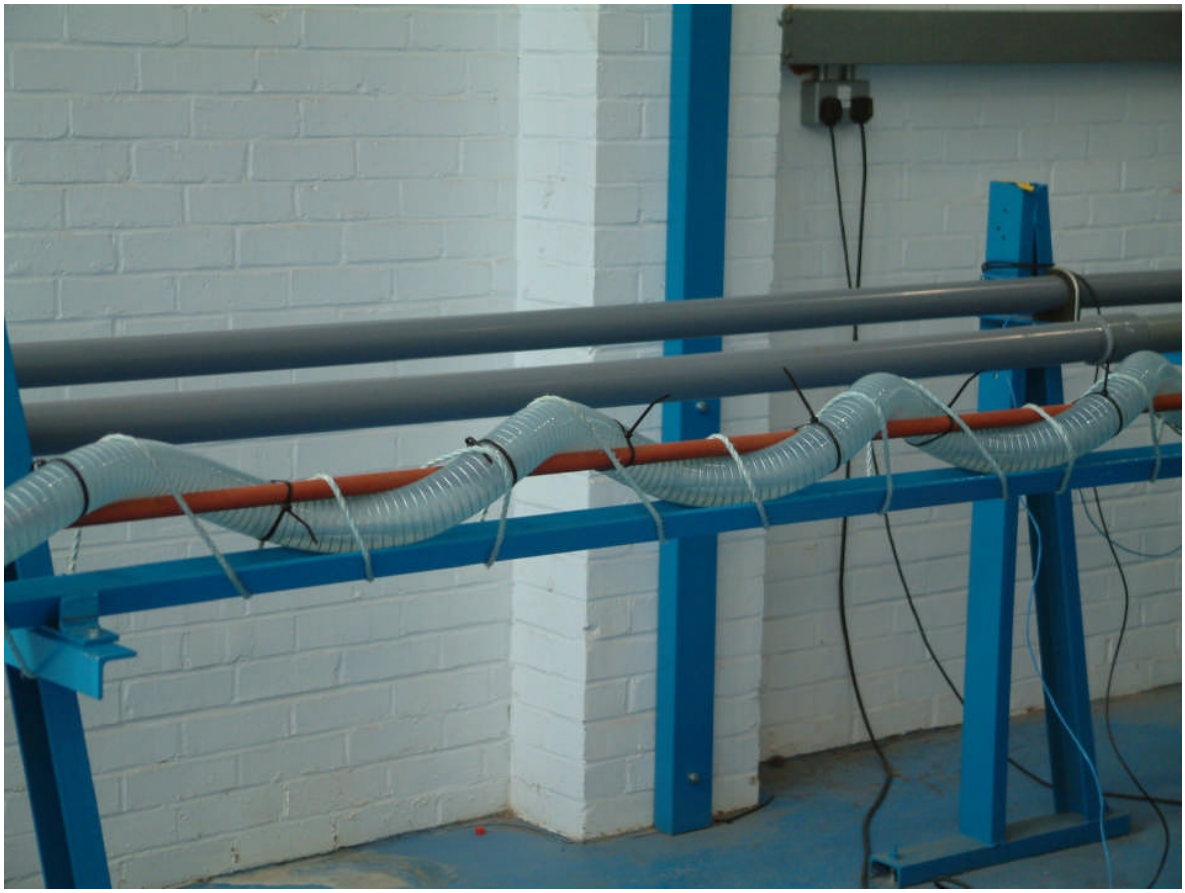

Figure 4-1: Side view of the 50 mm *helical pipe*

4.2 Experimental set-up

This section describes the basic apparatus and procedure employed for the experimental work on 50 mm internal diameter straight and *helical pipes*.

Cranfield University two-phase facility is described, with special attention given to key pieces of instrumentation, such as the pressure sensor, pressure drop sensor and conductivity probes which are discussed in detail in the

instrumentation section (4.2.3). In particular, the design and calibration process of the conductivity probes are discussed in section 4.2.3.2. Section 4.2.4 discuses the data acquisition system (DAS) that was used to collect data from the two-phase rig.

4.2.1 Two-phase facility

The Cranfield University's two-phase (air and water) facility was used to carry out this research. Figure 4-2 shows test-section of the two-phase test facility. *Helical pipe* test section and conductivity probes' positions on the installation are also shown. The two-phase (air and water) rig was built and located in the Multiphase laboratory of the Department of Process and System Engineering. A P & I diagram of the two-phase rig is shown in Appendix A with dimensions. It comprises the liquid supply, gas supply and test section.

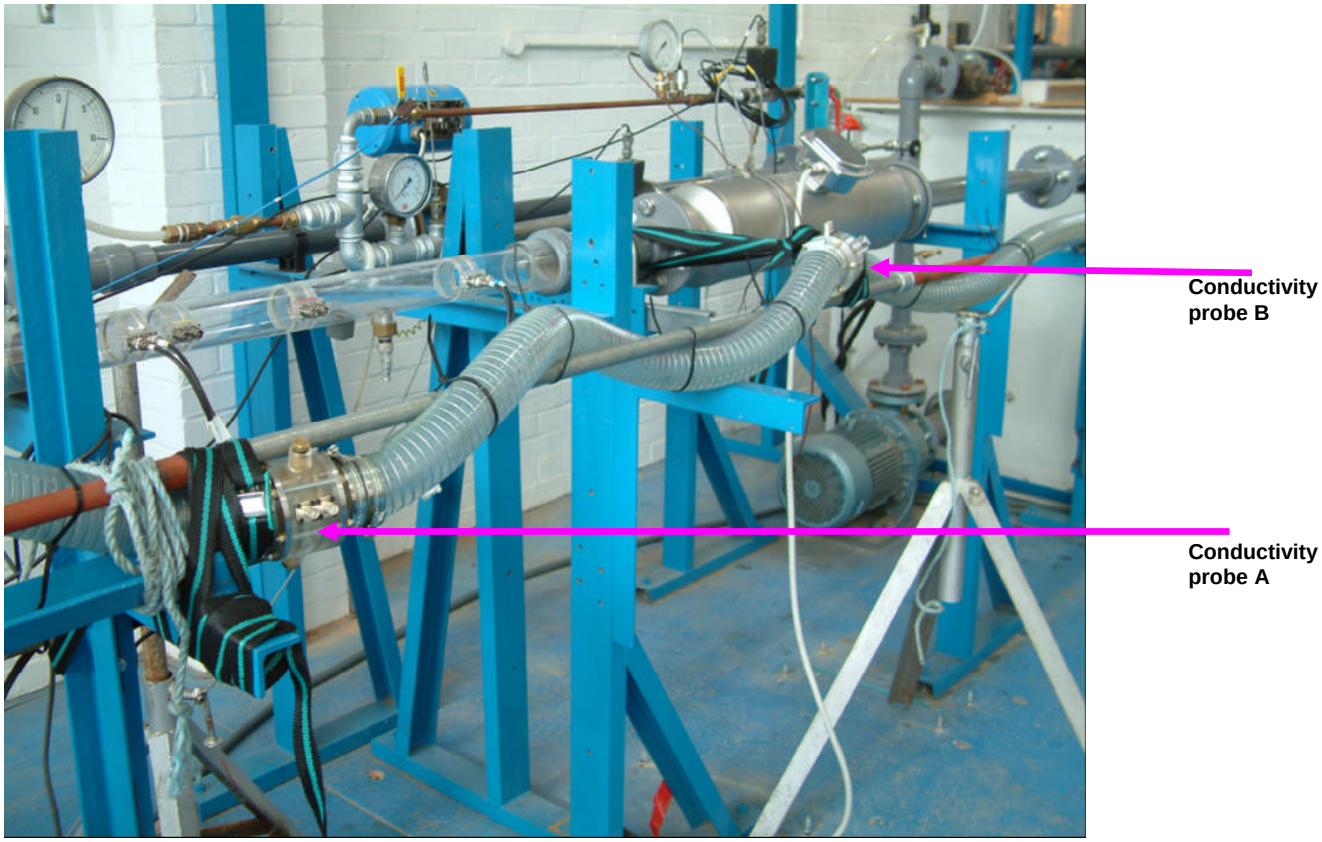

Figure 4-2: Two-Phase Facility Diagram showing test section

As shown in Figure 4-2, the inlet section was identical for both the straight and *helical pipes* experiments. The temperature of the water was between 20^{O} and 22^{O} Centigrade through out all the experiments. Since the research investigations described in this thesis involved a series of experiments over many months, great care was taken to minimise the changes between each series of experiments. In particular, a special effort was made to check each piece of instrumentation before any runs were started and where necessary, a new calibration was performed on the sensors. In this way, any measurement errors of each instrument were reduced.

4.2.2 Fluid supply system

The fluid supply system comprises liquid supply and gas supply lines. Each of the lines is described below.

4.2.2.1 Liquid-supply line

Water was stored in a tank of capacity 4.408 m^3 - see Figure 4-3. A Worthington Simpson centrifugal water-pump, of maximum capability, 40 m^3/hr and a maximum discharge pressure of 5 bar(g) was installed to pump water from the tank to the test section of the rig. A by-pass line was used to control the water flow from the pump; with the water outlet being directed back to the water tank via a valve. A Khrone Altoflux Series electromagnetic K280/0 AS model meter with $0 \rightarrow 4.524$ m^3/hr range was used to measure the water flow. The water from the pump flows to the mixing point, where it is combined with the gas and the mixture flowed to the test section. Water in the tank was regularly replaced, so that fresh water could be used during each experimental campaign. The water tank was regularly drained; the tank was also washed and filled with fresh water

Figure 4-3: Water-supply tank

4.2.2.2 Air supply line

Air was supplied from a compressor (Figure 4-4), which has a maximum supply capability of 400 m^3/hr Free Air Delivery and a maximum discharge-pressure of 10 bar(g). The air was passed to a 2.5 m^3 compressed air tank from the compressor outlet. Air from the receiver flowed to the gas metering system via a needle valve. The needle valve controlled the flow of air to the metering system, thus facilitating the maintenance of a constant mass flow for a given receiver pressure. It also stabilised the flow entering the test section. From the air metering system, the air passed to the mixing point, where it mixed with the water flow before entering the test section. In order to enhance the initial stratification of the two-phase flow mixtures, air was fed perpendicularly into the top of the pipeline.

The air metering system loop consists of a pressure regulator unit, instrument loading pressure and control valve, air filter and mass flow controller Bronkhorst

Hi-Tech Mass Flowmeter with a 0 →100 l/min range. Flow of the air was metered using a pair of Quadrina gas turbine flowmeters. There were two air flow lines (one for the low flows and the second for high flows).

Figure 4-4: Air-supply lines

4.2.2.3 Experimental method and test section

The procedure adopted for this experimental work was to select a fixed value of the liquid's superficial velocity and gradually increasing in incremental steps the air's superficial velocity. The fluid flow was fully developed before entering the test section. The flow patterns changed from one flow regime to another by increasing the air flow rate. The flow regime map (see Figure 2-10) for two-phase flow of the air-water mixture in the 2" pipeline proposed by Mandhane et al. (1974) was used to select values of the liquid and air superficial velocities used in this experimental study. An experimental matrix of flow conditions was

therefore compiled to cover a wide range of flow patterns for air–water mixture flows in the 50 mm internal-diameter horizontal pipe. Also in this study, the range of liquid superficial velocities was between 0.15 ms^{-1} and 3.02 ms^{-1} and air superficial velocities was between 0.15 ms^{-1} and 2.59 ms^{-1}.

The test section was made of a 50 mm internal-diameter semi-transparent pipeline. The pipeline was installed in horizontal (inclined at zero degree) position. The pipeline was attached to a horizontally hinged angle iron to prevent vibration of the pipeline particularly during experiments involving high gas and high liquid flows. The pipeline length was long enough (i) to allow the fluid flow to be fully developed and (ii) for stabilisation of the flow to occur before it entered the test section where various measurements were taken. The test section consisted of two pairs of flush-mounted ring electrodes. From the test section, water flowed back to the tank, while the associated air was discharged into the atmosphere.

4.2.3 Instrumentation

This section describes the basic apparatus and procedure employed. Both the pressure transducer and the conductivity probes are described in detail in this section. Table 4-1 also contains details of all the sensors used for this experimental study. The pressure and pressure drop were measured by pressure transducers with an accuracy of ±2% of full scale. The accuracy of the conductivity probes was also estimated as ± 2% of full scale.

4.2.3.1 Pressure transducer

Principally, there are two different ways of measuring pressure difference between two locations in a flow, i.e. is either by using two separate absolute pressure transducers connected to the system and recording the difference between their simultaneous readings or by using a device which can directly measure the pressure difference. Mechanical and electronic devices are used

for measuring pressure differences. Mechanical devices are inclined manometers and micro-manometers. They can measure small pressure differences accurately (down to fractions of 1 mm water). Their disadvantage is that the readings cannot be recorded on-line on a data acquisition system. Electronic devices, known as differential-pressure (DP) cells give their indications almost instantaneously (100Hz) and they can be connected online to a data acquisition system. DP cells are more suitable for time-dependent flows than mechanical devices. When absolute pressure transducers are used, two transducers can be connected directly to the two pressure tappings between which the pressure drop has to be measured. But, with this arrangement, the accuracy of the pressure difference is determined by the accuracy of the transducers, which usually in the best case is about 0.1% of their full range.

The pressure transducers used for this experimental study, were connected to the top of the pipeline. This arrangement was preferred because if the pressure transducer was connected to the bottom of the pipe, the static head of the liquid on the DP cell at the pipe bottom would have affected the pressure readings significantly in the range of pressure differences reported in this investigation. The pressure transducers were also calibrated prior to installing them on the pipeline. Linear plots were achieved from the calibration exercise for both the pressure transducer used to measure pressure drop and the gas line pressure transducer. The calibration plots are shown in Figures 4-5 and 4-6. From the regression (Equation 4-1) of the plot, Zero and gain values were evaluated from the calibration equations 4-1 and 4-2 and they were reflected on the labview as shown in Table 4-2.

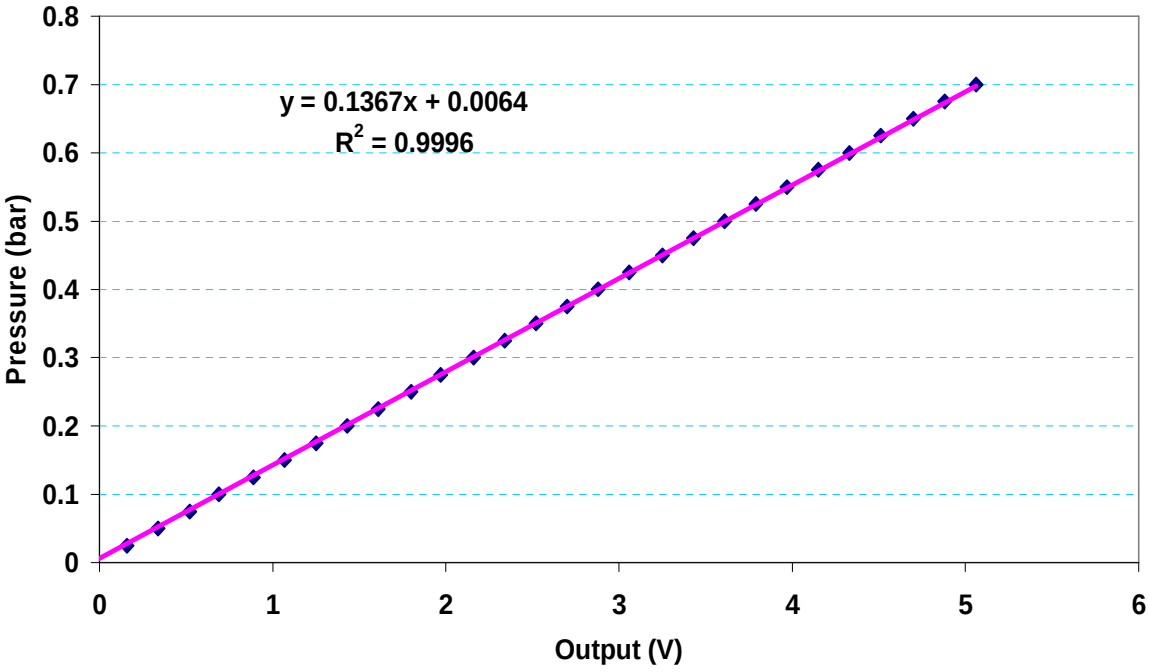

Figure 4-5: Pressure drop transducer calibration plot

$$y = 0.1367\,x + 0.0064 \qquad \textbf{Equation 4-1}$$

The pressure transducer used for the gas line was also calibrated - see Figure 4-6. Zero and gain were also evaluated from the resultant regression equation (Equation 4-2) and were reflected on the Labview (Table 4-2).

$$y = 1.3323\,x - 0.0155 \qquad \textbf{Equation 4-2}$$

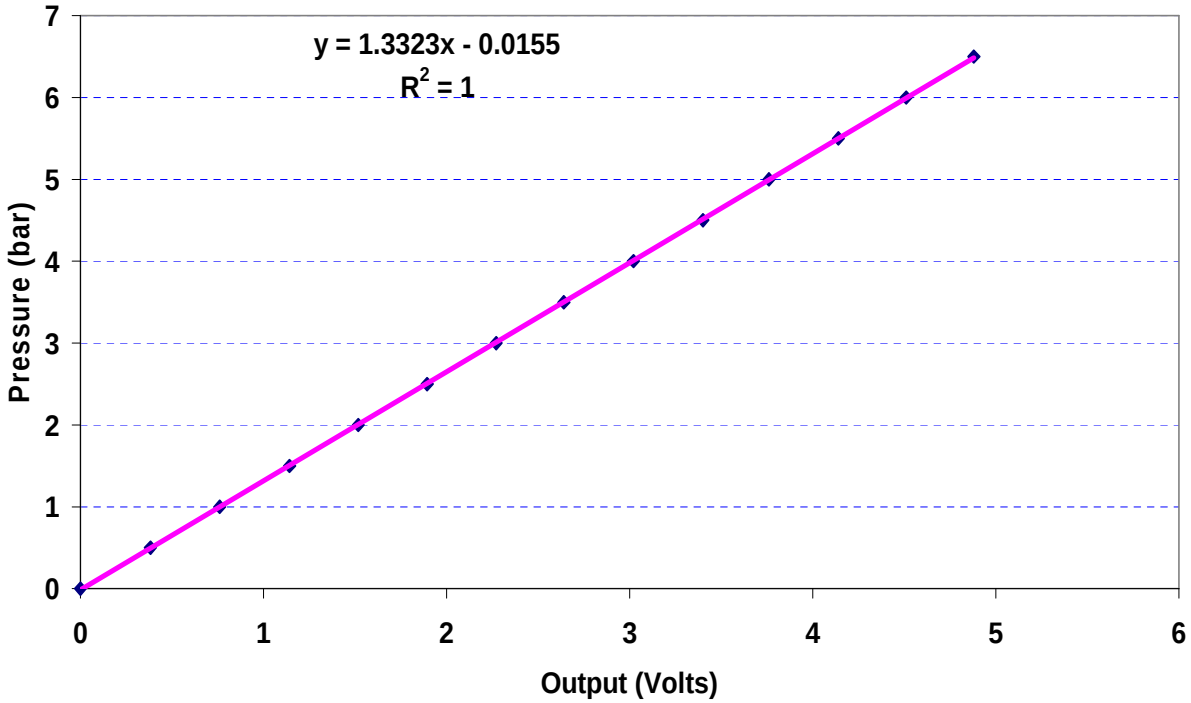

Figure 4-6: Gas-line pressure transducer calibration plot

Specifications of the instrumentation used for this experimental work are summarised in Table 4-1.

Sensor Designation	Sensor Description	Sensor Details	Range	Instrument Uncertainty
FL	Water Inlet Flowmeter (Reference meter)	Khrone Altoflux Elecotromagnetic Flowmeter Model K280/0 AS	0-4.524 m^3/hr	±1% of full scale
FG_L	Inlet Air Flowmeter (Low Flow)	Quadrina Turbine Meter, Model QFG/13B/EP1	1-8 m^3/hr	±1% of full scale
FG_H	Inlet Air Flowmeter (High Flow)	Quadrina Turbine Meter, Model QFG/25B/EP1	6-60 m^3/hr	±1% of full scale
P_L	FGL Reference Pressure Sensor	Pressure Gauge Transducer RS 286-671	0-5 bar(g)	±2% of full scale
P_H	FGH Reference Pressure Sensor	Pressure Gauge Transducer RS 286-671	0-5 bar(g)	±2% of full scale
P_{DP}	In-Line Pressure Drop Sensor	Gauge Style PMP 4110	0.7-7 bar(g)	±2% of full scale
P_M	In-Line Pressure Sensor	Gauge Style RS 286-671	0-5 bar(g)	±2% of full scale
T_1	FG1 Reference Temperature Sensor	RS Thermocouple	0-100 ^{o}C	±1% of full scale
T_2	FG2 Reference Temperature Sensor	RS Thermocouple	0-100 ^{o}C	±1% of full scale

Table 4-1: Two-Phase Facility Instrumentation

4.2.3.2 Conductance "O"-ring spool piece sensors

According to Miya (1970); Brown et al. (1978); Davies (1992); Strand (1993), Srichai (1994), Manolis (1995), a conductivity probe is a convenient way for measuring liquid holdup in two-phase flow of gas-liquid mixtures provided that the liquid electrical conductivity is sufficiently high. Ring electrodes were first employed by Asali et al. (1985) while Andreussi et al. (1988) and Tsochtzidis et al. (1992) developed the theoretical bases regarding the response of this electrode configuration. Other studies have been conducted by Brown et al. (1978), Karapantios et al. (1989) and Koskie et al. (1989) concerning the use and calibration of parallel wire probes for liquid film thickness measurements. Kang and Kim (1992) compared both theoretically and experimentally, the performance of flush mounted electrodes and wire electrodes in order to determine the spatial resolution of the probe when immersed in a wavy liquid film. Fossa (1998) has also reported that capacitance probes allow the evaluation of two-phase properties, even when exposed to non-conducting media, but that they usually need particular care during the calibration. Details about this technique and more references can be found in Hewitt (1978). Impedance probes can easily be used in large-scale experiments and in industrial applications such as continuous monitoring of the liquid holdup in a gas-liquid pipeline. This technique is based on the measurement of the electrical Impedance between two or more electrodes mounted on a specially-designed section of the pipe.

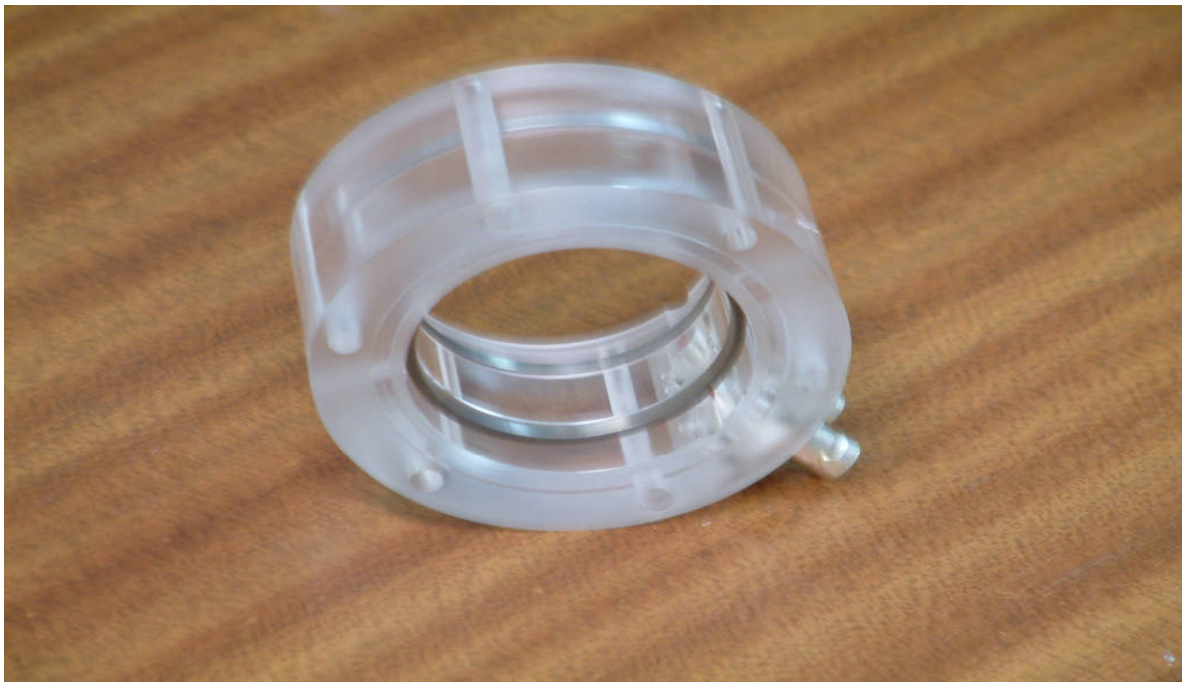

Figure 4-7: Side view of conductivity probe

In this work, a non-intrusive conductivity probes made of two ring electrodes mounted flush to the pipe wall, were applied to measure the mean liquid holdup under different flow-conditions. Figures 4-7 and 4-8 show a side view and end views of the probe respectively. Two sets of ring probes were used for this research. One (conductivity A, $\mathbf{C_A}$) was installed at the dip of the *helical pipe* while the second (conductivity B, $\mathbf{C_B}$) was installed at the top of the curvature of the pipe (Figure 4-2). Appendix D shows details of the conductivity-probe design. The probes comprise two stainless-steel ring electrodes, with a width of 4 mm, and they are spaced 18 mm apart.

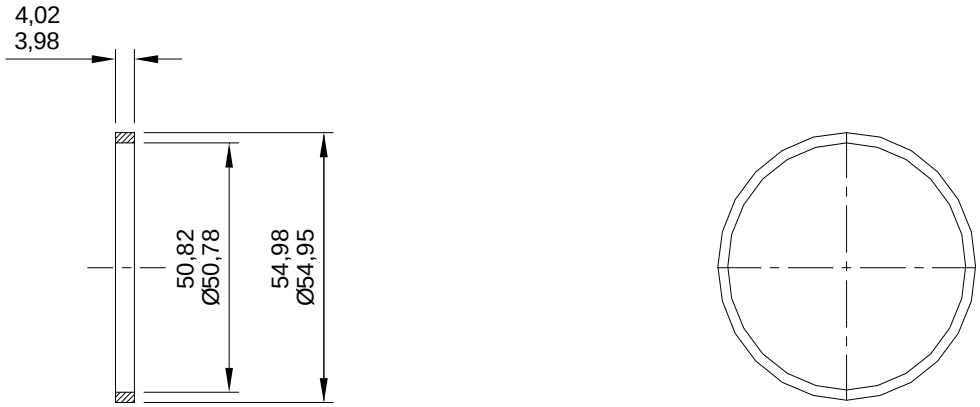

Figure 4-8: Conductivity electrode end views

(All measurements are in millimeters)

Each of the two conductivity probes was calibrated separately. The calibration exercise was carried out by connecting each probe to a conductivity electronic conditioning box.

In calibrating the conductivity probes, tap water was used as the liquid medium to fill the pipe. The pipe in which the probes were flushed mounted was carefully placed in a horizontal position, while great care was taken to check the inclination of the pipe for each measurement. In order to cover the liquid fraction range of 0 to 1, 44 measurements were made for conductivity probe $\mathbf{C_A}$ while 57 measurements were made for conductivity probe $\mathbf{C_B}$. The weight of the water excluding the weight of the conductivity ring and the corresponding value in volt were recorded. The conductance output of the probes in volts vis-à-vis the liquid holdup was normalised. As shown in Figures 4-9 and 4-10, a polynomial calibration curve for each conductivity probe was used at the end of the calibration exercise. From Figures 4-9 and 4-10, the liquid holdup regression equations as a function of the normalised output conductance for the two conductivity probes ($\mathbf{C_A}$ and $\mathbf{C_B}$) can be written as:

$$y = -0.9374x^4 + 0.7075x^3 + 0.8603x^2 + 0.3622x - 0.0006 \qquad \textbf{Equation 4-3}$$

$$y = -1.3456x^4 + 1.8808x^3 - 0.1494x^2 + 0.6238x - 0.0088$$ **Equation 4-4**

In both Equations 4-3 and 4-4, x = **V*.**

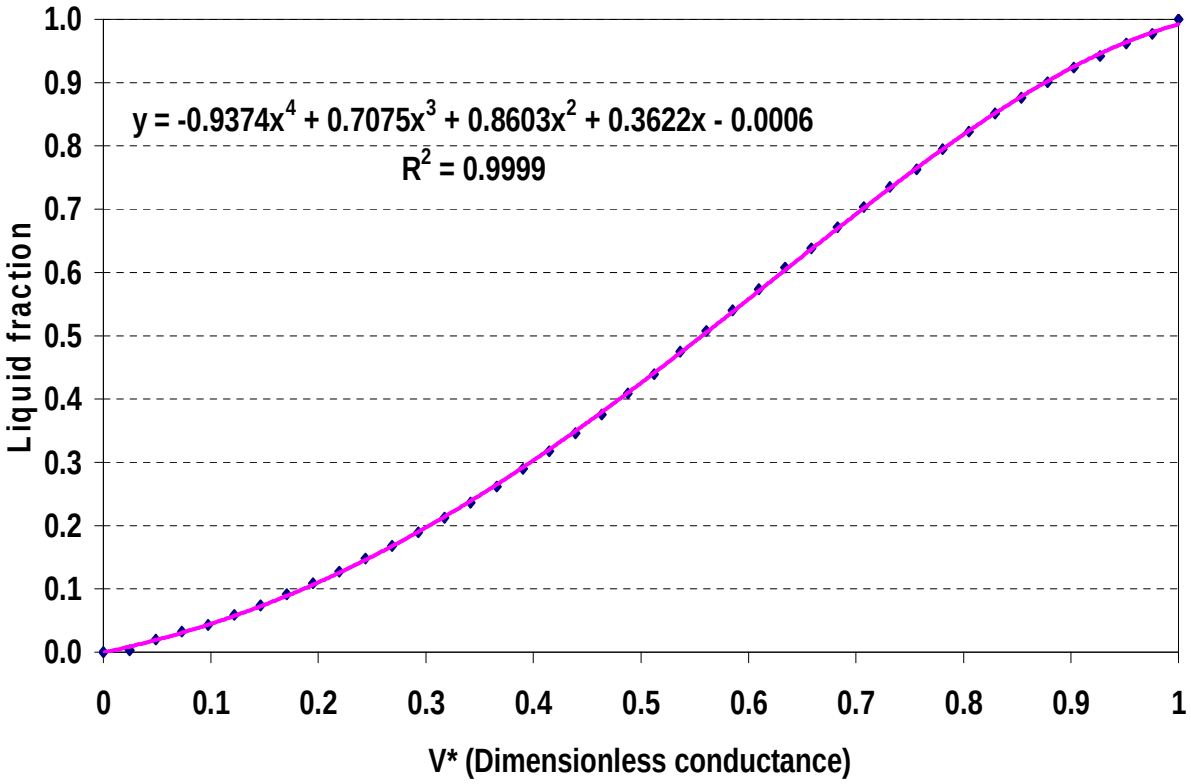

Figure 4-9: Calibration curve for conductivity probe CA

Figure 4-11 shows comparison of calibration curves for both probes $\mathbf{C_A}$ and $\mathbf{C_B}$. The relationship between the liquid holdup and the dimensionless conductance (**V***) plotted in both Figures 4-9 and 4-10 shows that liquid holdup increases as the conductivity probe values increase. This can be interpreted that the more the liquid the more the probes conduct.

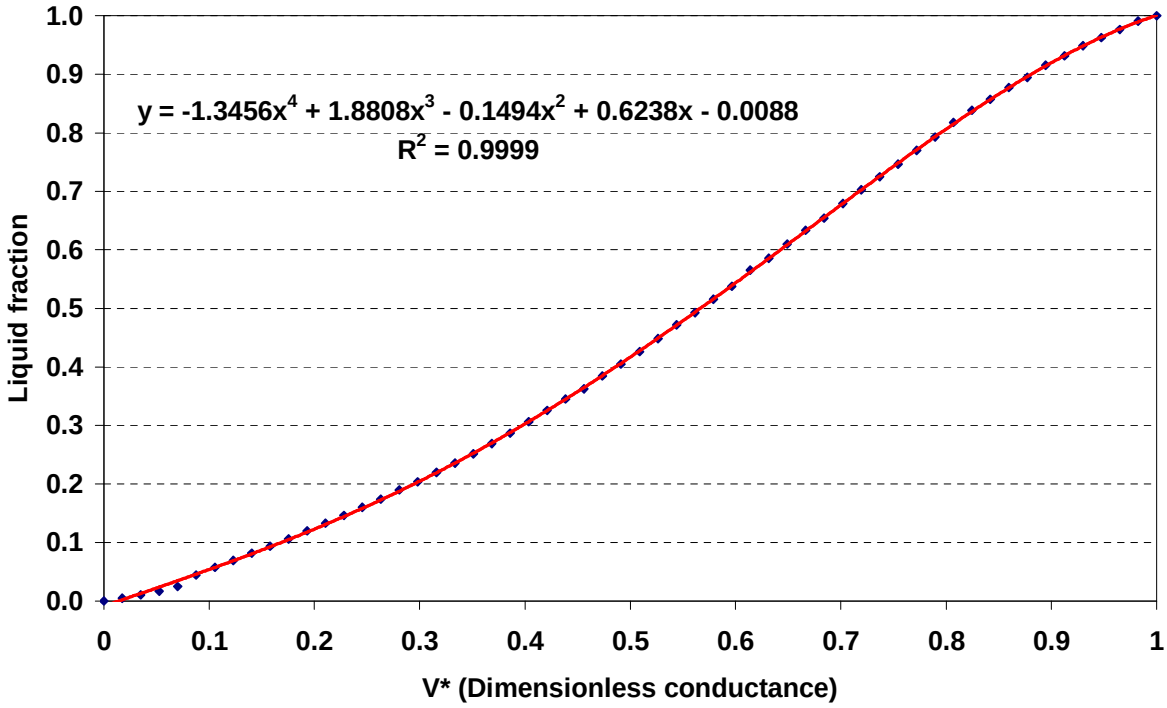

Figure 4-10: Calibration curve for conductivity probe CB

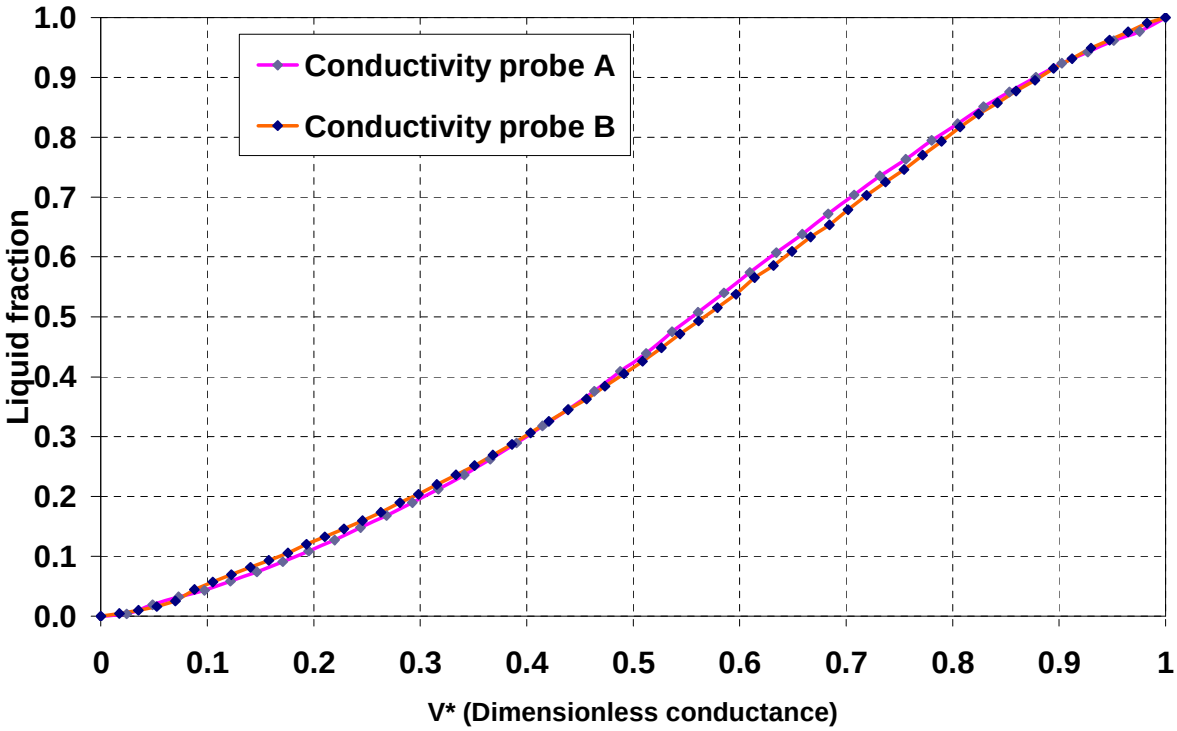

Figure 4-11: Calibration curves for conductivity probes C_A and C_B

Characteristics of the conductivity probes signal traces during some flow patterns are presented in section 4.3.4.

4.2.4 Data-acquisition system

Data from the two–phase (air-water) facility were acquired by a dedicated Personal Computer (PC) – based Data Acquisition System (DAS). The data acquisition system is shown in Figure 4-12

Figure 4-12: Two-phase facility Data-Acquisition *S*ystem (DAS)

The DAS hardware consisted of a series of custom-built Signal Conditioning units. Data were collected over a set of 12 channels; with a range of 0 to 10 V d.c. The incoming data were converted to appropriate digital signals and then transferred to the PC via the parallel port multiplexer (SCB-68).

A PC system (100 MHz Dell PC) with 10 GB (AMD Athlon) hard disk, running the Windows 2000 operating system was used to receive data from the

(SCB-68). A runtime version of Labview 'Virtual Instrument' was then used to gather data in real time from the DAS hardware and display the results on the computer screen for control purposes.

The DAS software took information from the raw voltage entering the computer from the DAS hardware and converted the information to engineering units for the corresponding instruments. The following equation was used in order to do this:

$$EU = K(V - V_0) \qquad \textbf{Equation 4-5}$$

where

EU is the required engineering unit

K is the gain

V is the voltage signal

V_0 is the voltage at the zero signal reading (where the measured variable is zero). This is usually referred to as the 'zero' or 'offset'. The required gains and zeros for each channel were held in a table and a text file that was accessed by the DAS software during execution. The Data-Acquisition System (DAS) is shown in Table 4-2.

Signal	Signal name	Zero	Gain	Units	Channel
FL	Water flow	0.5	6.27	l/s	1
FG_L	Air flow (low line)	0	26.88	l/min	2
FG_H	Air flow (high line)	0	60	l/min	3
P_L	Air pressure (low line)	-0.001	0.679	bar	4
P_H	Air pressure (high line)	0.012	1.332	bar	5
P_M	Mixture pressure	0.003	0.863	bar	6
DP	Pressure drop	-0.047	137	mbar	7
T_{Gi}	Air-inlet temperature	0	9.98	^{o}C	8
T_M	Mixture temperature	0	10.1	^{o}C	9
C_A	Conductivity probe A	0	1	V	11
C_B	Conductivity probe B	0	1	V	12

Table 4-2: Data-Acquisition *S*ystem Table

4.3 Experimental-data processing and analysis

Processing and analyses of the experimental data for both straight and *helical pipes* are discussed as follows. All data from the two-phase facility instrumentation were recorded by the Data-Acquisition System (already discussed in Section 4.2.4). At the gas-metering point, temperature and pressure were measured to calculate the volumetric flowrate of the gas in the test section. In line with the set objective of this study, the parameters measured include pressure, pressure drop and liquid holdup for both straight and *helical pipes*.

4.3.1 Pressure drop characteristics

Pressure drop was chosen to be investigated because it forms one of the key parameters for the design of pipelines. However, it was observed in the course of this research that pressure drop measurements are difficult due to the inherent variable nature of the two-phase flow. Brill & Beggs (1991) stated that the only method of evaluating various pressure gradient prediction methods is comparison of predicted pressure gradients with those actually measured.

Tables 4-3 to Tables 4-18 show the various combinations of air and water investigated. The values for pressure drop and liquid holdup are the experimental values downloaded through the DAS from the pressure drop sensor and conductivity probes respectively. However, liquid holdup values are time-averaged mean-values from the two conductivity probes. Details of the individual conductivity-probe traces are presented in 4.3.4. Figures 4-13 to 4-20 show the effects of increasing gas superficial velocity on the pressure drop while the effect of pressure drop on liquid holdup is shown on Figures 4-29 to 4-36.

Test	Liquid's superficial velocity, V_{SL} (ms^{-1})	Air's superficial velocity, V_{SG} (ms^{-1})	Observed flow regime	Pressure drop, DP (mbar)	Liquid holdup, H_L
1	0.15	0.60	Intermittent bubbly	3.43	0.29
2		1.0	Intermittent bubbly	3.81	0.24
3		1.59	Bubbly	4.19	0.21
4		2.01	Bubbly	4.42	0.19

Table 4-3: Observations for the straight pipe (V_{SL} = 0.15 ms^{-1})

Test	Liquid's superficial velocity, V_{SL} (ms^{-1})	Air's superficial velocity, V_{SG} (ms^{-1})	Observed flow regime	Pressure drop, DP (mbar)	Liquid holdup, H_L
1	0.15	0.63	Bubbly	27.86	0.25
2		1.04	Bubbly	28.71	0.21
3		1.57	Bubbly	29.24	0.19
4		2.03	Bubbly	29.29	0.18

Table 4-4: Observations for the *helical pipe* (V_{SL} = 0.15 ms^{-1})

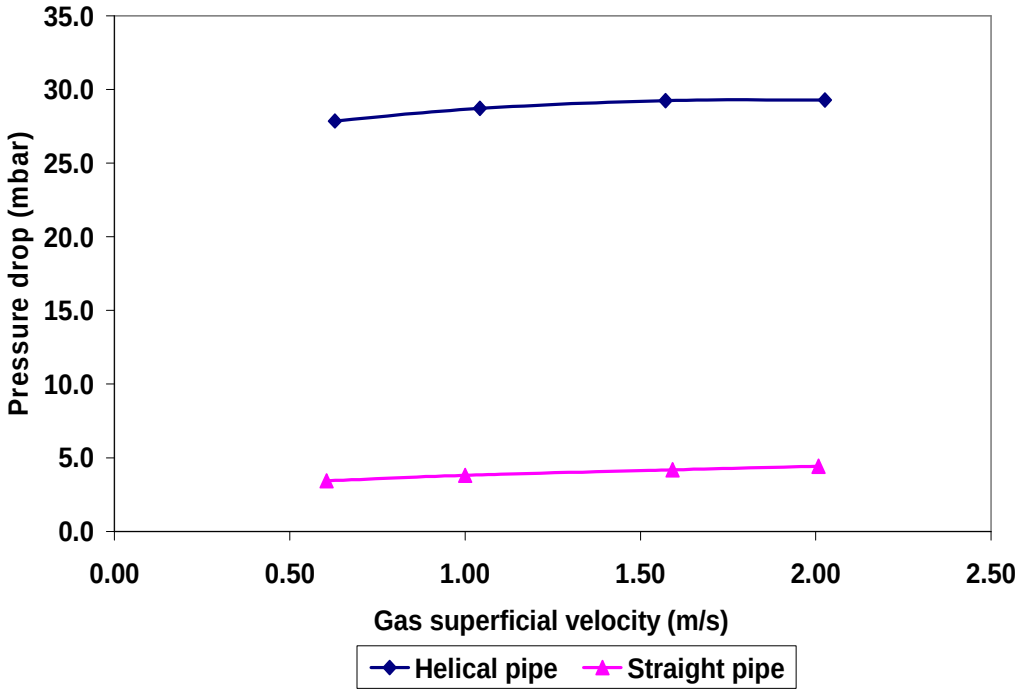

Figure 4-13: Pressure drop versus gas superficial velocity
(V_{SL} = 0.15 ms^{-1}, V_{SG} = 0.63 → 2.03 ms^{-1})

Test	Liquid's superficial velocity, V_{SL} (ms^{-1})	Air's superficial velocity, V_{SG} (ms^{-1})	Observed flow regime	Pressure drop, DP (mbar)	Liquid holdup, H_L
1	0.30	0.16	Growing slug	2.29	0.50
2		0.30	Growing slug	2.72	0.41
3		0.61	Growing slug	3.09	0.34
4		1.02	Bubbly	3.56	0.32
5		1.51	Bubbly	4.75	0.30
6		2.04	Bubbly	5.79	0.25
7		2.47	Bubbly	6.78	0.24

Table 4-5: Observations for the straight pipe (V_{SL} = 0.30 ms^{-1})

Test	Liquid's superficial velocity, V_{SL} (ms^{-1})	Air's superficial velocity, V_{SG} (ms^{-1})	Observed flow regime	Pressure drop, DP (mbar)	Liquid holdup, H_L
1	0.30	0.15	Bubbly	26.54	0.44
2		0.31	Bubbly	28.77	0.38
3		0.61	Bubbly	30.16	0.32
4		1.04	Bubbly	32.05	0.29
5		1.53	Bubbly	33.52	0.26
6		2.08	Bubbly	34.71	0.25
7		2.56	Bubbly	35.98	0.23

Table 4-6: Observations for the *helical pipe* (V_{SL} = 0.30 ms^{-1})

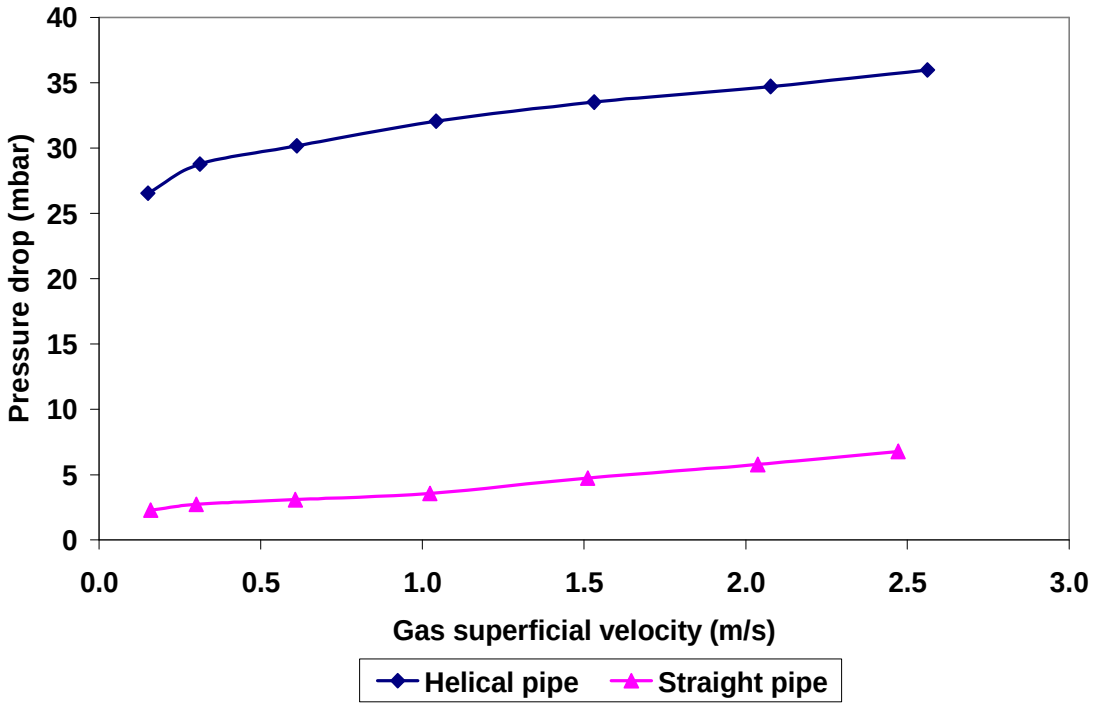

Figure 4-14: Pressure drop versus gas superficial velocity

(V_{SL} = 0.30 ms^{-1}, V_{SG} = 0.15 → 2.56 ms^{-1})

Test	Liquid's superficial velocity, V_{SL} (ms^{-1})	Air's superficial velocity, V_{SG} (ms^{-1})	Observed flow regime	Pressure drop, DP (mbar)	Liquid holdup, H_L
1	0.50	0.03	Slug	4.69	0.69
2		0.15	Slug	5.77	0.53
3		0.30	Slug	6.57	0.46
4		0.60	Slug	7.25	0.41
5		1.02	Growing slug	9.27	0.34
6		1.51	Dispersed bubbly	12.46	0.30
7		1.98	Dispersed bubbly	16.28	0.29
8		2.59	Dispersed bubbly	18.66	0.27

Table 4-7: Observations for the straight pipe (V_{SL} = 0.50 ms^{-1})

Test	Liquid's superficial velocity, V_{SL} (ms^{-1})	Air's superficial velocity, V_{SG} (ms^{-1})	Observed flow regime	Pressure drop, DP (mbar)	Liquid holdup, H_L
1	0.50	0.03	Bubbly	37.41	0.53
2		0.16	Bubbly	39.90	0.50
3		0.31	Bubbly	40.51	0.45
4		0.63	Bubbly	42.59	0.42
5		1.03	Bubbly	46.67	0.39
6		1.55	Bubbly	50.55	0.34
7		2.01	Bubbly	53.24	0.32
8		2.53	Bubbly	57.17	0.30

Table 4-8: Observations for the *helical pipe* (V_{SL} = 0.50 ms^{-1})

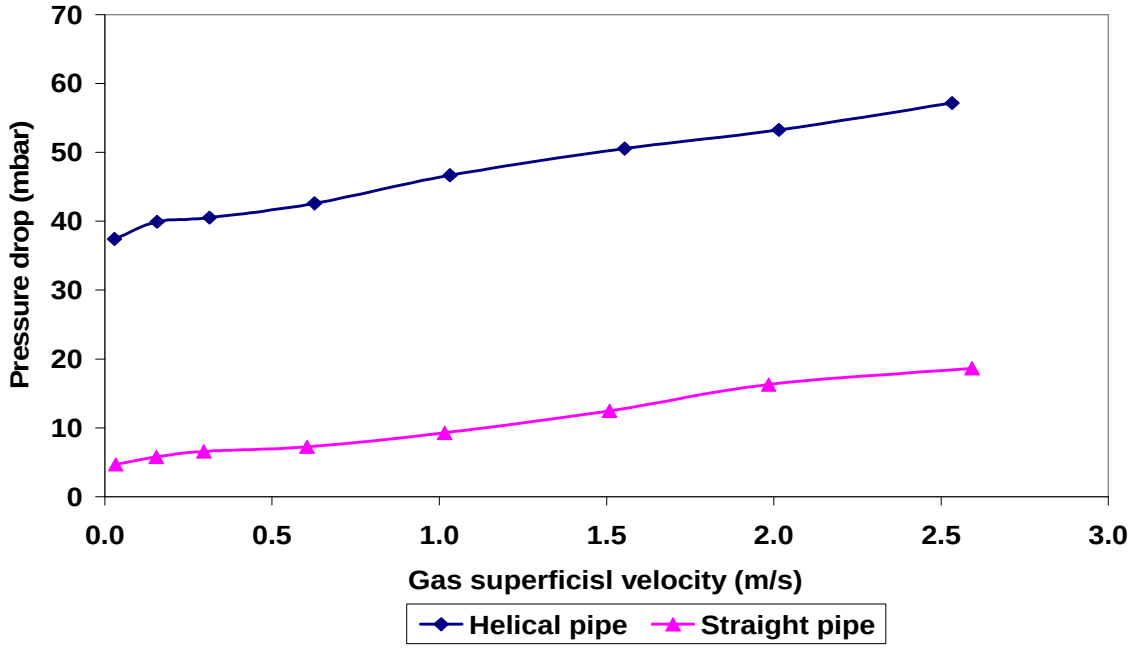

Figure 4-15: Pressure drop versus gas superficial velocity (V_{SL} = 0.50 ms^{-1}, V_{SG} = 0.03 → 2.59 ms^{-1})

Test	Liquid's superficial velocity, V_{SL} (ms^{-1})	Air's superficial velocity, V_{SG} (ms^{-1})	Observed flow regime	Pressure drop, DP (mbar)	Liquid holdup, H_L
1	1.0 → 1.01	0.04	Slug	9.73	0.76
2		0.15	Slug	11.30	0.66
3		0.31	Slug	13.06	0.56
4		0.60	Slug	17.44	0.48
5		1.03	Growing slug	24.98	0.43
6		1.48	Growing slug	32.28	0.38
7		2.0	Growing slug	37.95	0.33
8		2.48	Dispersed bubbly	45.39	0.28

Table 4-9: Observations for the straight pipe (V_{SL} = 1.0 → 1.02 ms^{-1})

Test	Liquid's superficial velocity, V_{SL} (ms^{-1})	Air's superficial velocity, V_{SG} (ms^{-1})	Observed flow regime	Pressure drop, DP (mbar)	Liquid holdup, H_L
1	1.0 → 1.02	0.04	Bubbly	32.80	0.77
2		0.16	Bubbly	36.22	0.73
3		0.31	Bubbly	38.74	0.67
4		0.62	Bubbly	44.92	0.59
5		1.05	Bubbly	52.72	0.54
6		1.56	Bubbly	66.15	0.49
7		2.09	Dispersed bubbly	71.23	0.45
8		2.56	Dispersed bubbly	81.63	0.41

Table 4-10: Observations for the *helical pipe* (V_{SL} = 1.0 → 1.02 ms^{-1})

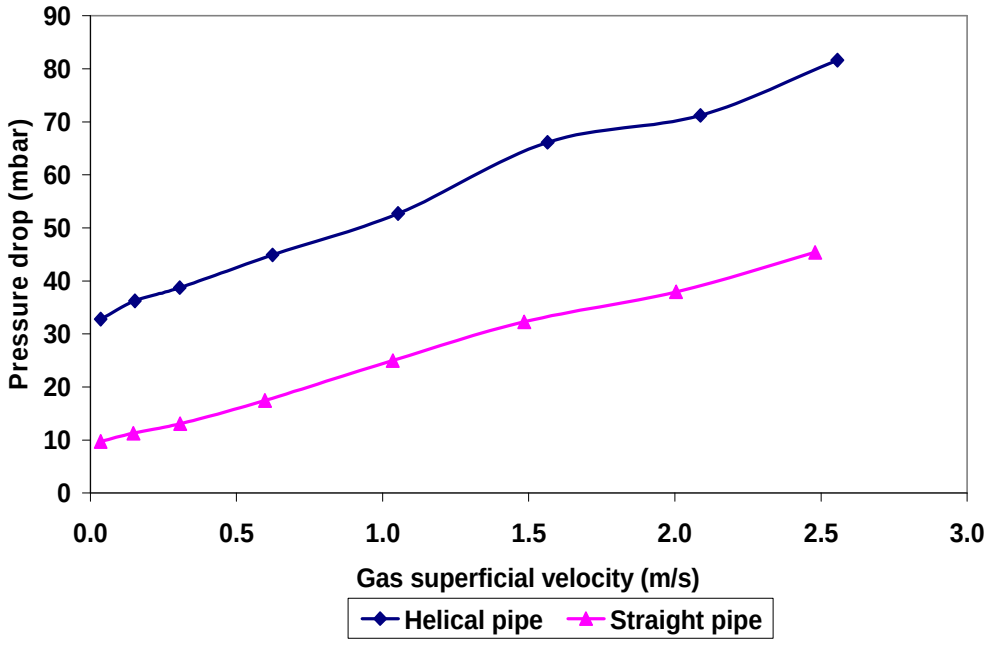

Figure 4-16: Pressure drop versus gas superficial velocity (V_{SL} = 1.0 → 1.02 ms^{-1}, V_{SG} = 0.04 → 2.56 ms^{-1})

Test	Liquid's superficial velocity, V_{SL} (ms^{-1})	Air's superficial velocity, V_{SG} (ms^{-1})	Observed flow regime	Pressure drop, DP (mbar)	Liquid holdup, H_L
1	1.49 → 1.51	0.03	Growing slug	16.02	0.84
2		0.15	Growing slug	18.75	0.73
3		0.29	Growing slug	21.35	0.66
4		0.60	Growing slug	27.60	0.56
5		1.0	Growing slug	38.88	0.48
6		1.50	Growing slug	53.89	0.41
7		2.02	Growing slug	63.86	0.37

Table 4-11: Observations for the straight pipe (V_{SL} = 1.49 → 1.53 ms^{-1})

Test	Liquid's superficial velocity, V_{SL} (ms^{-1})	Air's superficial velocity, V_{SG} (ms^{-1})	Observed flow regime	Pressure drop, DP (mbar)	Liquid holdup, H_L
1	1.50 → 1.53	0.03	Bubbly	50.69	0.89
2		0.15	Bubbly	55.22	0.82
3		0.32	Bubbly	59.04	0.76
4		0.64	Bubbly	67.18	0.67
5		1.06	Bubbly	73.35	0.61
6		1.55	Bubbly	81.95	0.56
7		2.04	Bubbly	91.89	0.53

Table 4-12: Observations for the *helical pipe* (V_{SL} = 1.49 → 1.53 ms^{-1})

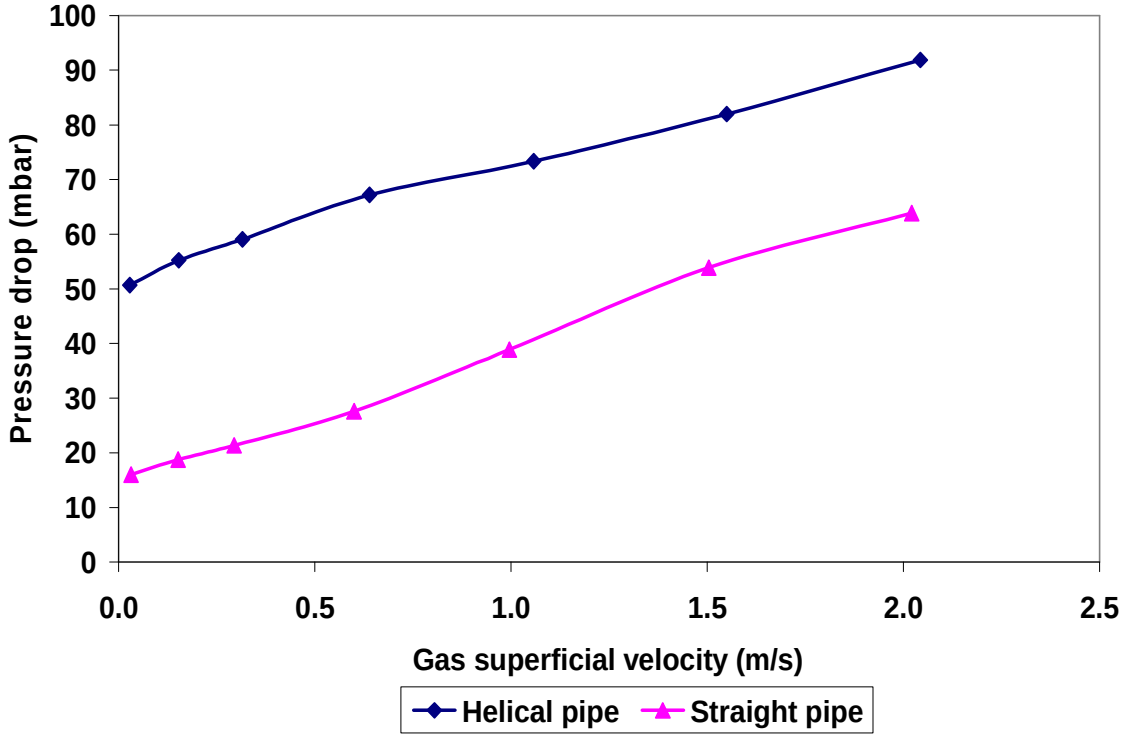

Figure 4-17: Pressure drop versus gas superficial velocity
(V_{SL} = 1.49 → 1.53 ms^{-1}, V_{SG} = 0.03 → 2.04 ms^{-1})

Test	Liquid's superficial velocity, V_{SL} (ms^{-1})	Air's superficial velocity, V_{SG} (ms^{-1})	Observed flow regime	Pressure drop, DP (mbar)	Liquid holdup, H_L
1	2.0 → 2.01	0.03	Growing slug	22.78	0.87
2		0.15	Growing slug	27.53	0.79
3		0.30	Growing slug	31.94	0.72
4		0.60	Growing slug	41.10	0.63
5		1.0	Growing slug	56.66	0.53
6		1.52	Growing slug	78.01	0.49

Table 4-13: Observations for the straight pipe (V_{SL} = 2.0 → 2.02 ms^{-1})

Test	Liquid's superficial velocity, V_{SL} (ms^{-1})	Air's superficial velocity, V_{SG} (ms^{-1})	Observed flow regime	Pressure drop, DP (mbar)	Liquid holdup, H_L
1	2.0 → 2.02	0.04	Bubbly	73.40	0.91
2		0.18	Bubbly	79.16	0.85
3		0.31	Bubbly	83.03	0.82
4		0.62	Bubbly	92.92	0.74
5		1.03	Bubbly	102.47	0.68
6		1.58	Dispersed bubbly	109.98	0.63

Table 4-14: Observations for the *helical pipe* (V_{SL} = 2.0 → 2.02 ms^{-1})

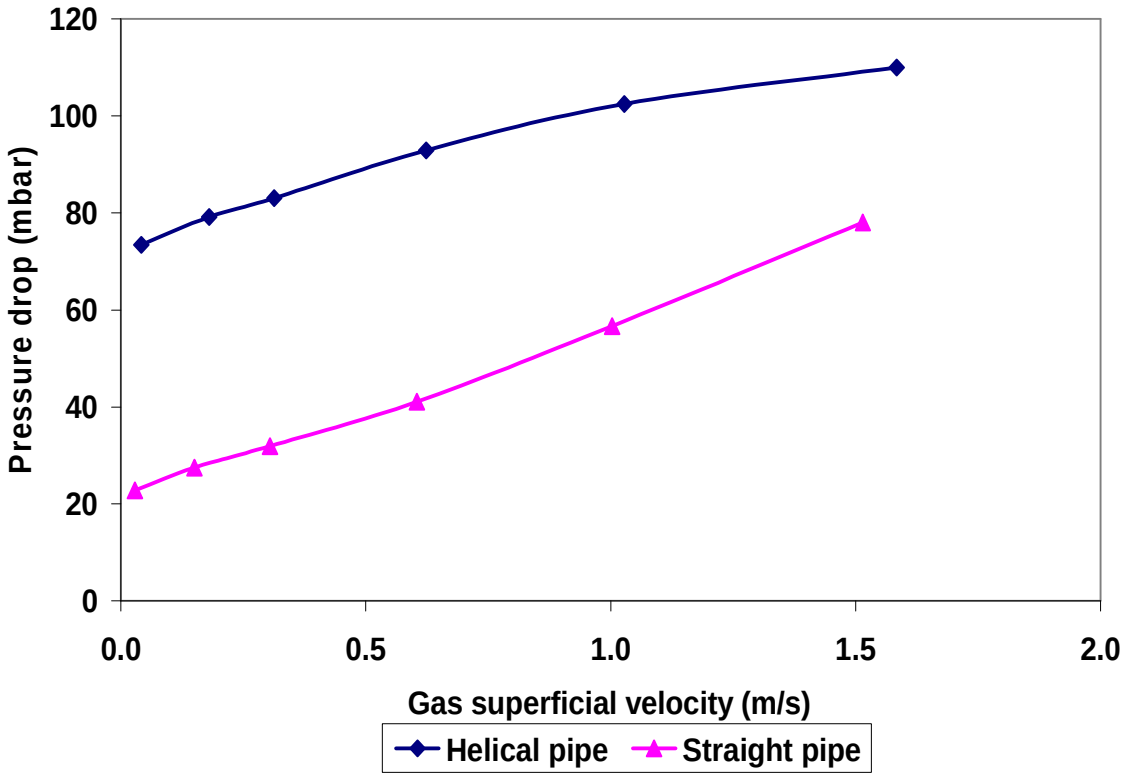

Figure 4-18: Pressure drop versus gas superficial velocity (V_{SL} = 2.0 → 2.02 ms^{-1}, V_{SG} = 0.03 → 1.58 ms^{-1})

Test	Liquid's superficial velocity, V_{SL} (ms^{-1})	Air's superficial velocity, V_{SG} (ms^{-1})	Observed flow regime	Pressure drop, DP (mbar)	Liquid holdup, H_L
1	2.50 → 2.51	0.03	Bubbly	30.65	0.90
2		0.15	Bubbly	37.43	0.81
3		0.30	Bubbly	43.55	0.76
4		0.60	Bubbly	54.45	0.68
5		1.0	Dispersed bubbly	72.37	0.63
6		1.50	Dispersed bubbly	98.37	0.48

Table 4-15: Observations for the straight pipe (V_{SL} = 2.49 → 2.52 ms^{-1})

Test	Liquid's superficial velocity, V_{SL} (ms^{-1})	Air's superficial velocity, V_{SG} (ms^{-1})	Observed flow regime	Pressure drop, DP (mbar)	Liquid holdup, H_L
1	2.49 → 2.52	0.04	Bubbly	82.69	0.94
2		0.17	Bubbly	89.90	0.90
3		0.31	Bubbly	95.32	0.88
4		0.61	Bubbly	106.56	0.84
5		1.05	Bubbly	125.22	0.77
6		1.56	Dispersed bubbly	141.68	0.74

Table 4-16: Observations for the *helical pipe* (V_{SL} = 2.49 → 2.52 ms^{-1})

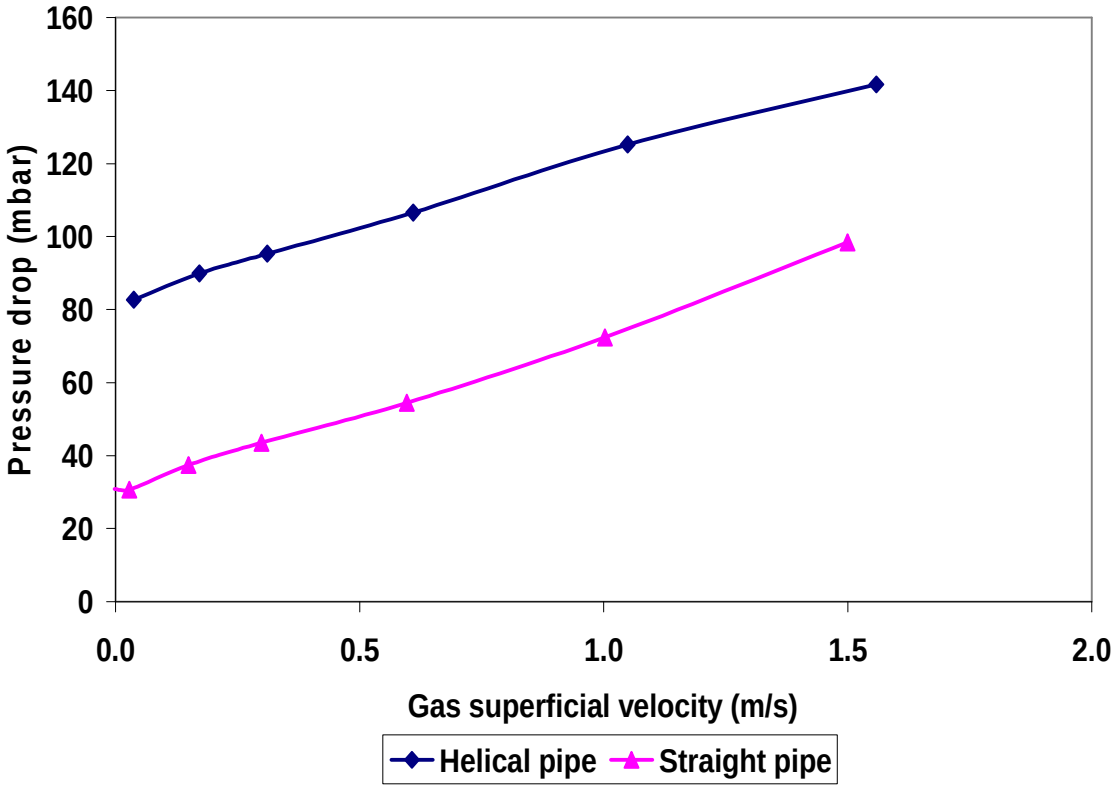

Figure 4-19: Pressure drop versus gas superficial velocity
(V_{SL} = 2.49 → 2.52 ms^{-1}, V_{SG} = 0.03 → 1.50 ms^{-1})

Test	Liquid's superficial velocity, V_{SL} (ms^{-1})	Air's superficial velocity, V_{SG} (ms^{-1})	Observed flow regime	Pressure drop, DP (mbar)	Liquid holdup, H_L
1	3.0 → 3.02	0.04	Bubbly	43.96	0.87
2		0.15	Bubbly	50.62	0.82
3		0.29	Bubbly	57.76	0.79
4		0.61	Dispersed bubbly	72.76	0.71
5		1.01	Dispersed bubbly	94.87	0.60

Table 4-17: Observations for the straight pipe (V_{SL} = 3.0 → 3.02 ms^{-1})

Test	Liquid's superficial velocity, V_{SL} (ms^{-1})	Air's superficial velocity, V_{SG} (ms^{-1})	Observed flow regime	Pressure drop, DP (mbar)	Liquid holdup, H_L
1	3.0 → 3.02	0.04	Bubbly	100.13	0.94
2		0.16	Bubbly	107.54	0.91
3		0.31	Bubbly	115.47	0.89
4		0.61	Dispersed bubbly	130.32	0.85
5		1.04	Dispersed bubbly	150.53	0.80

Table 4-18: Observations for the *helical pipe* (V_{SL} = 3.0 → 3.02 ms^{-1})

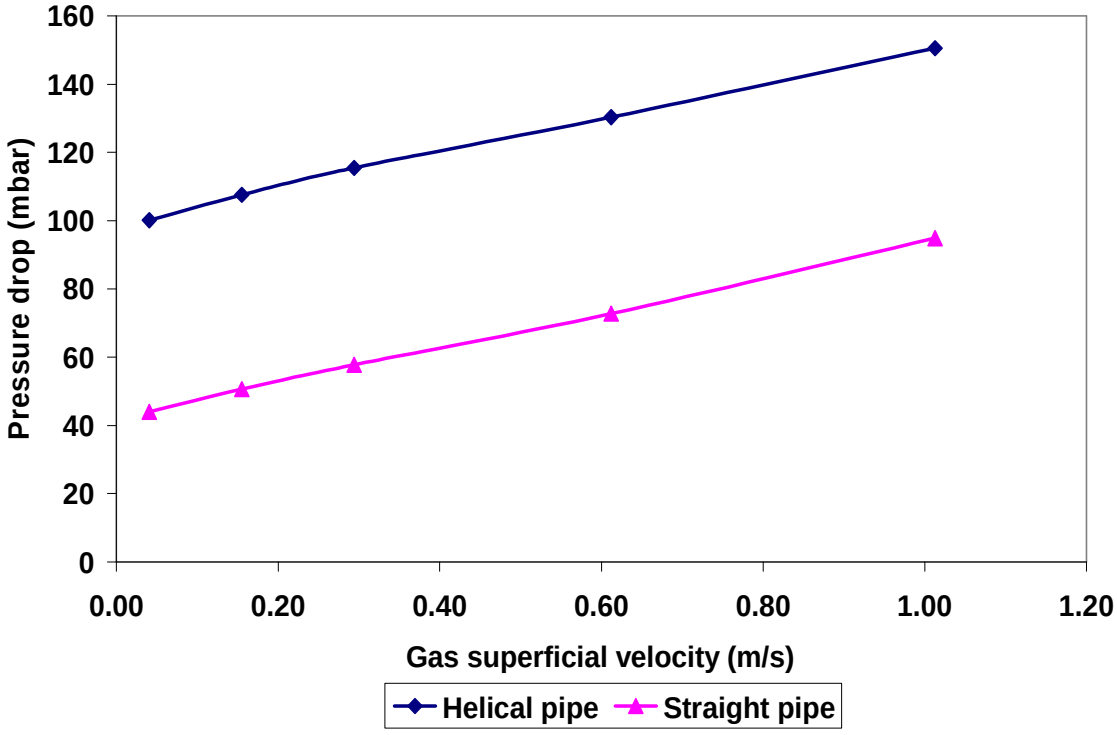

Figure 4-20: Pressure drop versus gas superficial velocity (V_{SL} = 3.0 → 3.02 ms^{-1}, V_{SG} = 0.04 → 1. 01 ms^{-1})

Pressure characteristics for both straight and *helical pipes* show that throughout the entire experimental campaign, the pressure drop has been higher for the *helical pipe* than for the straight pipe. The result is a confirmation of various previous studies. The graphical representation also shows that for liquid superficial velocities of 0.30, 0.5 and 1.0 ms^{-1}, the pressure drop gap between the values for the two pipes becomes large as the rate of air injection increases. But at liquid superficial velocities of 1.5, 2.0 and 2.5 ms^{-1}, the trend changed to opposite. That is, as the air-injection increases the pressure drop gap between the straight and *helical pipes* tends to reduce. At a liquid superficial velocity of 3.0 ms^{-1}, the pressure drop gap between the straight and *helical pipes* remains constant.

Details of the pressure drop signal plots, corresponding to the experimental matrix analysed in this thesis are presented in Appendix B.

4.3.2 Liquid holdup characteristics

The need to calculate the liquid content in the pipeline under various flow conditions, in order to design separation and slug catching facilities, has made it mandatory for the engineer to include liquid holdup as part of the parameters to be considered.

Mean liquid holdup data were obtained for each of the flowrate combinations from the conductivity “O” rings. To obtain the mean liquid holdup, the raw signal data from the conductivity sensor were normalised and converted to liquid holdup values by applying the calibration equation.

For each of the experimental matrices considered, the mean liquid holdup was plotted as a function of gas superficial velocity at a constant liquid superficial velocity. Tables 4-3 to 4-18 contain values of liquid holdup for various combinations of air and water. Figures 4-21 to 4-28 show liquid holdup plots against gas superficial velocity.

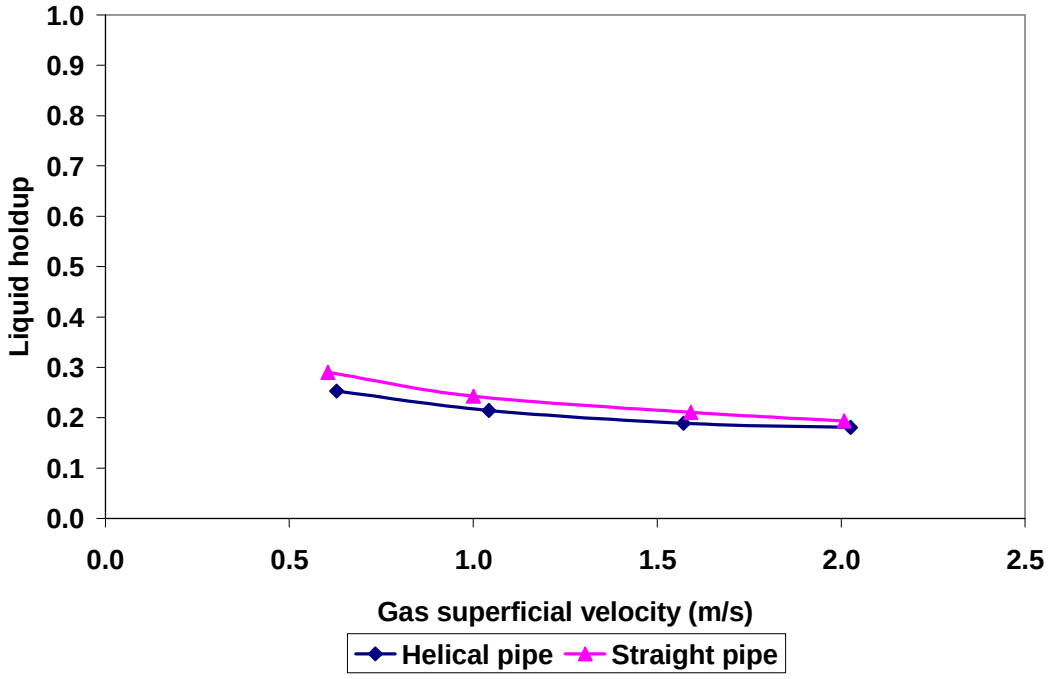

Figure 4-21: Liquid holdup versus gas superficial velocity

(V_{SL} = 0.15 ms^{-1}, V_{SG} = 0.63 → 2.03 ms^{-1})

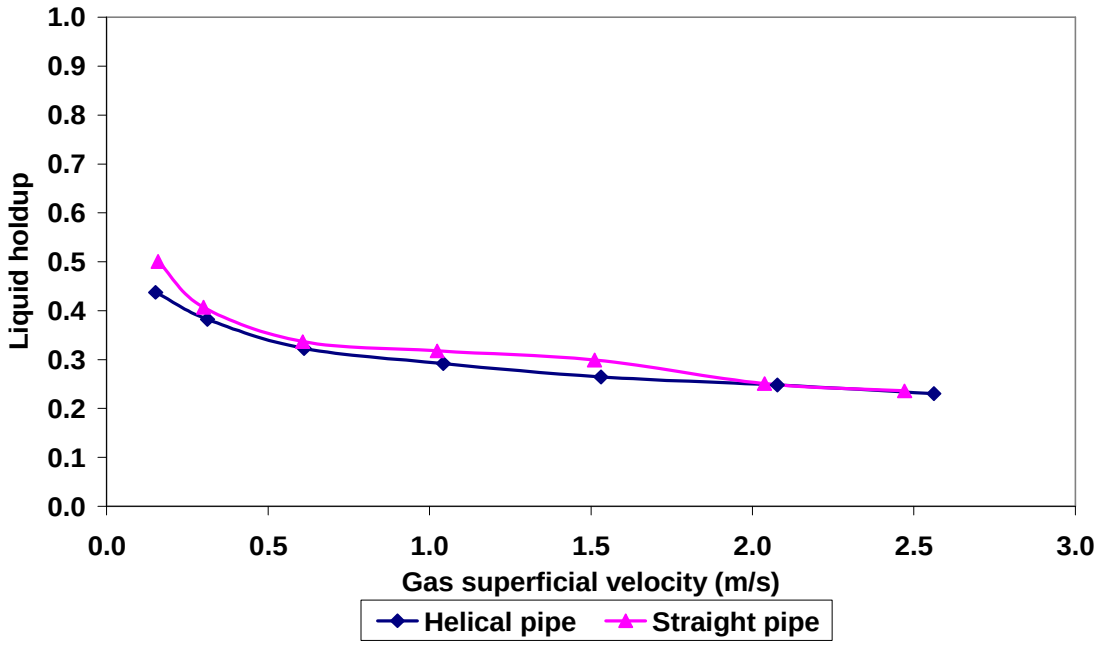

Figure 4-22: Liquid holdup versus gas superficial velocity

(V_{SL} = 0.30 ms^{-1}, V_{SG} = 0.15 → 2.56 ms^{-1})

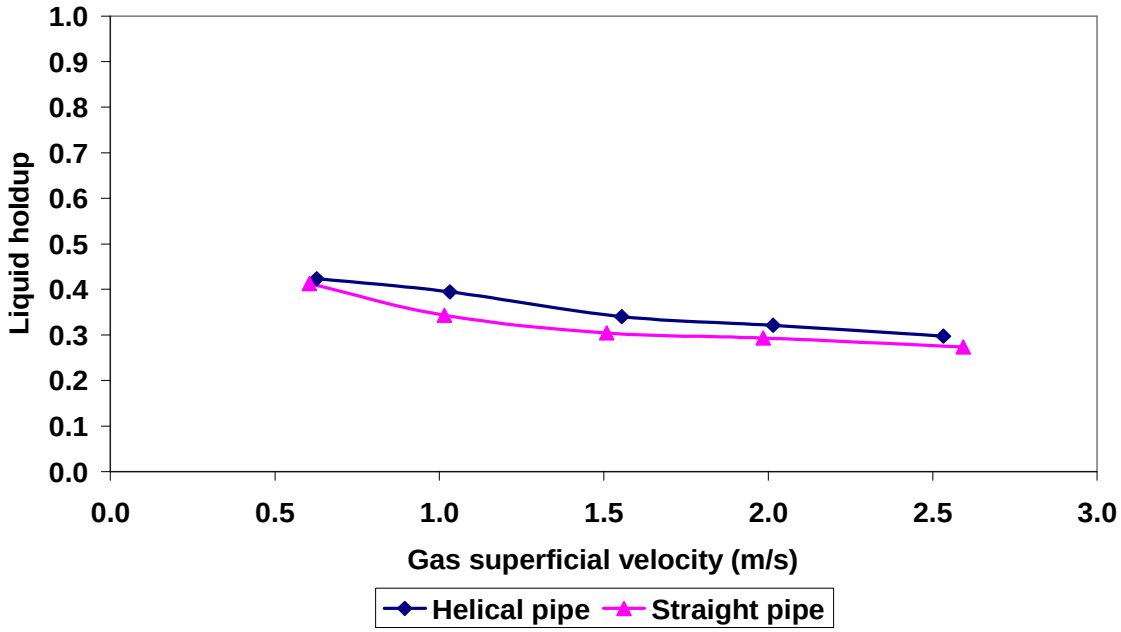

Figure 4-23: Liquid holdup versus gas superficial velocity

(V_{SL} = 0.50 ms^{-1}, V_{SG} = 0.03 →2.59 ms^{-1})

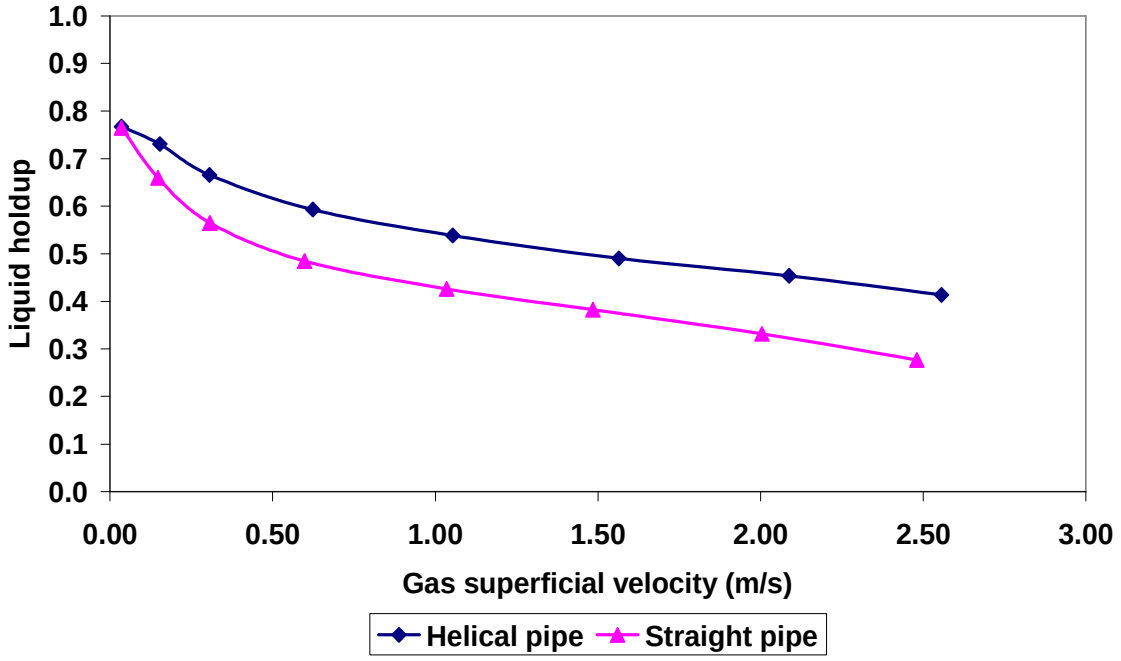

Figure 4-24: Liquid holdup versus gas superficial velocity

(V_{SL} = 1.0 → 1.02 ms^{-1}, V_{SG} = 0.04 → 2.56 ms^{-1})

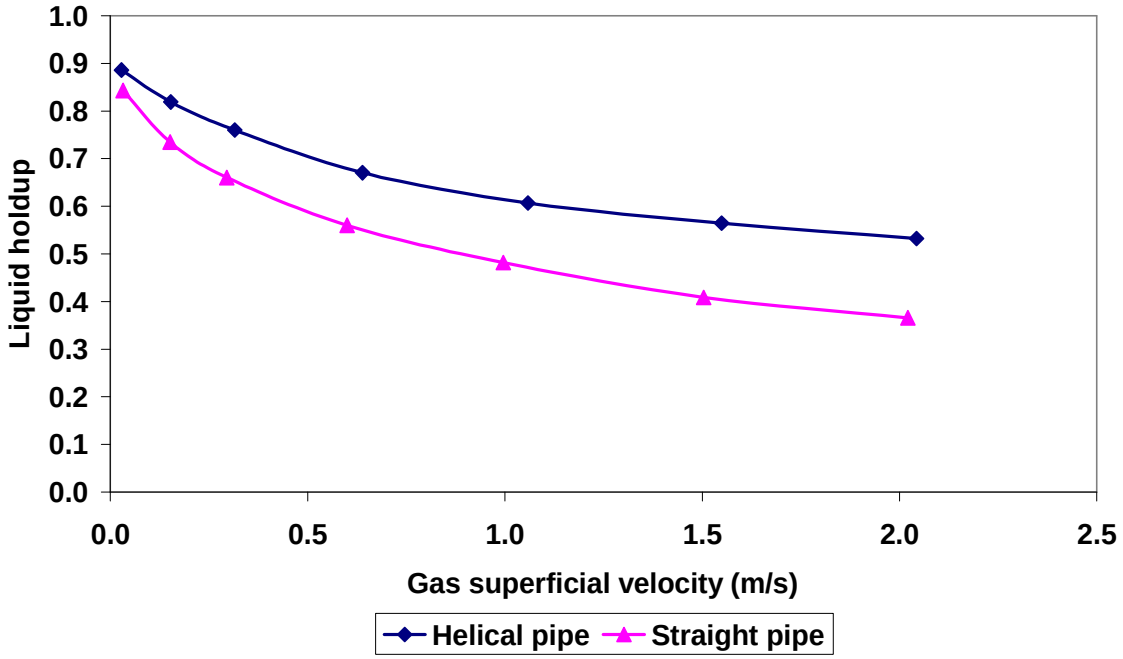

Figure 4-25: Liquid holdup versus gas superficial velocity

(V_{SL} = 1.49 → 1.53 ms^{-1}, V_{SG} = 0.03 → 2.04 ms^{-1})

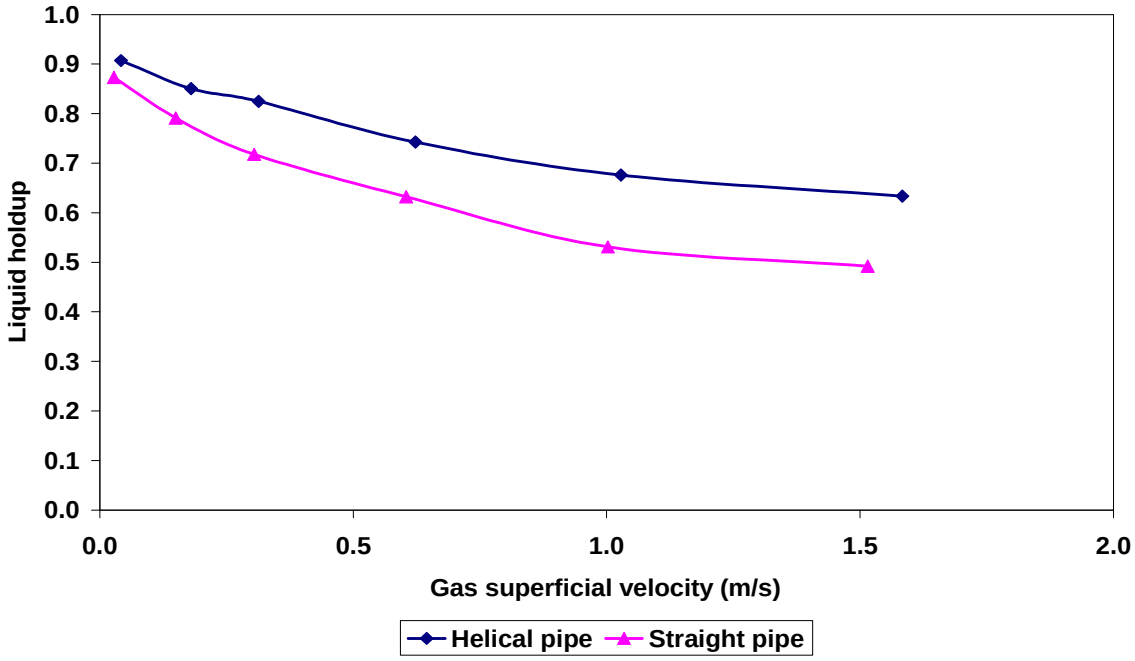

Figure 4-26: Liquid holdup versus gas superficial velocity

(V_{SL} = 2.0 → 2.02 ms^{-1}, V_{SG} = 0.03 → 1.58 ms^{-1})

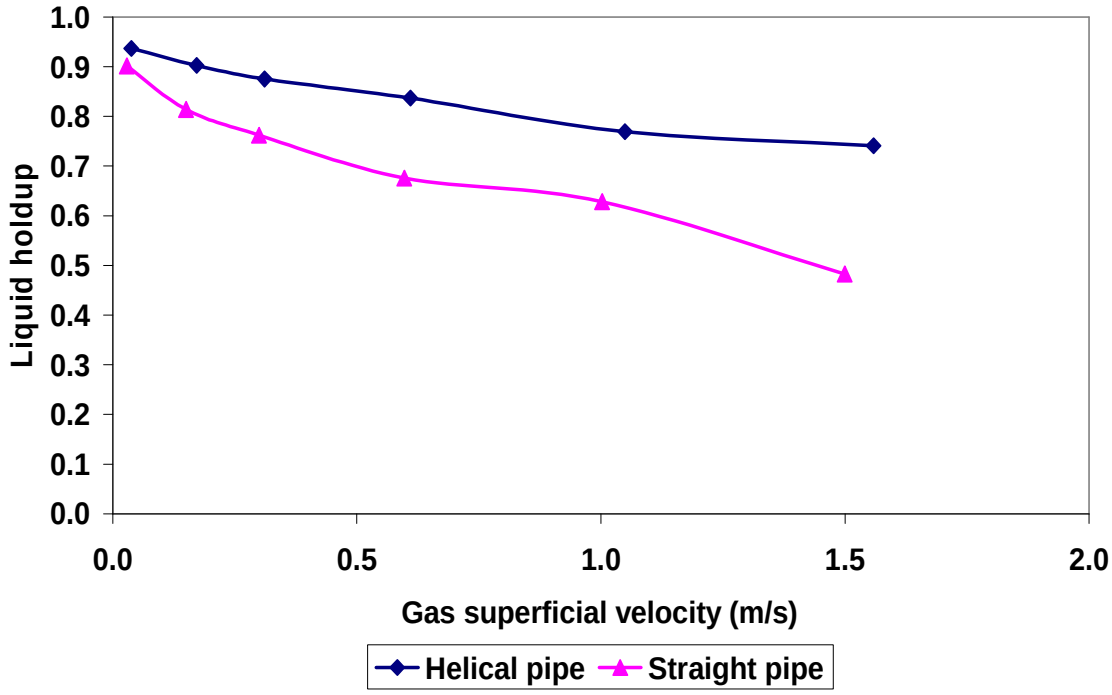

Figure 4-27: Liquid holdup versus gas superficial velocity

(V_{SL} = 2.49 → 2.52 ms^{-1}, V_{SG} = 0.03 → 1.50 ms^{-1})

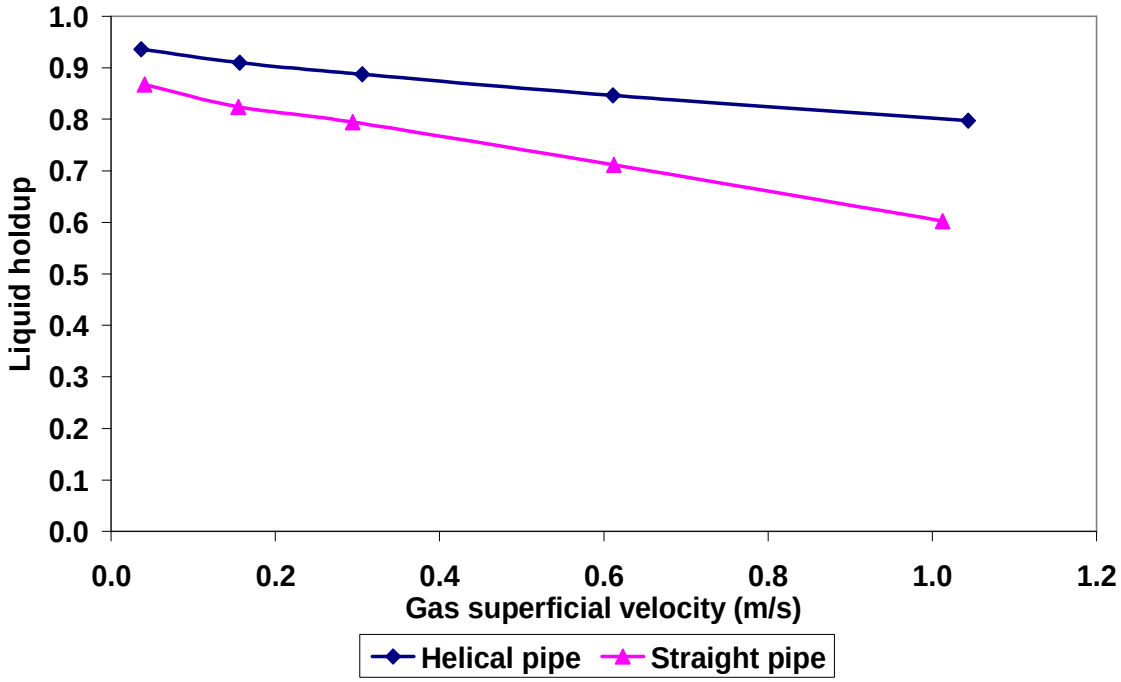

Figure 4-28: Liquid holdup versus gas superficial velocity

(V_{SL} = 3.0 → 3.02 ms^{-1}, V_{SG} = 0.04 → 1. 01 ms^{-1})

As expected, the liquid holdup decreases with increasing gas flowrate for all the experimental matrices. However, an interesting feature was observed as the liquid holdup characteristics (See Figures 4-21 and 4-22) have shown that at low liquid superficial velocities of 0.15 ms^{-1} and 0.30 ms^{-1} the liquid holdup in the straight pipe is slightly higher than that in the *helical pipe.* But for liquid superficial velocities of 0.5 ms^{-1} to 3.0 ms^{-1} (See Figures 4-23 to 4-28), the liquid holdup in the *helical pipe* is higher than that in the straight pipe.

4.3.3 Pressure drop effect on the liquid holdup

Figures 4-29 to 4-36 show the effect of pressure drop on liquid holdup

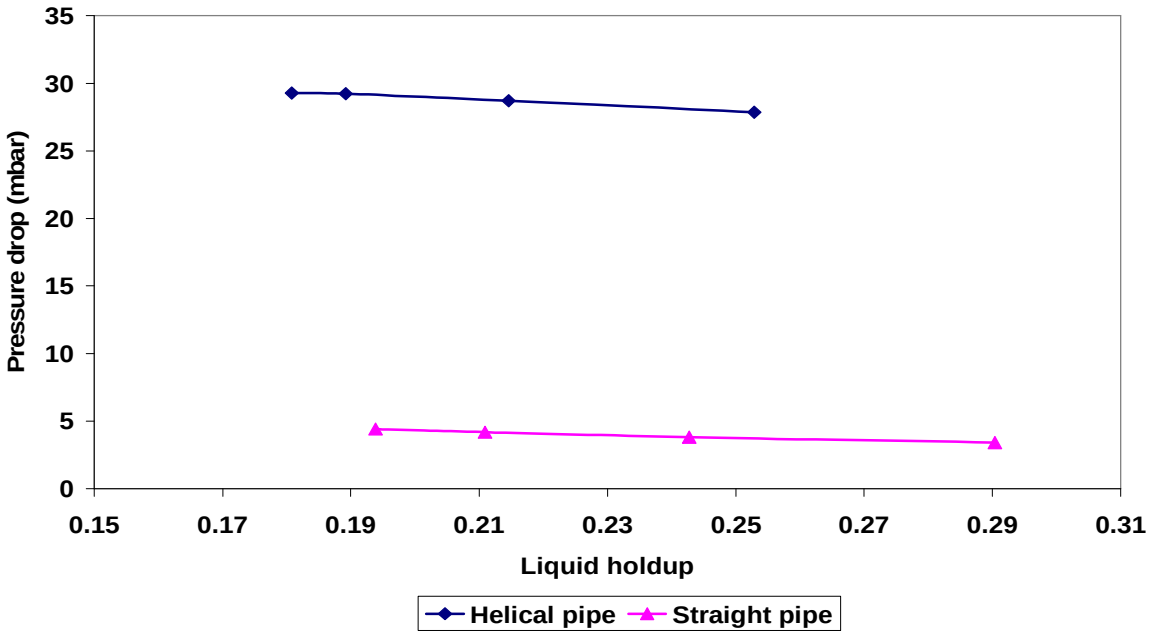

Figure 4-29: Liquid holdup versus pressure drop

(V_{SL} = 0.15 ms^{-1}, V_{SG} = 0.63 → 2.03 ms^{-1})

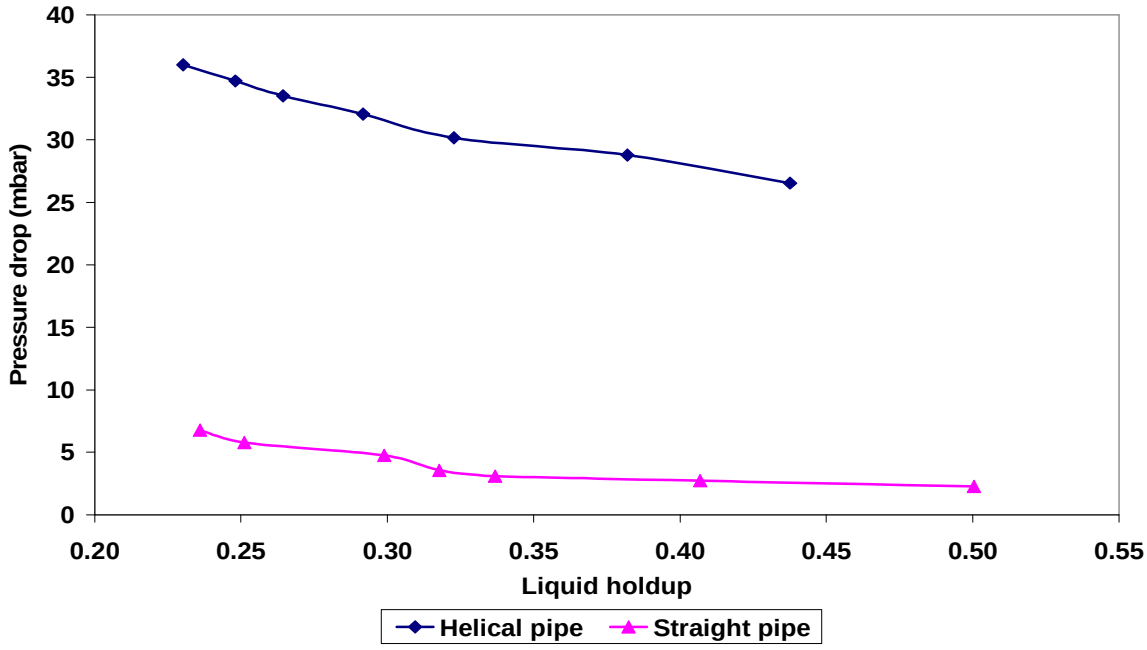

Figure 4-30: Liquid holdup versus pressure drop

(V_{SL} = 0.30 ms^{-1}, V_{SG} = 0.15 → 2.56 ms^{-1})

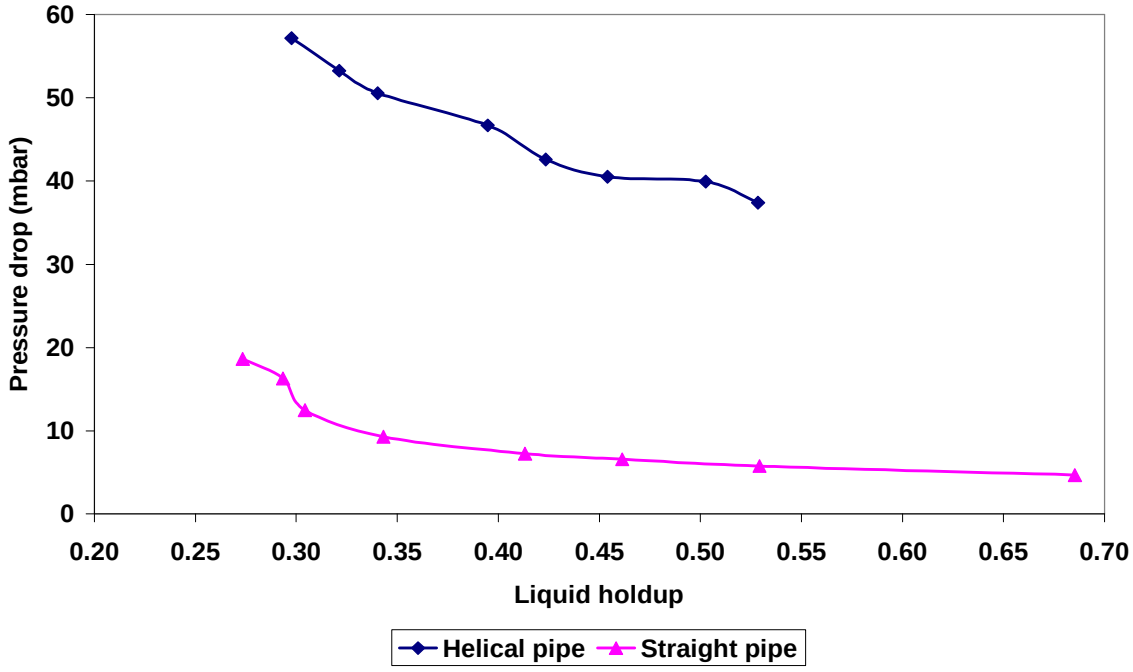

Figure 4-31: Liquid holdup versus pressure drop

(V_{SL} = 0.50 ms^{-1}, V_{SG} = 0.03 → 2.59 ms^{-1})

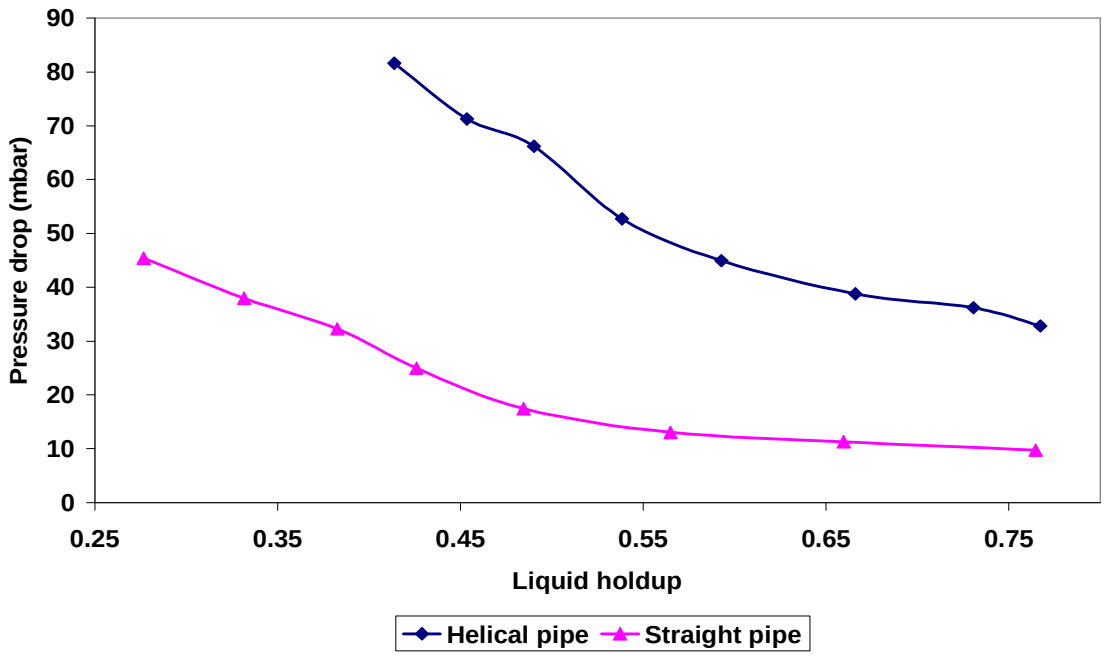

Figure 4-32: Liquid holdup versus pressure drop

(V_{SL} = 1.0 → 1.02 ms^{-1}, V_{SG} = 0.04 → 2.56 ms^{-1})

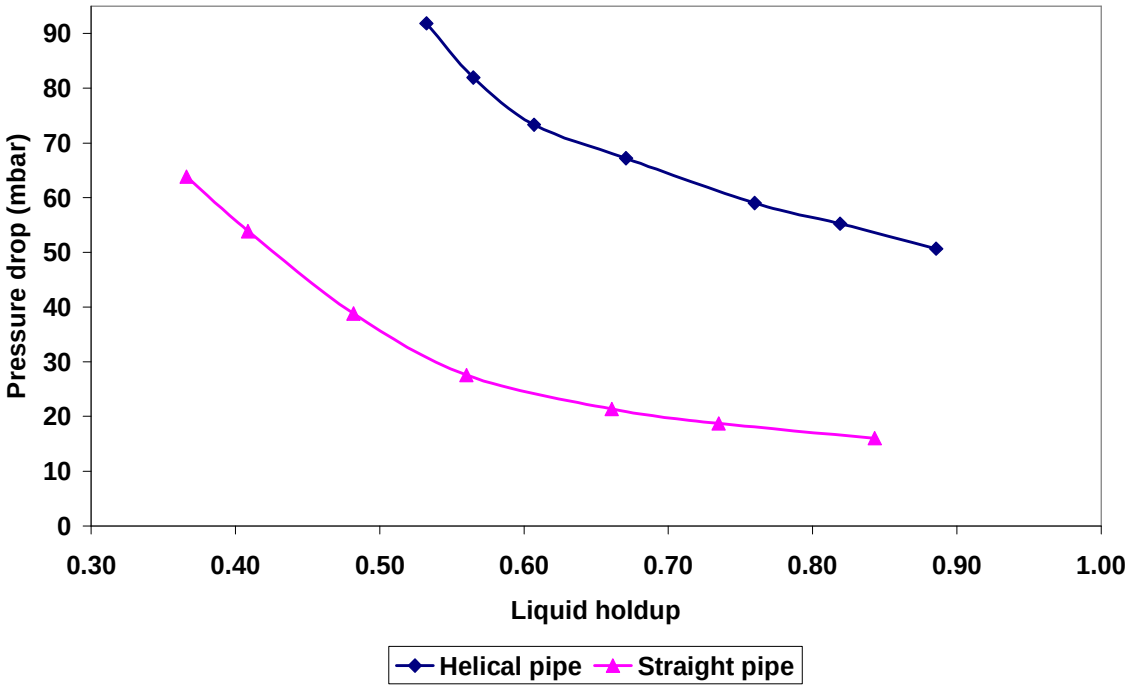

Figure 4-33: Liquid holdup versus pressure drop

(V_{SL} = 1.49 → 1.53 ms^{-1}, V_{SG} = 0.03 → 2.04 ms^{-1})

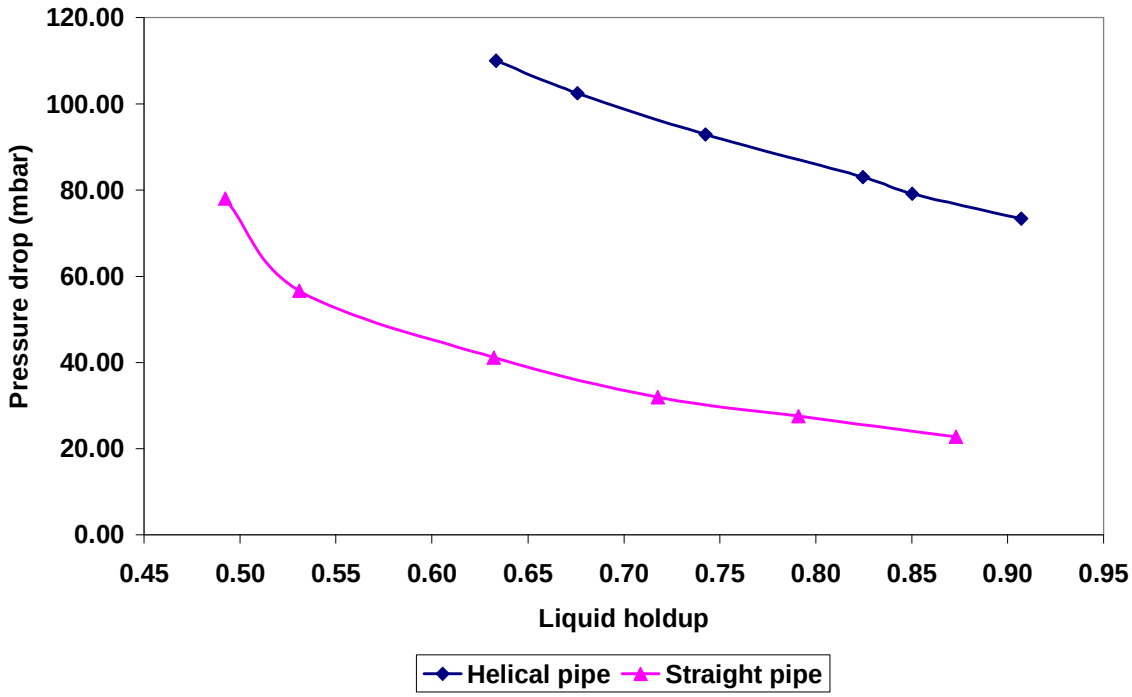

Figure 4-34: Liquid holdup versus pressure drop

(V_{SL} = 2.0 → 2.02 ms^{-1}, V_{SG} = 0.03 → 1.58 ms^{-1})

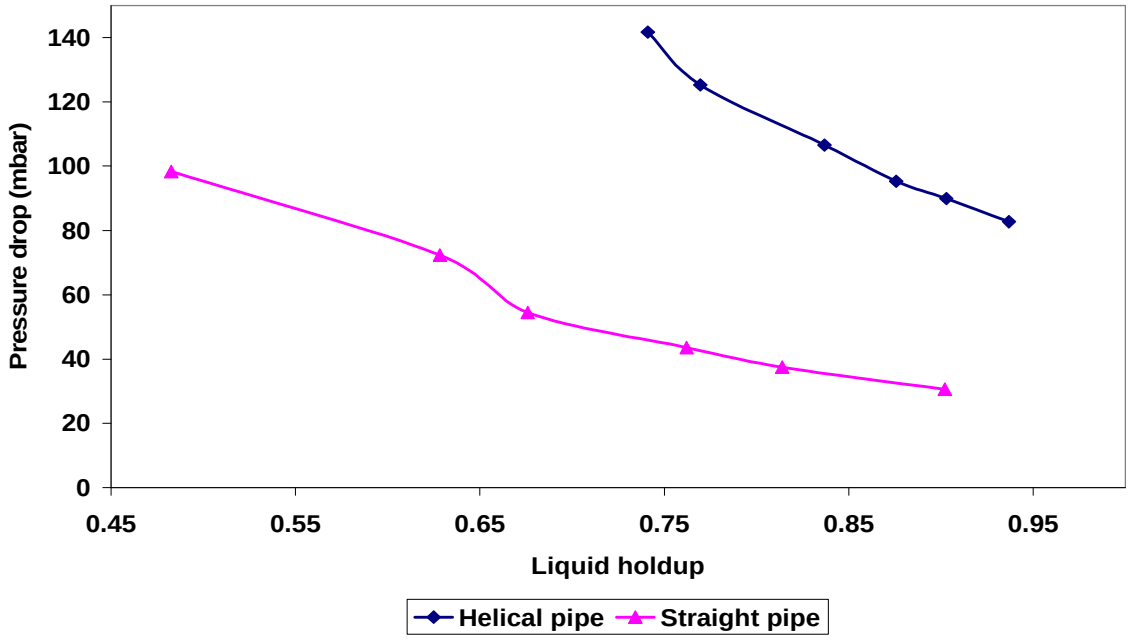

Figure 4-35: Liquid holdup versus pressure drop

(V_{SL} = 2.49 → 2.52 ms^{-1}, V_{SG} = 0.03 → 1.50 ms^{-1})

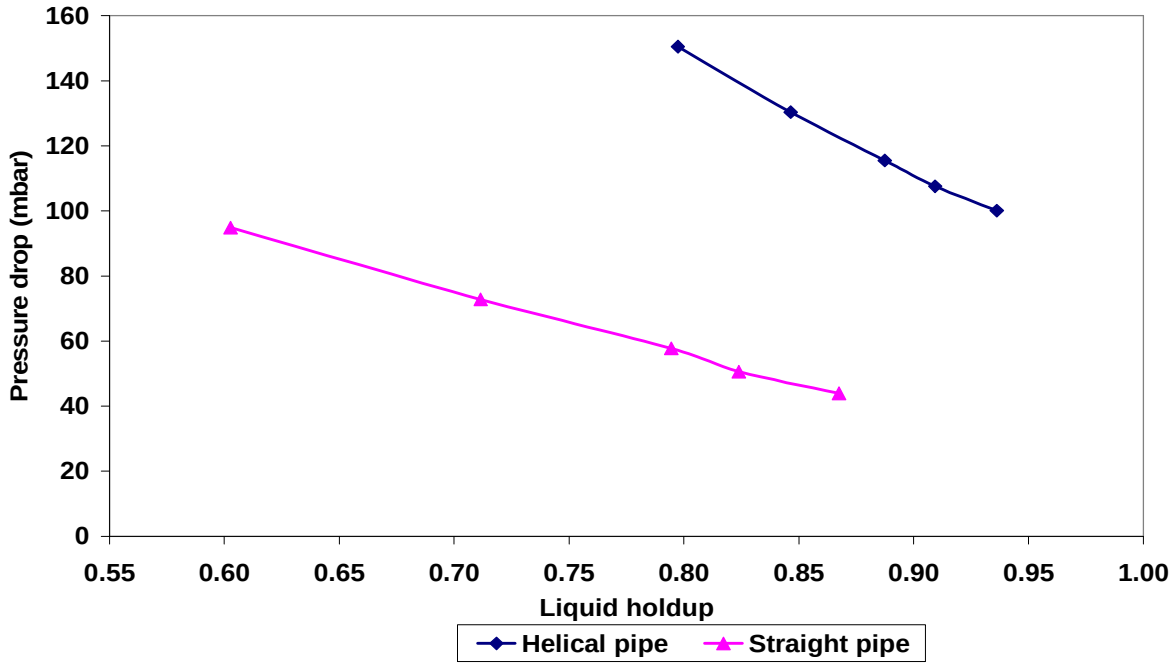

Figure 4-36: Liquid holdup versus pressure drop
(V_{SL} = 3.0 – 3.02 ms^{-1}, V_{SG} = 0.04 – 1. 01 ms^{-1})

The effects of pressure drop on liquid holdup are plotted in Figures 4-29 to 4-36. For all the superficial velocities of gas and liquid investigated, the liquid holdup increases as the pressure drop decreases. This effect manifests well in Figures 4-32 to 4-36.

4.3.4 Conductivity probe signal characteristics

Two conductivity probes labelled **A** and **B** were installed in the test section (down stream) of the experimental pipeline. Probe **A** was installed at the dip of the *helical pipe* while probe **B** was installed at the top of the curvature of the *helical pipe* (Figure 4-2). This probe arrangement was adopted to compare the values of liquid holdup at both locations on the *helical pipe*. Three flow regimes (stratified, slug and intermittent) have been selected to compare probes **A** and **B** signal characteristics in both straight and *helical pipes* (Table 4-19).

Pipe	V_{SL} (ms^{-1})	V_{SG} (ms^{-1})	Flow regime	Probe A: Liquid holdup	Probe B: Liquid holdup	Probes average (A+B): Liquid holdup	Pressure drop (mbar)
Straight	0.15	0.60	stratified	0.35	0.24	0.29	3.43
	0.50	0.15	Slug	0.55	0.51	0.53	5.77
	1.50	1.0	Bubbly	0.54	0.42	0.48	38.88
	3.01	1.01	Dispersed bubbly	0.68	0.53	0.60	94.87
Helical	0.15	0.63	Bubbly	0.25	0.25	0.25	27.86
	0.50	0.16	Bubbly	0.42	0.58	0.50	39.90
	1.50	1.0	Bubbly	0.55	0.66	0.61	73.35
	3.0	1.04	Dispersed bubbly	0.80	0.80	0.80	150.53

Table 4-19: Conductivity probe trace characteristics

4.3.4.1 Probes' signal trace characteristics for stratified and bubbly flows

Figures 4-37 and 4-38 show conductivity traces of both straight and *helical pipes* respectively. At a liquid superficial velocity of 0.15 ms^{-1} and air superficial velocity of 0.60 ms^{-1}, stratified flow occurred in the straight pipe (See Figure 4-37) whereas for the same combination of air and liquid [liquid superficial velocity (V_{SL}) of 0.15 ms^{-1} and air superficial velocity (V_{SG}) of 0.63 ms^{-1})], bubbly flow occurred in the *helical pipe* (Figure 4-38).

The signal trace in the straight pipe (Figure 4-37) shows that liquid holdup was higher in probe **A** than probe **B**. However, in the *helical pipe* (Figure 4-38); even though there is no clear indication confirming which of the two probes indicates a higher liquid holdup; but signal analysis shows that liquid holdup in the two probes **A** and **B** were the same. Comparing the average values for the two

pipes (straight and *helical*), liquid holdup was higher in the straight pipe than the *helical pipe* under identical applied conditions (Tables 4-19).

Figure 4-39 shows pressure drop signal for the straight pipe during stratified flow with V_{SL} = 0.15 ms^{-1} and V_{SG} = 0.60 ms^{-1}. Figure 4-40 shows the pressure drop signal for the *helical pipe* at V_{SL} = 0.15 ms^{-1} and V_{SG} = 0.63 ms^{-1} when the flow was bubbly. As shown in Table 4-19, the pressure drop was higher for the *helical pipe* than for the straight pipe.

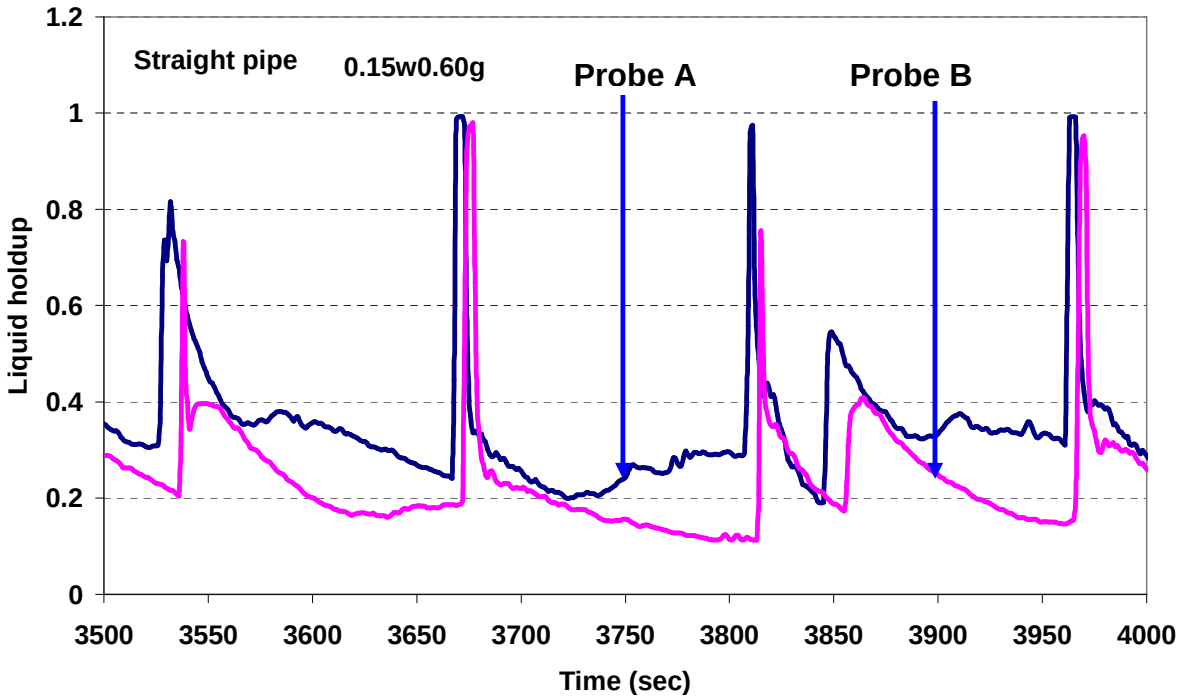

Figure 4-37: Straight pipe conductivity signal trace during stratified flow (V_{SL} = 0.15 ms^{-1}, V_{SG} = 0.60 ms^{-1})

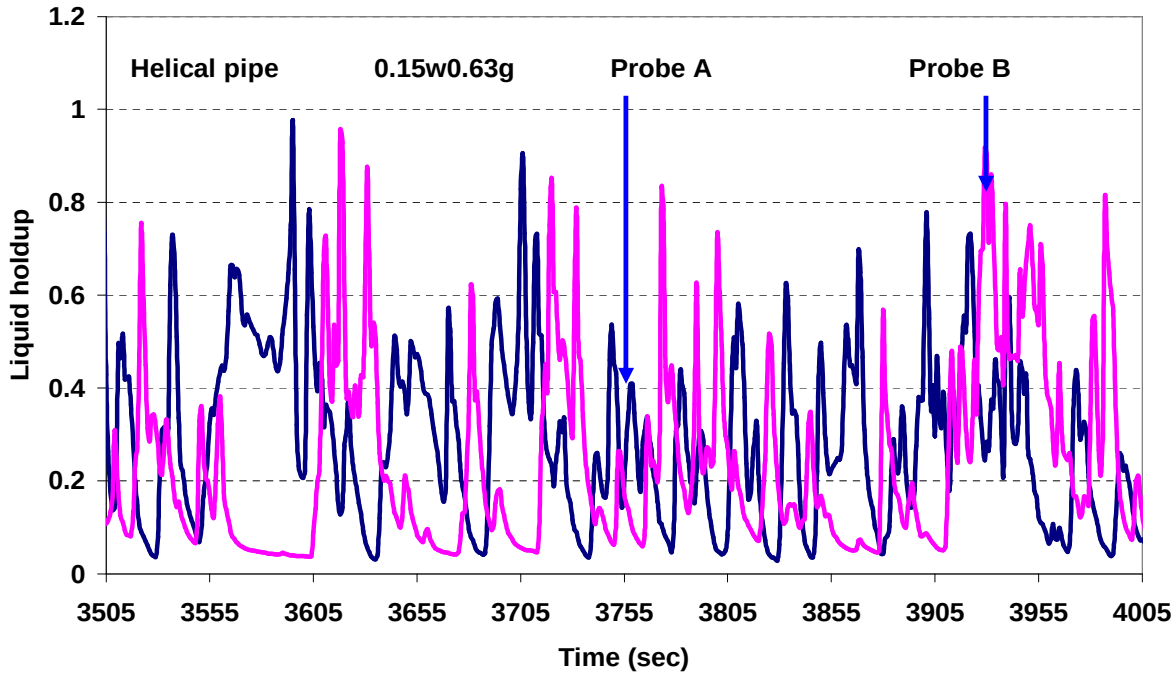

Figure 4-38: *Helical pipe* conductivity signal trace during bubbly flow (V_{SL} = 0.15 ms^{-1}, V_{SG} = 0.63 ms^{-1})

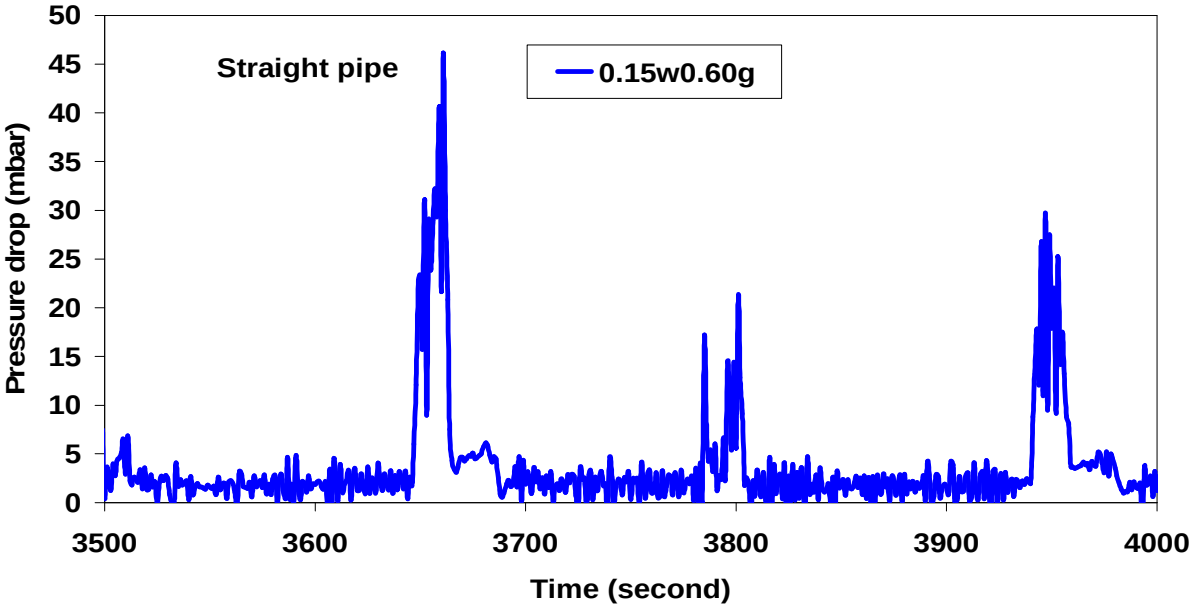

Figure 4-39: Straight pipe pressure drop signal trace during stratified flow (V_{SL} = 0.15 ms^{-1}, V_{SG} = 0.60 ms^{-1})

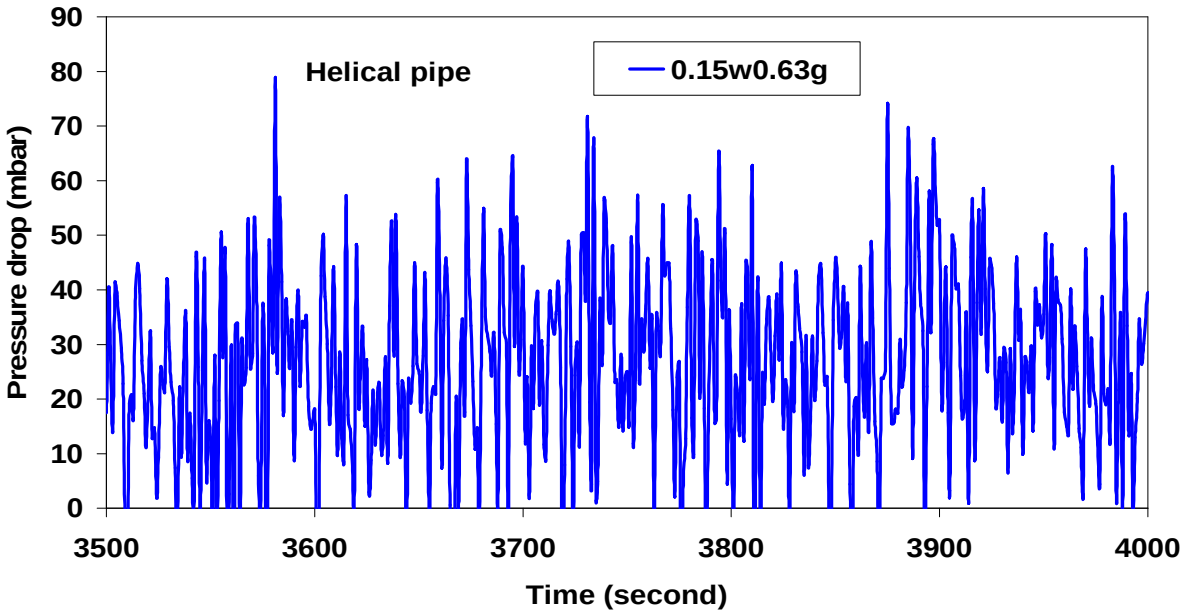

Figure 4-40: *Helical pipe* pressure drop signal trace during bubbly flow (V_{SL} = 0.15 ms^{-1}, V_{SG} = 0.63 ms^{-1})

4.3.4.2 Probes' signal trace characteristics for slug and bubbly flows

Figures 4-41 and 4-42 show characteristics of the probes' signal traces when the fluid flow in the straight pipe was slug and in the *helical pipe* was bubbly at a liquid superficial velocity of 0.5 ms^{-1} and an air superficial velocity of 0.15 ms^{-1}. Figure 4-41 shows that liquid holdup for probe **A** was higher during the slug flow pattern than for probe **B**. In the *helical pipe*, the flow was bubbly (Figure 4-42) and liquid holdup in probe **B** was much higher than for probe **A**.

The average liquid holdup value was slightly higher (0.53) in the straight pipe than the *helical* (0.50).

From the conductivity probes' signal analysis, a slug pattern occurred in the straight pipe at a liquid superficial velocity of 0.5 ms^{-1} and air superficial velocity of 0.15 ms^{-1} whereas at the same superficial velocities of air and water in *helical pipe,* slug flow does not occur: instead bubbly flow ensued.

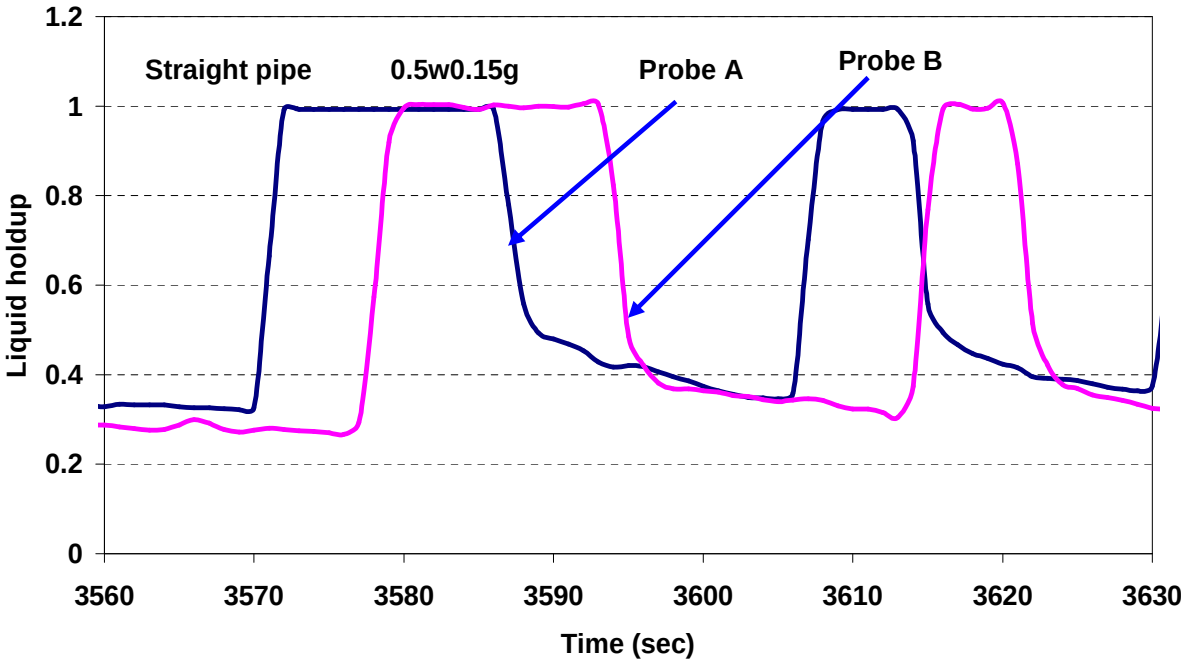

Figure 4-41: Straight pipe conductivity signal trace during slug flow (V_{SL} = 0.5 ms^{-1}, V_{SG} = 0.15 ms^{-1})

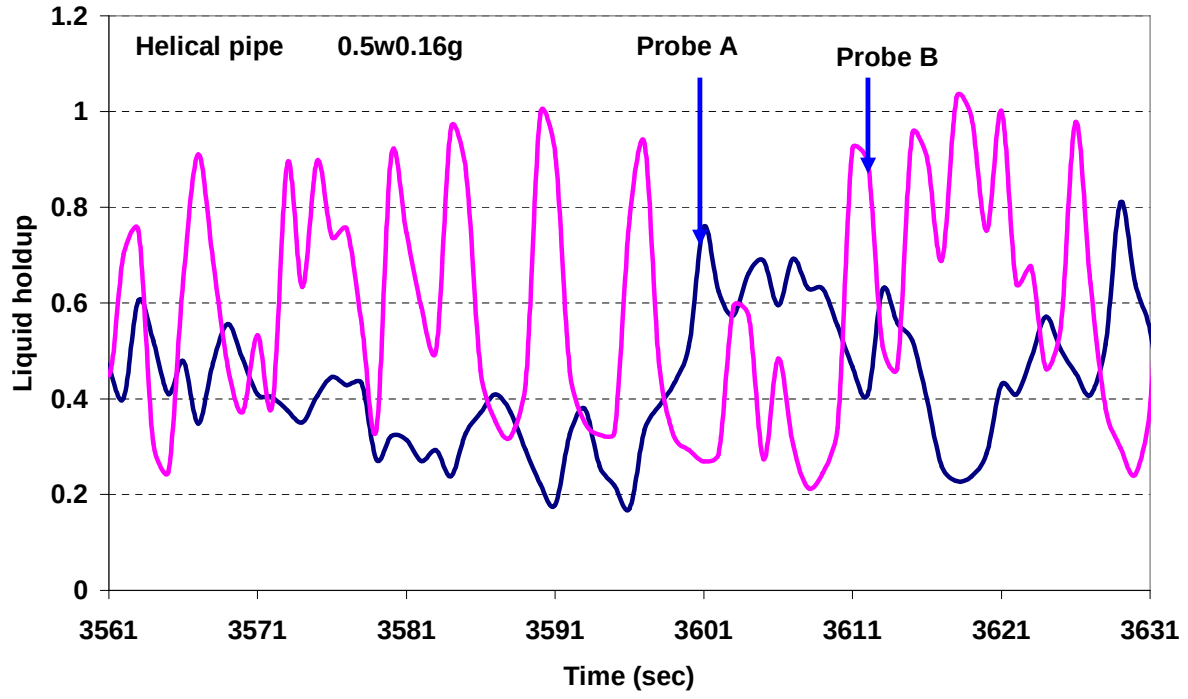

Figure 4-42: *Helical pipe* conductivity signal trace during bubbly flow (V_{SL} = 0.5 ms^{-1}, V_{SG} = 0.16 ms^{-1})

Figure 4-43 shows the pressure drop signal for the straight pipe during the slug flow at V_{SL} = 0.50 ms^{-1} and V_{SG} = 0.15 ms^{-1}. Figure 4-44 shows the pressure drop signal for the *helical pipe* when the flow was bubbly at V_{SL} = 0.5 ms^{-1} and V_{SG} = 0.16 ms^{-1}. Again, the pressure drop was higher for the *helical pipe* than for the straight pipe.

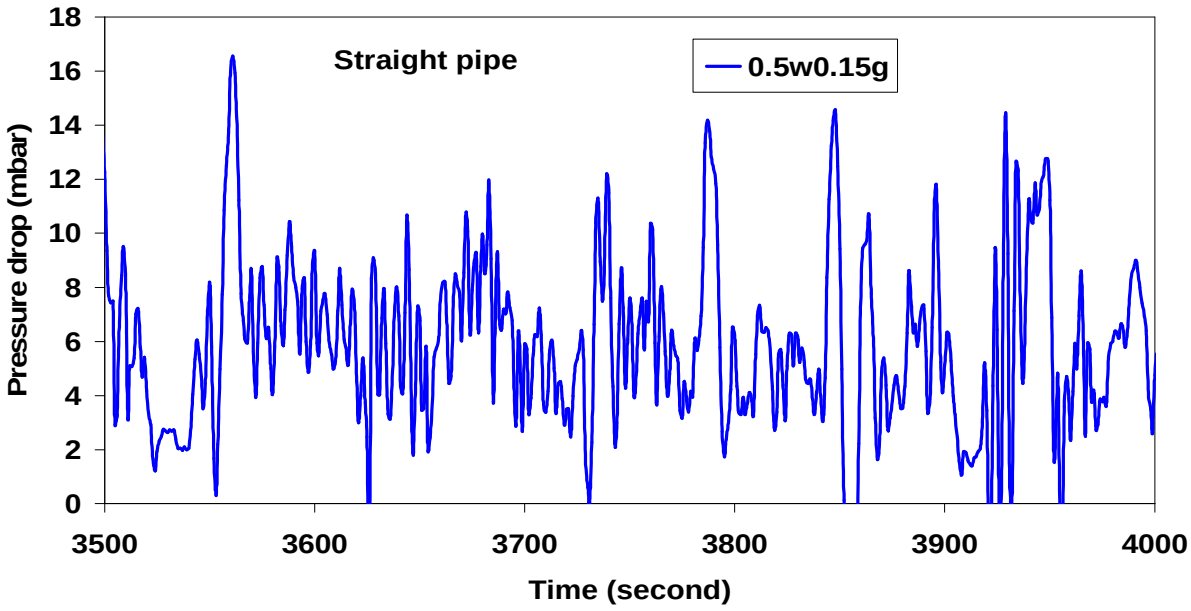

Figure 4-43: Straight pipe pressure drop signal trace during slug flow (V_{SL} = 0.5 ms^{-1}, V_{SG} = 0.15 ms^{-1})

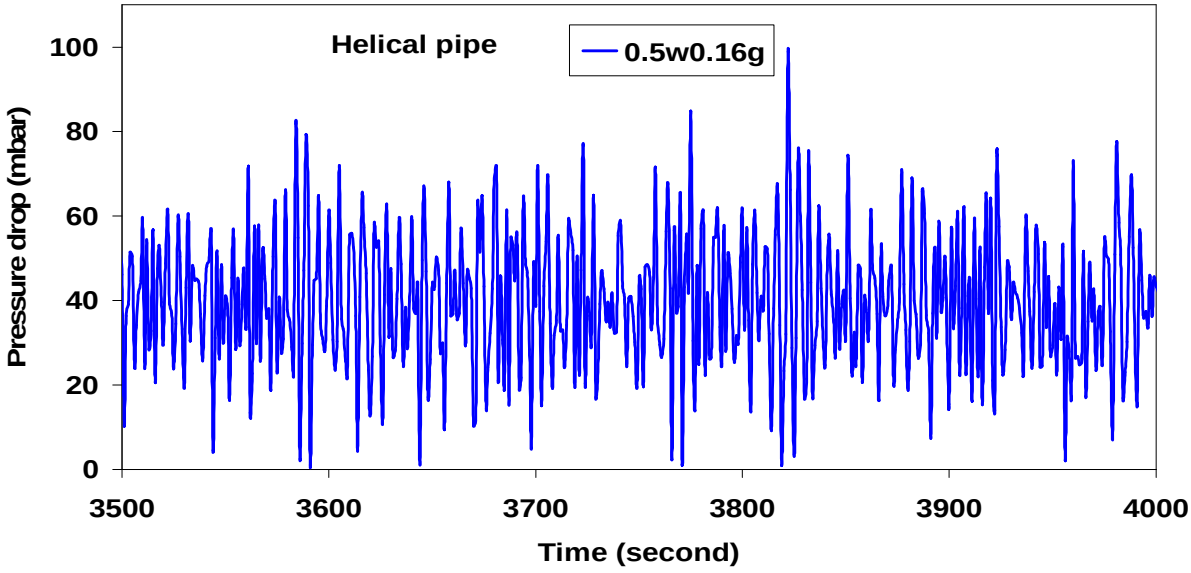

Figure 4-44: *Helical pipe* pressure drop signal trace during bubbly flow (V_{SL} = 0.5 ms^{-1}, V_{SG} = 0.16 ms^{-1})

4.3.4.3 Probes' signal trace characteristics for bubbly flows

Figures 4-45 and 4-46 show the characteristics of the probes' signal traces when the fluid flow in both straight and *helical pipes* was bubbly. During this flow regime, Figure 4-45 shows that the liquid holdup in probe **A** was higher than in probe **B** whereas in the *helical pipe*, where the flow was also bubbly (Figure 4-46), the liquid holdup in probe **B** was higher than probe **A**.

On average, the liquid holdup value in the straight pipe was much lower (0.48) than for the *helical pipe* (0.61).

Figure 4-47 shows the pressure drop signal for the straight pipe. Figure 4-48 shows the pressure drop signal for the *helical pipe*. The pressure drop was higher (73.35 mbar) in the *helical pipe* than the straight pipe (38.88 mbar).

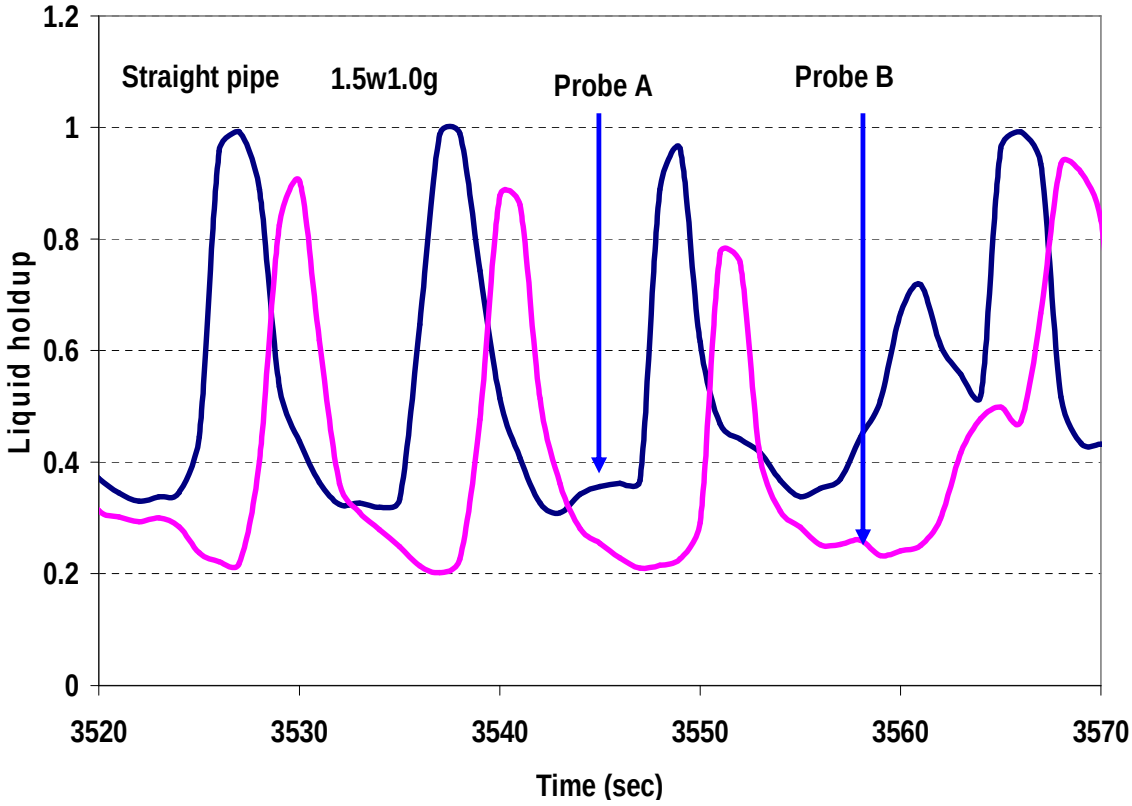

Figure 4-45: Straight pipe conductivity signal trace during bubbly flow (V_{SL} = 1.5 ms^{-1}, V_{SG} = 1.0 ms^{-1})

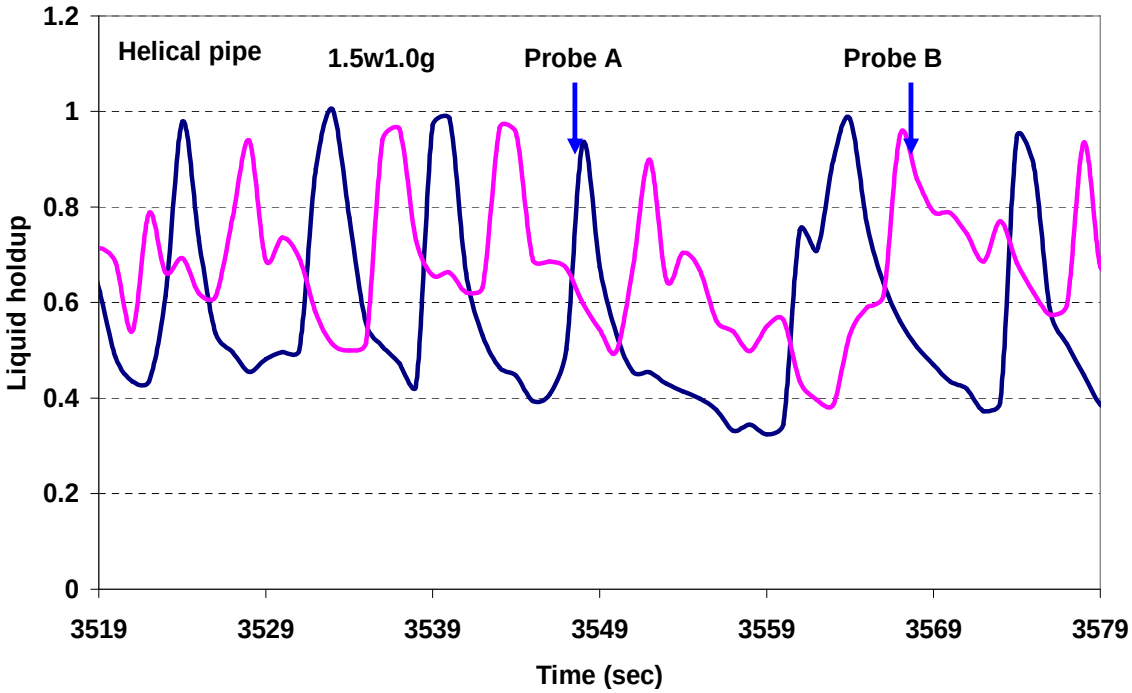

Figure 4-46: *Helical pipe* conductivity signal trace during bubbly flow (V_{SL} = 1.5 ms^{-1}, V_{SG} = 1.0 ms^{-1})

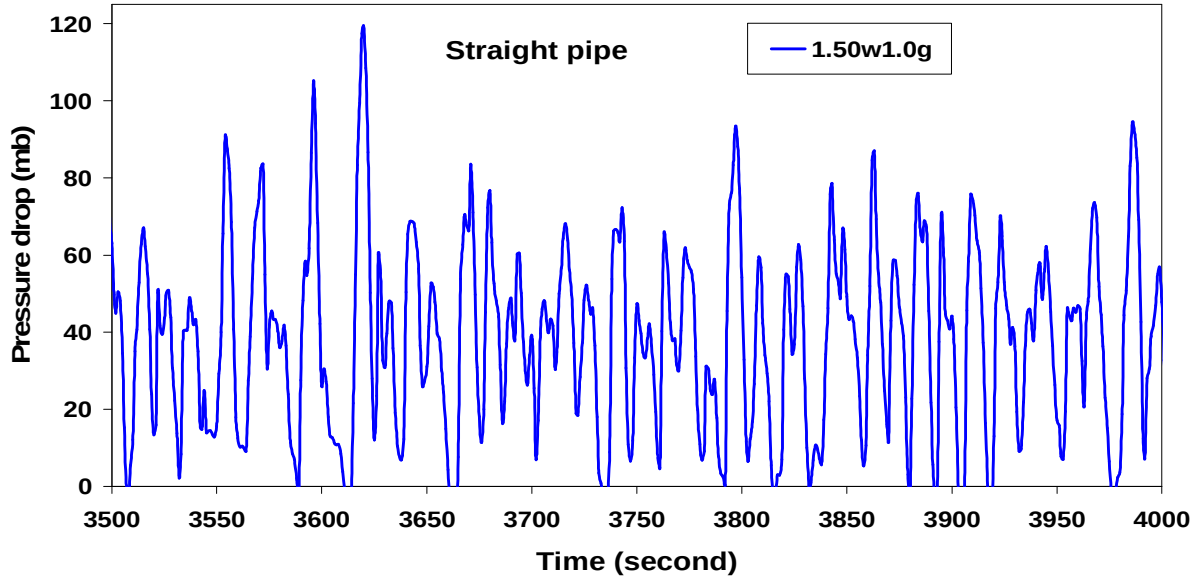

Figure 4-47: Straight pipe pressure drop signal trace during bubbly flow (V_{SL} = 1.5 ms^{-1}, V_{SG} = 1.0 ms^{-1})

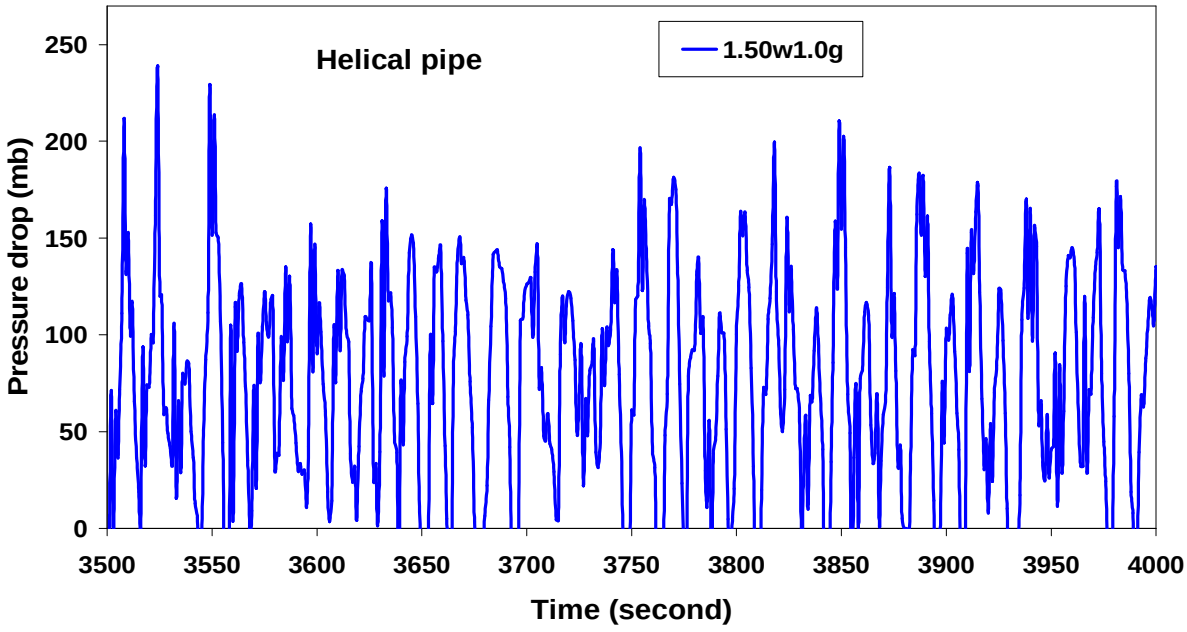

Figure 4-48: *Helical pipe* pressure drop signal trace during bubbly flow (V_{SL} = 1.5 ms^{-1}, V_{SG} = 1.0 ms^{-1})

4.3.4.4 Probes' signal trace characteristics for dispersed bubbly flows

Figures 4-49 and 4-50 show characteristics of the probes' signal traces when the fluid flow in both the straight and *helical pipes* consisted of dispersed bubble. During this flow regime (dispersed bubbles) both Figures 4-49 and 4-50 show that the liquid holdup for probe **A** was higher than for probe **B** in both straight and *helical pipes*. However, it can be observed that the signal trace of probe **A** in the *helical pipe* has both maximum and minimum liquid holdups. On average, both probes **A** and **B** in *helical pipe* have the same value (0.80) of liquid holdup (Table 4-19). Comparing the average values in both straight and *helical pipes*, the liquid holdup in the *helical pipe* was much higher (0.80) than in the straight pipe (0.60). It can also be observed from both Figures 4-49 and 4-50 that the minimum liquid holdup was also higher for the *helical pipe* than for the straight pipe.

Figures 4-51 and 4-52 show the pressure drop signal for both straight and *helical pipes* during dispersed bubbly flow at V_{SL} = 3.0 ms^{-1} and V_{SG} = 1.0 ms^{-1}. The pressure drop was still higher in the *helical pipe* than in the straight pipe. Numerical values to corroborate this fact and all the above discussions on the conductivity probes' trace characteristics for both the straight and *helical pipes* are presented in Table 4-19.

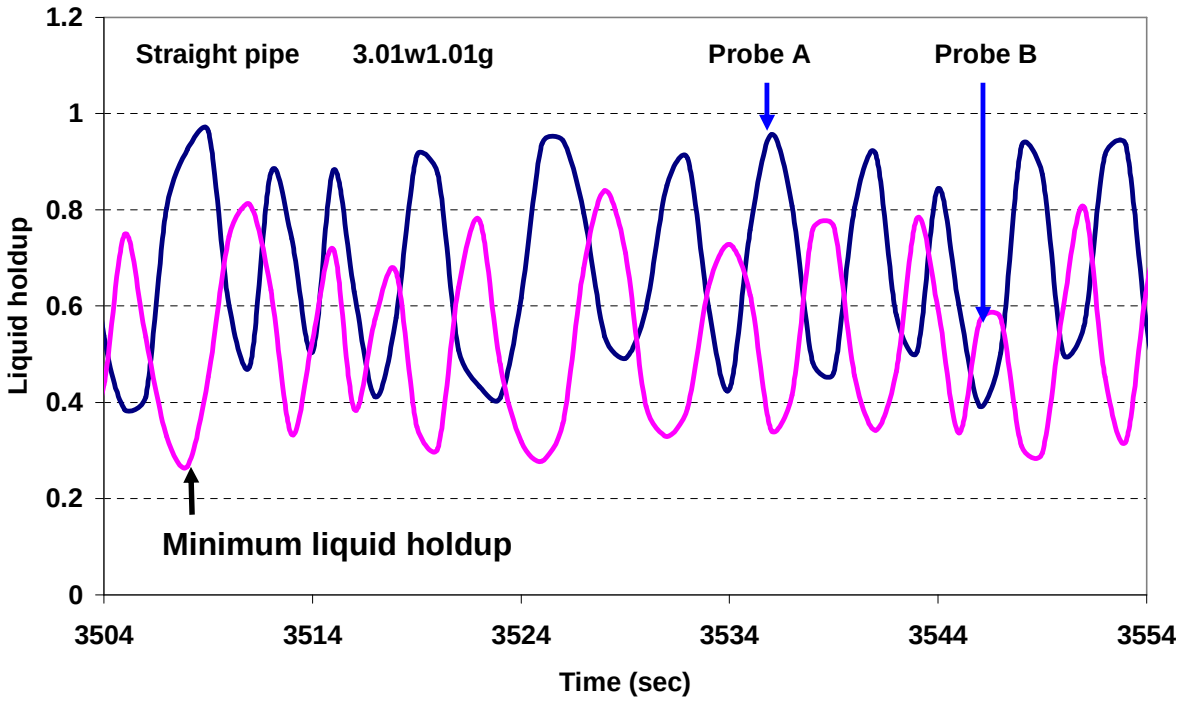

Figure 4-49: Straight pipe conductivity signal trace during dispersed bubbly flow (V_{SL} = 3.01 ms^{-1}, V_{SG} = 1.01 ms^{-1})

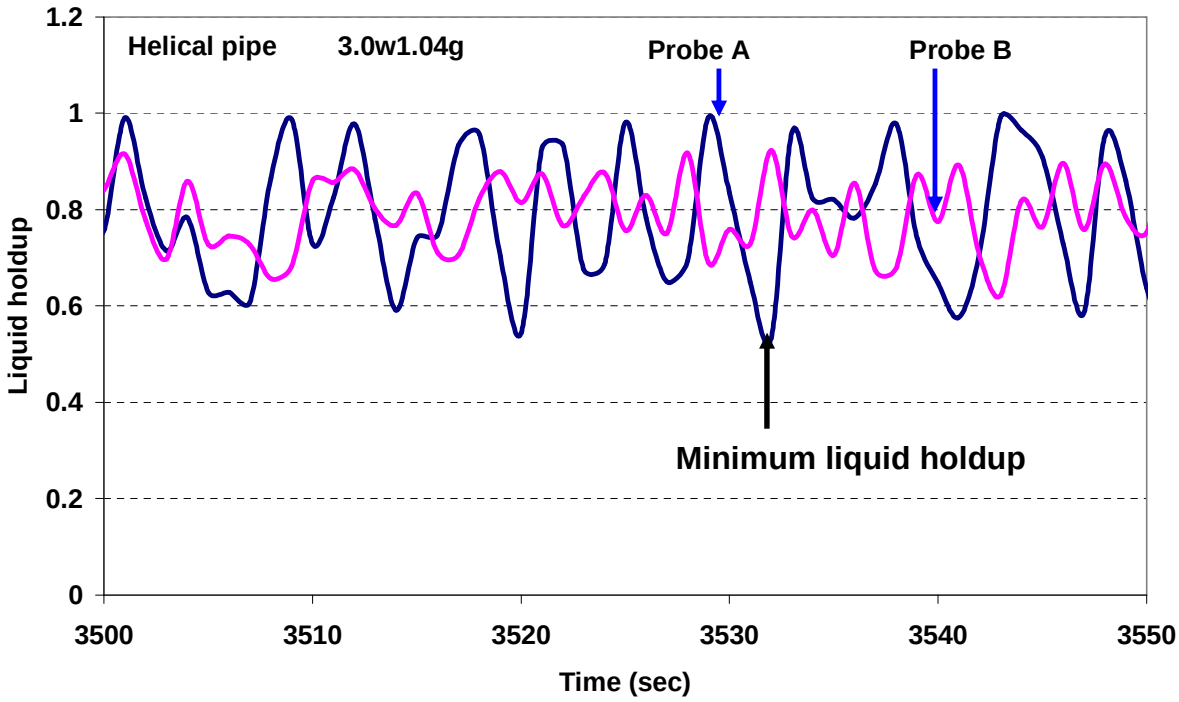

Figure 4-50: *Helical pipe* conductivity signal trace during dispersed bubbly flow (V_{SL} = 3.0 ms^{-1}, V_{SG} = 1.04 ms^{-1})

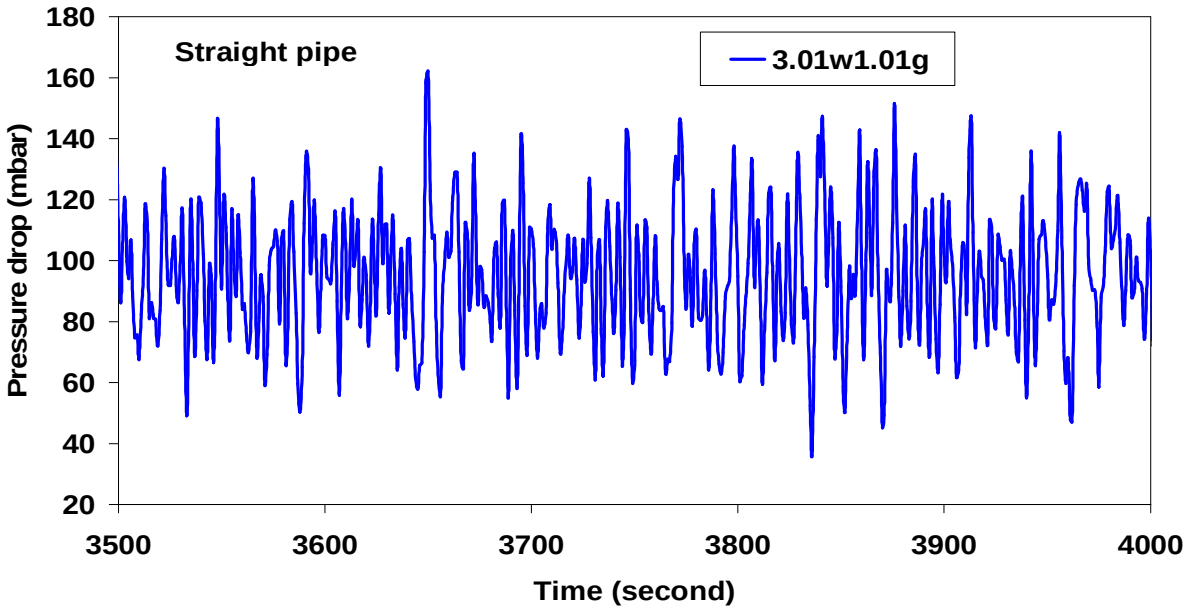

Figure 4-51: Straight pipe pressure drop signal trace during dispersed bubbly flow (V_{SL} = 3.01 ms^{-1}, V_{SG} = 1.01 ms^{-1})

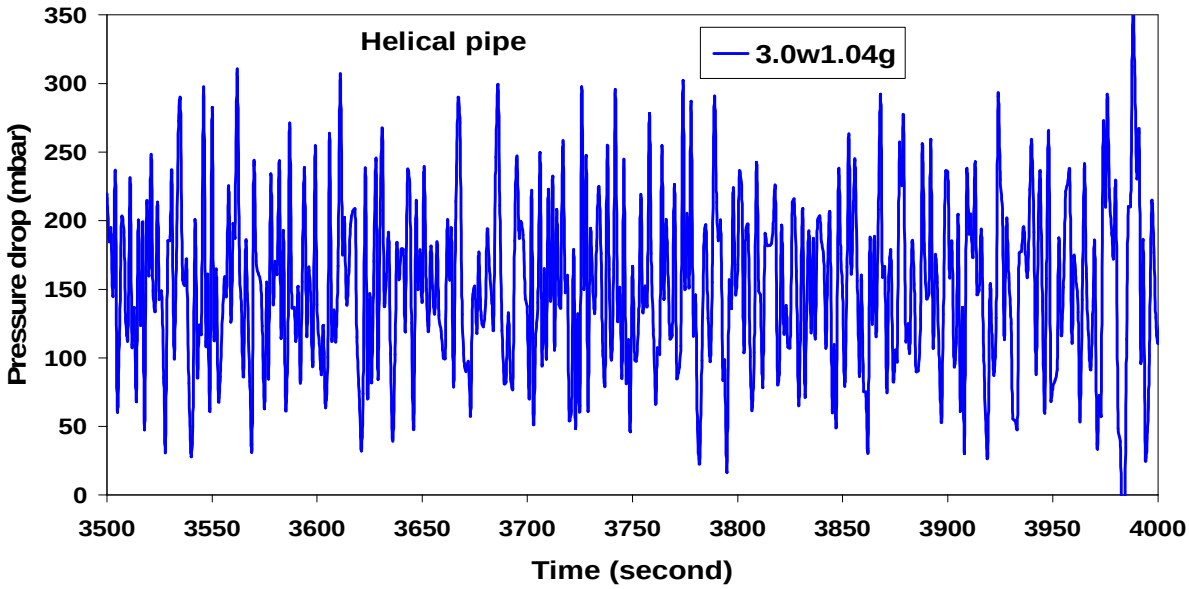

Figure 4-52: *Helical pipe* pressure drop signal trace during dispersed bubbly flow (V_{SL} = 3.0 ms^{-1}, V_{SG} = 1.04 ms^{-1})

Detailed signal analyses for the two conductivity-probes data are presented in Appendix C.

4.3.4.5 Flow visualization

Flow visualization for all the experimental tests was undertaken simultaneously with the quantitative measurements. The flow regime that occurred for each combination of air and water, for both straight and *helical pipes,* are reported in section 4.3.1. A summary of some unique characteristics of the flows in both configurations (i.e. straight and *helical pipes*) are presented in Table 4-19.

It was observed that, by virtual of the design of *helical pipes*, swirl was generated which encouraged radial mixing of air and water. In particular, when gas and liquid mixture flow occurs, the flow pattern in the straight pipe was stratified where air (lighter phase) travels on top of the liquid, whereas air tends to travel at the centre of the pipe in *helical pipe* flows and stratified flow did not occur instead bubbly flow ensued.

4.3.5 Evaluation of friction factor

4.3.5.1 Single-phase

Friction factor for single-phase (water) flow was evaluated for both straight and *helical pipes*. Equation 4-6 was used to calculate the friction factor.

$$f = \frac{2d\Delta P}{\rho l v^2} \qquad \textbf{Equation 4-6}$$

where

f is the friction factor

d is the pipe's internal-diameter

ΔP is the pressure drop

ρ is the fluid's (water) density

l is the pipes' length

v is the fluid's (water) velocity

Table 4-20 shows the calculated values of the friction factor and Reynolds number at the studied liquid velocities.

Pipe	Liquid velocity, V_L (ms^{-1})	Friction factor	Reynolds number (10^3)
Helical	1.0	0.1290	50
	1.5	0.0902	76
	2.0	0.0716	101
	2.5	0.0555	126
	3.0	0.0472	151
Straight	1.0	0.0419	51
	1.5	0.0281	76
	2.0	0.0265	100
	2.5	0.0245	126
	3.0	0.0244	150

Table 4-20: Single-phase friction factor and Reynolds number values

Figure 4-53 shows the relationship between the friction factor and Reynolds number for the single-phase flow at different liquid velocities for the two pipes (namely straight and *helical*). At all the liquid velocities studied (1.0 ms^{-1}, 1.5 ms^{-1}, 2.0 ms^{-1}, 2.5 ms^{-1} and 3.0 ms^{-1}), friction factor for the *helical pipe* is higher than friction factor for the straight pipe. This confirms the result obtained from the 25.4 mm (preliminary experiments) single-phase experiments presented in chapter 3.

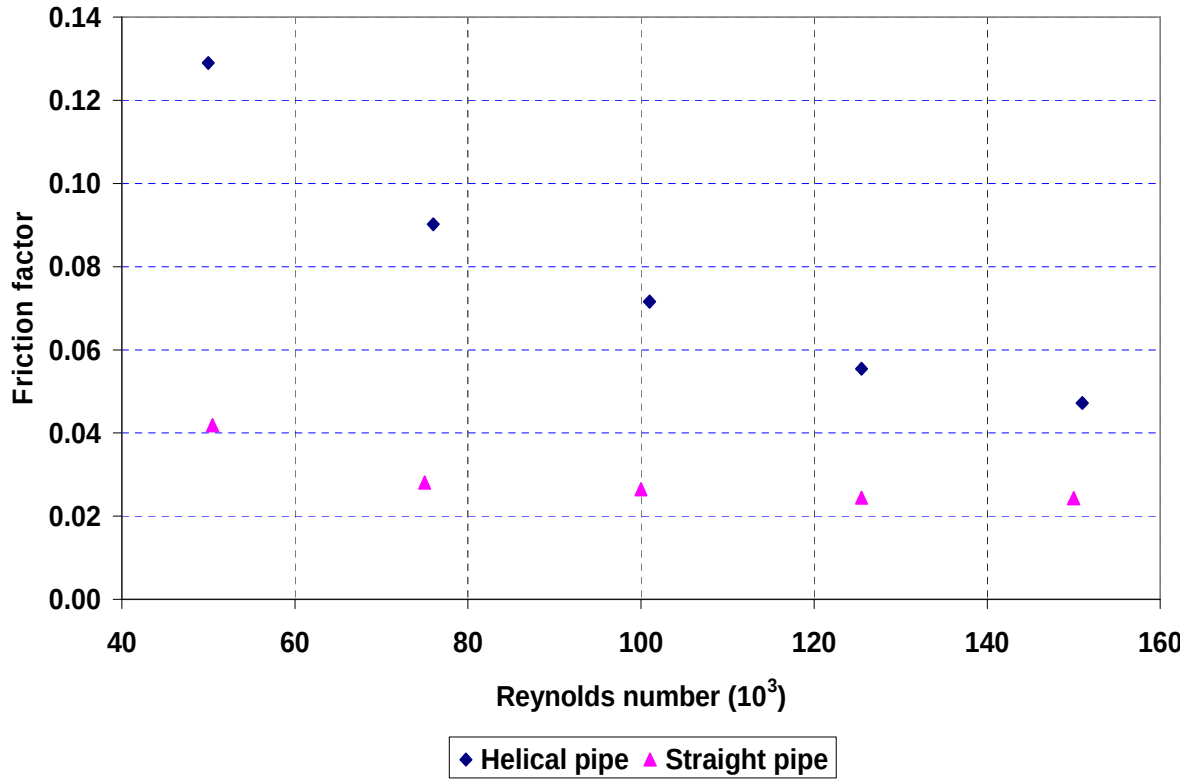

Figure 4-53: *Helical* and straight pipes' single-phase friction factor versus Reynolds number chart (V_L= 1.0, 1.5, 2.0, 2.5 and 3.0 ms^{-1})

4.3.5.2 Two-phase

Friction factors for different two-phase flow patterns for both straight and *helical* pipes were calculated using Equation 4-7 after Brill and Beggs (1991). In evaluating the two-phase flow friction factor, a homogeneous flow was assumed. That is, the gas and liquid were assumed to be travelling at the same velocity in the pipe. The flow regime was also not considered. The two-phase density was calculated based on this no-slip assumption

$$f_n = \frac{1}{\left[2\log\left(N_{\mathrm{Re}\,n} \Big/ \left(4.5233\log N_{\mathrm{Re}\,n} - 3.8215\right)\right)\right]^2} \qquad \textbf{Equation 4-7}$$

$$N_{\mathrm{Re}\,n} = \frac{\rho_n V_m d}{\mu_n} \qquad \textbf{Equation 4-8}$$

$$\rho_n = \rho_L \lambda_L + \rho_G (1 - \lambda_L)$$ **Equation 4-9**

$$V_m = V_{SL} + V_{SG}$$ **Equation 4-10**

$$\mu_n = \mu_L \lambda_L + \mu_G \lambda_G$$ **Equation 4-11**

where

f_n is the no-slip friction factor

$N_{\mathrm{Re}\,n}$ is the Reynolds number

ρ_n is the two-phase density

ρ_L is the liquid density

ρ_G is the gas density

V_m is the mixture velocity in the two-phase flow

V_{SL} is the liquid superficial velocity

V_{SG} is the gas superficial velocity

λ is the non-slip liquid holdup

The ratio of the two-phase friction factor to no-slip friction factor was calculated from Equation 4-12 after Brill and Beggs (1991).

$$\frac{f_{tp}}{f_n} = e^s$$ **Equation 4-12**

$$s = \frac{[In(y)]}{\left\{-0.0523 + 3.182 In(y) - 0.8725 [In(y)]^2 + 0.1853 [In(y)]^4\right\}}$$ **Equation 4-13**

$$y = \frac{\lambda_L}{H_L{}^2}$$ **Equation 4-14**

where

f_{tp} is the two-phase friction factor

e^S is the empirically determined 2-phase multiplier

y is the ratio of non-slip liquid holdup to slip liquid holdup

H_L is the slip liquid holdup

Equations 2-44 and 2-47 were therefore used to calculate the two-phase density and viscosity respectively. The two-phase Reynolds number Re_M was also defined by equation 2-50. The liquid holdup values from the conductivity probes were also used to calculate the two-phase density terms.

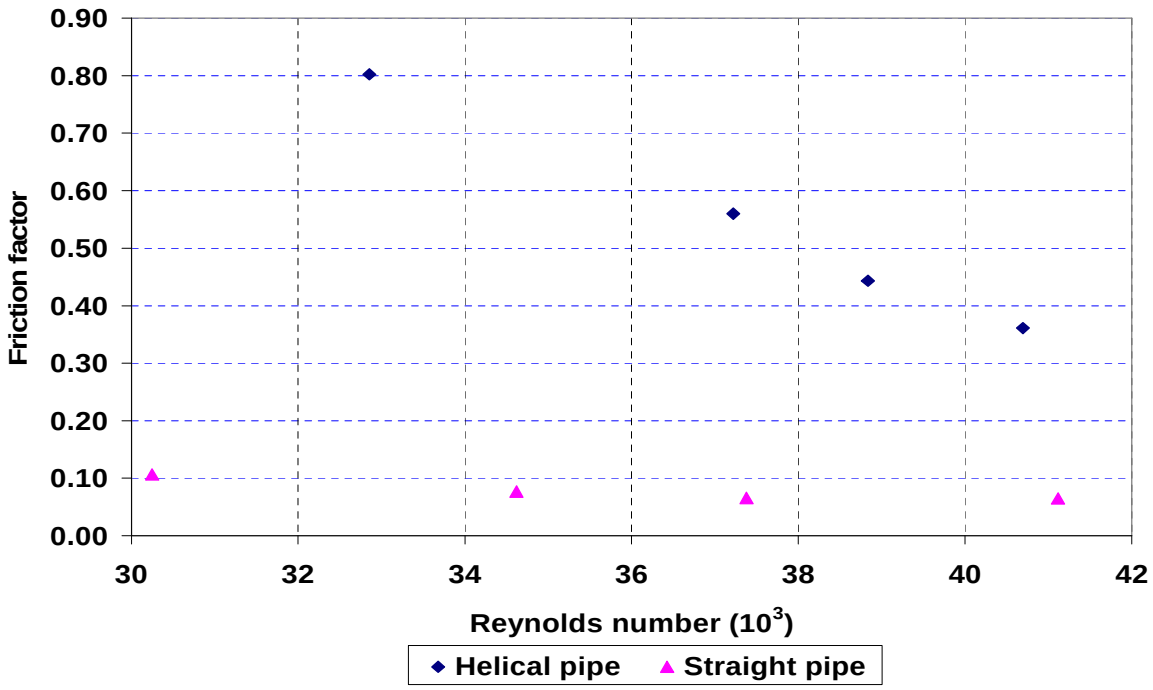

Figure 4-54: Friction factor versus Reynolds number chart at V_{SL} = 0.15 ms^{-1}

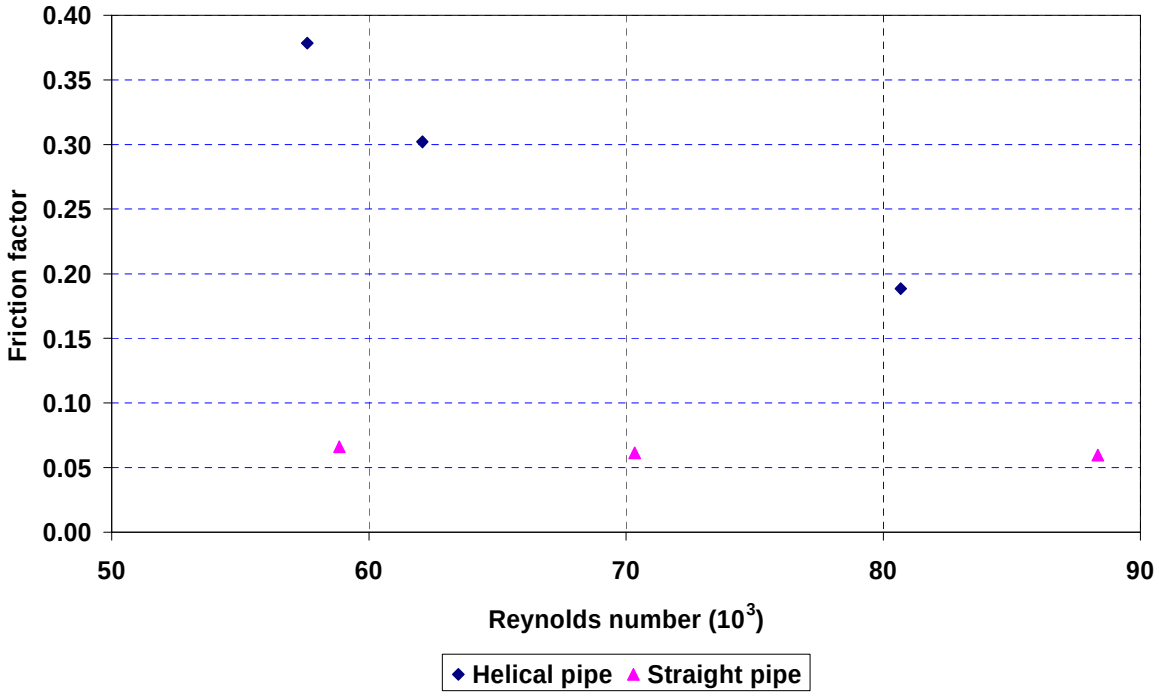

Figure 4-55: Friction factor versus Reynolds number chart at V_{SL} = 0.5 ms^{-1}

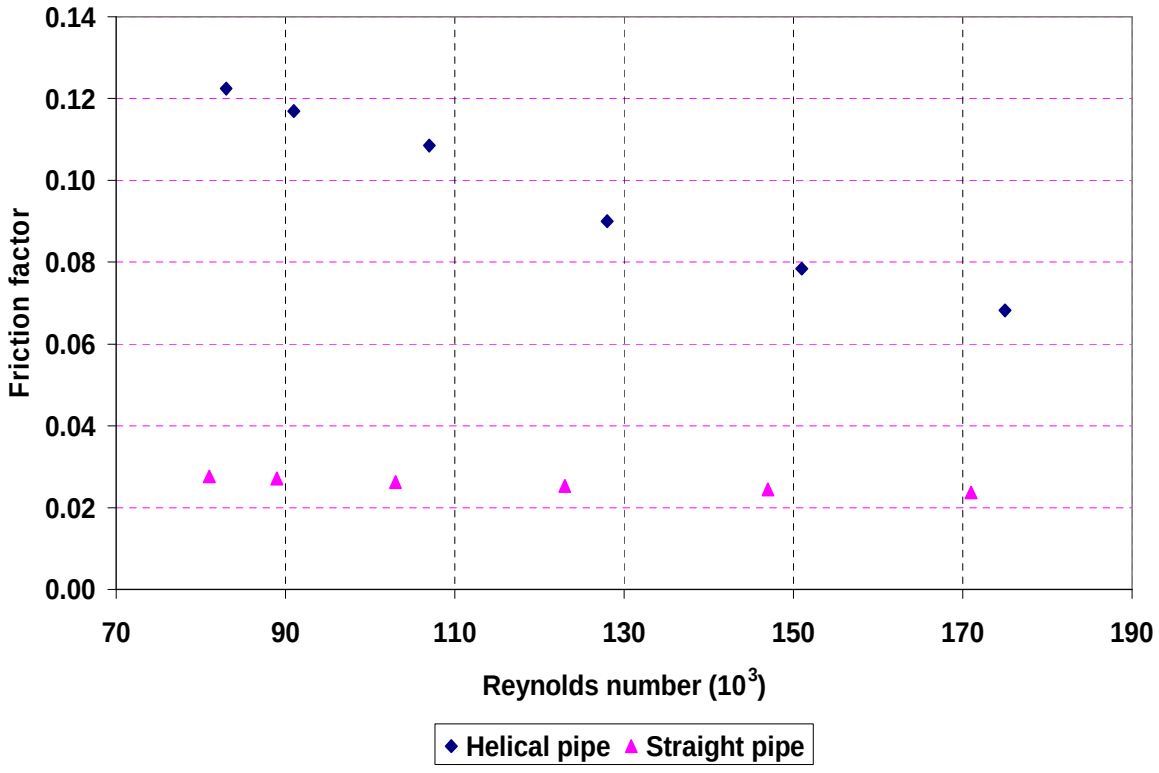

Figure 4-56: Friction factor versus Reynolds number chart at V_{SL} = 1.5 ms^{-1}

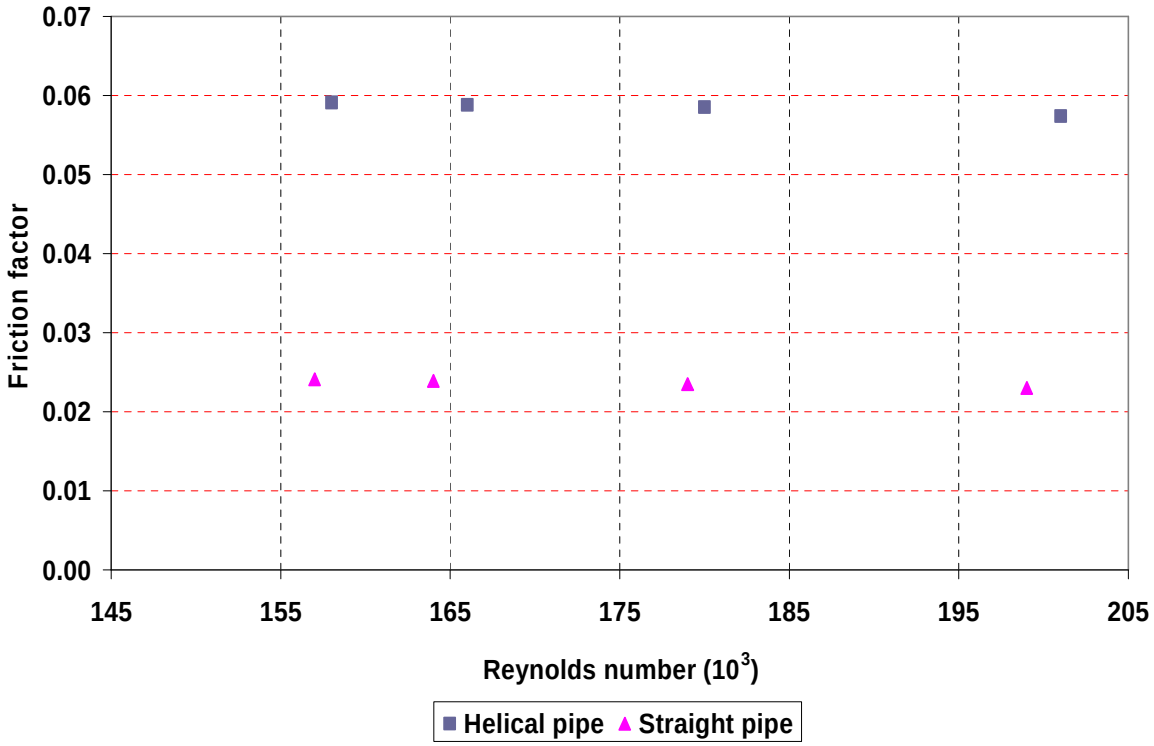

Figure 4-57: Friction factor versus Reynolds number chart at V_{SL} = 3.0 ms^{-1}

Figures 4-54 to 4-57 show the relationship between friction factor and Reynolds number at different flow patterns for the two-phase flow. Again, at all the gas and liquid superficial velocities studied, the friction factor for the *helical pipe* is higher than friction factor for the straight pipe. This also confirms the results obtained from both 25.4 mm (preliminary experiments) single-phase experiments presented in chapter 3 and the single-phase experiments for this 0.05 m internal-diameter pipes. However, the friction factor gaps between the straight and *helical pipes* in both the single-phase and the two-phase results studied in this chapter (for the 0.05 m internal-diameter pipes) have been noticed to be much higher whereas in the results of the 25.4 mm internal-diameter single-phase experiments, the values between the two pipes (straight and *helical*) are very close to each other.

Another feature of the friction factor charts discussed for both single-phase and two-phase flows (Figures 4-53, 4-54 to 4-57, 4-58 and 4-59) reported in this

chapter is that as the gas and liquid superficial velocities increase, the friction factor values reduce, particularly for the *helical pipe*. The friction factor also seems to remain constant at high fluid superficial velocities. This was particularly observed for the dispersed bubbly flow regime. See Figure 4-59 for the straight pipe and Figure 4-57 for the *helical pipe*.

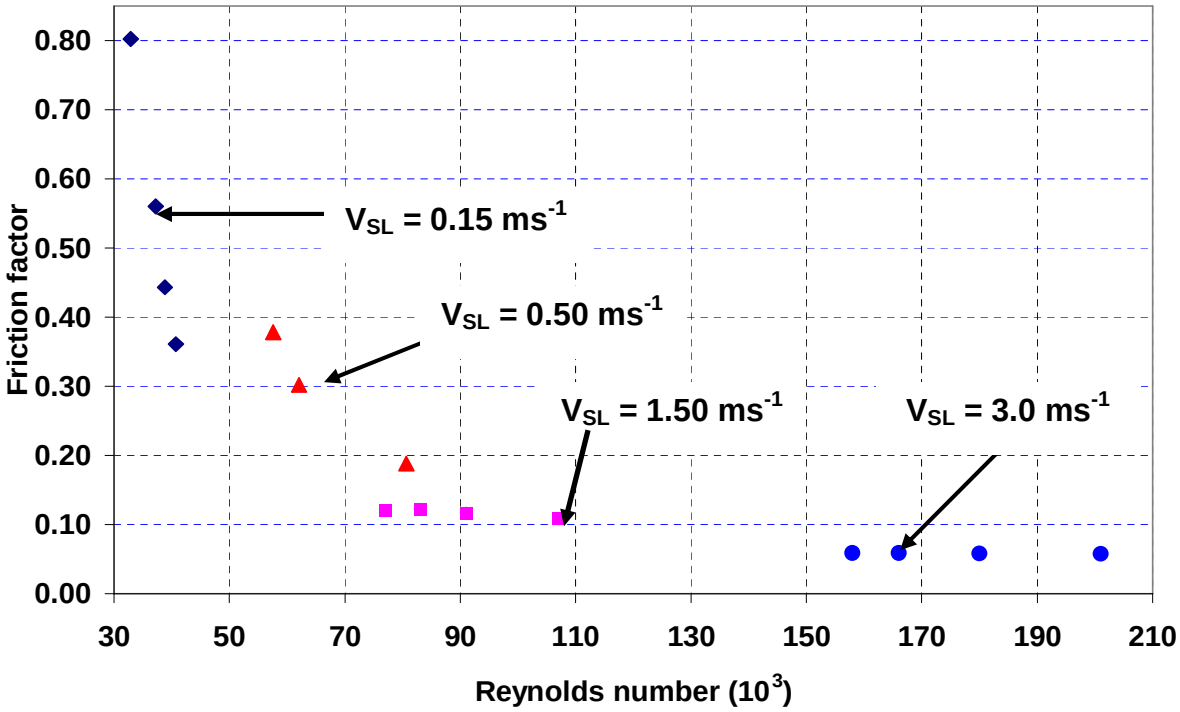

Figure 4-58: *Helical pipe* friction factor versus Reynolds number chart (V_{SL}= 0.15, 0.5, 1.50 and 3.0 ms^{-1})

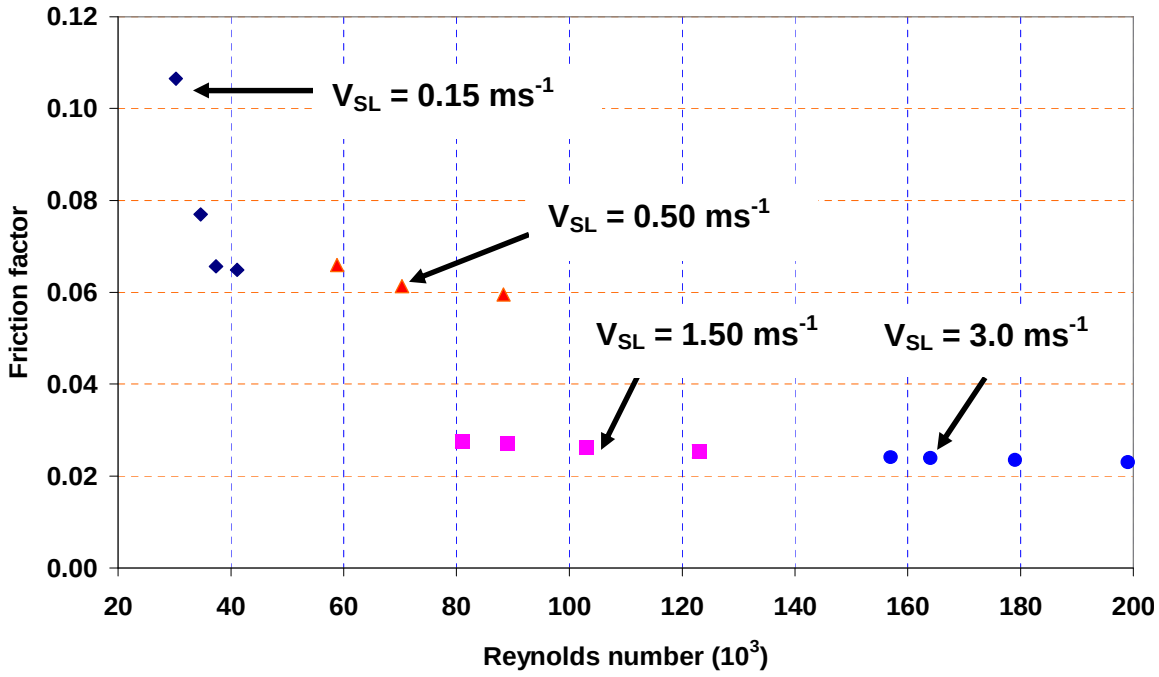

Figure 4-59: Straight pipe friction factor versus Reynolds number chart (V_{SL}= 0.15, 0.5, 1.50 and 3.0 ms^{-1})

4.3.6 Comparison of experimental values of liquid holdup with theoretical values

The measured experimental values of the liquid holdup obtained by the conductivity probes were compared with theoretical values at liquid superficial velocities of 0.15 ms^{-1}, 0.5 $ms^{-1,}$ 1.5 ms^{-1}, and 3.0 ms^{-1} and at various gas superficial velocities. Equation 4-15 after Beggs & Brill (1991) was applied to calculate the theoretical values.

$$\lambda_L = \frac{V_{SL}}{V_{SL} + V_{SG}} \qquad \textbf{Equation 4-15}$$

A comparison of the experimental and theoretical results is presented in Table 4-21.

Pipe	V_{SL} (ms^{-1})	V_{SG} (ms^{-1})	Experimental average (probes A+B): liquid holdup value	Theoretical liquid holdup value	% Error
Straight	0.15	0.60	0.29	0.20	30.71
	0.50	0.15	0.53	0.77	-44.74
	1.50	1.0	0.48	0.60	-25.0
	3.01	1.01	0.60	0.75	-24.22
Helical	0.15	0.63	0.25	0.19	23.80
	0.50	0.16	0.50	0.76	-51.40
	1.50	1.0	0.61	0.59	2.70
	3.0	1.04	0.80	0.74	6.94

Table 4-21: Experimental and theoretical error comparison for holdup values

4.3.7 Comparison of experimental results with published correlations

The experimental results have been compared with some of the published correlations discussed in this thesis.

4.3.7.1 Single-phase

Figure 4-60 shows a comparison of single-phase friction factors obtained from these *helical pipe* (internal-diameter 0.05m) experiments. Published correlations from Czop et al. (1994), Ito (1959), Kubair & Varrier (1961/1962), Mishra & Gupta (1979) and White (1932) have been compared with the experimental results.

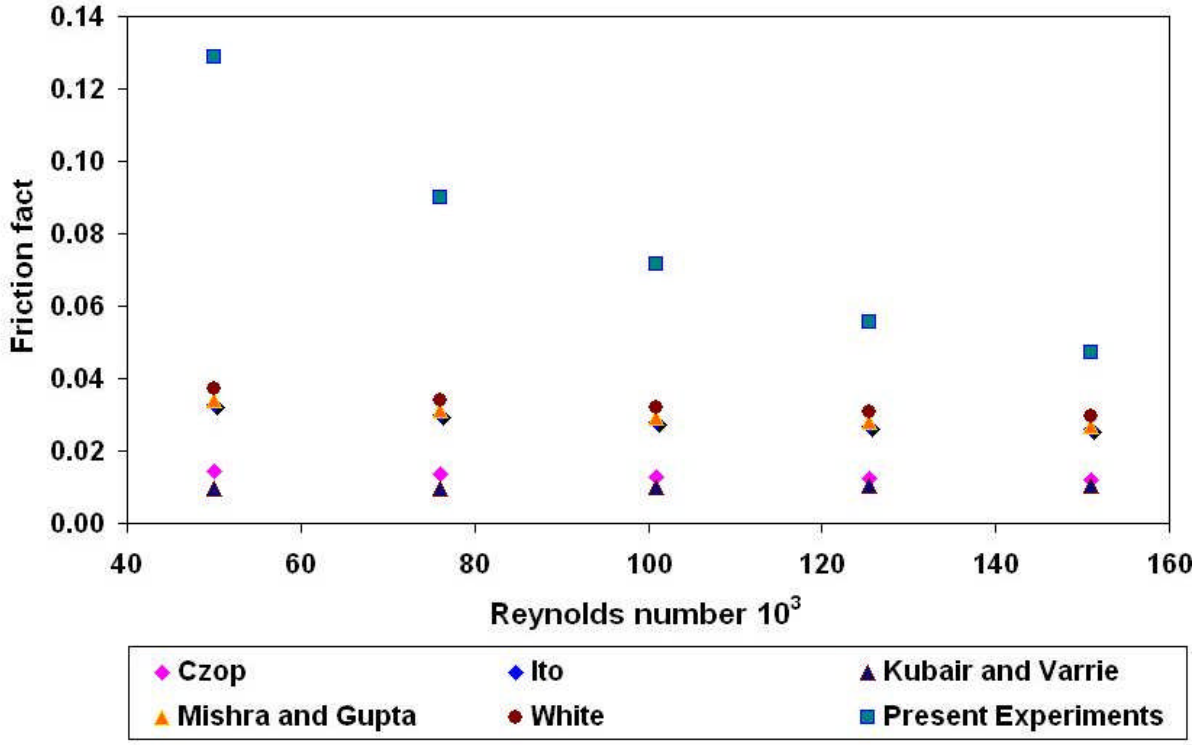

Figure 4-60: Comparison of single-phase friction factor with correlations

Czop and Kubair & Varrier correlations are very much lower than the experimental results. Ito, Mishra & Gupta and White correlations although are higher than Czop and Kubair & Varrier correlations but also lower than the experimental results. The experimental results become closer to the correlations as the Reynolds numbers increase.

4.3.7.2 Two-phase

Figure 4-61 shows a comparison of Lockhart and Martinelli parameter (**X**) with two-phase pressure drop multiplier (ϕ). The measured experimental values of the pressure drop for single-phase (water) at liquid superficial velocities of 0.5 ms^{-1}, 1.5 ms^{-1}, and 3.0 ms^{-1} were used to calculate the Lockhart and Martinelli parameter (**X**) and the two-phase multiplier (ϕ). These three liquid superficial velocities were selected to represent water flows at low, medium and high superficial velocities.

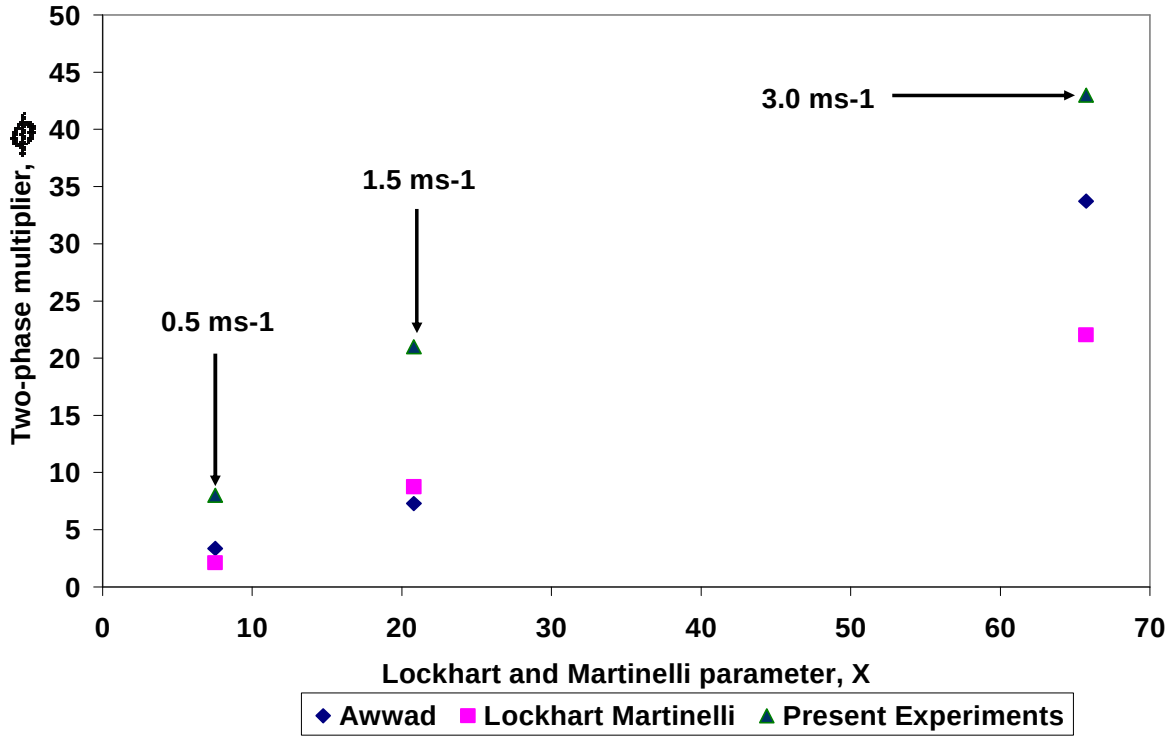

Figure 4-61: Comparison of two-phase pressure drop with correlations

Awwad et al. (1995a) and Lockhart and Martinelli (1949) correlations were compared with the present experimental results. Equation 2-171 (quoted below)

$$\phi_L = \left(\frac{X}{9.63F_d^{\,0.61}}\right)\left(1+\frac{12}{X}+\frac{1}{X^2}\right)^{\frac{1}{2}}$$

was used to calculate **Φ**. In evaluating the Lockhart and Martinelli parameter, **X** equation 2-75 (also quoted below) was applied.

$$X = \sqrt{\frac{-\Delta P_L}{-\Delta P_G}}$$

As shown in Figure 4-61, at all the liquid superficial velocities, the experimental results are higher than the two correlations. At liquid superficial velocity of 0.5 ms^{-1}, the experimental result and the correlations are closer than at 1.5 and 3.0 ms^{-1} and Lockhart and Martinelli correlation is the lowest. However, at 1.5 ms^{-1} liquid superficial velocity, Awwad correlation is the lowest and at the liquid superficial velocity of 3.0 ms^{-1}, Lockhart and Martinelli correlation is the lowest.

4.4 Conclusions

The following conclusions can be drawn from the experimental results presented in this chapter:

- The pressure drop is higher in the *helical pipe* than in the straight pipe.
- Liquid holdup increases as the pressure drop decreases in both pipes.
- At low liquid superficial velocities, liquid holdup is slightly higher in the straight pipe than in the *helical pipe*. But at relatively higher superficial velocities, the liquid holdup is higher in the *helical pipe* than in the straight pipe.
- Slug flow occurred in the straight pipe at certain superficial velocities of air and water, whereas at the same superficial velocities of air and water, slug flow did not occur in the *helical pipe* - instead bubbly flow ensued.
- Stratified flow occurred in the straight pipe at very low superficial velocities of air and water. But at the same very low superficial velocities of air and water, stratified flow did not occur in the *helical pipe* - instead bubbly flow occurred.
- The friction factor is higher in the *helical pipe* than in the straight pipe for both single-phase and two-phase flows.

Chapter 5

5 Applications of *helical pipes*

5.1 Severe slugging

One important area of application of *helical pipe*s discovered during the course of this research study is severe slugging mitigation. Severe slugging can be defined as a highly undesirable flow behaviour that has to be avoided in any multiphase flow transport system. It is caused by instabilities of the flow in a pipeline: it is a phenomenon that involves the build-up of liquid slugs equal to or longer than one riser length. Its formation normally consists of four phases, viz: slug formation, slug production, blow-out, and liquid fall back. It should be noted that cyclic flow instability in the riser with the build-up of slugs shorter than one riser height can also occur, but these are normally of a less severe nature because a complete blockage of the gas does not occur. Two types of slugging do commonly occur in multiphase flows. The first is hydrodynamic slugging, which normally occurs in the horizontal part of the flow line. It may also occur in wells and risers. It is usually a frequently appeared slug but relatively short. The inlet separator of any process plant will, in most cases, handle the hydrodynamic type of slugging, because the amount of liquid in the slug is small compared with the free volume in the separator. The second type is riser slugging, which can be generated by gravity forces. Riser slugging contains a lot of liquid and can represent a major challenge for the downstream processing systems. It has been observed that, when production rates vary, separator levels and compressor flows oscillate.

Severe slugging is also a phenomenon which may occur in systems where a horizontal pipeline segment with a downward inclination is followed by vertical

segment (riser) regardless of the water depth. For such a system, at low liquid and gas rates, liquid accumulates in the riser and the pipeline, so blocking the passage of the gas flow. This results in a compression of the gas in the pipeline. As air continues to enter the flowline, and the pressure could not increase further, the air volume in the flowline then pushes the air-water interface towards the riser base. When the interface reaches the base of the riser, it triggers the gas blowdown resulting in a rapid decrease in riser pressure difference.

Severe slugging will cause periods of no liquid and gas production in the separator followed by very high liquid and gas flow rates. This phenomenon is highly undesirable due to the large pressure and flow rate fluctuations it causes. The large liquid production might cause overflow and shut down of the separator. Fluctuations in gas production might cause operational problems during flaring, and the high pressure fluctuations might reduce the production capacity of the field. Increased mechanical stresses may occur as a result of high velocities and the highly fluctuating liquid inventory in the riser. This can also reduce the operating life of the riser. Increased average riser base pressure usually occurs due to the severe slugging formation. This leads to increases in backpressure, which also reduces the flow of hydrocarbon products from the well. The increase in backpressure in some cases may be sufficient to totally kill the well.

Many studies have been carried out in the last couple of decades, to achieve an understanding of the phenomenon and to develop mitigation methods to overcome severe slugging. Yocum (1973) identified several severe slugging control methods that are still being considered today. These include the reduction of the line diameter; the splitting of the flow into dual or multiple streams; gas injection into the riser; the use of mixing devices at the riser base; as well as choking and back-pressure increase. He observed that increased back-pressure could eliminate severe slugging, but would seriously reduce the

flow capacity. He also claimed that choking would cause severe reductions in the flow capacity.

Contrary to Yocum's claim, Schmidt (1977) and Schmidt et al. (1979) noted that severe slugging in a pipeline-riser system could be eliminated or minimized by choking at the riser top, which will eventually cause little or no changes in flow rates and pipeline pressure. Schmidt also indicated that the elimination of severe slugging could be achieved by gas injection, but concluded that it is not an economically viable option due to the costs of a compressor to pressurize the gas for injection, and of the piping required to transport the gas to the base of the riser.

Pots et al. (1985) investigated the use of gas injection as an elimination method of severe slugging. Their conclusion was that the severity of the slugging cycle was considerably lower for riser injection of about 50% inlet-gas flow. It was observed that severe slugging did not completely disappear even with 300% injection. Taitel (1986) provided a theoretical explanation for the success of choking to stabilize the flow as reported by Schmidt (1977). Jansen (1996) investigated different elimination methods such as back-pressure increase, choking, gas-lifting and combination of choking and gas-lifting. He then proposed the stability and the quasi-equilibrium models for the analysis of the above elimination methods. He presented the following experimental observations: a very high back-pressure was required to eliminate severe slugging; careful choking was needed to stabilize the flow with a minimal back-pressure increase; large amounts of injected gas were needed to stabilize the flow with the gas-lifting method and the choking and gas- lifting combination was the best elimination method. The stability criteria for choking and gas-lifting were developed by modifying the original Taitel et al. (1990) model. Hill (1989 and 1990) described the riser base gas-injection tests performed at the S.E. Forties field to eliminate severe slugging. He concluded that gas injection was shown to reduce the extent of severe slugging. He also stated that the condition for eliminating severe slugging was to bring the flow pattern in the riser to

annular flow by preventing liquid accumulation at the riser base. Therefore, large amount of injection gas was needed to completely stabilize the flow.

Kaasa's (1990) proposal for eliminating severe slugging involved a second riser to connect the pipeline to the platform. A downward-sloping pipeline acted like a slug catcher because the prevailing flow pattern is mostly stratified at low flow rates. The second riser was placed at such a point on the pipeline that all the gas was diverted to it and the original riser transported all the liquid. The second riser was equipped with a pressure control valve to control the pressure fluctuations. This method has two disadvantages namely: the original riser will be almost full of liquid so imposing a considerable back-pressure on the system, which can result in a significant reduction in production capacity. Secondly, the installation of second riser was not economically viable.

McGuinness and Cooke (1993) undertook a field trial in St. Joseph field, Sabah, Malaysia operated by Shell. The severe slugging problem was observed when a new satellite field was brought on stream with its increased pipeline volume. Severe slugging resulted in higher back-pressure and reduced the production capacity of the system. Their solution to the problem was the separation of the fluids at a satellite platform and transporting the liquid and gas in separate flow lines to the main production platform. A minimum back-pressure was achieved by the utilization of a surge vessel operating at atmospheric pressure for the liquid stream rather than a low-pressure separator.

Wyllie and Brackenridge (1994) proposed a retrofit solution to reduce the severe slugging effects. Their solution requires a small-diameter pipe insert into the riser, thereby creating an annulus that can be used for gas injection. This was initially considered to be a good retrofit solution when there was no provision for severe slugging on the existing riser. But, on the other hand, conceptually, it was a restriction to the flow that might pose problems for operations such as pigging. Wyllie (1994) filed a patent application in the UK for a very similar device. The modified device was retrievable, but still required a

complimentary operation for the retrieval. It was claimed these variable-diameter pigs could pass through it. But no details have been given on how to size and design such a device.

Barbuto (1995) proposed a different approach to eliminate severe slugging. The proposal involved the pipeline and riser being connected to each other to transmit the pipeline gas to the riser at a predetermined position. This point was said to be at one-third of the total riser height from the riser base. Different control schemes on the by-pass line were discussed. The main theme of this technique was to keep the pipeline pressure under control.

Hollenberg et al. (1995) proposed a topside flow-control system to eliminate severe slugging. The principle of the system was to keep the mixture's flow-rate constant throughout the operation by means of a control valve. The authors realized that it was not possible to utilize the control valve in this way because of difficulties in measuring the two-phase mixture velocity, which was the parameter of interest for achieving the required control. They solved the problem by replacing the control valve with a small control separator so allowing (i) the separation of phases and (ii) the measurements of the flow rates. They conducted laboratory tests using an experimental facility of 2 inch internal diameter, 328 feet long pipeline and with a 54 feet high riser. Although their control system was shown to work for all the cases investigated, the riser's base-pressures were tripling which indicated that a tremendous back-pressure occurred upstream.

Courbot (1996) proposed an automatic-control scheme to prevent severe slugging in a 16-inch multiphase pipeline. The riser base pressure was kept constant by a valve upstream of the separator to control the flow. The field proved that the control scheme was a success, although considerable increases at the riser base pressure were observed. Courbot considered other severe slugging elimination techniques. The only other viable alternative method he considered was gas-lifting, which was found to be expensive due to high capital

expenditures (CAPEX). Controlling the separator pressure or separator fluid level was found to be ineffective as a result of simulation studies performed with the OLGA software.

Hassanein and Fairhurst (1998) presented the challenges in mechanical and hydraulic aspects of riser design for deepwater developments. They pointed out that flow-rate variations would be larger due to the bigger hydrodynamic-slugs expected owning to the larger flow-line diameters. Besides, the longer flow lines combined with the risers may increase the possibility of severe slugging. The larger system volume can lead to more severe surges during transient operations. Severe slugging, if allowed, is expected to create very large flow-rate variations. They have suggested Riser Base Gas Lift (RBGL) and foaming as viable methods for severe slugging elimination.

Johal et al. (1997) pointed out that the Riser Base Gas Lift technique may cause additional problems due to Joule-Thompson cooling of the injected gas. Gas acts like a heat sink and lowers the temperature of the fluids making the flow conditions more susceptible for the wax and hydrate formation-problems. Therefore, operators would need either to heat the gas before injecting or use chemicals to prevent the formation of paraffin and hydrates. They proposed an alternative technique, called Multiphase Riser Base Lift (MRBL), for deepwater developments. MRBL is based on the idea of diverting the nearby multiphase flow-stream to the pipeline-riser system which is experiencing severe slugging. This will help to alleviate the severe slugging problem without exposing the system to other potential problems. A proof-of-concept study was conducted using PipeLine Analysis Code (PLAC). The authors claimed that using MRBL would save up to $8,000,000.00 in CAPEX alone compared with using a conventional Riser Base Gas Lift (RBGL). Song and Kouba (2000) recently proposed sub-sea separation of gas and liquid as a method of prevention of severe slugging. After separation, the gas and liquid are transported to a separator. A liquid pump is used to overcome the hydrostatic head, thereby

preventing a capacity reduction due to back-pressure. They also conducted a proof-of-concept study using OLGA software.

5.2 Severe slugging Formation

Severe slugging formation is a process involving four stages. Figures 5-1 to 5-4 describe a typical severe slugging formation cycle. The basic unrestricted (no elimination) severe slugging cycle has been studied and its behaviour explained by several investigators (Yocum 1973, Schmidt et al. 1980, Boe 1981; Schmidt et al. 1985; Taitel et al. 1986, Fabre et al. 1987; Fuchs 1987; Pots et al. 1987; 1990).

Stage 1 – Slug generation: Figure 5-1 shows the first stage of a severe slugging cycle. This is the beginning of the formation of a typical severe slugging incident. During this stage, liquid coming from the pipeline accumulates at the riser base and the base of the riser is blocked.

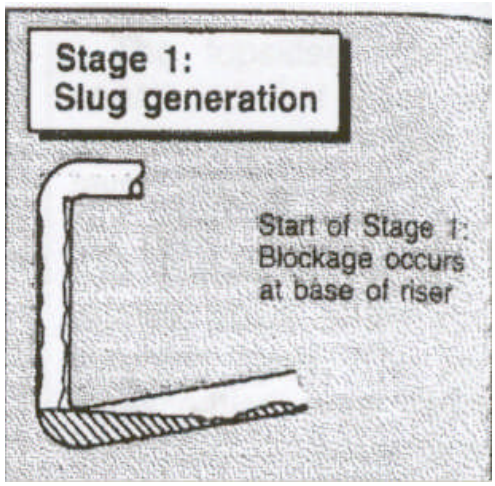

Figure 5-1: Slug Generation Hill (1990)

Stage 2 – Slug Production: This is the second stage of severe slugging formation, when the liquid level in the riser increases and the liquid slug reaches the top of the riser. As the gas passage is blocked, the pressure in the flow line

increases. The riser pressure is also at its maximum value and also remains constant and the gas in the pipeline tends to push the liquid into the separator. When the liquid reaches the top of the riser, there will be a period of relatively-steady production and the hydrostatic pressure at the base of the riser would also remain constant. This stage is shown in Figure 5-2

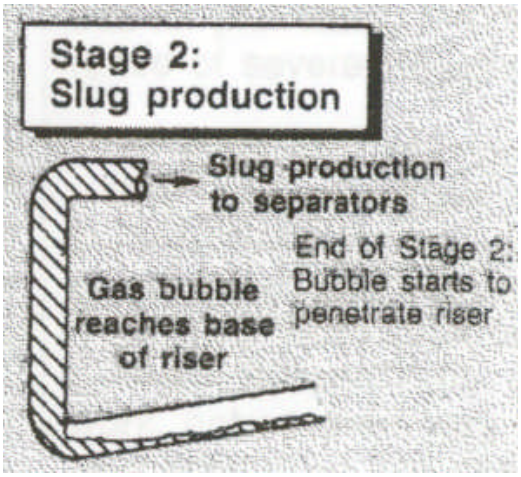

Figure 5-2: Slug Production Hill (1990)

Stage 3 – Bubble Penetration: The third step begins when the incoming gas pushes the gas/liquid interface in the flowline towards the base of the riser and the gas starts to penetrate the riser. As the gas/liquid interface reaches the riser base, the gas continues to push the liquid into the riser proper, as shown in Figure 5-3. A series of bubbles are formed and accelerate along the riser. The bubbles then displace further liquid from the riser, expanding and thus reducing the pressure difference over the riser.

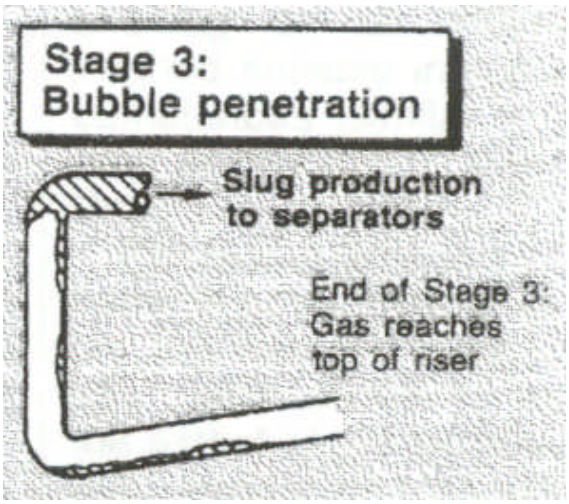

Figure 5-3: Slug Penetration Hill (1990)

Stage 4 – Gas Blowdown and Liquid Fallback: This last stage of severe slugging is gas blowdown and liquid fallback. The drop in pressure difference over the riser during the third stage reduces the riser's base-pressure. When the pressure drops to below a certain level, the gas will no longer have sufficient energy to carry the liquid phase and induce acceleration of the pipeline gas into the riser. This, in turn, increases the rate of change in the pressure difference, so effectively feeding back into the gas inflow process. In this way, there is a spontaneous sweep-out of the liquid slug and depressurisation or gas blowdown of the pipeline. Liquid will then reverse down the riser causing an accumulation and blockage at the riser base. A new severe slugging cycle then begins again. This stage is characterised by a large liquid delivery, followed by a rapid gas-delivery, and carrying the remaining liquid in an annular flow.

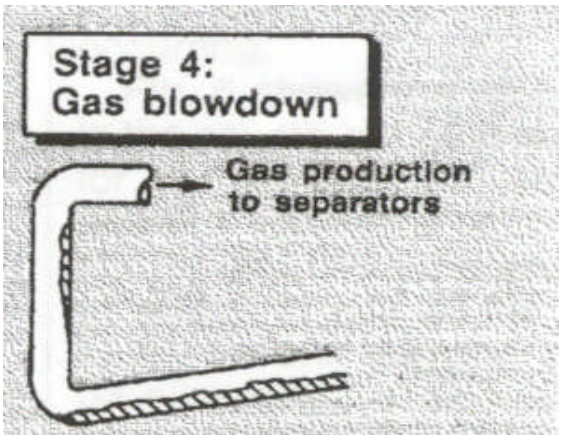

Figure 5-4: Gas Blowdown Hill (1990)

It must be noted that, towards the end of the gas blowdown period, the gas flow into the separator decreases. The reduction in momentum transfer is not sufficient to support the upward motion of the liquid on the riser walls, which begins to fall under gravity and in counter-current conditions into the riser base. The liquid then accumulates, so blocking the riser base to the passage of gas and thus initiating the formation of the next slug. Figure 5-4 shows this stage of severe slugging formation.

5.3 Severe slugging Criteria

The question of when will severe slugging occur has been answered by the development of steady-state models. These seek to model a particular process required for severe slugging and hence predict the likelihood of severe slugging and, as such, the models provide criteria for severe slugging. The results of the criteria can be depicted as a region of a flow regime map which indicates the region of severe slugging.

The work of Schmidt et al. (1980) formed the basis of much pertinent early studies. They suggested that, for severe slugging to occur, the following three conditions were required:

- a pipeline laid with a downward inclination

- stratified flow in the pipeline
- the rate of hydrostatic-head accumulation at the riser base being greater than the rate of pipeline's gas-pressure increase.

5.3.1 The stratified-flow criterion

Schmidt et al. (1980) asserted that for severe slugging to occur, stratified flow must be present in the main pipeline. Previous work of Taitel and Duckler (1976) developed a criterion for the onset of severe slugging phenomenon. They developed a criterion for stratified flow in horizontal and near horizontal pipelines. Many authors, including Boe (1981), Pots et al. (1985) and Taitel (1986) used this criterion as it was not explicitly developed as a severe slugging criterion. Using the inviscid Kelvin-Helmholtz theory (Milne-Thompson, 1960), the condition for small wave growth between parallel plates was:

$$U_{SG} > \left[\frac{g(\rho_L - \rho_G)h_G}{\rho_G}\right]^{\frac{1}{2}} \qquad \textbf{Equation 5-1}$$

where U is the velocity, ρ the density and h the height occupied by a given phase between the plates. The subscripts L and G refer to the liquid and gaseous phases respectively. Below the gas velocity prescribed by Equation 5-1, stratified flow occurs and hence severe slugging is possible in the pipeline/riser.

Equation 5-1 was also extended to flows in a circular cross-section pipeline, taking into account the suppression of the wave formation by gas acceleration over the wave crest. This yields a criterion for stratified flow:

$$U_{SG} < C_2\left[\frac{(\rho_L - \rho_G)g\cos\beta A_G}{\rho_G dA_L / dh_{LP}}\right]^{\frac{1}{2}} \qquad \textbf{Equation 5-2}$$

where $C_2 \approx A_G / A_L$, A is the flow area, β is the angle of inclination and h is the height of the phase occupying the pipe cross-section. The change in liquid flow-area with liquid height dA_L / dh_L is given by Taitel and Duckler (1976) as:

$$\frac{dA_L}{dh_L} = D\sqrt{1-\left(2\frac{h_L}{D}-1\right)^{\frac{1}{2}}} \qquad \textbf{Equation 5-3}$$

Goldzberg and Mckee (1987) considered the formation of slugs in a pipeline through the sweep-out of accumulated liquid. Their approach was centred on a criterion for wave growth to form a slug as the gas accelerated over the interface. The analysis of the Bernoulli equation over the surface became reduced to Equation 5-2. A plot of this criterion is shown in Figure 5-5. The region of stratified flow is the region below the transition line as indicated on the graph.

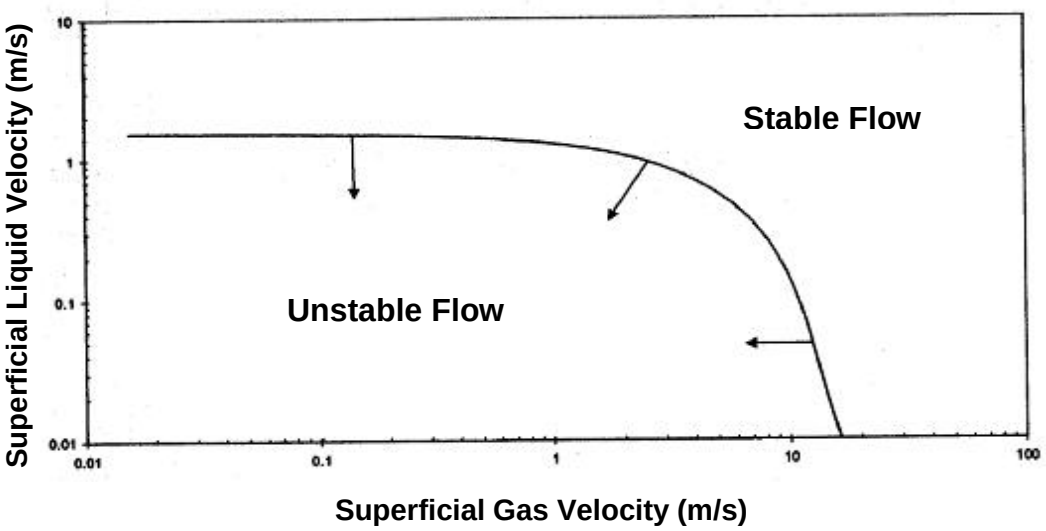

Figure 5-5: Stratified-Flow Criterion: Taitel and Duckler (1976)

5.3.2 The Boe Criterion

A criterion for severe slugging to ensue was developed by Boe (1981a), based on the assertion of Schmidt et al. (1980) that the rate of head accumulation at

the riser base must be greater than the rate of pipeline gas-pressure increase for severe slugging to form. This may be summarised as:

$$\frac{\partial(\Delta P_{HYD})}{\partial t} > \frac{\partial(P_P)}{\partial t} \qquad \textbf{Equation 5-4}$$

where P is the pressure and t the time, the subscripts HYD and p refer to hydrostatic and pipeline pressures respectively. Based upon constant inlet flowrates, a pressure balance over the riser and the gas mass balance in the pipeline, the criterion, Equation 5 - 4 was resolved to give:

$$U_{SL} \geq \frac{P_P}{\rho_L g(1-\varepsilon_L) L \sin\alpha} U_{SG} \qquad \textbf{Equation 5-5}$$

It must be noted here that the inclination α of the riser is accounted for: with a vertical riser, sin α = 1. In the initial work of Boe, the no-slip condition for the pipeline liquid holdup was used as:

$$\varepsilon_L = \frac{U_{SL}}{U_{SL} + U_{SG}} \qquad \textbf{Equation 5-6}$$

Combining Equations 5-5 and 5-6, yields a straight line above which severe slugging occurred as shown in Figure 5-6. Other correlations for liquid holdup yielded an envelope region, where severe slugging would take place. The most common correlation employed is that suggested by Taitel (1986), using liquid velocity to calculate first the single-phase gas pressure drop and then relating this to the liquid holdup. The Boe criterion, using this correlation, is shown in Figure 5-6. The arrows show the region of unstable flow to the left of the transition lines.

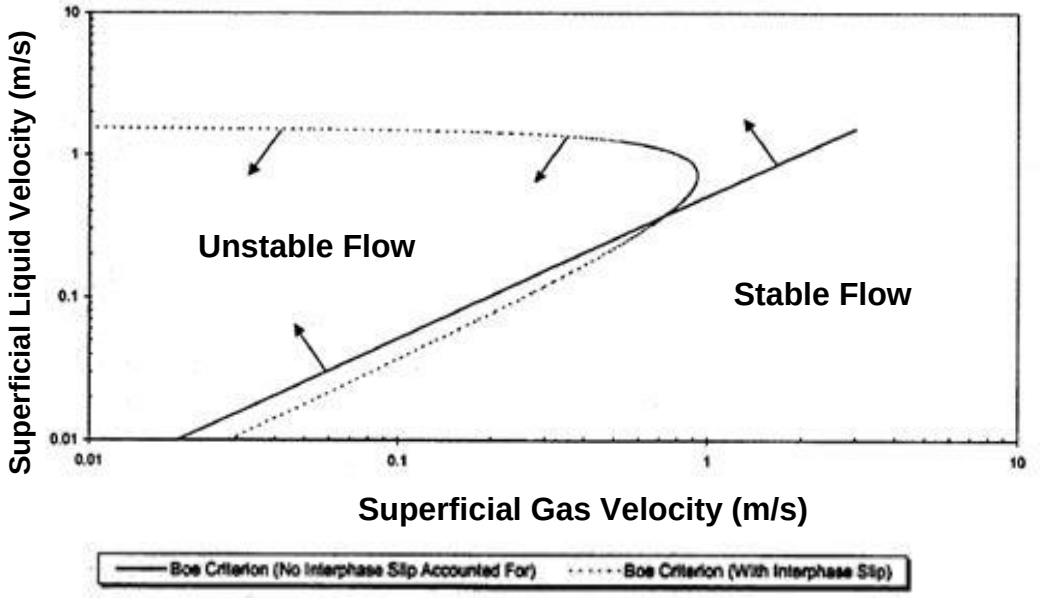

Figure 5-6: Boe (1981) Criterion

5.3.3 The Taitel Criterion

The aim of the Taitel (1986) criterion was to quantify the effect of separator pressure on the likelihood of severe slugging occurring. It was based on considerations of the blowdown of the pipeline/riser. In the analysis, Taitel supposed that, in order for blowdown to occur, the liquid column in the riser must be unstable. Such an unstable column was spontaneously blown-out of the riser as soon as Taylor bubbles penetrated the riser base. Taitel showed that the condition for instability was:

$$\frac{\partial(\Delta F)}{\partial y} > 0 \qquad \textbf{Equation 5-7}$$

For $y = 0$, ΔF is the force difference over the riser as a bubble penetrates the riser base. It has been noted that, in the original work, the criterion was for stable flow and hence the inequality was reversed. A force balance over the liquid column was given as:

$$\Delta F = \left[\left(P_{Sep} + \rho_L g h_R \right) \frac{\varepsilon_{GP} L}{\varepsilon_{GP} L + \varepsilon'_G L} \right] - \left[P_{Sep} + \rho_L g \left(h_R - y \right) \right]$$ **Equation 5-8**

where ε'_G is the gas holdup immediately behind the penetrating Taylor bubble front. Combining Equations 5-7 and 5-8 gives the final form of the criterion (with respect to atmospheric conditions):

$$\frac{P_{sep}}{P_0} < \frac{\left(\varepsilon_{GP} / \varepsilon'_G \right) L - h_g}{P_G / \rho_L g}$$ **Equation 5-9**

Examining Equation 5-9, most of the parameters are specified by the pipeline/riser geometry and operating conditions. The remaining variables are the gas holdup in the pipeline and behind the bubble front. Thus, in order to plot the results on a flow regime map, an expression for the pipeline gas holdup, ε_{GP} is required. Taitel (1986) provided a correlation for gas holdup as a function of the liquid velocity at the inlet.

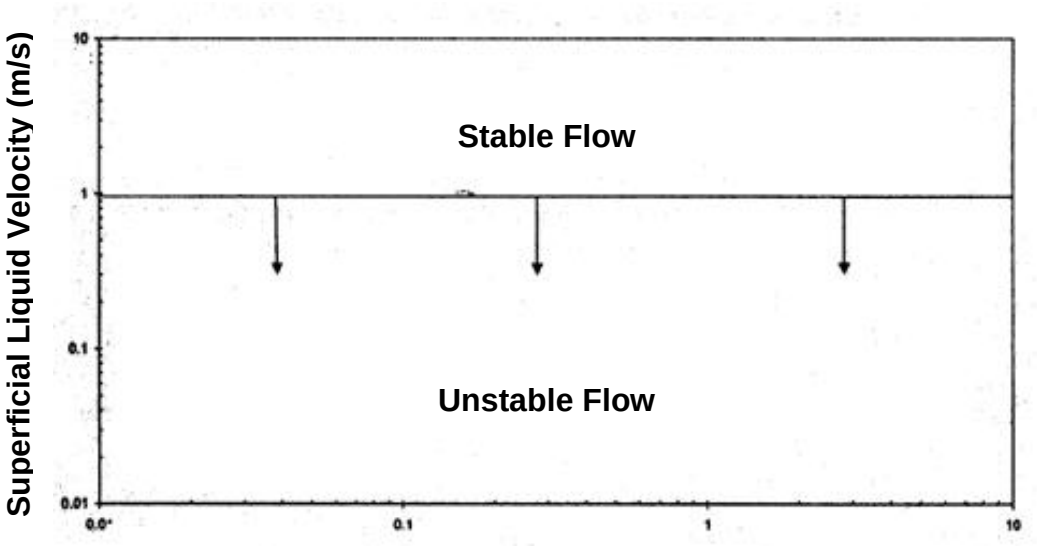

Figure 5-7: Taitel (1986) Criterion

Using this correlation, the Taitel criterion becomes a function of the liquid velocity only. As only a single value of ε_{GP} is obtained for any given separator pressure, the Taitel criterion gives a single limiting liquid velocity for severe slugging, as per Figure 5-7 above. Taitel also modified the criterion to account for the non-zero gas fraction in the body of the slug, taking this fraction as ε_{SL}, Equation 5–9 then becomes:

$$\frac{P_{sep}}{P_0} < \frac{\varepsilon_{SL}\left[\left(\varepsilon_G / \varepsilon'_G\right)L - h_g\right]}{P_0/\rho_L g} \qquad \textbf{Equation 5-10}$$

In the referenced work of Taitel (1986), the successful application of the developed criterion to data collected by Schmidt et al. (1980) was shown.

5.3.4 Fuchs' Pressure-Criterion

A criterion, developed by Fuchs (1987), was based on the considerations of the 'release' of a severe slug equivalent to the blowdown of the riser. The basic form of the criterion for the acceleration of a gas bubble entering the riser base was:

$$\frac{d\left(P_{Ustr} - P_{Dstr}\right)}{dt} > \frac{d\left(\Delta P_{HYD}\right)}{dt} \qquad \textbf{Equation 5-11}$$

In Equation 5-11, the subscripts *Ustr* and *Dstr* refer to upstream and downstream conditions respectively, at points removed from the riser. In certain cases, these can be approximated by the pipeline and separator conditions (Fuchs 1987). Differentiating the mass balances for the upstream and downstream volumes, V_{Ustr} and V_{Dstr}, the left-hand side of Equation 5-11 was resolved. Using the Ideal gas equation-of-state (EOS), the pressure change was related to changes in the mass of gas and volume:

$$\frac{dP_{Ustr}}{dt} = \frac{P_{Ustr}A}{V_{GUstr}}\left[\left(U_{SGP} - U_{SGR}\right) + \left(U_{SLP} - U_{SLR}\right)\right] \qquad \textbf{Equation 5-12}$$

For the upstream and downstream gases:

$$\frac{dP_{Dstr}}{dt} = \frac{P_{Dstr} A}{V_{GDstr}} \left[\left(U_{SGP} - U_{SGR} \right) + \left(U_{SLP} - U_{SLR} \right) \right] \qquad \textbf{Equation 5-13}$$

The right-hand side of Equation 5-11 was evaluated from considerations of the bubble penetration, giving:

$$\frac{d\left(\Delta P_{HYD}\right)}{dt} = -g \sin\beta \left(\rho_L - \rho_G \right) \left(\varepsilon_L - \varepsilon'_L \right) \frac{dy}{dt} \qquad \textbf{Equation 5-14}$$

Combining Equations 5-12 and 5-14 and resolving in terms of the gas velocity entering the riser base (Fuchs, 1987) gave the final form of the criterion as:

$$\frac{\left(\frac{P_S A}{V_{G\,UStr}} \right) + \left(\frac{P_P A}{V_{G\,DStr}} \right)}{g \sin\alpha \left(\rho_L - \rho_G \right)} < \frac{\varepsilon_L - \varepsilon'_L}{1 - \varepsilon'_L} \frac{U_{SGB}}{\left(U_{SGB} + U_{SLB} \right) - \left(U_{SGI} + U_{SLI} \right)} \qquad \textbf{Equation 5-15}$$

In Equation 5-15, the subscripts GB and LB refer respectively to the gas and liquid entering at the riser base. The left-hand side of the equation is the characteristic severe slugging parameter for the system. The right-hand side relates to the 'stiffness' of the system according to Fuchs (1987). As it is an experimentally determined quantity, it reduces the applicability of the criterion. The exact values of the riser-based velocities $U^S{}_{GR}$ and $U^S{}_{LR}$ were considered to be the maximum velocities experienced during the severe slugging process. Fuchs (1987) showed the equivalence of his approach with that of earlier authors, under which assumptions this analysis became reduced to those of Boe (1981) and Taitel (1986).

5.4 Review of Current Methods of Mitigating Severe slugging

5.4.1 Background

Some of the factors to be considered when assessing the severity of slugging in any pipeline flow are flow-line pressure, rates of producing gas and liquid and flow-line topography.

However, few systematic studies have been conducted to account for the changes in the operational conditions when applying methods to eliminate severe slugging (Yocum 1973, Schmidt et al. 1979; Pots et al. 1987, Hill 1989, 1990; Jansen et al. 1990, 1994;) recognized that choking can eliminate severe slugging. However, no complete analysis of the choking behaviour was presented. Choking has been found to eliminate severe slugging by increasing the back-pressure proportionally to the velocity increase at the choke. If the acceleration of the gas front up the riser is stabilized before reaching the choke, steady flow will eventually occur.

Many active and passive methods have been proposed to mitigate the menace of severe slugging. There are basically three methods namely: gas-lifting, choking and back-pressure increase that have been adopted to control severe slugging. All other proposed techniques are based on these three basic elimination methods.

5.4.2 Gas-lifting

This is a method of eliminating severe slugging. In gas-lifting, external gas is injected either into the riser or pipeline at the riser bottom to reduce the hydrostatic head in the riser or to increase the gas flow rate in the pipeline. The gas-lifting technique has been employed since the 1950s to improve the well flow by reducing the fluid density, thereby increasing the flow along the production line. Riser base gas-injection is a development of gas lift that was first used to control hydrodynamic slugging in vertical risers Schmidt et al.

(1981). In using the gas- lifting method to control severe slugging, the local fluid density is reduced thus promoting an upward flow and limiting liquid fallback. In turn, it prevents the accumulation of a stagnant mass of liquid at the riser base, which leads to severe slugging formation.

The application of riser base gas-lift to control severe slugging was first described by Hill (1989). Initial experiments in a 50 m long and 15 m high pipeline-riser of 50 mm internal diameter at atmospheric pressure provided data on the application of gas lift to control severe slugging. These studies were used to predict the required quantity of gas for the full-scale operation. The gas-lifting system was then installed on the offshore platform and proved to be successful in start-up conditions and in re-starting a well that had been killed-off by the backpressure from the riser.

However, Schmidt et al. (1979) and Yocum (1973) in their studies considered gas lift to be too expensive. Pots et al. (1987) and Hill (1989, 1990) also studied the effect of gas injection on severe slugging characteristics in a pipeline-riser system. The drawback of gas lift is the large gas-volumes needed to obtain a satisfactory stability of the flow in the riser. The primary benefit of gas injection is to reduce the hydrostatic head in the riser and thus, reduce the pipeline pressure. The injected gas also tends to carry the liquid and, thus, keep the liquid moving up the riser. When sufficient gas is injected, the liquid will be continuously lifted and a steady flow will occur.

Tengesdal et al. (2003) did some work on severe slugging using the gas-lifting technique. They presented a steady-state model that predicts the acceptable range of pressure drops across the gas-bypass line for successful operation of the gas-lift severe slugging elimination method. Figure 5-8 shows a schematic of self-lifting elimination technique they proposed.

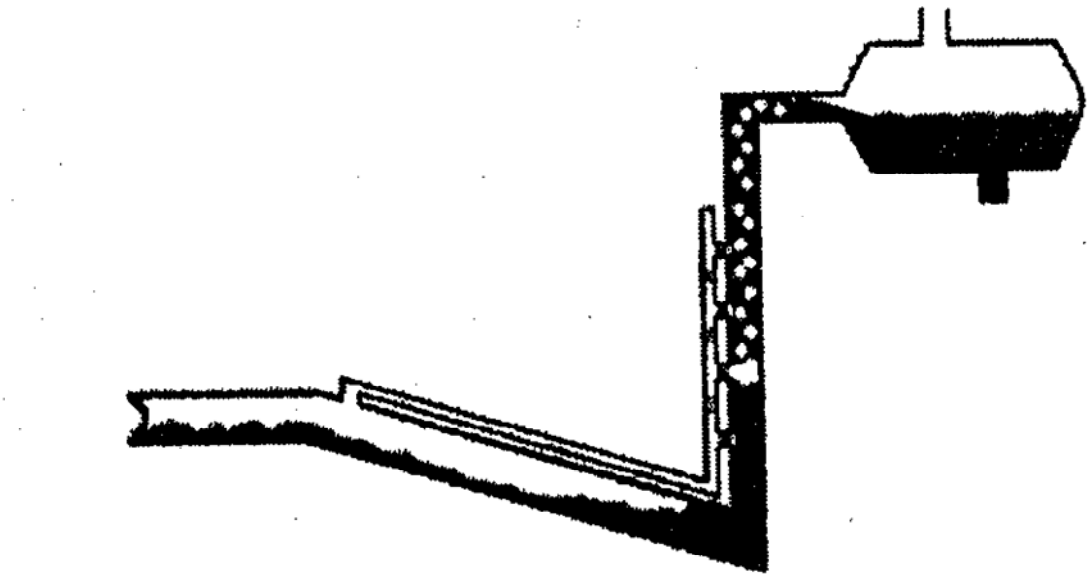

Figure 5-8: Schematic of self-lifting elimination technique.
Tengesdal et al. (2003)

They also proposed a simplified model as a criterion for continuous flow. In their model, they assumed for the flow system that the frictional pressure drop is negligible. They also assumed that, in the section of the pipeline/riser/separator system they considered, pressure and temperature variations are small enough that gas and liquid PVT and flow properties like densities and holdups can be considered to be approximately constant and that gravitational pressure drop in the gas bypass is ignored. Figure 5-9 shows a schematic of the pipeline/riser system they modelled. In the simplified model, there is no pressure drop between points A and B regardless of whether the liquid or gas legs are considered.

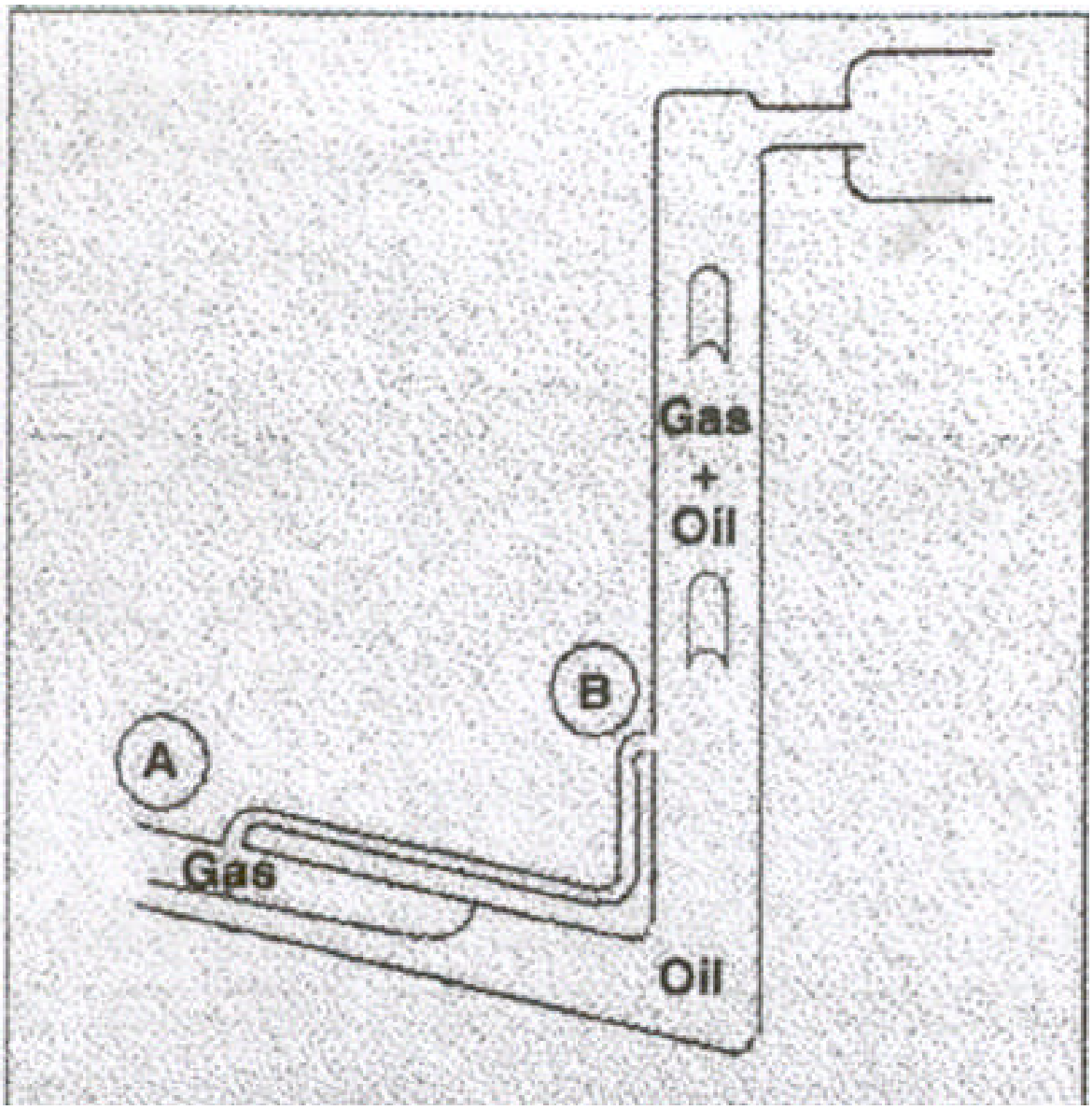

Figure 5-9: Simplified model of pipeline/riser system. Denney (2003)

5.4.3 Topside Riser Choking

This method increases the backpressure in proportion to the velocity increase in the riser. According to Schmidt et al. (1980b), topside riser choking was one of the first methods proposed to control severe slugging-see Figure 5-10.

Choking was applied manually using an actuated valve, induced bubble-flow or normal slug-flow in the riser by increasing the effective backpressure at the riser outlet. The technique is a modification of the Yocum (1973) method that used a choke to control hydrodynamic slug flow in a vertical riser. Schmidt et al. (1985) described the mechanism by which choking controls severe slugging particularly with reference to the flow-regime prediction. The increase in backpressure effectively prevents the spontaneous blow out of the liquid column in the riser by increasing the pressure drop through the riser relative to the gas velocity. In effect, there is an increase in the retarding force acting on bubbles penetrating the riser, thus preventing it from accelerating to such a velocity as to cause blowdown of the pipeline/riser.

Courbot (1996) reported the successful implementation of this technique based on feedback control from a measurement of the riser's base-pressure. Jansen et al. (1996) also carried out theoretical and experimental investigations of this technique by modifying the Taitel (1986) criterion to account for the additional backpressure of choking. The choke backpressure upstream was given by P_U

$$P_{UStr} = P_{Sep} + CU^{2}_{SL} \qquad \textbf{Equation 5-16}$$

where C is an experimentally determined parameter. As the gas bubbles penetrate the riser base, an incremental jump in the upstream of the choke was incorporated into Equation 5-16 thus giving:

$$P_{UStr} - \left(P_{Sep} + CU^{2}_{SL}\right) = K_Y \qquad \textbf{Equation 5-17}$$

where K is a constant of proportionality. Equation 5-17 was substituted into the pressure balance used in Taitel's (1986) analysis, so that, with choking in operation, the criterion for severe slugging became:

$$\frac{P_{Sep} + CU^{2}_{SL}}{P_o} < \frac{\frac{\varepsilon_G L}{\varepsilon'_G}\left(1 - \frac{K}{\rho_L g}\right)}{P_O / \rho_L g}$$

Equation 5-18

Predictions were compared with experimental data collected from a 25.4 mm vertical riser/pipeline rig with the pipeline inclined at -1^0 to the horizontal and opened to the atmosphere. The results obtained compared favourably with the criterion predictions for different choke-settings.

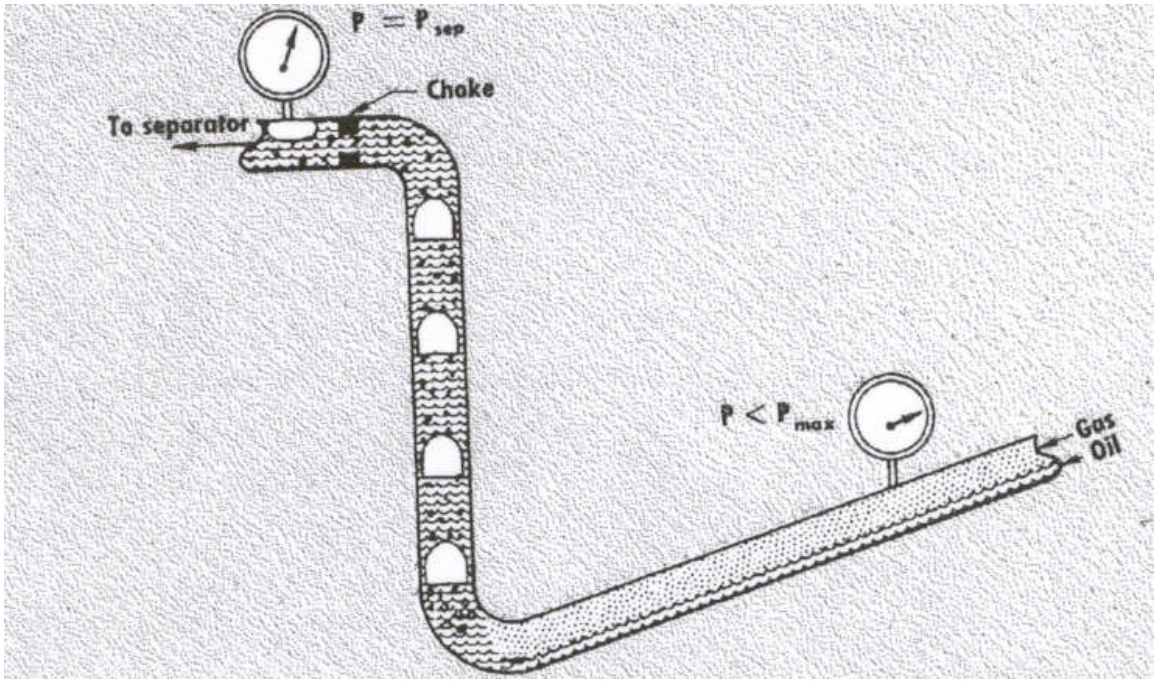

Figure 5-10: Schematic of Pipeline/riser System with a Choke. Schmidt et al. (1979)

5.4.4 Backpressure Increase

The backpressure increase method eliminates severe slugging by increasing the system pressure and thereby significantly reducing the production capacity. This method of eliminating severe slugging is not a viable option even for shallow-water systems since the production capacity reduction is experienced

due to the backpressure imposed. The reduction in production capacity is therefore expected to be worse for deepwater production systems.

5.5 Other Techniques of Preventing Severe slugging

Several other methods proposed to eliminate severe slugging in a pipeline/riser system have their working principles similar to, or are derivatives from the three methods described above. For example, increased pipeline pressure and topside riser choking methods appear to have been used as retrofit solutions to unexpected operating problems. Both of these techniques are field specific and may not be effective in many cases. Moreover, both tend to reduce well productivity by increasing the pipeline pressure and so may restrict production.

5.5.1 Internal Riser Insert System (IRIS)

This is a new technique to eliminate severe slugging in the pipeline/riser system. It is a retrofit combination technique of riser base gas injection and reduced riser diameter. It involves inserting a sleeve into an existing riser to reduce the effective internal diameter and allow gas to be injected at the base of the riser. The use of this technique allows the elimination of severe slugging in multiphase production risers. It also extends satellite well-life by reducing hydrostatic backpressure. The technique can be installed from the platform topside and requires no subsea intervention into the riser or flowline. IRIS is suitable for existing production facilities or as part of the design basis for a new installation to optimise pipeline efficiency over field life.

It comprises a simple lightweight sleeve suspended by a hanger spool within the existing riser. Figure 5-11 shows the system. Generally, IRIS can be said to achieve two aims namely a reduction in the riser's effective bore and formation of an annulus between the riser pipe and the sleeve route-gas to the base of the riser, where it is injected into the multiphase produced fluid stream. In this way,

the superficial gas velocity in the riser can be raised to a level whereby severe slugging will not occur.

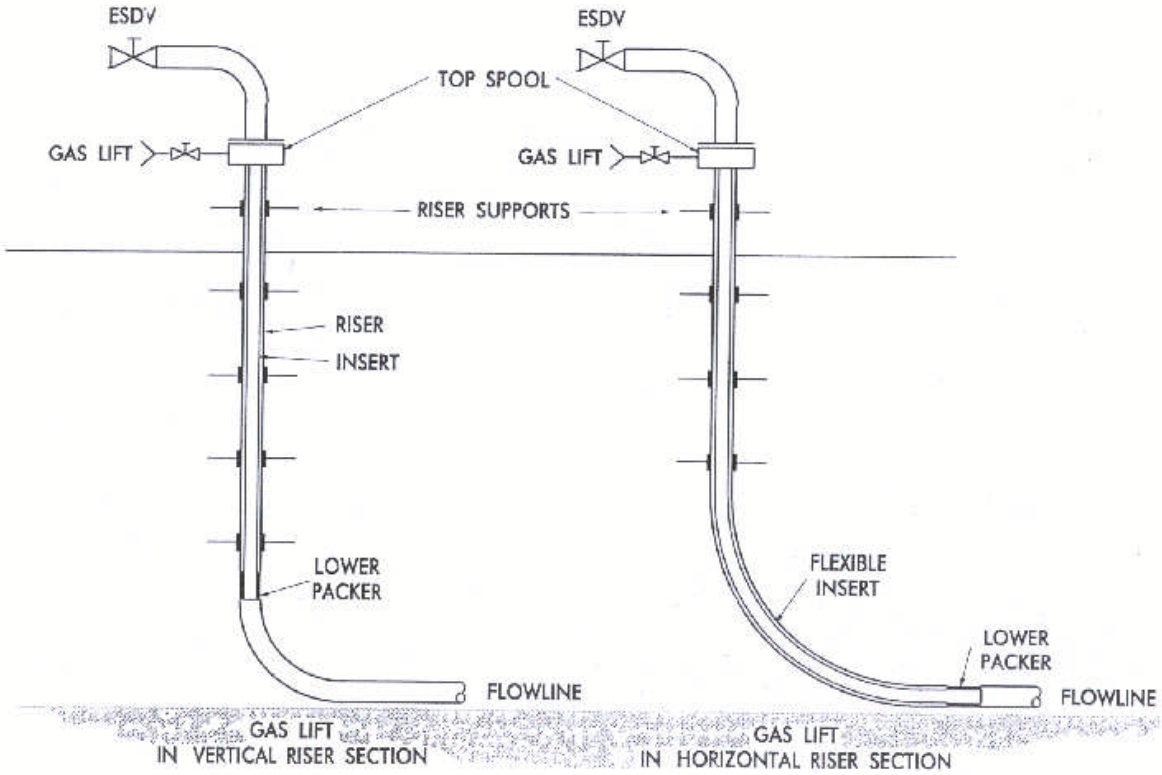

Figure 5-11: Schematic of Riser Layout with IRIS Installed. Wyllie (1994)

The insert sleeve is suspended from a hanger spool at the top of the riser which also serves as the gas-supply point. A packer is used at the bottom of the riser to secure the sleeve and withstand the impact of any slug load or multi-diameter pigs passing through the pipeline. The sleeve can be made of lightweight materials and is designed to be piggable and removable if required.

The required gas injection in the IRIS varies depending on the location of the gas-injection point. First, if the gas injection is above the riser base, the gas velocity in the riser is increased, such that the flow moves out of the slugging/churn flow region into the annular flow. This is shown in Figure 5-12. The reduction in riser bore and hence volume also tends to increase the gas

velocity in the riser. This again helps to move the operating point towards the annular flow and significantly reduce the gas-injection rate required.

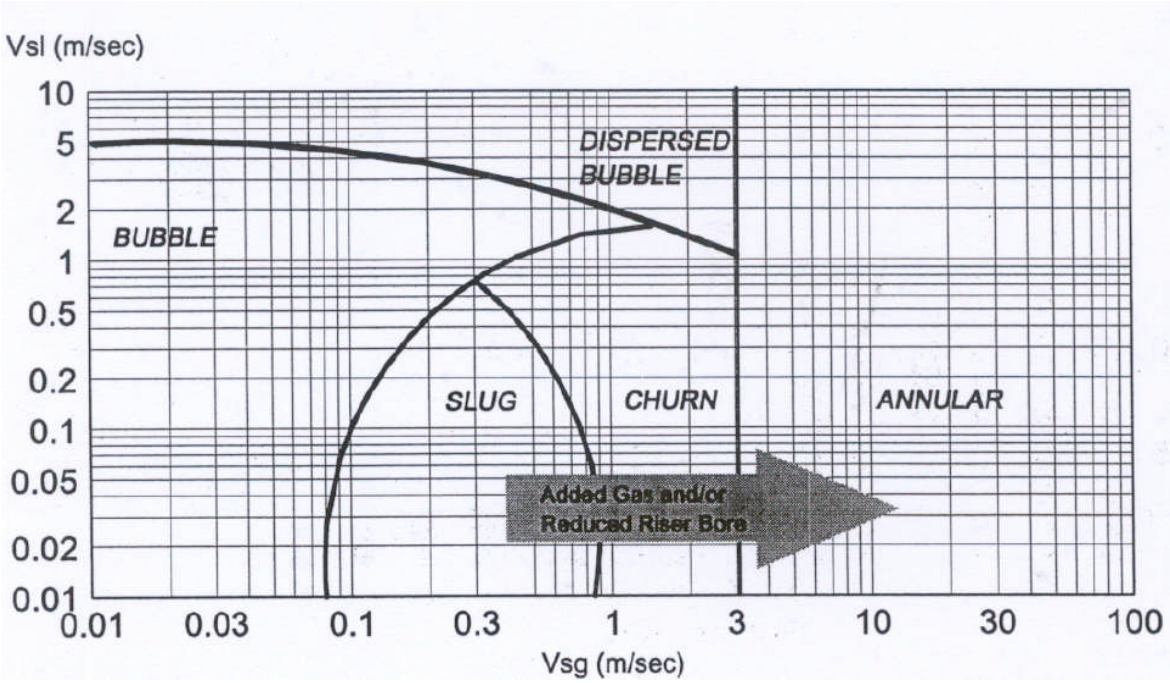

Figure 5-12: Effect of Gas Injection on Riser Flow Regime. Wyllie (1994)

Secondly, if the gas is injected into the pipeline upstream of the riser base liquid blockage, the rate of gas pressure build-up behind the slug will be increased and along with the reduction in riser's effective volume, this will tend to reduce the slug size.

Wyllie, M. W. J. & Brackenridge, A. (1994) reported that one of the additional benefits of IRIS is that the additional gas-fraction in the riser has the effect of significantly reducing the static head on the subsea production wells, thereby allowing increased well draw-down. They quoted that, for typical water depths and pipeline lengths, static-pressure reductions of around 5 bar have been observed in simulations. A typical well draw-down of between 50 and 100 bpd/bar was considered and it was reported that the reduction in backpressure alone could allow an extra 250 to 500 bpd to be produced in some cases.

Figure 5-13 shows an example of how IRIS can extend hydrocarbon field-life by eliminating slugging and reducing backpressure.

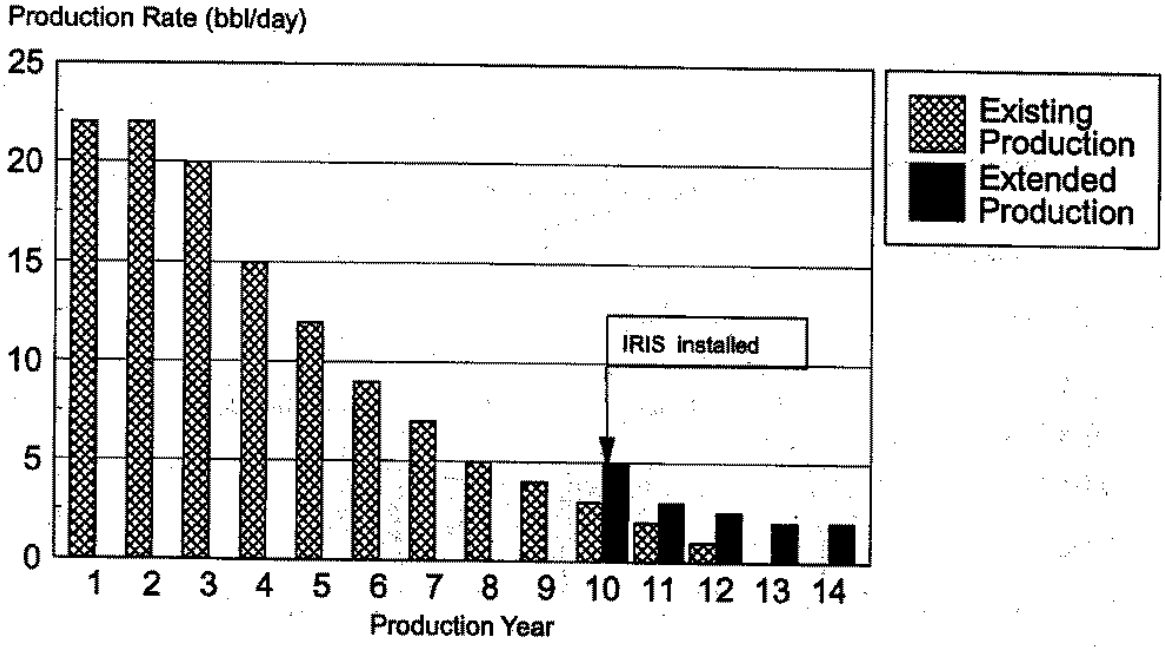

Figure 5-13: Typical IRIS Impact On Production Rates. Wyllie (1994

The main problem of this technique is the reduction in riser's diameter: it has two opposing effects as reported by Wyllie & Brackenridge (1994). If the diameter is reduced in the case of downstream injection, it will lead to an increase in riser gas velocity and so reduce the amount of gas required to meet the critical minimum velocity. For upstream injection, a reduction of IRIS bore will increase the rate of hydrostatic head rise in the riser and so require an increased amount of gas injection to overcome this. So the optimum location for gas injection for either upstream or downstream of the riser base bend has to be determined.

5.5.2 Gas Injection at Riser Base

Gas injection at the riser base is a development of the gas-lift method, which was first used to control hydrodynamic slugging in vertical risers (Schmidt et al.

1981). Hill (1990) reported that topside simulations were undertaken on a 50 mm internal diameter with a 50 m length pipeline and a 15 m high riser-see Figure 5-14. During these investigations, it was concluded that there was a remote chance of high liquid-level alarms and of liquid carry-over from the separation system during the production stage of the severe slugging cycle. Then it was concluded that the preferred method for the first investigation was that of riser base injection. The initial experiments were at atmospheric pressure and provided data on the application of gas lift to severe slugging. The studies were used to predict the required quantity of gas for the full-scale operation. As part of the work described on choking, Jansen et al. (1996) also investigated the riser base gas-injection method. They extended the Taitel (1986) criterion for severe slugging to include steady-state gas injection into the base of the riser. A criterion for severe slugging was then given as:

$$\frac{P_S}{P_O} \angle \frac{(\varepsilon_{GP} / \varepsilon'_G) L - h_g}{P_O / \varepsilon_{GR} \rho_L g} \qquad \textbf{Equation 5-19}$$

where ε_{GR} is the void fraction in the riser due to the gas lift and it is calculated using a simple bubble-flow model as:

$$\varepsilon_{GR} = 1 - \frac{U_{SGR}}{U_{BUB}} \qquad \textbf{Equation 5-20}$$

$$U_{BUB} = C_O U_M + U_D \qquad \textbf{Equation 5-21}$$

where C_O is the drift parameter and equals to 1.2 and U_D is the bubble's drift velocity, $0.35\sqrt{gD}$. A quasi-equilibrium model was also developed to simulate the time-dependent nature of the flow: the model was based on the work of Taitel et al. (1990). Comparisons of these models were carried out against experimental data from a 25.4 mm internal diameter, 9.1 m long and 3 m high pipeline/riser rig. The experiments demonstrated that severe slugging could be mitigated by using the gas-lift method. However, it was found that a large

amount of gas was required to eliminate pressure cycling altogether. Jansen et al. (1996) indeed found that the flow in the riser must approach annular flow before steady riser-flow is achieved. The successful prediction of the severe slugging region and the severe slugging characteristics by the criterion and the quasi-equilibrium model were demonstrated.

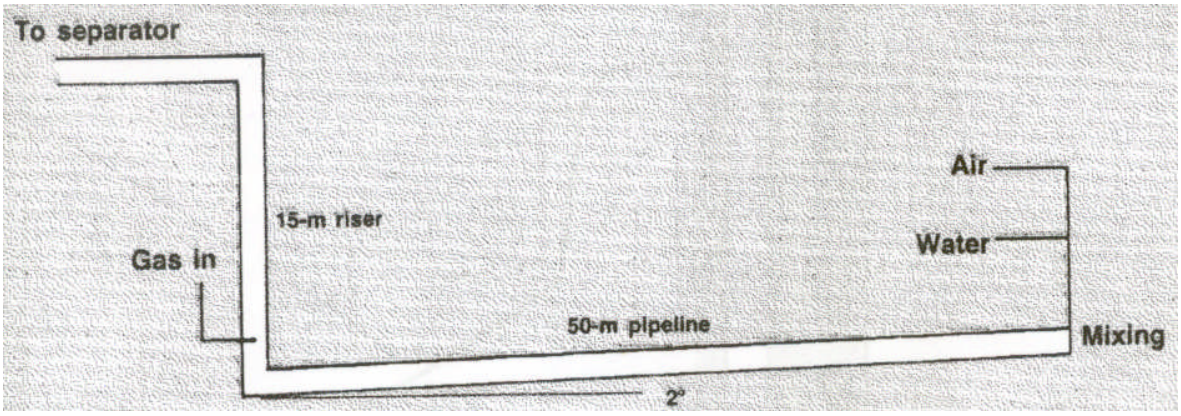

Figure 5-14: Schematic of Gas injection at Riser base Hill (1990)

5.5.3 Active Feedback Control

Havre and Dalsmo (2002) introduced a technique called Active Feedback Control as a method that can be used to prevent severe slugging in a pipeline/riser system.

They presented the results of their findings from field tests as well as those from dynamic multiphase flow simulations. The results from their simulations, with feed back control, show that stable processs conditions at both the pipeline inlet and outlet in all cases, whereas without control, severe slugging flow would be experienced. Pipeline profile plots of the liquid volume fraction through a slug flow cycle were compared with corresponding plots with feed back control applied. They used the comparison to justify the internal stability of the pipeline.

It is a technique that can detect the formation of slug and try to limit its size in order to restrict the effect on the separator train and compressors at the

production facility. The method involves the active actuation of the production choke in which it is moved in accordance with a dynamic feedback-control algorithm. It is reported that by applying feedback control from the pressure upstream of where the slug is generated, it is possible to avoid slugging with an average pipeline pressure lower than pressure typically introduced by a simple constant-choke. Furthermore, it is possible to achieve a stable pipeline inlet-pressure that is less than the peak inlet-pressure with severe-slug flow.

5.5.4 Active Bypass Method

This is another method proposed by Duret et al. (2004) to prevent the occurrence of severe slugging in the pipeline/riser system. Figure 5-15 shows a schematic of the technique. It is a method which involves stabilising the flow by maintaining the pipeline gas front, which is upstream of the riser base at a constant position. This implies that the flow remains in the second step of the cycle of severe slugging and never enters the third step, which is “blowout”. In view of this, a gas bypass is created at the bottom point by removing gas from the pipeline and re-injecting it at a given height of the riser.

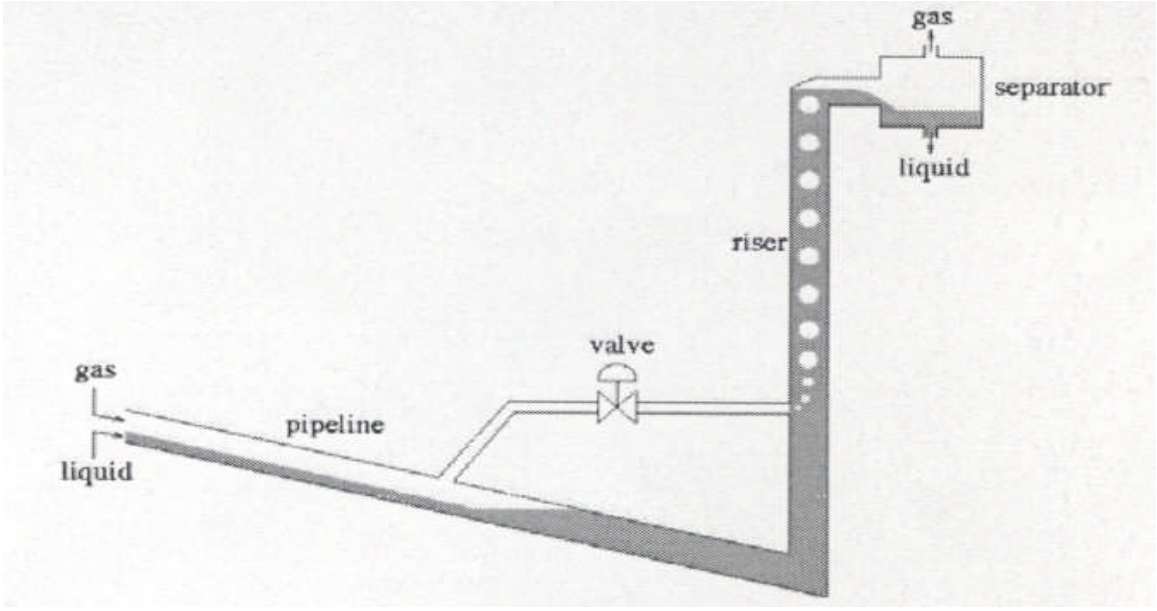

Figure 5-15: Schematic of Active Bypass Controller. Duret et al (2004)

As shown in Figure 5-15, a valve is added to the bypass which can be controlled to regulate the gas mass-flow rate. The re-injected gas in the riser also enables one to reduce the riser's hydrostatic-head without using gas lift, while a steady dispersed or intermittent flow at the exit of the riser is guaranteed.

5.6 The proposed novel (*helical pipe* installation) method

The proposed novel method involved the installation of *helical pipes* of 6 m and 3 m lengths and both are 0.1 m internal diameter up-stream of a catenary-shaped riser base. Two-phase (air and water) experiments were performed in the catenary shaped riser which was also 0.1 m internal diameter and 10.5 m high. Various combinations of air and water flowrates were investigated. The pressure at the outlet of the riser was maintained at 1barg and a 55 m long flowline prior to the riser was at -2 degrees to the horizontal. The 6 m and 3 m lengths of *helical pipes* were investigated in order to study the length effect on the effectiveness of the *helical pipe*.

Figure 5-16 shows a side view of the 0.1 m internal diameter *helical pipe* used for the experiments performed. The *helical pipe* was made by 'wrapping' a reinforced flexible translucent pipe round a 1.5 inch mandrel. Flange adaptors were provided at both ends of the *helical pipe* to connect to Cranfield University's 0.1 m flowline of the riser rig.

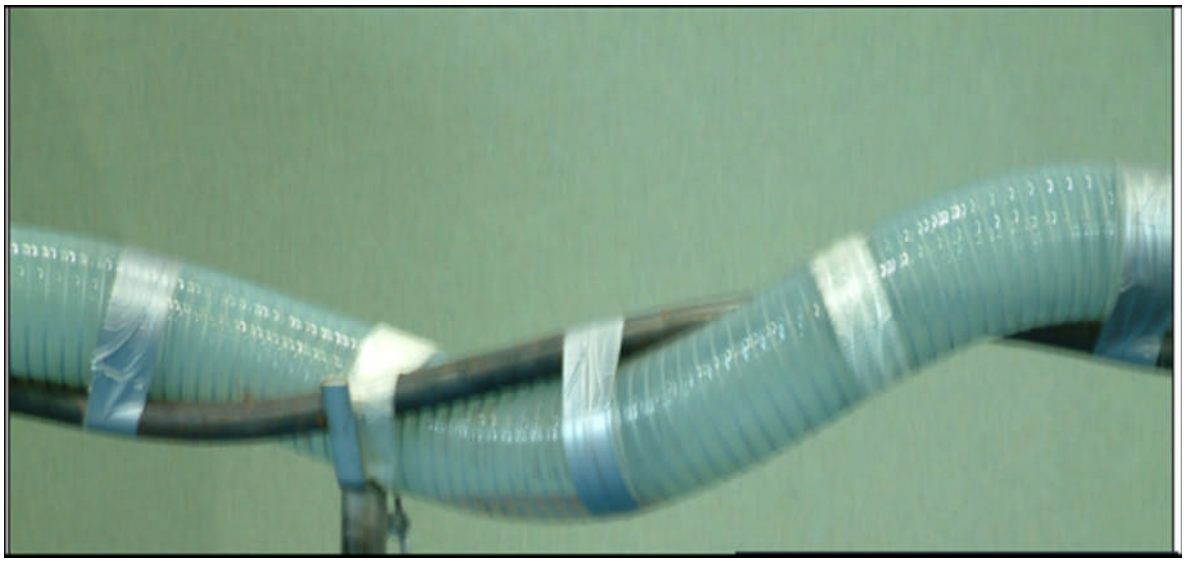

Figure 5-16: Side view of a low amplitude *helical pipe*

The aim and objective of installing the *helical pipe* on the riser experiments are stated in chapter 6 of this Thesis. The experimental facilities together with the experimental results and associated discussion including the fluid flow characteristics in *helical pipe* during severe slugging, visual observations, overall behaviour and effect of *helical pipe* on severe slugging formation and the experimental conclusions are also detailed in chapter 6. The method proved to be successful in reducing the severity of slugging in the catenary riser system investigated. It will also be more economical to adopt as a method of controlling severe slugging in any pipeline/riser system than any of the existing methods in that the *helical pipe* section will form an integral part of the flowline segment. It will not require either a separate pipeline system or the installation of any additional components on the pipeline/riser.

Chapter 6

6 Riser Experiments

6.1 Introduction

The aim of the experiment was to investigate the effects of installing a section of *helical pipe* at a short distance from the base of the riser with the particular objective of controlling severe slugging in a pipeline-riser system. The objective of the experiment was to improve production and transportation of hydrocarbon products (oil and gas) particularly in the sub-sea environment, where severe slugging has been a major problem.

Analyses of the experimental results for both with and without *helical pipes* are discussed in two parts. The first part describes the characteristics of severe slugging in the pipeline/riser system in terms of pressure difference over the riser, liquid holdup and liquid production. Comparisons between the two (straight and *helical*) pipes are made. The second part is concerned with flow regime maps for the straight and *helical pipes* under severe slugging.

6.2 Experimental facilities and methods

Figure 6-1 shows the Cranfield University's Three-Phase Facility, which was used for the riser experiments. The test facility can be divided into three zones – the metering area, test area and the separation area. Each area is described briefly below. It must be noted that, although Cranfield University's test facility is a three-phase (air, water and oil) facility, the experiments performed were two-phase (air and water). Nevertheless, the description below is for the three-phase (air, water and oil) facility. For all the experiments performed, the maximum pressure at the base of the riser was about 2.1 barg during severe

slugging, when the riser was completely filled with water. In all the experiments performed, water flowrates were kept constant while air flowrates were varied. The test procedure is also discussed. A process and instrumentation (P & I) diagram of the three-phase test facility and flowline/riser profile and Coordinates are shown in APPENDIX A.

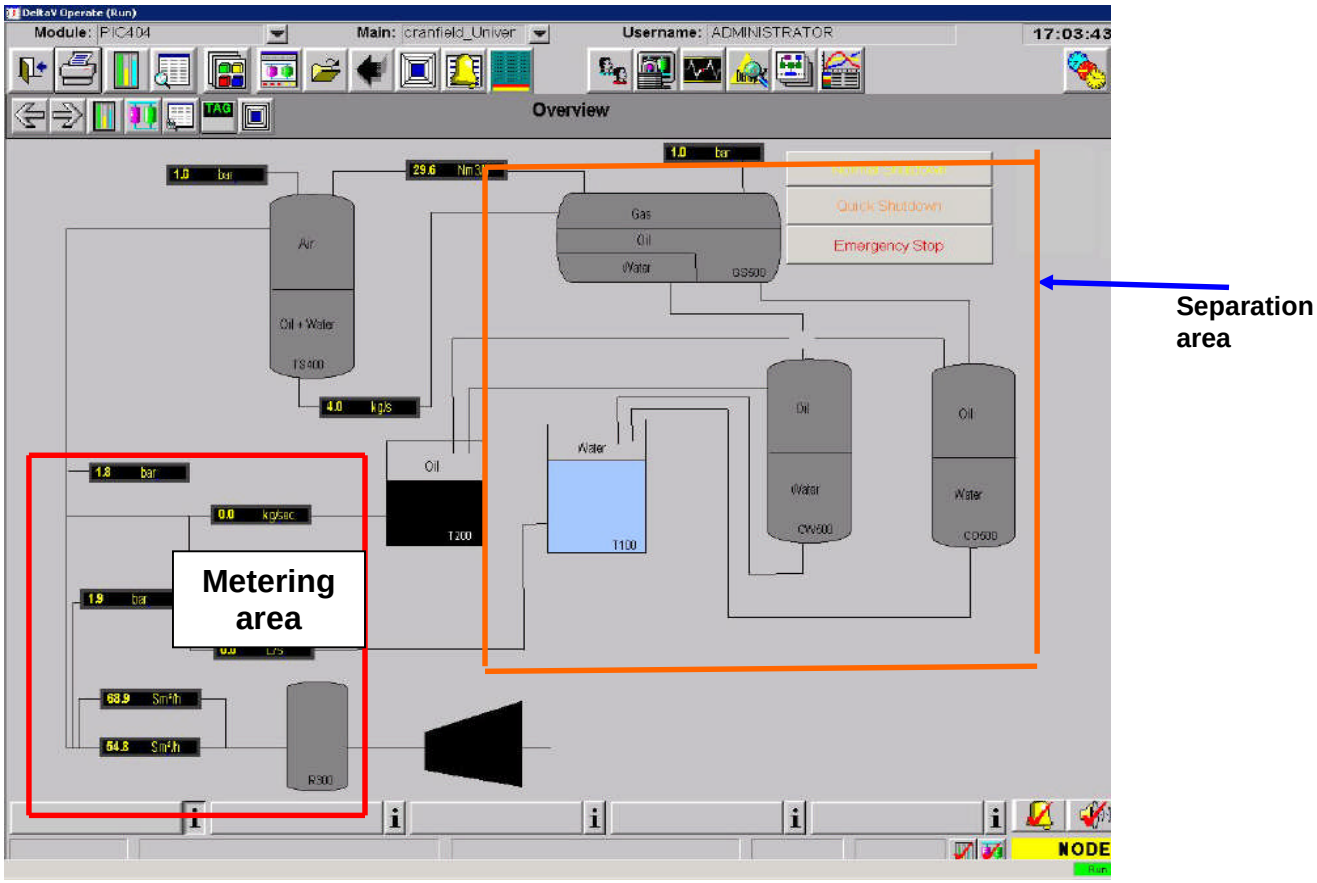

Figure 6-1: Cranfield University Three-phase Facility

The facility consists of a three-phase gravity separator, oil and water coalescers, storage tanks, oil and water pumps, compressor and air clean-up equipment. The liquid flows from the facility are metered and the density was measured online by a number of Coriolis mass-flow meters. The pressure of the three-phase separator was controlled by using the gas-outlet valve. The oil and water liquid levels were maintained by using the valves between the separator and the coalescer. The facility is controlled by a DeltaV© distributed control-

system (DCS) to ensure the desired operation conditions were achieved at the test rig.

6.2.1 Flow metering area

Air and water were supplied in a controlled manner from the three-phase facility. Figure 6-2 shows the metering area of the three-phase test facility. Air was supplied from a bank of four compressors connected in parallel. When all the 4 compressors were run in parallel, a maximum air flowrate of 4250 m^3/hr free air delivery (FAD) at 7 barg can be supplied. The air from all four compressors was accumulated in a large air receiver to reduce the pressure fluctuation from the compressor. Air from the receiver passed through a bank of three filters (coarse, medium and fine) and then through a cooler, where debris and condensates present in the air were stripped from the air before it flowed into the flowmeters. However, only one compressor was commissioned (at the time these experiments were being performed and it was supplying a maximum flowrate of 1275 m^3/hr FAD at 7 barg). The compressor was started manually, but can be shut down remotely from the control room or through the supervisory control and data acquisition (SCADA) software during shutdown.

Water was supplied from a 12,500-litres capacity water-tank while oil was supplied from a tank of similar capacity. The water tank was situated in the laboratory, while the oil tank was situated outside the laboratory for safety reasons. The water and oil were supplied to the flow loop by two multistage Grundfos CR90-5 pumps. Both water and oil pumps were identical and have a duty of over 100 m^3/hr at 10 barg. Speed control was achieved using inverters. The pumps were operated remotely using DeltaV.

6.2.1.1 Metering section

The flowrates of the air, water and oil were regulated by their respective control valves. The water flowrate was metered by a 1” Rosemount 8742 Magnetic flowmeter while the oil flowrate was metered by a 1” Micro Motion Mass

flowmeter. The air was metered by a bank of two Rosemount Mass Probar flowmeters of ½" and 1" diameter respectively. The smaller air flowmeter measured the lower air flowrate while the larger air flowrate metered the higher air flowrate. Additional two Foxboro 3" Coriolis meter and control valves were added later.

The metering section not only metered the flowrates of air, water and oil but also supplied the flow of air, water and oil constantly in a controlled manner as determined by the operator (or necessary, by a preset sequence input through another computer or software).

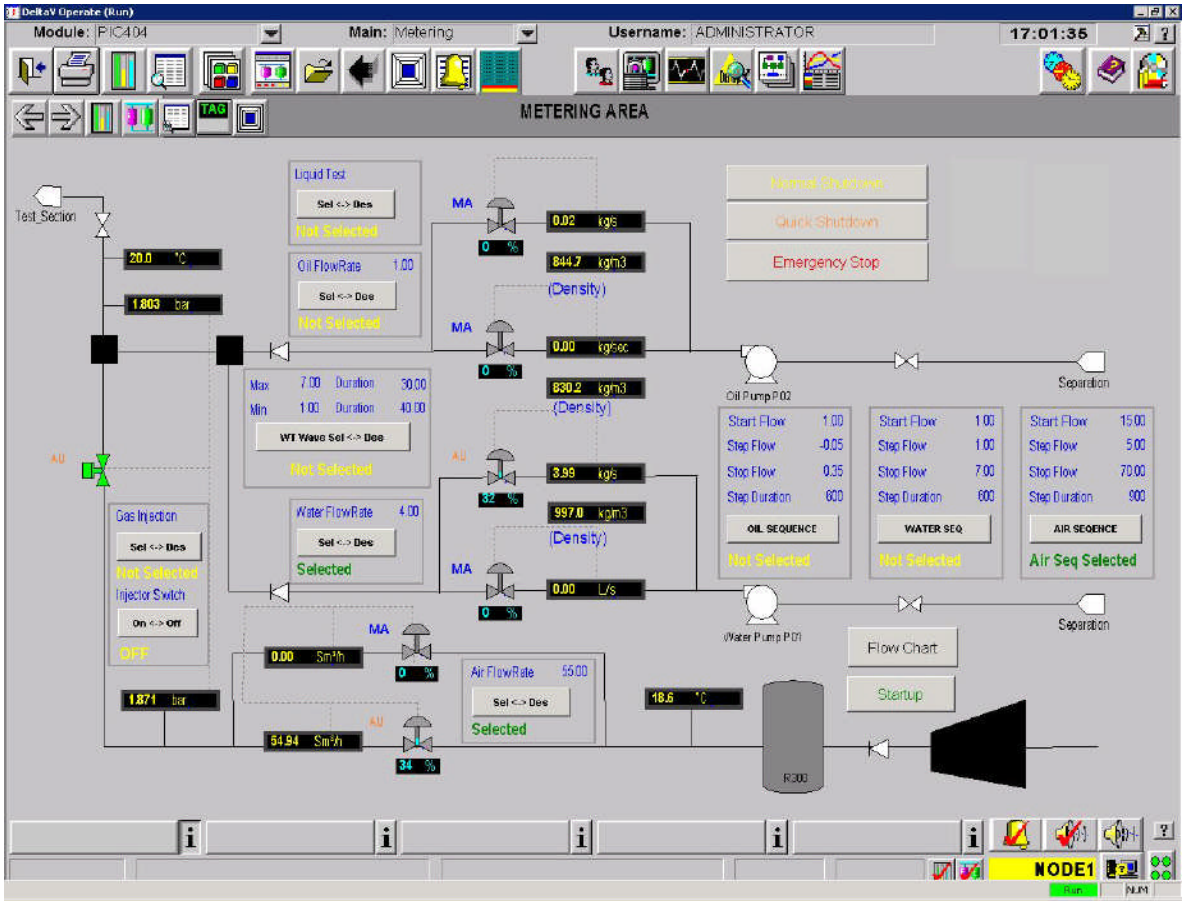

Figure 6-2: Flow metering area of the three-phase facility

6.2.1.1.1 Air supply

There were two air flow metering loops, each comprising a set of control valves and flow meters to meter high and low flowrates (0 to 100 Sm^3/hr for low flowrates and 95 to 4250 Sm^3/hr for high flowrates). The operator will normally specify a certain flowrate of air to flow into the test section. DeltaV will then select the suitable air metering loop. Due to the nature of the experiments, the air flowrate was expected to fluctuate (sometimes violently). Hence, the control valve was expected to control and keep the flow steady at the specified flowrate.

6.2.1.1.2 Water supply

Initially, there was only one water metering loop, comprising a control valve and a flow meter metering a flow from 0 to 26.4 m^3/hr, but later a second loop was added. DeltaV software was installed in order to select the suitable water metering loop when the operator specified the flowrate of water. There was only one pump supplying water into the metering loop(s). An inverter was used to control the speed of the pump to prevent overworking and overheating of the pump. Hence a flow controller was installed to control the valve and the speed of the pump, so that the specified flowrate of water can be supplied into the test section without overheating the pump. That can be achieved by starting the pump at the lowest operational speed whilst monitoring the flowrate of the fluid entering the flowmeter and percentage opening of the valve. If the percentage opening of the valve exceeded 80% without reaching the required flowrate, the pump speed will be increased by one step. The pump speed could be increased one step at a time until the required flowrate was achieved. Ideally, the valve opening should be between 70% and 80% at the required flowrate. Due to the nature of the experiments, the water flowrate was also expected to fluctuate. Hence, the control valve was tuned to control and keep the flow steady at any specified flowrate.

6.2.2 Test area

The test section comprises a 55 m long, 2° downward inclined, 0.1 m (4”) nominal diameter flow line, a 10.5 m high catenary riser and a vertical two-phase separator. The installation was designed to encourage stratified flows in the flowline and hence promote severe slugging in the riser.

Figure 6-3 shows a test section of the straight pipe, where both the flowline and the riser are made of straight pipes. Figure 6-4 shows a test section of the *helical pipe* where a 6 m *helical pipe* was installed at some distance upstream of the riser base. In both cases, air and water were mixed in a mixer before entering the test area.

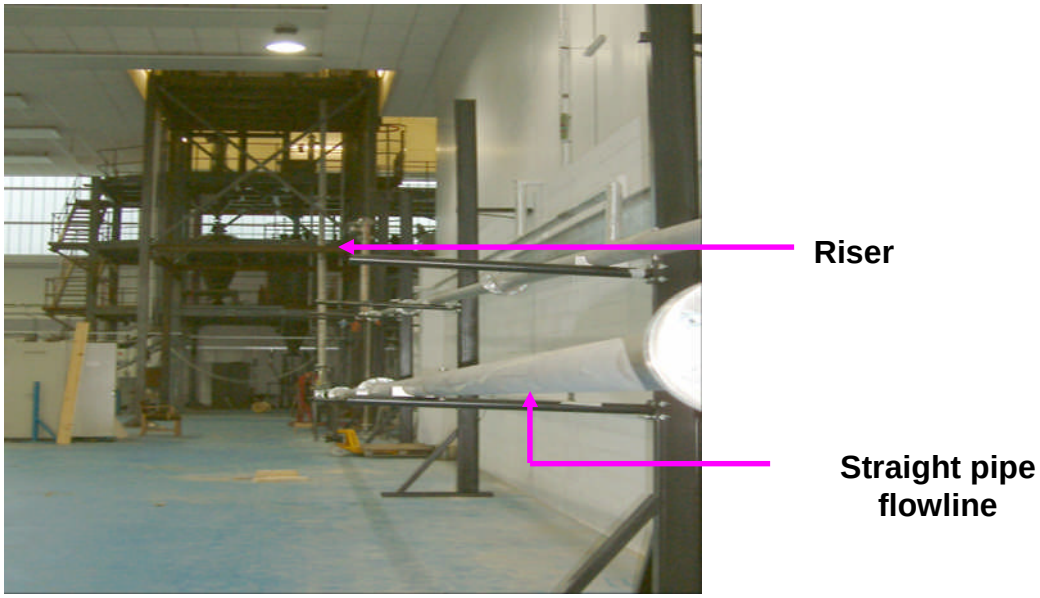

Figure 6-3: Straight pipe flowline and riser test section

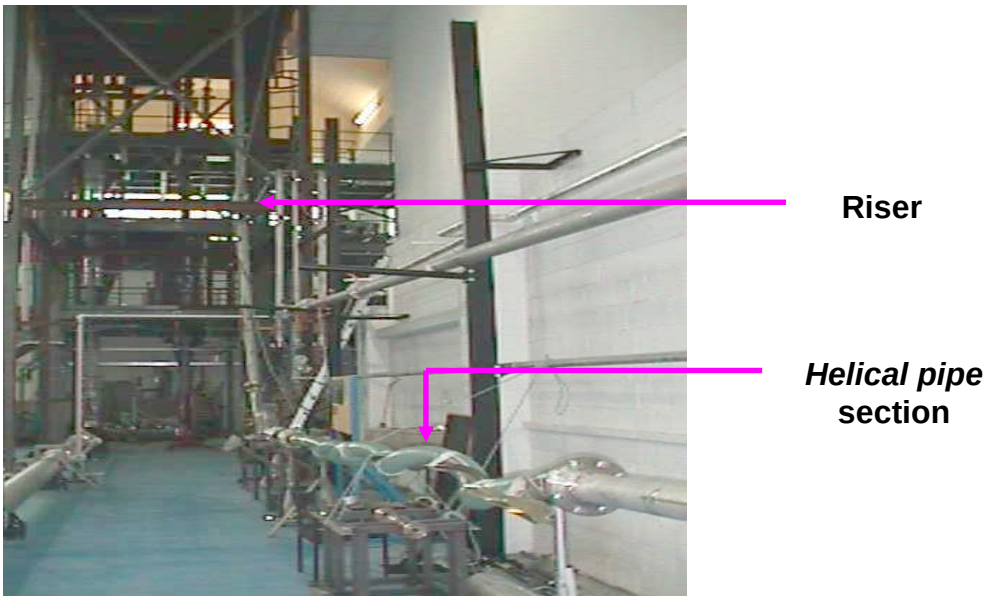

Figure 6-4: Flowline with *helical pipe* section and riser test section

The pressure and liquid level are controlled in the two-phase separator by a pressure controller and radar gauge level-controller maintained by the DeltaV control system. The separated air and water mixture then flow through separate air and liquid lines into the three-phase gravity separator for phase separation and cleaning. Air from the vertical two-phase separator is metered by a 1" Rosemount Vortex flowmeter while the water/oil mixture is metered by a 2" Micro Motion Mass flowmeter.

All the controls (for pressure and level) in the test area were located at the topside separator. Figure 6-5 shows instrument layout of the test area.

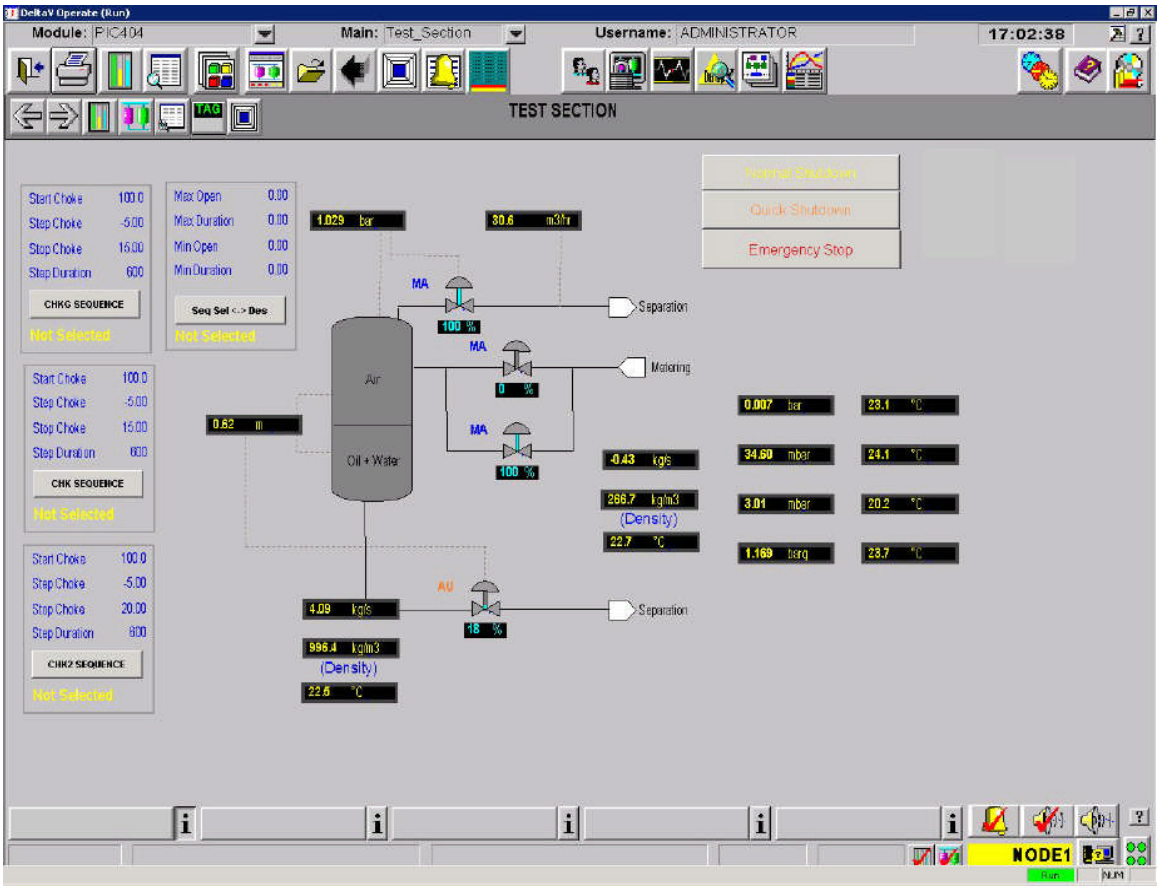

Figure 6-5: Test area instrument layout of the three-phase facility

6.2.3 Phase-separation area

The outlet air-flow from the riser exit was measured by a vortex flow-meter and the water by a Coriolis meter. The air and water were returned to the three-phase separator. The pressure in the topside separator was controlled using the gas outlet-valve between the topside separator and the three-phase separator. The liquid level was maintained by the liquid outlet-valve of the topside separator. A 'near straight tube' Coriolis meter was installed at the near vertical section at the top of the riser. The meter can be used to give an indication of the fluid mass-flow and density at the riser exit. The riser exit liquid flow can also be determined by totalizing the topside separator liquid-outlet flow and the liquid that accumulated in the separator.

The pressure, oil/water interface level and air/oil interface level were controlled by a pressure controller and two level-displacer type level controller maintained by the DeltaV control system.

Air was exhausted into the atmosphere after separation and cleaning in the three-phase separator. Water and oil from the three-phase separator entered their respective coalescers, where liquids were further cleaned before returning to their respective tanks. There were two flow-control valves of different sizes (1” and 3”) for each of the water and oil return lines. They were installed in a split range flow control to keep the oil/water and air/oil interfaces stable in the three-phase separator. For example, the smaller valve was operating when a small amount of water or oil exited the separator and vice versa. The phase-separation section comprised a 3-phase separator and two coalescers.

6.2.3.1 Three-phase separator

There were three sets of controls, namely, pressure control, oil-water interface level control and an oil-air level control. Each level controller adjusted two different control-valves of different sizes, that is, one for low flowrates and the other for high flowrates. Figure 6-6 shows the phase-separation area of the three-phase facility.

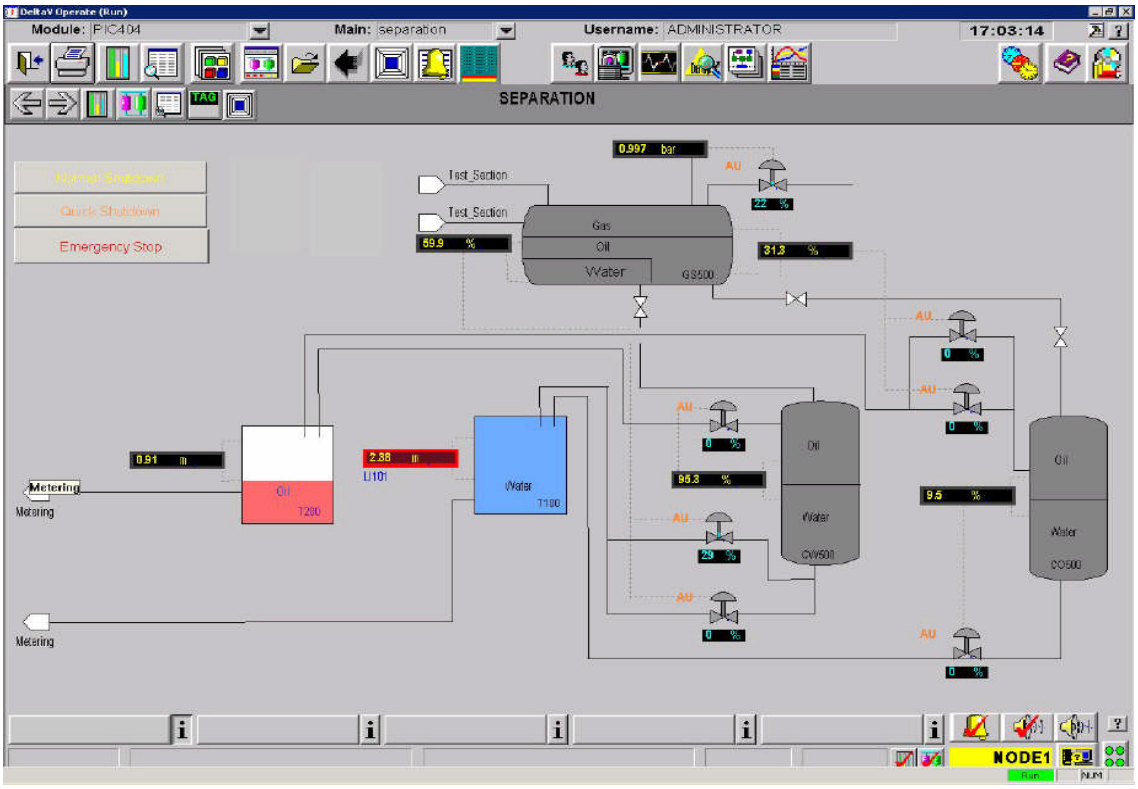

Figure 6-6: Phase separation area of the three-phase facility

6.2.3.2 Coalescers

The water and oil from the three-phase separator entered their respective coalescers, where they were further cleaned before returning to their respective tanks. The air was however exhausted into the atmosphere. Each of the coalescers has an oil-water level controller.

6.3 Experimental results and discussions

Some of the fluids' (air and water) matrices, for the straight and the *helical pipes'* riser experiments are shown in Table 6-1 and Table 6-2 respectively.

Test	Liquid's superficial velocity, V_{SL} (ms^{-1})	Air's superficial velocity, V_{SG} (ms^{-1})	Flow regime
1	0.05	0.36	Ordinary slugging (S)
2	0.06	0.18	Severe Slugging SS1
3	0.13	0.09, 0.18, 0.27, 0.32, 0.34, 0.36	Severe Slugging SS1
		0.38	Severe Slugging SS
		0.45, 0.54	Ordinary slugging S
4	0.25	0.36	Severe Slugging SS1
		0.45, 0.50, 0.54	Severe Slugging SS
		0.63, 0.71	Ordinary slugging S
5	0.38	0.09, 0.18, 0.27, 0.36	Severe Slugging SS1
		0.45, 0.54, 0.62, 0.71, 0.78, 0.83, 0.89	Severe Slugging SS
		1.07, 1.24	Ordinary slugging S
6	0.57	0.36, 0.71. 0.80,	Severe Slugging SS1
		0.86, 0.89, 0.92	Severe Slugging SS

Table 6-1: Fluids matrix for the straight pipe riser experiments

Test	Liquid's superficial velocity, V_{SL} (ms^{-1})	Air's superficial velocity, V_{SG} (ms^{-1})	Flow regime
1	0.13	0.18, 0.27	Severe Slugging SS1
		0.34	Severe Slugging SS
		0.45, 0.54	Ordinary slugging S
2	0.38	0.18, 0.36	Severe Slugging SS1
		0.44, 0.53, 0.62	Severe Slugging SS
		0.71, 0.80, 0.88, 1.06, 1.23	Ordinary slugging S
3	0.51	0.45, 0.54	Severe Slugging SS

Table 6-2: Fluids matrix for the *helical pipe* riser experiments

6.3.1 Visual observations

Fluid-flow visualization was made during these riser experiments through a Perspex viewing section, which was installed downstream of the *helical pipe* section. Figure 6-7 shows the Perspex viewing-section on installation.

Figure 6-7: Perspex viewing-section

It was observed that the *helical pipe* section had two main effects on the flow. First, it acted as a series of 'sumps' where the water settled and stratified flow could not be maintained in the pipe. The settled-water at the bottom of each dip blocked the passage of the air until the pressure was built up sufficiently (this could be only a very small increase in pressure) to cause a 'mini blow out'. Thus water and air travelled through the *helical pipe* section in pulses of 'mini slugs'. The flows at the start and at the end of each pulse were also highly aerated. Secondly, the *helical pipe* section imparted swirl to the liquid causing even more air entrainment (or bubbles) as it 'poured' over the top of each turn of the pipe. After the *helical pipe* section, the fluid naturally tried to revert to stratified flow in the straight section immediately upstream of the riser. However, it was observed at the viewing section that the air water separation was incomplete and there were still bubbles in the water.

6.3.2 Pressure difference characteristics

Figures 6-8 and 6-9 show characteristics of the pressure difference cycle between the base and the top of the riser during the occurrence of severe slugging for both straight and *helical pipes* respectively.

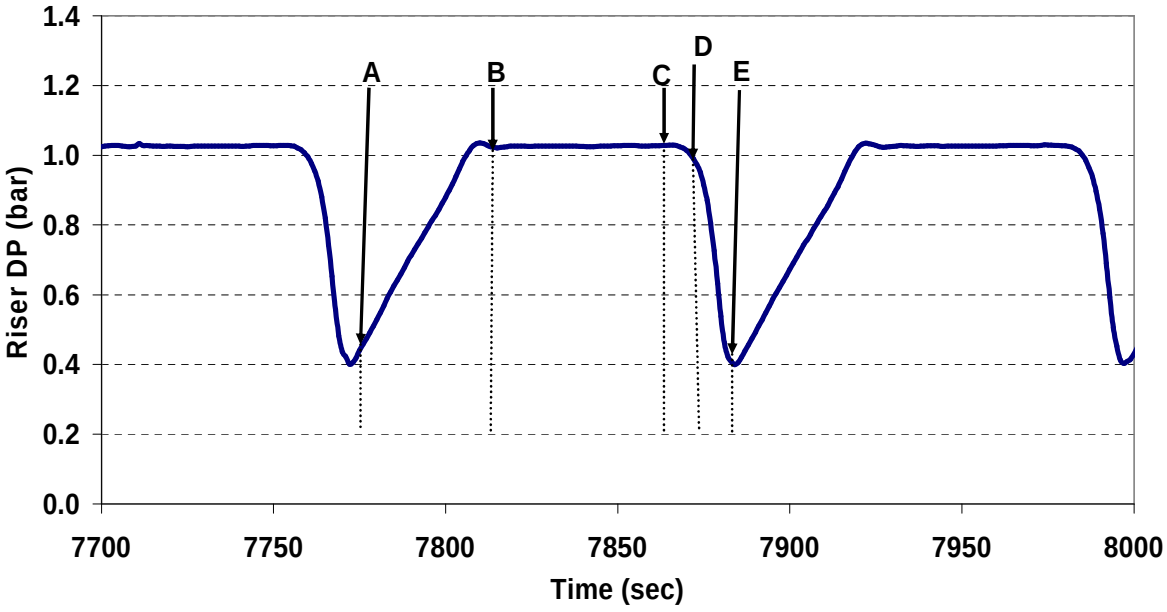

Figure 6-8: Straight pipe pressure difference cycle characteristics

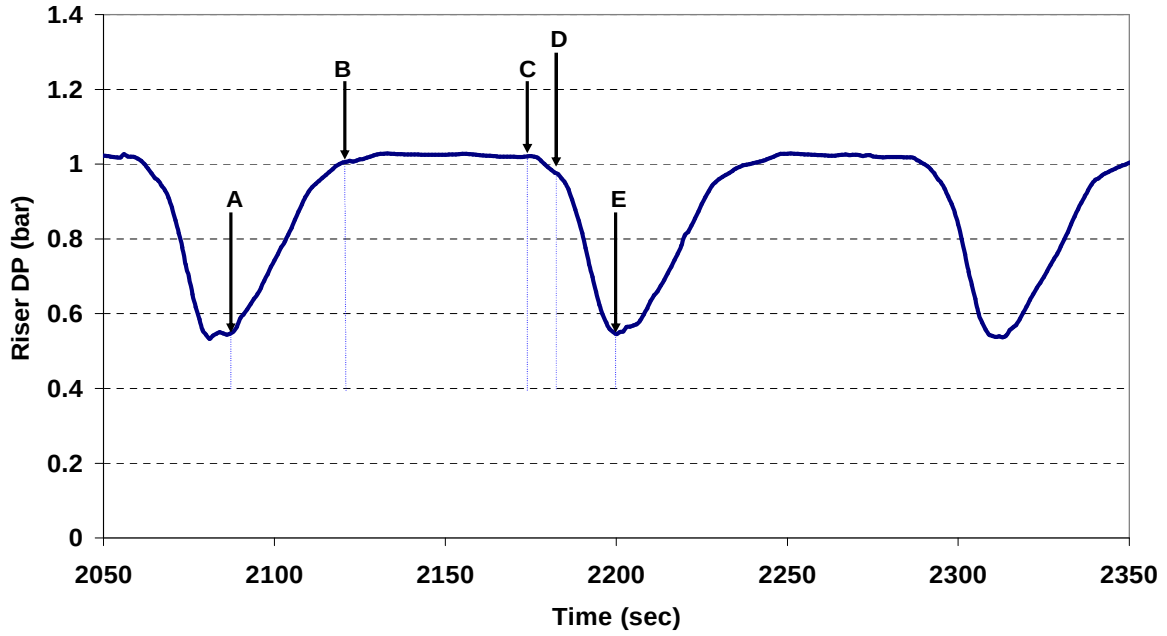

Figure 6-9: *Helical pipe* riser pressure difference cycle characteristics

As shown in Figures 6-8 and 6-9, as the liquid starts to accumulate at the base of the riser, pressure difference between the base and the top of the riser increases steadily (section **AB**). This is usually called slug build up period.

The second stage of severe slugging formation, which is normally regarded as slug production is shown in section **BC** in both Figures 6-8 and 6-9. During this period, the pressure difference over the riser is constant and at its maximum value.

The bubble-penetration stage is shown in section **CD** in Figures 6-8 and 6-9, and at this stage, pressure difference over the riser begins to drop.

The last stage of severe slugging formation (i.e. gas blowdown) is shown in section **DE** in Figures 6-8 and 6-9. The beginning of the pressure drop over the riser during the bubble-penetration stage reduces the riser base pressure, so inducing acceleration of the pipeline gas into the riser.

6.3.3 Liquid holdup characteristics

A gamma densitometer was installed at the base of the pipeline/riser experimental rig to give values of the density of the fluid at that section. The gamma densitometer reading also gave the liquid holdup characteristics. When the section was 100% full of water, the density was around 1 kg/l. Figures 6-10 and 6-11 show gamma density characteristics cycle for both straight and *helical pipes'* configurations. The fluctuating nature of the traces in all the sections (**AB, BC, CD and DE)** in Figure 6-11 shows that air always escaped with liquid in the *helical pipe*.

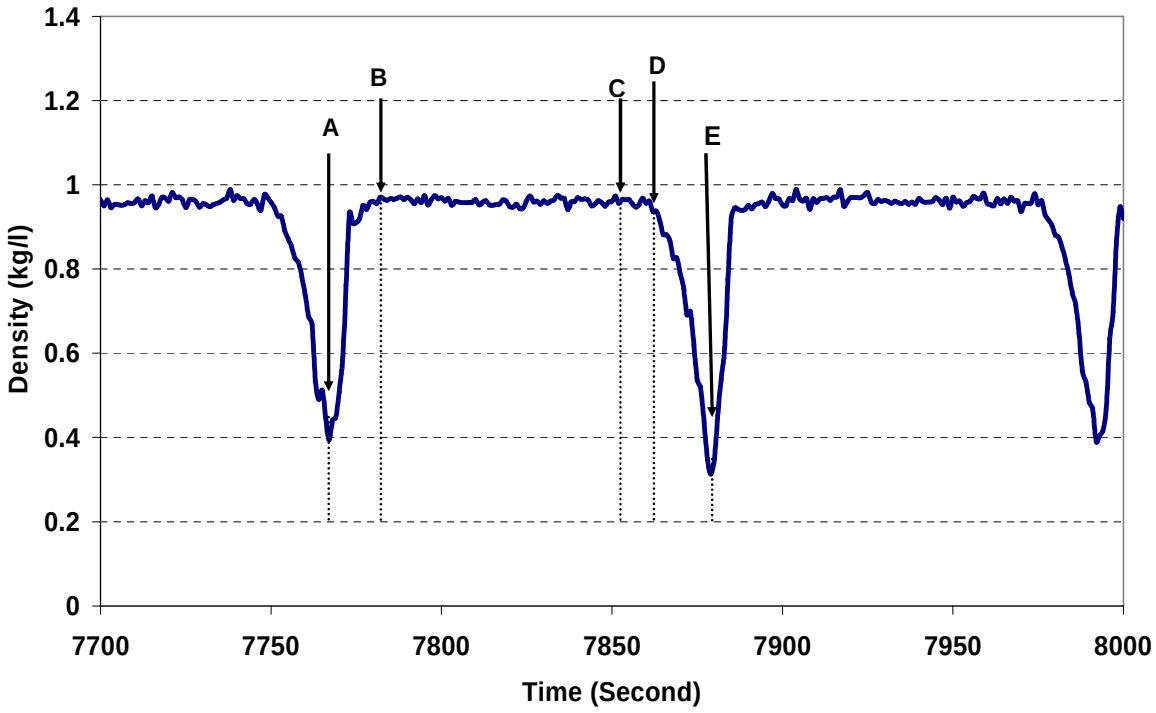

Figure 6-10: Riser base gamma densitometer cycle characteristics for the straight pipe's configuration during severe slugging

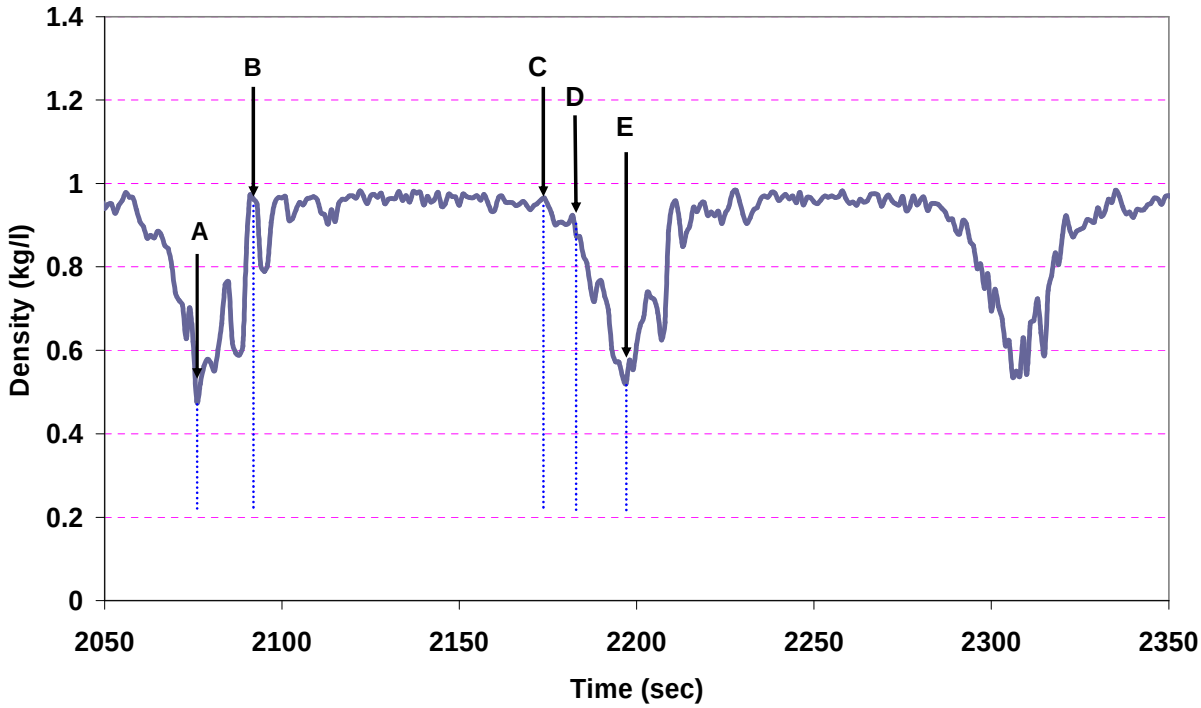

Figure 6-11: Riser base gamma densitometer cycle characteristics for the *helical* pipe's configuration during severe slugging

Comparing Figures 6-10 and 6-11 (riser base gamma densitometer cycle characteristics), there is a major difference between the behaviours of both straight and *helical pipes*' configurations. Firstly, during the slug production phase **BC**, the gamma densitometer reading for the straight pipe is more constant than that of the *helical pipe* which remains fluctuating so indicating that the riser base is not full of water but has air passing through it. Also for the *helical pipe's* configuration, the riser base fluid-density drops rapidly during the gas blowdown stage section **DE** and thereafter the riser base density increases (section **AB**) in an up and down pattern (this is attributed to the passage of pockets of air that escaped with the liquid).

6.3.4 Liquid production characteristics

Figures 6-12 and 6-13 show liquid production cycle characteristics behaviour during severe slugging (SS1) for both straight and *helical pipes* respectively.

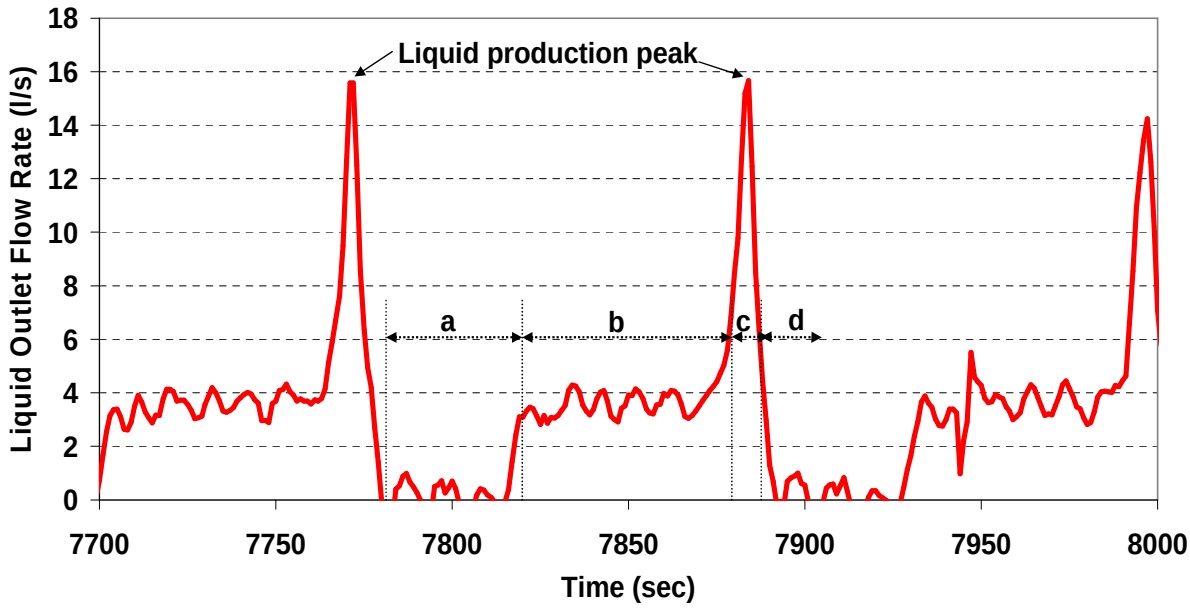

Figure 6-12: Straight pipe liquid production cycle characteristics

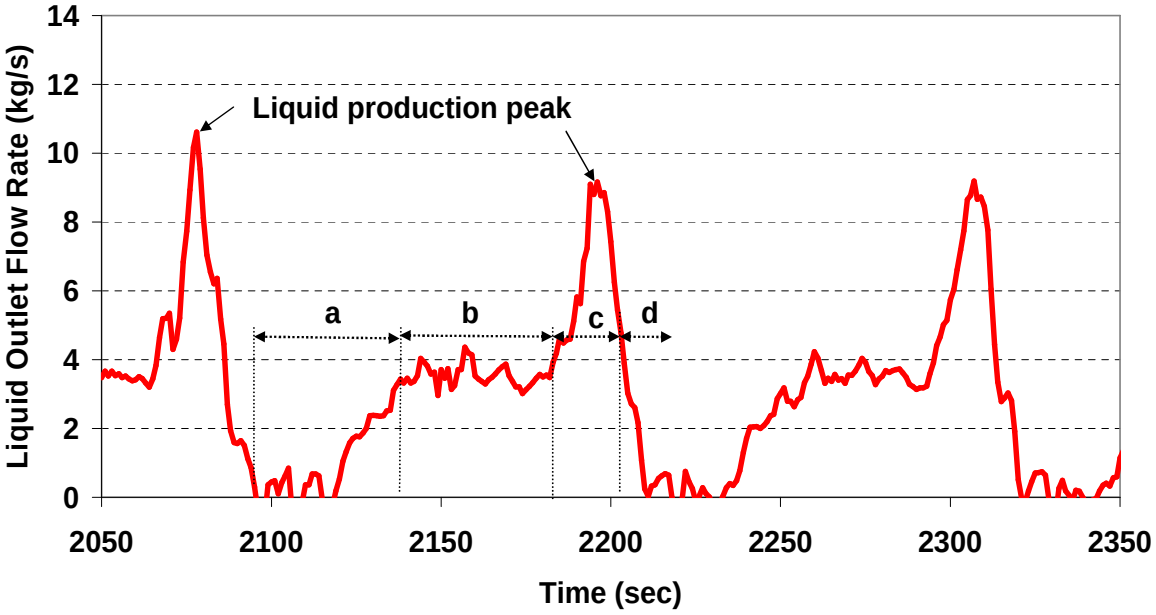

Figure 6-13: *Helical pipe* liquid production cycle characteristics

Comparing Figures 6-12 and 6-13, liquid outlet flow rate is higher in the straight pipe riser than in the *helical pipe* riser. This can be attributed to the presence of air at all times in the *helical pipe* riser. One of the detrimental features of severe slugging class1 (SS1) is a sudden increase in liquid production which usually leads to overflow of the topside separator. As a result of overflow, the separator can shut down or other platform processing devices will be damaged. Moreover, pressure fluctuations resulting from the large liquid production can slow down the hydrocarbon field's productivity. So the net effect of less increase in liquid production in *helical pipe* riser is that all these problems will be reduced.

6.3.5 Overall behaviours of straight and helical pipes

6.3.5.1 Severe slugging class 1(SS1)

Figure 6-14 shows a typical severe slugging class1 (SS1) behaviour of a 0.1 m straight pipe riser (i.e. without the *helical pipe*) with gas superficial (U_G) and liquid superficial (U_W) velocities at 0.18 ms^{-1} and 0.38 ms^{-1} respectively. The pressure difference (i.e. between the base and the top of the riser), liquid

holdup at the base of the riser and liquid production (outlet flow) characteristics are shown in Figure 6-14.

After the gas blowdown stage, the energy of the air was insufficient to support the liquid in the riser and the liquid will fall back down and collect at the riser base. The gamma densitometer reading will usually indicate that the bottom of the riser was almost blocked by the water (the density at the bottom was nearly 1kg/l). The pressure difference increased slowly until the water reached the top of the riser and the pressure difference then remained constant. During the period of constant pressure difference, the gamma densitometer will indicate that the riser base was full of water. It must be noted that the oscillation of liquid flow during this 'constant' production period was due to numerical errors from differentiation of the separator liquid level to calculate the flow from the riser. This is a period of constant liquid-production and it means that the flow at the outlet of the riser is roughly constant. As air continuously entered the flowline, but the pressure cannot increase further, the increased air volume in the flowline will push the air/ water interface towards the riser base. When the interface reached the base of the riser, as indicated by a drop in the gamma densitometer reading, it triggered the gas blowdown resulting in a rapid decrease in riser pressure difference. As the liquid was pushed out of the riser, a surge in liquid production ensued and was followed by a surge in gas flow.

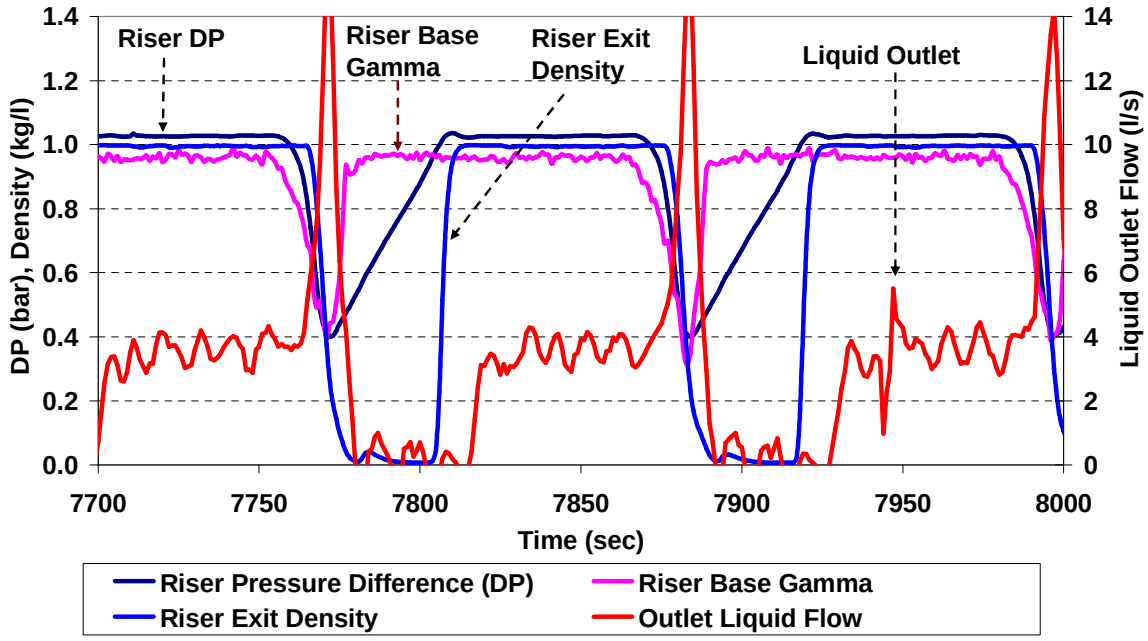

Figure 6-14: Severe slugging class 1 (SS1) cycle characteristics of 0.1 m straight riser (U_G = 0.18 ms^{-1}, U_W = 0.38 ms^{-1})

The overall behaviour of the riser with the *helical pipe* section under similar conditions as straight pipe is shown in Figure 6-15. The major difference, which distinguishes the *helical pipe* section riser from the straight pipe riser, is the constant escape of air up the riser. This was shown by the riser base gamma densitomer trace. After the gas blowdown stage of severe slugging formation, the riser base density increased in a 'zigzag' manner (due to the passing 'pockets' of gas). During the slug production stage (when the riser DP was approximately constant at 1.04bar), the gamma densitomer reading remained fluctuating, indicating the riser base was not full of water but had a small amount of air passing through. The riser base fluid-density also dropped rapidly during gas blow-down. The minimum liquid holdup is much higher than that of the straight pipe riser. The minimum pressure difference across the riser with the *helical pipe* section was also much higher than the straight pipe riser so indicating there was more liquid in the former case. It can be postulated that the 'gas energy' available to 'push' the liquid out of the riser with the *helical pipe* section will be much less than the straight pipe riser. This could be attributed to the *helical pipe* having a higher friction factor than the straight pipe. The net

effect is that the blow down process will be less severe with the installation of the *helical pipe* section. The peak liquid and gas velocities are also much lower and hence will lead to much better conditions for the topside facilities from both process and mechanical considerations.

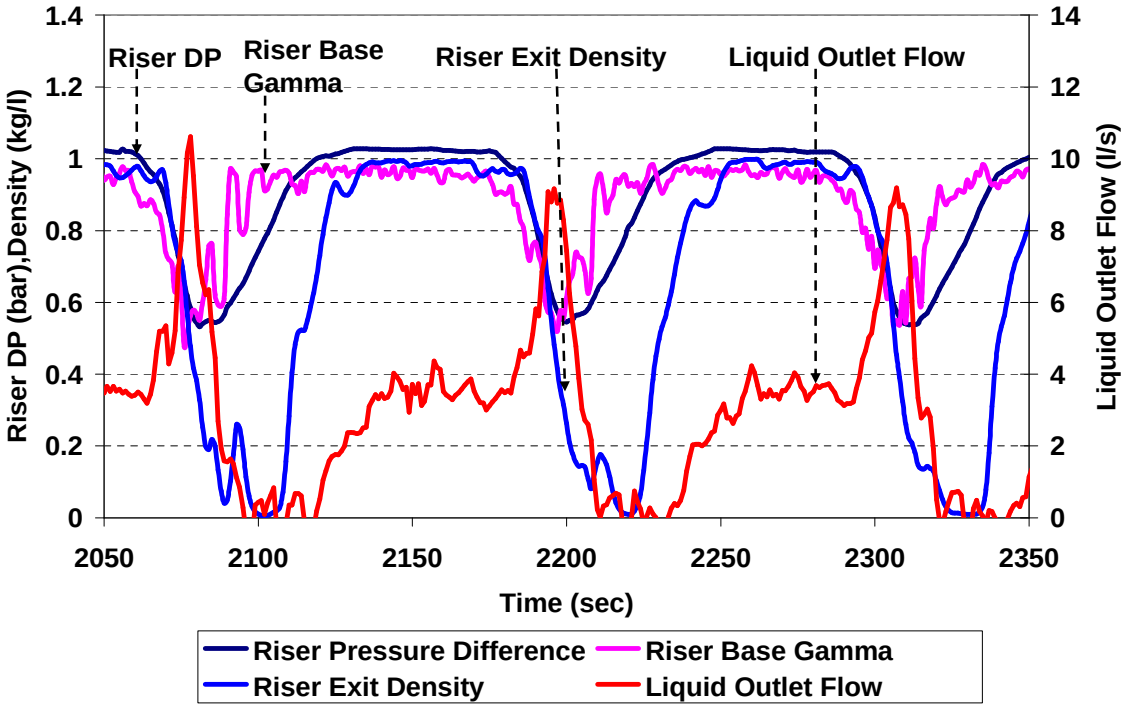

Figure 6-15: Severe slugging class 1 (SS1) cycle characteristics for the installation of 0.1 m *helical pipe* section (U_G = 0.18 ms^{-1}, U_W = 0.38 ms^{-1})

6.3.5.2 Severe slugging class 2 (SS)

As the air flowrate was increased and water flowrate was kept constant, the flow regime changed from severe slugging with constant liquid production (SS1) to severe slugging with variable liquid production (SS) and slug flows (S). Figures 6-16 and 6-17 (for both straight and *helical pipes* respectively) show the typical characteristic behaviour of severe slugging with variable liquid production (SS). For the *helical pipe,* severe slugging class 2 (SS) occurred at the same liquid superficial velocity (0.38 ms^{-1}) severe slugging class 1 (SS1) occurred but at an increased gas superficial velocity of 0.55 ms^{-1} (Figure 6-17). For the straight

pipe, severe slugging class 2 (SS) occurred at liquid superficial velocity of 0.51 ms^{-1} and gas superficial velocity of 0.71 ms^{-1} (Figure 6-16).

Whilst there was no constant liquid production in this class of severe slugging (SS), the riser could be completely filled with liquid as indicated by the maximum pressure difference of 1.04bar. Thus the liquid slug will be equal to or longer than the length of the riser (hence the severe slugs). The regular passing of gas pockets up the riser was clearly evidenced from the pulsations in the gamma densitometer readings at both the base and top of the riser (Figure 6-17). It was also observed that the frequency at which pressure, density and liquid production occurred increased more than in severe slugging class SS1.

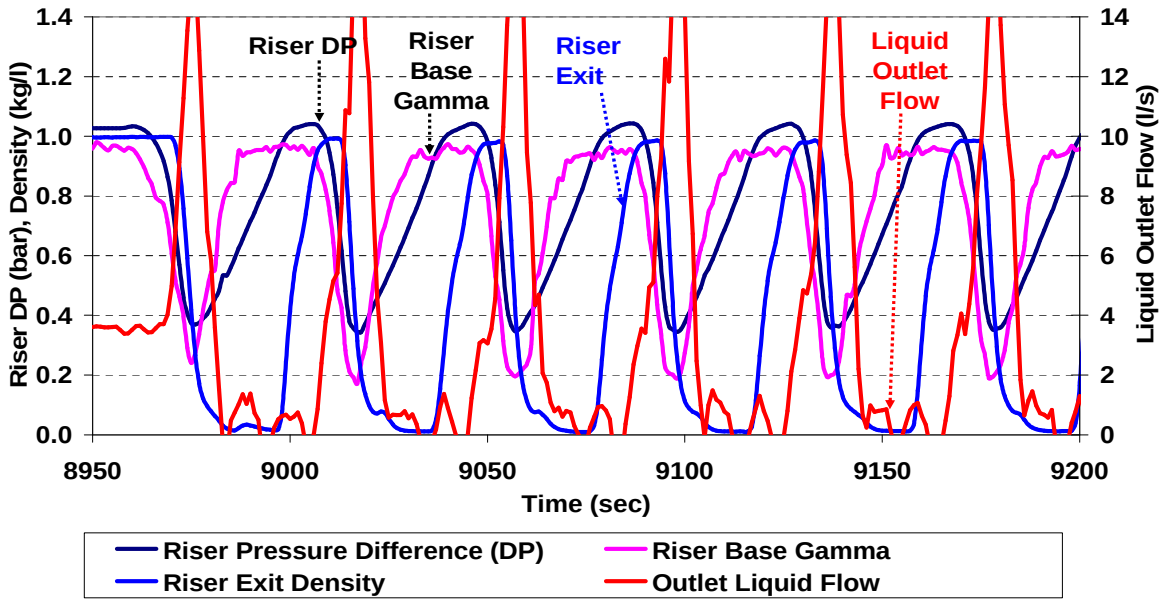

Figure 6-16: Severe slugging class 2 (SS) cycle characteristics of 0.1 m straight riser (U_G = 0.71 ms^{-1}, U_W = 0.51 ms^{-1})

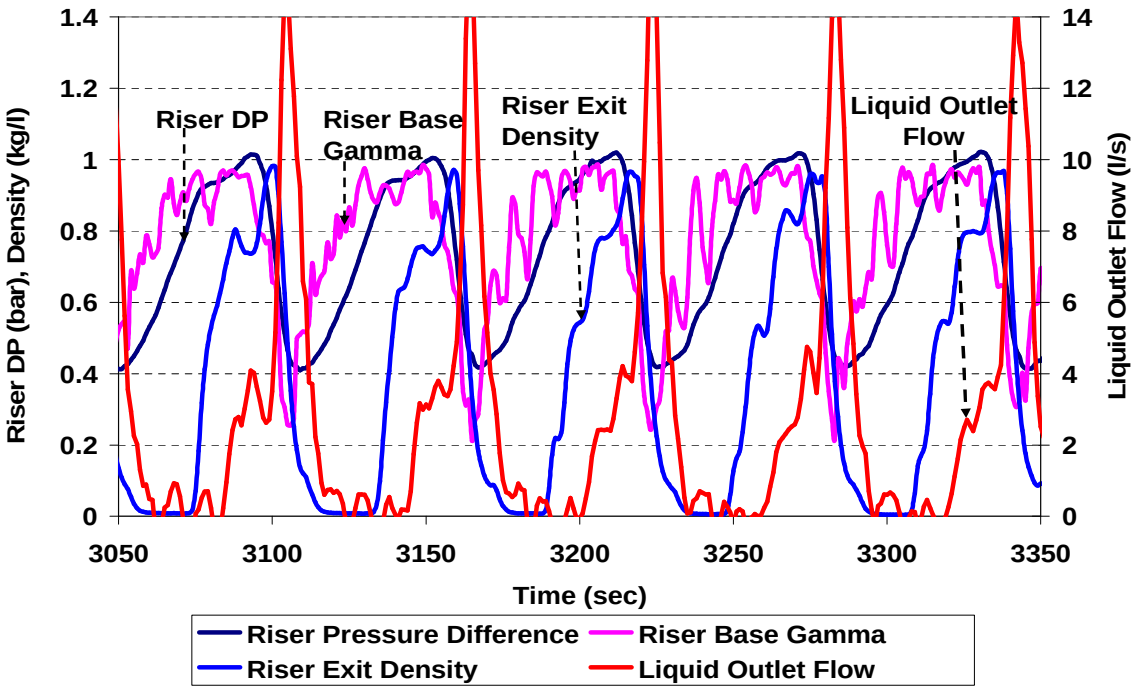

Figure 6-17: Severe slugging class 2 (SS) cycle characteristics with installation of 0.1 m *helical pipe* section (U_G = 0.55 ms^{-1}, U_W = 0.38 ms^{-1})

6.3.5.3 Ordinary slug (S)

Figure 6-18 shows an ordinary slug flow regime for the straight pipe. This class of slug (S) occurred for the straight pipe as gas superficial velocity was increased further from 0.71 ms^{-1} to 0.89 ms^{-1} at the same liquid superficial velocity (0.51 ms^{-1}) of severe slugging class 2 (SS).

At the same liquid superficial velocity (0.38 ms^{-1}) of severe slugging class 2 (SS) for the *helical pipe* and as the gas superficial velocity was increased further from 0.55 ms^{-1} to 0.80 ms^{-1} , the flow regime also changed from severe slugging class 2 (SS) to ordinary slug (S). This is shown in Figure 6-19. During this class of slug flow, the riser was never full of water and the maximum pressure difference was less than 1 bar (0.92bar). The frequency at which pressure, density and liquid production occurred also increased more than in severe slugging class SS.

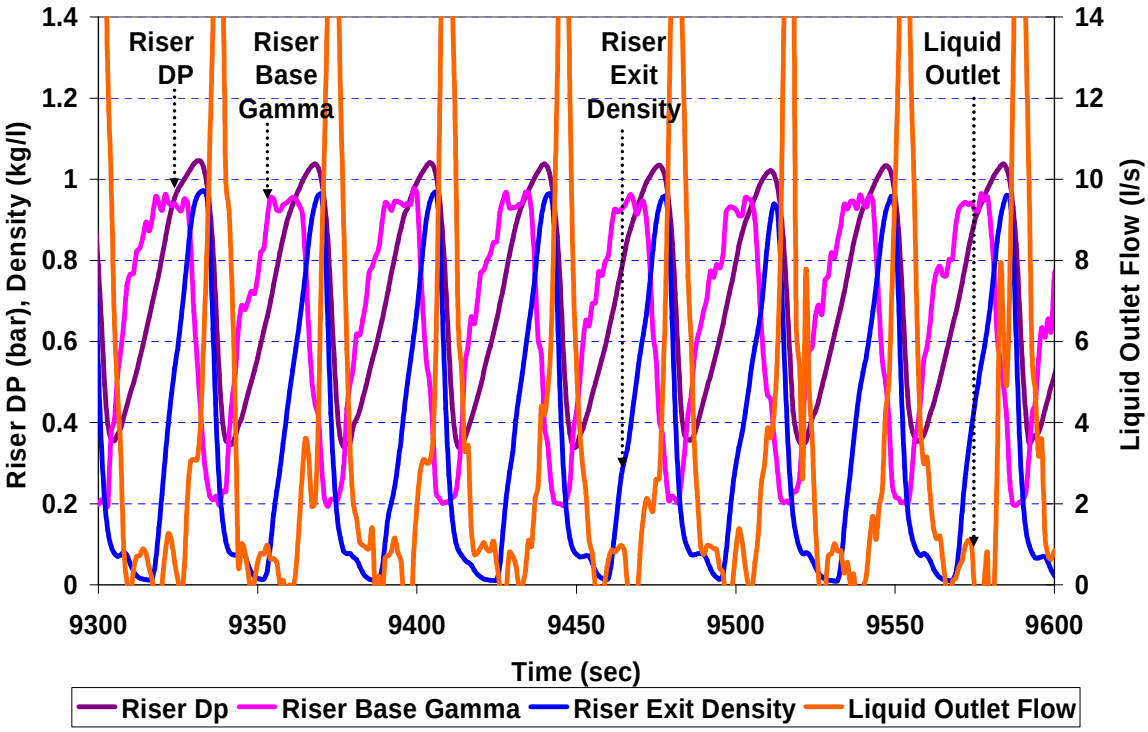

Figure 6-18: Ordinary slug (S) cycle characteristics with installation of 01 m Internal-diameter straight riser (U_G = 0.89 ms^{-1}, U_W = 0.51 ms^{-1})

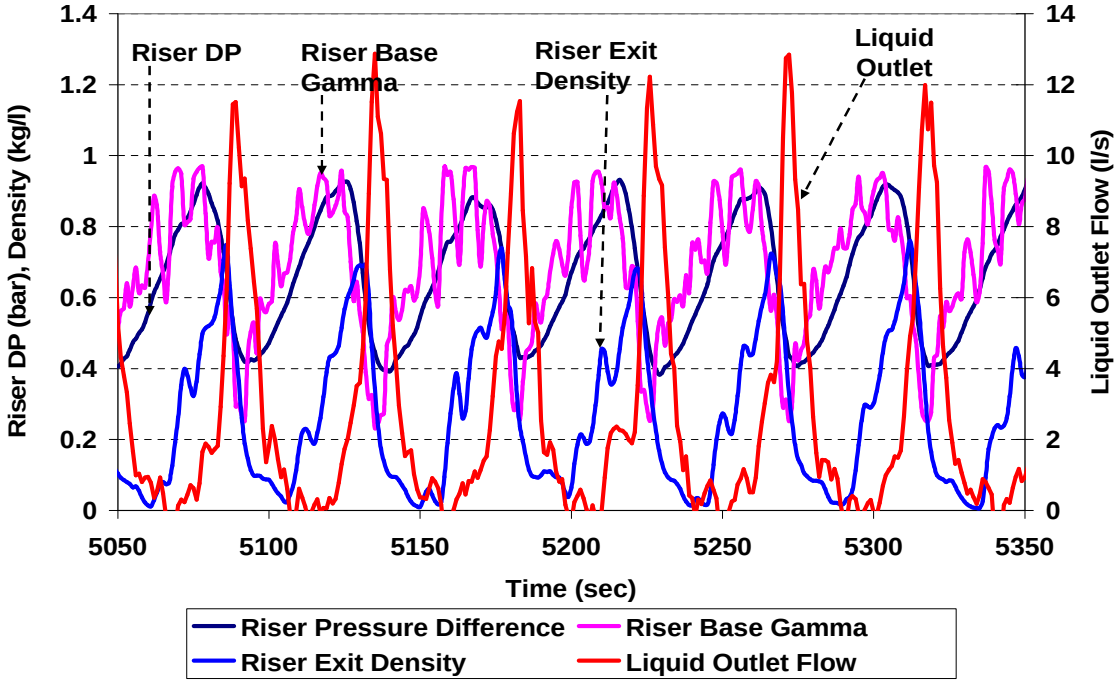

Figure 6-19: Ordinary slug (S) cycle characteristics with installation of 0.1 m *helical pipe* section (U_G = 0.80 ms^{-1}, U_W = 0.38 ms^{-1})

6.3.5.4 Summary of experimental results

In order to summarise discussions on the experimental results, Figure 6-20 was plotted (riser pressure difference against air superficial velocity) to show the differences between severe slugging in the riser, with and without the *helical pipe* section of 6 m length, at a liquid superficial velocity (U_W) of 0.38 ms^{-1}.

As shown in Figure 6-20, at air superficial velocities between 0.4 ms^{-1} and 1.4 ms^{-1}, both risers experienced severe slugging (SS1). Although the maximum pressure differences for both scenarios (pipes) were the same during the severe slugging (SS1), the minimum pressure difference for the *helical pipe* section was higher than for the straight pipe. This is because the gas blowdown stage in the *helical pipe* was less severe during slugging formation than for the straight pipe. Figure 6-20 also shows that as the air superficial velocity increases, the maximum pressure difference drastically reduces for the *helical pipe* which shows that the riser was not full of water as the severe slugging flow regime changes to ordinary slug flow. Further increase in air superficial velocity resulted in small pressure differences and the flow regime changed from slug flow to bubble flow.

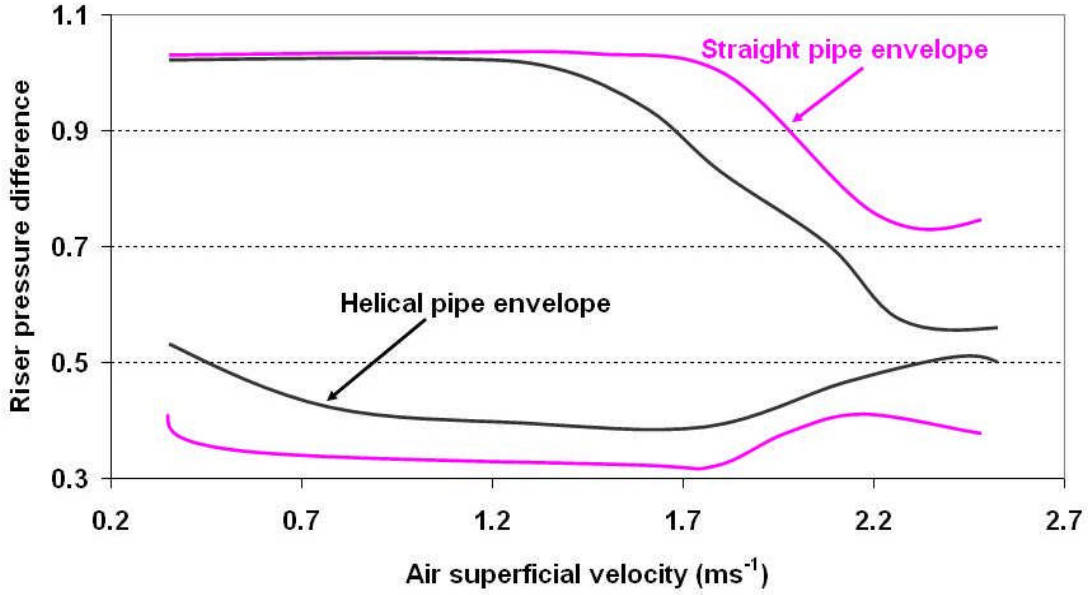

Figure 6-20: Riser pressure difference with increase in gas flow (U_W 0.38 ms^{-1})

The plot in Figure 6-20 shows severe slugging envelopes for both straight and *helical pipe*s. Experimental data points that are joined together by lines are shown in Appendix A.

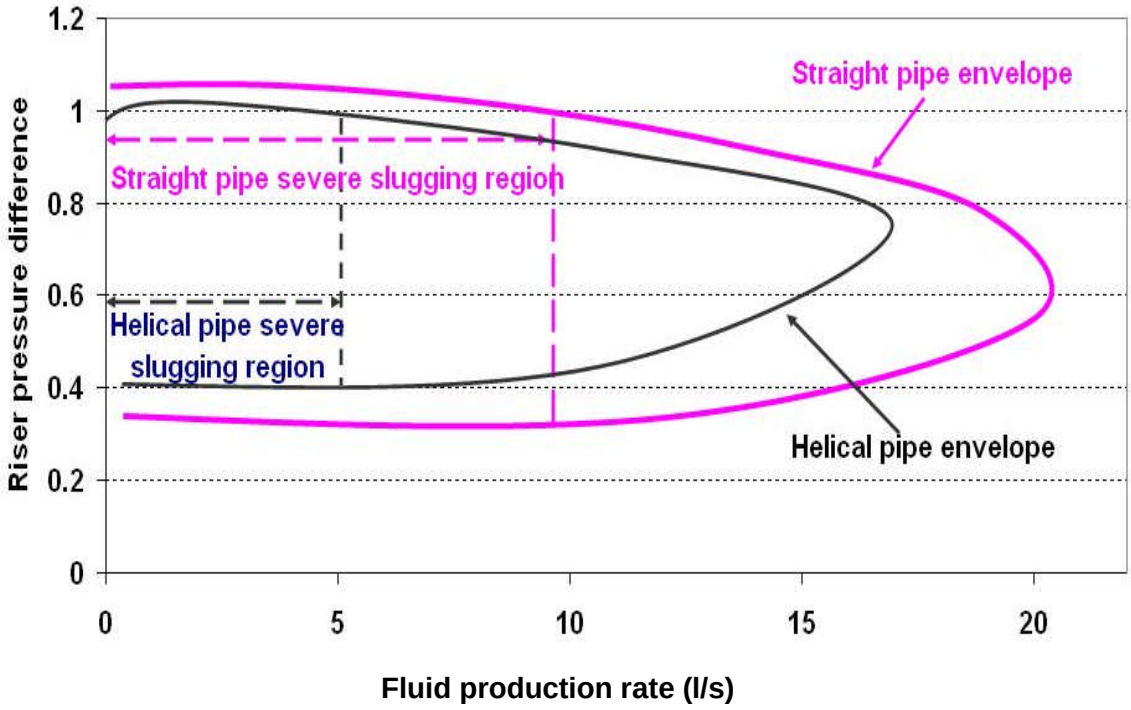

Figure 6-21: Riser pressure difference with fluid production rate

Figure 6-21 shows a relationship between riser pressure difference and fluid production rate. The figure shows a similar behaviour to riser pressure difference with increase in gas superficial velocity (Figure 6-20). As the fluid production rate increases, the severity of the liquid slugging changes from SS1 to ordinary slug (S). Again, the figure shows that severe slugging classes SS1 and SS (indicated by the maximum pressure difference of 1.04 bar) occur at a lower fluid production rate for the riser with the *helical pipe* section. In addition to this, even in the severe slugging (SS1) region, the minimum pressure difference for the *helical pipe* section was higher than the straight pipe riser at the same fluid production rate.

It is also evident from Figure 6-21 that the change from one flow regime to another occurred at a lower fluid production rate for the *helical pipe* section than for the straight pipe riser. Experimental data points that are joined together by lines for Figure 6-21 are also shown in Appendix A.

6.3.5.5 Riser instantaneous liquid production

Figure 6-22 shows traces of the riser instantaneous liquid production for both the straight and the *helical pipes*. Again, the data points that are joined together by lines for this figure (Figure 6-22) are shown in Appendix A.

As shown in the Figure (6-22), traces of the riser outlet fluid flows for the straight and *helical pipe*s are compared for different inlet air flow conditions. The water flow was maintained at a superficial velocity of 0.38 ms^{-1}. The Figure also shows that the outlet fluid flows in the severe slugging region increases with the inlet air flow. One of the most challenging conditions the topside separator is always facing is the severe slugging boundary where the instantaneous riser liquid outlet flow is the highest. These instantaneous liquid production comparative studies between the straight and the *helical pipes* (Figure 6-22), show that with the installation of a 6 m *helical pipe* section, the maximum liquid flow at the outlet was 17 l/s as compared with that of straight pipe which was 21l/s. This also proves that the use of *helical pipes* to mitigate severe slugging will be beneficial than using the straight pipes.

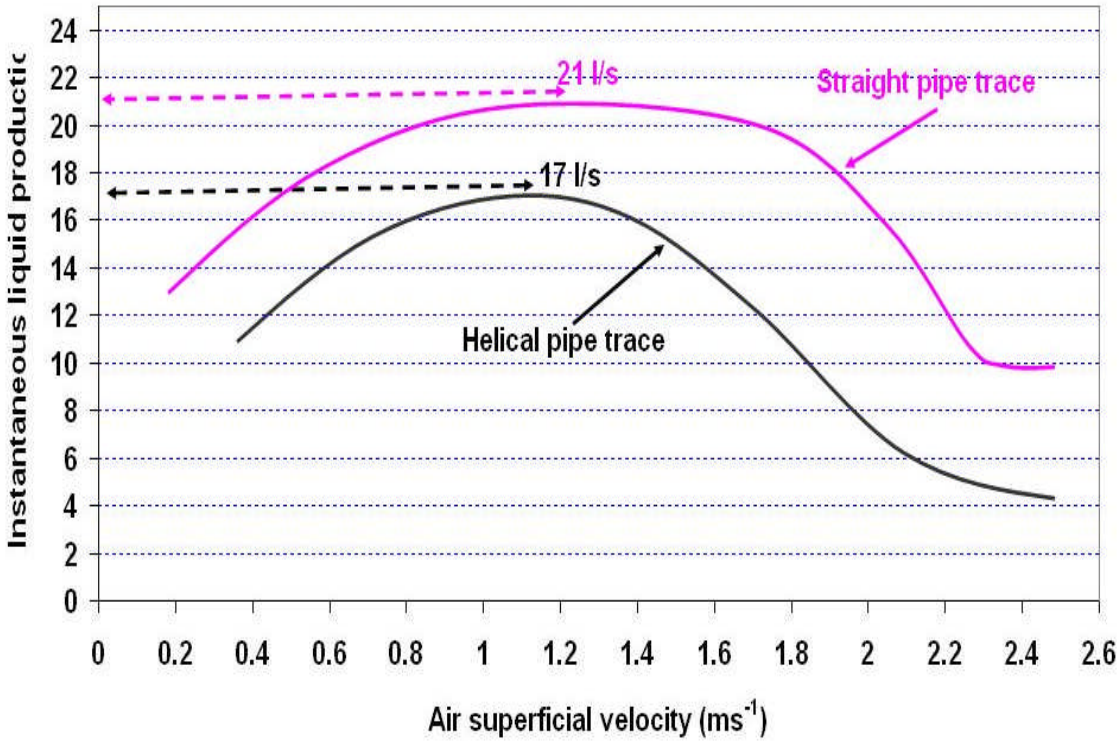

Figure 6-22: Liquid instantaneous production

All these experimental results clearly confirm that the riser with the *helical pipe* section will be better than the straight pipe riser by having a larger operational envelope.

6.3.5.6 Effect of reducing the *helical pipe* length

Having established that the installation of the *helical pipe* upstream of the riser base will reduce the menace of severe slugging, the 6 m length *helical pipe* was reduced to 3 m. The aim was to study how effective a 3 m length of the *helical pipe* will reduce severe slugging compared with the 6 m length. Figure 6-23 shows the result of the length effect on the severe slugging envelopes.

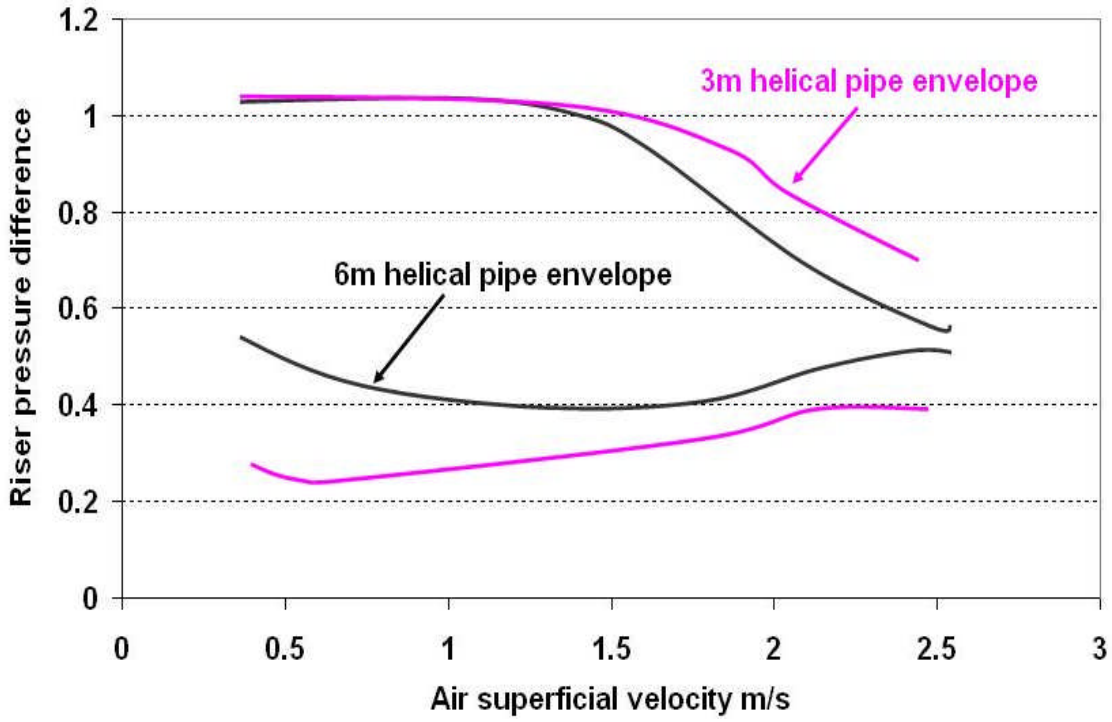

Figure 6-23: Effect of the *helical pipe* length on severe slugging control

As shown in Figure 6-23, the effect of 3 m length *helical pipe* is less than for the 6 m length *helical pipe* particularly at high air superficial velocities. This may be attributed to the fact that the longer the length of the *helical pipe*, the more the number of pitches and the more air is entrained in the pipe. Experimental data points that are joined together by lines for Figure 6-23 are shown in Appendix A.

The gaps in the groups of experimental data that are joined together by lines shown in Appendix A were due to time delays whenever the air flow rate was increased.

All the experimental data points were sampled at intervals of one second (1 sec) through the test matrix.

6.3.5.7 Flow regime maps

These were developed from the experimental test results. Figures 6-24 and 6-25 show the flow regime maps for the riser with the straight pipe and riser with a 6 m *helical pipe* section upstream of the riser. It is pertinent to state that, although the regime boundary is drawn as a line, the transition between one flow regime and another is a gradual process. Comparing both flow regime maps (Figures 6-24 and 6-25), it is clear that the severe slugging region for the 6 m *helical pipe* section riser (Figure 6-25) is much smaller than the straight pipe riser (Figure 6-24). Also at a liquid superficial velocity of 0.38 ms^{-1}, the gas superficial velocity for severe slugging (SS) to slug flow (S) transition was around 0.67 ms^{-1} for the *helical pipe* section riser which compared with 0.93 ms^{-1} for the straight riser. The area for bubbly/slug flow is also much larger than for the *helical pipe* section riser.

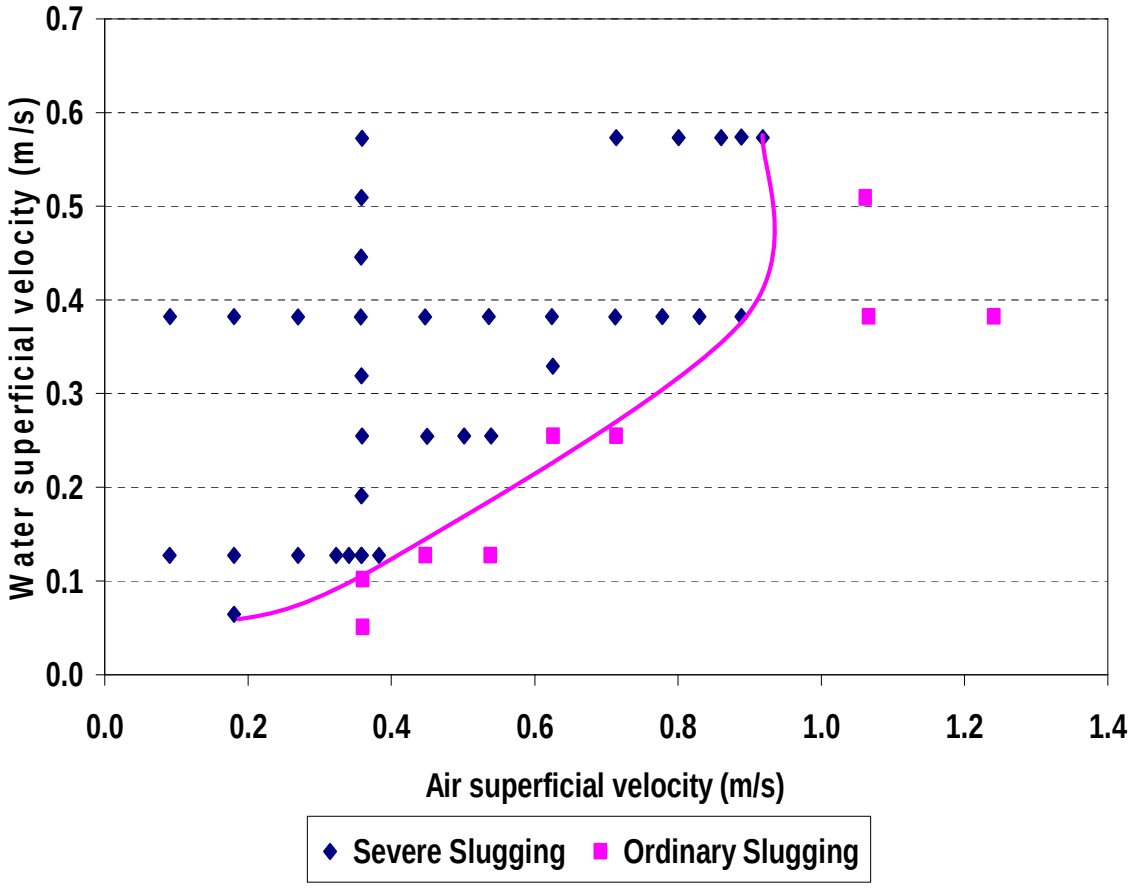

Figure 6-24: Flow regime map for the straight pipe

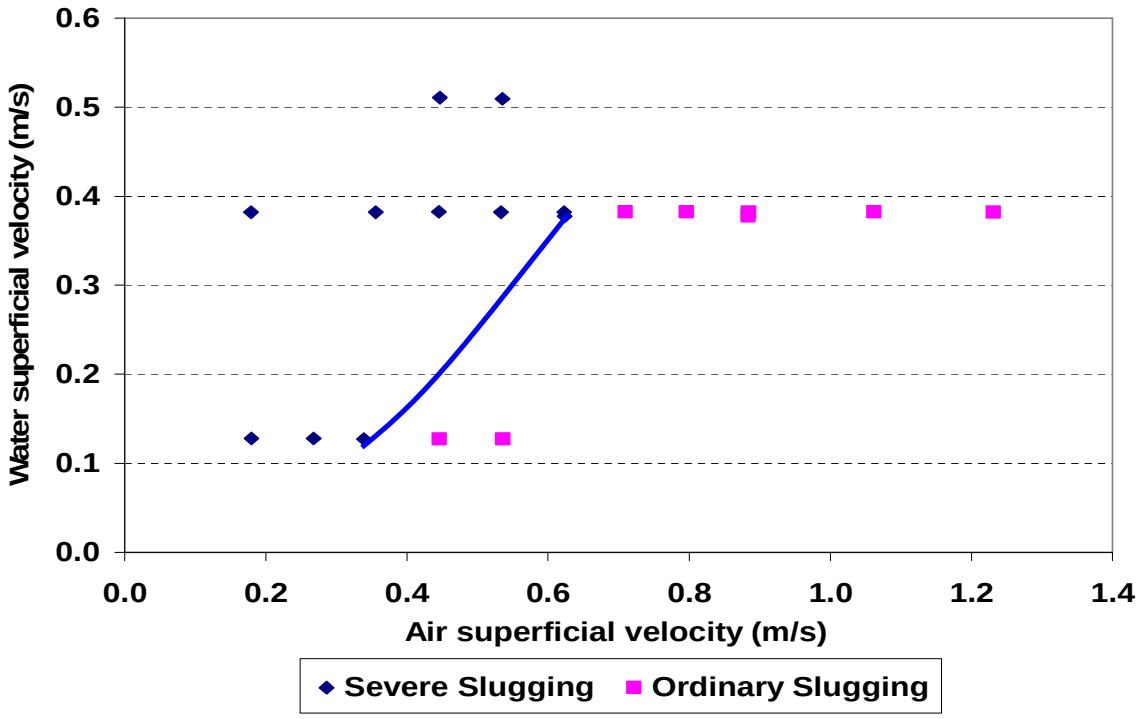

Figure 6-25: Flow regime map with the *helical pipe* section of 6 m

6.4 Conclusions

Based on the experimental evidence presented in this chapter, the following conclusions are drawn:

- The *helical pipe* section destroys the conventional stratified flow regime which normally occurs in a straight pipe in the slightly downward inclined pipeline. As the flow negotiates the 'peaks and troughs' of the *helical pipe* section, gas is entrained in the liquid which makes it impossible for a stratified flow regime to be established. Also, by the time the flow reaches the base of the riser, stratified flow has not been re-established. This leads to the release of bubbles up the riser and the lower likelihood for the riser base to be blocked by liquid.

- The *helical pipe* section reduces the region of severe slugging by about 76.2% in comparison with a straight pipe riser, thus enlarging the operating envelope.

- Even in the severe slugging regime, the severity of the liquid production, liquid blowdown and pressure oscillation are reduced, which in effect will lead to better conditions for the topside process facilities.

- The cost of installing a section of *helical pipe* upstream of a riser base to control severe slugging will be far cheaper than any of the existing methods (discussed in chapter 5 of this Thesis) of reducing severe slugging formation. This is because the section of the *helical pipe* will form an integral part of the flowline. No additional components (valves, gas line or sleeves) are required to be installed or external gas to be injected either into the riser or pipeline. The installation will also be easier.

Chapter 7

7 Conclusions and Recommendations

The studies in this thesis have reviewed the correlations for fluid flows through *helical pipes*. Three different *helical pipe* geometries have been experimentally investigated. Details of the three pipe geometries are presented in Appendix A. Three straight pipes, of the same internal-diameters as the *helical pipes,* were also experimentally investigated. The results for each of the *helical pipes* investigated have also been compared with their counterparts for the straight pipes.

7.1 Conclusions

7.1.1 Research summary

1. Review of *helical pipe* correlations. This has established that most previous studies on *helical pipe*s have been for pipes with small internal-diameters (0.9 mm to 17.5 mm) and high amplitude (i.e. high value of internal-diameter, **d** to *helical pipe* diameter, **D**).

2. *Helical pipes* with low amplitude and internal–diameters 25.4 mm, 50 mm and 100 mm have been investigated experimentally. This new research direction, in the study of hydrodynamics, has applications with particular reference to transporting hydrocarbon products from their reservoirs or wells to the process plant.

3. Experiments were performed on single-phase (water) fluid-flow in 25.4 mm internal-diameter straight and *helical pipe*s in horizontal and vertical

positions. The main aim of these experiments was to measure and compare pressures and pressure drops in both the straight and *helical pipe*s. Visual observations were also undertaken.

4. Experiments were also performed on single-phase (water) and two-phase (water and air) in 50 mm internal-diameter straight and *helical pipe*s for a mean horizontal position. The main aim of performing these experiments was to study hydrodynamic characteristics of two-phase (air and water) flows in straight and *helical pipes* with the main objective of investigating the effectiveness of the *helical pipe* in destroying hydrodynamic slugs, which usually occur in fluid flows in horizontal straight pipes. Visual observations were recorded while the experiments were being performed.

5. A comprehensive review of severe slugging formation in order to determine the criteria for their formation and the control methods to inhibit their initiation were carried out. The objectives of the review were to discuss the menace of severe slugging in pipeline-riser systems and on the other hand to discuss the proposed novel method of installing sections of *helical pipe*s of 6 m and 3 m lengths up-stream of a catenary shaped riser base.

6. For the first time, sections (6 m and 3 m lengths) of *helical pipes* of internal-diameter 0.1 m were installed at some distance from the base of a catenary riser. The aim of installing the *helical pipe sections* was to experimentally study their effects on riser behaviour with a particular reference to controlling severe slugging in pipeline riser systems. The objective of the experiments was to improve the conveyance of hydrocarbon products, particularly from wells and reservoirs in the sub-sea environment to process plants on-shore.

7.1.2 Conclusions

The complexity of fluid flows in *helical pipe*s mainly stems from the gas-liquid interface changing randomly and instantaneously inside the *helical pipe*s: this change is geometry dependent. The following conclusions can be drawn from the results of this research study.

1. In single-phase (water) flows, the *helical pipe* has a higher head loss than the straight pipe. This confirmed the results of previous investigations by several authors. This conclusion also shows that irrespective of the size (big or small) of internal-diameter, pitch and amplitude, single-phase fluid flows in *helical pipe*s will always exhibit higher head losses or pressure drops than equivalent straight pipes. This is due to the centrifugal force which the fluid flow in the *helical pipes* experiences and which also causes a swirling motion of the fluid in the *helical pipe*s. The head loss has also been confirmed to be higher in fluids flowing in horizontal pipes than fluids flowing in similar pipes but in the vertical position.

2. The results of investigations on hydrodynamic characteristics of single-phase (water) and two-phase (air and water) flows in straight and *helical pipes* of 50 mm internal-diameter and in horizontal position show that:

    I. the pressure drop is higher in the *helical pipe* than in the straight pipe for both single-phase and two-phase flows;

    II. the liquid holdup increases as the pressure drop decreases in both straight and *helical pipes*;

    III. at relatively higher fluids' superficial velocities, the liquid holdup is higher in the *helical pipe* than in the straight pipe; and

IV. at very low superficial velocities of air and water, stratified flow occurred in the straight pipe, but at the same very low superficial velocities of air and water, stratified flow did not occur in the *helical pipe*; instead a bubbly flow occurred.

3. Slug flow occurred in the straight pipe at certain superficial velocities of air and water, whereas, at the same superficial velocities of air and water, slug flow did not occur in the *helical pipe*; instead bubbly flow occurred.

4. The friction factor is higher in the *helical pipe* than in the straight pipe for both single-phase and two-phase flows.

5. For severe slugging conditions, the *helical pipe* section installed at some distance from the base of the riser destroys the conventional stratified flow regime which normally occurs in straight pipes in the slightly downward inclined pipeline. As the fluids flow up and down the *helical pipe* section, gas is trapped in the liquid which makes it impossible for a stratified flow regime to be established. Also, by the time the flow reaches the base of the riser, stratified flow has not been re-established. This leads to the release of bubbles up the riser and the lower likelihood for the riser base to be blocked by liquid.

6. Flow regime maps showing the occurrence of severe slugging were developed for both straight and *helical pipe*s from the analysed experimental data. The developed flow regime maps showed that installation of a *helical pipe* section, at some distance from the base of a riser, reduces the region of severe slugging by about 76.2% in comparison with a straight pipe riser, thus enlarging the operating envelope. Also, in the severe slugging regime, the severity of the liquid production, liquid blowdown and pressure oscillation are reduced, which in effect will lead to better conditions for the topside process facilities.

7. The cost of installing a section of *helical pipe* upstream of a riser base in order to control severe slugging will be far cheaper than any of the existing methods of reducing severe slugging formation. This is because the section of the *helical pipe* will form an integral part of the flowline. No additional components (valves, gas line or sleeves) are required to be installed or external gas to be injected either into the riser or pipeline. The installation will also be easier.

8. Flow visualization for all the experimental tests was undertaken simultaneously with the quantitative measurements. This has revealed that in two-phase (gas-liquid) fluid flows in *helical pipe*s, the gas phase travels in the middle of the *helical pipe*. This can be postulated as the main reason why at low fluids' (gas and liquid) superficial velocities, a stratified flow pattern does not occur in the *helical pipe*s.

7.2 Recommendations

As already mentioned, this study has opened up a new direction in the design of pipeline systems particularly in transporting hydrocarbon products from both on-shore and off-shore wells and reservoirs. However, many pertinent questions are still to be answered and the following are recommended for further investigations:

1. This study has shown that the flow pattern in *helical pipe* does not include stratified and slug flows and that predominantly the flow regimes in *helical pipe* are bubbly and dispersed. However, there is a need to investigate the phase interactions (transition between these two flow regimes). This will enable comparisons to be made with studies already undertaken with respect to phase interactions between one flow regime and another in straight pipes.

2. The combination of straight and *helical pipes* should be investigated in pipeline riser systems in order to confirm the optimal pipeline system that

will reduce the menace of severe slugging in the off-shore environment with a view to improving the production and transportation of hydrocarbon products.

3. This study was on two-phase (gas-liquid) flows. Other fluid phases including three-phase (oil-water-gas, oil-water-solid) should be investigated. In order to maintain flow assurance, the study of fluid phase including solids (sand, grit and dirt) is recommended as they tend to accumulate in the pipes and cause fluid-flow blockages. If the pipelines are free of these solid elements, the frequency of pigging (which is always expensive and always requires plant to be shut down and hence reduces productivity), of the pipelines will be greatly reduced.

4. In order to also maintain flow assurance of hydrocarbon products in the pipelines; there is a need for a better understanding of heat transfer phenomena particularly in *helical pipe*s with low amplitude. Thermal management of pipeline systems to ensure that temperatures remain above the relevant hydrate and wax deposition temperatures is a widely used technology. However, further investigations of heat transfer in *helical pipes* are strongly recommended.

5. The development of flow patterns and maps for *helical pipes*. Most of the existing fluid-flow regime maps have been developed for straight pipes. With the evolvement of *helical pipe*s' applications in the oil-and-gas industry, there will be a need to develop similar flow patterns for *helical pipe*s. H*elical pipes* with different configurations (helix angles, pitches, amplitudes, internal-diameters, helical-diameters, etc.) should also be investigated with a view to developing flow regime maps for a wide range of *helical pipes*.

6. These studies have been mainly concerned with horizontal pipes. Other pipes' positions (vertical and angular inclinations) should be investigated,

in particular, to study the effects of acceleration due to gravity in fluids flowing vertically and also the effects of fluids flowing downward and upward. These investigations are necessary because most of the pipelines go through combinations of these positions. The pipe position also has effects on parameters such as the liquid holdup and pressure drop.

7 Boundary-layer development is an important concept in fluid flows in pipeline and should be investigated for *helical pipes*. This will enable fluid flow velocity profiles to be generated for *helical pipe*s and compared with fluid flow velocity profile for straight pipes.

8 *Helical pipes* with various helix angles, pitches and amplitudes should be studied experimentally with a view to deducing the best *helical pipe* geometry that will reduce the menace of severe slugging in the pipeline-riser systems.

9 Computer simulation of the effectiveness of the *helical pipe* section in reducing severe slugging should be carried out and simulation predictions compared with experimental results. Computational Fluid Dynamics (CFD) of fluid flow in straight and *helical pipe*s and in both horizontal and vertical pipe positions should also be studied and the predictions compared with the corresponding experimental results.

References

Adedigba, A. G. O. (1988), "*Design of district-heating pipelines",* Master of Science Thesis, Cranfield Institute of Technology, Cranfield, UK.

Adler, M. (1934), "Stromung in gekrummten rohren. Z. Agnew", *Mathematics. Mechanical,* vol. 14, no. 5, pp. 257-275.

Akagawa, K, Sakaguchi, T. and Ueda, M. **(1971),** "Study on a gas- liquid two-phase flow in helically coiled tubes", *Bulletin JSME,* vol. 14, no. 72, pp. 564-571.

Ali, S. and Seshadri, C. V. (1971), "Pressure drop in Archimedian spiral tubes", *Industrial & Engineering Chemistry Process Design and Development,* vol. 10, no. 3, pp. 328-332.

Awwad, A., Xin, R. C., Dong, Z. F., Ebadian, M. A. and Soliman, H. M. (1995a), "Flow patterns and pressure drop in air/water two-phase flow in horizontal helicoidal pipes", *Journal of Fluids Engineering, Transactions of the ASME,* vol. 117, no. 4, pp. 720-726.

Awwad, A., Xin, R. C., Dong, Z. F., Ebadian, M. A. and Soliman, H. M. (1995b), "Measurement and correlation of the pressure drop in air-water two-phase flow in horizontal helicoidal pipes", *International Journal of Multiphase Flow,* vol. 21, no. 4, pp. 607-619.

Babus'Haq, R. F., Daly, L. M., Probert, S. D. and Adedigba, A. G. O. (1989), "Heat losses from horizontal pipes embedded in trenches filled with granular materials", *American Institute of Chemical Engineers Symposium Series,* vol. 85, no. 269, pp. 350-355.

Baker, O. (1954), "Designing for simultaneous flow of oil and gas", *Oil and Gas Journal,* vol. 53, no. 12, pp. 185-195.

References

Banerjee, S., Rhodes, E. and Scott, D. S. (1969), "Studies on cocurrent gas-liquid flow in helically coiled tubes- 1", *Canadian Journal of Chemical Engineering,* vol. 47, no. 5, pp. 445-453.

Barbuto, F. A. A. and Caetano, E. F. (**1991),** "On the occurrence of severe slugging phenomenon in Pargeo-1 Platform, Campos Basin, Offshore Brazil", *Proceedings 5th International Conference on Multiphase Production*, BHR Group, pp 491-503".

Barnea, D., Shoham, O. and Taitel, Y. (1982), "Flow pattern transition for downward inclined two phase flow; horizontal to vertical", *Chemical Engineering Science,* vol. 37, no. 5, pp. 735-740.

Barnea, D., Shoham, O. and Taitel, Y. (1980), "Flow pattern characterization in two phase flow by electrical conductance probe", *International Journal Multiphase Flow,* vol. 6, no. 5, pp. 387-397.

Baroczy, C. J. (1966), "A systematic correlation for two-phase pressure drop", *Chemical Engineering Progress,* vol. 62, no. 44, pp. 232-249.

Barua, S. N. (1963), "On secondary flow in stationary curved pipes", *Quarterly journal of mechanics and applied mathematics,* vol. 16, pp. 61-77.

Beattie, D. R. H. and Whalley, P. B. **(1982),** "A simple two-phase frictional pressure drop calculation method", *International Journal of Multiphase Flow,* vol. 8, no. 1, pp. 83-87.

Beggs, H. D. and Brill, J. R. (1973), "Study of two-phase flow in inclined pipes", *Journal of Petroleum Technology,* vol. 25, pp. 607-617.

Boe, A. (1981), "Severe slugging characteristics, part 1, flow regime for severe slugging, *Presented at Special Topics in Two Phase Flow*," Trondheim, Norway.

Boyce (1969), "Hold-up and pressure drop measurement in the two phase flow of air-water mixing tubes in helical coils", in RHODES E (ed.), *International*

symposium on research in concurrent gas and liquid flow, New York, Plenum press, New York, pp. 203.

Brill, J. R. and Beggs, H. D. (1991), "Two-phase flow in pipes", Sixth Edition, Third Printing.

Brown, R. C., Andreussi, P. and Zanelli, S. (1978), "The use of wire probes for the measurement of liquid film thickness in annular gas liquid flows", *Canadian Journal of Chemical Engineering.,* vol. 56, no. 6, Dec.1978, pp. 754-757.

Chen Xue Jun and Zhou Fang Teh (1982), "Investigation of flow pattern and frictional pressure drop characteristics of air-water two-phase flow in helical coils", Alternative Energy Sources: *Proceedings of the Miami International Conference on Alternative Energy*, pp. 69-84.

Chen, J. J. J. and Spedding, P. L. (1983), "Analysis of holdup in horizontal two-phase gas-liquid flow", *International Journal of Multiphase Flow,* vol. 9, no. 2, pp. 147-159.

Chisholm, D. (1967), "A theoretical basis for the Lockhart-Martinelli correlation for two phase flows", *International Journal of Heat and Mass Transfer,* vol. 10, pp. 1767-1778.

Chisholm, D. (1973), "Research note: Void fraction during two-phase flow", *Journal of Mechanical Engineering Science,* vol. 15, no. 3, pp. 235-236.

Collins, W. M. and Dennis, S. C. R. (1975), "Steady motion of a viscous fluid in a curved tube", *Quarterly Journal of Mechanics and Applied Mathematics,* vol. 28, no. 2, pp. 133-156.

Coulson, J. M. and Richardson, J. F. (1998), "*Chemical engineering volume 1 (Fluid flow, heat and mass transfer)",* 4th Edition, Pergamon.

References

Coulson, J. M. and Richardson, J. F. (1993), "*Chemical engineering volume 1 (Fluid flow, heat and mass transfer)",* 4th Edition, Pergamon.

Courbot, A., (1996), "*Prevention of severe slugging in the Dunbar 16 inches multiphase pipeline"*.

Czop, V., Barbier, D. and Dong, S. (1994), "Pressure drop, void fraction and shear stress measurements in an adiabatic two-phase flow in a coiled tube", *Nuclear Engineering and Design,* vol. 149, pp. 323-333.

Davies, S. R. (1992), "*Studies of two-phase intermittent flow in pipelines",* PhD Thesis, Imperial College of Science, Technology & Medicine, Department of Chemical Engineering and Chemical Technology, London, England.

Dean, W. R. (1928), "The streamline motion in a curved pipe", *Philosophical magazine,* vol. 5, pp. 673-695.

Dean, W. R. (1927), "Note on the motion of fluid in a curved pipe", *Philosophical magazine,* vol. 4, pp. 208-231.

Delhaye, J. M. and Jones Jr., O. C. (1975), "Measurement techniques for transient and statistical studies of two-phase, gas liquid flows", *American Society of Mechanical Engineers (Paper),* no. 75-Ht-10.

Douglas, J. F. and Gasiorek, J. M. and Swaffield, J. A. (1998), "*Fluid mechanics",* 3rd Edition, Longman Singapore Publishers Ltd, Singapore.

Dukler, A. E. (1964), "Frictional pressure drop in two-phase flow: A. comparison of existing correlations for pressure loss and holdup", *American Institute of Chemical Engineers Journal,* vol. 10, no. 1, pp. 38-43.

Duret, E., Peysson, Y., Tran, Q. and Rouchon, P. (2004), "Active bypass to eliminate severe slugging in multiphase production", *4th North American Conference on Multiphase Technology,* pp. 205-223.

References

Eaton. B. A., Andrews, D. E., Knowles, C. R., Silberberg, I. H. and Brown, K. E. (1967), "The prediction of flow patterns, liquid holdup and pressure losses occurring during continuous two-phase flow in horizontal pipelines", *Journal of Petroleum Technology* .

Eustice, J. (1911), "Experiments on steam-line motion in curved pipes", *Proceedings of the Royal Society of London, Series A,* vol. 85, pp. 107-118.

Eustice, J. (1910), "Flow of water in curved pipes", *Proceedings of the Royal Society of London, Series A,* vol. 84, pp. 119-131.

Forsdyke, I. N., (1997), "*Flow assurance in multiphase environments"*.

Friedel, L. (1979), "Improved friction pressure drop correlations for horizontal and vertical two-phase pipe flow", *European Two Phase Flow Group Meeting, No. E2, Ispra, Italy*.

Friedel, L. (1980), "Pressure drop during gas/vapor-liquid flow in pipes", *International chemical engineering,* vol. 20, no. 3, pp. 352-367.

Fuchs, P. (1987), "The pressure limit for terrain slugging", *Proceedings 3rd International Journal of Multiphase Production, BHR Group*, pp. 65-71.

Goldzberg, V. and Mckee, F (1987), "Model predicts liquid accumulation, severe terrain-induced slugging for two-phase lines", *Oil and Gas Journal,* pp. 105-109.

Goldzberg, V. and McKee, F. E. (1985), "Model predicts liquid accumulation, severe terrain-induced slugging for two-phase lines." *Oil and Gas Journal,* vol. 83, no. 33, pp. 105-106, 108.

Govier, G. W. and Fogarasi, M. (1975), "Pressure drop in wells producing gas and condensate", *Journal of Canadian Petroleum Technology,* vol. 14, no. 44, pp. 28-41.

References

Haaland, S. E. (1983), "Simple and explicit formulas for the friction factor in turbulent pipe flow", *Journal of Fluids Engineering, Transactions of the ASME,* vol. 105, no. 1, pp. 89-90.

Hall, A. R. W., (1992), "*Multiphase flow of oil, water and gas in horizontal pipe"* Ph.D. Thesis, Imperial College of Science, Technology & Medicine, Department of Chemical Engineering and Chemical Technology, University of London, England.

Hart, J., Ellenberger, J. and Hamersma, P. J. (1988), "Single- and two-phase flow through helically coiled tubes", *Chemical Engineering Science,* vol. 43, no. 4, pp. 775-783.

Hassanein, T. and Fairhurst, P. (1998), "Challenges in the mechanical and hydraulic aspects of riser design for deepwater developments", *Presented at Deepwater Technology Conference, Oslo.*

Havre, K. and Dalsmo, M. (2002), "Active feedback control as a solution to severe slugging", *SPE Production and Facilities,* vol. 17, no. 3, pp. 138-148.

Hewitt, G. F., Hall, A. R., Pan, L. (1995), "Three-phase liquid–liquid gas flow: A new challenge", in: Celata, G. P., Shah, R. K. (Eds), *Two-Phase Flow Modelling and Experimentation,* vol. 1, no. Edizioni, ETS, pp. 53-63.

Hewitt, G. F. (1978), "Measurement of two phase flow parameters."

Hill, T. J. (1990), "Gas injection at riser base solves slugging, flow problems", *Oil and Gas Journal,* vol. 88, no. 9, pp. 88-92.

Hill, T. J. (1989), "Riser-base gas injection into the SE Forties lines".

Hill, T. J., (1997), "*Gas-liquid flow challenges in oil and gas production"*.

Hollenberg, J. F. and DeWolf, S. and Meiring, W. J. (1995), "A method to suppress severe slugging in flowline riser systems", *Proceeding 7th International Conference on Multiphase Flow,* pp. 89-103.

Hughmark, G. A. **(1962),** "Pressure drop in horizontal and vertical co-current gas-liquid flow", *IEC Fund,* vol. 2, pp. 315.

Ito, H. (1959), "Friction factors for turbulent flow in curved pipes", *Transactions of the ASME-Journal of basic engineering,* vol. 81, pp. 123-134.

Jansen, F. E., Shoham, O. and Taitel, Y. (1996), "The elimination of severe slugging - experiments and modelling", *International Journal of Multiphase Flow,* vol. 22, no. 6, pp. 1055-1072.

Johal, K. S., Teh, C. E. and Cousins, A. R., (1997), "*Alternative economic method to riser base gas lift for deep water subsea oil/gas field developments"*.

Jones Jr., O. C. and Zuber, N. (1975), "Interrelation between void fraction fluctuations and flow patterns in two-phase flow", *International Journal of Multiphase Flow,* vol. 2, no. 3, pp. 273-306.

Kaasa, O. (1990), "A subsea slug catcher to prevent severe slugging", *6th Underwater Technology International Conference.*

Kasturi, G. and Stepanek, J. B. (1972), "Two phase flow - 1, 2.", *Chemical Engineering Science,* vol. 27, no. 10, pp. 1871-1891.

Kubair, V. (1966), "Heat transfer to Newtonian fluids in coiled pipes in laminar flow." *International Journal of Heat and Fluid Flow,* vol. 9, pp. 63-75.

Kubair, V. and Kuloor, N. R. (1965), "Non-isothermal pressure drop data for liquid flow in helical coils", *Indian Journal of Technology,* vol. 3, pp. 5-7.

Kubair, V. and Varrier, C. B. S. (1961-62), "Pressure drop for liquid flow in helical coils", *Transactions of the IIChE,* vol. 14, pp. 93-97.

Laflin, G. C., Oglesby, K. D., (1976), "*Experimental investigation of the effect of a constriction on turbulent pipe flow"* (Bachelor's Thesis, University of Tulsa), Tulsa, USA.

Laskey, S. J. (2002), "*A study of single and two-phase flows in devices with narrow flow passages"*. PhD Thesis, Cranfield University, Cranfield, UK.

Lissenburg, R. C. D., Hinze, J. O. and Leijdens, H. (1975), "Experimental investigation of the effect of a constriction on turbulent pipe flow", *Applied Scientific Research (The Hague),* vol. 31, no. 5, pp. 343-362.

Liu, S., Afacan, A. and Nasr-El-din, H. A. and Masliyah, J. H. (1994), "An experimental study of pressure drop in helical pipes", *Proceedings of the Royal Society of London, A,* vol. 444, pp. 307-316.

Lockhart, R. W. and Martinelli, R. C. (1949), "Proposed correlation of data for isothermal two-phase, two – component flow in pipes", *Chemical Engineering Progress,* vol. 45, no. 1, pp. 39-48.

Lockin, D. W. (1950), "Energy losses in 90-degree duct elbows", *Transactions American society of heating and ventilating engineers,* vol. 56, pp. 479-502.

Maddock, C. and Lacey, P. M. C. and Patrick, M. A. (1974), "The structure of two-phase flow in a curved pipe", *Institute of Chemical Engineers Symposium,* vol. Series No. 38, Multiphase flow systems.

Malinowsky, M. S., (1975), "*An experimental study of oil–water and air–oil–water flowing mixture in horizontal pipes"*. M.Sc. Thesis, University of Tulsa, Tulsa, USA.

Mandhane, J. M., Gregory, G. A. and Aziz, K. (1974), "A flow pattern map for gas-liquid flow in horizontal pipes", *International Journal of Multiphase Flow,* vol. 1, pp. 537-553.

Mandhane, J. M., Gregory, G. A. and Aziz, K. **(1975),** "Critical evaluation of holdup prediction methods for gas-liquid flow in horizontal pipes", *Journal of Petroleum Technology,* vol. 27, pp. 1017-1026.

Manlapaz, R. L. and Churchill, S. W. (1980), "Fully developed laminar flow in a helically coiled tube of finite pitch", *Chemical Engineering Communications,* vol. 7, no. 1-3, pp. 57-78.

Manolis, I. G. (1995), "*High pressure gas-liquid slug flow*" PhD Thesis, Imperial College of Science, Technology & Medicine, Department of Chemical Engineering and Chemical Technology, London, England.

McAdams, W. H. (1942), "Vapourisation inside horizontal tubes, 2: Benzene-Oil mixtures", *Transactions of the ASME,* vol. 64, pp. 193-200.

McGuinness, M. and Cooke, D., (1993), "*Partial stabilisation at St. Joseph"*.

Miller, D. S. (1990), "Internal flow systems". 2nd Edition BHRA (Information services), Cranfield, UK.

Miller, D. S. (1978), "Internal flow systems", BHRA Fluid Engineering, Cranfield, UK.

Milne-Thompson (1960), "*Theoretical Hydrodynamics"*, The Mac-Millan Company, New York.

Minami, K. and Brill, J. P. (1987), "Liquid holdup in wet-gas pipelines", *Society of Petroleum Engineers, Production Engineering,* vol. 2, no. 1, pp. 36-44.

Mishra, P. (1979), "Momentum transfer in curved pipes. 1. Newtonian fluids", *Industrial and Engineering Chemistry. Process Design and Development,* vol. 18, no. 1, pp. 130-137.

Miya, M. (1970), "*Properties of roll waves"*. PhD Thesis, University of Illinois, Illinois, USA.

Montgomery, J. (2002), "*Severe slugging and unstable flows in an S-shaped riser".* PhD Thesis, Cranfield University, Cranfield, UK.

Mori, Y. and Nakayama, W. (1967b), "Study on forced convective heat transfer in curved pipes. (3rd report, theoretical analysis under the condition of uniform wall temperature and practical formulae)." *International journal of heat and mass transfer,* vol. 10, pp. 681-695.

Mori, Y. and Nakayama, W. (1967a), "Study on forced convective heat transfer in curved pipes. (2nd report, turbulent region)." *International Journal of Heat and Mass Transfer,* vol. 10, pp. 37-59.

Mori, Y. and Nakayama, W. (1965), "Study on forced convective heat transfer in curved pipes. (1st report, laminar region)." *International journal of heat and mass transfer,* vol. 8, pp. 67-82.

Mujawar, B. A. and Raja Rao, M. (1981), "Gas-non-Newtonian liquid two-phase flow in helical coils", *Industrial & Engineering Chemistry Process Design and Development,* vol. 20, no. 2, pp. 391-397.

Pan, L. (1996), "*High pressure three-phase (gas/liquid/liquid) flow*" PhD Thesis, Imperial College of Science, Technology & Medicine, Department of Chemical Engineering and Chemical Technology, London, England.

Patel, R. P. (1974), "Note on fully developed turbulent flow down a circular pipe", *Aeronautical Journal,* vol. 78, no. 758-759, pp. 93-97.

Perry, R. H. and Green, D. (1984), *"Chemical Engineers' Handbook",* 6th Edition, McGraw-Hill.

Pots, B. F. M., Bromilow, I. G. and Konijn, M. J. W. F. (1987), "Severe slug flow in offshore flowline/riser systems", *Society of Petroleum Engineers Production Engineering,* vol. 2, no. 4, pp. 319-324.

Pots, B. I. M., Bromilow, I. G. and Konijn, M. J. W. F. (1985), "Slug flow in offshore flowline/riser systems", *Society of Petroleum Engineers of AIME, (Paper),* pp. 347-356.

Prandtl, L. (1954), "Essentials of fluid dynamics." *Blackie & Son Limited, London and Glasgow.*

Premoli A., Di Francesco D. and Prina A. (1971), "A imensional correlation for evaluating two- phase mixture density, (Una correlazione adminensionale per la determinazione della densita di miscele bifasiche)", *Termotecnica (Milan),* vol. 25, no. 1, pp. 17-26.

Rangacharyulu, K. and Davies, G. S. (1984), "Pressure drop and holdup studies of air-liquid flow in helical coils", *Chemical engineering journal,* vol. 29, no. 1, pp. 41-46.

Rippel, G. R., Eidt Jr., C. M. and Jordan Jr., H. B. (1966), "Two-phase flow in a coiled tube: Pressure drop, holdup, and liquid phase axial mixing", *Industrial & Engineering Chemistry. Process Design and Development,* vol. 5, no. 1, pp. 32-39.

Saxena, A. K., Schumpe, A., Nigam, K. D. P. and Deckwer, W. D. **(1990),** "Flow regimes, hold-up and pressure drop for two-phase flow in helical coils", *Canadian Journal of Chemical Engineering,* vol. 68, no. 4, pp. 553-559.

Schmidt, E. F. (1967), "Warmeubergang and druckverlust in rohrschlangen.", *Chemie ingenieur technik,* vol. 39, no. 13, pp. 781-789.

Schmidt, Z. (1977), "*Experimental study of two-phase slug flow in a pipeline riser pipe system".* PhD thesis, University of Tulsa, Tulsa, USA.

Schmidt, Z. and Brill, J. P. and Beggs, D. H. (1981), "Experimental study of normal slug flow in a two-phase flow pipeline-riser pipe system", *Journal of Energy Resources Technology,* vol. 103, pp. 67-75.

Schmidt, Z., Brill, J. P. and Beggs, H. D. (1980), "Experimental study of severe slugging in a two-phase-flow pipeline-riser pipe system", *Society of Petroleum Engineers journal,* no. 5, pp. 407-414.

Schmidt, Z., Brill, J. P. and Beggs, H. D. (1979), "Choking can eliminate severe pipeline slugging", *Oil and Gas Journal,* vol. 77, no. 46.

Schmidt, Z., Doty, D. R. and Dutta-Roy, K. (1985), "Severe slugging in offshore pipeline riser-pipe systems", *Society of Petroleum Engineers journal,* vol. 25, no. 1, pp. 27-38.

Shoham, O. (1982), "*Flow pattern transition and characterisation in gas-liquid two-phase flow in inclined pipes"*. PhD Thesis, Tel-Aviv University, Tel-Aviv.

Sobocinski, D. P, (1953), "*Horizontal co-current flow of water, gas–oil and air"* Master's Thesis, University of Oklahoma, Oklahoma, USA.

Srichia, S. (1994), "*High pressure separated two-phase flow*". PhD Thesis, Imperial College of Science, Technology & Medicine, Department of Chemical Engineering and Chemical Technology, London, England.

Srinivasan (1968), "Pressure drop and heat transfer in coils", *The chemical engineer*, pp. CE113-CE119.

Stapelburg, H. H. and Mewes, D., (1994), "The flow of two-immiscible liquids in horizontal pipes", *International Journal of Multiphase Flow,* vol. 20, no. 2, pp. 285.

Strand, O. (1993), "*An experimental investigation of stratified two-phase flow in horizontal pipes"*. Thesis presented for the degree of DOCTOR SCIENTIARUM, University of Oslo, Mechanics division, Department of Mathematics, Oslo.

Taitel, Y., Vierkandt, S., Shoham, O. and Brill, J. P. (1990), "Severe slugging in a riser system. Experiments and modelling", *International Journal of Multiphase Flow,* vol. 16, no. 1, pp. 57-68.

References

Taitel, Y. (1986), "Stability of severe slugging", *International Journal of Multiphase Flow,* vol. 12, no. 2, pp. 23-217.

Taitel, Y. and Dukler, A. E. (1976), "Model for predicting flow regime transitions in horizontal and near horizontal gas-liquid flow", *American Institute of Chemical Engineers Journal,* vol. 22, no. 1, pp. 47-55.

Taylor, G. I. (1929), "The criterion for turbulence in curved pipes", *Proceedings of the Royal Society of London, Series A,* vol. 124, pp. 243-249.

Tengesdal, J.Ø, Thompson, L. and Sarica, C., (2003), "*A design approach for "self-lifting" method to eliminate severe slugging in offshore production systems"*.

Townsend, A. A. (1976), "The structure of turbulent shear flow".

Van Dyke, M. (1978), "Extended Stokes Series: Laminar flow through a loosely coiled pipe", *Journal of Fluid Mechanics,* vol. 86, no. pt 1, pp. 129-145.

Weisman J., Duncan D., Gibson J. and Crawford T. (1979), "Effects of fluid properties and pipe diameter on two-phase flow patterns in horizontal lines", *International Journal of Multiphase Flow,* vol. 5, no. 6, pp. 437-462.

Whalley, P. B. (1980), "Air-water two-phase flow in helically coiled tube", *International Journal of Multiphase Flow,* vol. 6, pp. 345-356.

White, C. M. (1932), "Fluid friction and its relation to heat transfer.", *Transactions of the Institute of Chemical Engineers,* no. 10, pp. 66-86.

White, C. M. (1929), "Streamline flow through curved pipes", *Proceedings of the Royal Society of London, A,* vol. 123, pp. 645-663.

Wyllie, M. W. J. and Brackenridge, A. (1994), "A retrofit solution to reduce slugging effects in multiphase subsea pipelines – The Internal Riser Insert System (IRIS)", *Subsea International Conference*.

References

Xin, R. C., Awwad, A., Dong, Z. F. and Ebadian, M. A. (1997), "An experimental study of single-phase and two-phase flow pressure drop in annular helicoidal pipes", *International Journal of Heat and Fluid Flow,* vol. 18, no. 5, pp. 482-488.

Xin, R. C., Awwad, A., Dong, Z. F., Ebadian, M. A. and Soliman, H. M. (1996), "An investigation and comparative study of the pressure drop in air-water two-phase flow in vertical helicoidal pipes", *International Journal of Heat and Mass Transfer,* vol. 39, no. 4, pp. 735-743.

Yocum, B. T. (1973), "Offshore riser slug flow avoidance: Mathematical models for design and optimizations", *Society of Petroleum Engineers AIME Prepr*, no. SPE 4312.

APPENDIX A

Details of helical pipes, two-phase and three-phase test facilities, riser profile and summary of riser experimental results

APPENDIX A

25.4 mm internal-diameter *helical pipe* test section

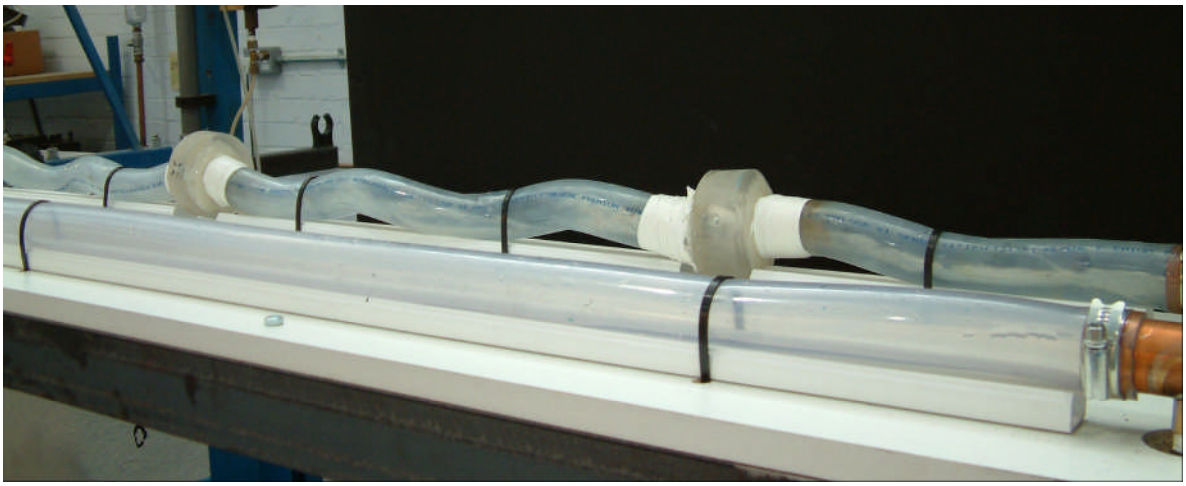

Amplitude, A_p is 21.25 mm

- Helical diameter, D is 42.5 mm
- Internal diameter d, is 25.4 mm
- Length l, is 2100 mm
- Pitch is 250 mm

50 mm internal-diameter *helical pipe* side view

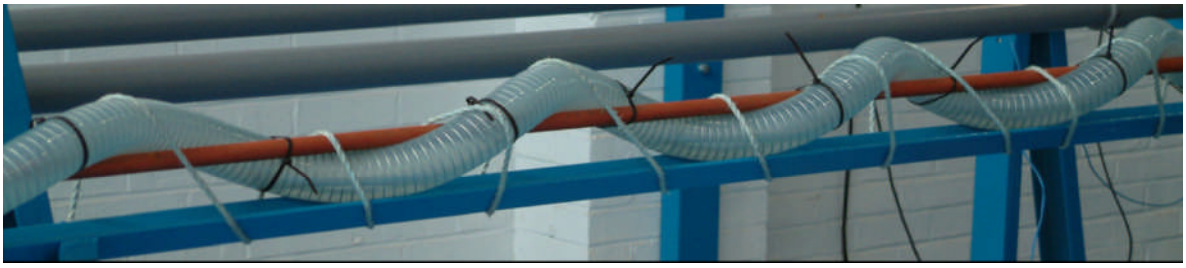

- Amplitude, A_p is 75.5 mm
- Helical diameter, D is 150 mm
- Internal diameter d, is 50 mm
- Length l, is 2000 mm
- Pitch is 550 mm

Two-phase facility

APPENDIX A

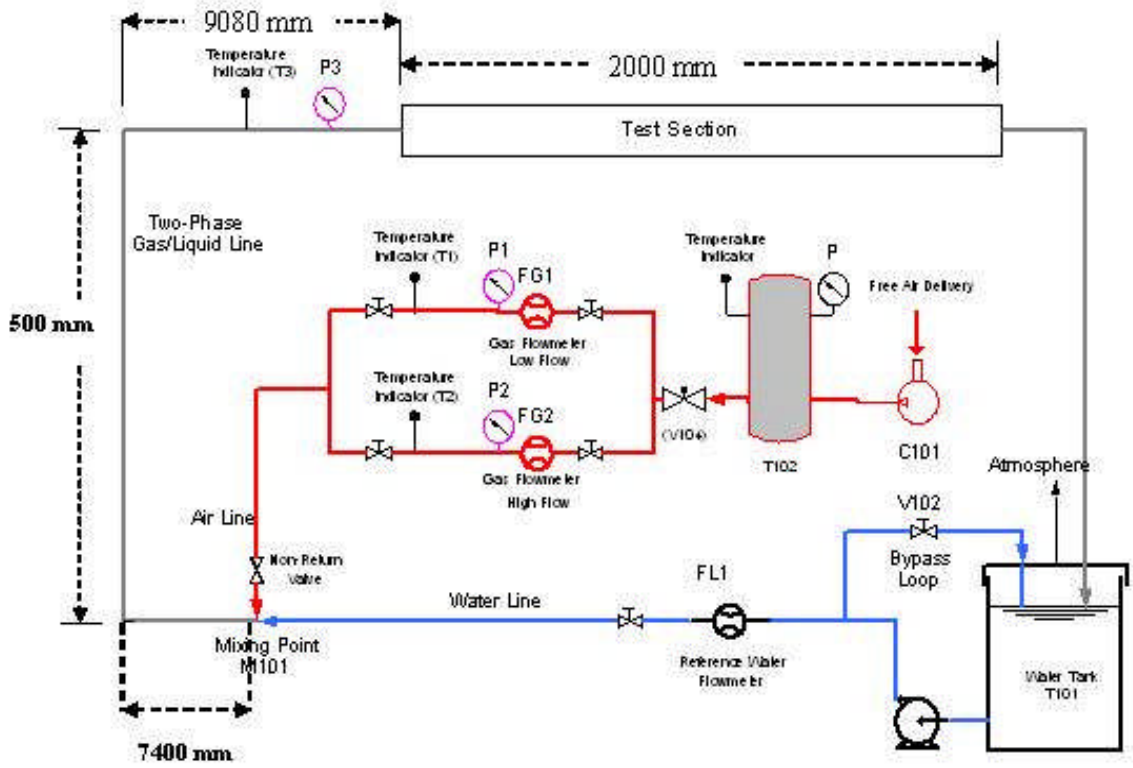

Cranfield University two- phase facility P & I diagram

100 mm internal-diameter *helical pipe* side view

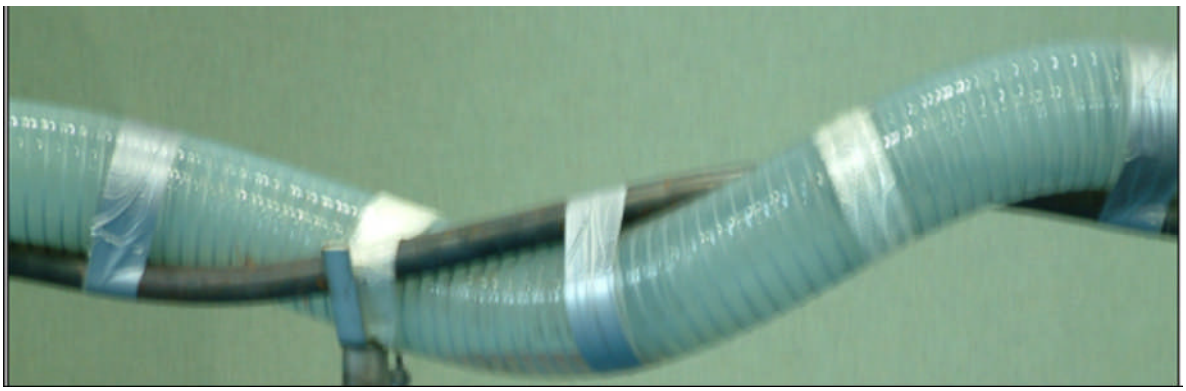

- Amplitude, A_p is 105 mm
- Helical diameter, D is 210 mm
- Internal diameter d, is 100 mm
- Length l, is 6000 mm
- Pitch is 1000 mm

Three-phase facility

APPENDIX A

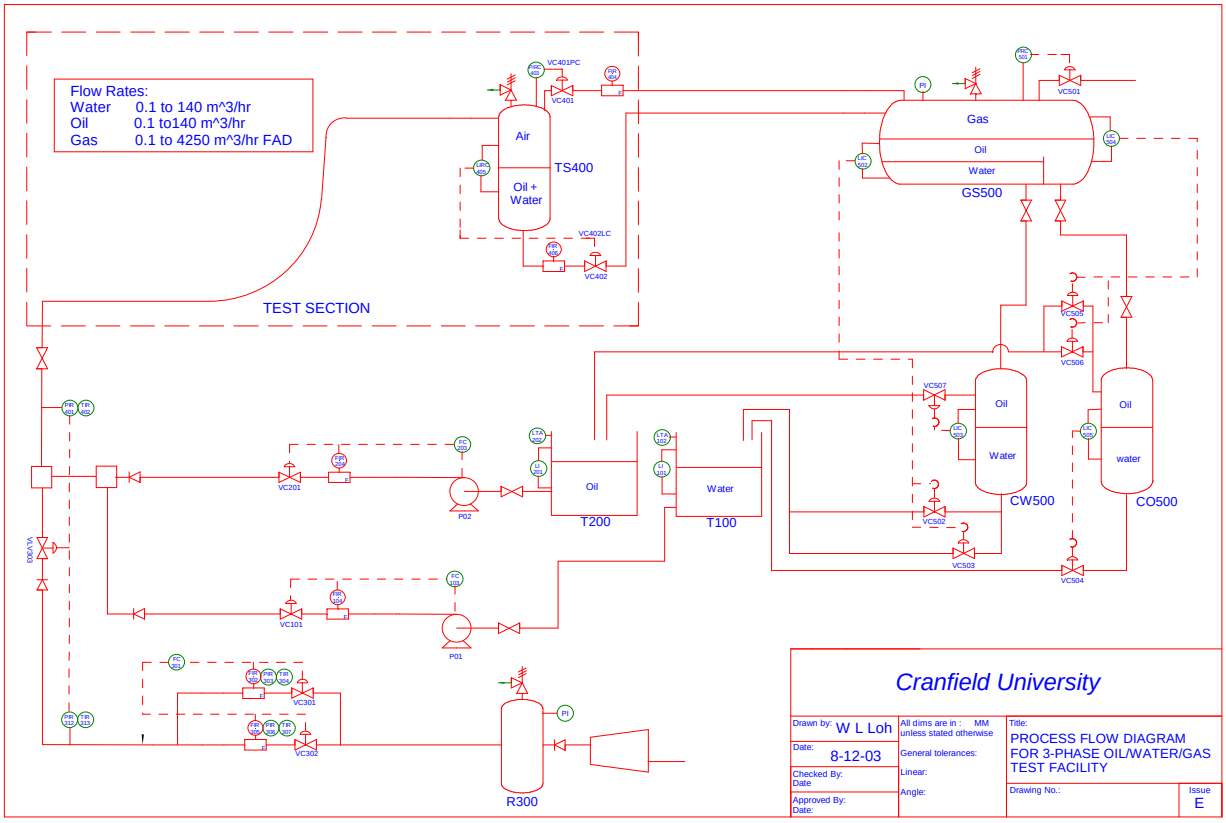

Cranfield University three phase facility P & I diagram

Catenary-shaped riser profile

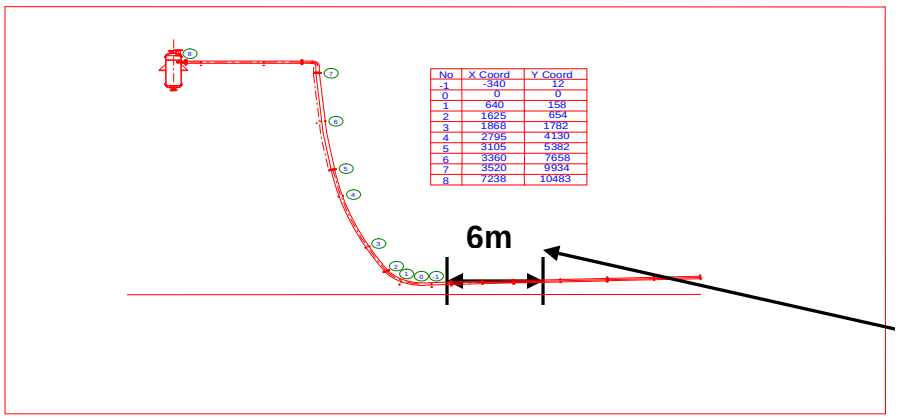

A section of the straight pipeline replaced by a 6 m helical pipe

Test area and profile of the catenary-shaped riser

Summary of riser experimental results

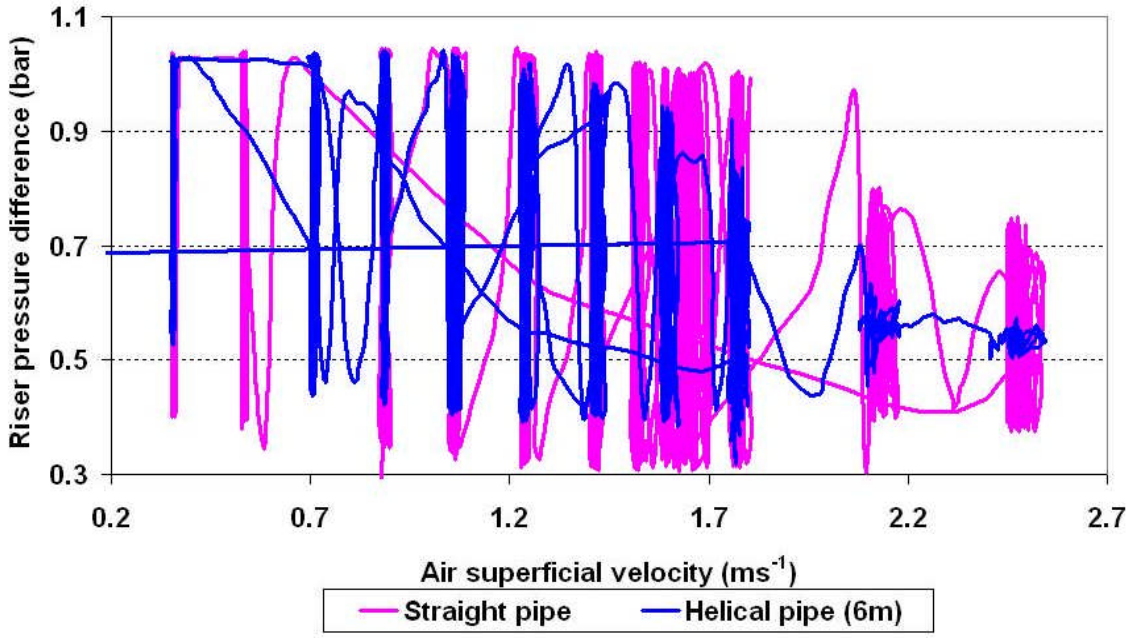

Riser pressure difference with increase in gas flow (U_W 0.38 ms^{-1})

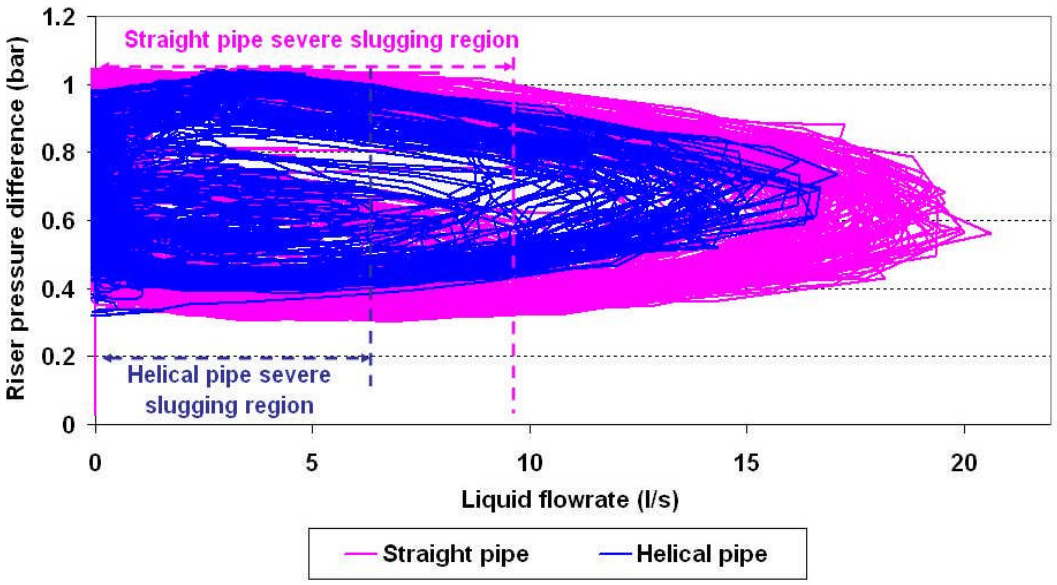

Riser pressure difference with fluid production rate

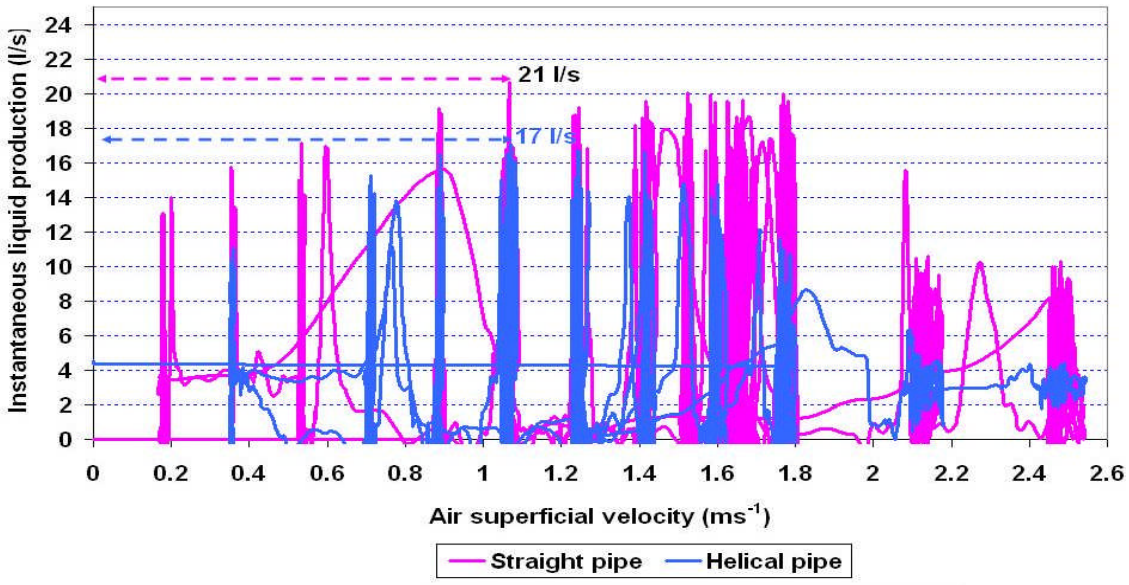

Liquid instantaneous production

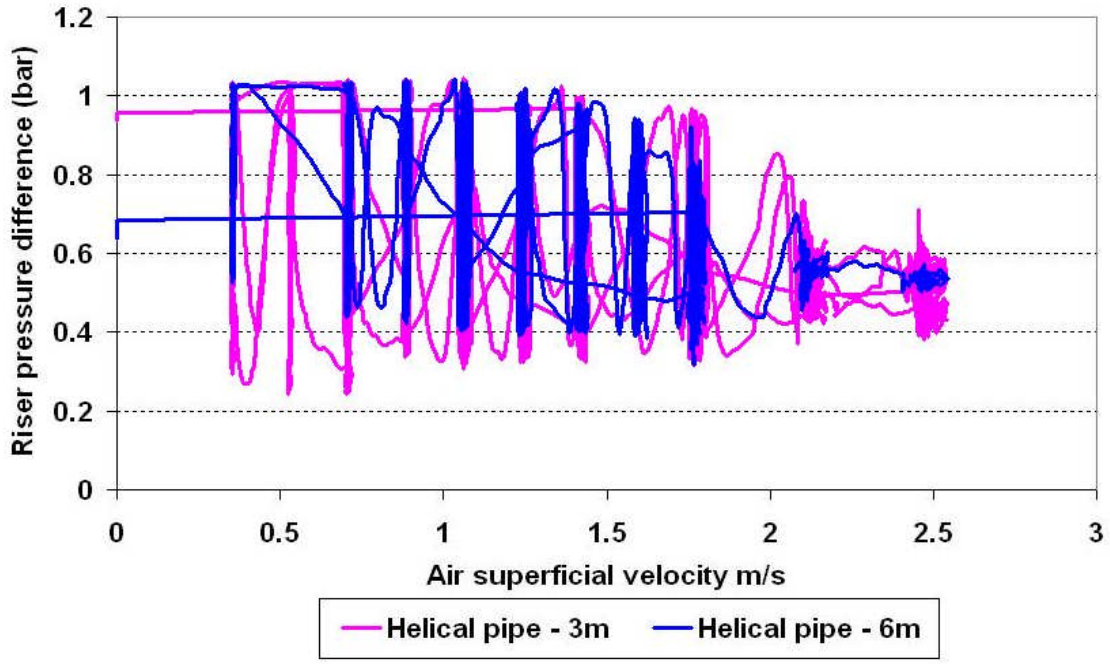

Effect of the *helical pipe* length on severe slugging control

APPENDIX B

Pressure drop signals

APPENDIX B

Pressure drop signals

Legend:

w **is the water superficial velocity**
g **is the air superficial velocity**

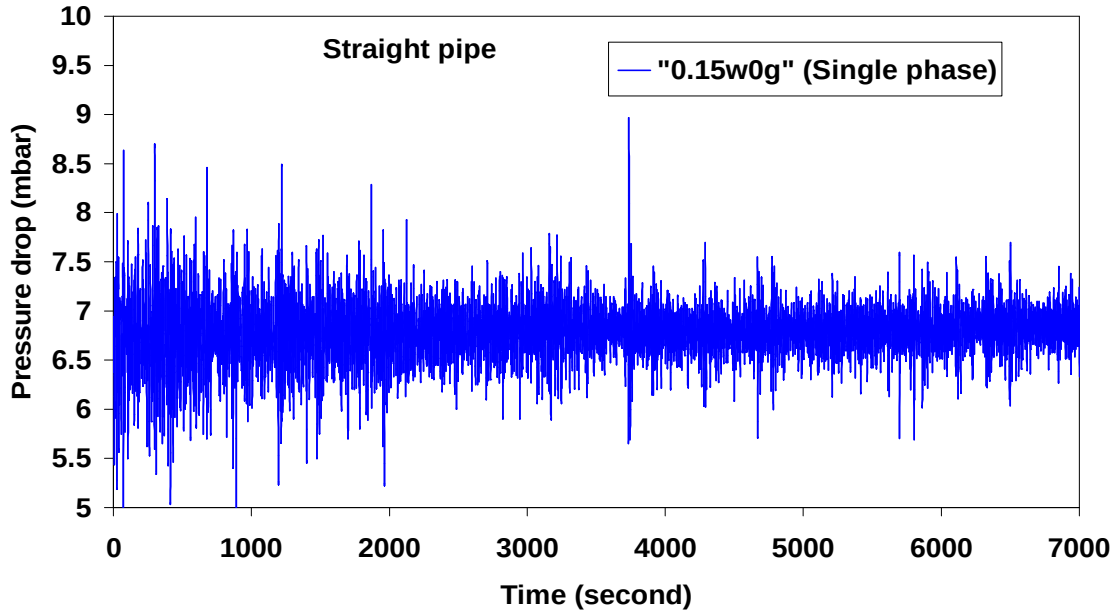

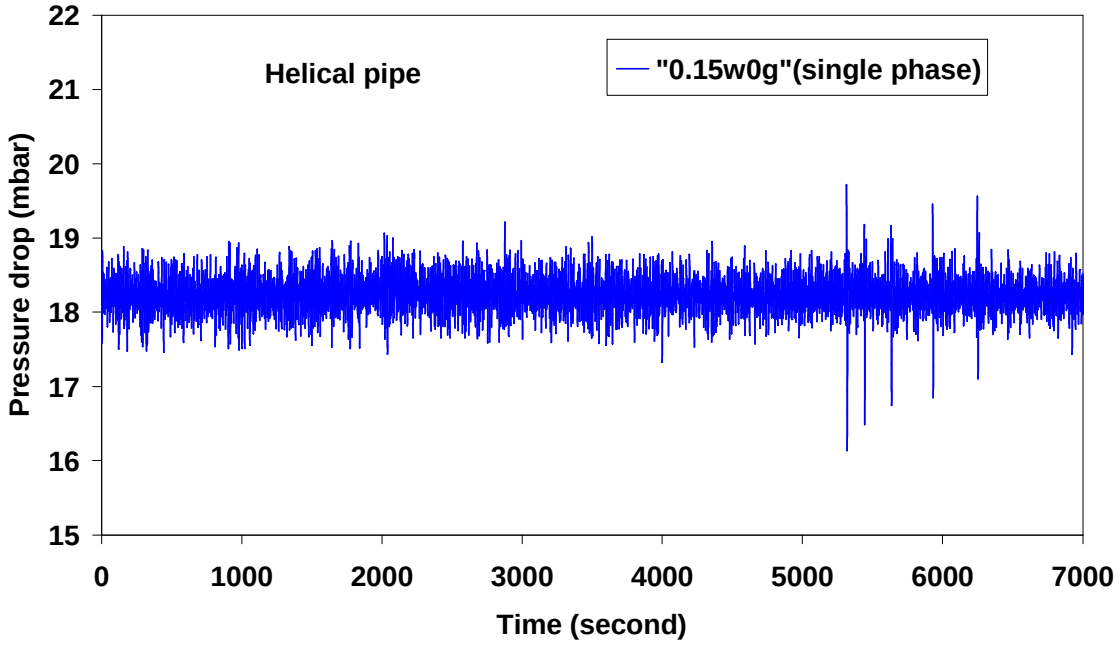

APPENDIX B

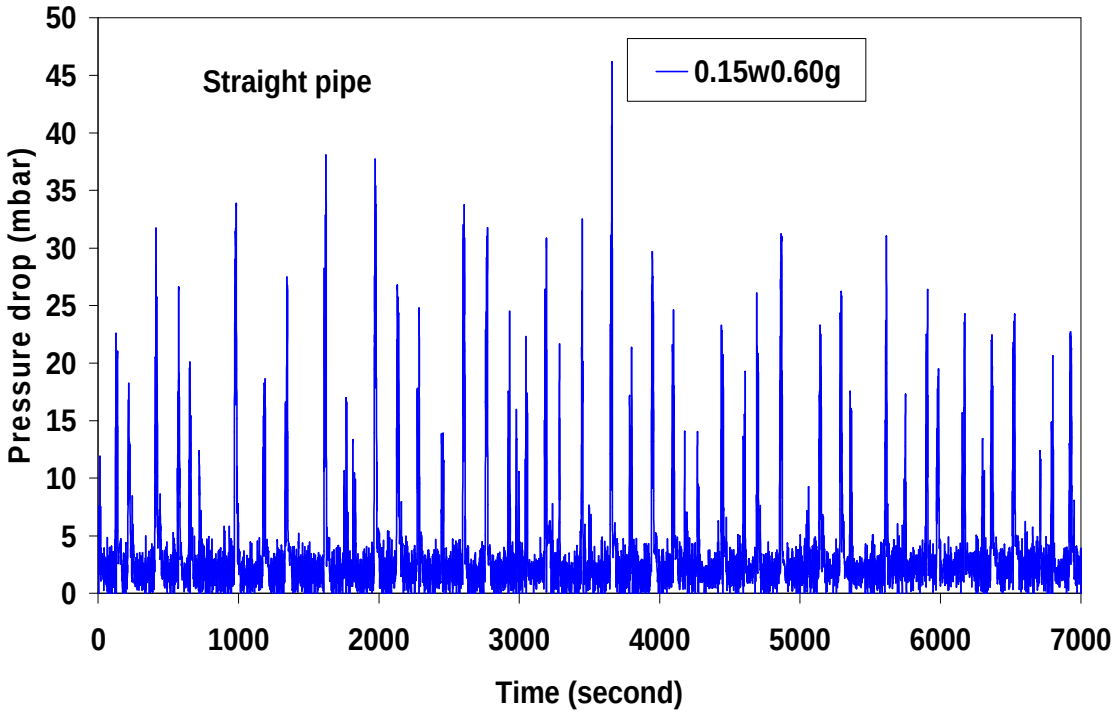
Straight pipe
0.15w0.60g
Pressure drop (mbar)
Time (second)
0
5
10
15
20
25
30
35
40
45
50
0
1000
2000
3000
4000
5000
6000
7000

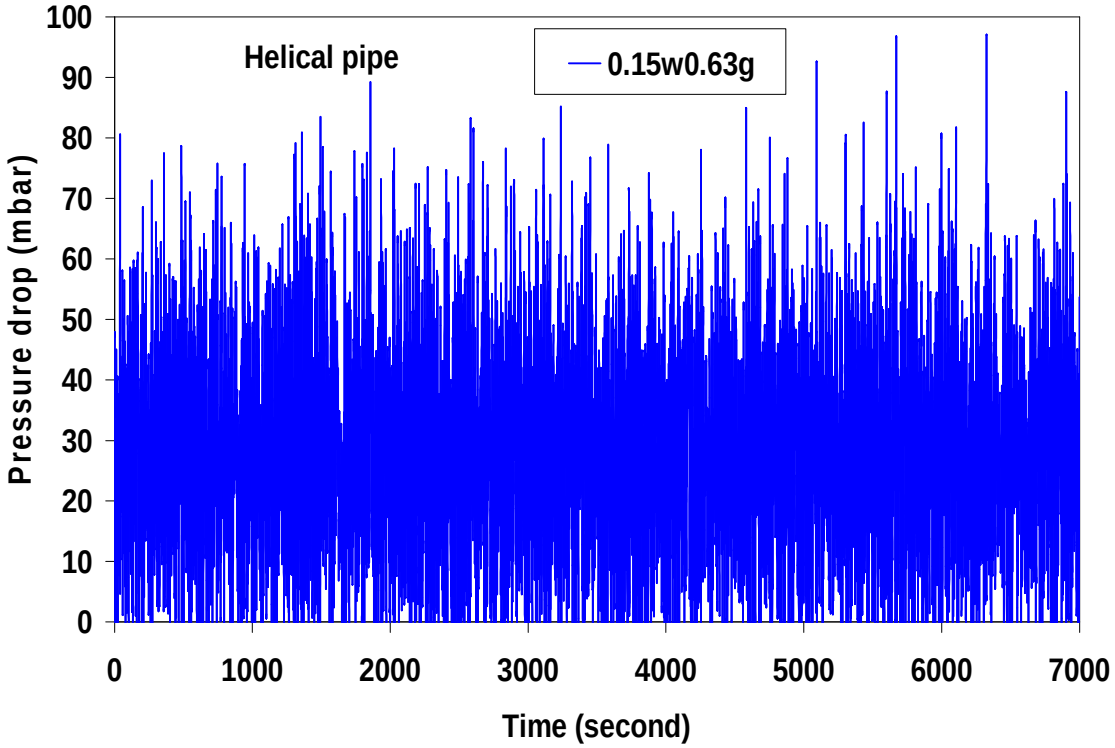
Helical pipe
0.15w0.63g
Pressure drop (mbar)
Time (second)
0
10
20
30
40
50
60
70
80
90
100
0
1000
2000
3000
4000
5000
6000
7000

APPENDIX B

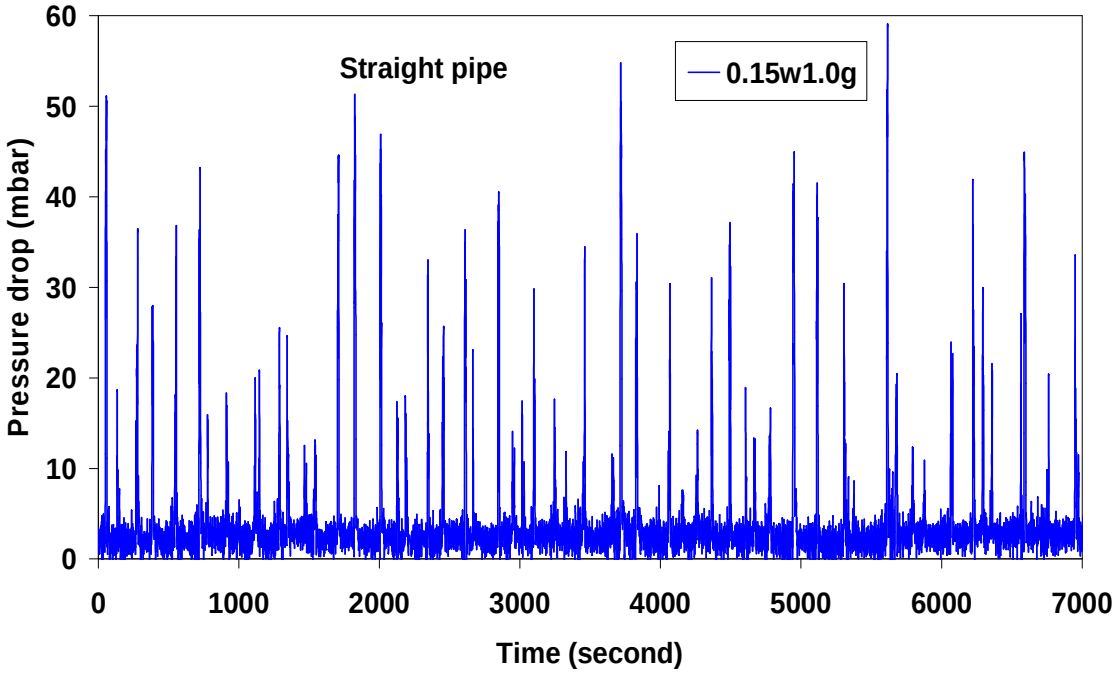
Straight pipe
0.15w1.0g
Pressure drop (mbar)
Time (second)
0
10
20
30
40
50
60
0
1000
2000
3000
4000
5000
6000
7000

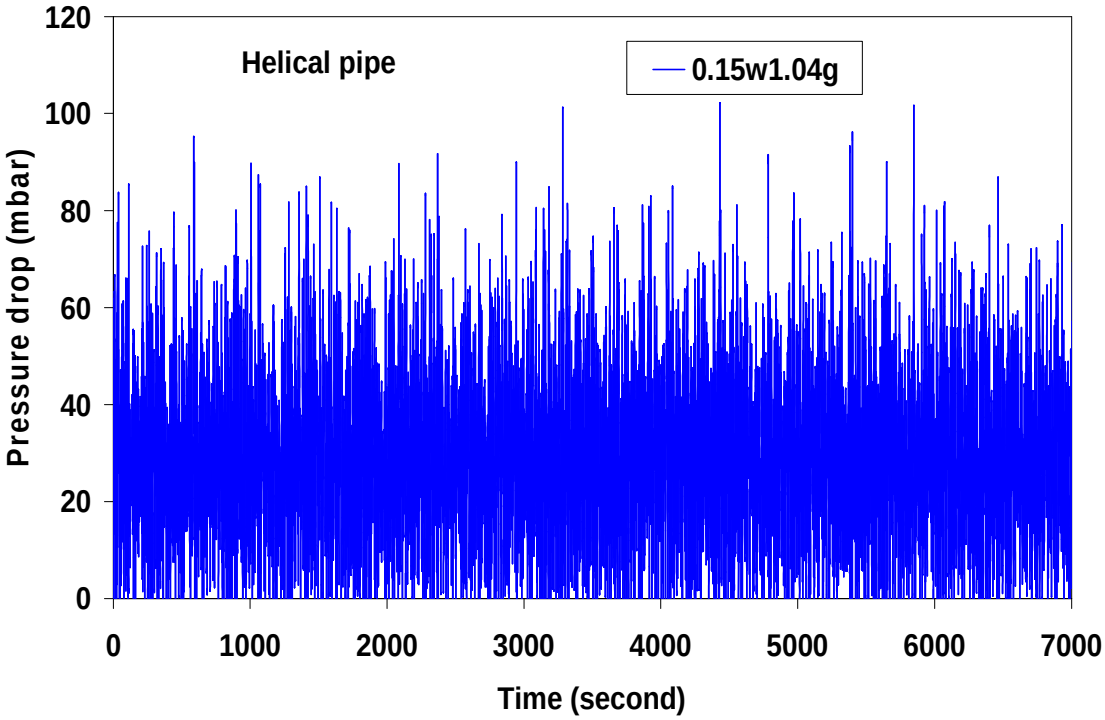
Helical pipe
0.15w1.04g
Pressure drop (mbar)
Time (second)
0
20
40
60
80
100
120
0
1000
2000
3000
4000
5000
6000
7000

APPENDIX B

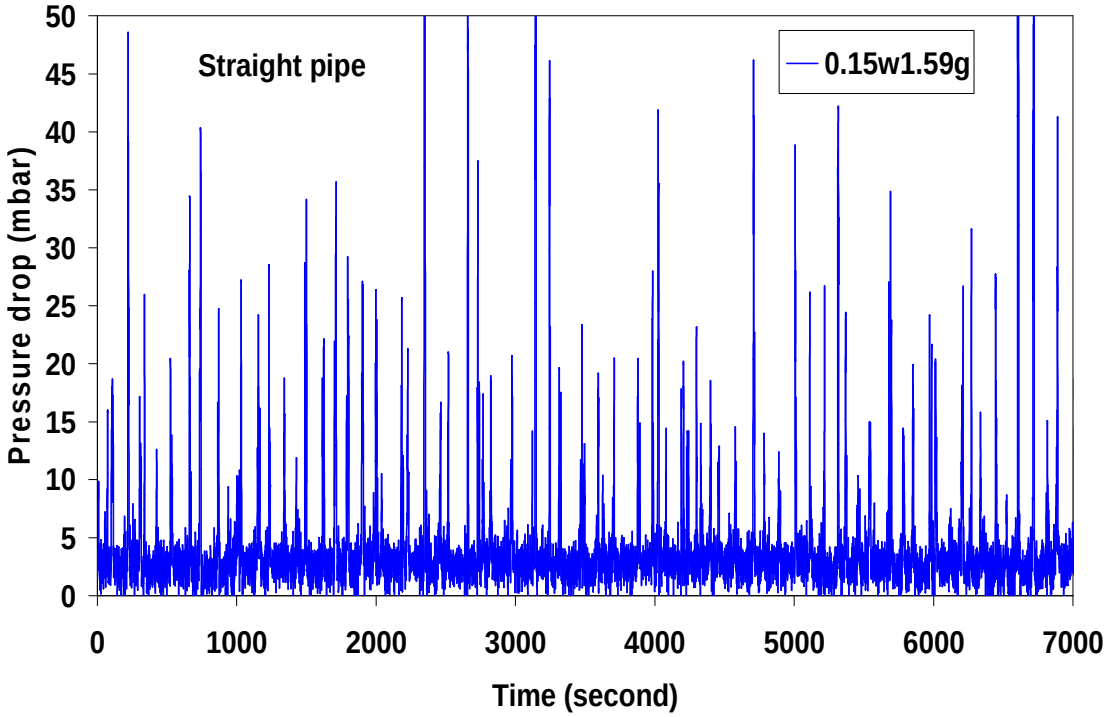
Straight pipe
0.15w1.59g
Pressure drop (mbar)
Time (second)
0
5
10
15
20
25
30
35
40
45
50
0
1000
2000
3000
4000
5000
6000
7000

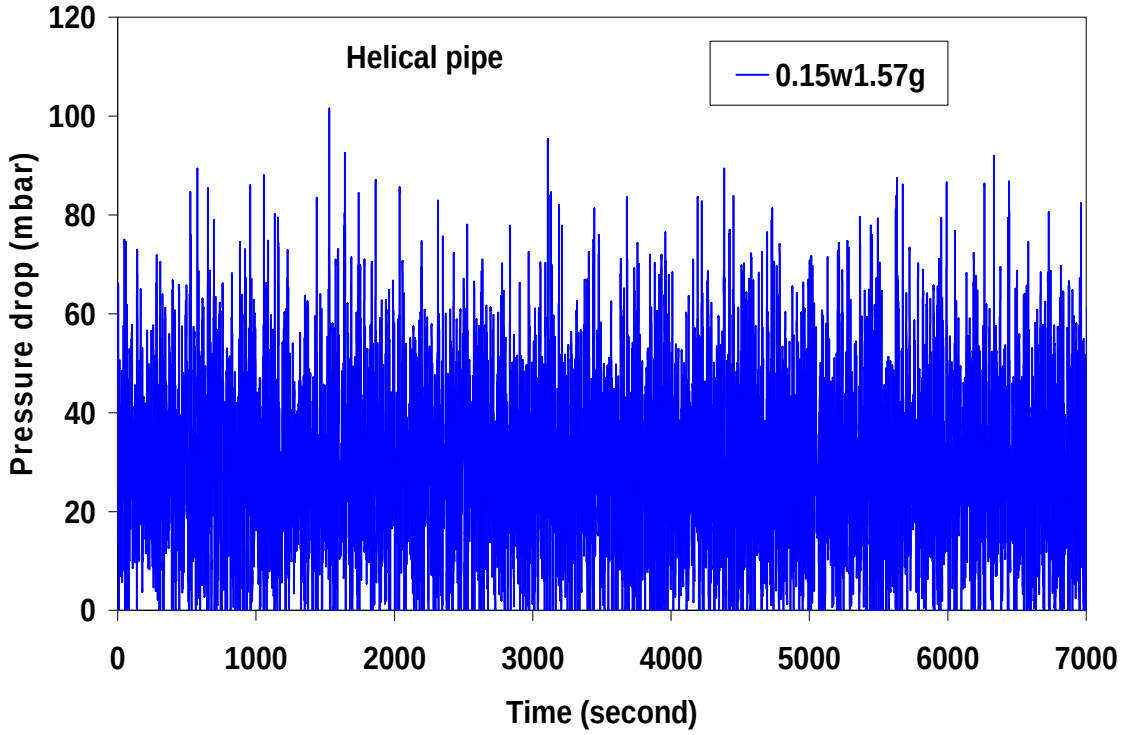
Helical pipe
0.15w1.57g
Pressure drop (mbar)
Time (second)
0
20
40
60
80
100
120
0
1000
2000
3000
4000
5000
6000
7000

APPENDIX B

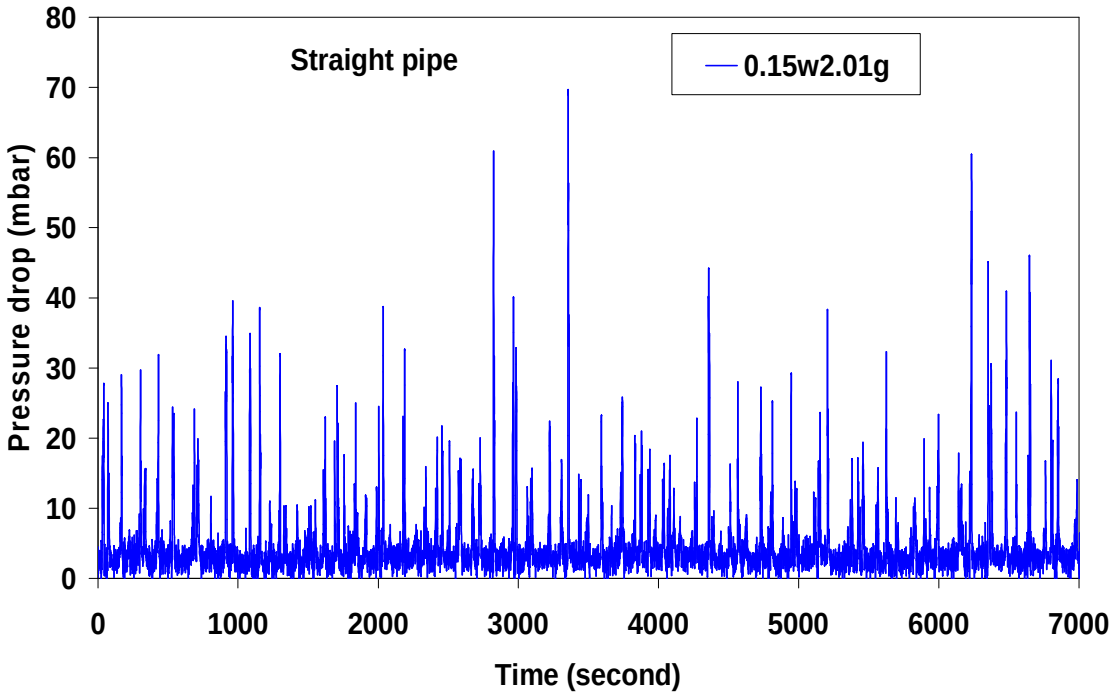
Straight pipe
0.15w2.01g
Pressure drop (mbar)
Time (second)
0
10
20
30
40
50
60
70
80
0
1000
2000
3000
4000
5000
6000
7000

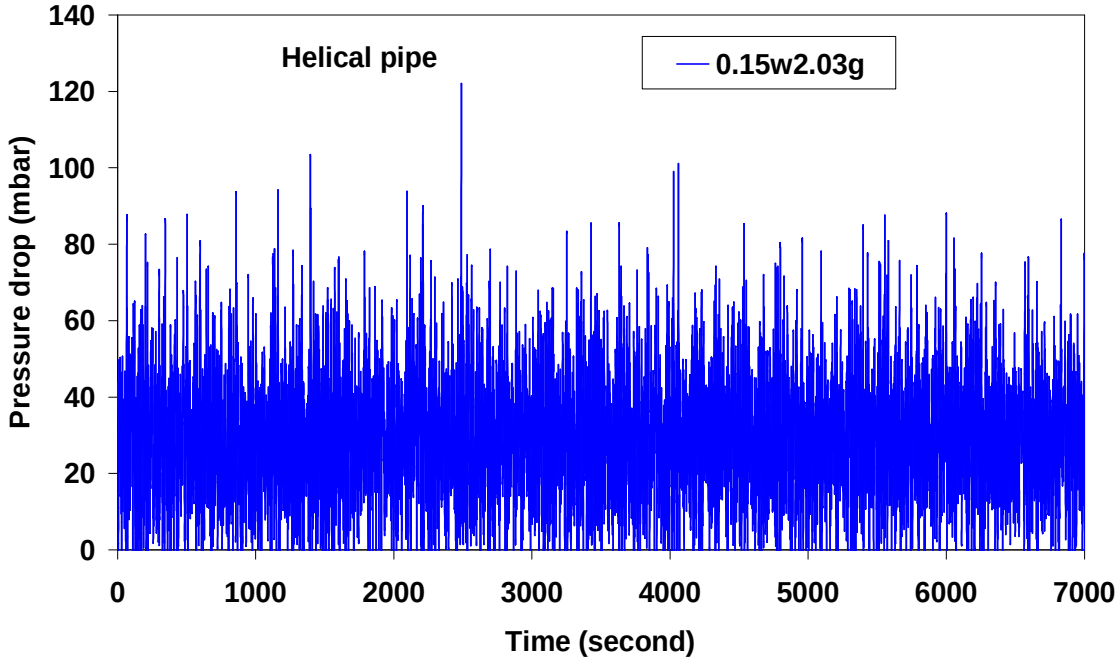
Helical pipe
0.15w2.03g
Pressure drop (mbar)
Time (second)
0
20
40
60
80
100
120
140
0
1000
2000
3000
4000
5000
6000
7000

APPENDIX B

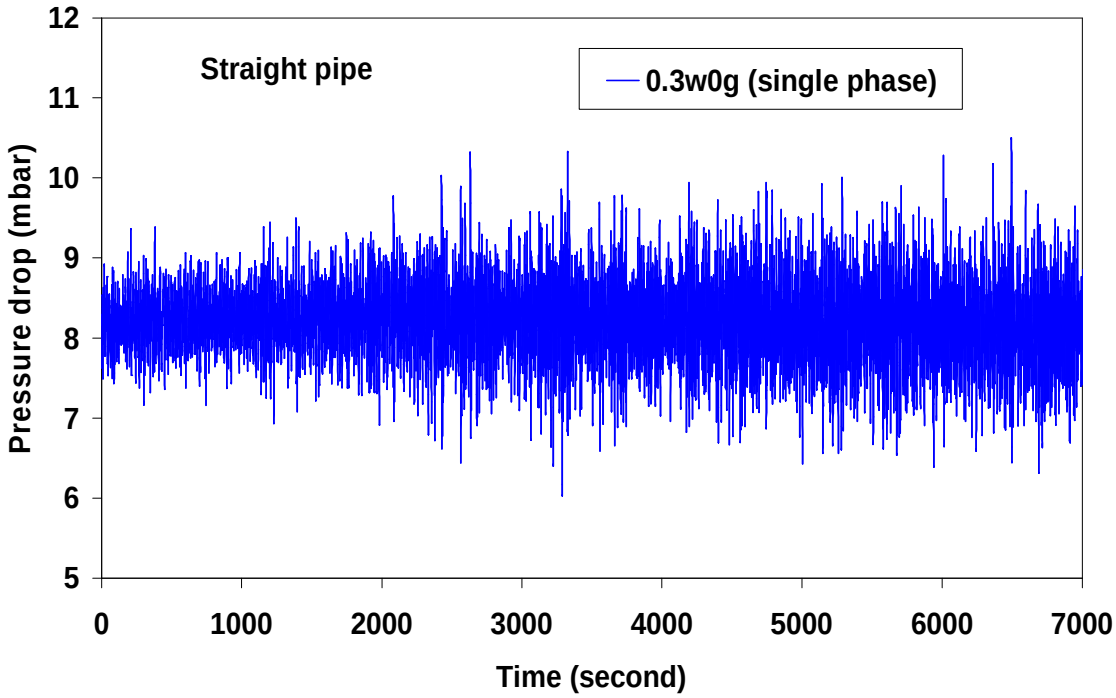
Straight pipe
0.3w0g (single phase)
Pressure drop (mbar)
12
11
10
9
8
7
6
5
0
1000
2000
3000
4000
5000
6000
7000
Time (second)

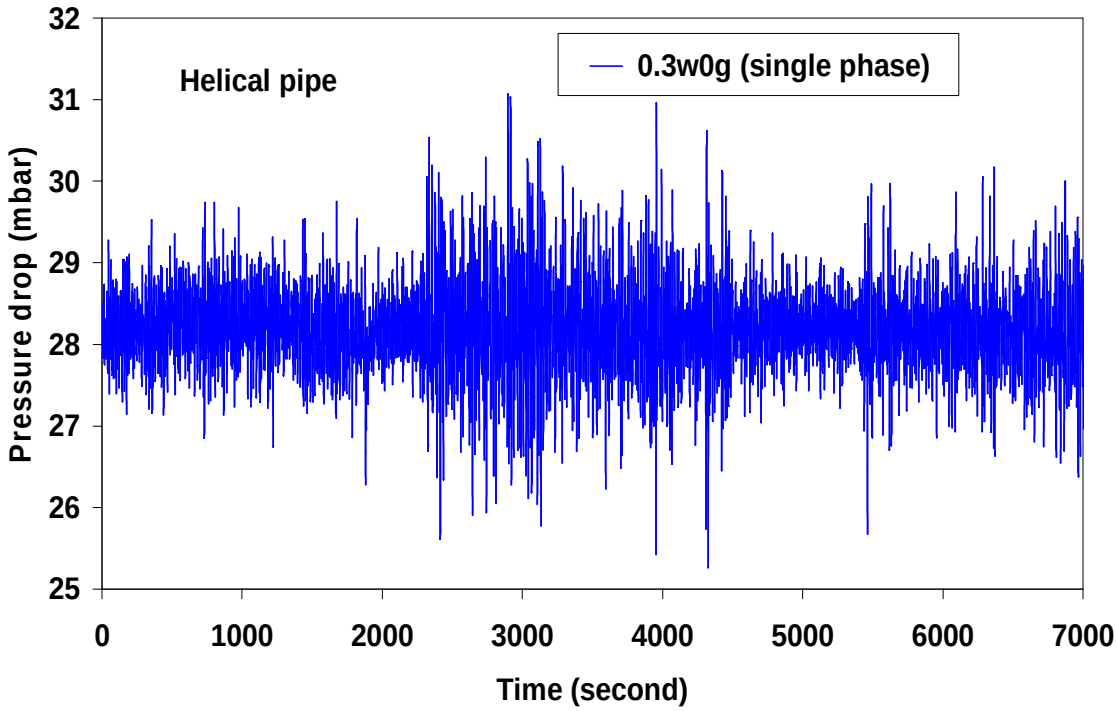
Helical pipe
0.3w0g (single phase)
Pressure drop (mbar)
32
31
30
29
28
27
26
25
0
1000
2000
3000
4000
5000
6000
7000
Time (second)

APPENDIX B

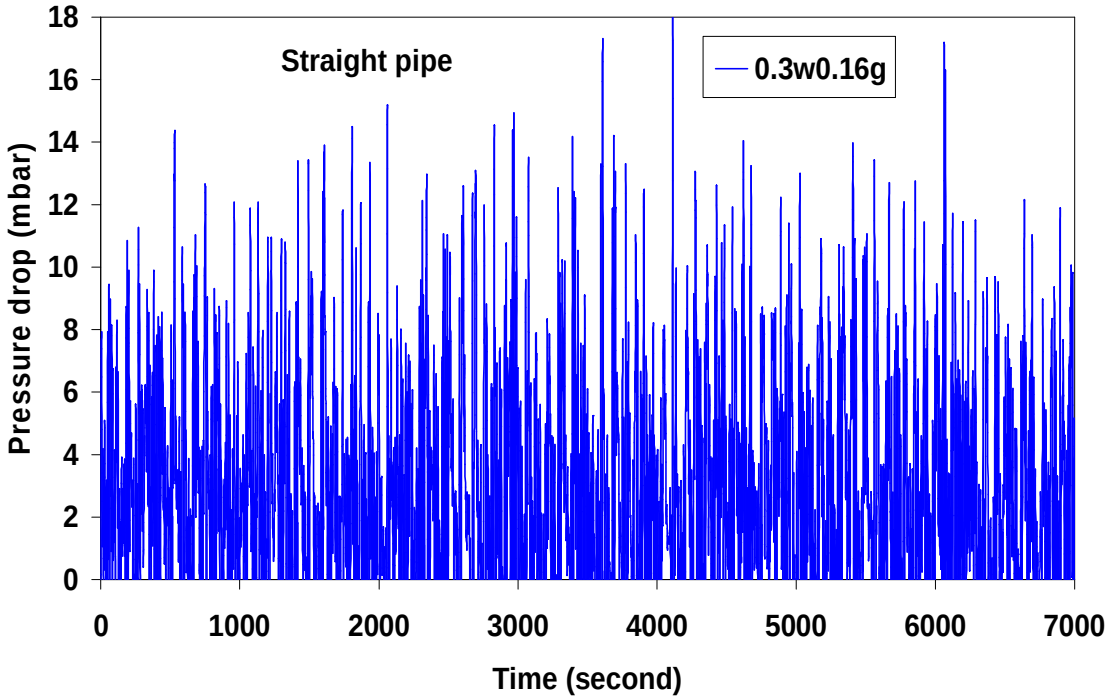
Straight pipe
0.3w0.16g
Pressure drop (mbar)
Time (second)
0
2
4
6
8
10
12
14
16
18
0
1000
2000
3000
4000
5000
6000
7000

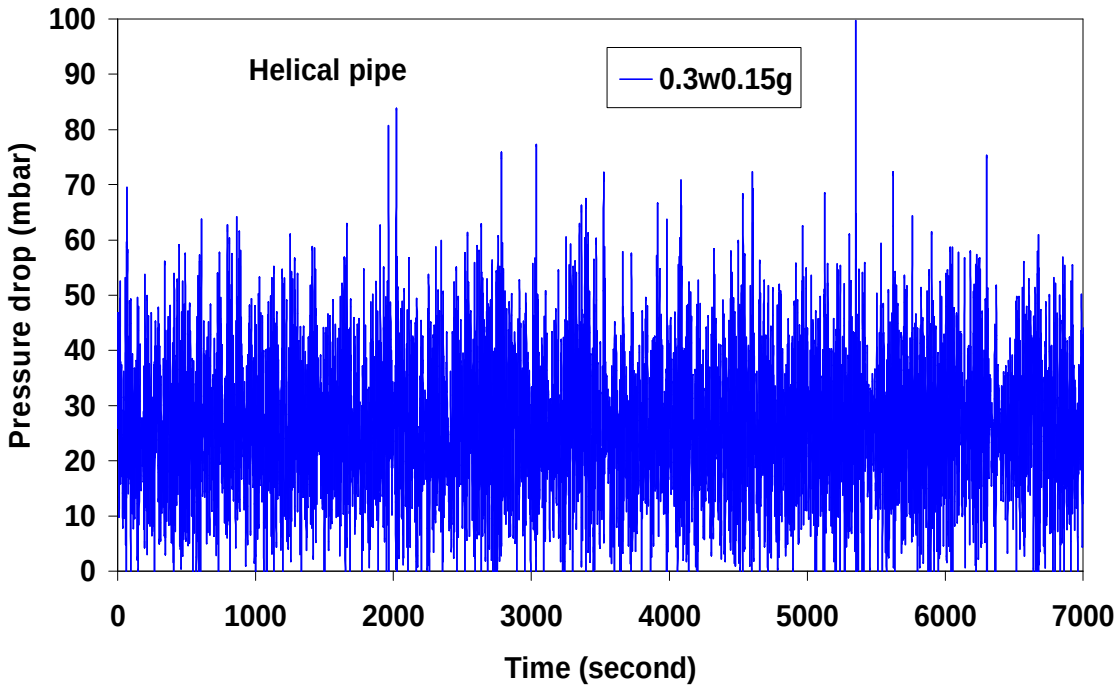
Helical pipe
0.3w0.15g
Pressure drop (mbar)
Time (second)
0
10
20
30
40
50
60
70
80
90
100
0
1000
2000
3000
4000
5000
6000
7000

APPENDIX B

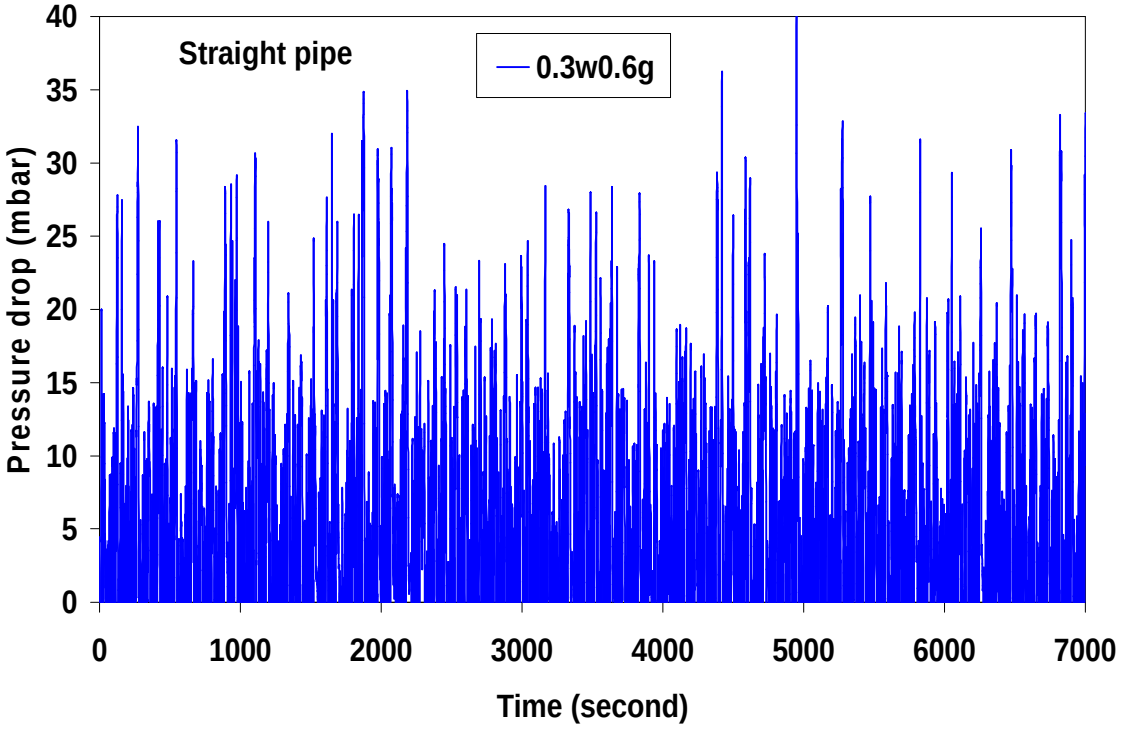
Straight pipe
0.3w0.6g
Pressure drop (mbar)
0
5
10
15
20
25
30
35
40
0
1000
2000
3000
4000
5000
6000
7000
Time (second)

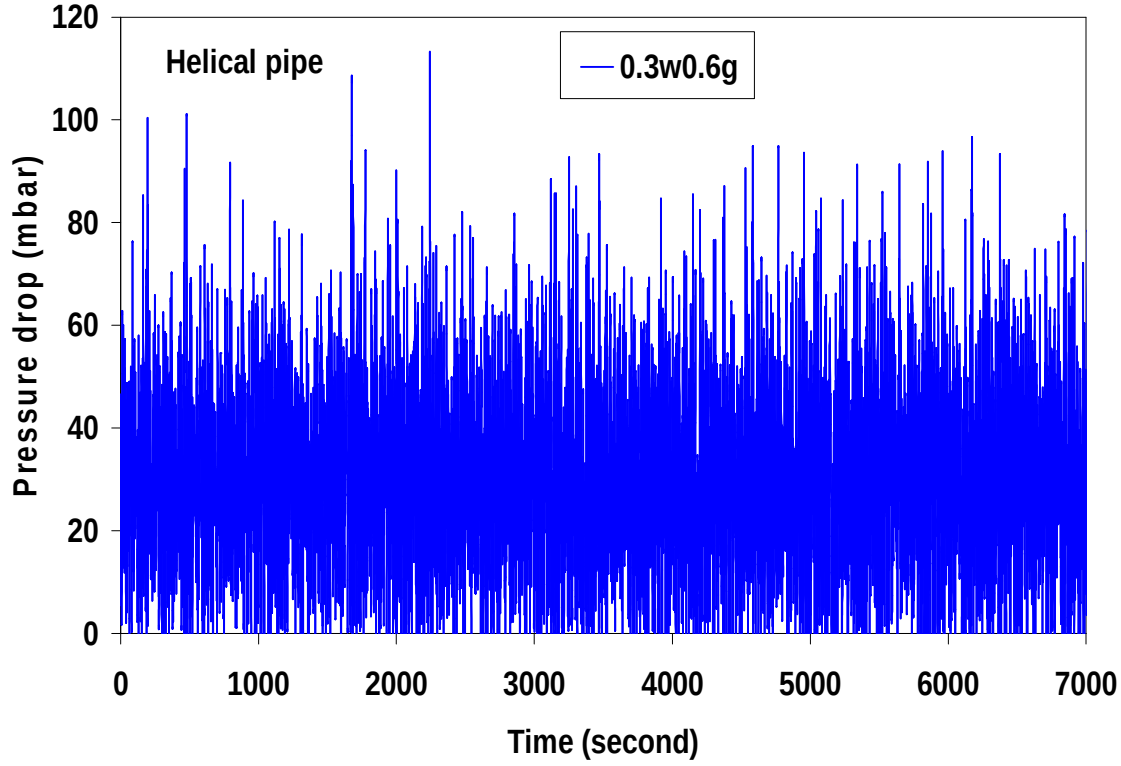
Helical pipe
0.3w0.6g
Pressure drop (mbar)
0
20
40
60
80
100
120
0
1000
2000
3000
4000
5000
6000
7000
Time (second)

APPENDIX B

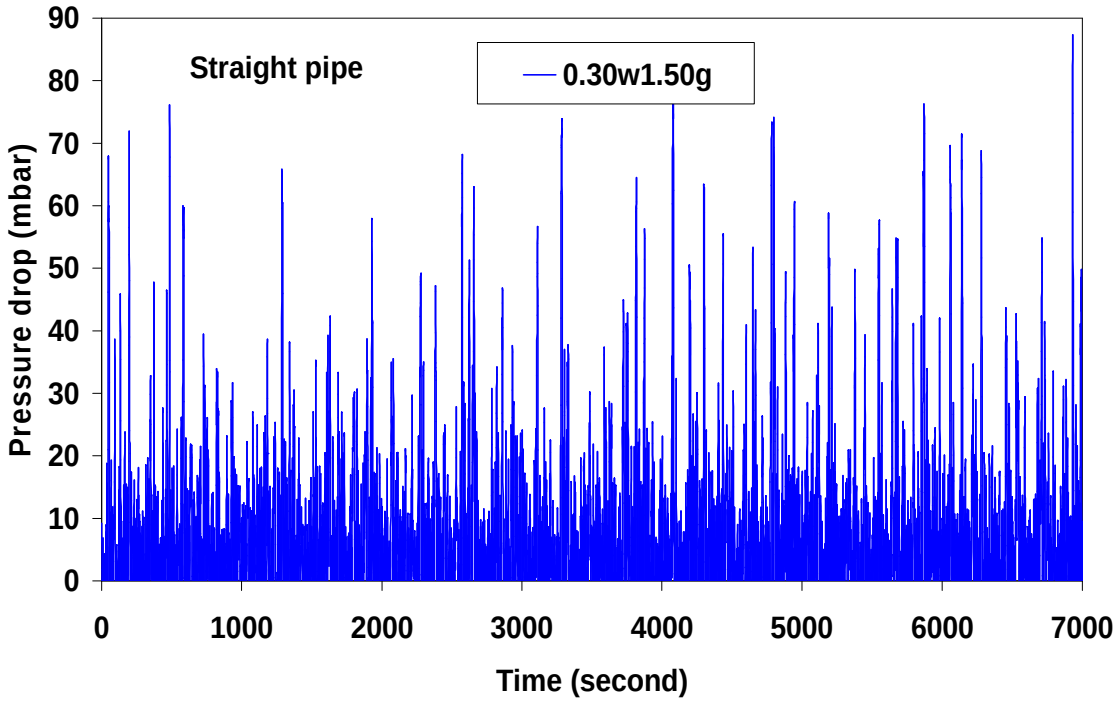
Straight pipe
0.30w1.50g
Pressure drop (mbar)
Time (second)
0
10
20
30
40
50
60
70
80
90
0
1000
2000
3000
4000
5000
6000
7000

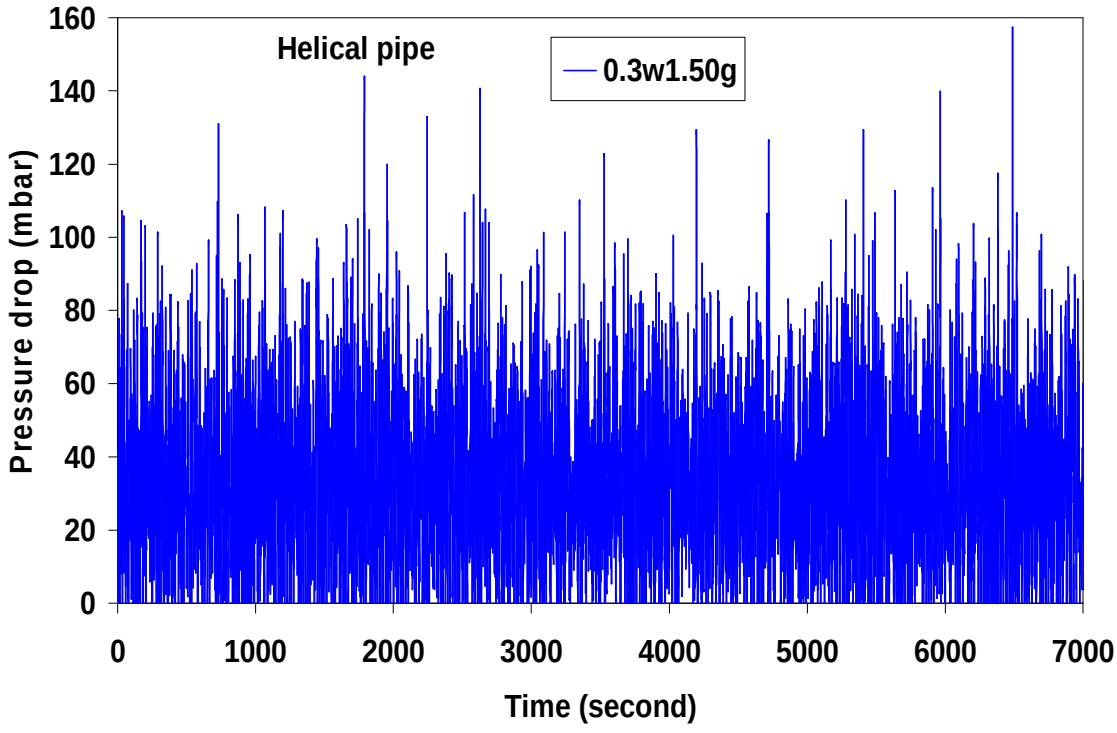
Helical pipe
0.3w1.50g
Pressure drop (mbar)
Time (second)
0
20
40
60
80
100
120
140
160
0
1000
2000
3000
4000
5000
6000
7000

APPENDIX B

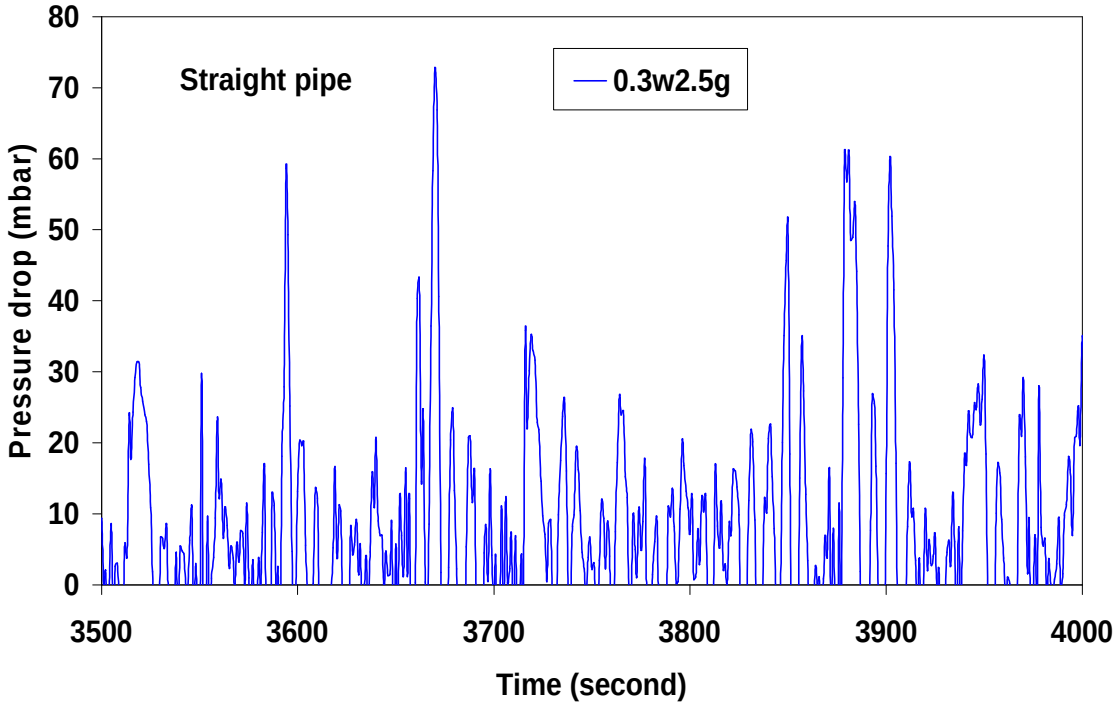
Straight pipe
0.3w2.5g
Pressure drop (mbar)
Time (second)
0
10
20
30
40
50
60
70
80
3500
3600
3700
3800
3900
4000

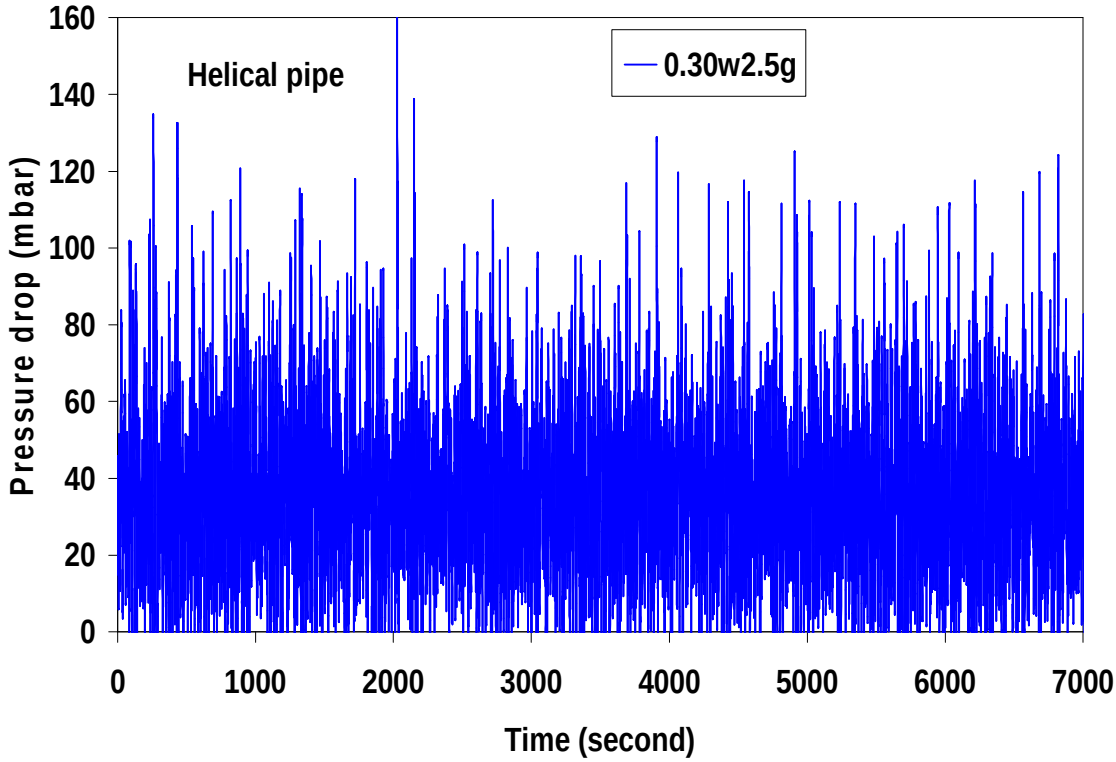
Helical pipe
0.30w2.5g
Pressure drop (mbar)
Time (second)
0
20
40
60
80
100
120
140
160
0
1000
2000
3000
4000
5000
6000
7000

APPENDIX B

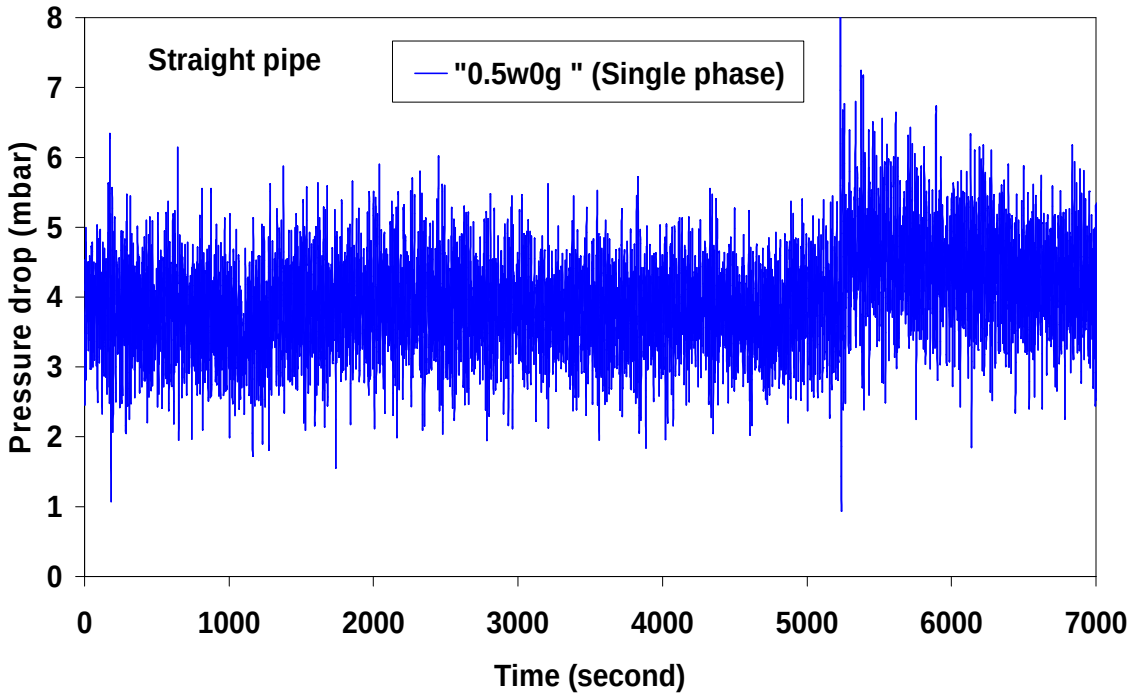
Straight pipe
"0.5w0g " (Single phase)
Pressure drop (mbar)
Time (second)
0
1
2
3
4
5
6
7
8
0
1000
2000
3000
4000
5000
6000
7000

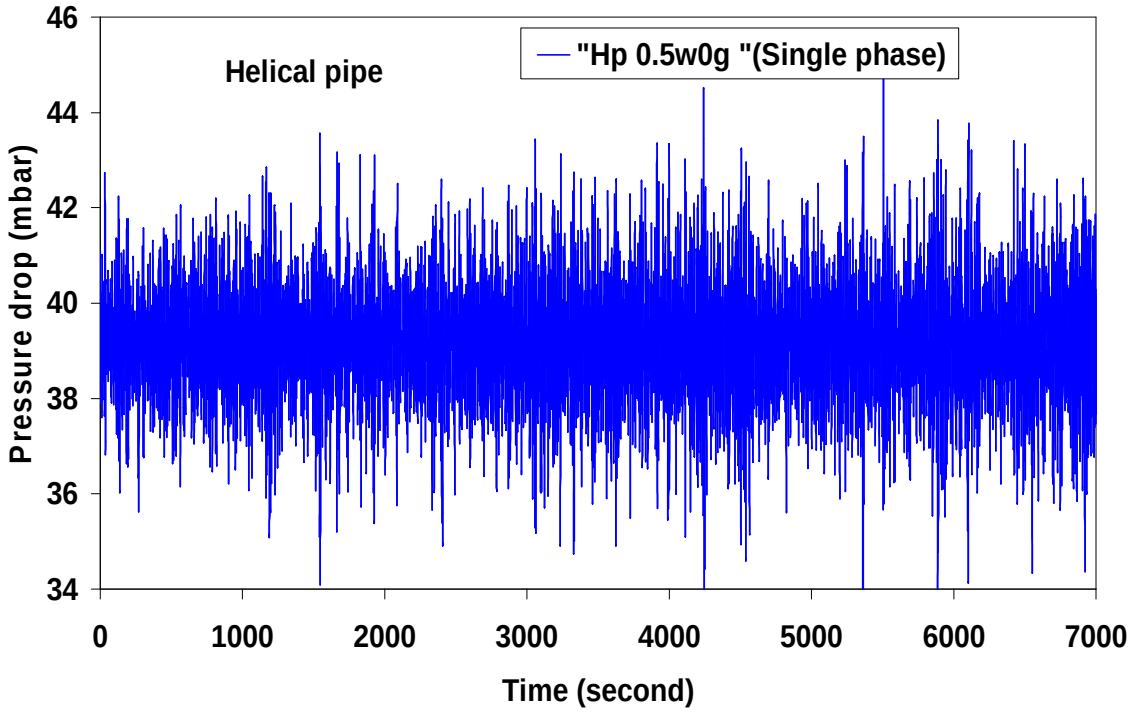
Helical pipe
"Hp 0.5w0g "(Single phase)
Pressure drop (mbar)
Time (second)
34
36
38
40
42
44
46
0
1000
2000
3000
4000
5000
6000
7000

APPENDIX B

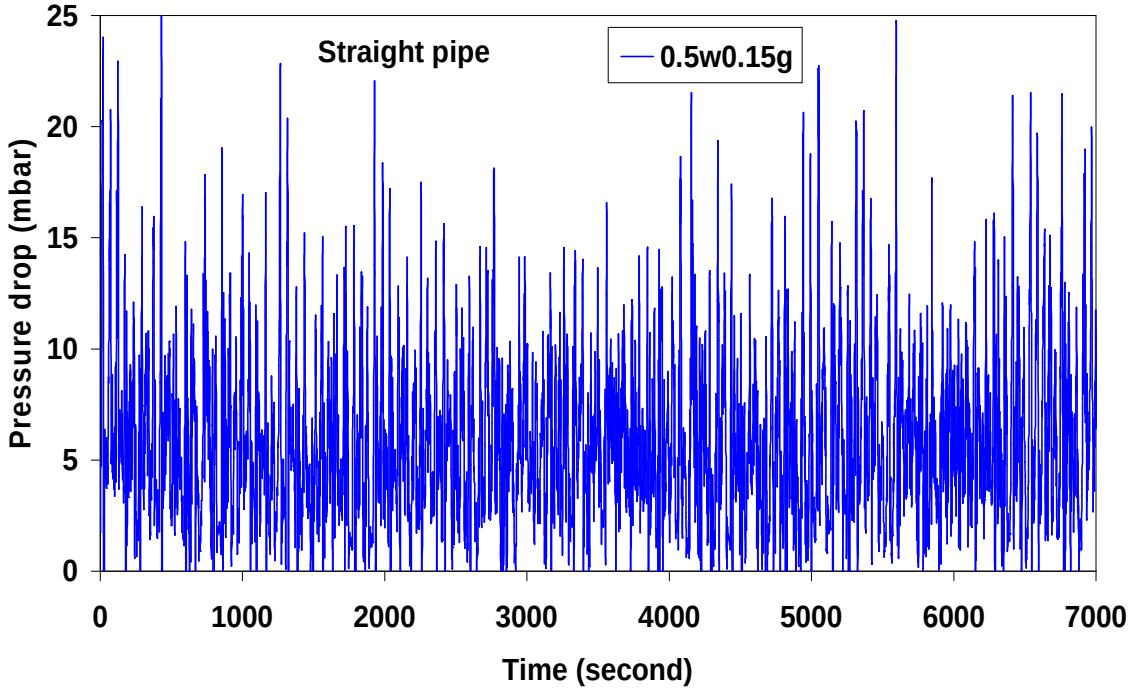
Straight pipe
0.5w0.15g
Pressure drop (mbar)
Time (second)
0
5
10
15
20
25
0
1000
2000
3000
4000
5000
6000
7000

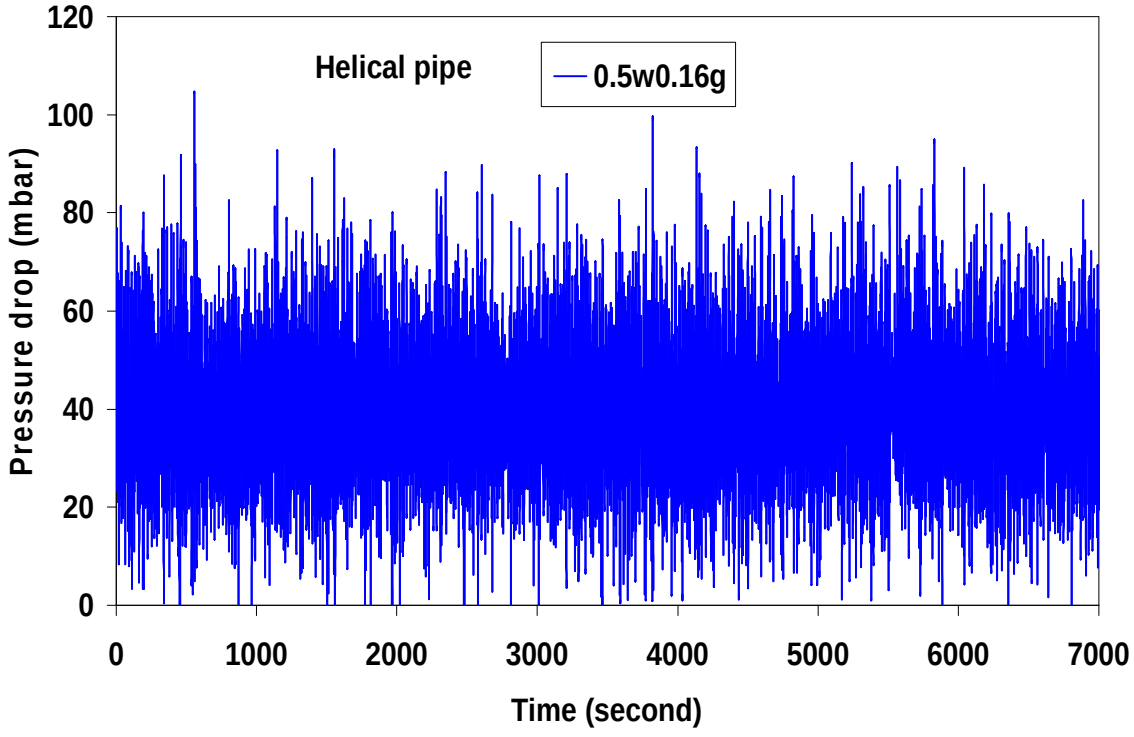
Helical pipe
0.5w0.16g
Pressure drop (mbar)
Time (second)
0
20
40
60
80
100
120
0
1000
2000
3000
4000
5000
6000
7000

APPENDIX B

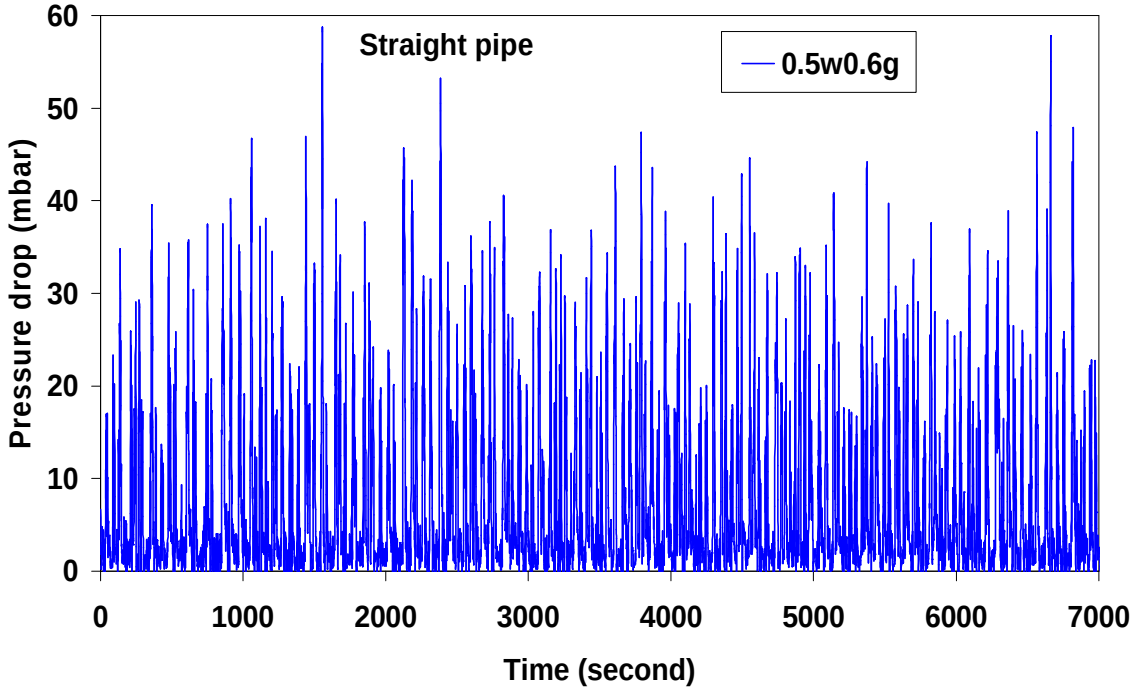
Straight pipe
0.5w0.6g
Pressure drop (mbar)
Time (second)
0
10
20
30
40
50
60
0
1000
2000
3000
4000
5000
6000
7000

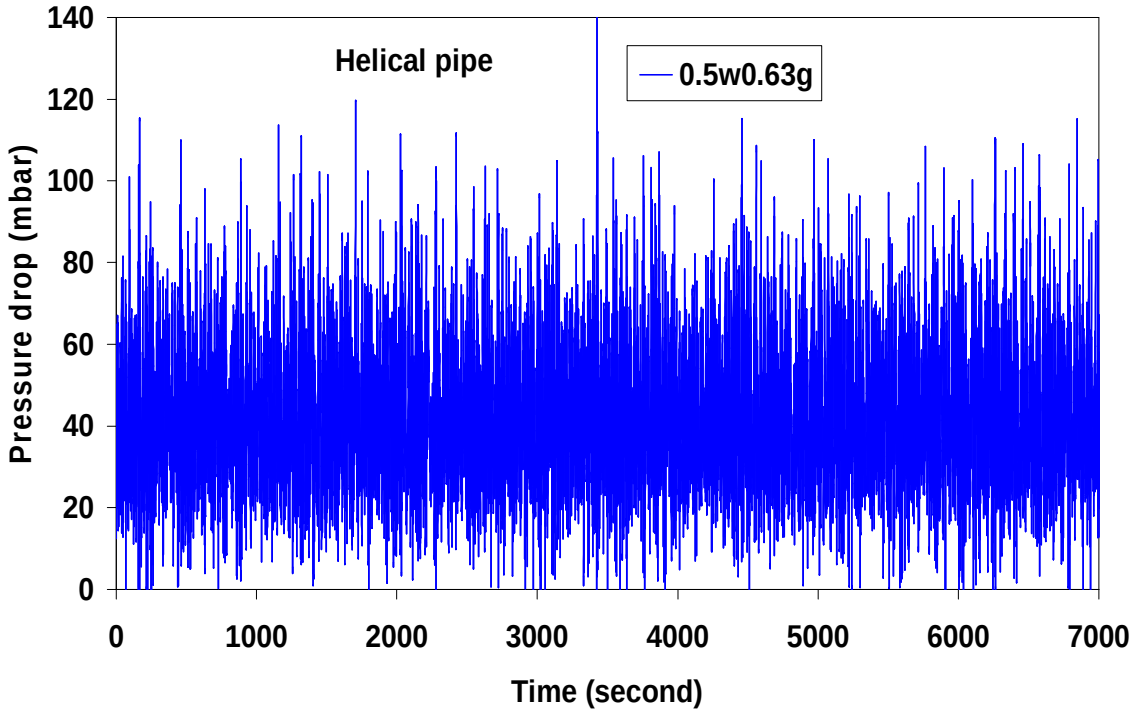
Helical pipe
0.5w0.63g
Pressure drop (mbar)
Time (second)
0
20
40
60
80
100
120
140
0
1000
2000
3000
4000
5000
6000
7000

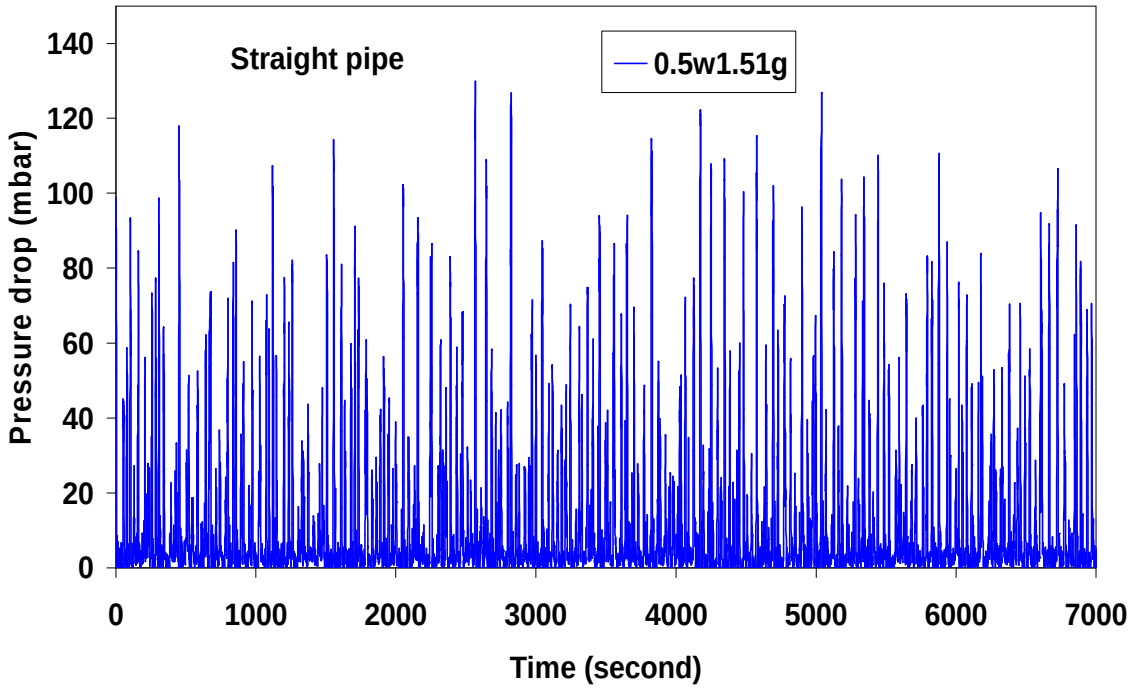
Straight pipe
0.5w1.51g
Pressure drop (mbar)
0
20
40
60
80
100
120
140
0
1000
2000
3000
4000
5000
6000
7000
Time (second)

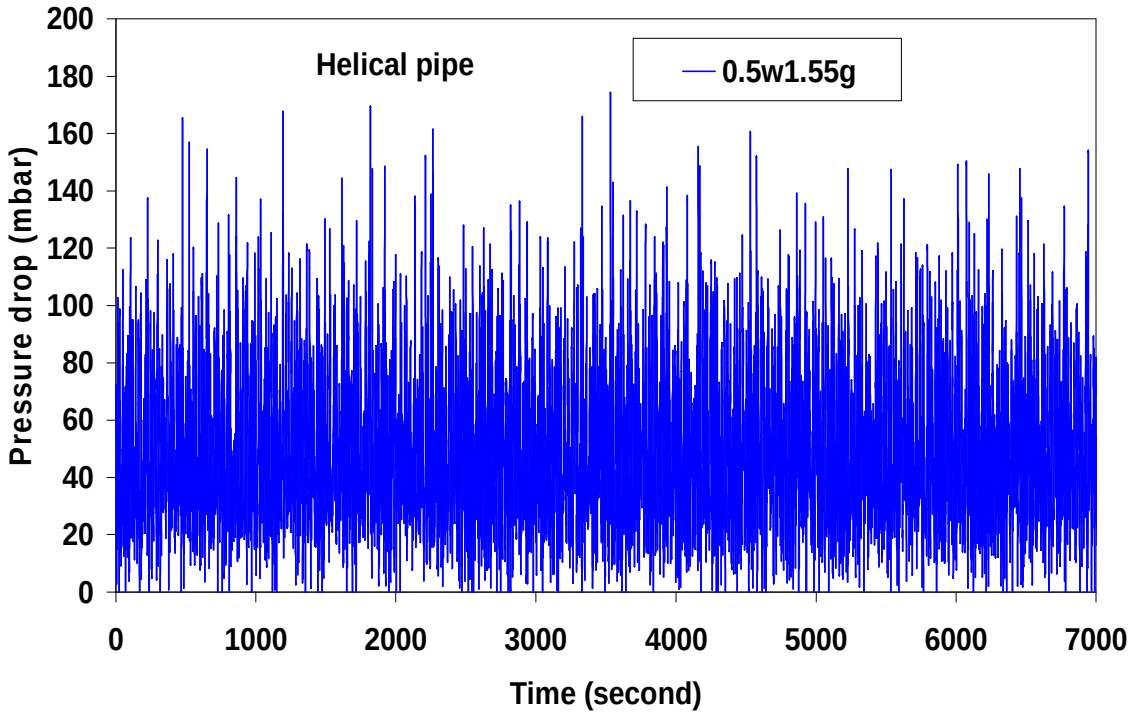
Helical pipe
0.5w1.55g
Pressure drop (mbar)
0
20
40
60
80
100
120
140
160
180
200
0
1000
2000
3000
4000
5000
6000
7000
Time (second)

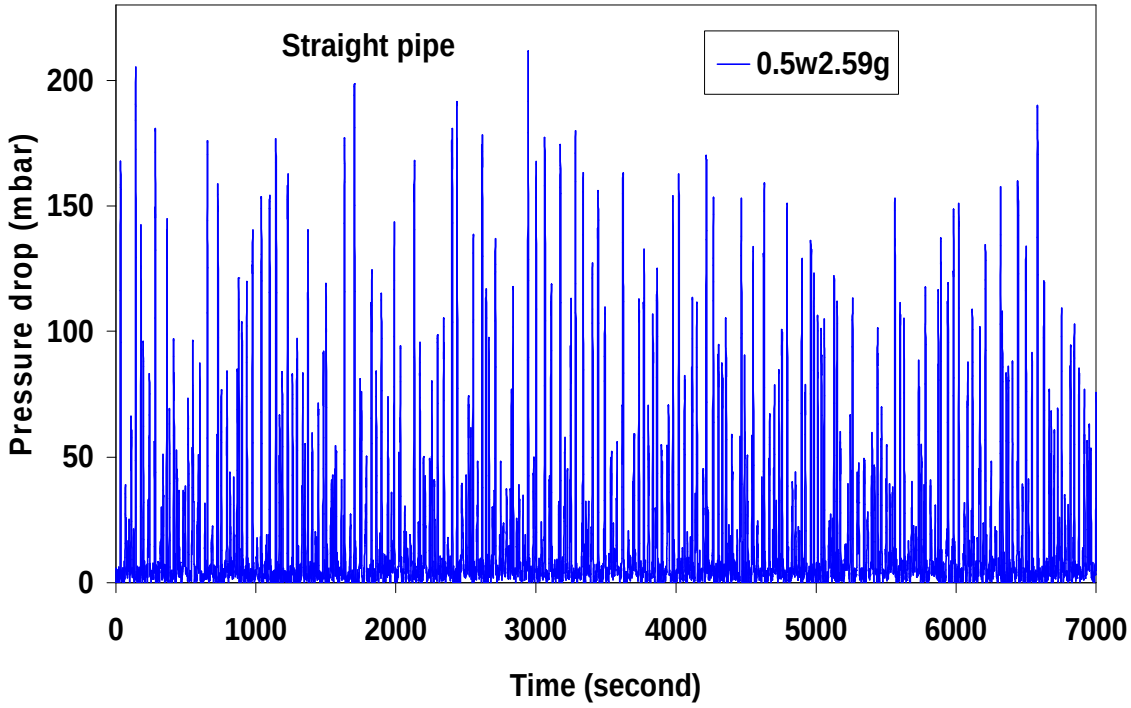
Straight pipe
0.5w2.59g
Pressure drop (mbar)
0
50
100
150
200
0
1000
2000
3000
4000
5000
6000
7000
Time (second)

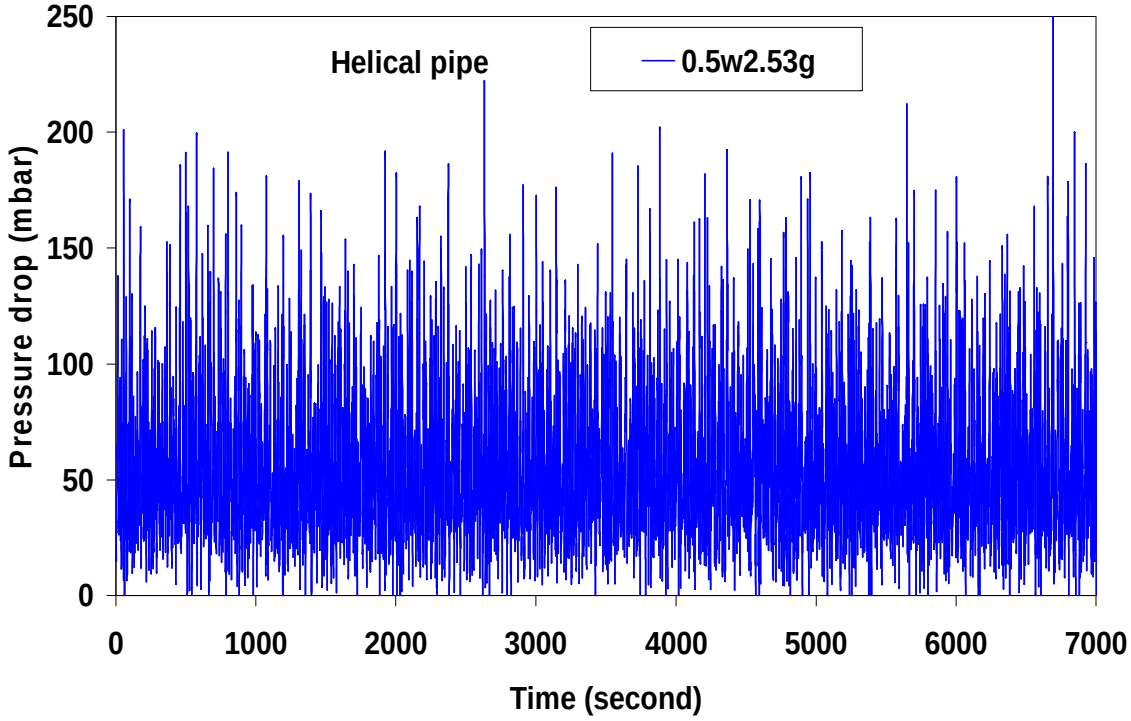
Helical pipe
0.5w2.53g
Pressure drop (mbar)
0
50
100
150
200
250
0
1000
2000
3000
4000
5000
6000
7000
Time (second)

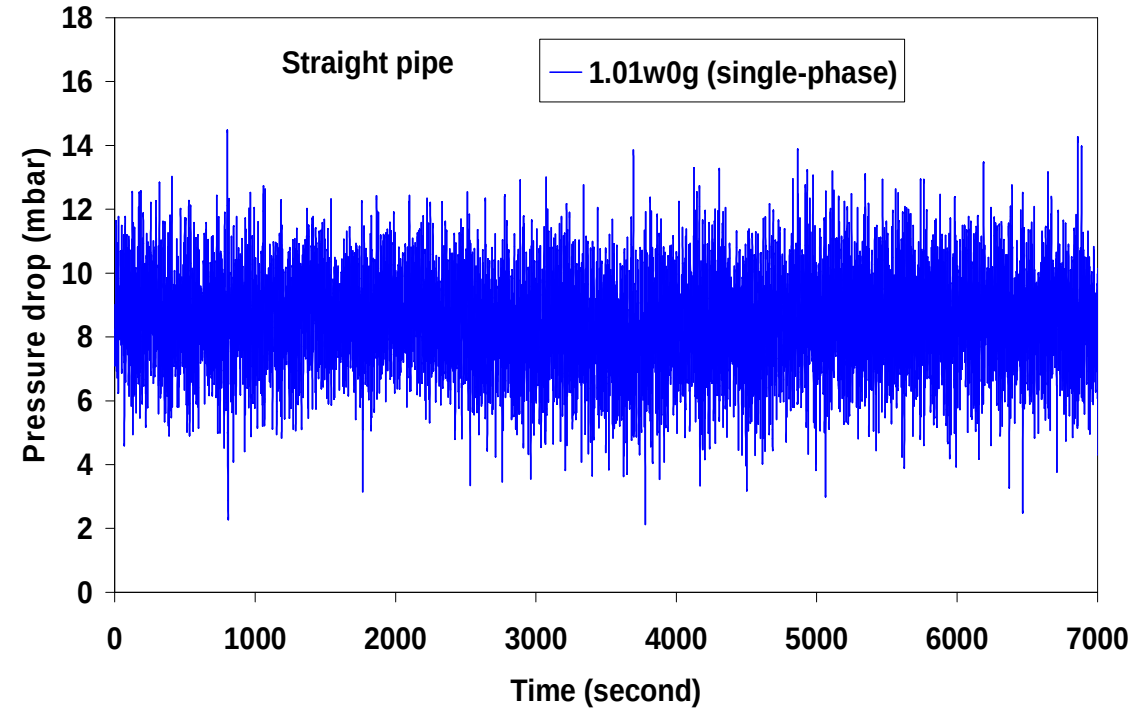
Straight pipe
1.01w0g (single-phase)
Pressure drop (mbar)
Time (second)
0
2
4
6
8
10
12
14
16
18
0
1000
2000
3000
4000
5000
6000
7000

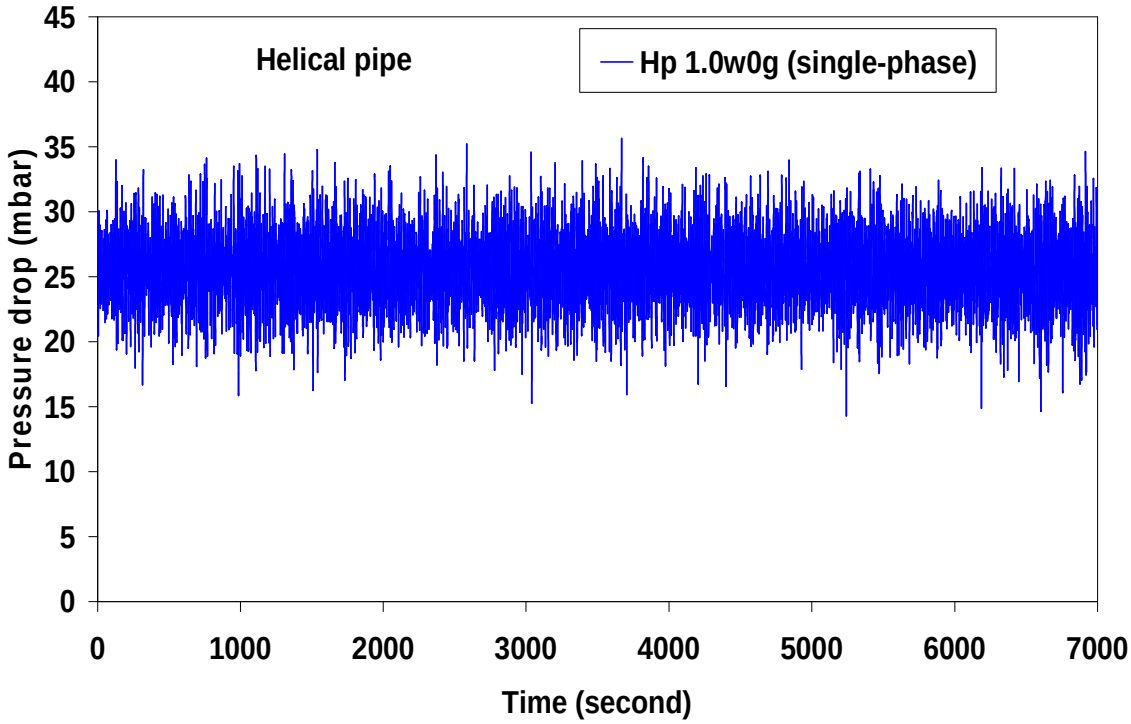
Helical pipe
Hp 1.0w0g (single-phase)
Pressure drop (mbar)
Time (second)
0
5
10
15
20
25
30
35
40
45
0
1000
2000
3000
4000
5000
6000
7000

APPENDIX B

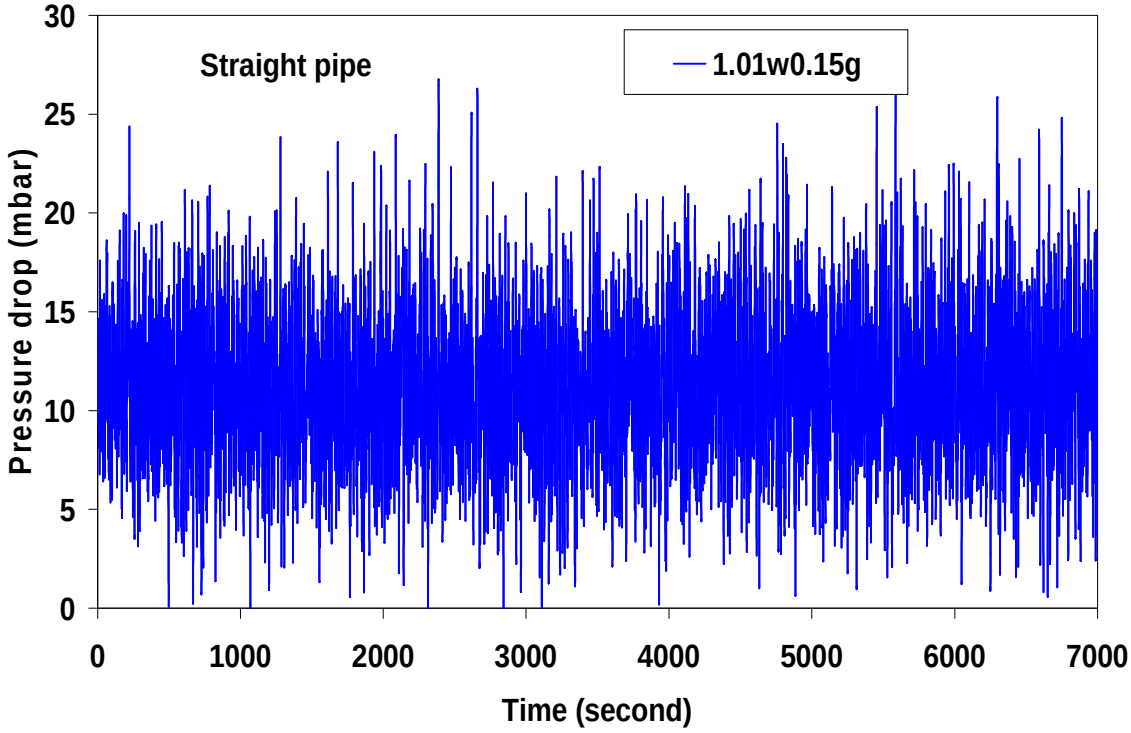
Straight pipe
1.01w0.15g
Pressure drop (mbar)
Time (second)
0
5
10
15
20
25
30
0
1000
2000
3000
4000
5000
6000
7000

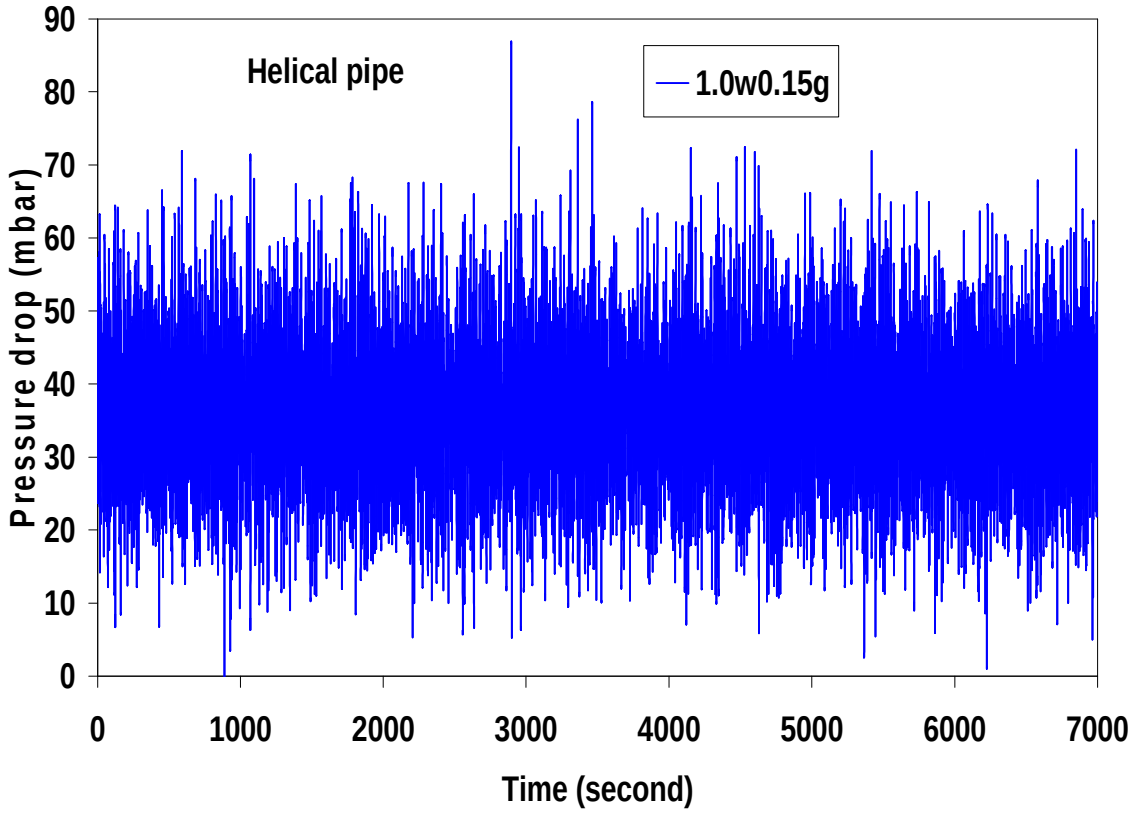
Helical pipe
1.0w0.15g
Pressure drop (mbar)
Time (second)
0
10
20
30
40
50
60
70
80
90
0
1000
2000
3000
4000
5000
6000
7000

APPENDIX B

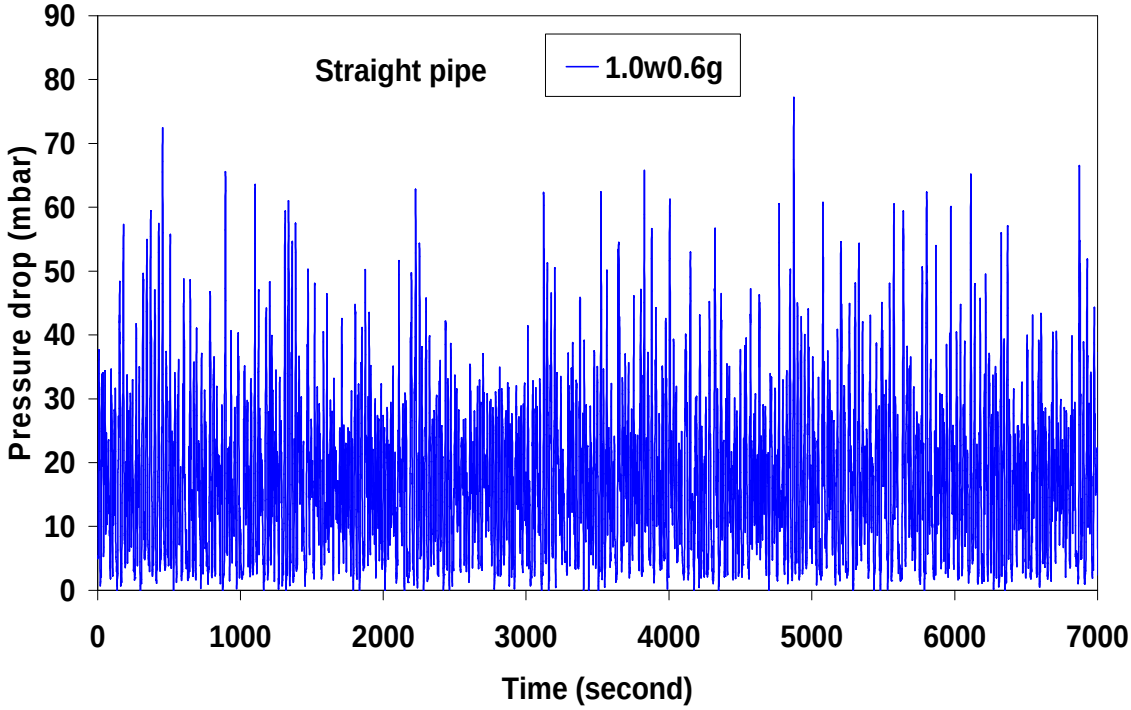
Straight pipe
1.0w0.6g
Pressure drop (mbar)
Time (second)
0
10
20
30
40
50
60
70
80
90
0
1000
2000
3000
4000
5000
6000
7000

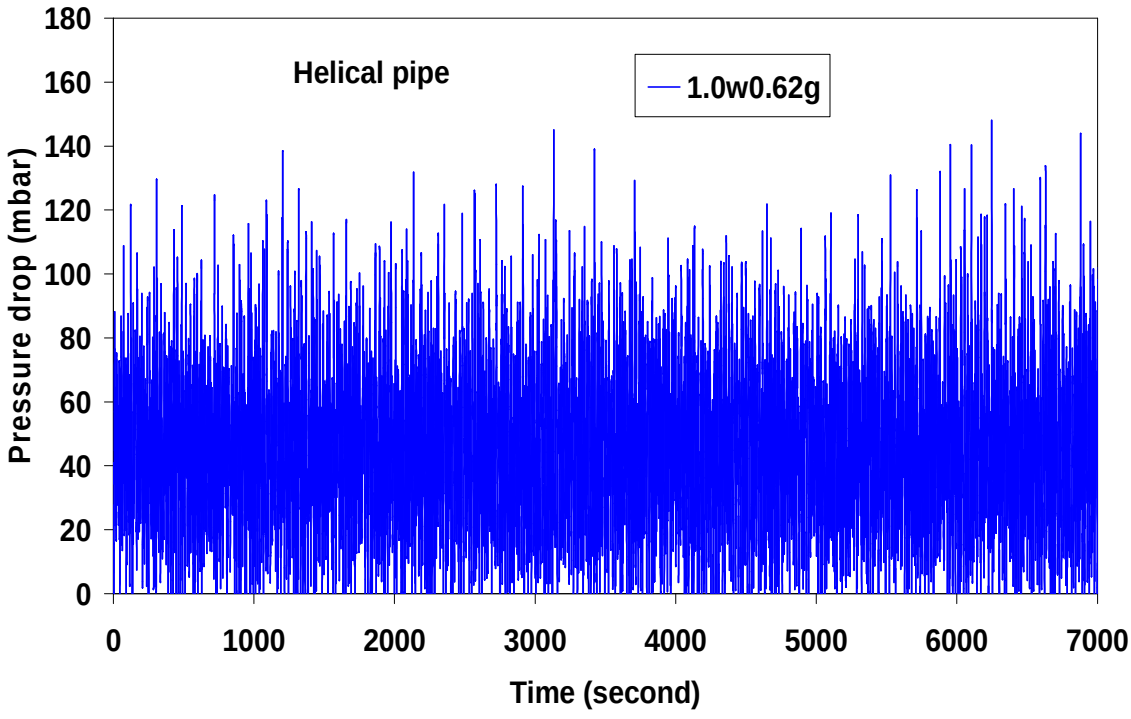
Helical pipe
1.0w0.62g
Pressure drop (mbar)
Time (second)
0
20
40
60
80
100
120
140
160
180
0
1000
2000
3000
4000
5000
6000
7000

APPENDIX B

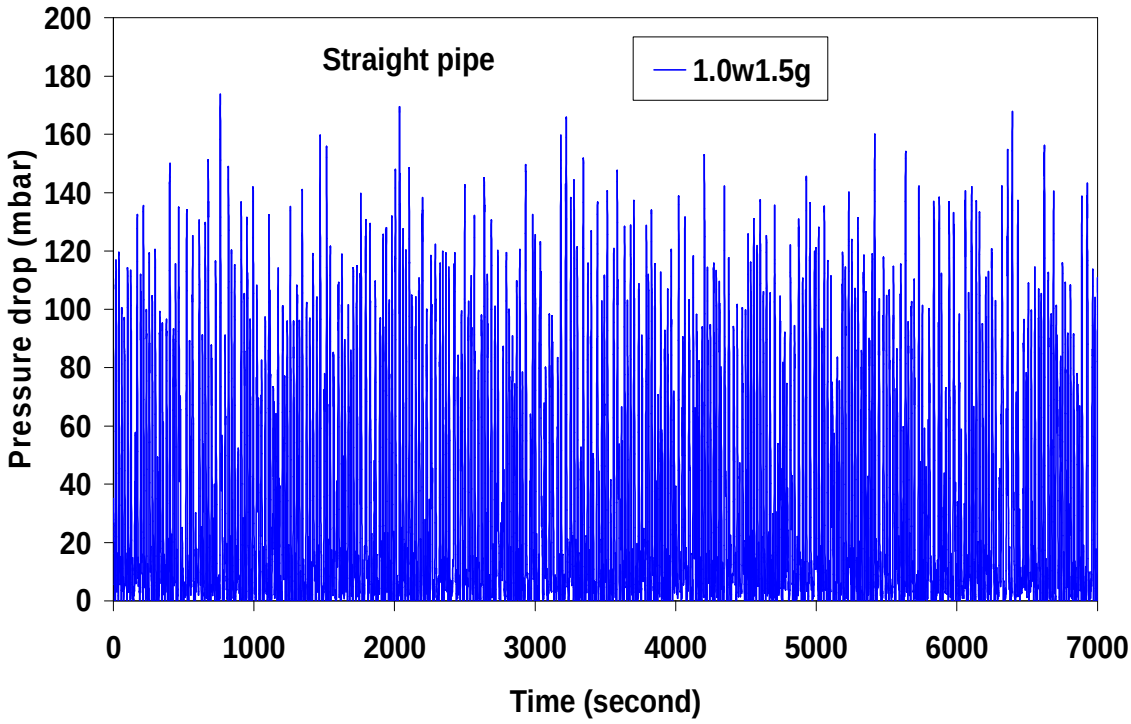
Straight pipe
1.0w1.5g
Pressure drop (mbar)
Time (second)
0
20
40
60
80
100
120
140
160
180
200
0
1000
2000
3000
4000
5000
6000
7000

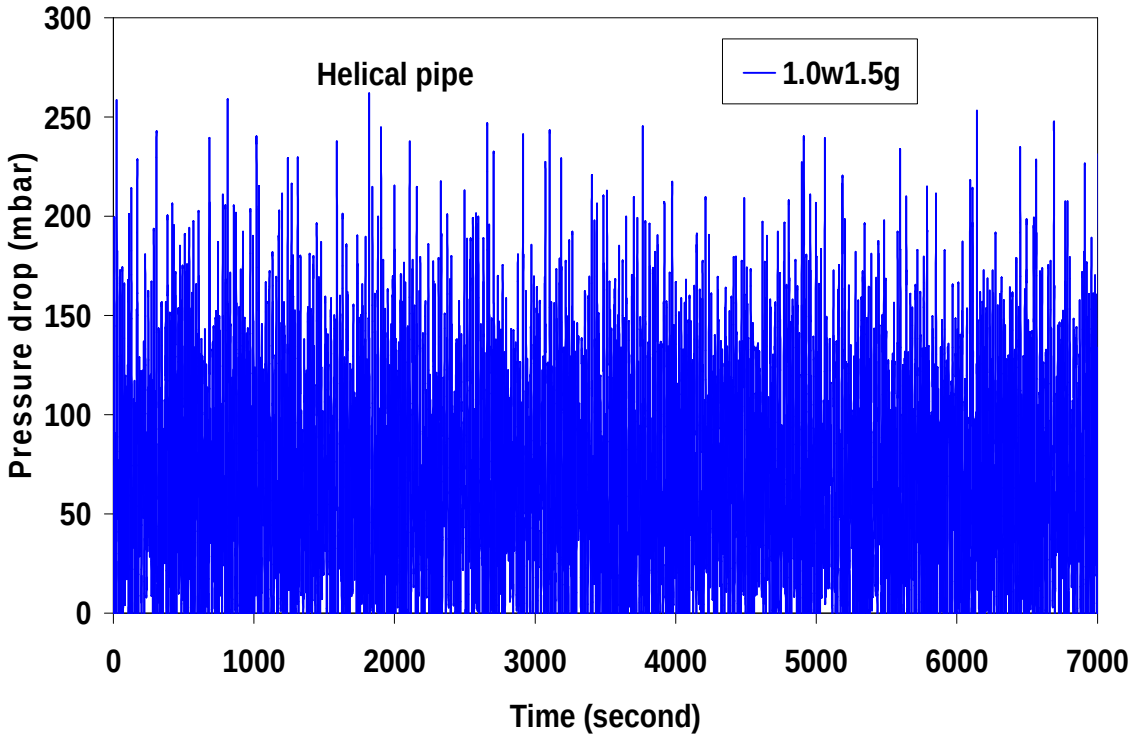
Helical pipe
1.0w1.5g
Pressure drop (mbar)
Time (second)
0
50
100
150
200
250
300
0
1000
2000
3000
4000
5000
6000
7000

APPENDIX B

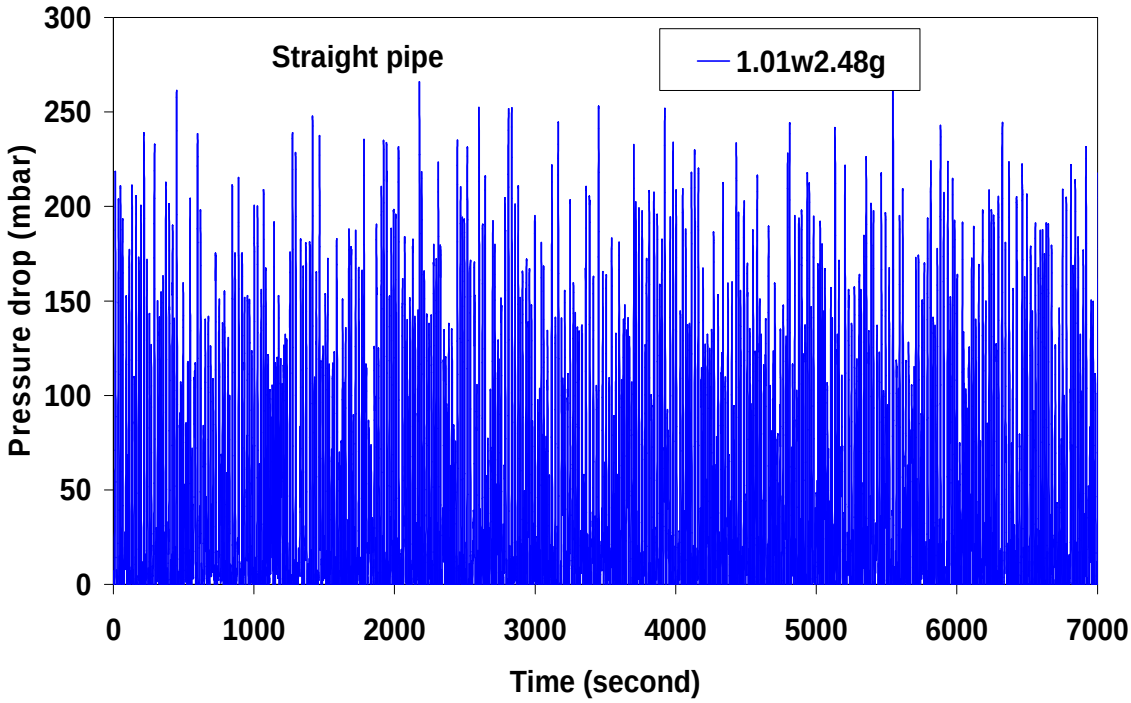
Straight pipe
1.01w2.48g
Pressure drop (mbar)
300
250
200
150
100
50
0
0
1000
2000
3000
4000
5000
6000
7000
Time (second)

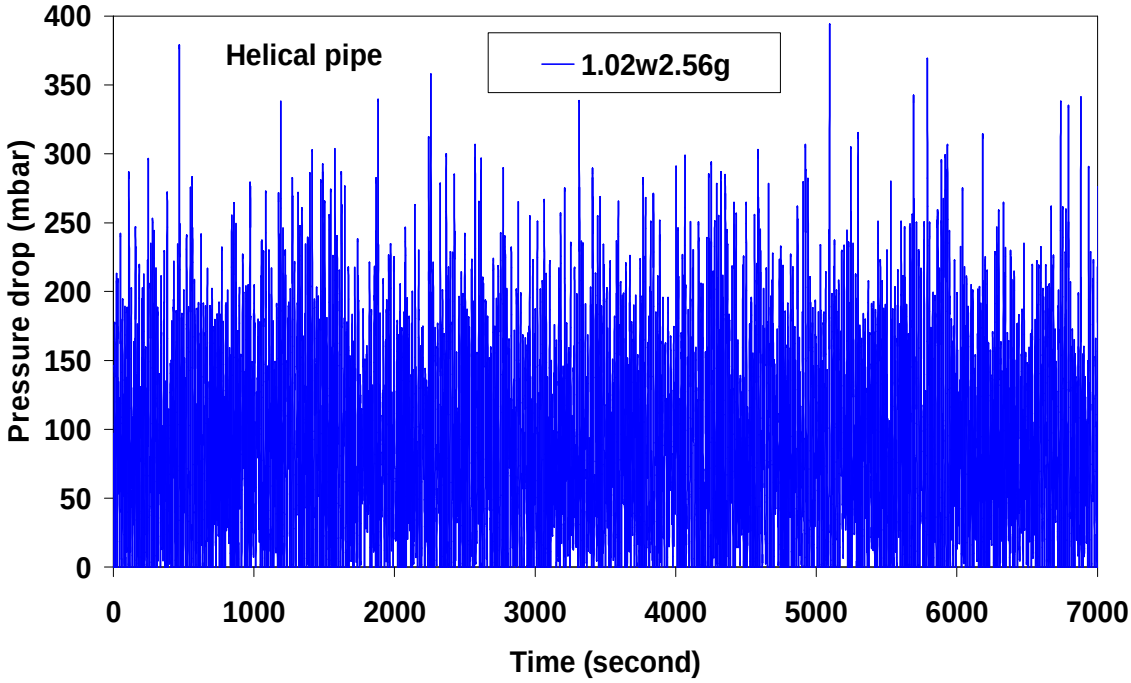
Helical pipe
1.02w2.56g
Pressure drop (mbar)
400
350
300
250
200
150
100
50
0
0
1000
2000
3000
4000
5000
6000
7000
Time (second)

APPENDIX B

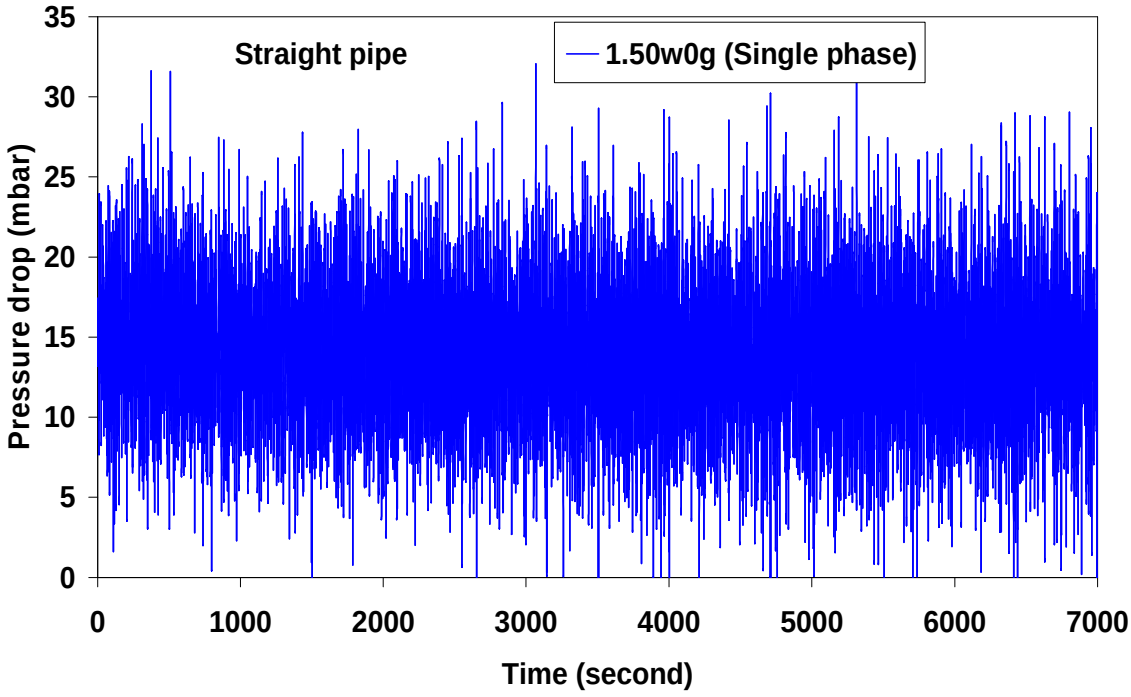
Straight pipe
1.50w0g (Single phase)
Pressure drop (mbar)
Time (second)
0
5
10
15
20
25
30
35
0
1000
2000
3000
4000
5000
6000
7000

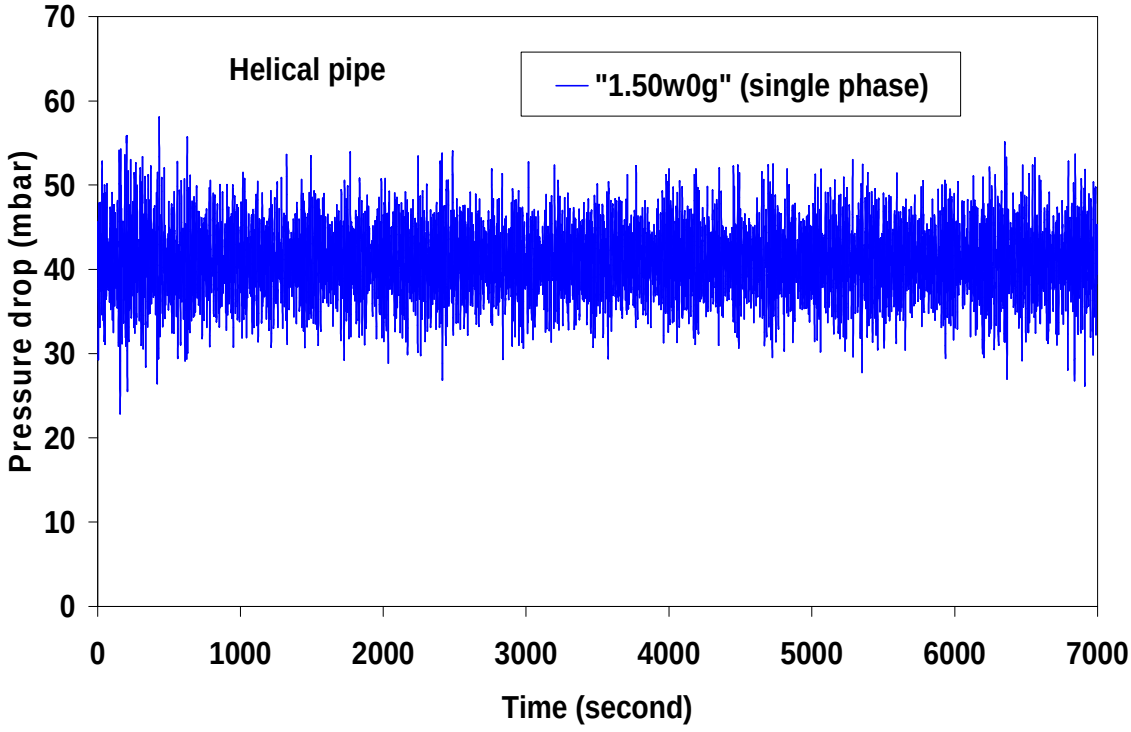
Helical pipe
"1.50w0g" (single phase)
Pressure drop (mbar)
Time (second)
0
10
20
30
40
50
60
70
0
1000
2000
3000
4000
5000
6000
7000

APPENDIX B

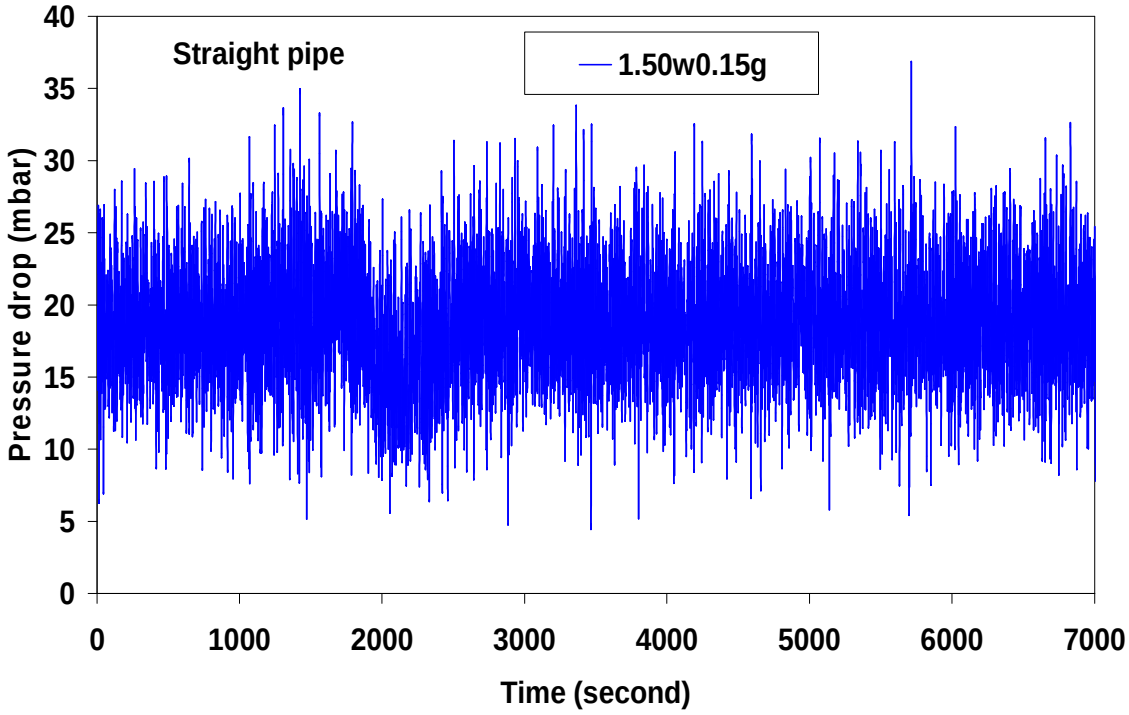
Straight pipe
1.50w0.15g
Pressure drop (mbar)
Time (second)
0
5
10
15
20
25
30
35
40
0
1000
2000
3000
4000
5000
6000
7000

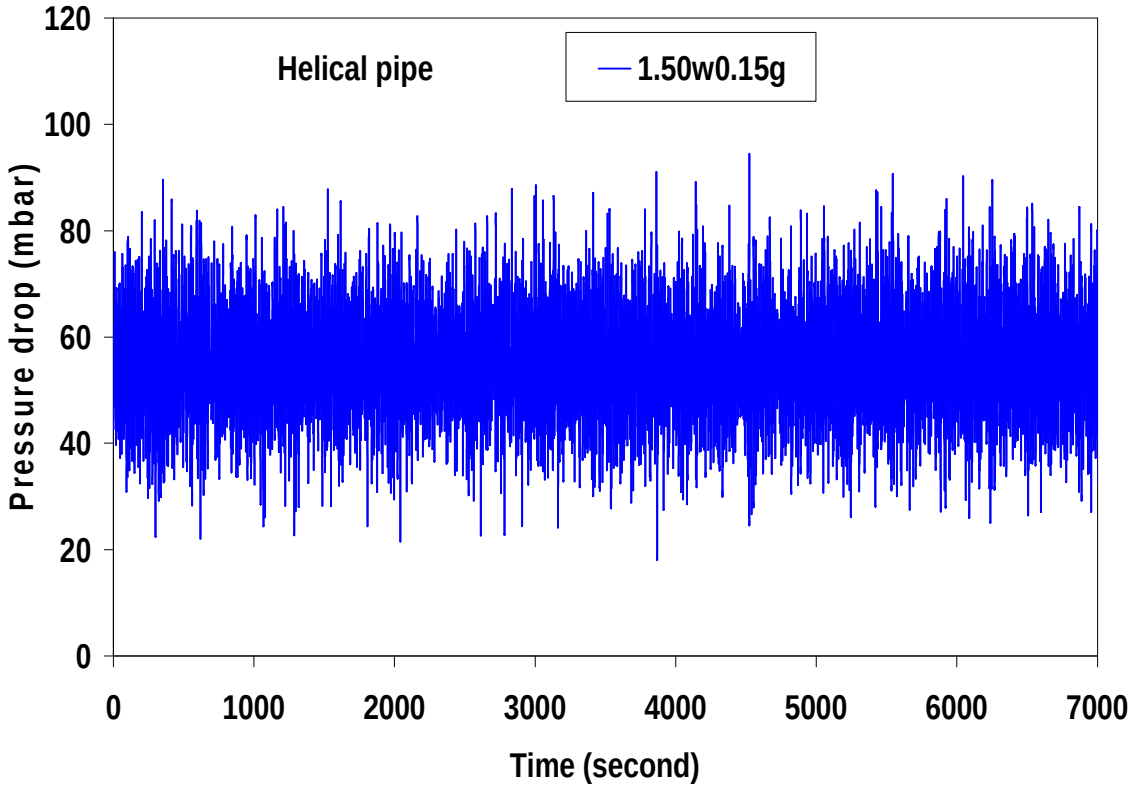
Helical pipe
1.50w0.15g
Pressure drop (mbar)
Time (second)
0
20
40
60
80
100
120
0
1000
2000
3000
4000
5000
6000
7000

APPENDIX B

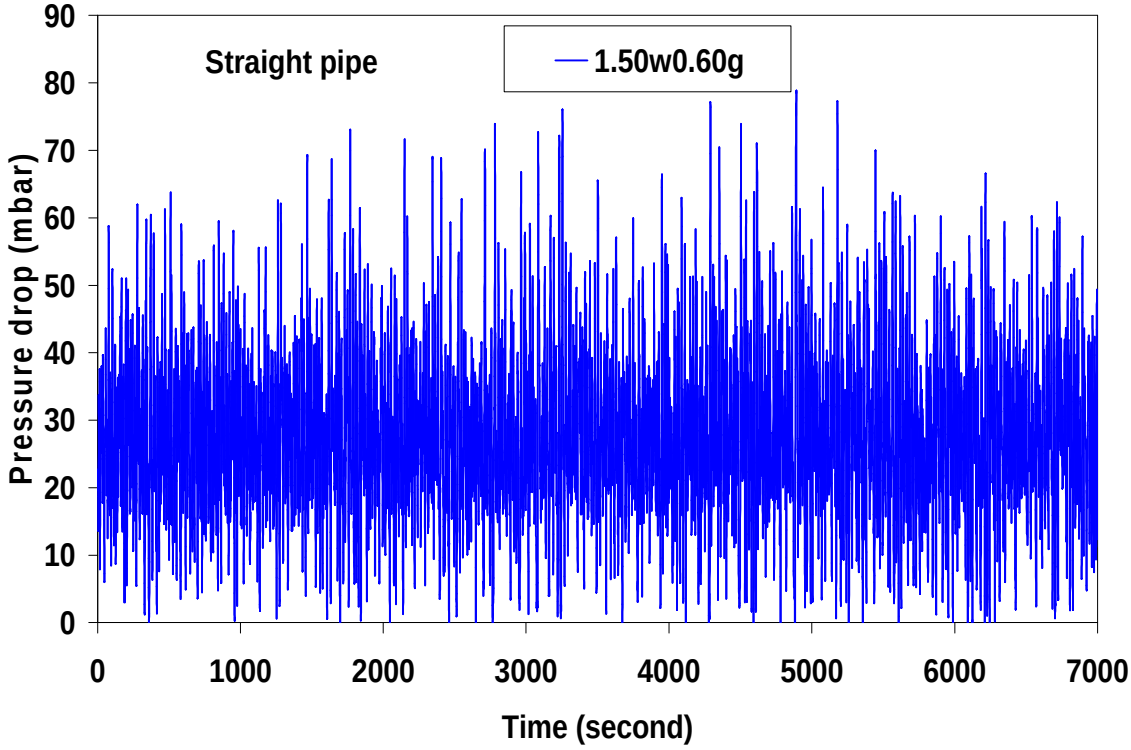
Straight pipe
1.50w0.60g
Pressure drop (mbar)
Time (second)
0
10
20
30
40
50
60
70
80
90
0
1000
2000
3000
4000
5000
6000
7000

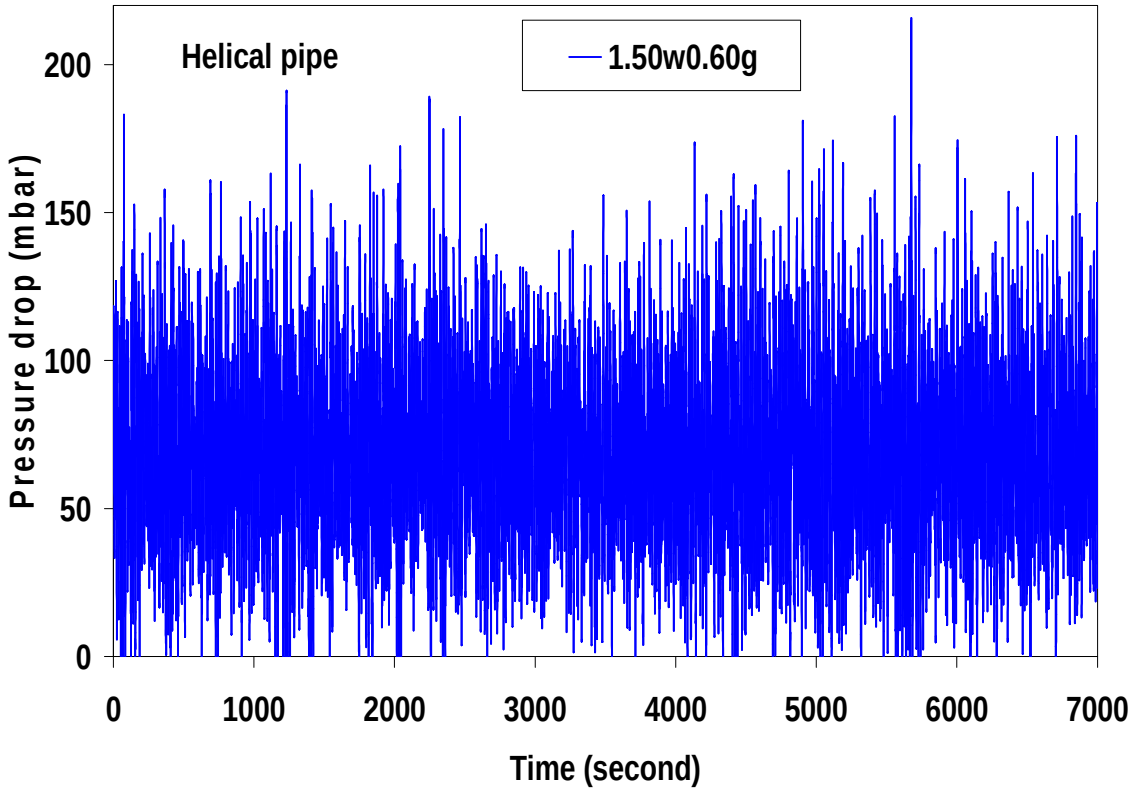
Helical pipe
1.50w0.60g
Pressure drop (mbar)
Time (second)
0
50
100
150
200
0
1000
2000
3000
4000
5000
6000
7000

APPENDIX B

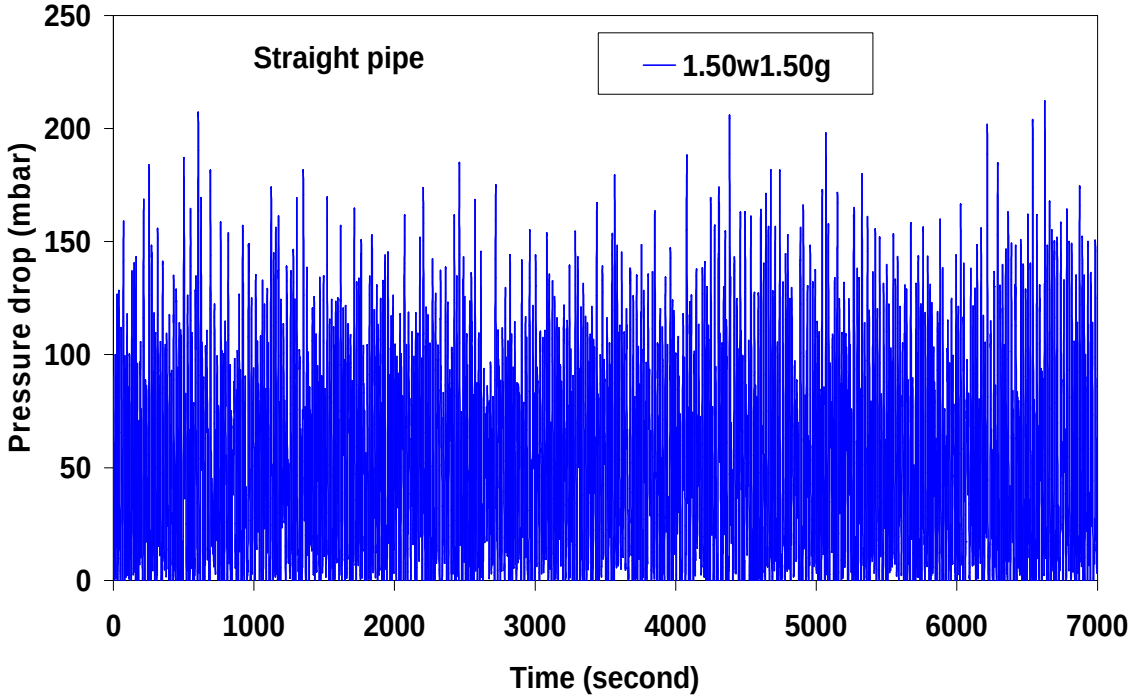
Straight pipe
1.50w1.50g
Pressure drop (mbar)
250
200
150
100
50
0
0
1000
2000
3000
4000
5000
6000
7000
Time (second)

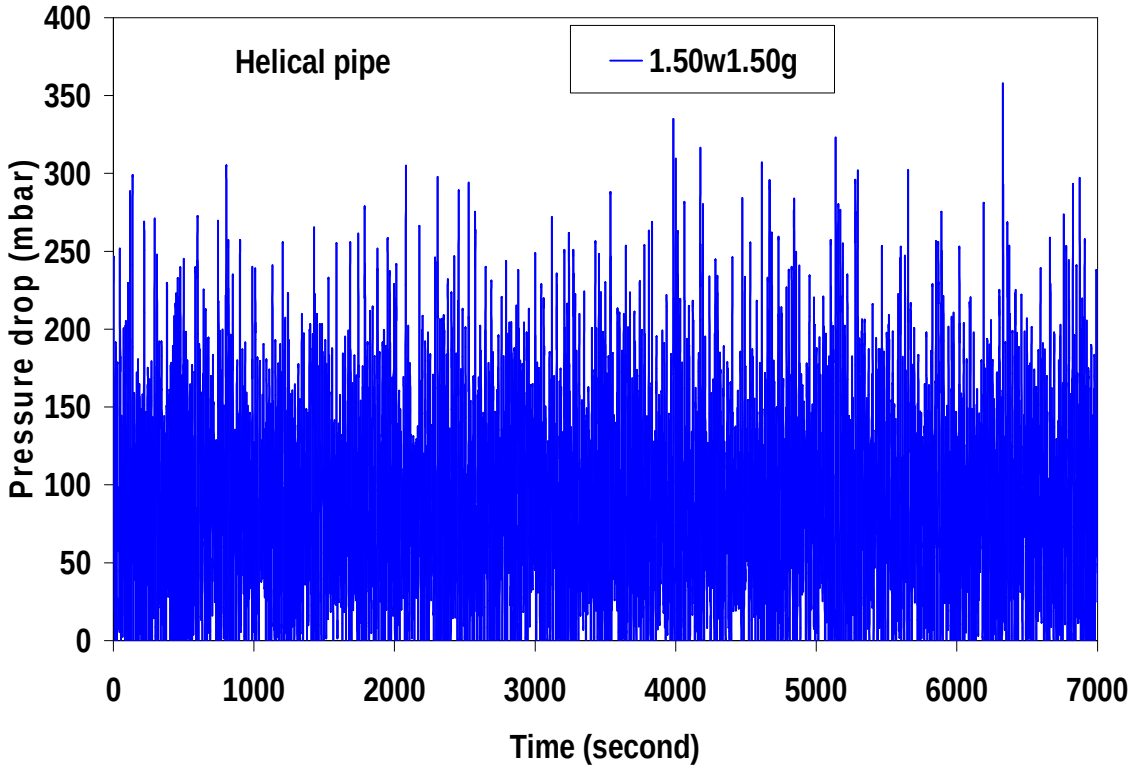
Helical pipe
1.50w1.50g
Pressure drop (mbar)
400
350
300
250
200
150
100
50
0
0
1000
2000
3000
4000
5000
6000
7000
Time (second)

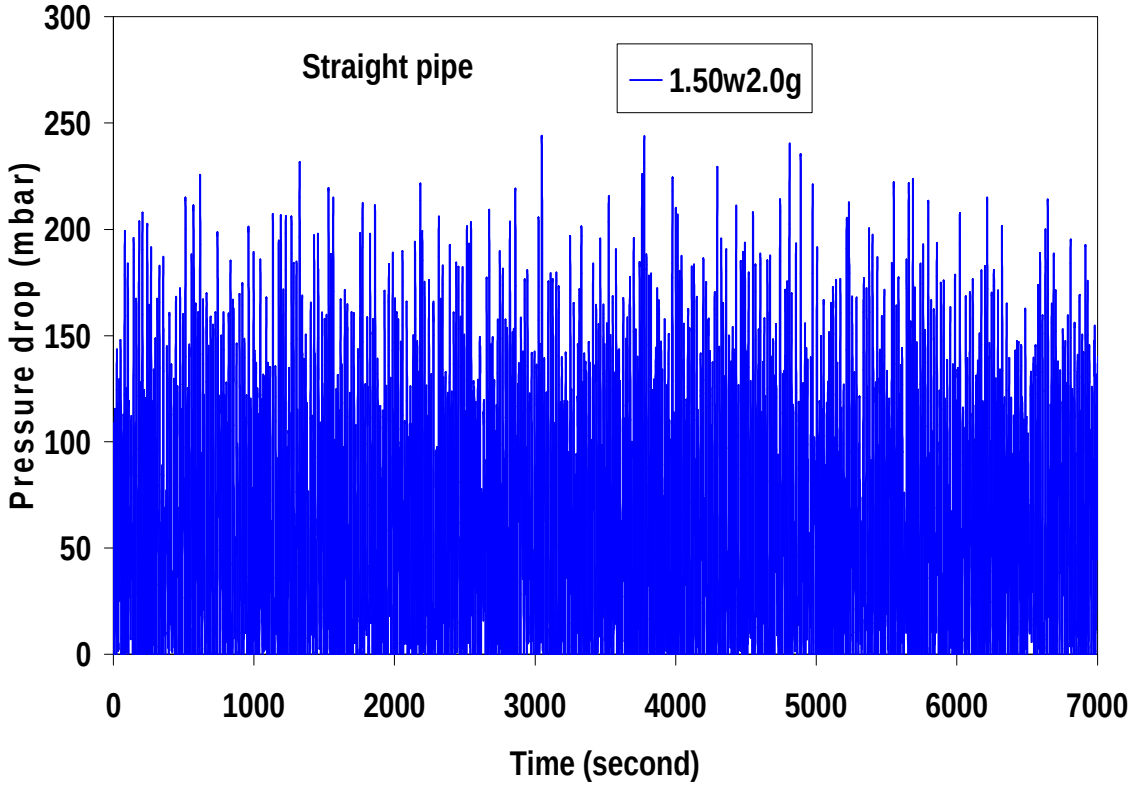
Straight pipe
1.50w2.0g
Pressure drop (mbar)
300
250
200
150
100
50
0
0
1000
2000
3000
4000
5000
6000
7000
Time (second)

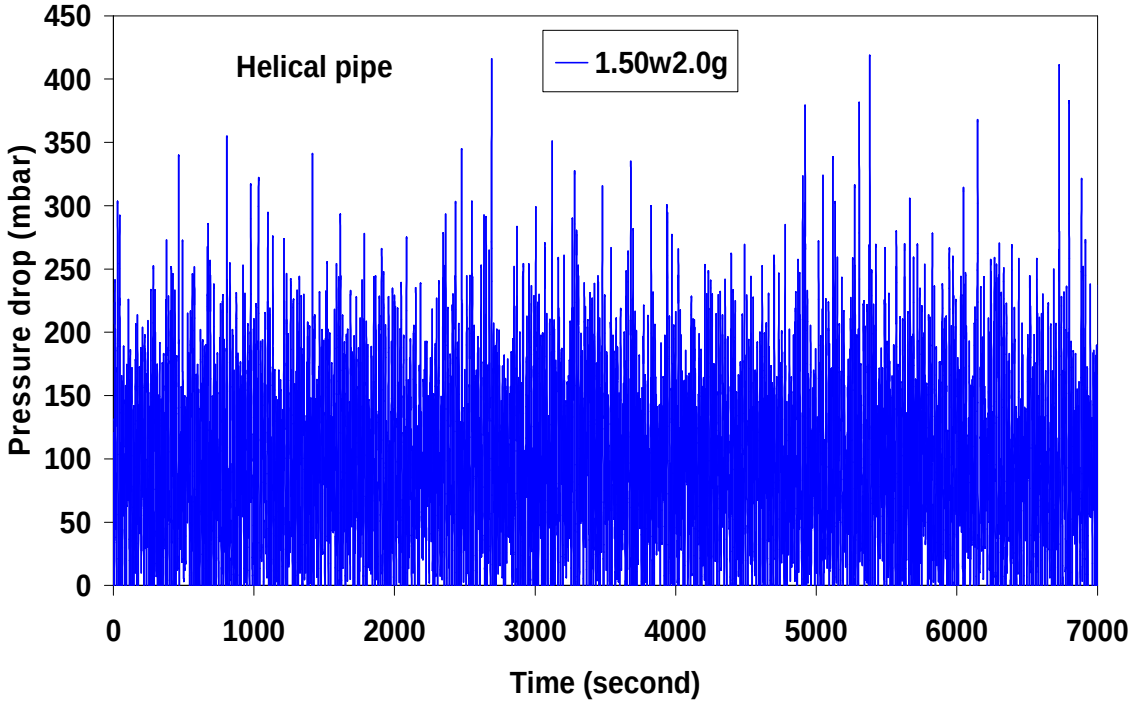
Helical pipe
1.50w2.0g
Pressure drop (mbar)
450
400
350
300
250
200
150
100
50
0
0
1000
2000
3000
4000
5000
6000
7000
Time (second)

APPENDIX B

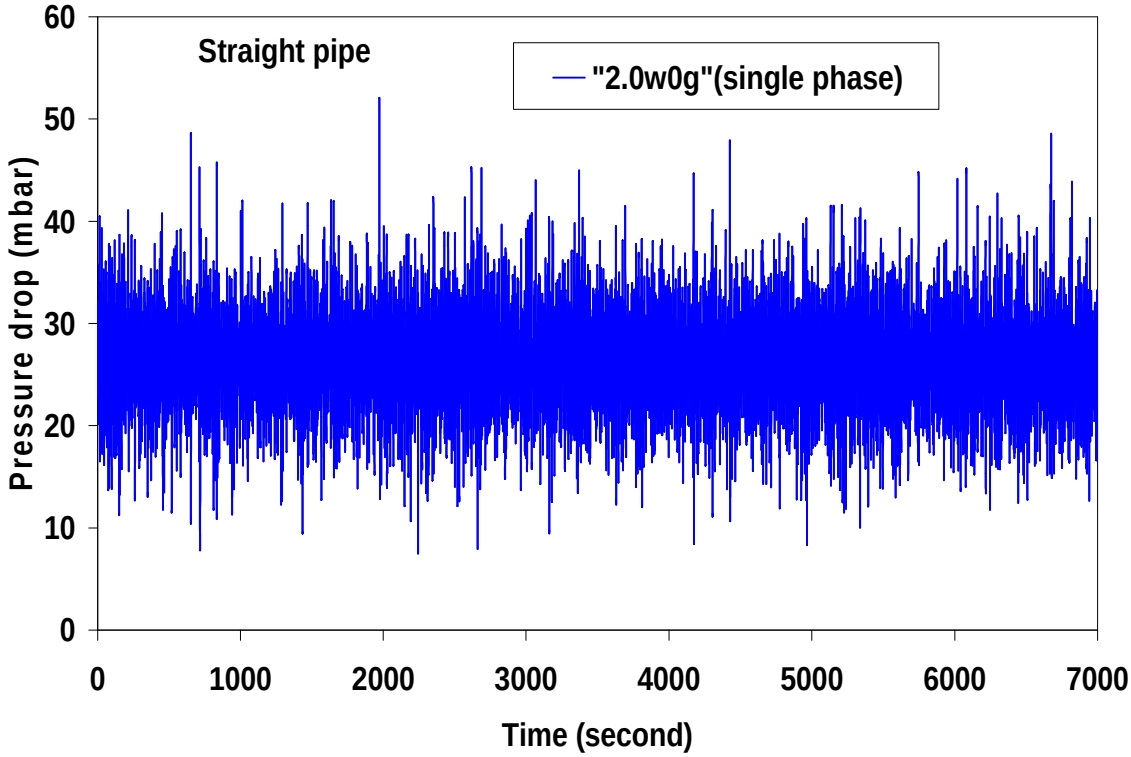
Straight pipe
"2.0w0g"(single phase)
Pressure drop (mbar)
Time (second)
0
10
20
30
40
50
60
0
1000
2000
3000
4000
5000
6000
7000

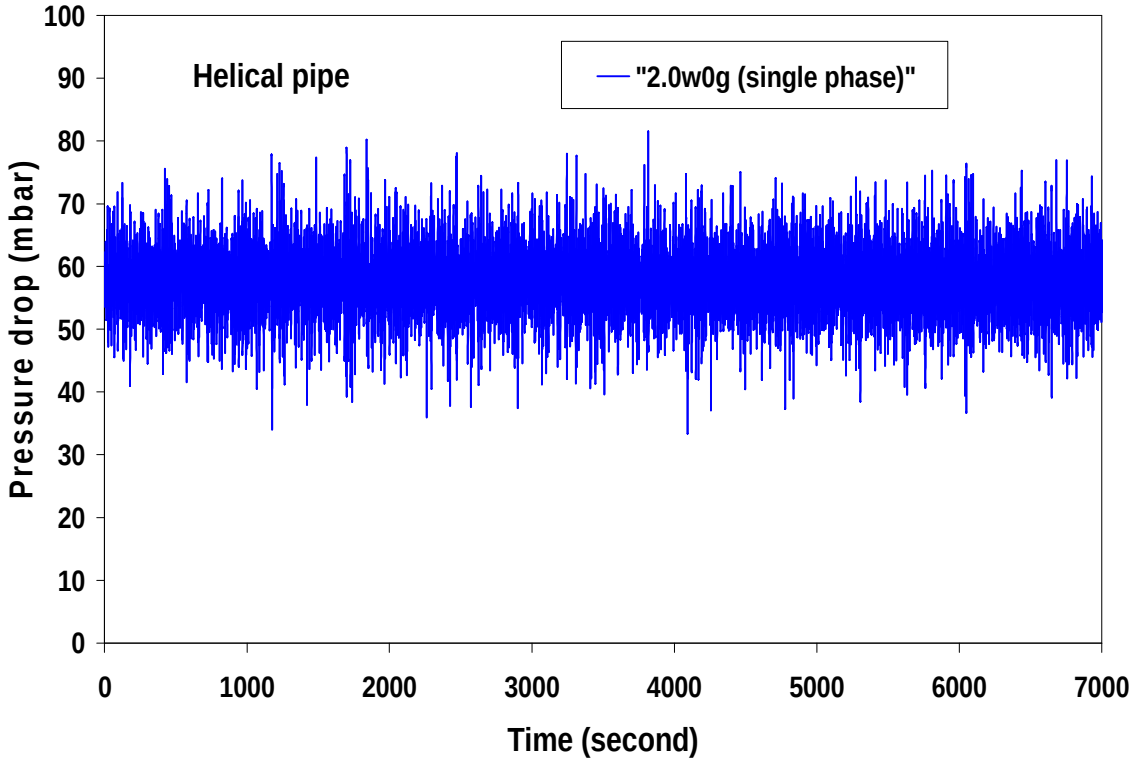
Helical pipe
"2.0w0g (single phase)"
Pressure drop (mbar)
Time (second)
0
10
20
30
40
50
60
70
80
90
100
0
1000
2000
3000
4000
5000
6000
7000

APPENDIX B

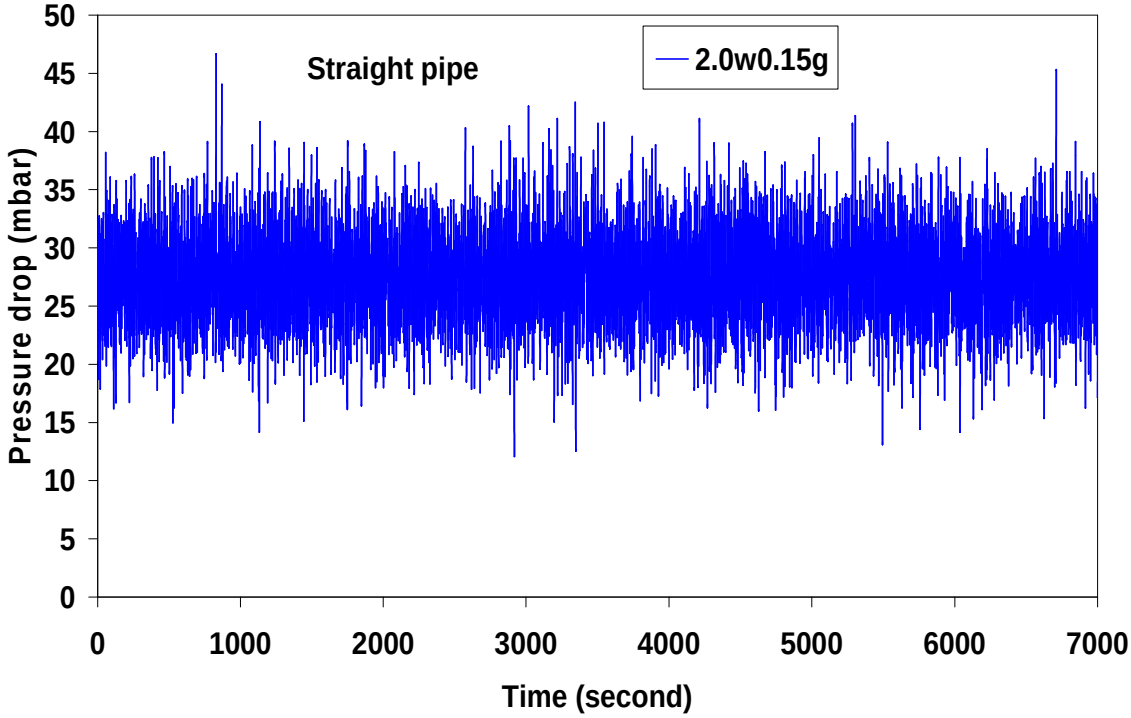
Straight pipe
2.0w0.15g
Pressure drop (mbar)
Time (second)
0
5
10
15
20
25
30
35
40
45
50
0
1000
2000
3000
4000
5000
6000
7000

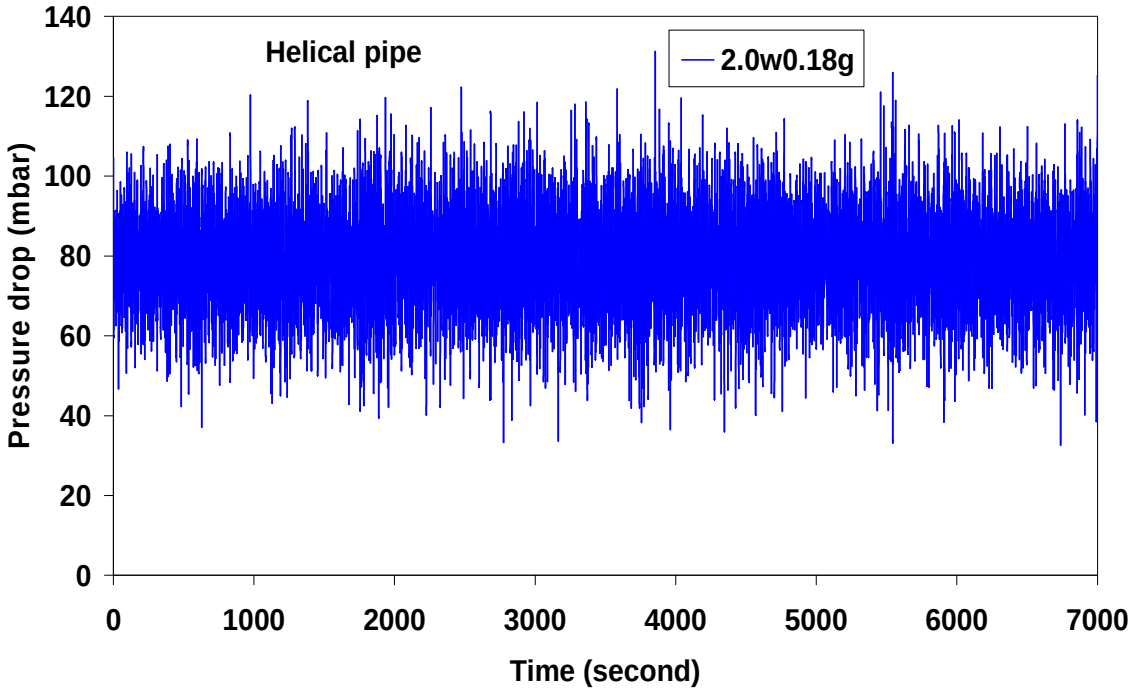
Helical pipe
2.0w0.18g
Pressure drop (mbar)
Time (second)
0
20
40
60
80
100
120
140
0
1000
2000
3000
4000
5000
6000
7000

APPENDIX B

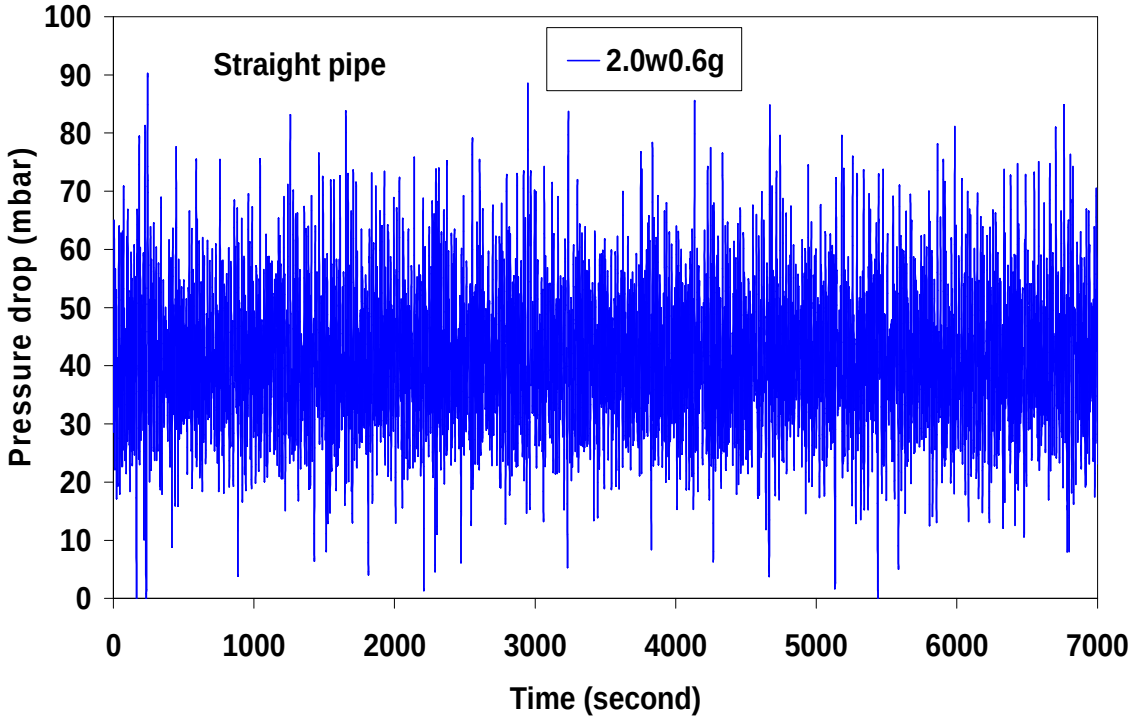
Straight pipe
2.0w0.6g
Pressure drop (mbar)
Time (second)
0
10
20
30
40
50
60
70
80
90
100
0
1000
2000
3000
4000
5000
6000
7000

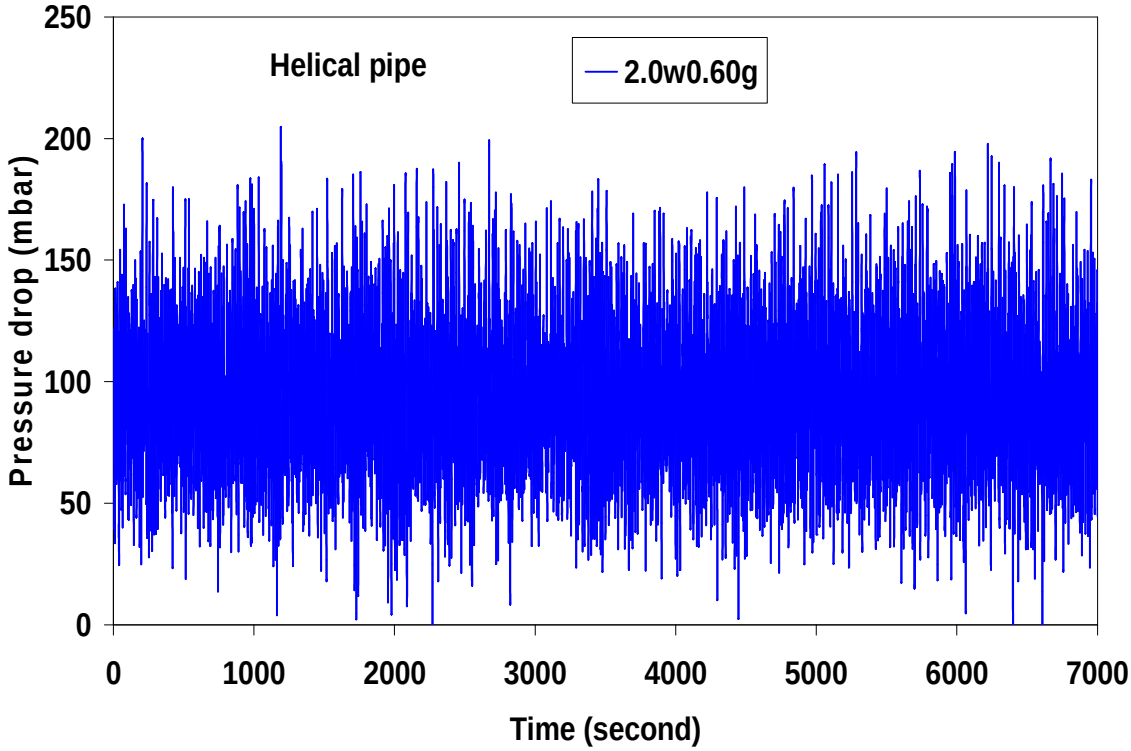
Helical pipe
2.0w0.60g
Pressure drop (mbar)
Time (second)
0
50
100
150
200
250
0
1000
2000
3000
4000
5000
6000
7000

APPENDIX B

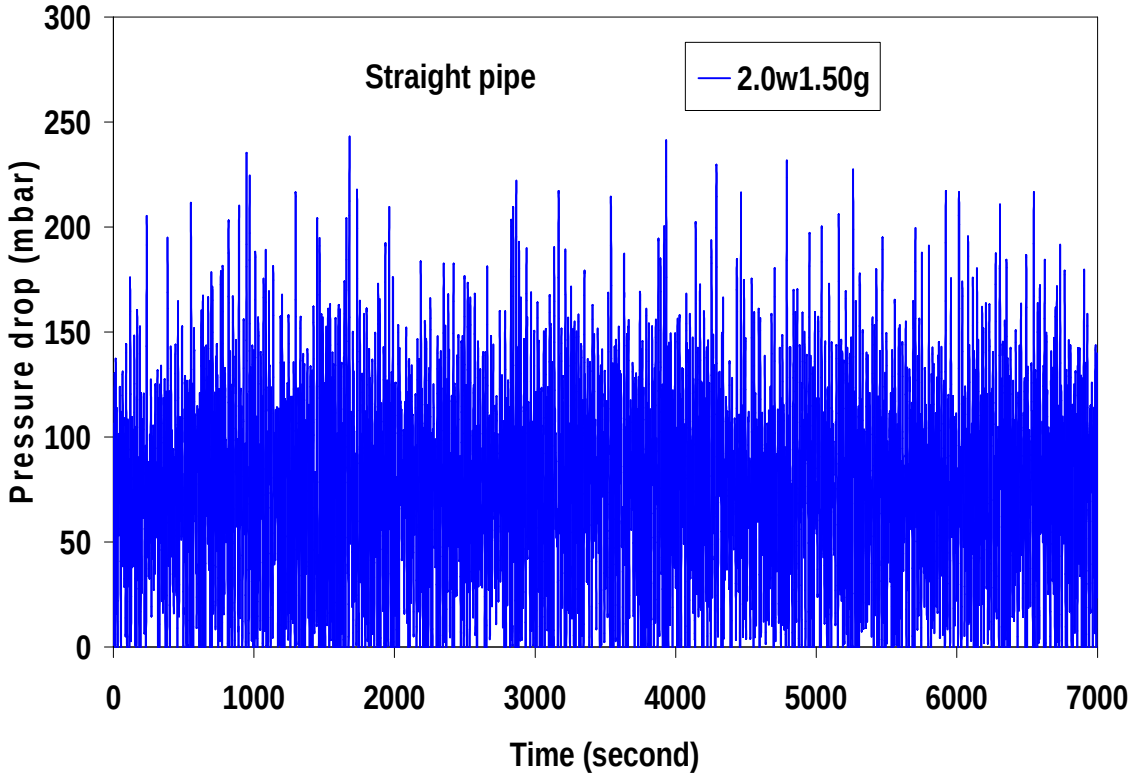
Straight pipe
2.0w1.50g
Pressure drop (mbar)
300
250
200
150
100
50
0
0
1000
2000
3000
4000
5000
6000
7000
Time (second)

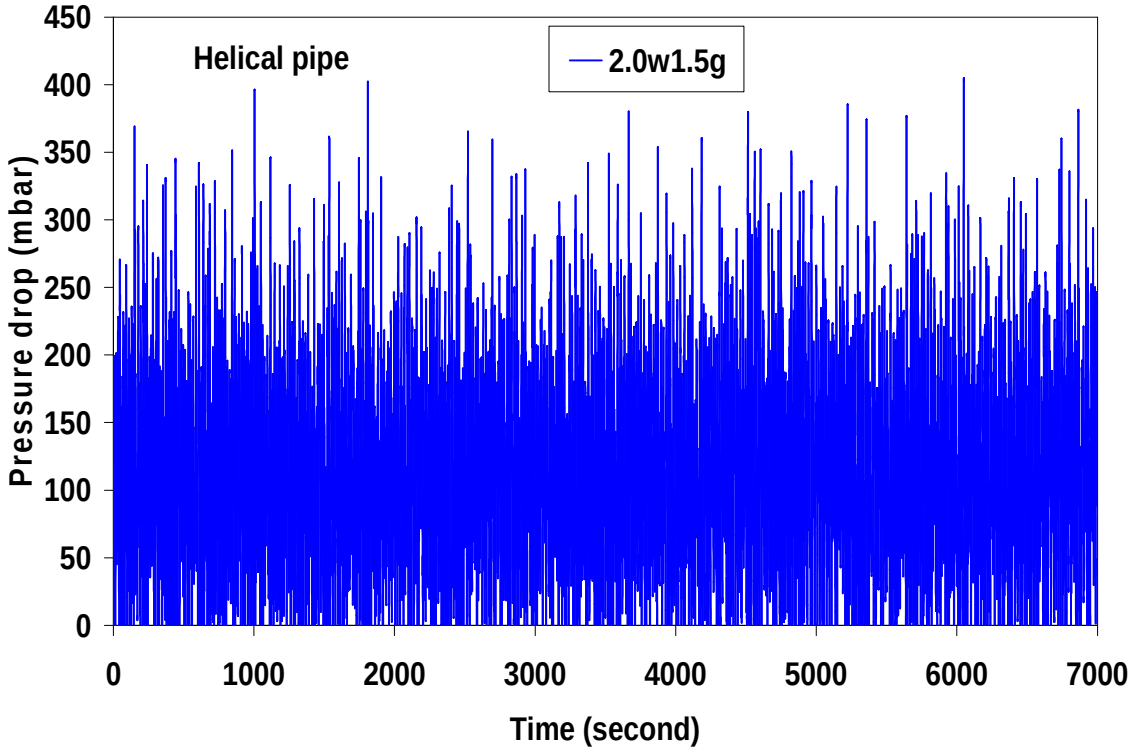
Helical pipe
2.0w1.5g
Pressure drop (mbar)
450
400
350
300
250
200
150
100
50
0
0
1000
2000
3000
4000
5000
6000
7000
Time (second)

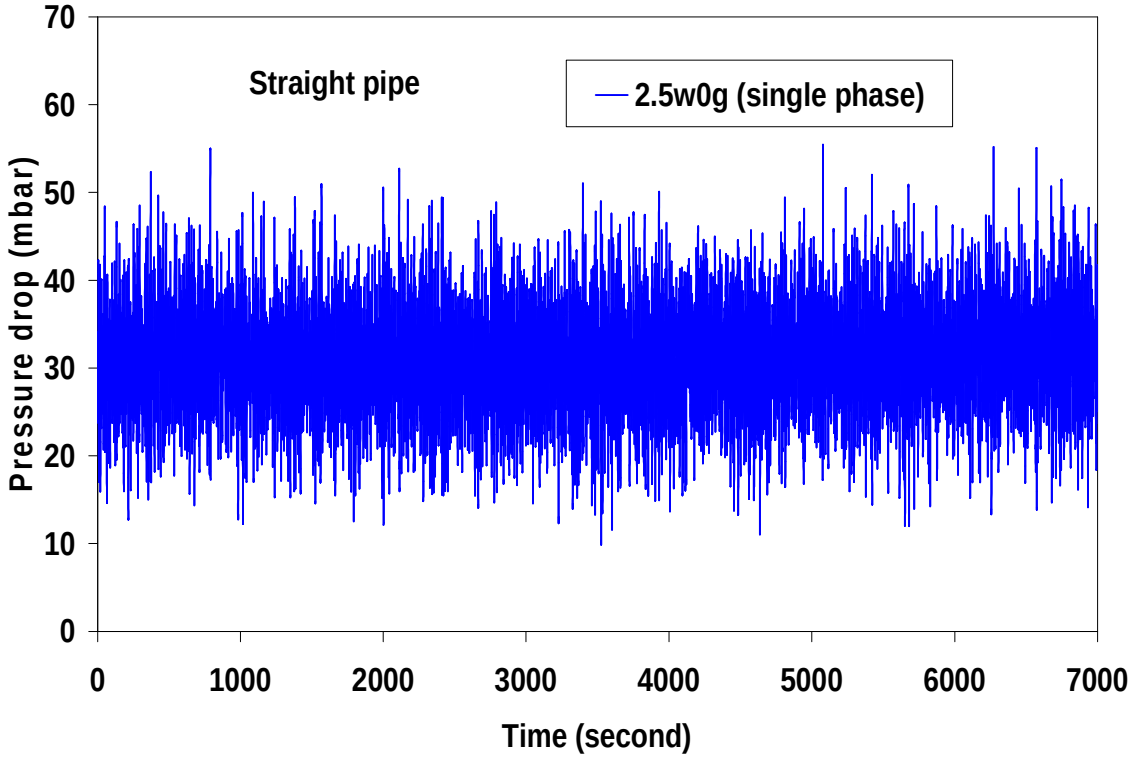
Straight pipe
2.5w0g (single phase)
Pressure drop (mbar)
Time (second)
0
10
20
30
40
50
60
70
0
1000
2000
3000
4000
5000
6000
7000

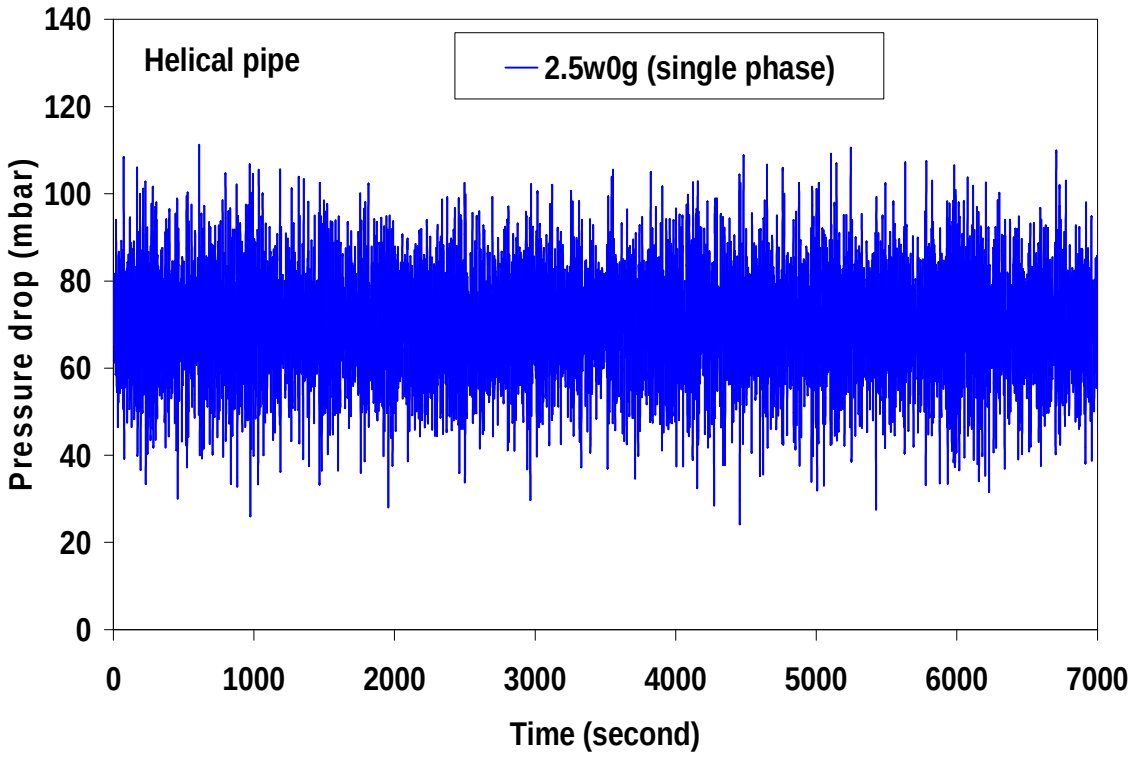
Helical pipe
2.5w0g (single phase)
Pressure drop (mbar)
Time (second)
0
20
40
60
80
100
120
140
0
1000
2000
3000
4000
5000
6000
7000

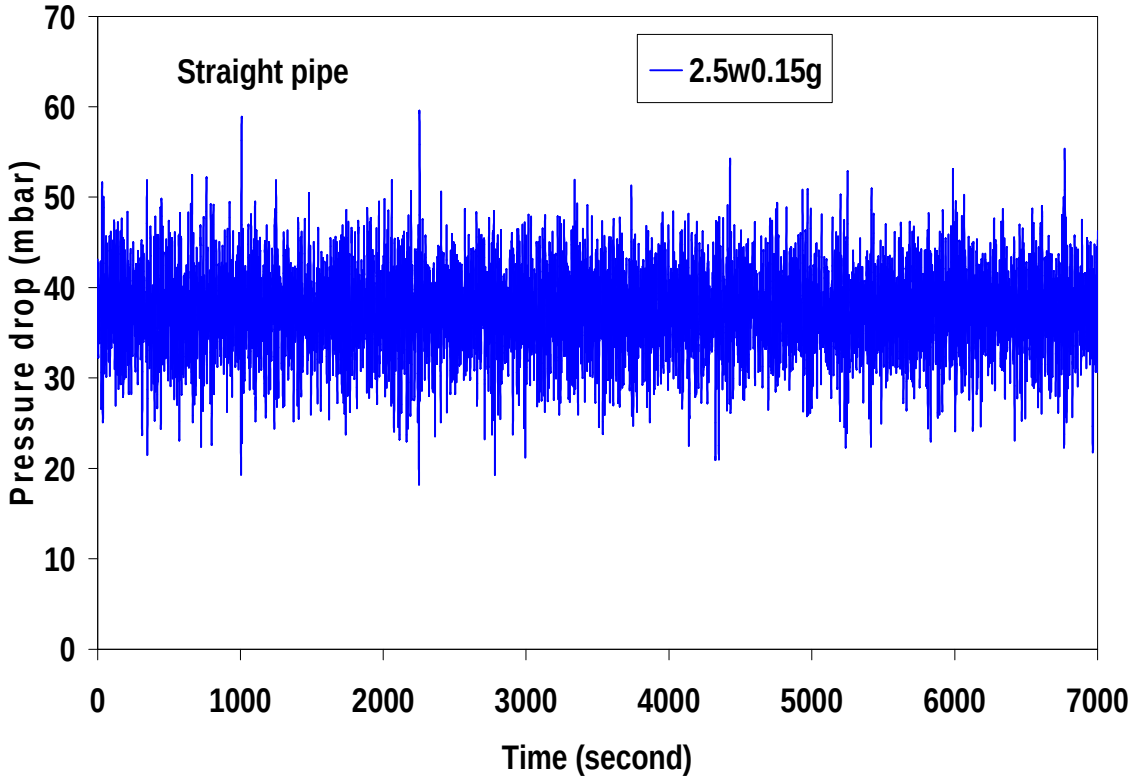
Straight pipe
2.5w0.15g
Pressure drop (mbar)
Time (second)
0
10
20
30
40
50
60
70
0
1000
2000
3000
4000
5000
6000
7000

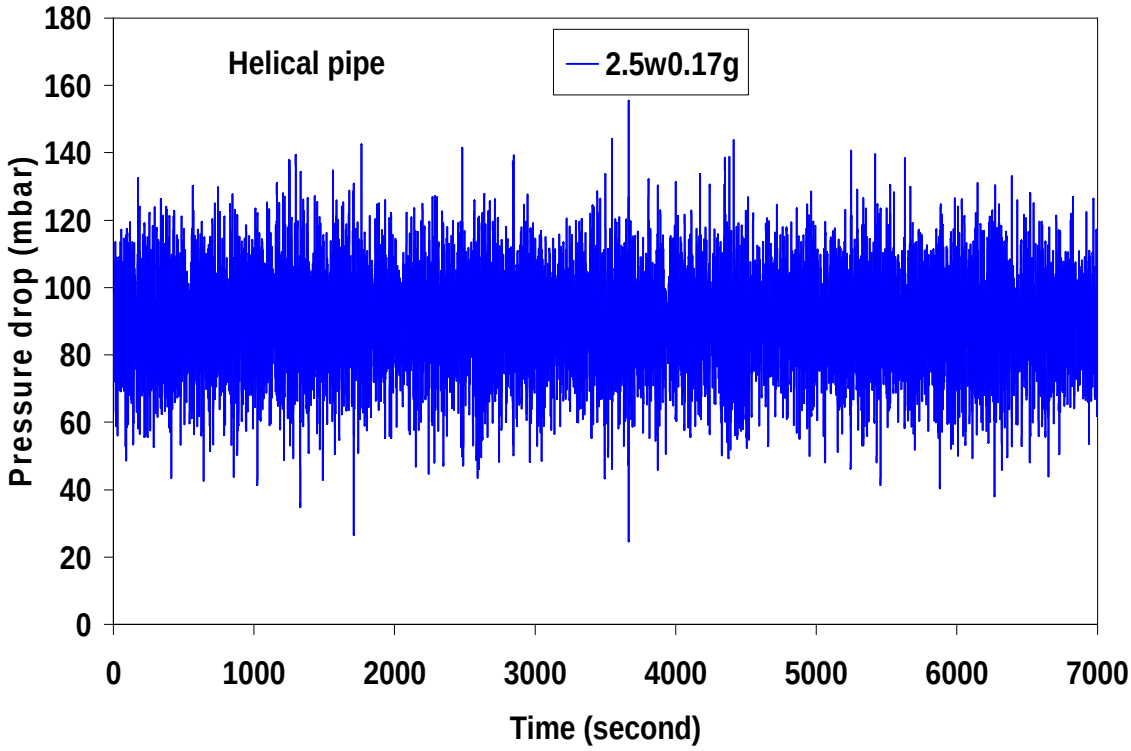
Helical pipe
2.5w0.17g
Pressure drop (mbar)
Time (second)
0
20
40
60
80
100
120
140
160
180
0
1000
2000
3000
4000
5000
6000
7000

APPENDIX B

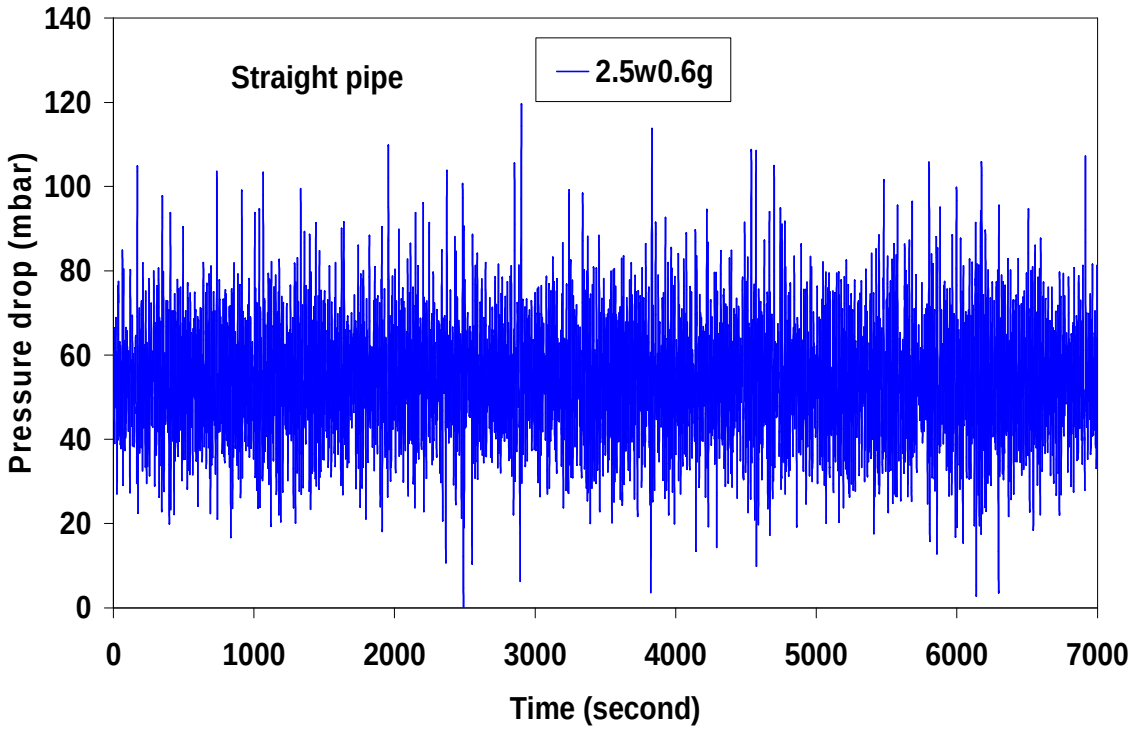
Straight pipe
2.5w0.6g
Pressure drop (mbar)
Time (second)
0
20
40
60
80
100
120
140
0
1000
2000
3000
4000
5000
6000
7000

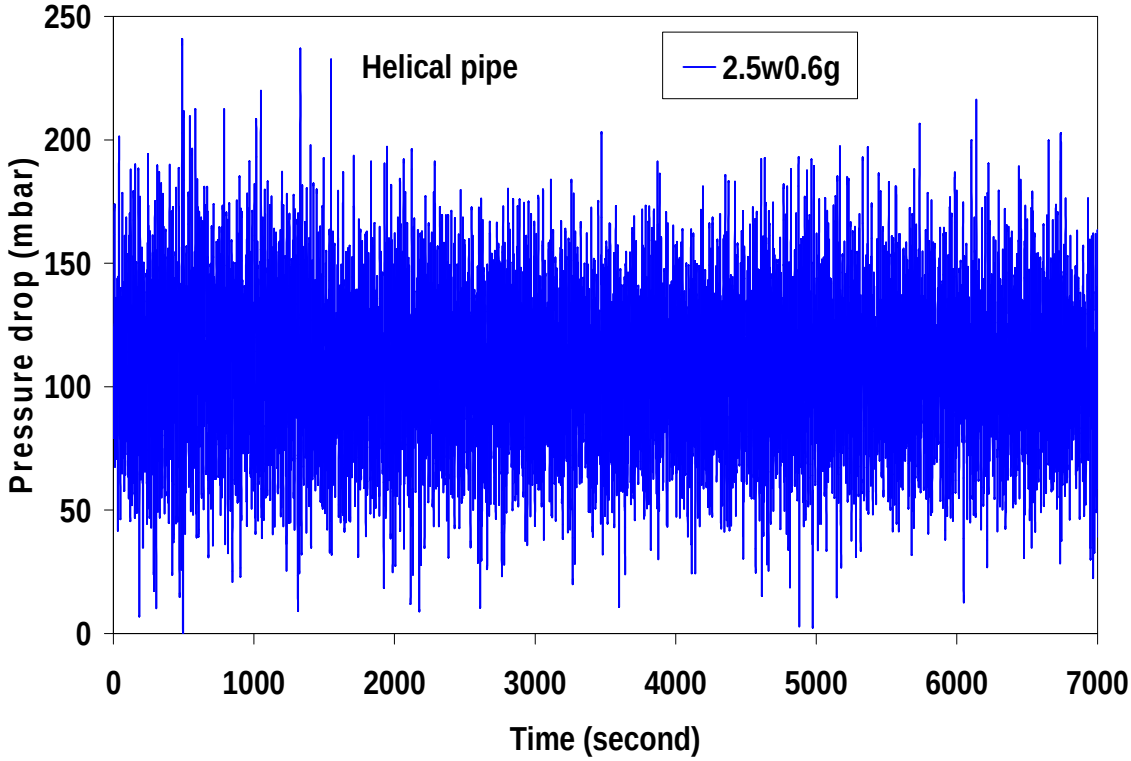
Helical pipe
2.5w0.6g
Pressure drop (mbar)
Time (second)
0
50
100
150
200
250
0
1000
2000
3000
4000
5000
6000
7000

APPENDIX B

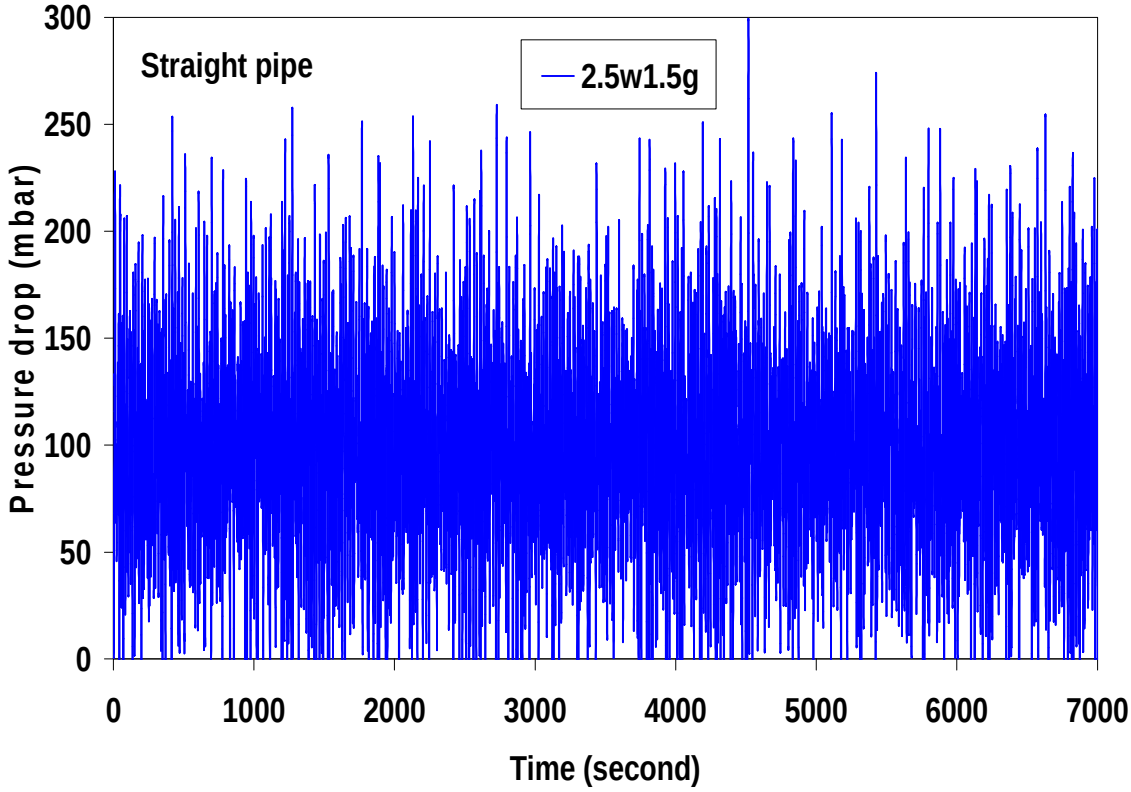
Straight pipe
2.5w1.5g
Pressure drop (mbar)
300
250
200
150
100
50
0
0
1000
2000
3000
4000
5000
6000
7000
Time (second)

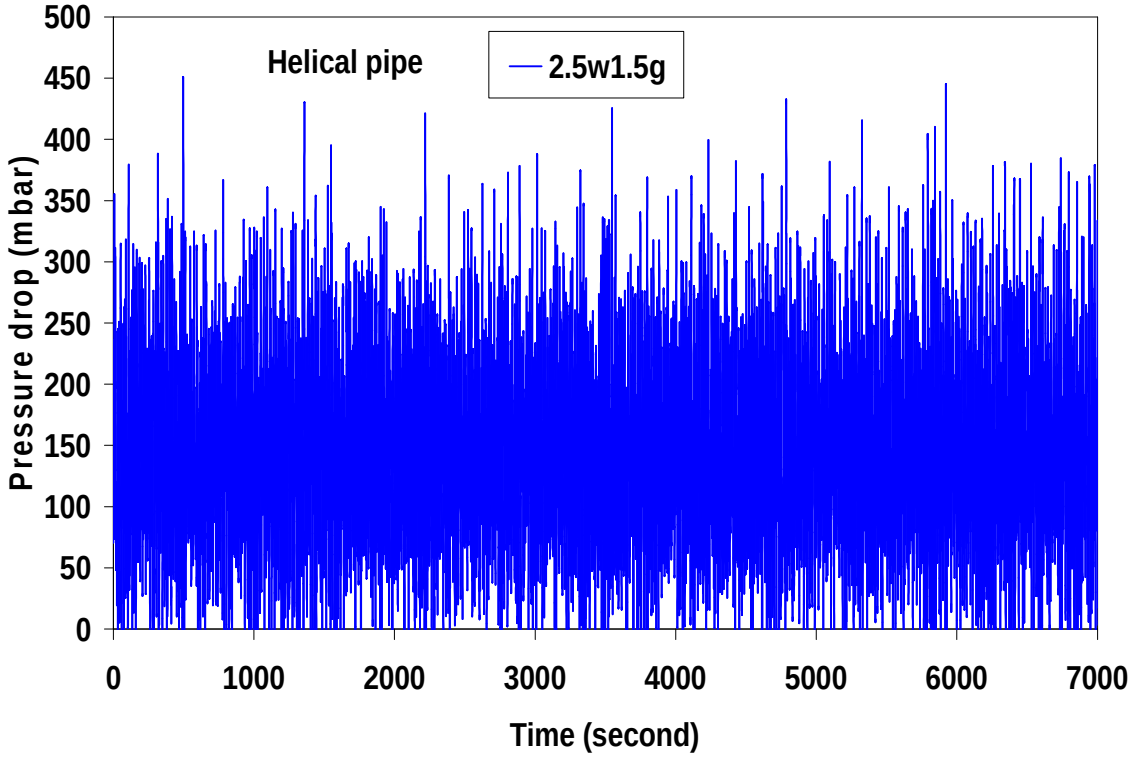
Helical pipe
2.5w1.5g
Pressure drop (mbar)
500
450
400
350
300
250
200
150
100
50
0
0
1000
2000
3000
4000
5000
6000
7000
Time (second)

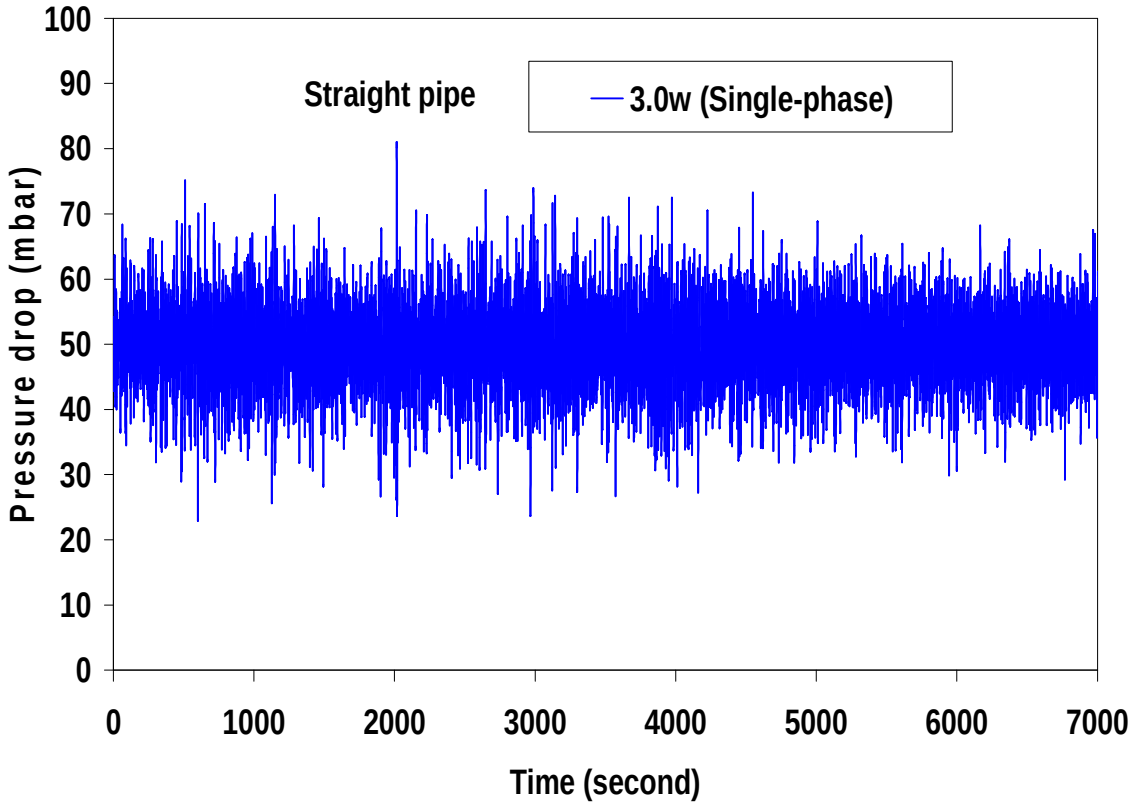
Straight pipe
3.0w (Single-phase)
Pressure drop (mbar)
Time (second)
100
90
80
70
60
50
40
30
20
10
0
0
1000
2000
3000
4000
5000
6000
7000

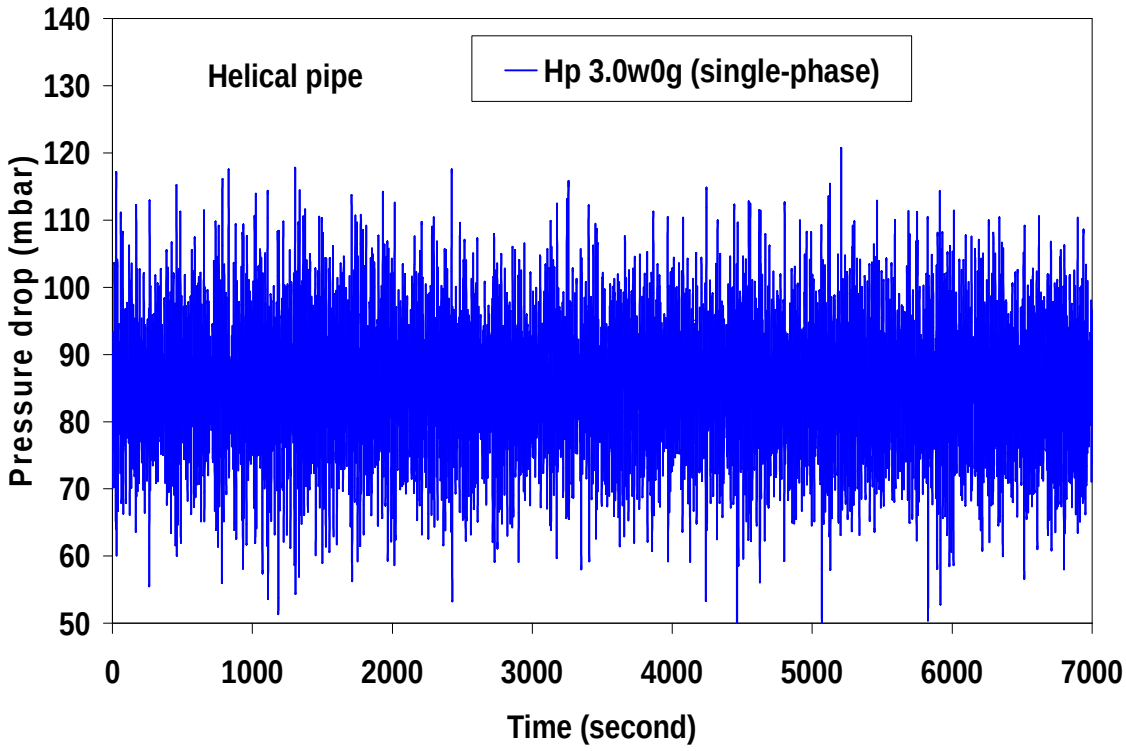
Helical pipe
Hp 3.0w0g (single-phase)
Pressure drop (mbar)
Time (second)
140
130
120
110
100
90
80
70
60
50
0
1000
2000
3000
4000
5000
6000
7000

APPENDIX B

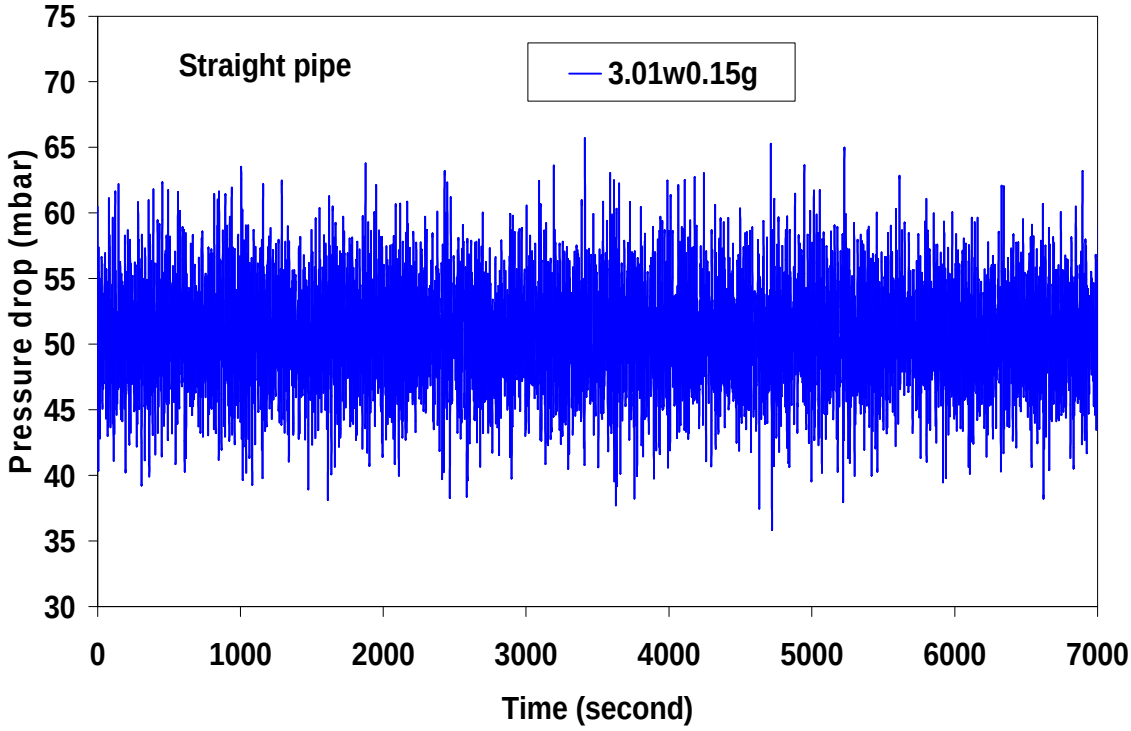
Straight pipe
3.01w0.15g
Pressure drop (mbar)
75
70
65
60
55
50
45
40
35
30
0
1000
2000
3000
4000
5000
6000
7000
Time (second)

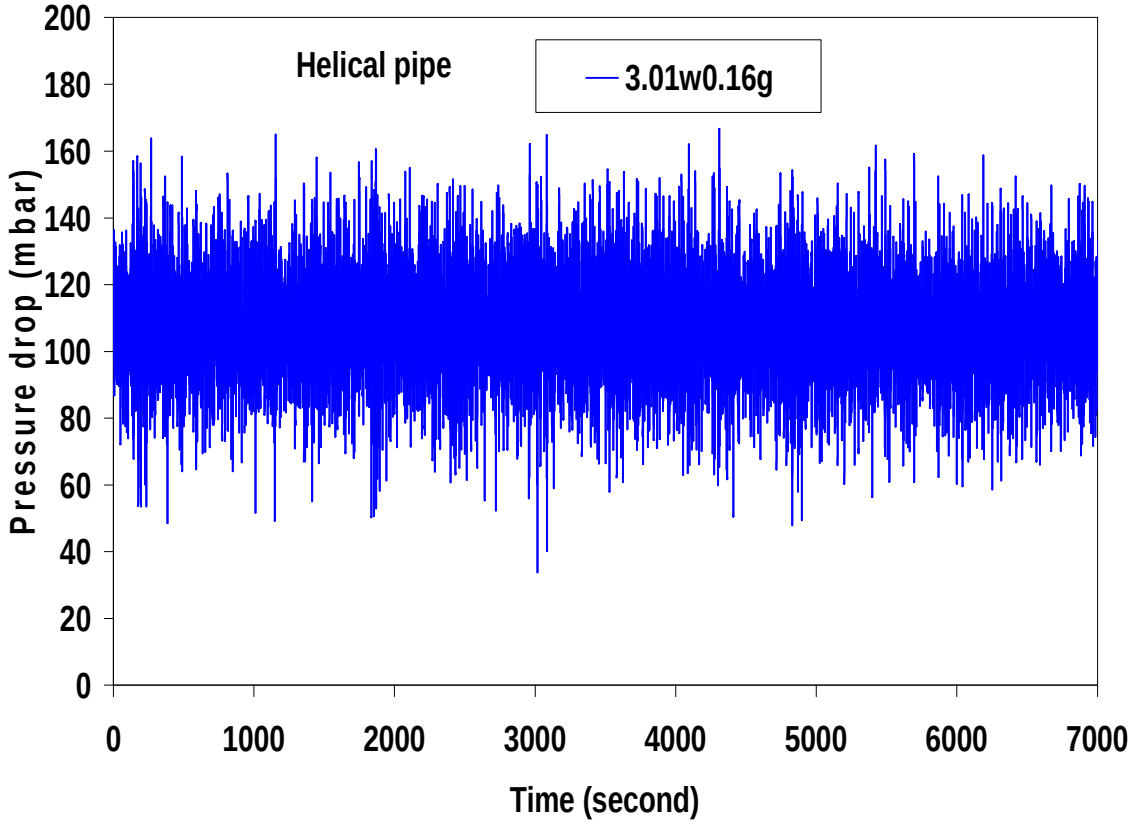
Helical pipe
3.01w0.16g
Pressure drop (mbar)
200
180
160
140
120
100
80
60
40
20
0
0
1000
2000
3000
4000
5000
6000
7000
Time (second)

APPENDIX B

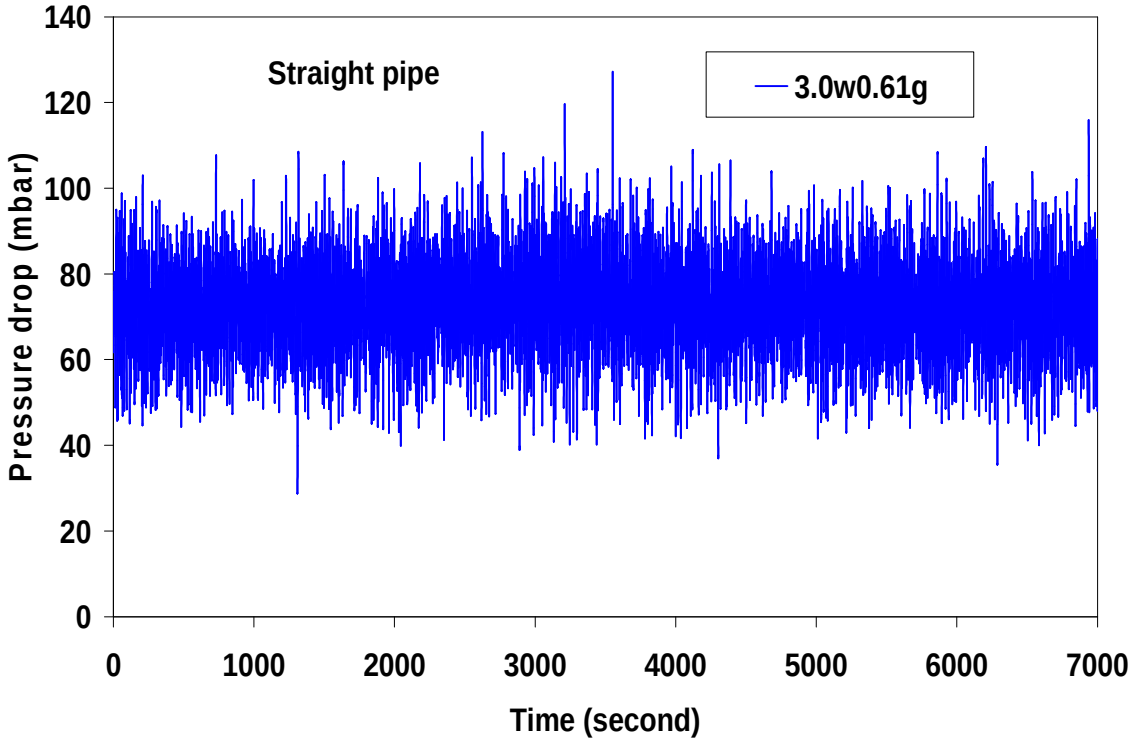
Straight pipe
3.0w0.61g
Pressure drop (mbar)
Time (second)
0
20
40
60
80
100
120
140
0
1000
2000
3000
4000
5000
6000
7000

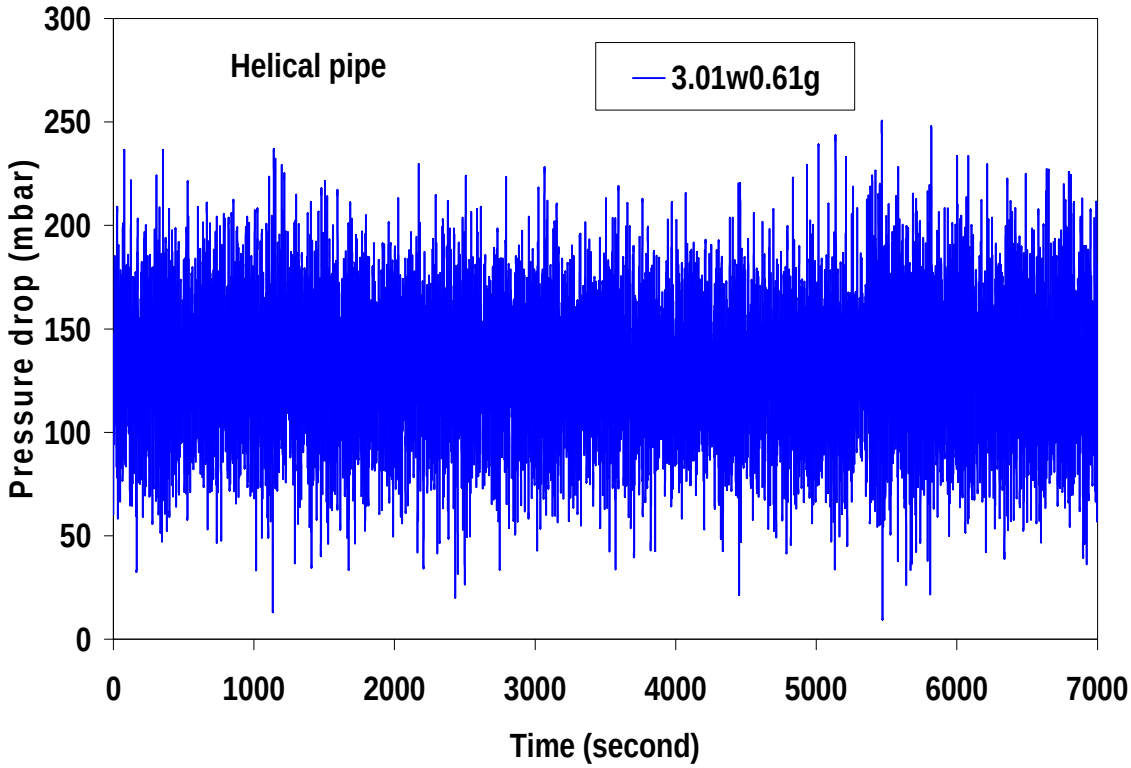
Helical pipe
3.01w0.61g
Pressure drop (mbar)
Time (second)
0
50
100
150
200
250
300
0
1000
2000
3000
4000
5000
6000
7000

APPENDIX B

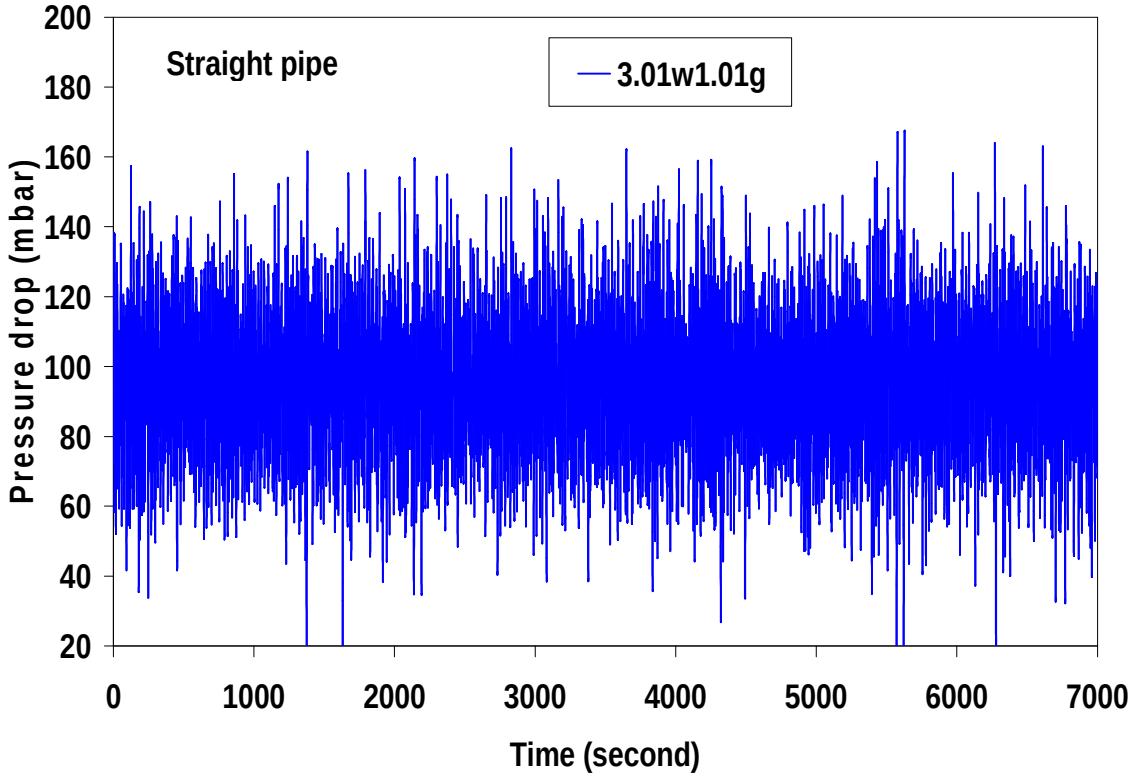
Straight pipe
3.01w1.01g
Pressure drop (mbar)
200
180
160
140
120
100
80
60
40
20
0
1000
2000
3000
4000
5000
6000
7000
Time (second)

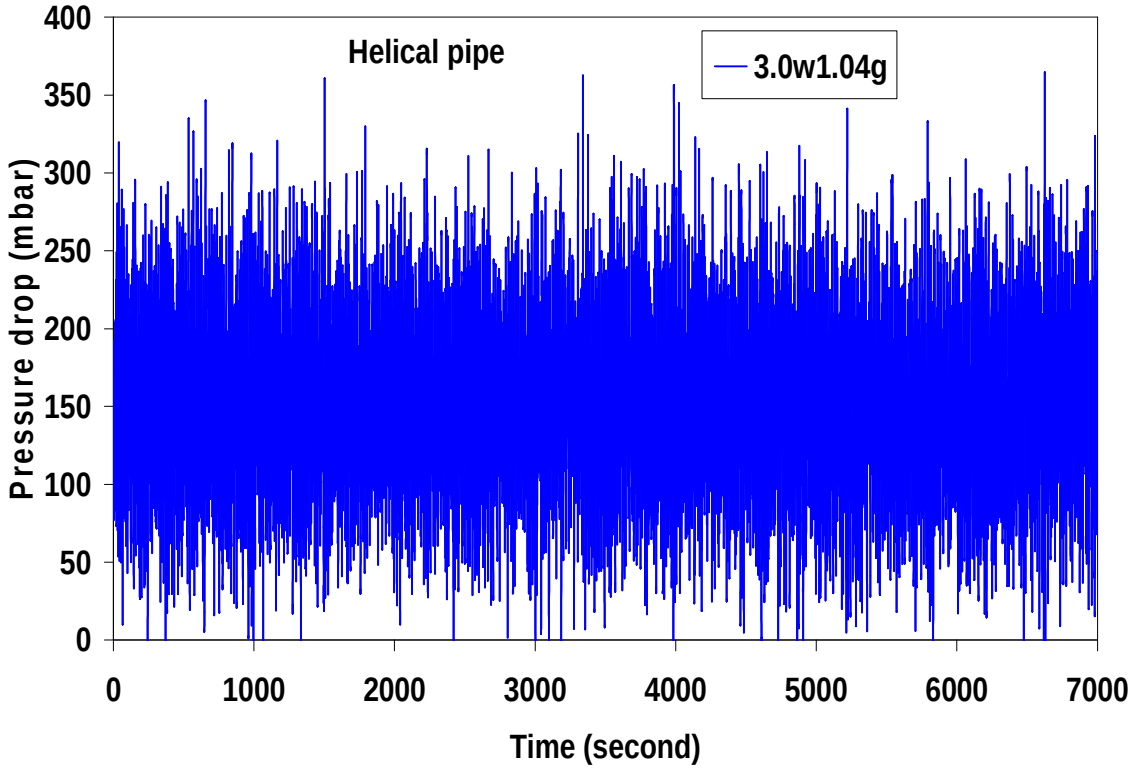
Helical pipe
3.0w1.04g
Pressure drop (mbar)
400
350
300
250
200
150
100
50
0
0
1000
2000
3000
4000
5000
6000
7000
Time (second)

APPENDIX C

Conductivity probe signals

APPENDIX C

Conductivity probe signals

Legend:

w **is the water superficial velocity**
g **is the air superficial velocity**

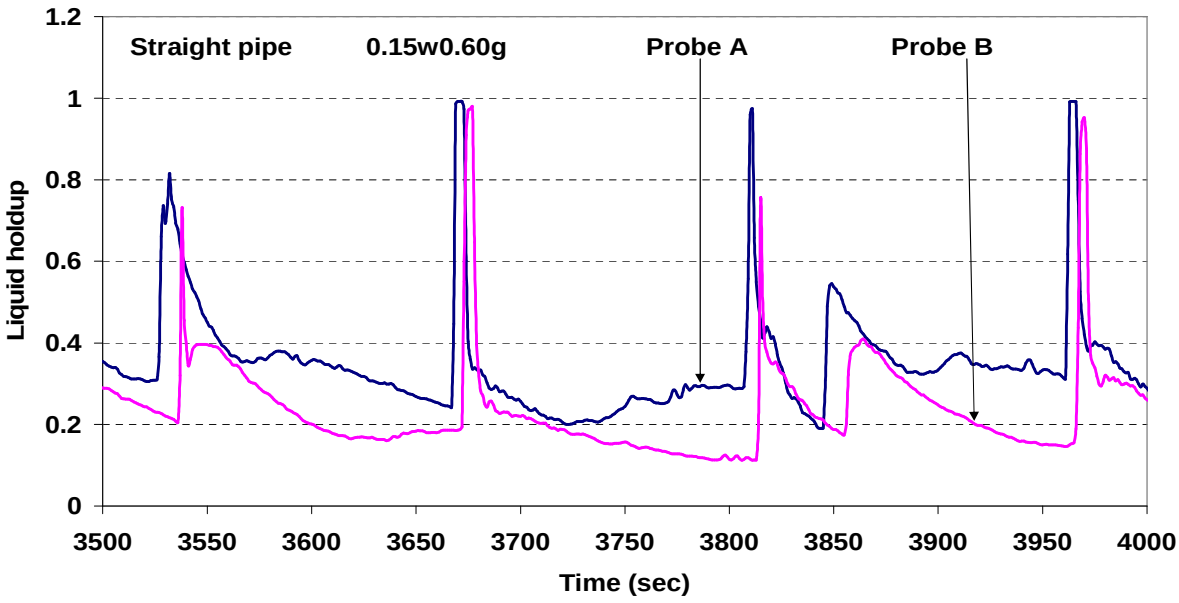

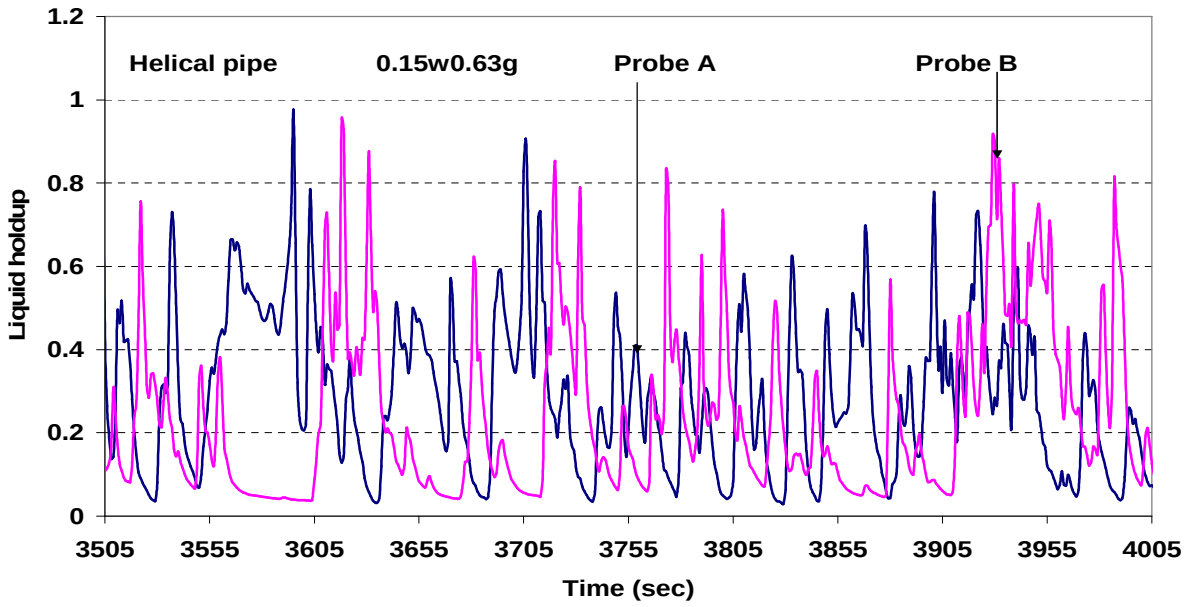

APPENDIX C

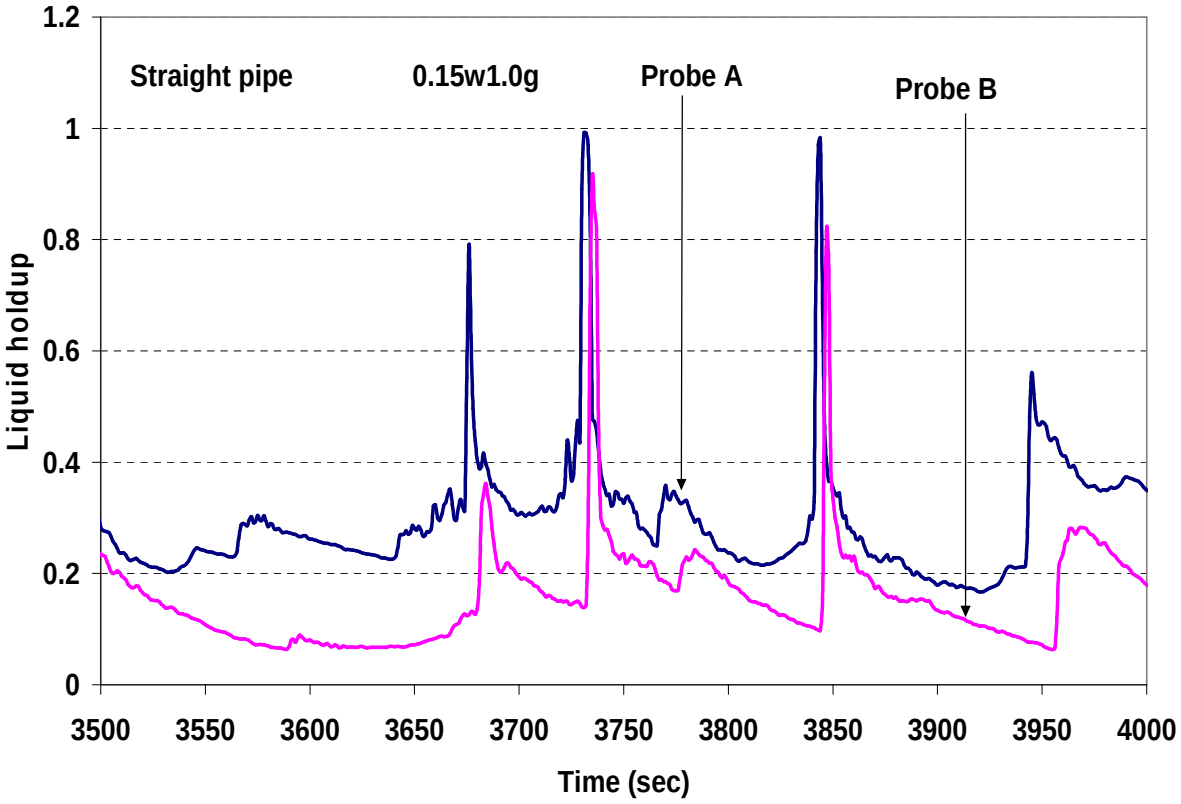
Straight pipe
0.15w1.0g
Probe A
Probe B
Liquid holdup
Time (sec)
1.2
1
0.8
0.6
0.4
0.2
0
3500
3550
3600
3650
3700
3750
3800
3850
3900
3950
4000

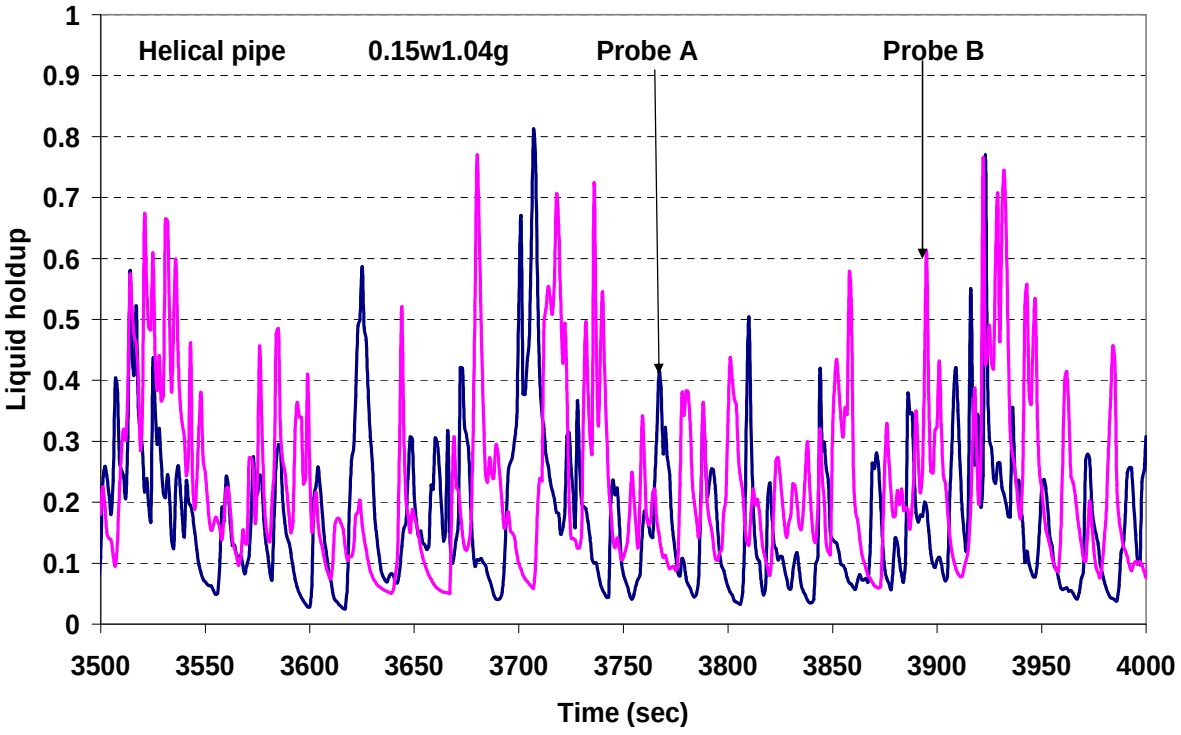
Helical pipe
0.15w1.04g
Probe A
Probe B
Liquid holdup
Time (sec)
1
0.9
0.8
0.7
0.6
0.5
0.4
0.3
0.2
0.1
0
3500
3550
3600
3650
3700
3750
3800
3850
3900
3950
4000

APPENDIX C

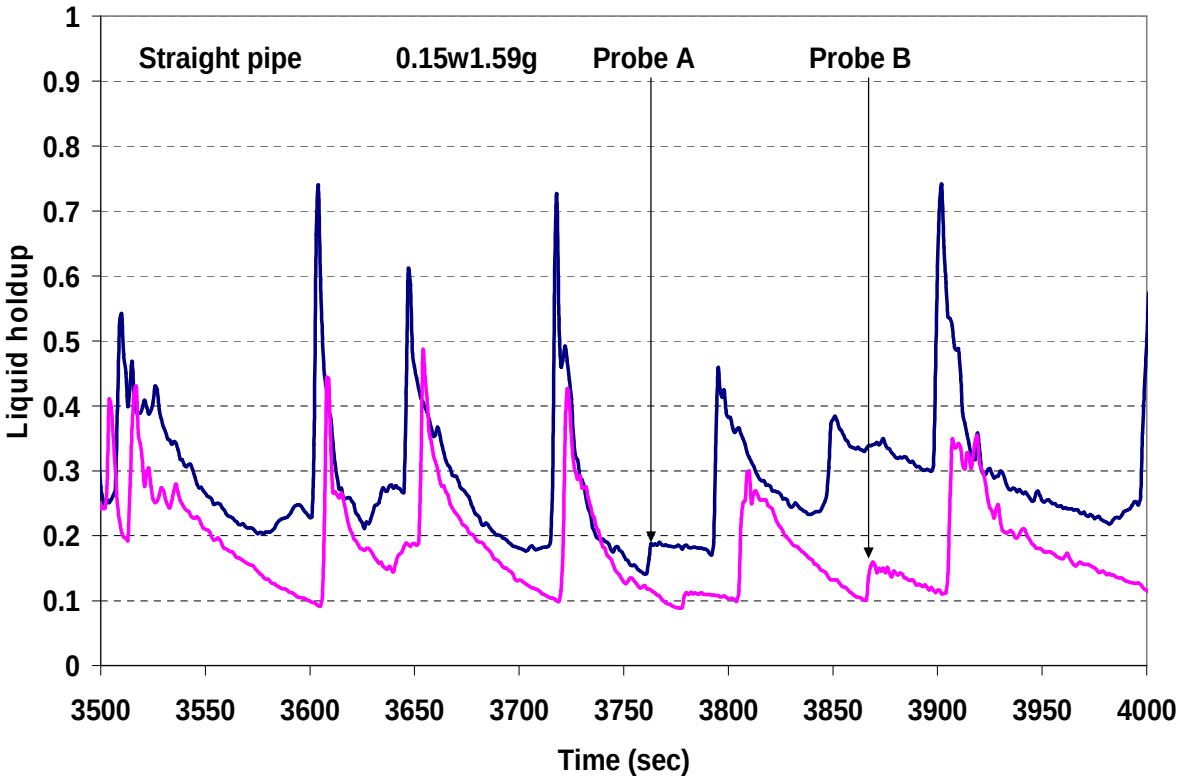
Straight pipe
0.15w1.59g
Probe A
Probe B
Liquid holdup
Time (sec)
1
0.9
0.8
0.7
0.6
0.5
0.4
0.3
0.2
0.1
0
3500
3550
3600
3650
3700
3750
3800
3850
3900
3950
4000

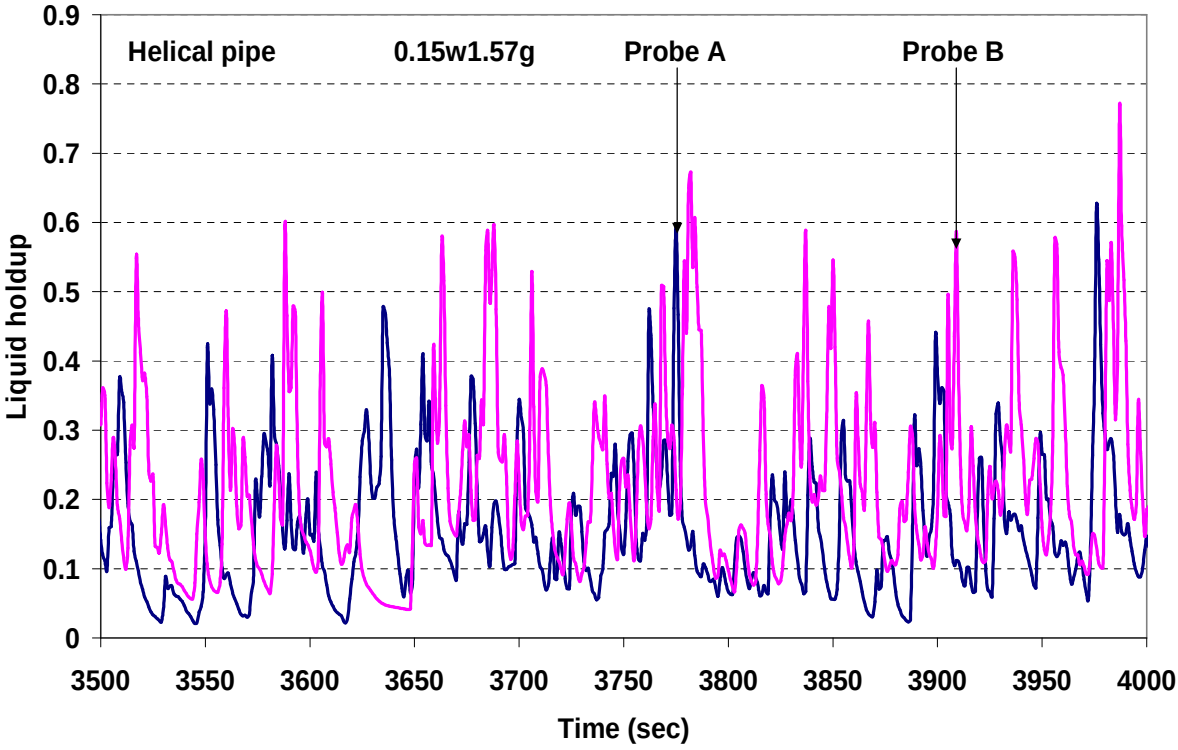
Helical pipe
0.15w1.57g
Probe A
Probe B
Liquid holdup
Time (sec)
0.9
0.8
0.7
0.6
0.5
0.4
0.3
0.2
0.1
0
3500
3550
3600
3650
3700
3750
3800
3850
3900
3950
4000

APPENDIX C

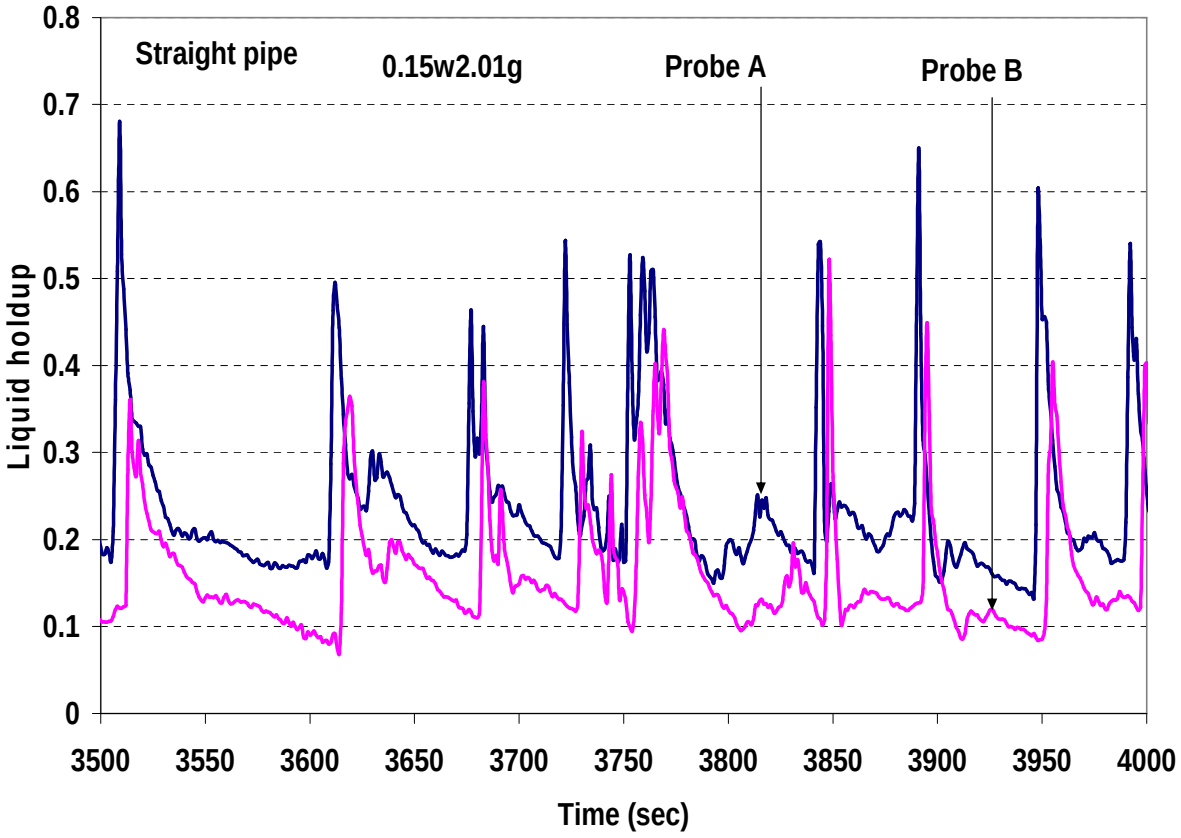
Straight pipe
0.15w2.01g
Probe A
Probe B
Liquid holdup
0.8
0.7
0.6
0.5
0.4
0.3
0.2
0.1
0
3500
3550
3600
3650
3700
3750
3800
3850
3900
3950
4000
Time (sec)

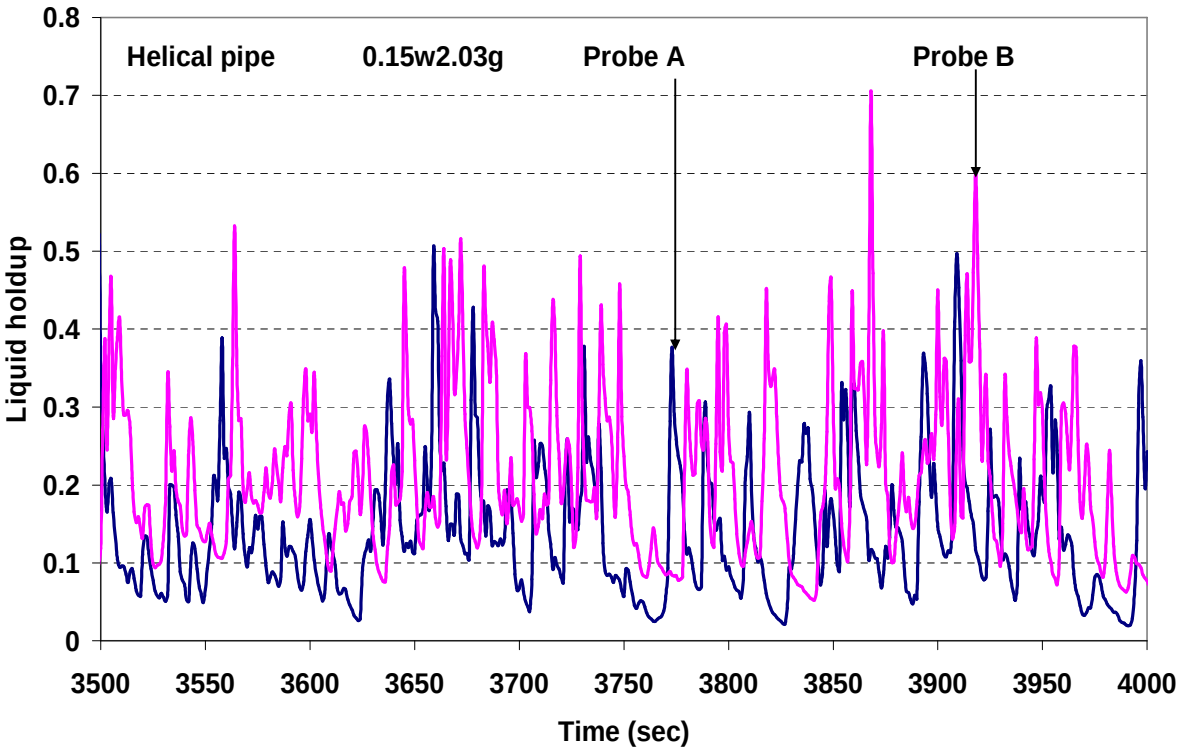
Helical pipe
0.15w2.03g
Probe A
Probe B
Liquid holdup
0.8
0.7
0.6
0.5
0.4
0.3
0.2
0.1
0
3500
3550
3600
3650
3700
3750
3800
3850
3900
3950
4000
Time (sec)

APPENDIX C

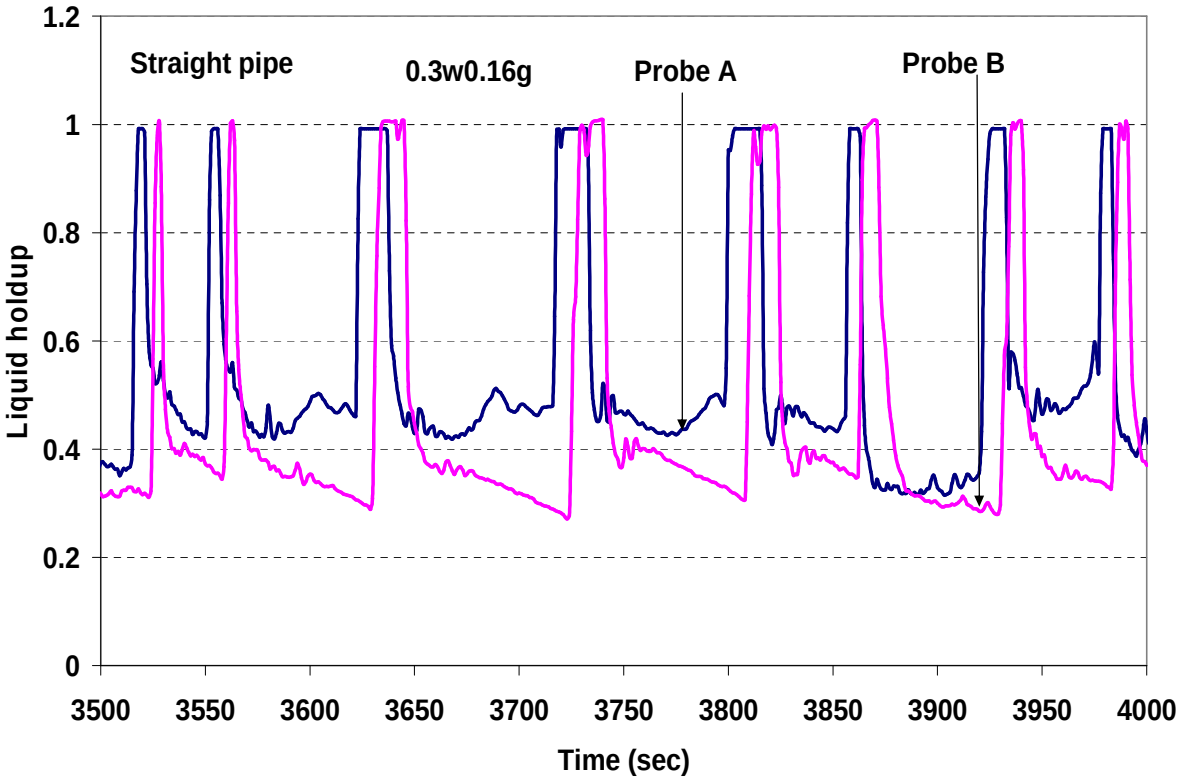
Straight pipe
0.3w0.16g
Probe A
Probe B
Liquid holdup
Time (sec)
1.2
1
0.8
0.6
0.4
0.2
0
3500
3550
3600
3650
3700
3750
3800
3850
3900
3950
4000

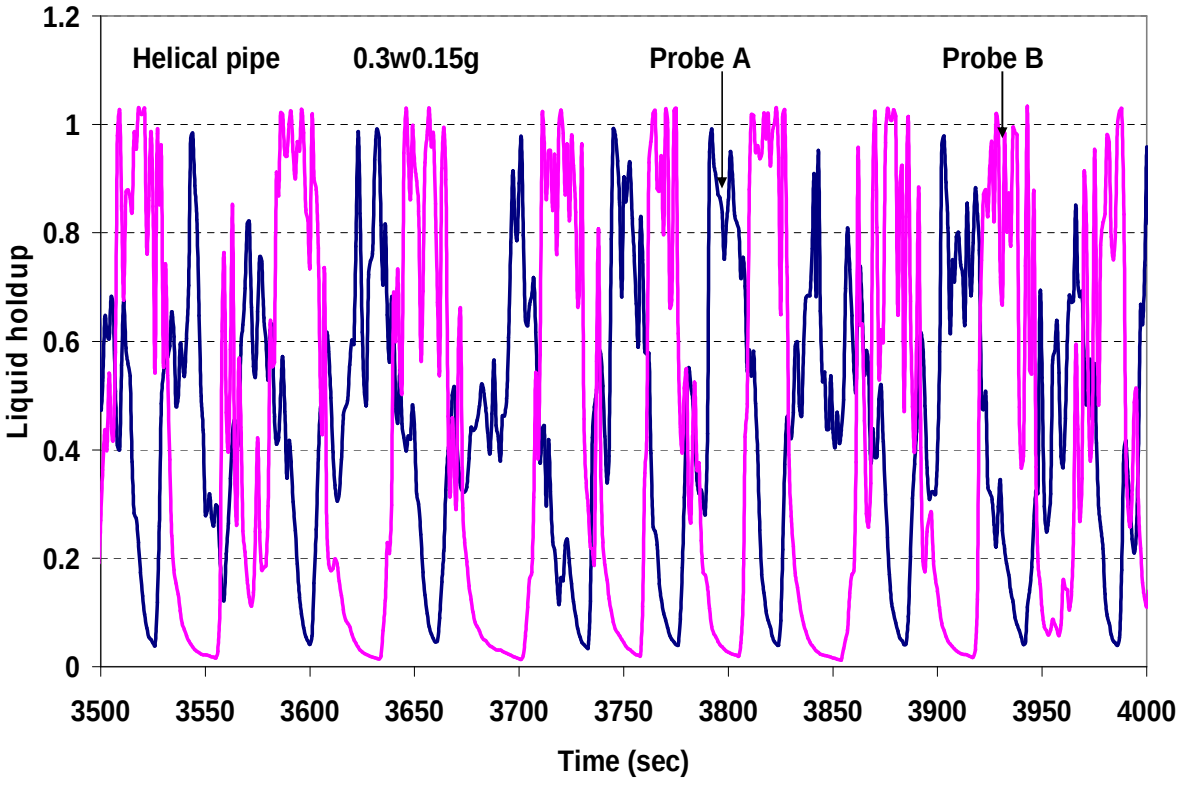
Helical pipe
0.3w0.15g
Probe A
Probe B
Liquid holdup
Time (sec)
1.2
1
0.8
0.6
0.4
0.2
0
3500
3550
3600
3650
3700
3750
3800
3850
3900
3950
4000

APPENDIX C

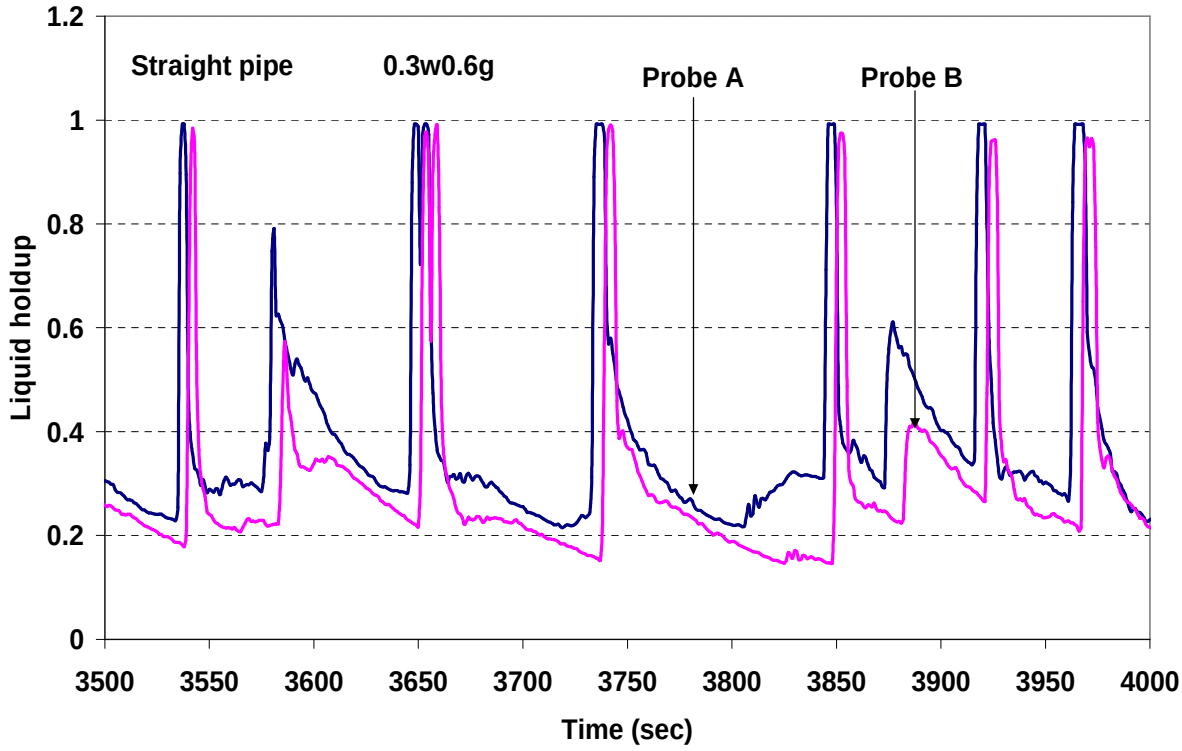
Straight pipe
0.3w0.6g
Probe A
Probe B
Liquid holdup
Time (sec)
1.2
1
0.8
0.6
0.4
0.2
0
3500
3550
3600
3650
3700
3750
3800
3850
3900
3950
4000

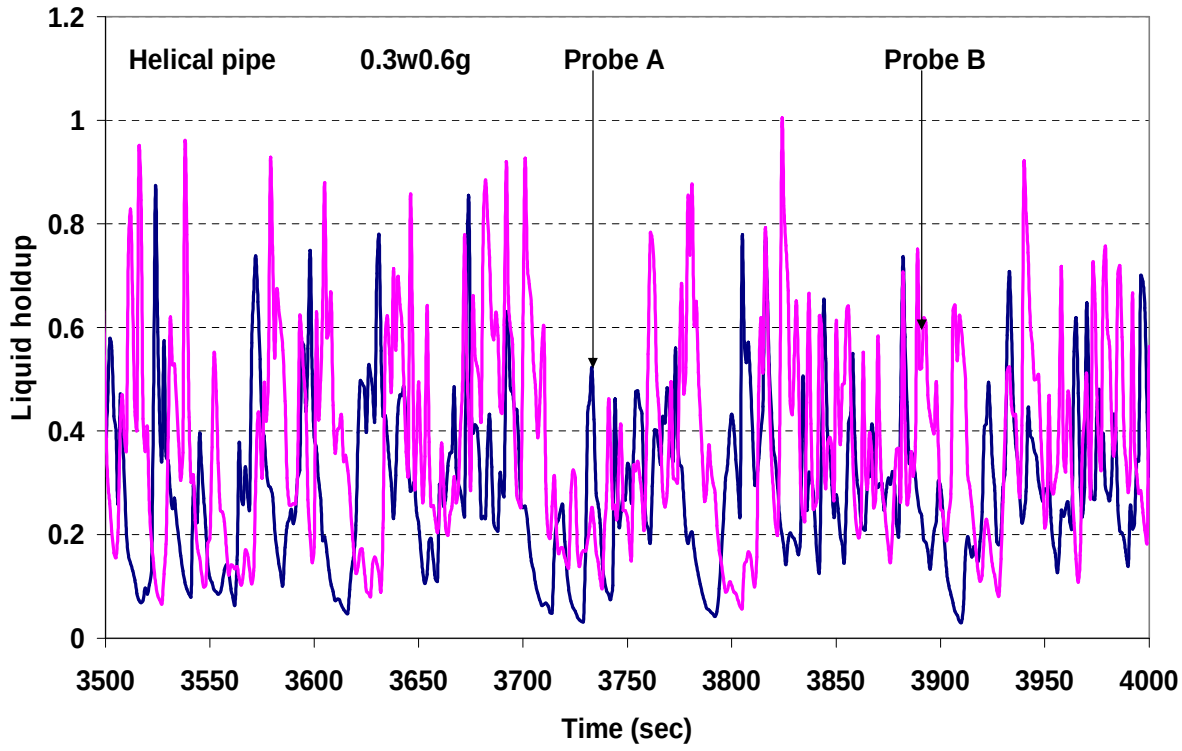
Helical pipe
0.3w0.6g
Probe A
Probe B
Liquid holdup
Time (sec)
1.2
1
0.8
0.6
0.4
0.2
0
3500
3550
3600
3650
3700
3750
3800
3850
3900
3950
4000

APPENDIX C

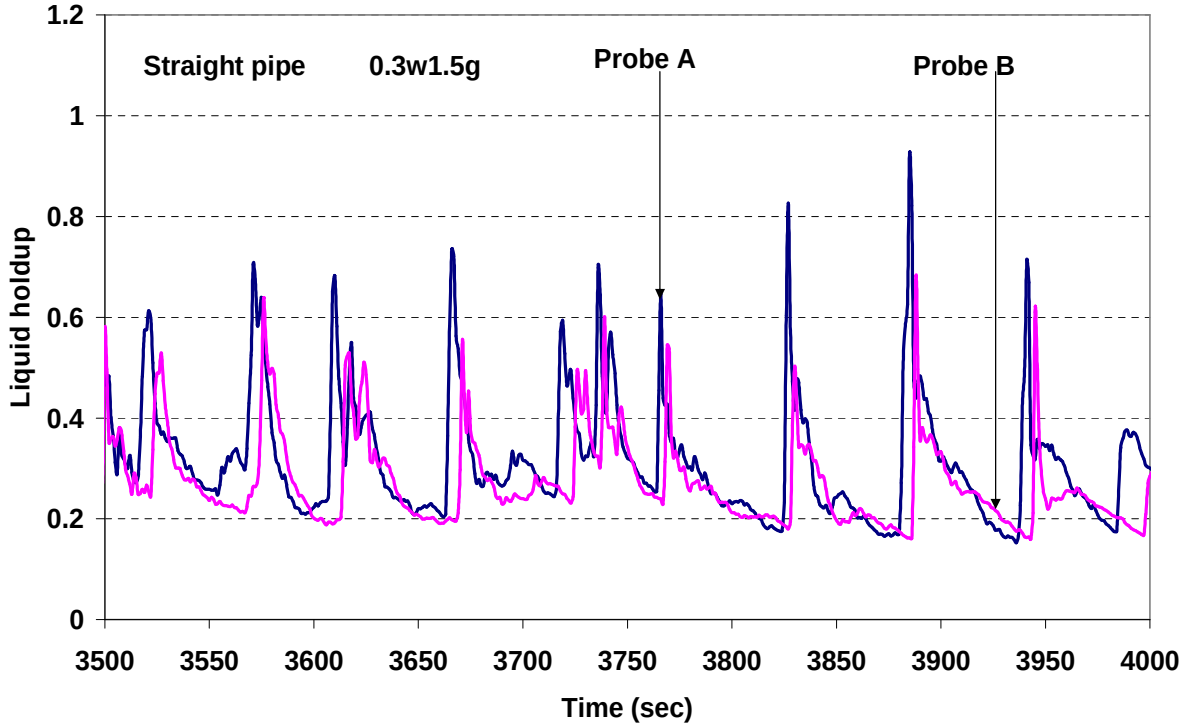
Straight pipe
0.3w1.5g
Probe A
Probe B
Liquid holdup
Time (sec)
1.2
1
0.8
0.6
0.4
0.2
0
3500
3550
3600
3650
3700
3750
3800
3850
3900
3950
4000

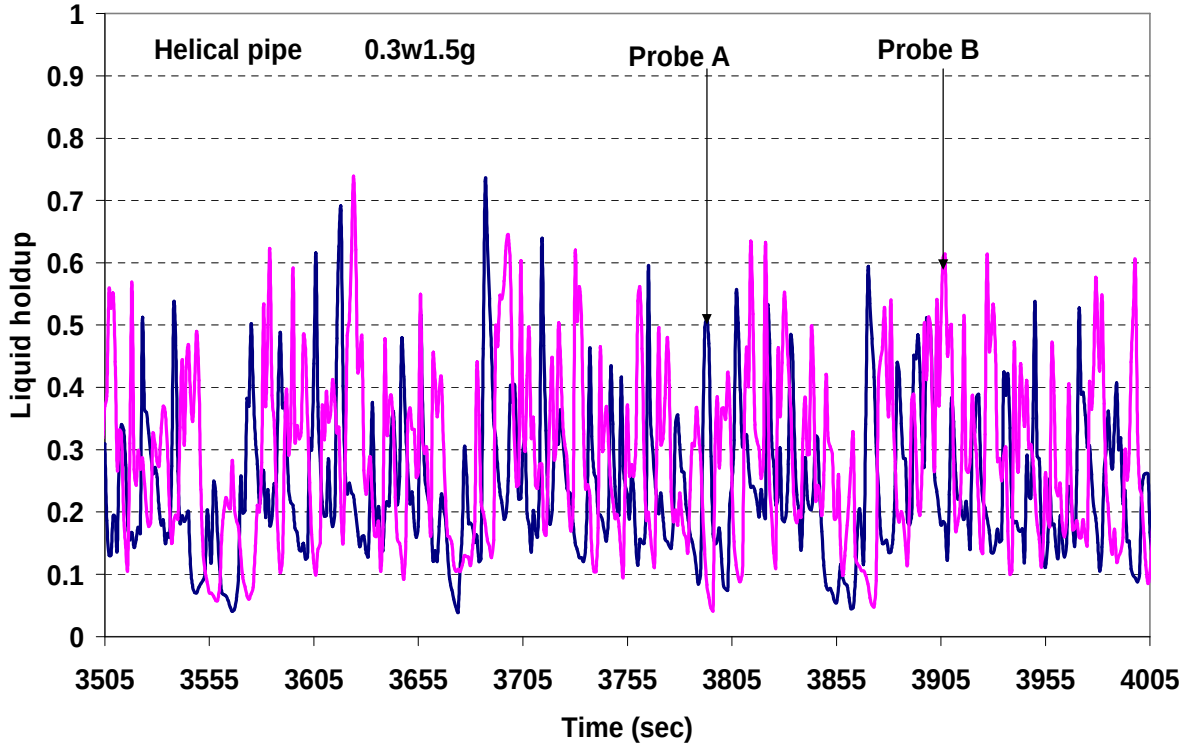
Helical pipe
0.3w1.5g
Probe A
Probe B
Liquid holdup
Time (sec)
1
0.9
0.8
0.7
0.6
0.5
0.4
0.3
0.2
0.1
0
3505
3555
3605
3655
3705
3755
3805
3855
3905
3955
4005

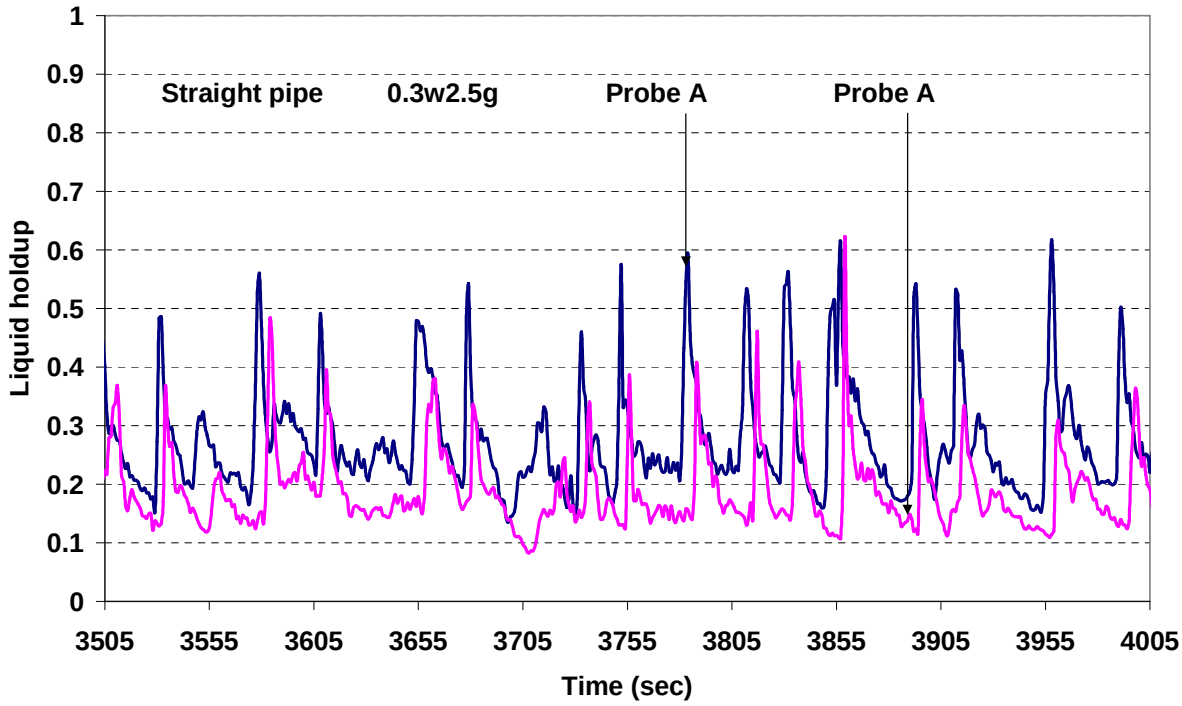
Straight pipe
0.3w2.5g
Probe A
Probe A
Liquid holdup
Time (sec)
1
0.9
0.8
0.7
0.6
0.5
0.4
0.3
0.2
0.1
0
3505
3555
3605
3655
3705
3755
3805
3855
3905
3955
4005

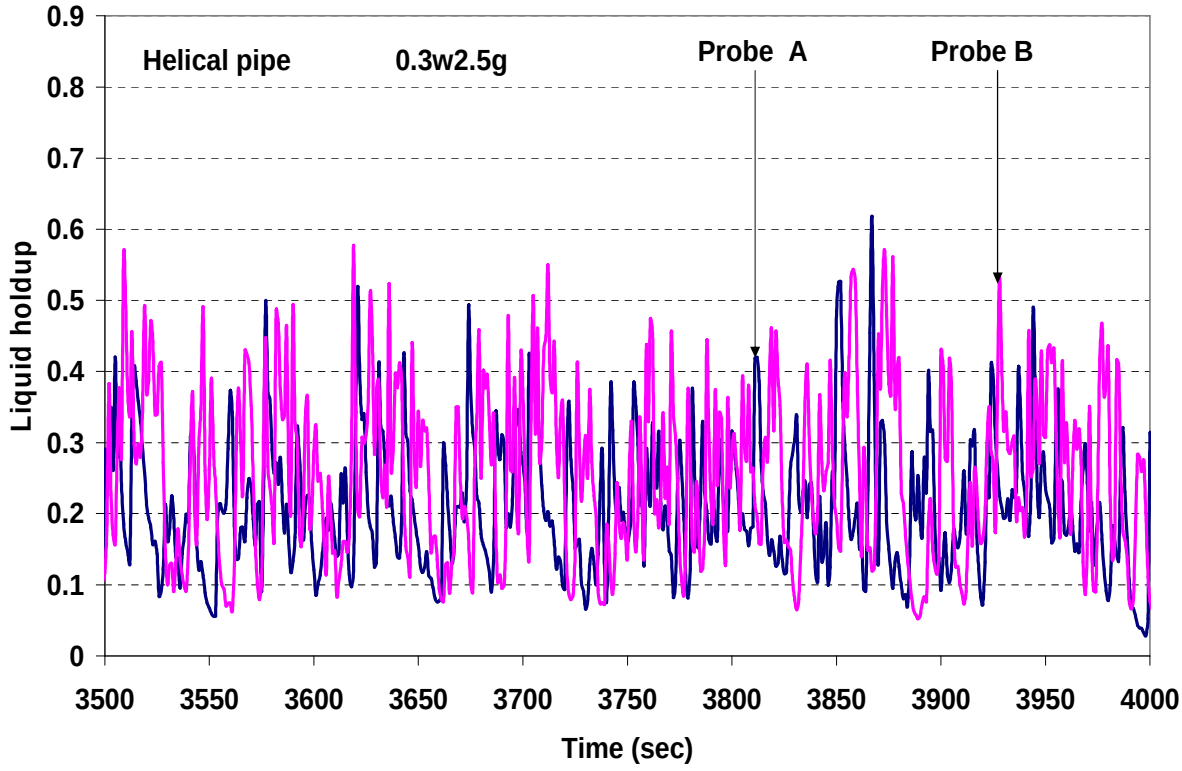
Helical pipe
0.3w2.5g
Probe A
Probe B
Liquid holdup
Time (sec)
0.9
0.8
0.7
0.6
0.5
0.4
0.3
0.2
0.1
0
3500
3550
3600
3650
3700
3750
3800
3850
3900
3950
4000

APPENDIX C

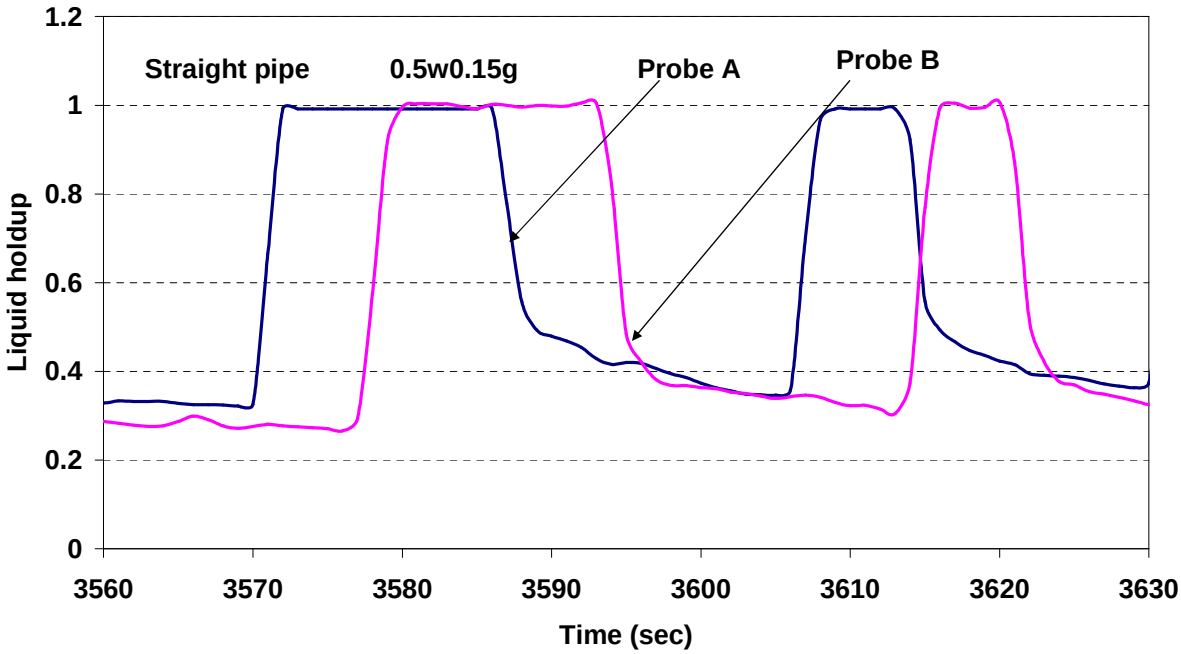
Straight pipe
0.5w0.15g
Probe A
Probe B
Liquid holdup
Time (sec)
1.2
1
0.8
0.6
0.4
0.2
0
3560
3570
3580
3590
3600
3610
3620
3630

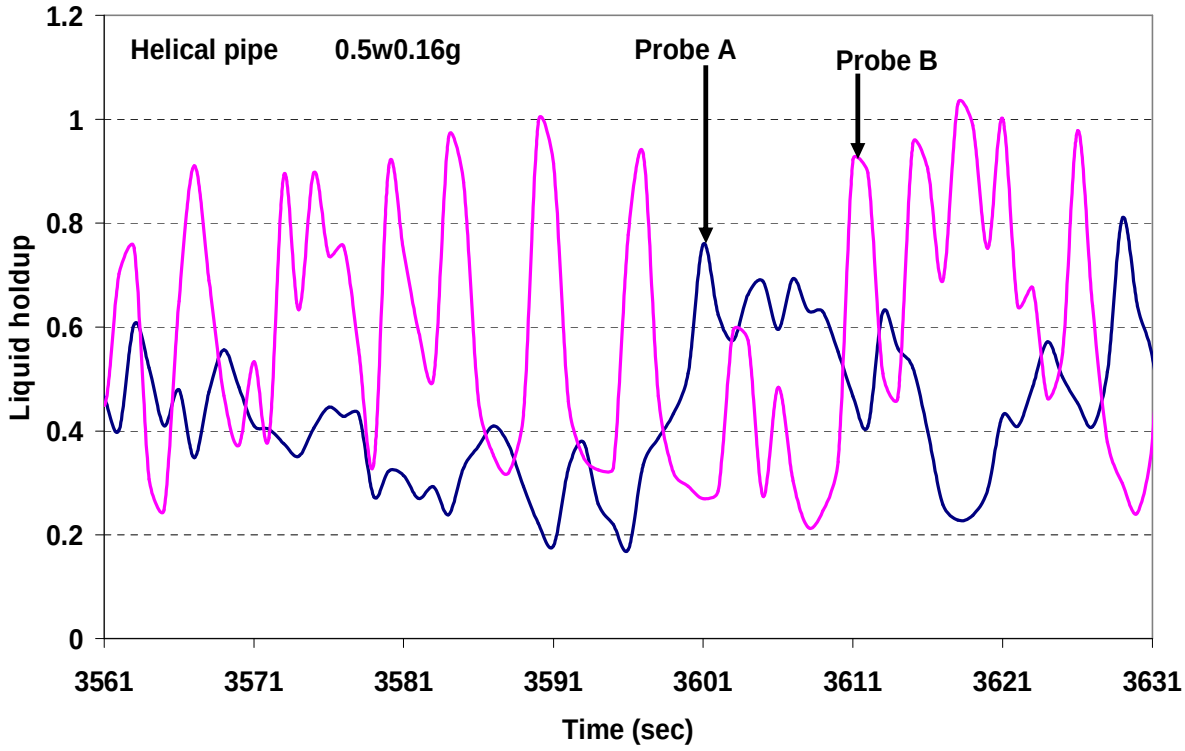
Helical pipe
0.5w0.16g
Probe A
Probe B
Liquid holdup
Time (sec)
1.2
1
0.8
0.6
0.4
0.2
0
3561
3571
3581
3591
3601
3611
3621
3631

APPENDIX C

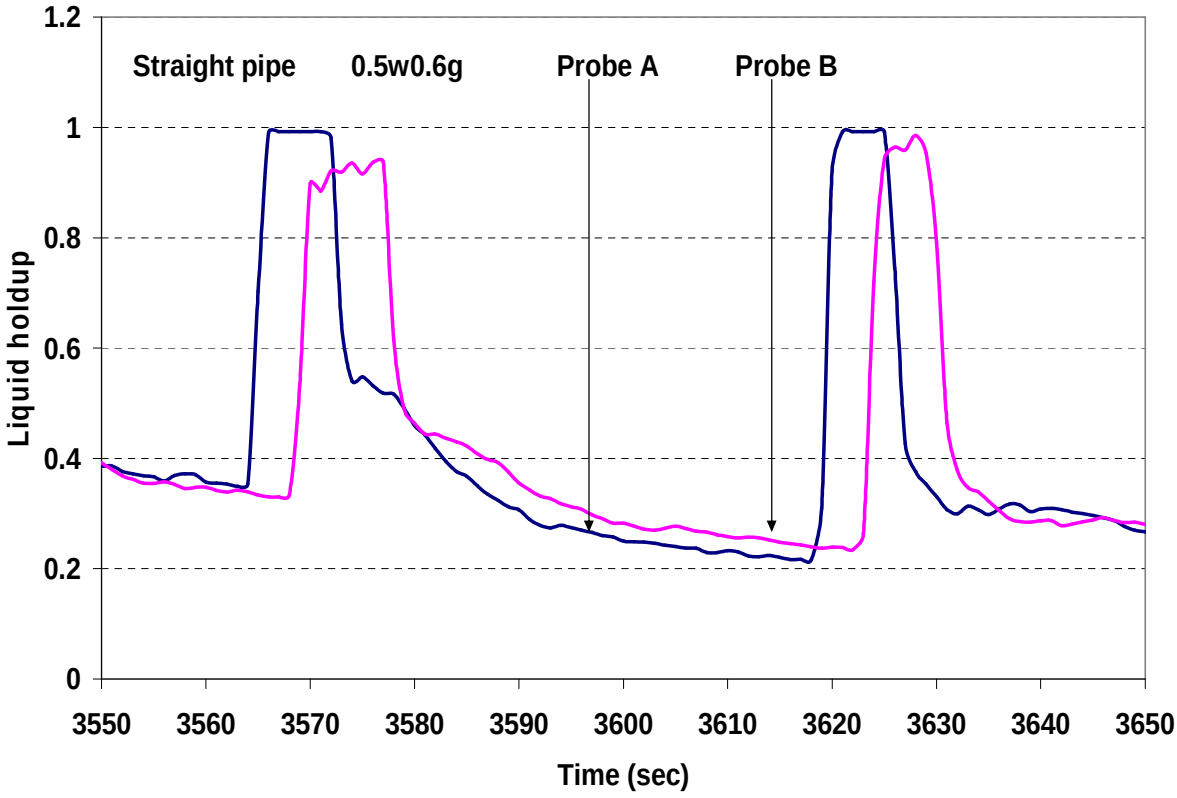
Straight pipe
0.5w0.6g
Probe A
Probe B
Liquid holdup
Time (sec)
1.2
1
0.8
0.6
0.4
0.2
0
3550
3560
3570
3580
3590
3600
3610
3620
3630
3640
3650

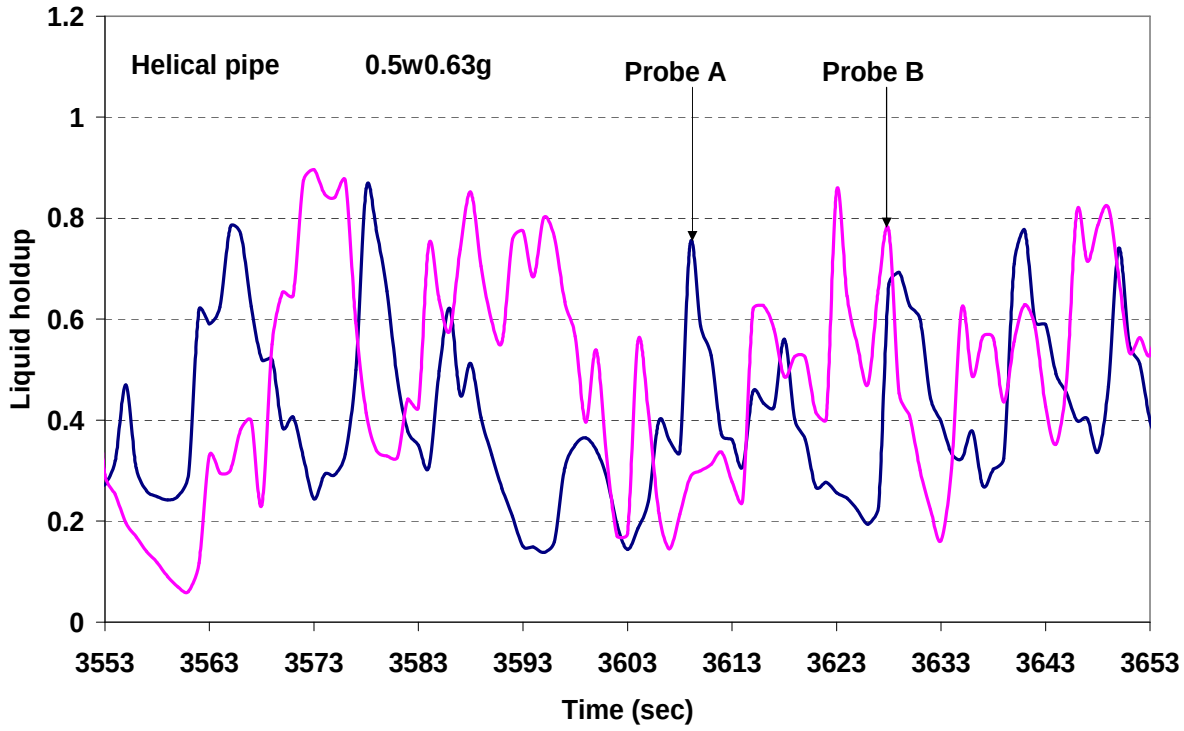
Helical pipe
0.5w0.63g
Probe A
Probe B
Liquid holdup
Time (sec)
1.2
1
0.8
0.6
0.4
0.2
0
3553
3563
3573
3583
3593
3603
3613
3623
3633
3643
3653

APPENDIX C

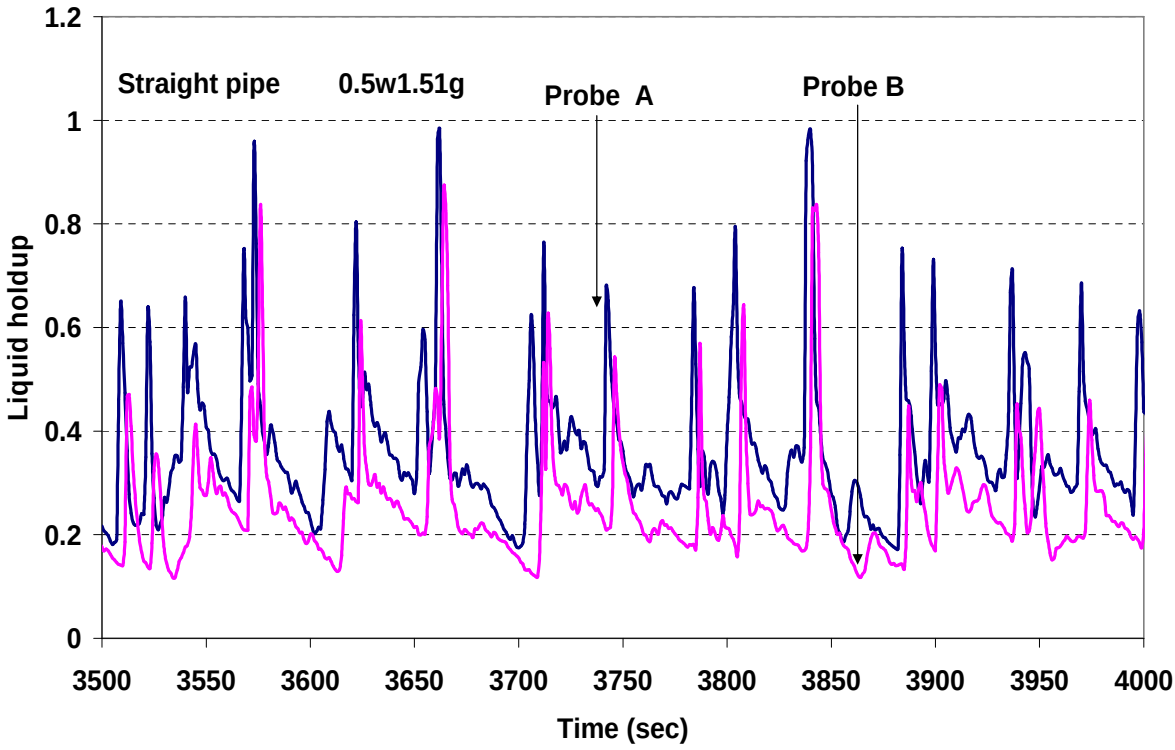
Straight pipe
0.5w1.51g
Probe A
Probe B
Liquid holdup
Time (sec)
1.2
1
0.8
0.6
0.4
0.2
0
3500
3550
3600
3650
3700
3750
3800
3850
3900
3950
4000

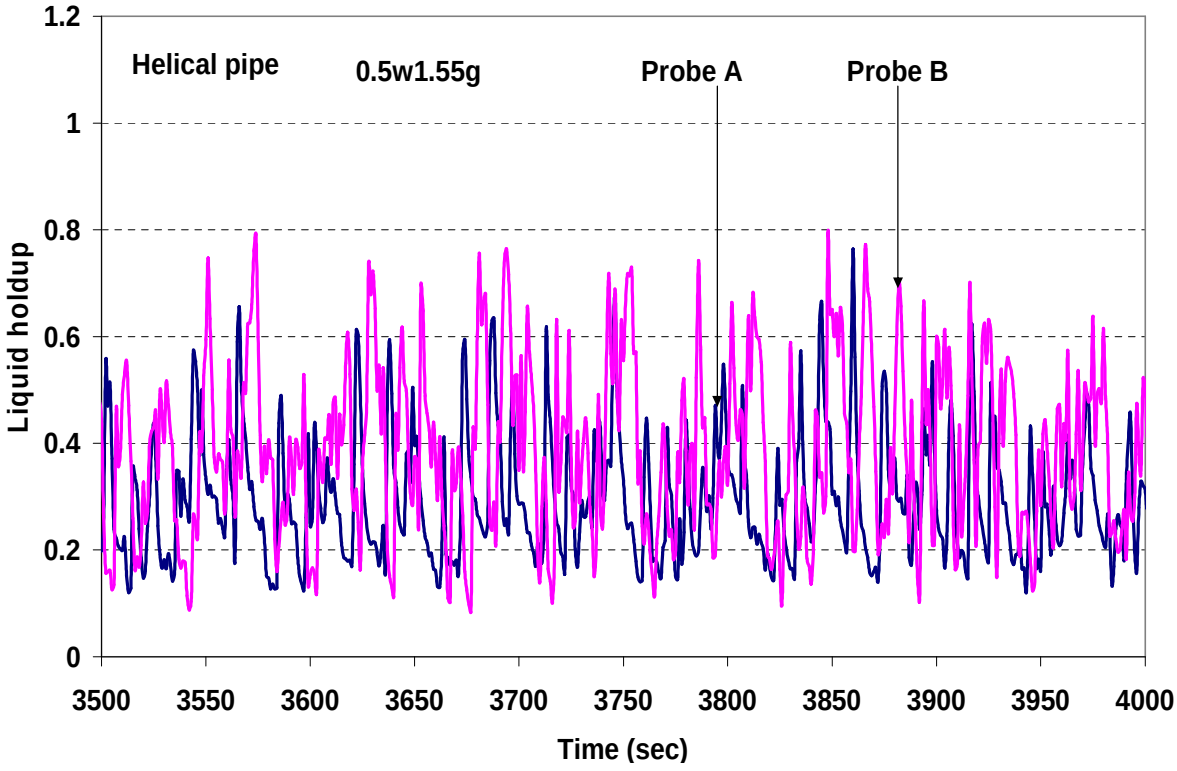
Helical pipe
0.5w1.55g
Probe A
Probe B
Liquid holdup
Time (sec)
1.2
1
0.8
0.6
0.4
0.2
0
3500
3550
3600
3650
3700
3750
3800
3850
3900
3950
4000

APPENDIX C

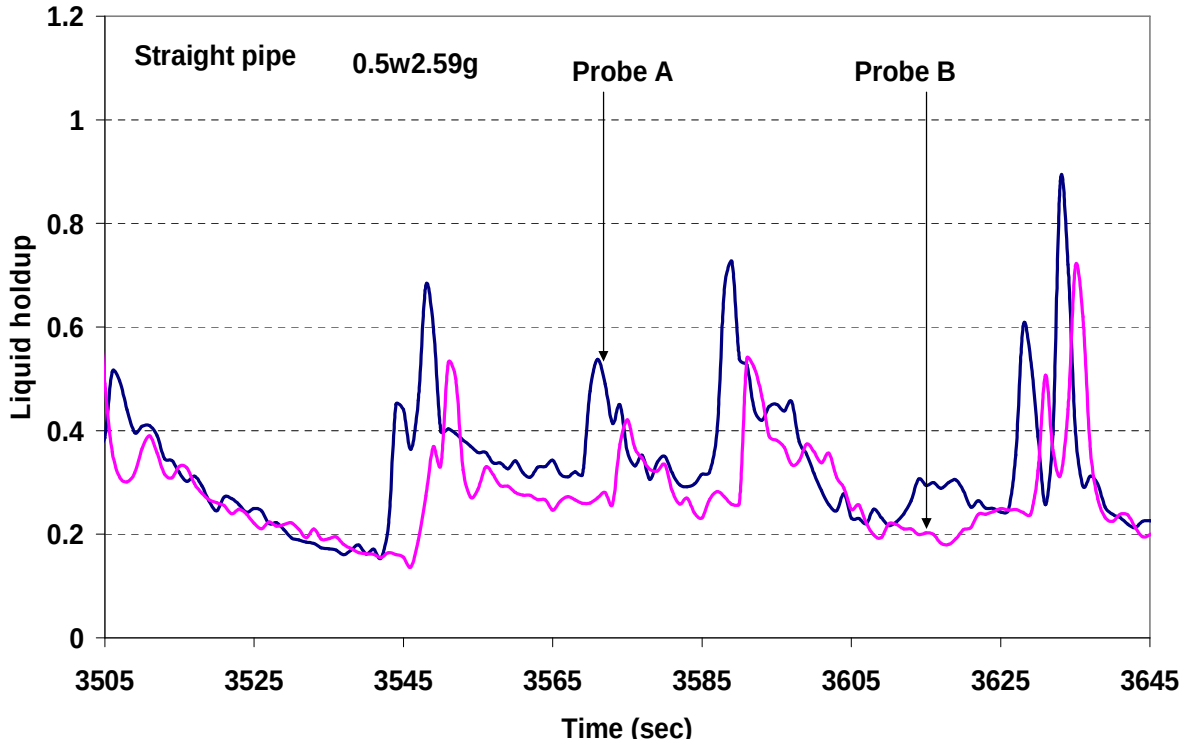
Straight pipe
0.5w2.59g
Probe A
Probe B
Liquid holdup
1.2
1
0.8
0.6
0.4
0.2
0
3505
3525
3545
3565
3585
3605
3625
3645
Time (sec)

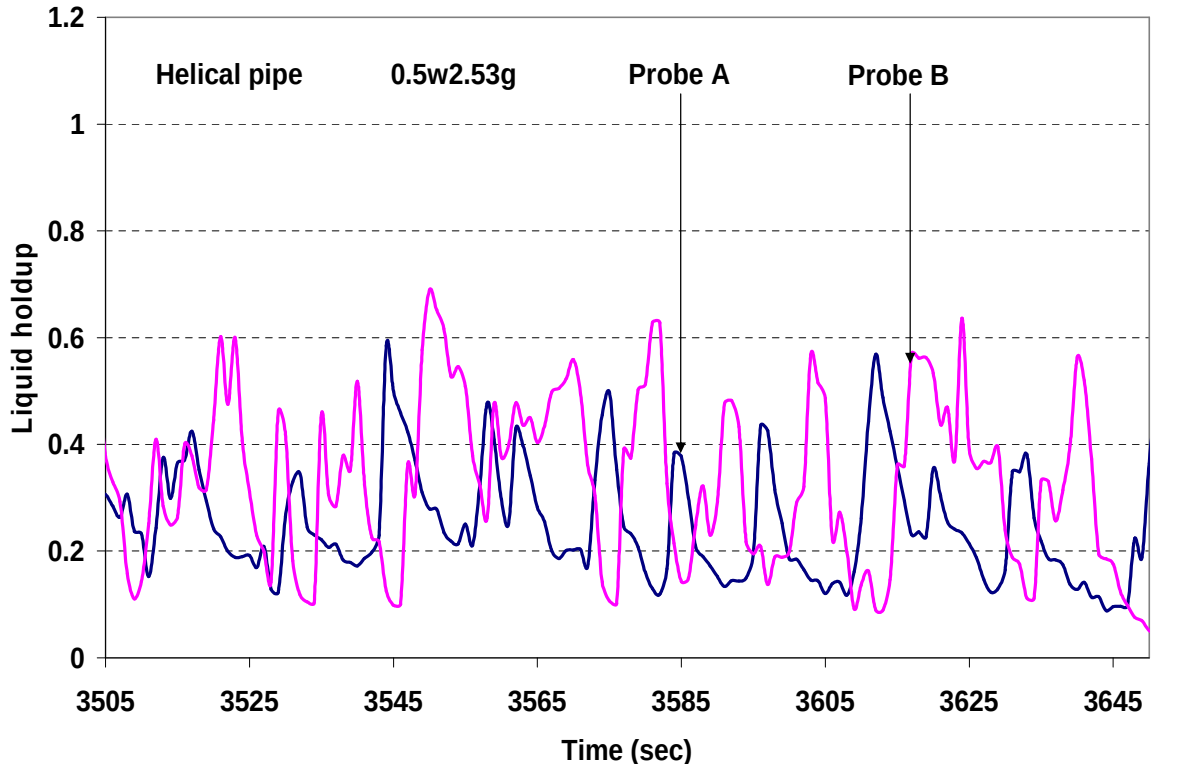
Helical pipe
0.5w2.53g
Probe A
Probe B
Liquid holdup
1.2
1
0.8
0.6
0.4
0.2
0
3505
3525
3545
3565
3585
3605
3625
3645
Time (sec)

APPENDIX C

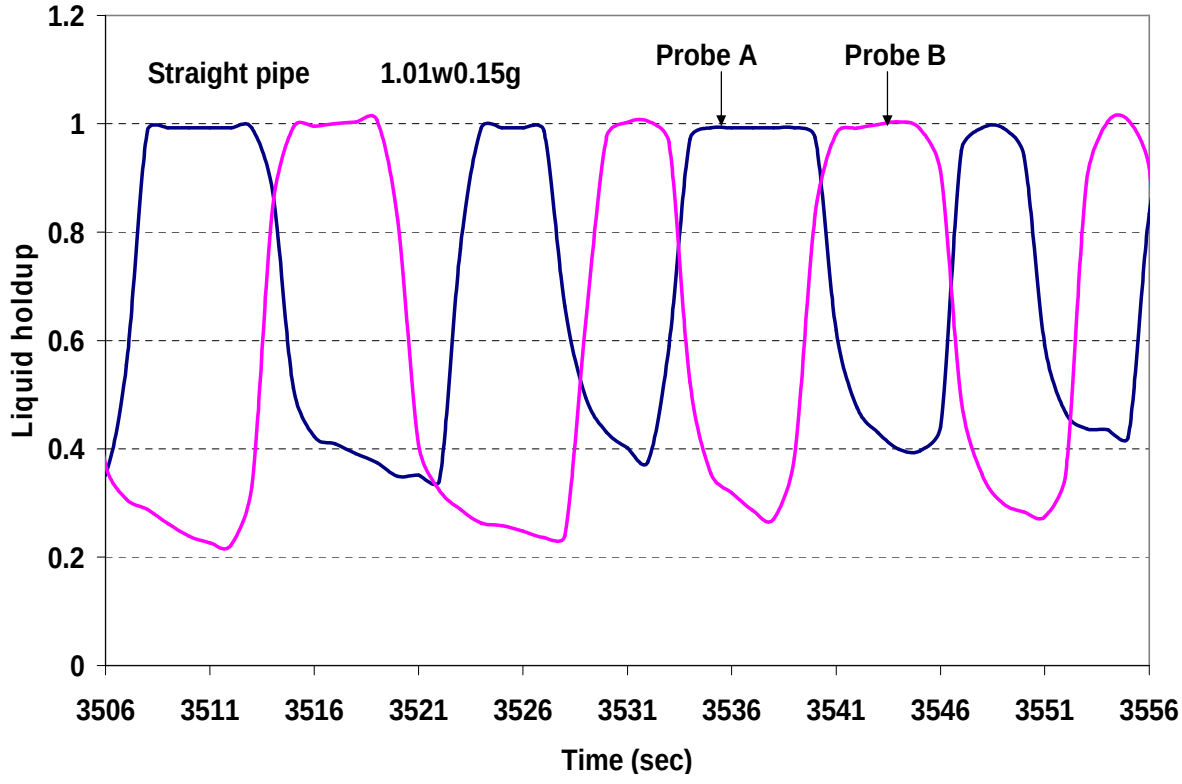
Straight pipe
1.01w0.15g
Probe A
Probe B
Liquid holdup
Time (sec)
1.2
1
0.8
0.6
0.4
0.2
0
3506
3511
3516
3521
3526
3531
3536
3541
3546
3551
3556

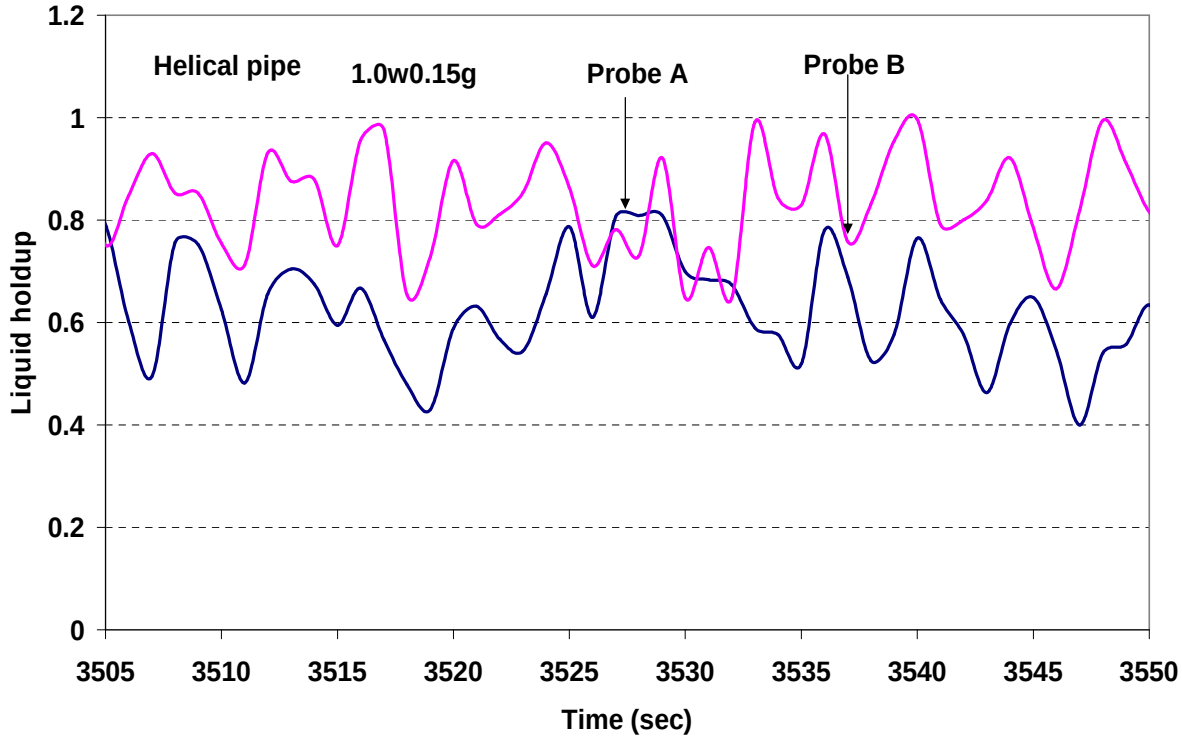
Helical pipe
1.0w0.15g
Probe A
Probe B
Liquid holdup
Time (sec)
1.2
1
0.8
0.6
0.4
0.2
0
3505
3510
3515
3520
3525
3530
3535
3540
3545
3550

APPENDIX C

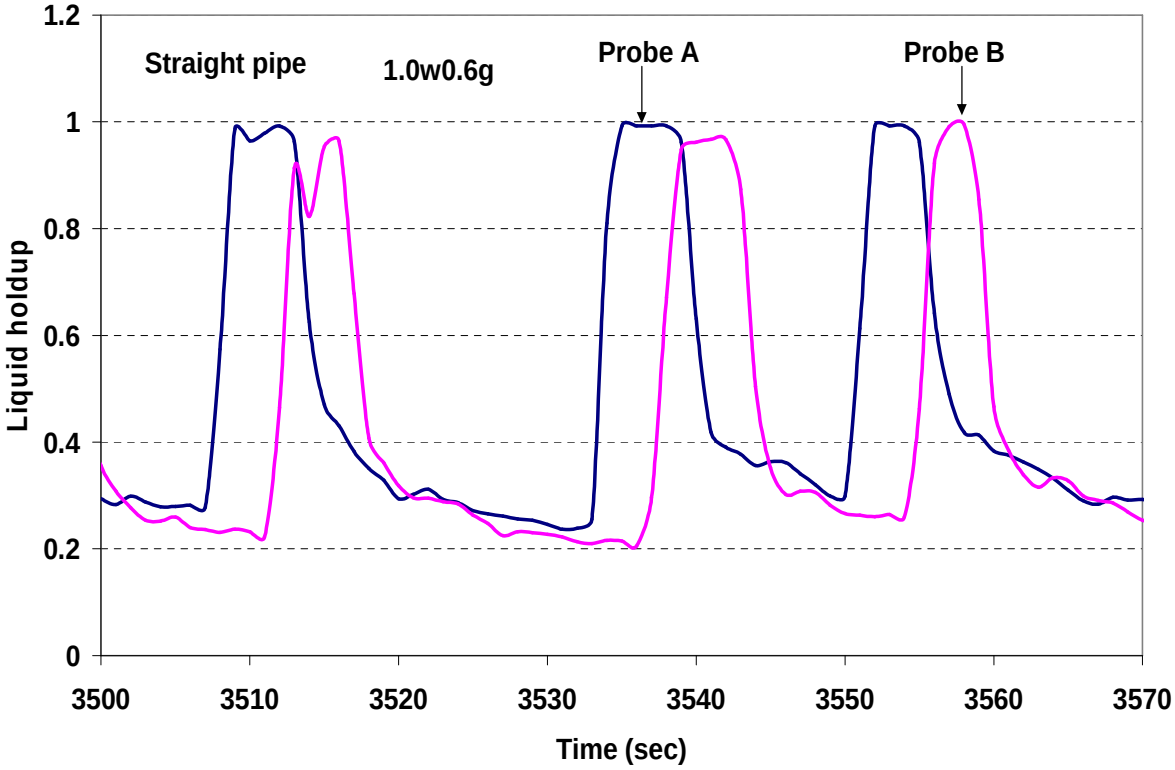
Straight pipe
1.0w0.6g
Probe A
Probe B
Liquid holdup
Time (sec)
1.2
1
0.8
0.6
0.4
0.2
0
3500
3510
3520
3530
3540
3550
3560
3570

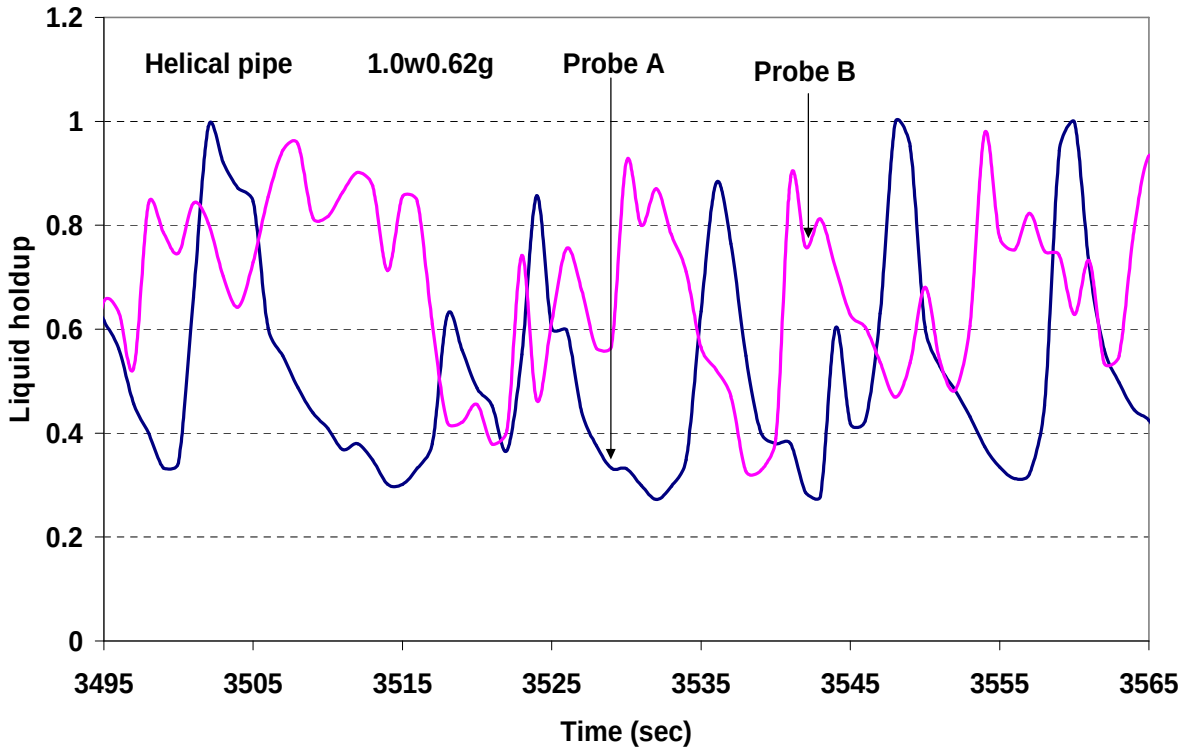
Helical pipe
1.0w0.62g
Probe A
Probe B
Liquid holdup
Time (sec)
1.2
1
0.8
0.6
0.4
0.2
0
3495
3505
3515
3525
3535
3545
3555
3565

APPENDIX C

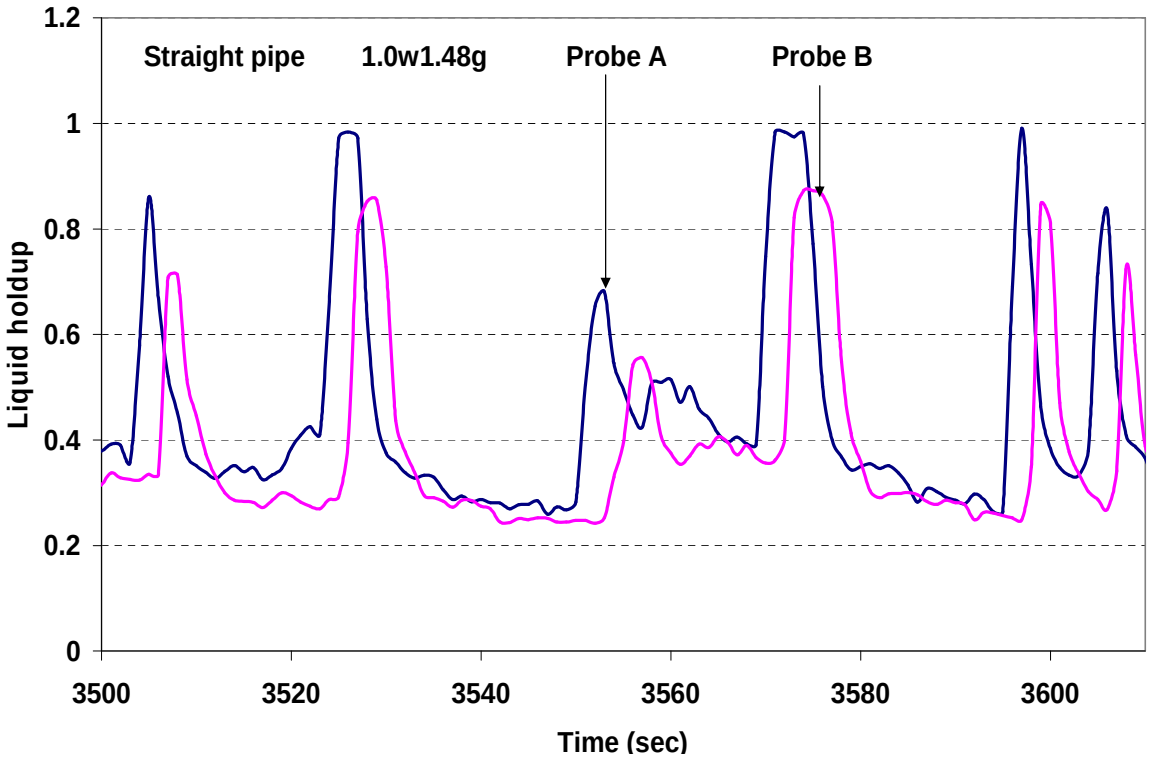
Straight pipe
1.0w1.48g
Probe A
Probe B
Liquid holdup
Time (sec)
1.2
1
0.8
0.6
0.4
0.2
0
3500
3520
3540
3560
3580
3600

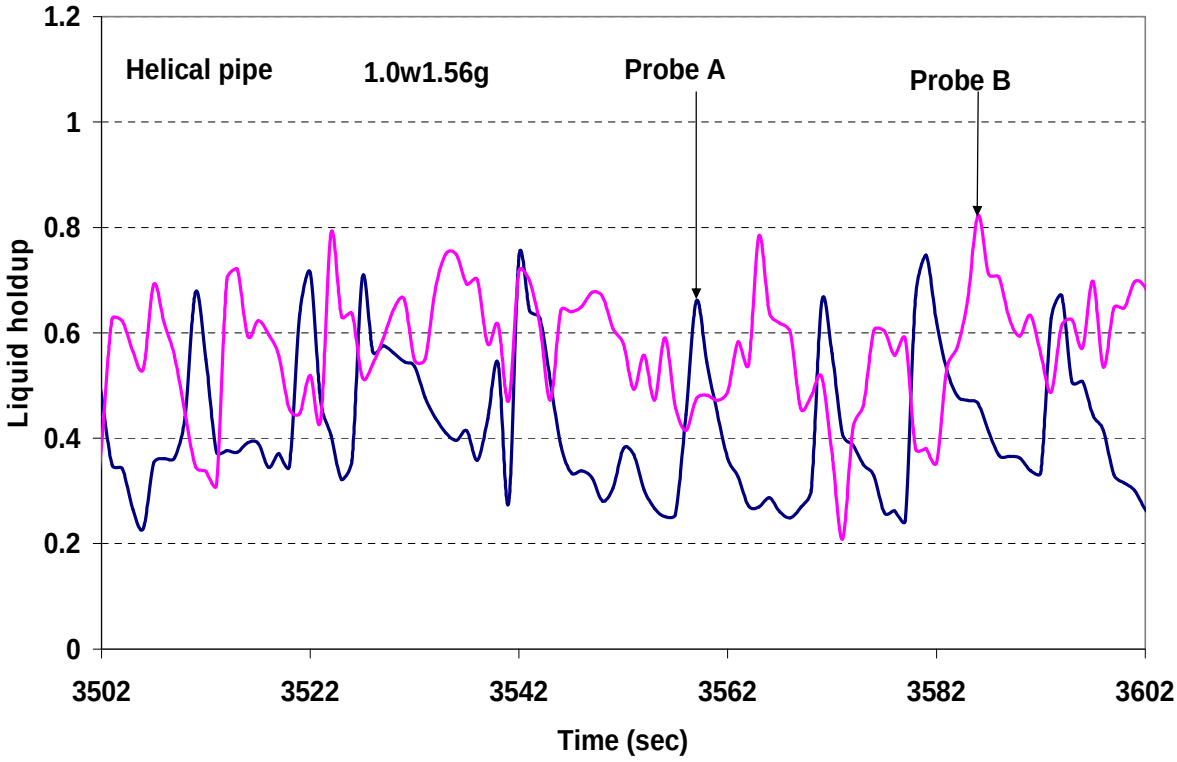
Helical pipe
1.0w1.56g
Probe A
Probe B
Liquid holdup
Time (sec)
1.2
1
0.8
0.6
0.4
0.2
0
3502
3522
3542
3562
3582
3602

APPENDIX C

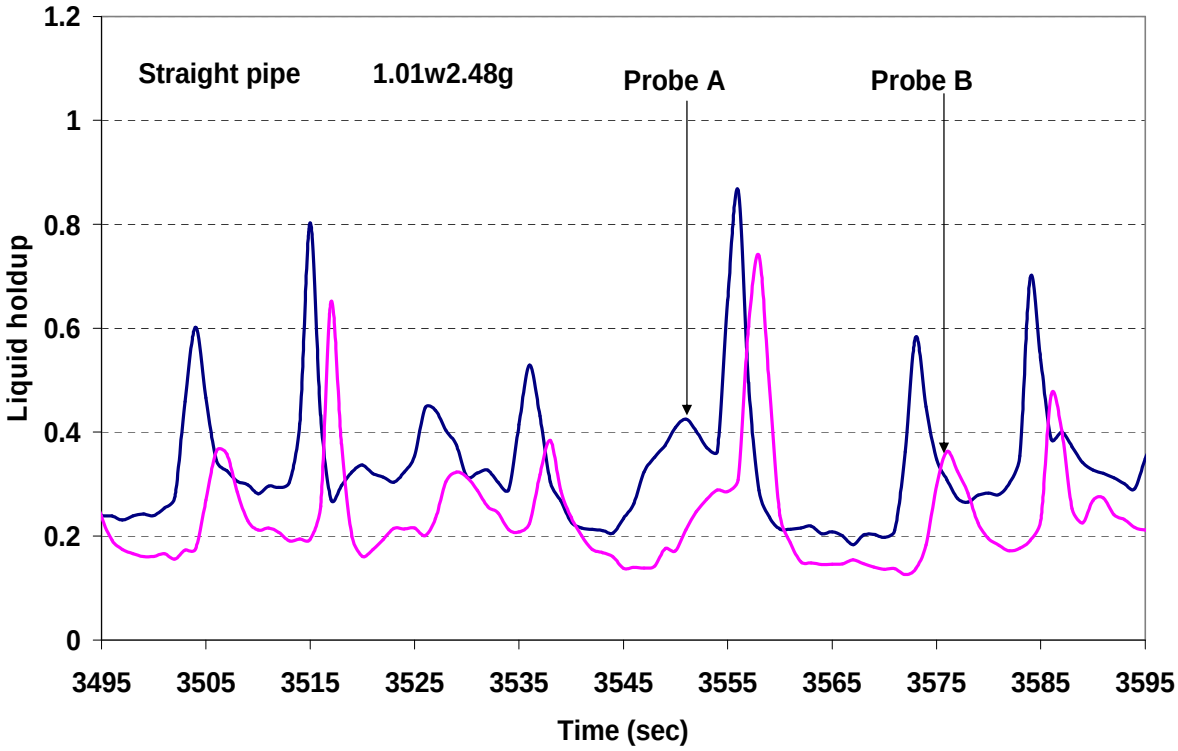
Straight pipe
1.01w2.48g
Probe A
Probe B
Liquid holdup
1.2
1
0.8
0.6
0.4
0.2
0
3495
3505
3515
3525
3535
3545
3555
3565
3575
3585
3595
Time (sec)

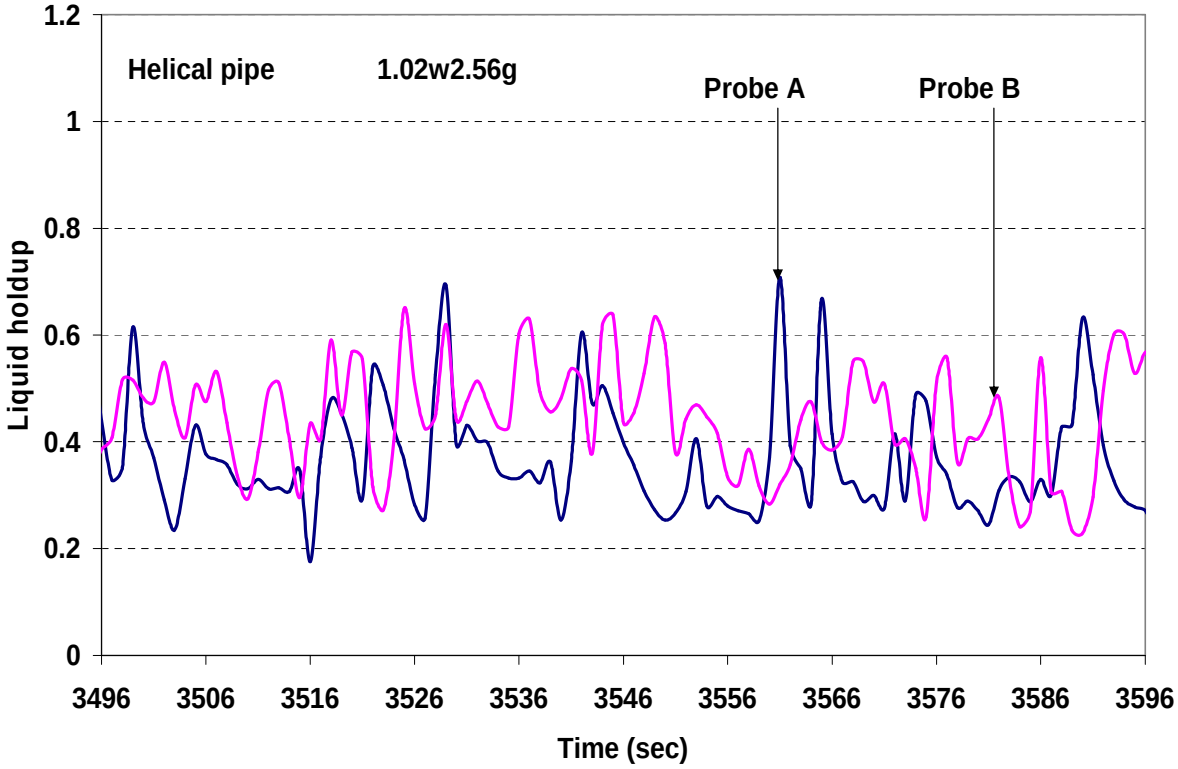
Helical pipe
1.02w2.56g
Probe A
Probe B
Liquid holdup
1.2
1
0.8
0.6
0.4
0.2
0
3496
3506
3516
3526
3536
3546
3556
3566
3576
3586
3596
Time (sec)

APPENDIX C

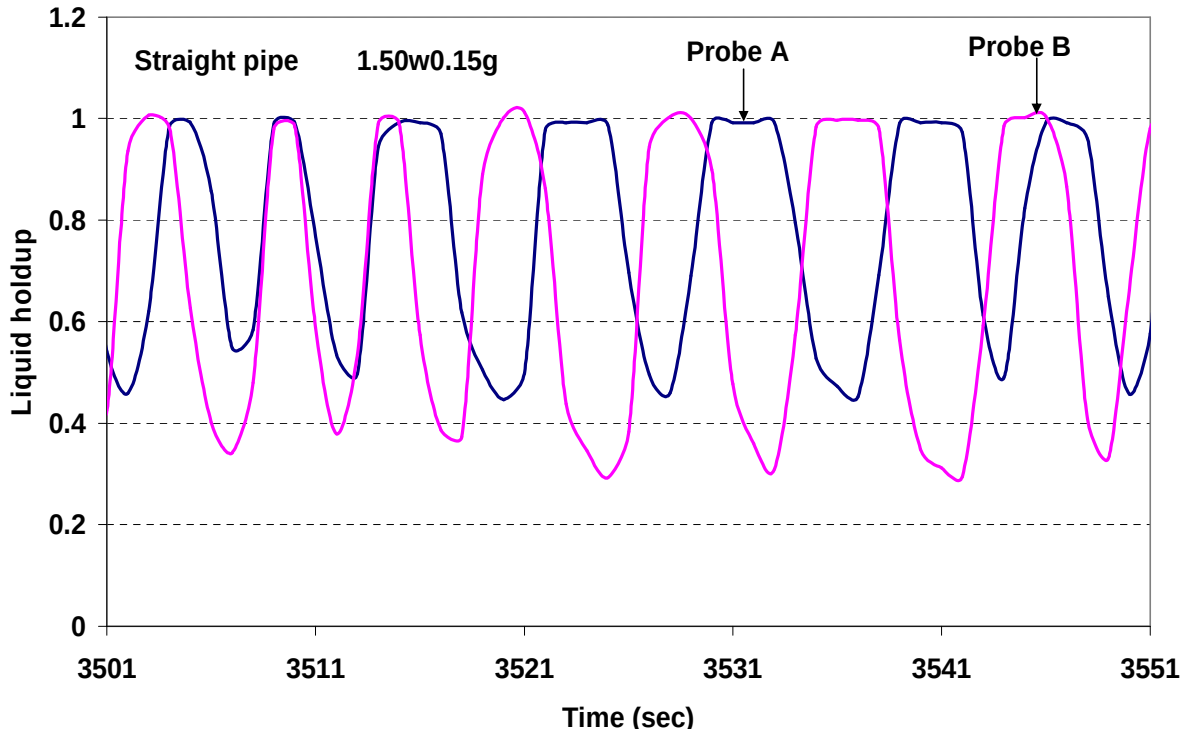
Straight pipe
1.50w0.15g
Probe A
Probe B
Liquid holdup
1.2
1
0.8
0.6
0.4
0.2
0
3501
3511
3521
3531
3541
3551
Time (sec)

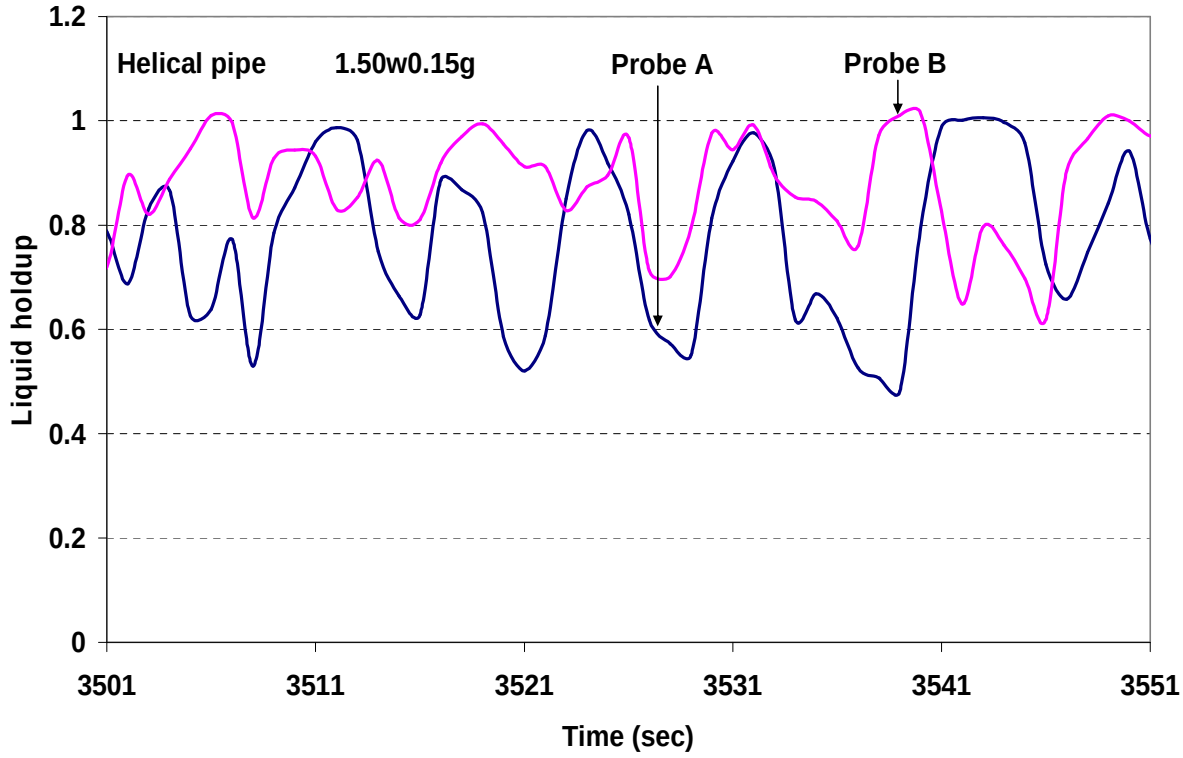
Helical pipe
1.50w0.15g
Probe A
Probe B
Liquid holdup
1.2
1
0.8
0.6
0.4
0.2
0
3501
3511
3521
3531
3541
3551
Time (sec)

APPENDIX C

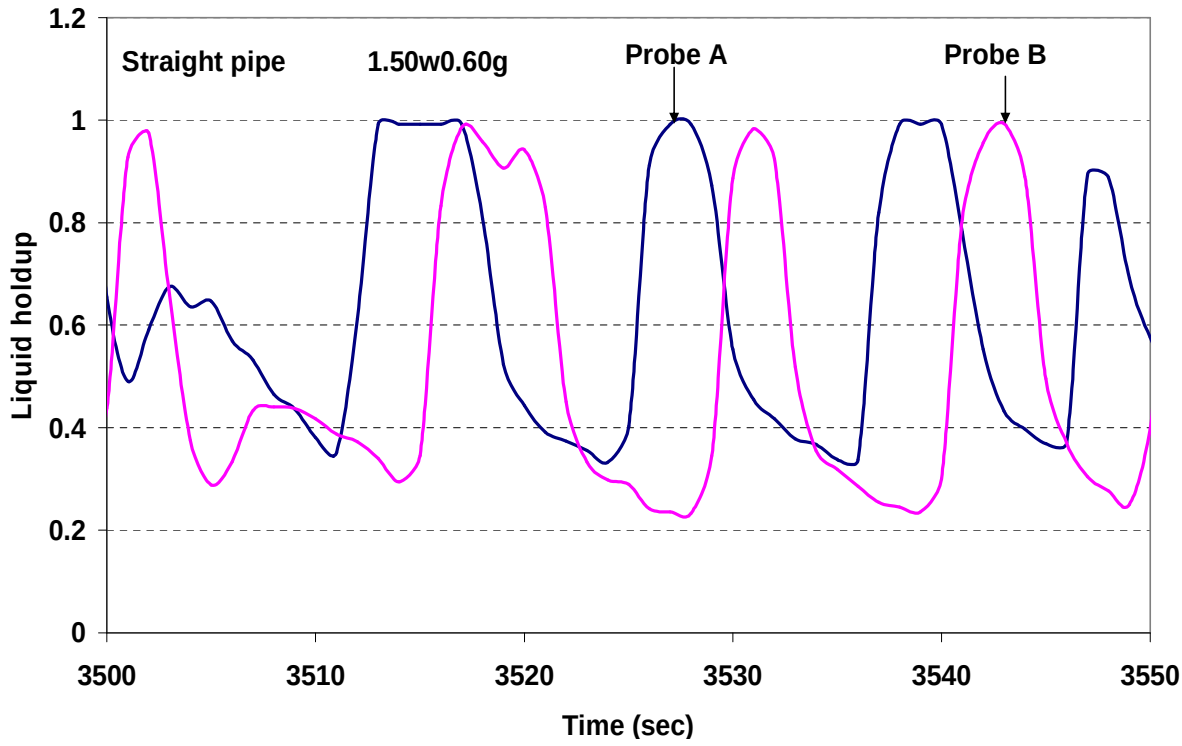
Straight pipe
1.50w0.60g
Probe A
Probe B
Liquid holdup
Time (sec)
1.2
1
0.8
0.6
0.4
0.2
0
3500
3510
3520
3530
3540
3550

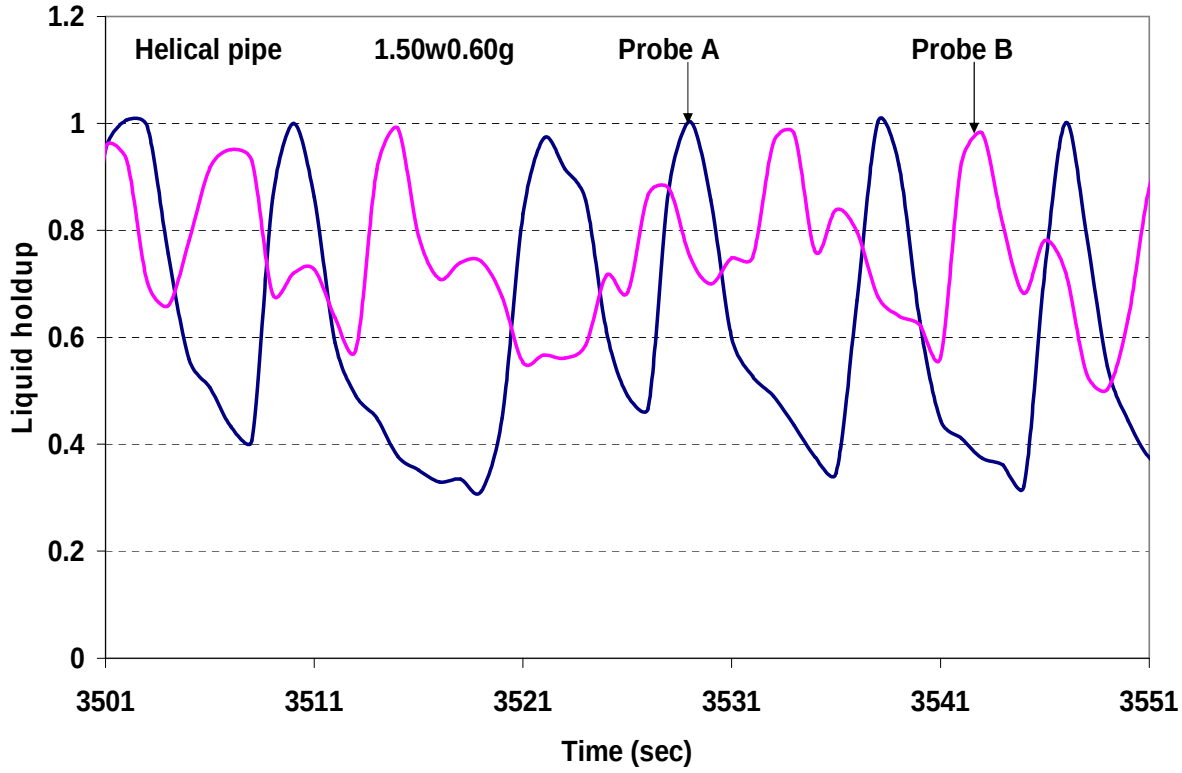
Helical pipe
1.50w0.60g
Probe A
Probe B
Liquid holdup
Time (sec)
1.2
1
0.8
0.6
0.4
0.2
0
3501
3511
3521
3531
3541
3551

APPENDIX C

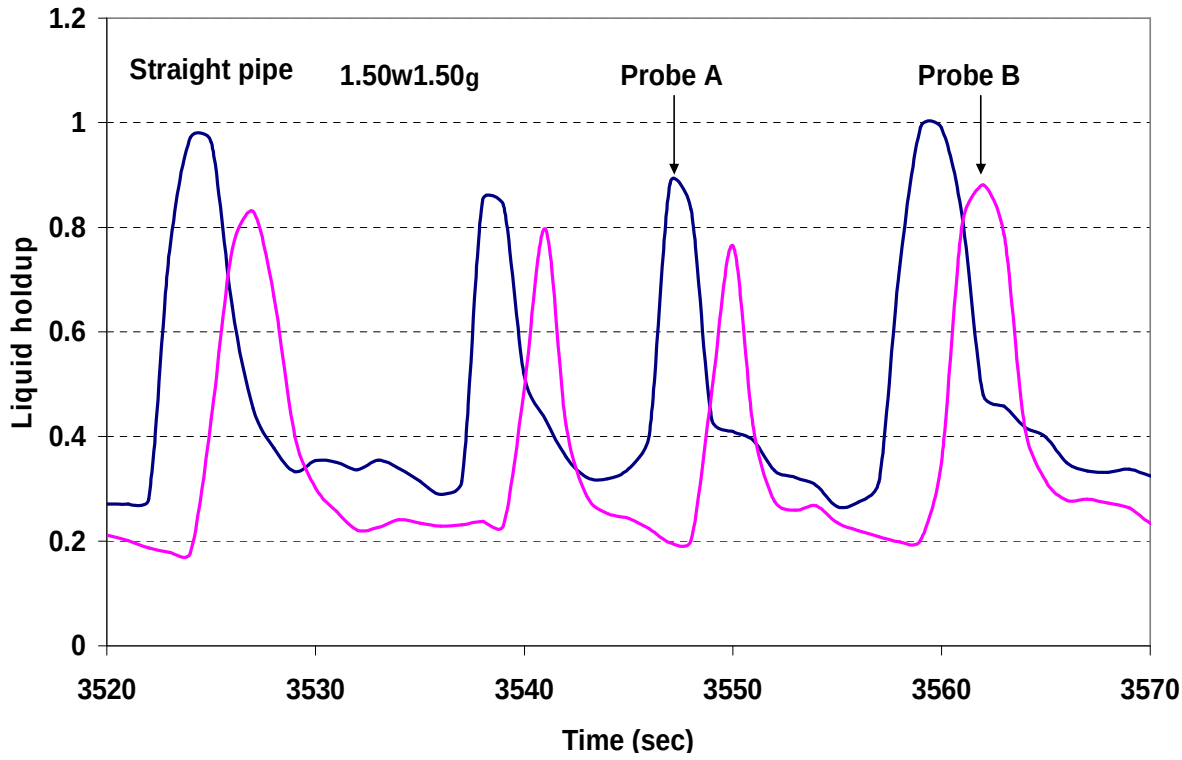
Straight pipe
1.50w1.50g
Probe A
Probe B
Liquid holdup
1.2
1
0.8
0.6
0.4
0.2
0
3520
3530
3540
3550
3560
3570
Time (sec)

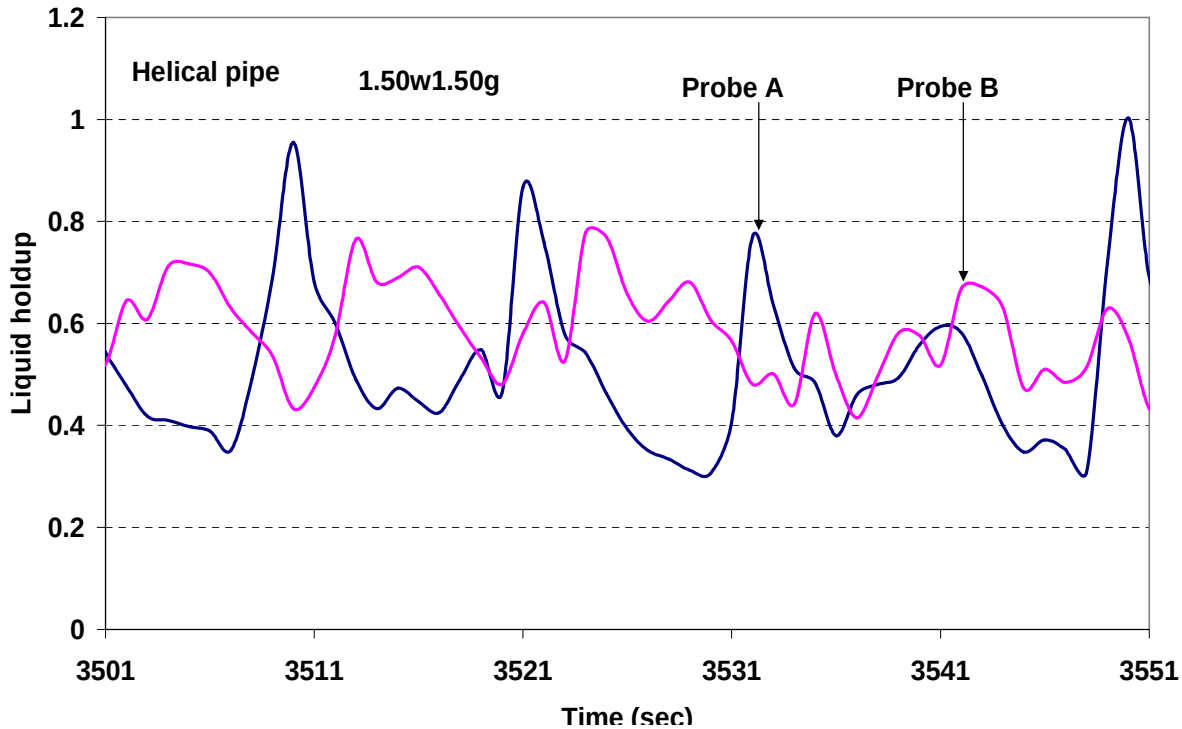
Helical pipe
1.50w1.50g
Probe A
Probe B
Liquid holdup
1.2
1
0.8
0.6
0.4
0.2
0
3501
3511
3521
3531
3541
3551
Time (sec)

APPENDIX C

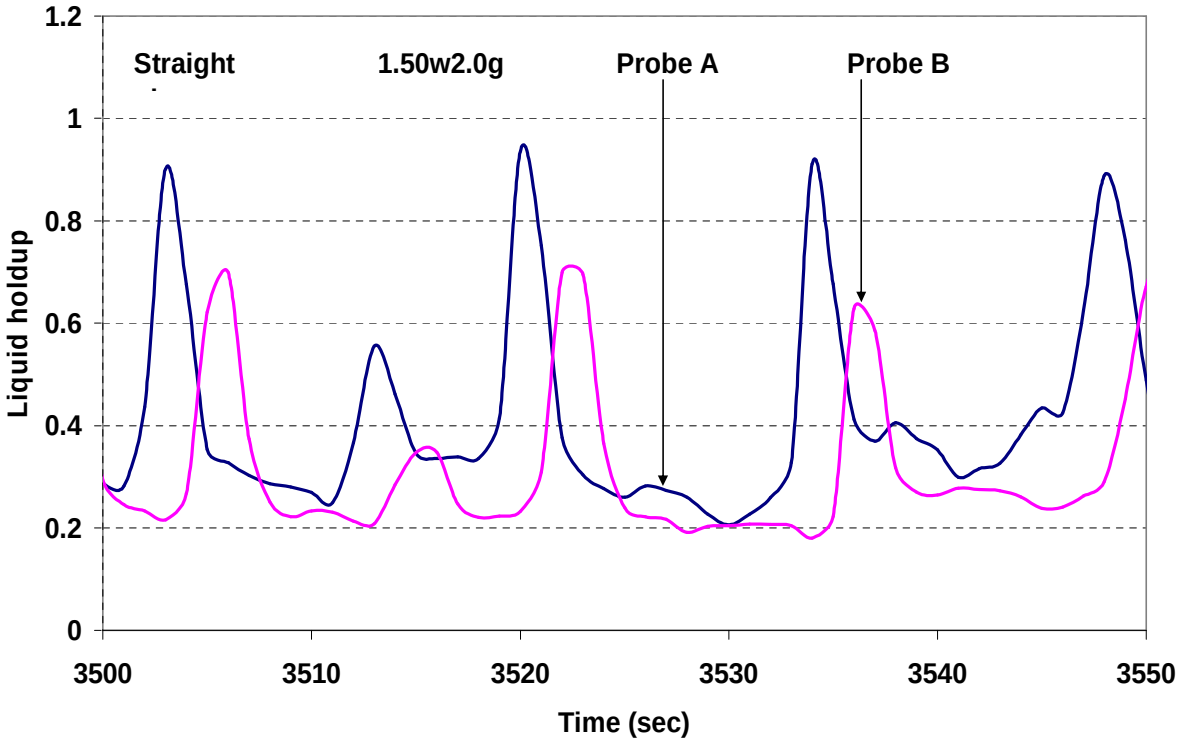
Straight
1.50w2.0g
Probe A
Probe B
Liquid holdup
Time (sec)
1.2
1
0.8
0.6
0.4
0.2
0
3500
3510
3520
3530
3540
3550

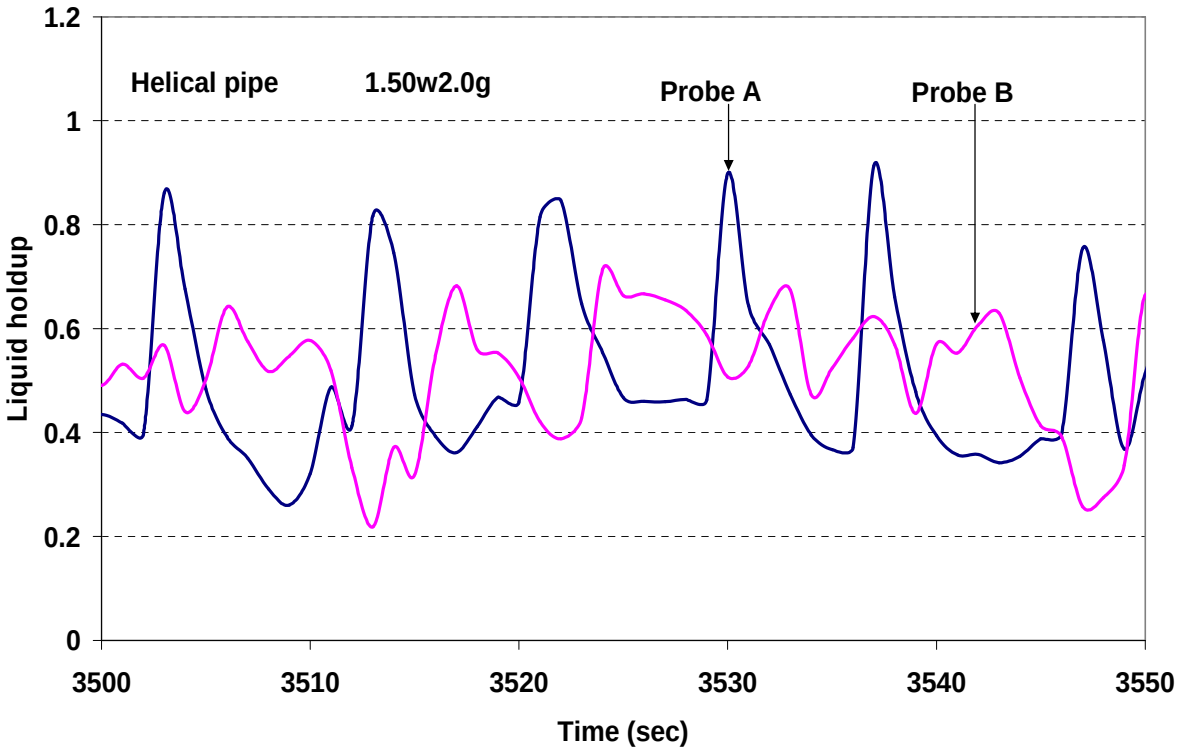
Helical pipe
1.50w2.0g
Probe A
Probe B
Liquid holdup
Time (sec)
1.2
1
0.8
0.6
0.4
0.2
0
3500
3510
3520
3530
3540
3550

APPENDIX C

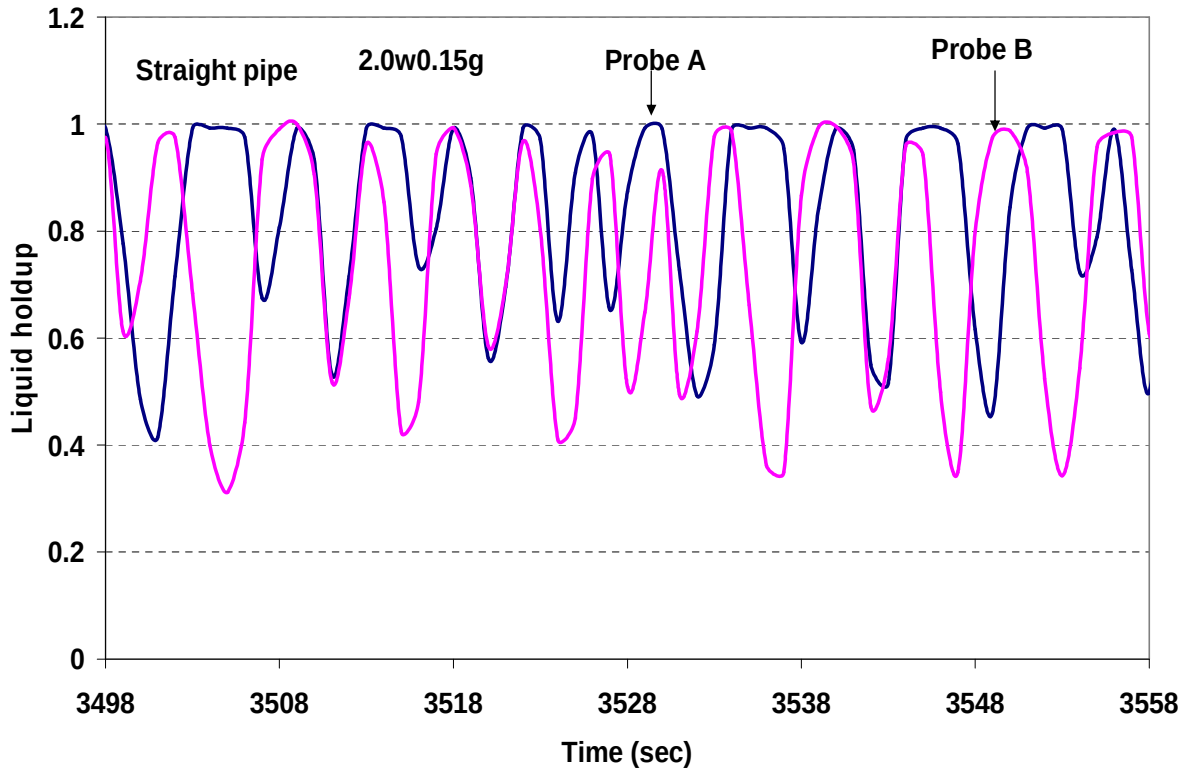
Straight pipe
2.0w0.15g
Probe A
Probe B
Liquid holdup
1.2
1
0.8
0.6
0.4
0.2
0
3498
3508
3518
3528
3538
3548
3558
Time (sec)

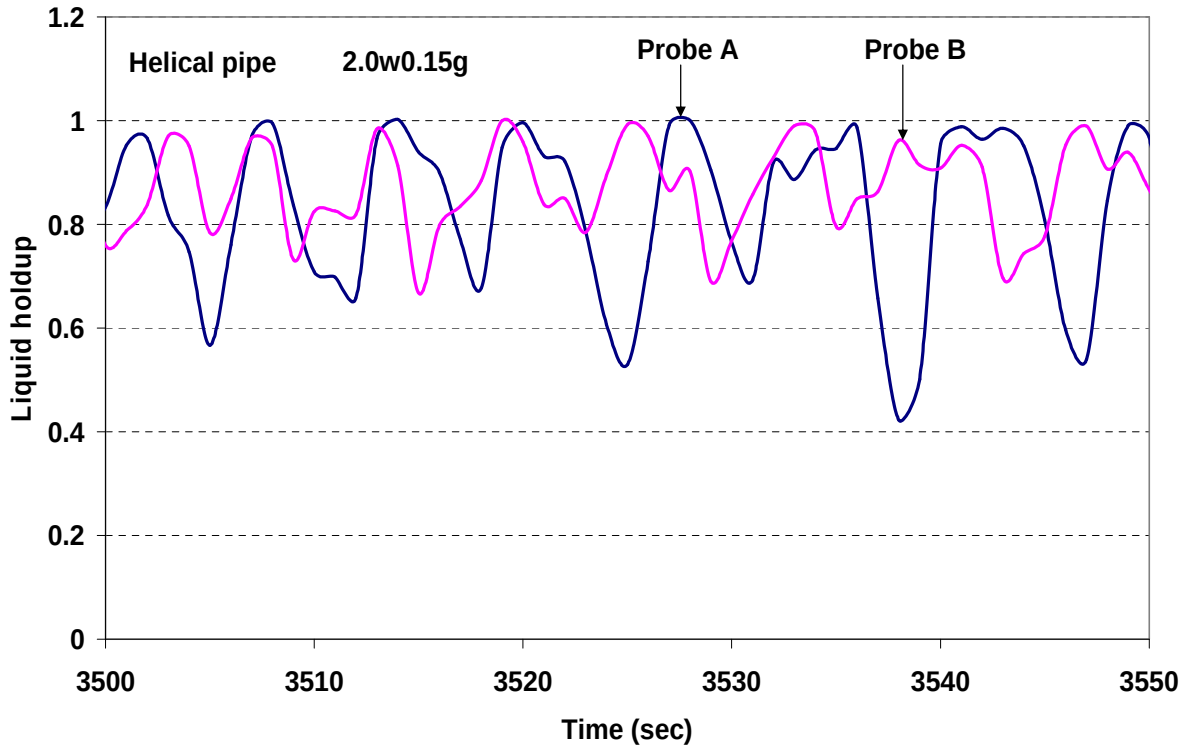
Helical pipe
2.0w0.15g
Probe A
Probe B
Liquid holdup
1.2
1
0.8
0.6
0.4
0.2
0
3500
3510
3520
3530
3540
3550
Time (sec)

APPENDIX C

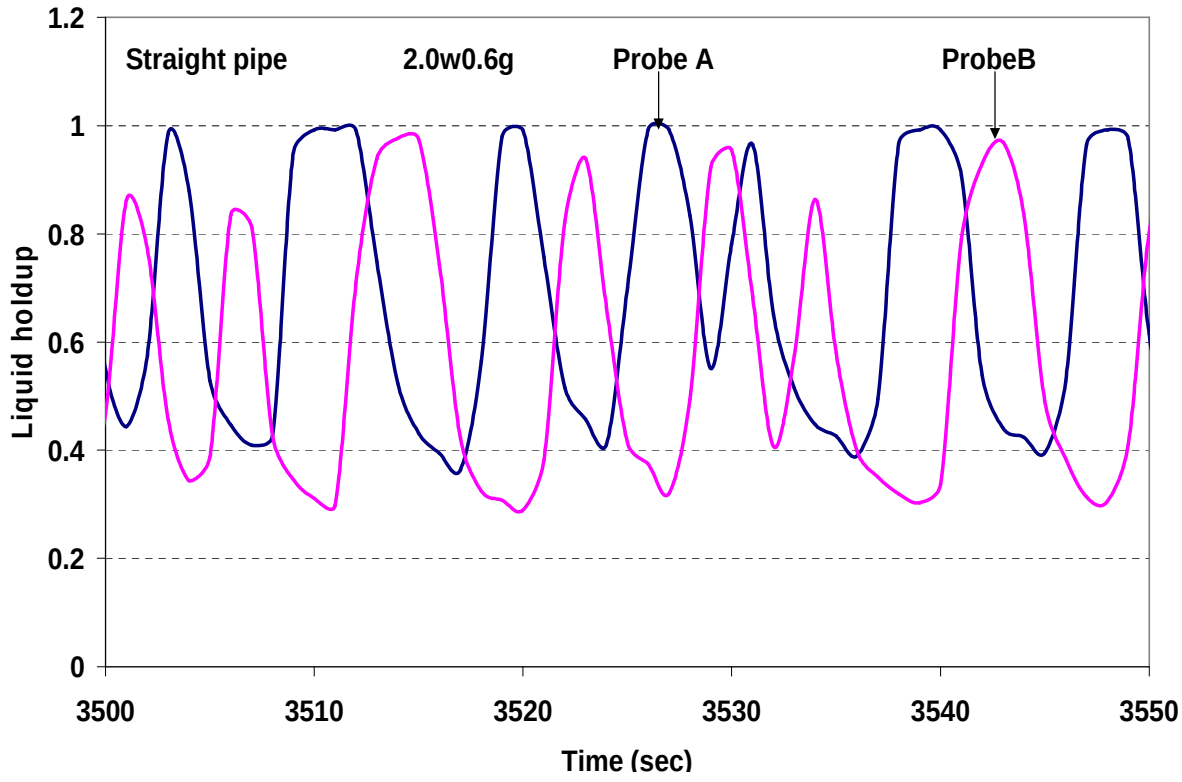
Straight pipe
2.0w0.6g
Probe A
ProbeB
Liquid holdup
Time (sec)
1.2
1
0.8
0.6
0.4
0.2
0
3500
3510
3520
3530
3540
3550

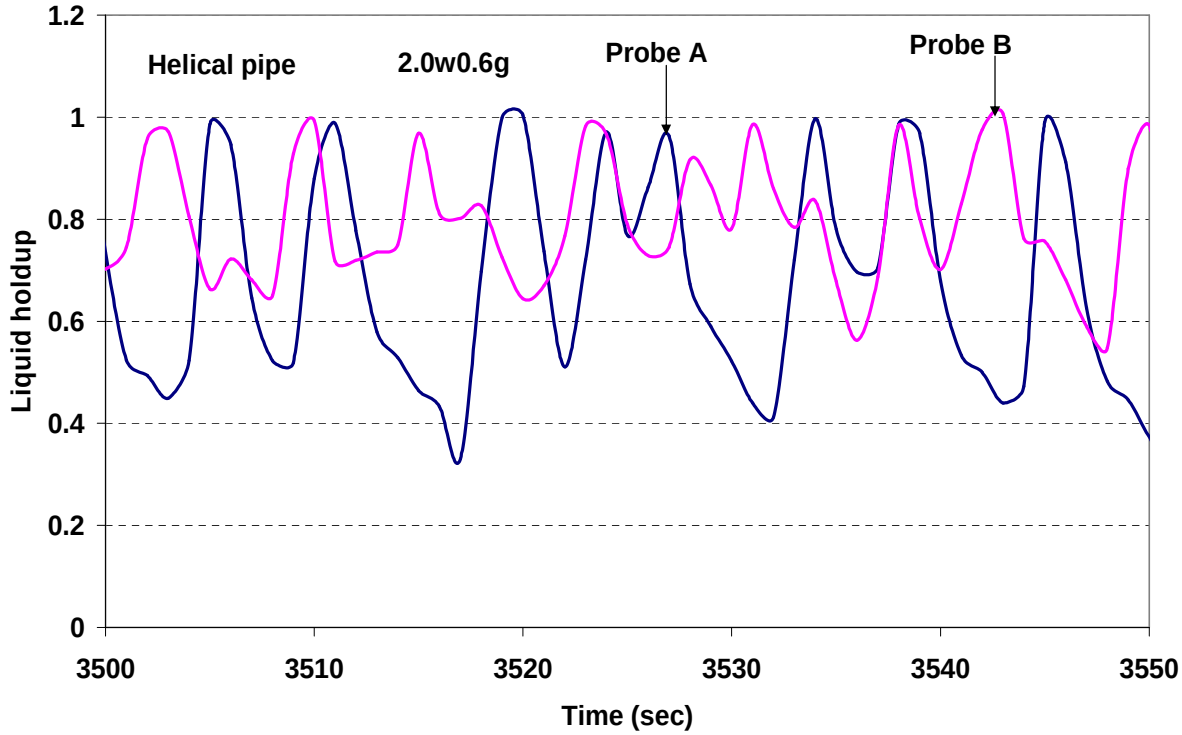
Helical pipe
2.0w0.6g
Probe A
Probe B
Liquid holdup
Time (sec)
1.2
1
0.8
0.6
0.4
0.2
0
3500
3510
3520
3530
3540
3550

APPENDIX C

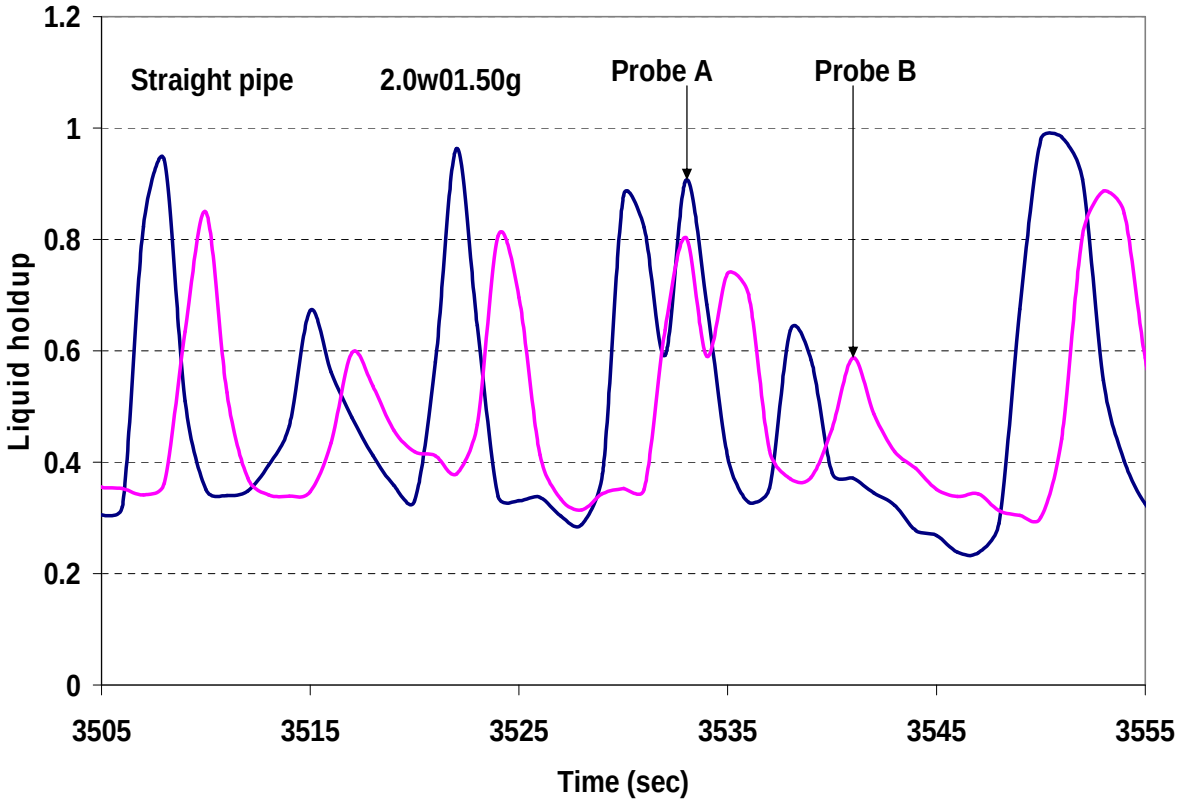
Straight pipe
2.0w01.50g
Probe A
Probe B
Liquid holdup
Time (sec)
1.2
1
0.8
0.6
0.4
0.2
0
3505
3515
3525
3535
3545
3555

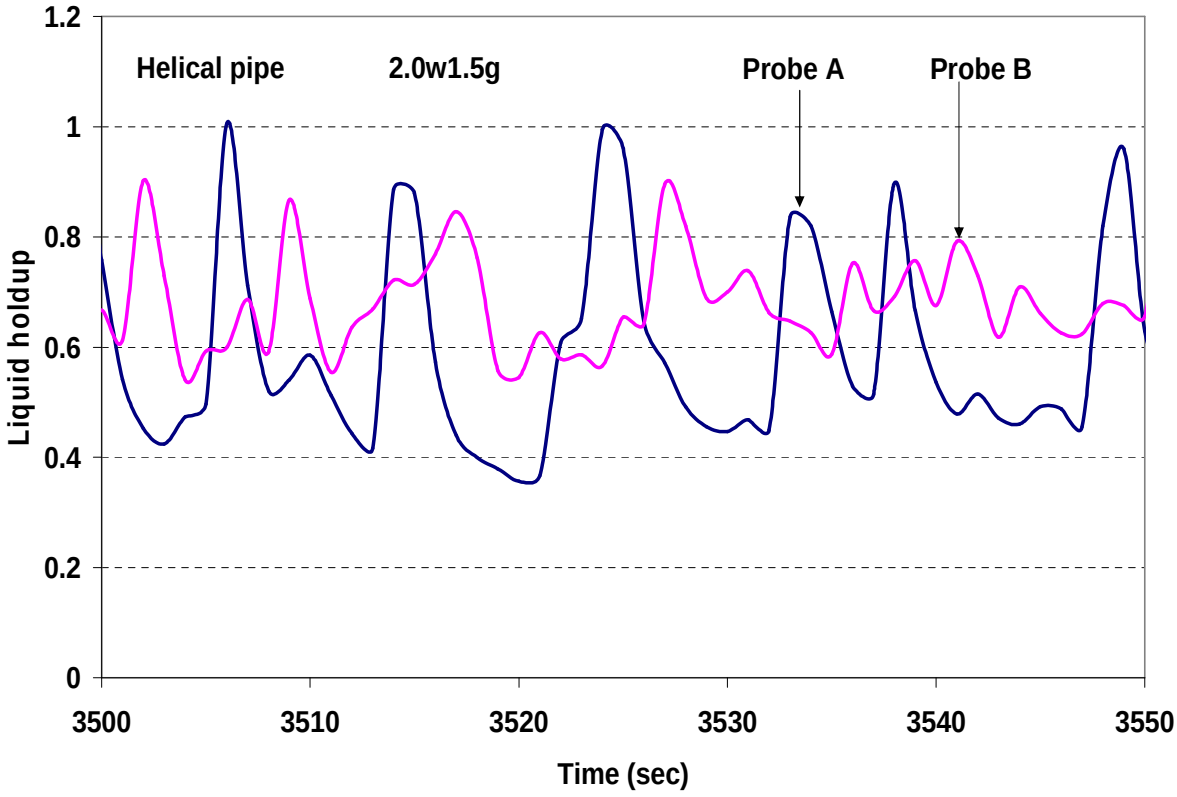
Helical pipe
2.0w1.5g
Probe A
Probe B
Liquid holdup
Time (sec)
1.2
1
0.8
0.6
0.4
0.2
0
3500
3510
3520
3530
3540
3550

APPENDIX C

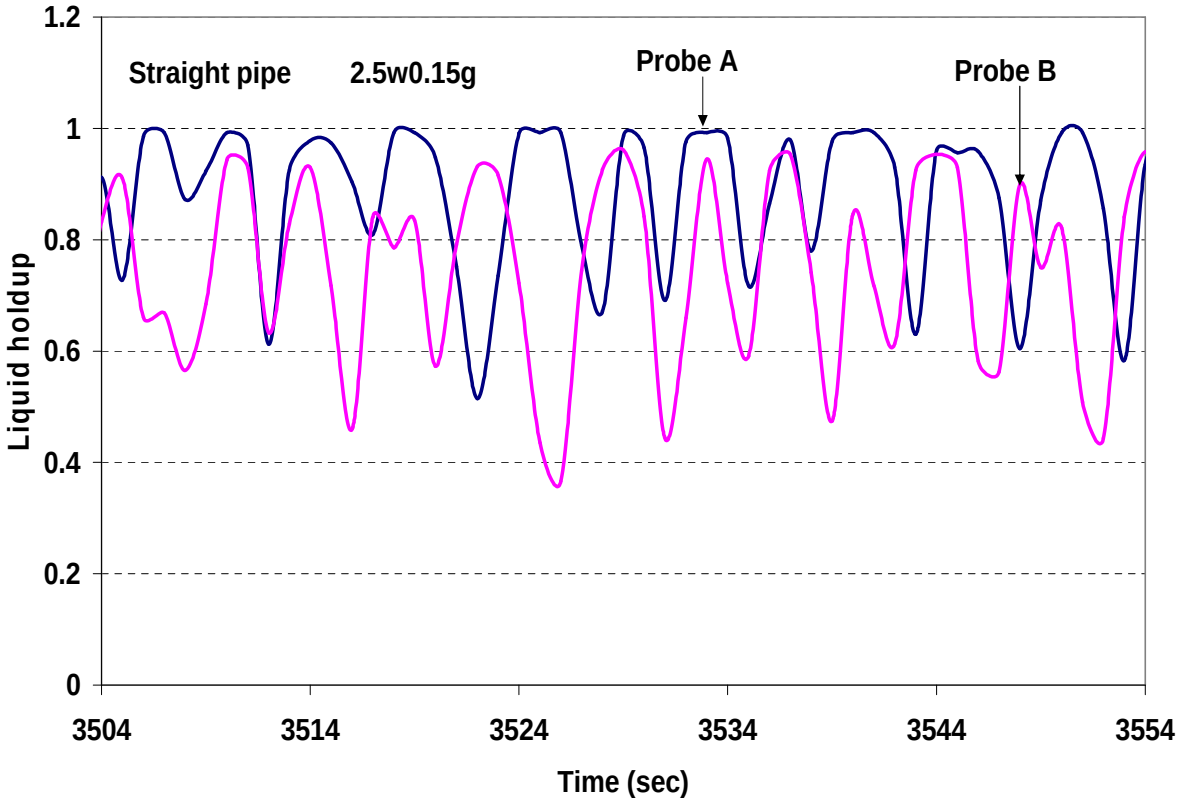
Straight pipe
2.5w0.15g
Probe A
Probe B
Liquid holdup
Time (sec)
1.2
1
0.8
0.6
0.4
0.2
0
3504
3514
3524
3534
3544
3554

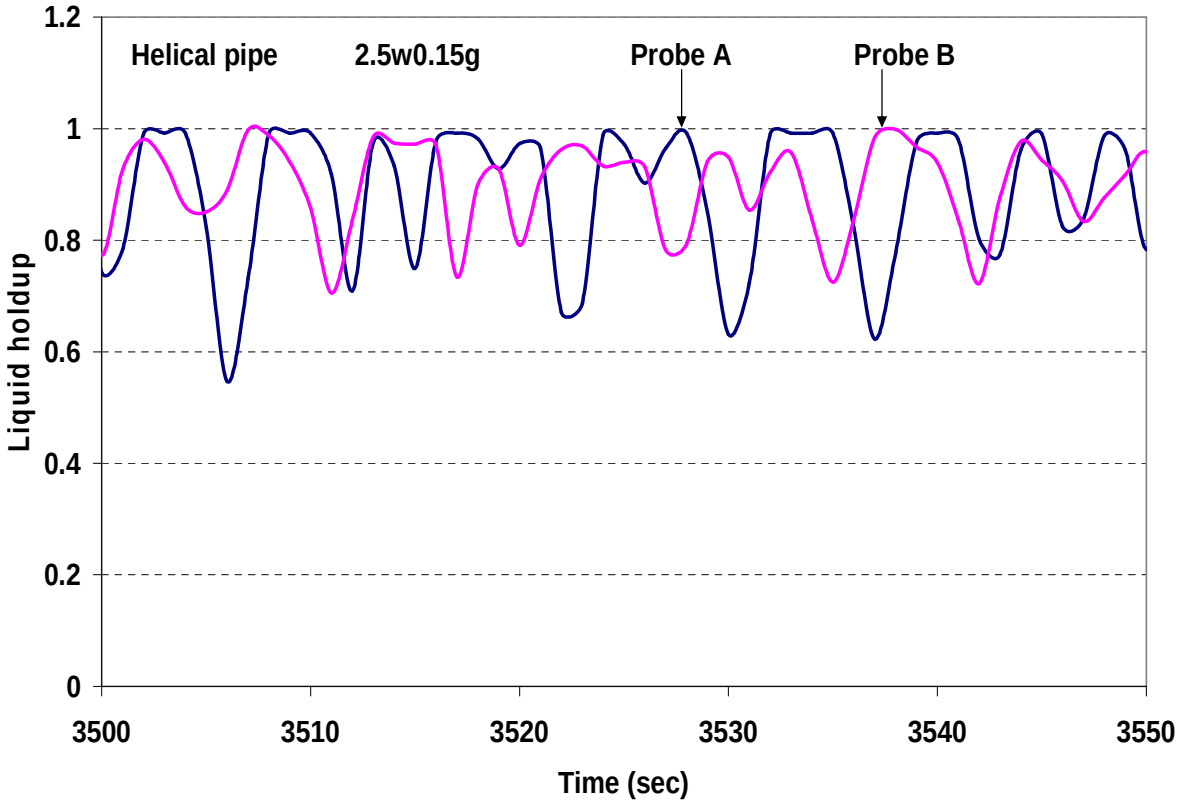
Helical pipe
2.5w0.15g
Probe A
Probe B
Liquid holdup
Time (sec)
1.2
1
0.8
0.6
0.4
0.2
0
3500
3510
3520
3530
3540
3550

APPENDIX C

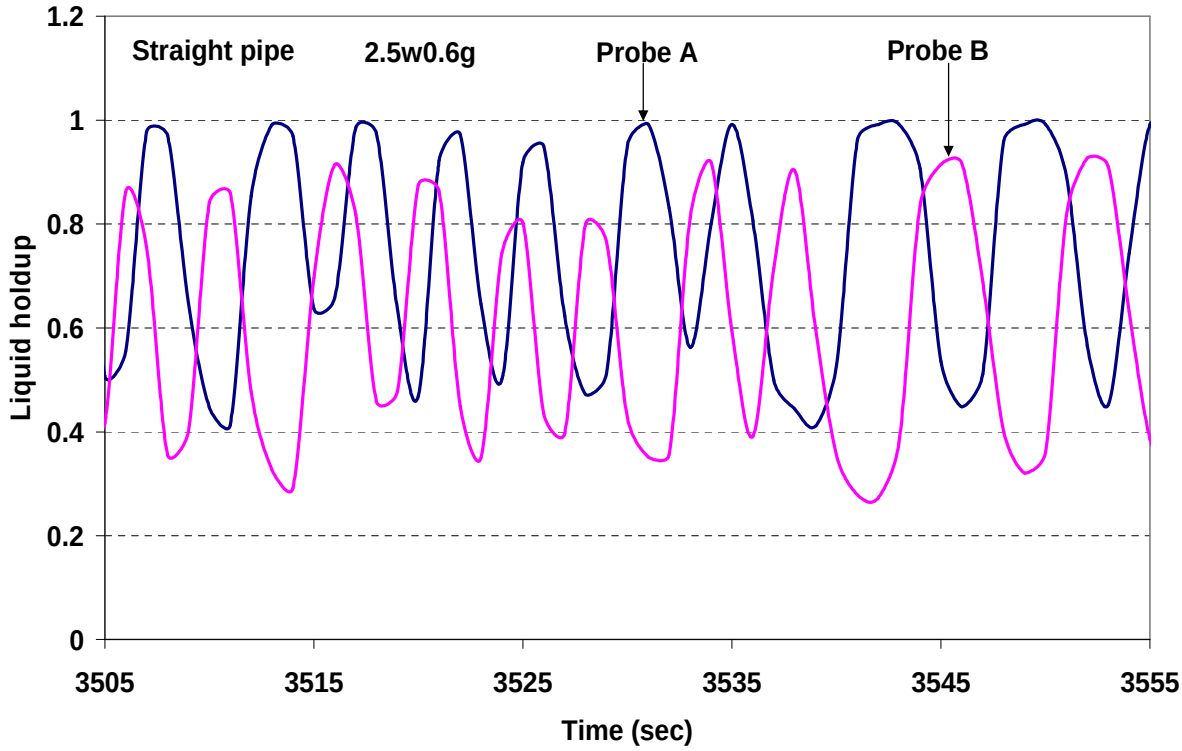
Straight pipe
2.5w0.6g
Probe A
Probe B
Liquid holdup
1.2
1
0.8
0.6
0.4
0.2
0
3505
3515
3525
3535
3545
3555
Time (sec)

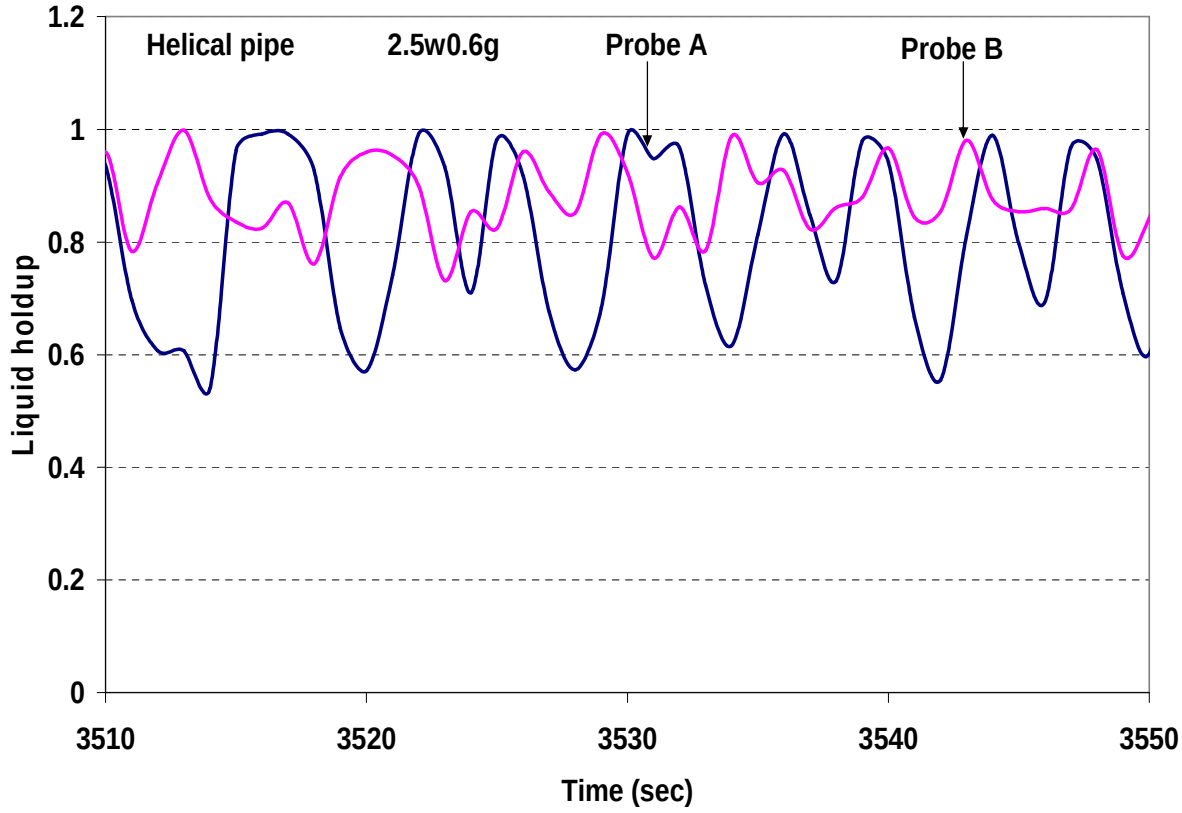
Helical pipe
2.5w0.6g
Probe A
Probe B
Liquid holdup
1.2
1
0.8
0.6
0.4
0.2
0
3510
3520
3530
3540
3550
Time (sec)

APPENDIX C

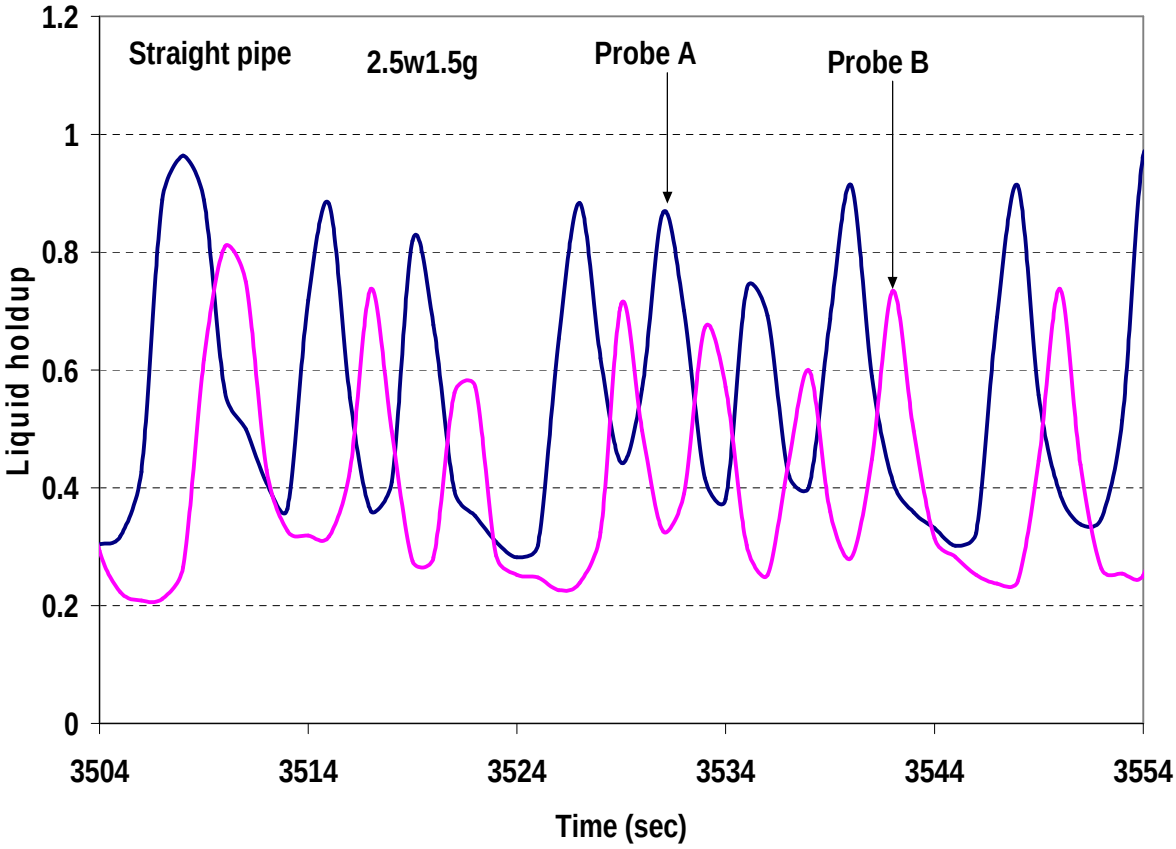
Straight pipe
2.5w1.5g
Probe A
Probe B
Liquid holdup
1.2
1
0.8
0.6
0.4
0.2
0
3504
3514
3524
3534
3544
3554
Time (sec)

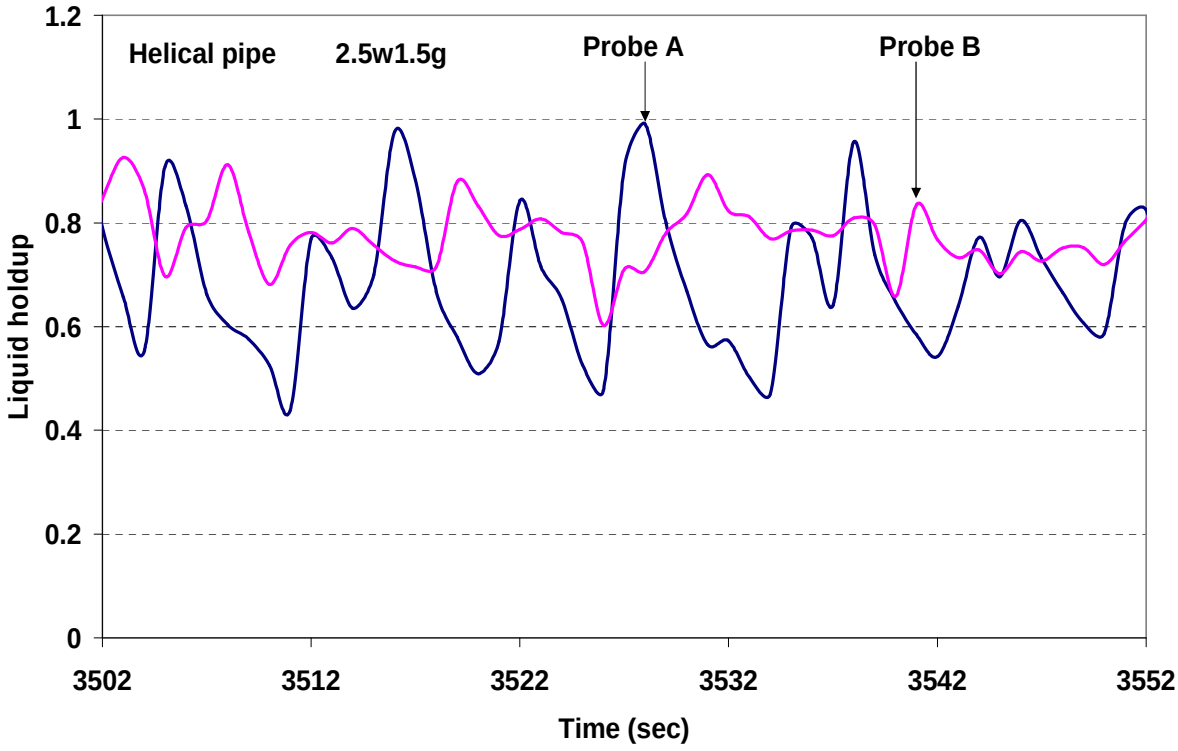
Helical pipe
2.5w1.5g
Probe A
Probe B
Liquid holdup
1.2
1
0.8
0.6
0.4
0.2
0
3502
3512
3522
3532
3542
3552
Time (sec)

APPENDIX C

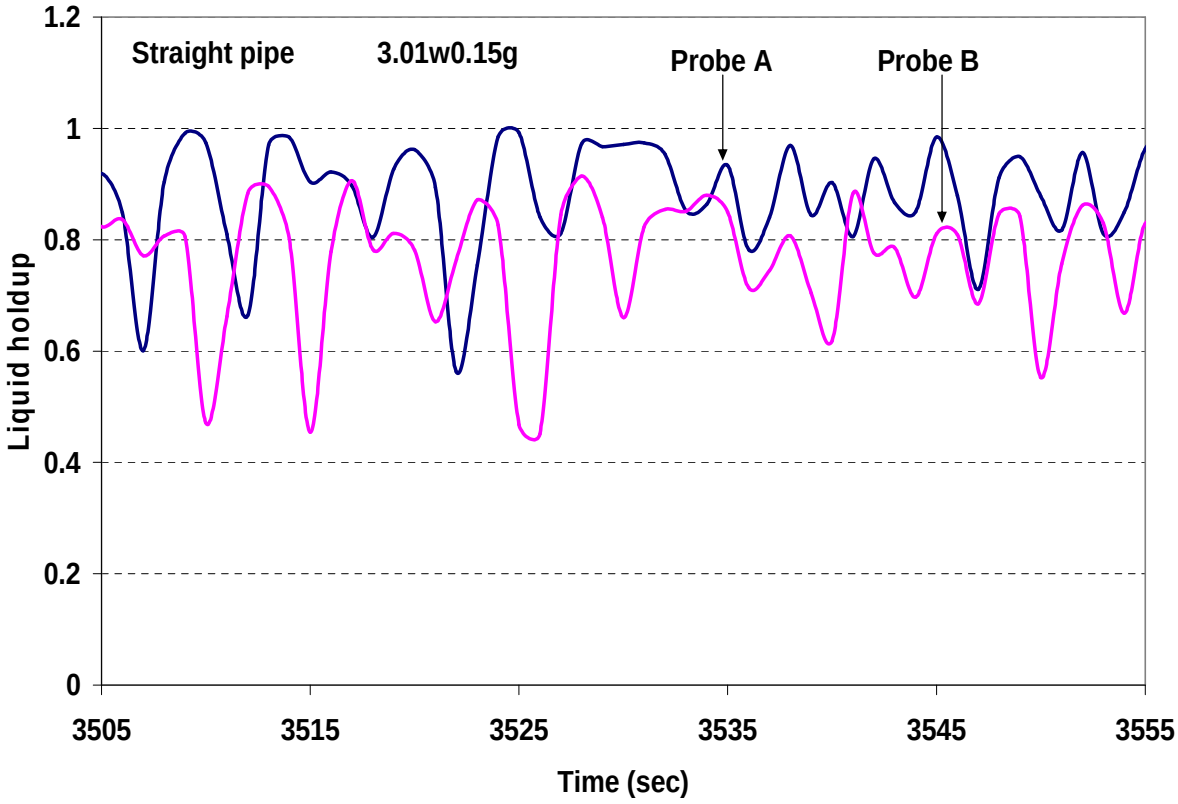
Straight pipe
3.01w0.15g
Probe A
Probe B
Liquid holdup
1.2
1
0.8
0.6
0.4
0.2
0
3505
3515
3525
3535
3545
3555
Time (sec)

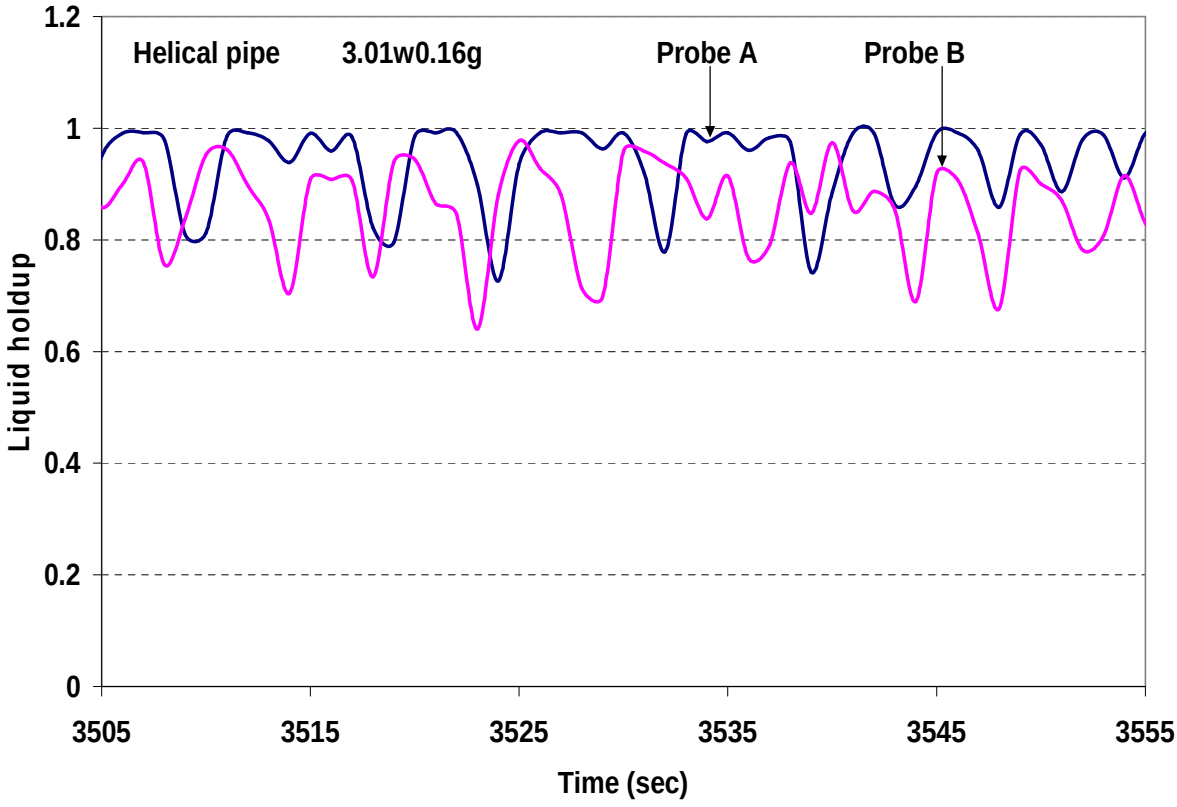
Helical pipe
3.01w0.16g
Probe A
Probe B
Liquid holdup
1.2
1
0.8
0.6
0.4
0.2
0
3505
3515
3525
3535
3545
3555
Time (sec)

APPENDIX C

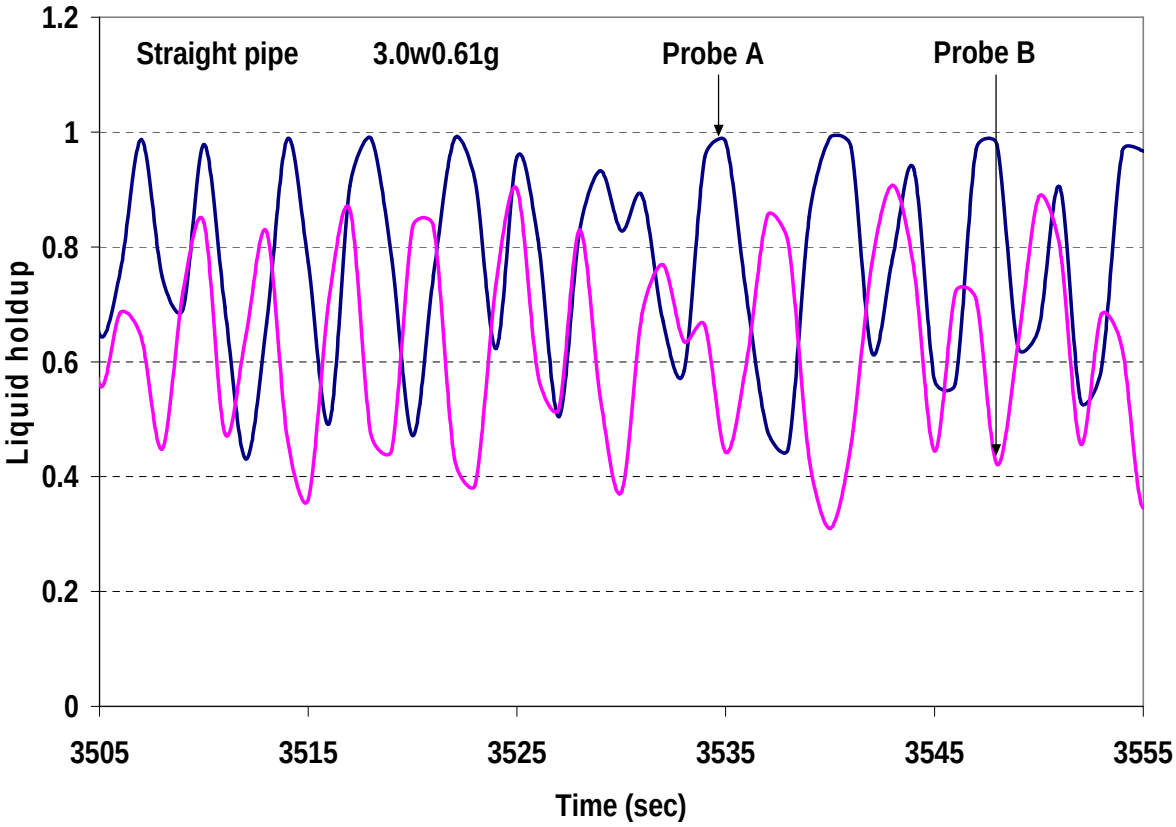
Straight pipe
3.0w0.61g
Probe A
Probe B
Liquid holdup
1.2
1
0.8
0.6
0.4
0.2
0
3505
3515
3525
3535
3545
3555
Time (sec)

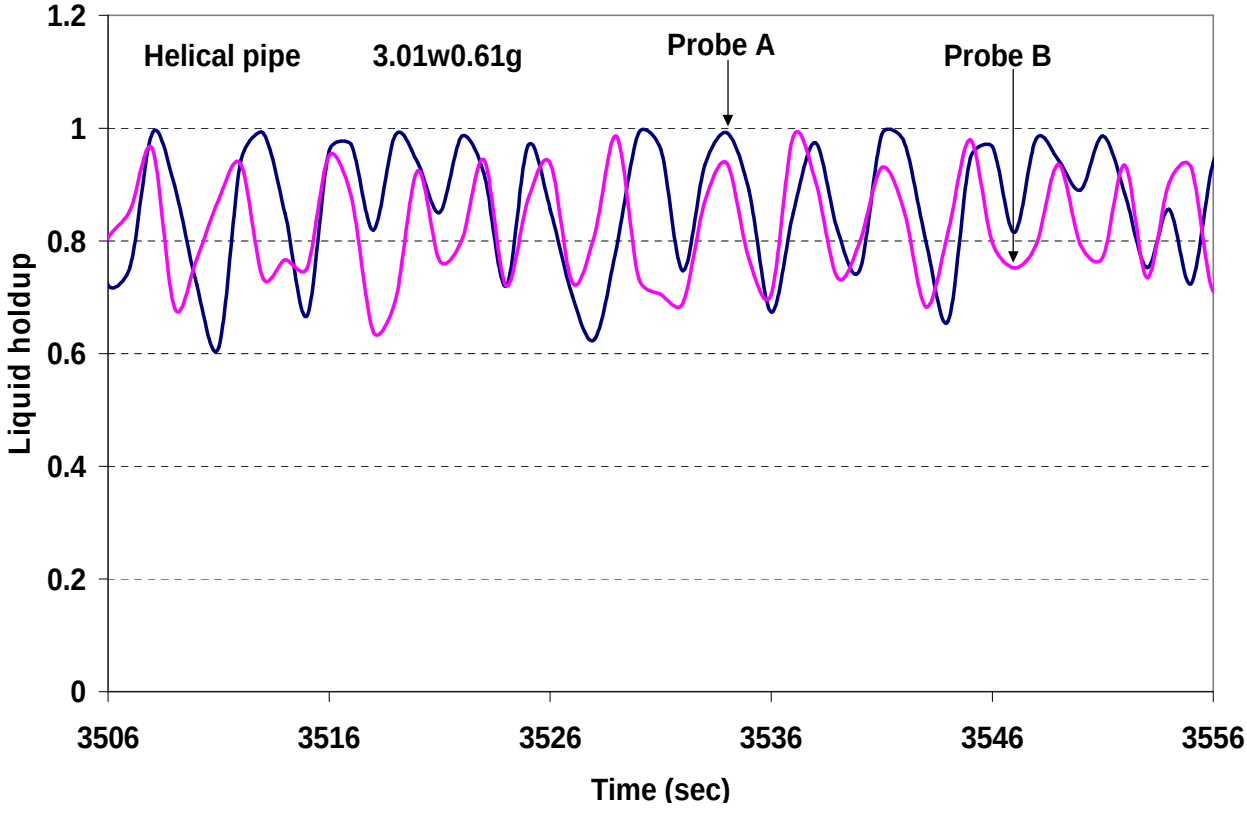
Helical pipe
3.01w0.61g
Probe A
Probe B
Liquid holdup
1.2
1
0.8
0.6
0.4
0.2
0
3506
3516
3526
3536
3546
3556
Time (sec)

APPENDIX C

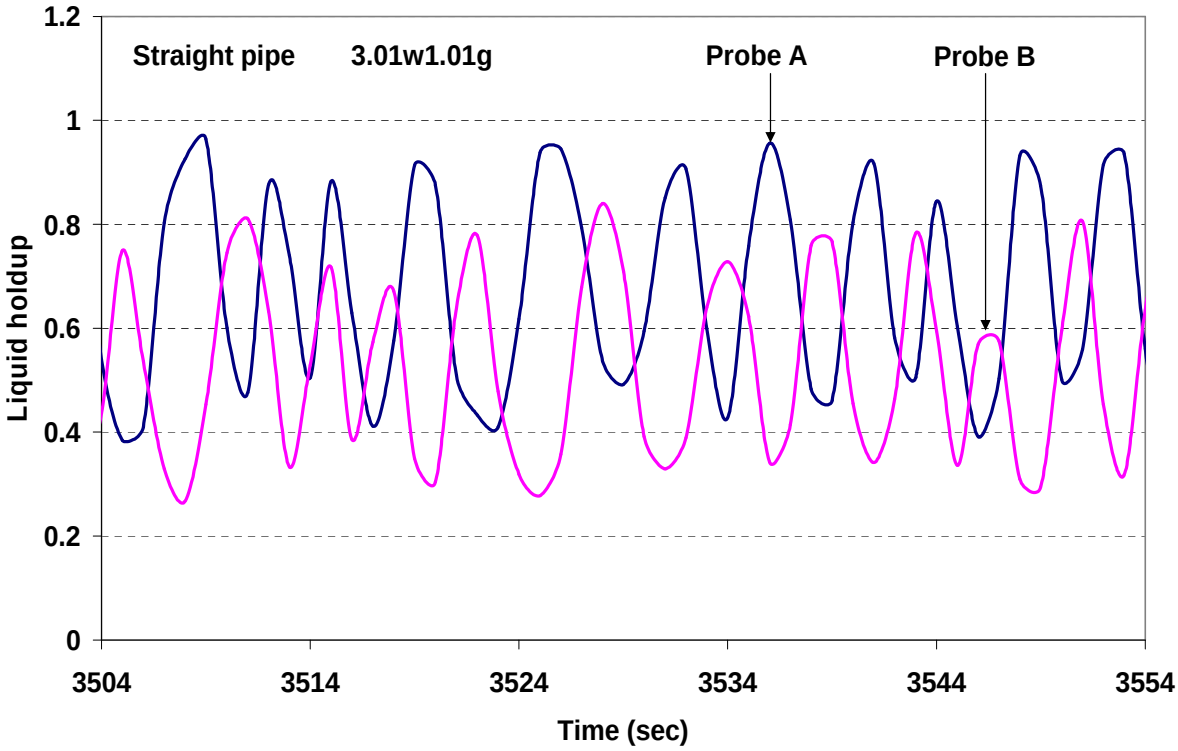
Straight pipe
3.01w1.01g
Probe A
Probe B
Liquid holdup
1.2
1
0.8
0.6
0.4
0.2
0
3504
3514
3524
3534
3544
3554
Time (sec)

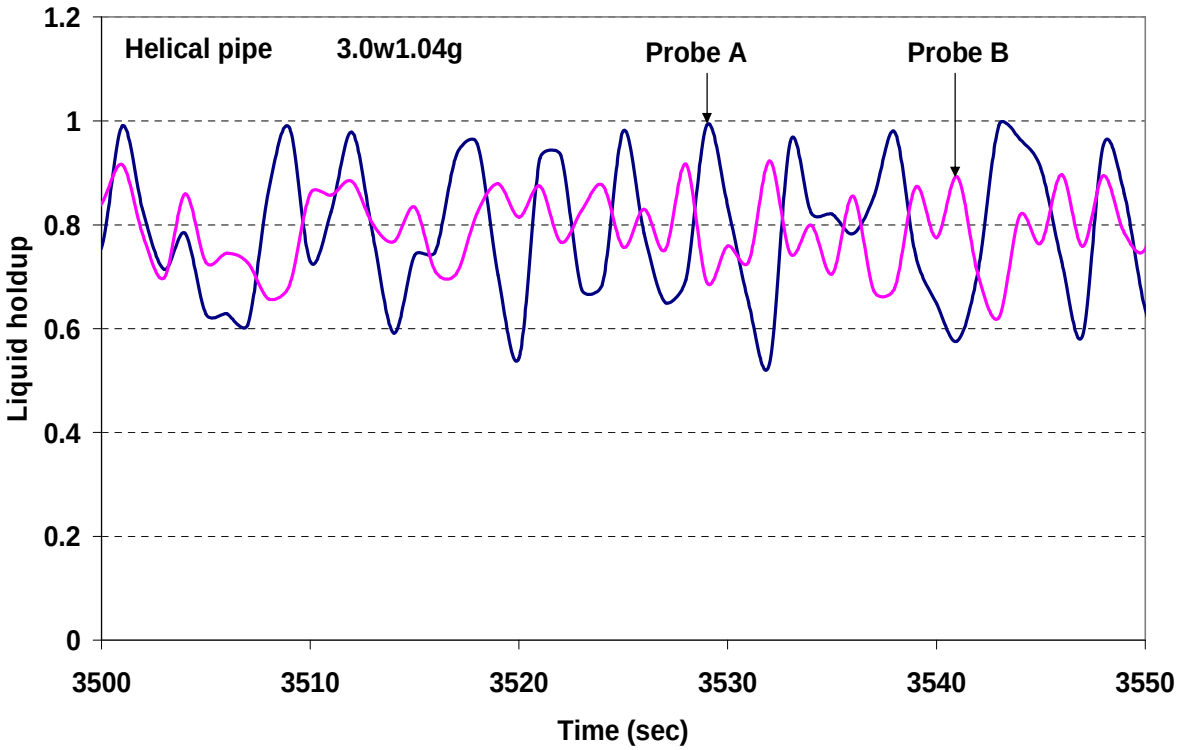
Helical pipe
3.0w1.04g
Probe A
Probe B
Liquid holdup
1.2
1
0.8
0.6
0.4
0.2
0
3500
3510
3520
3530
3540
3550
Time (sec)

APPENDIX D

Conductivity ring drawings

APPENDIX D

DRAWING No. ME/A3/35826	
ISSUE	MODIFICATION
A	———

ALL DIMENSIONS IN MILLIMETRES UNLESS OTHERWISE STATED

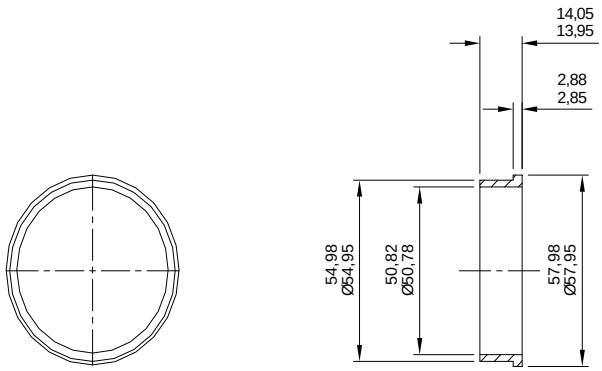

NOTE

REMOVE ALL SHARP EDGES

THIRD ANGLE PROJECTION			SHEET SIZE A3	1	A3/35826	LOCATION SPIGOT	4	PERSPEX		
				ITEM	PART No.	DESCRIPTION	No. OFF	MATL.	SPEC.	REMARKS
GENERAL TOLERANCE ON DIMENSIONS MACHINED ±0,2 UNMACHINED OTHER DIMENSIONS AS STATED	COST CODE	No. OF SETS REQ.	SCALE FULL SIZE	DRAWN	CHKD.	APPVD.	STRESS APPVD.	TITLE	SMAHT RISER LOCATION SPIGOT	
	R63006	1		E CLARK	A H					
				12/08/05	12/08/05					
WELD WHERE SHOWN THUS //////			FINISH	SCHOOL OF ENGINEERING CRANFIELD UNIVERSITY				DRAWING No. ME/A3/35826		
MACHINE WHERE SHOWN THUS	USED ON DRG. ME/A2/35829		SELF					SHT. 1 OF 1 SHEETS		

Appendix D1

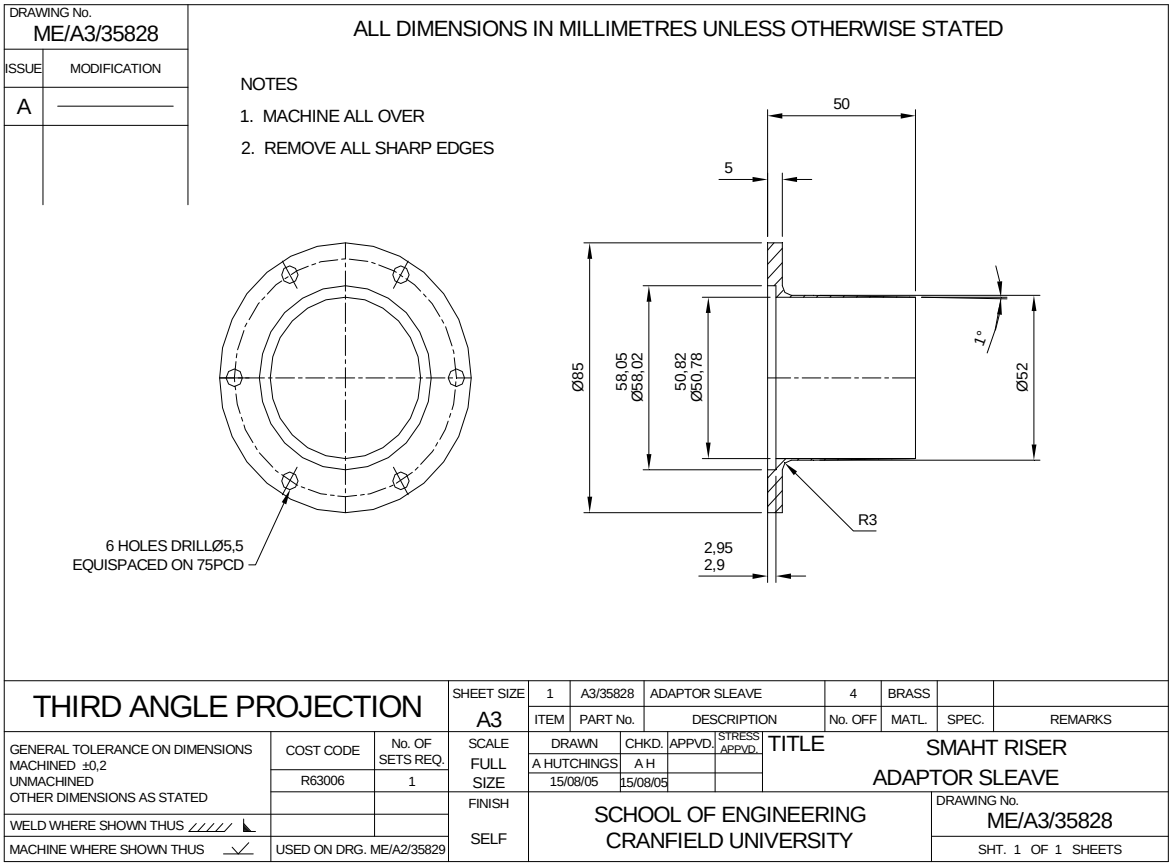
DRAWING No.
ME/A3/35828
ISSUE
MODIFICATION
A
ALL DIMENSIONS IN MILLIMETRES UNLESS OTHERWISE STATED
NOTES
1. MACHINE ALL OVER
2. REMOVE ALL SHARP EDGES
50
5
Ø85
58,05
Ø58,02
50,82
Ø50,78
1°
Ø52
R3
2,95
2,9
6 HOLES DRILLØ5,5
EQUISPACED ON 75PCD
THIRD ANGLE PROJECTION
SHEET SIZE
A3
ITEM
PART No.
DESCRIPTION
No. OFF
MATL.
SPEC.
REMARKS
1
A3/35828
ADAPTOR SLEAVE
4
BRASS
GENERAL TOLERANCE ON DIMENSIONS
MACHINED ±0,2
UNMACHINED
OTHER DIMENSIONS AS STATED
COST CODE
No. OF SETS REQ.
R63006
1
SCALE
FULL
SIZE
DRAWN
CHKD.
APPVD.
STRESS APPVD.
A HUTCHINGS
A H
15/08/05
15/08/05
TITLE
SMAHT RISER
ADAPTOR SLEAVE
WELD WHERE SHOWN THUS
MACHINE WHERE SHOWN THUS
USED ON DRG. ME/A2/35829
FINISH
SELF
SCHOOL OF ENGINEERING
CRANFIELD UNIVERSITY
DRAWING No.
ME/A3/35828
SHT. 1 OF 1 SHEETS

Appendix D2

DRAWING No. ME/A3/35833	
ISSUE	MODIFICATION
A	———

ALL DIMENSIONS IN MILLIMETRES UNLESS OTHERWISE STATED

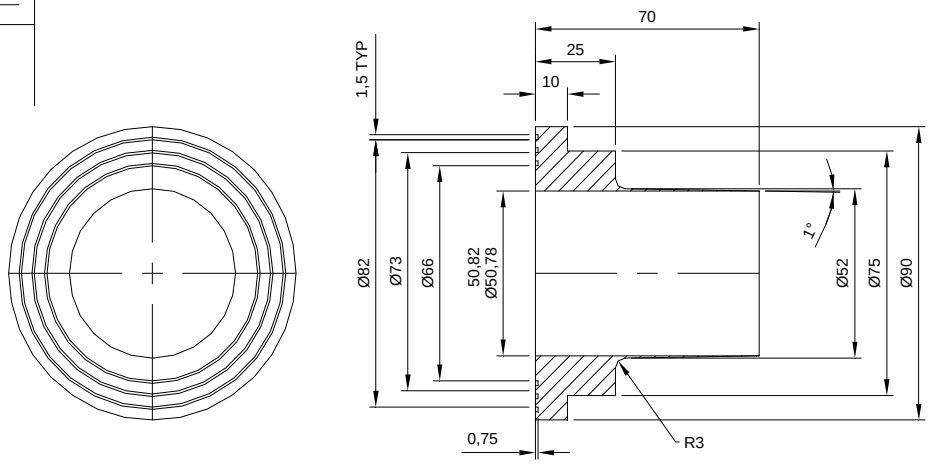

NOTES

1. MACHINE ALL OVER
2. REMOVE ALL SHARP EDGES

THIRD ANGLE PROJECTION	SHEET SIZE A3	ITEM	PART No.	DESCRIPTION	No. OFF	MATL.	SPEC.	REMARKS
		1	A3/35833	ADAPTOR FLANGE	1	BRASS		

GENERAL TOLERANCE ON DIMENSIONS MACHINED ±0,2 UNMACHINED OTHER DIMENSIONS AS STATED	COST CODE	No. OF SETS REQ.	SCALE FULL SIZE	DRAWN	CHKD.	APPVD.	STRESS APPVD.	TITLE
	R63006	1		E CLARK	A H			SMAHT RISER ADAPTOR FLANGE
				12/12/05	12/12/05			
WELD WHERE SHOWN THUS			FINISH SELF	SCHOOL OF ENGINEERING CRANFIELD UNIVERSITY				DRAWING No. ME/A3/35833
MACHINE WHERE SHOWN THUS	USED ON DRG. ME/A?/?????							SHT. 1 OF 1 SHEETS

Appendix D3

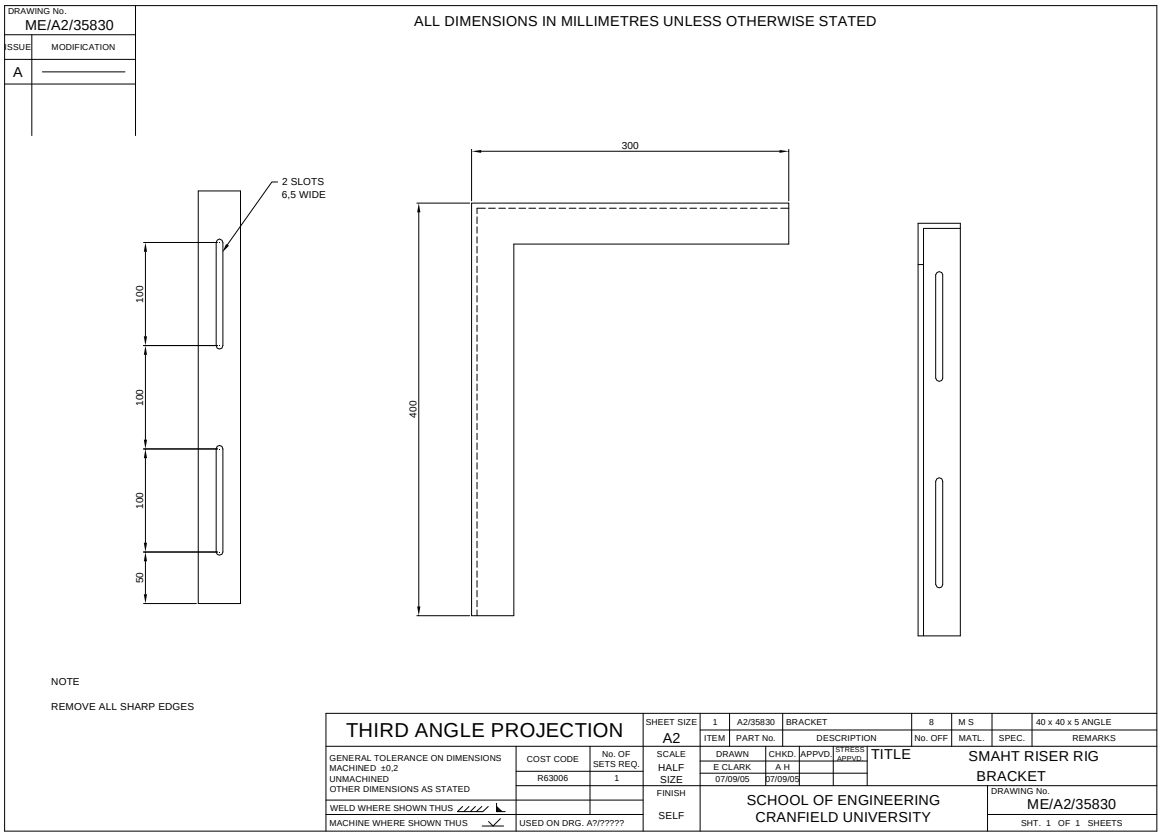
DRAWING No.
ME/A2/35830
ISSUE
MODIFICATION
A
ALL DIMENSIONS IN MILLIMETRES UNLESS OTHERWISE STATED
2 SLOTS
6,5 WIDE
300
400
100
100
100
50
NOTE
REMOVE ALL SHARP EDGES
THIRD ANGLE PROJECTION
SHEET SIZE
A2
1
A2/35830
BRACKET
8
M S
40 x 40 x 5 ANGLE
ITEM
PART No.
DESCRIPTION
No. OFF
MATL.
SPEC.
REMARKS
GENERAL TOLERANCE ON DIMENSIONS
MACHINED ±0,2
UNMACHINED
OTHER DIMENSIONS AS STATED
COST CODE
No. OF SETS REQ.
R63006
1
SCALE
HALF
SIZE
DRAWN
E CLARK
07/09/05
CHKD.
A H
07/09/05
APPVD.
STRESS APPVD.
TITLE
SMAHT RISER RIG
BRACKET
FINISH
SELF
SCHOOL OF ENGINEERING
CRANFIELD UNIVERSITY
DRAWING No.
ME/A2/35830
WELD WHERE SHOWN THUS
MACHINE WHERE SHOWN THUS
USED ON DRG. A?/?????
SHT. 1 OF 1 SHEETS

Appendix D4

DRAWING No. ME/A3/35827	
ISSUE	MODIFICATION
A	———

ALL DIMENSIONS IN MILLIMETRES UNLESS OTHERWISE STATED

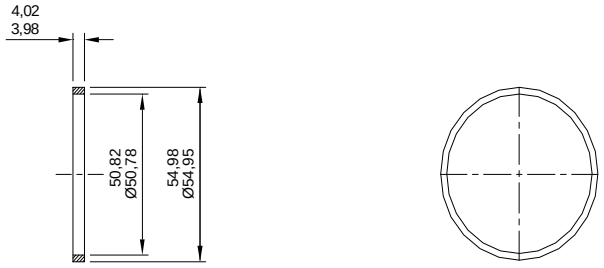

NOTES

1. WIRE ERODE FROM FLAT PLATE
2. REMOVE ALL SHARP EDGES

THIRD ANGLE PROJECTION	SHEET SIZE A3	ITEM	PART No.	DESCRIPTION	No. OFF	MATL.	SPEC.	REMARKS
		1	A3/35827	ELECTRODE	4	S S	316L	

GENERAL TOLERANCE ON DIMENSIONS MACHINED ±0,2 UNMACHINED OTHER DIMENSIONS AS STATED	COST CODE	No. OF SETS REQ.	SCALE FULL SIZE	DRAWN	CHKD.	APPVD.	STRESS APPVD.	TITLE
	R63006	1		E CLARK 12/08/05	A H 12/08/05			SMAHT RISER ELECTRODE
WELD WHERE SHOWN THUS //////			FINISH	SCHOOL OF ENGINEERING CRANFIELD UNIVERSITY				DRAWING No. ME/A3/35827
MACHINE WHERE SHOWN THUS	USED ON DRG. ME/A2/35829		SELF					SHT. 1 OF 1 SHEETS

Appendix D5

APPENDIX D

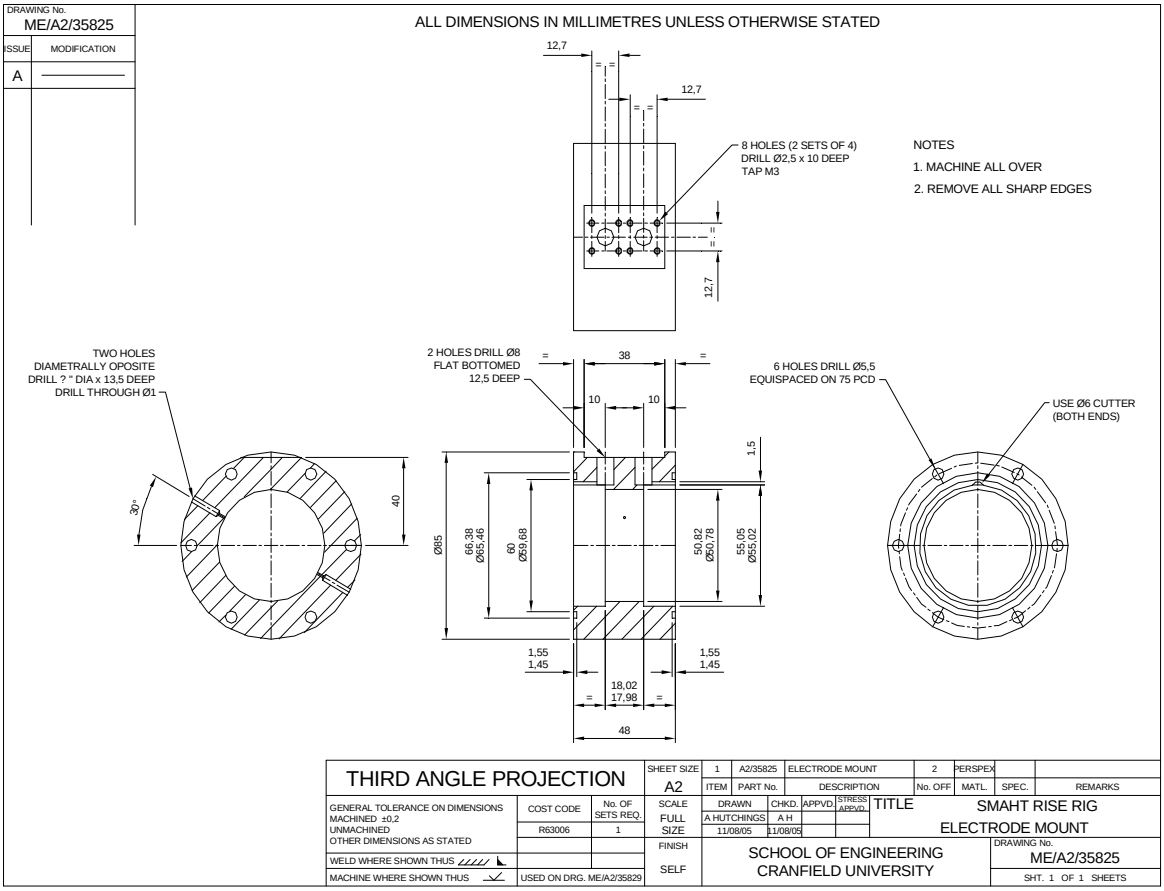

Appendix D6

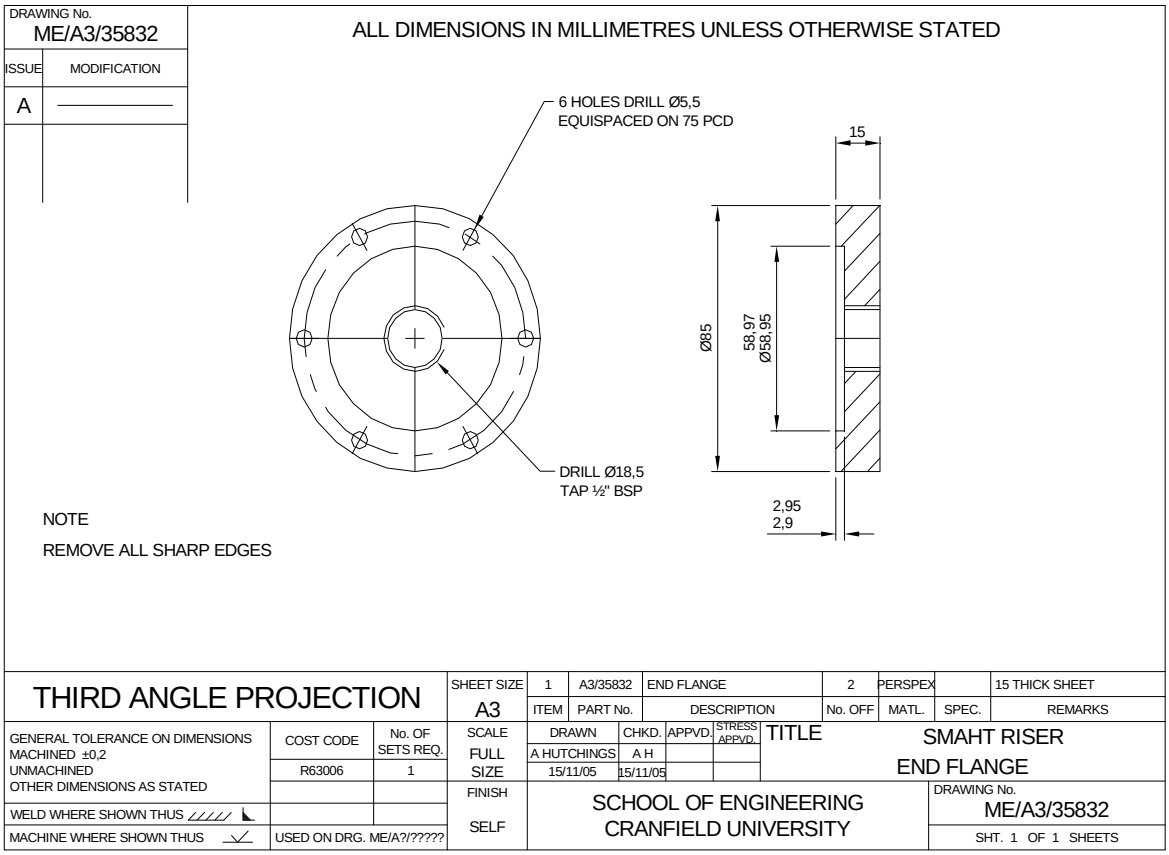
DRAWING No.
ME/A3/35832
ISSUE
MODIFICATION
A
ALL DIMENSIONS IN MILLIMETRES UNLESS OTHERWISE STATED
6 HOLES DRILL Ø5,5
EQUISPACED ON 75 PCD
15
Ø85
58,97
Ø58,95
DRILL Ø18,5
TAP ½" BSP
2,95
2,9
NOTE
REMOVE ALL SHARP EDGES
THIRD ANGLE PROJECTION
SHEET SIZE
A3
1
A3/35832
END FLANGE
2
PERSPEX
15 THICK SHEET
ITEM
PART No.
DESCRIPTION
No. OFF
MATL.
SPEC.
REMARKS
GENERAL TOLERANCE ON DIMENSIONS
MACHINED ±0,2
UNMACHINED
OTHER DIMENSIONS AS STATED
COST CODE
No. OF SETS REQ.
R63006
1
SCALE
FULL
SIZE
DRAWN
CHKD.
APPVD.
STRESS APPVD.
A HUTCHINGS
A H
15/11/05
15/11/05
TITLE
SMAHT RISER
END FLANGE
WELD WHERE SHOWN THUS
MACHINE WHERE SHOWN THUS
USED ON DRG. ME/A?/?????
FINISH
SELF
SCHOOL OF ENGINEERING
CRANFIELD UNIVERSITY
DRAWING No.
ME/A3/35832
SHT. 1 OF 1 SHEETS

Appendix D7

APPENDIX D

DRAWING No. ME/A2/35829

ISSUE	MODIFICATION
A	———

ALL DIMENSIONS IN MILLIMETRES UNLESS OTHERWISE STATED

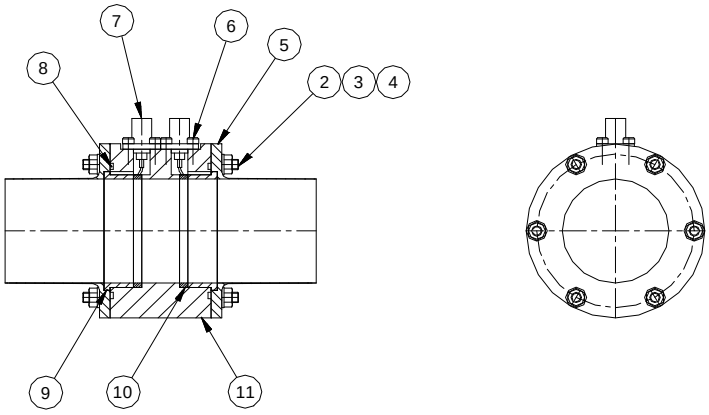

ITEM	PART No.	DESCRIPTION	No. OFF	MATL.	SPEC.	REMARKS
11	A3/35825	ELECTRODE MOUNT	1			
10	A3/35827	ELECTRODE	2			
9	A3/35826	LOCATION SPIGOT	2			
8		'O' RING	2	NITRILE		204-060
7		BNC PANEL SOCKET	2			
6		SKT. HD. CAP SCREW	8	SS		M3 x 10 LONG
5	A3/35828	ADAPTOR SLEAVE	2			
4		NUT	12	SS		M5
3		WASHER	12	SS		M5
2		STUDDING	6	SS		M5 x 74 LONG
1	A2/35829	PROBE ASSEMBLY	1			

THIRD ANGLE PROJECTION

SHEET SIZE A2

SCALE FULL

SIZE

FINISH SELF

	DRAWN	CHKD.	APPVD	STRESS APPVD.
A HUTCHINGS	A H			
16/08/05	16/08/05			

TITLE: SMAHT RISER PROBE ASSEMBLY

SCHOOL OF ENGINEERING
CRANFIELD UNIVERSITY

DRAWING No. ME/A2/35829

SHT. 1 OF 1 SHEETS

GENERAL TOLERANCE ON DIMENSIONS
MACHINED ±0,2
UNMACHINED
OTHER DIMENSIONS AS STATED

COST CODE	No. OF SETS REQ.
R63006	1

WELD WHERE SHOWN THUS

MACHINE WHERE SHOWN THUS

USED ON DRG. A?/?????

Appendix D8

APPENDIX D

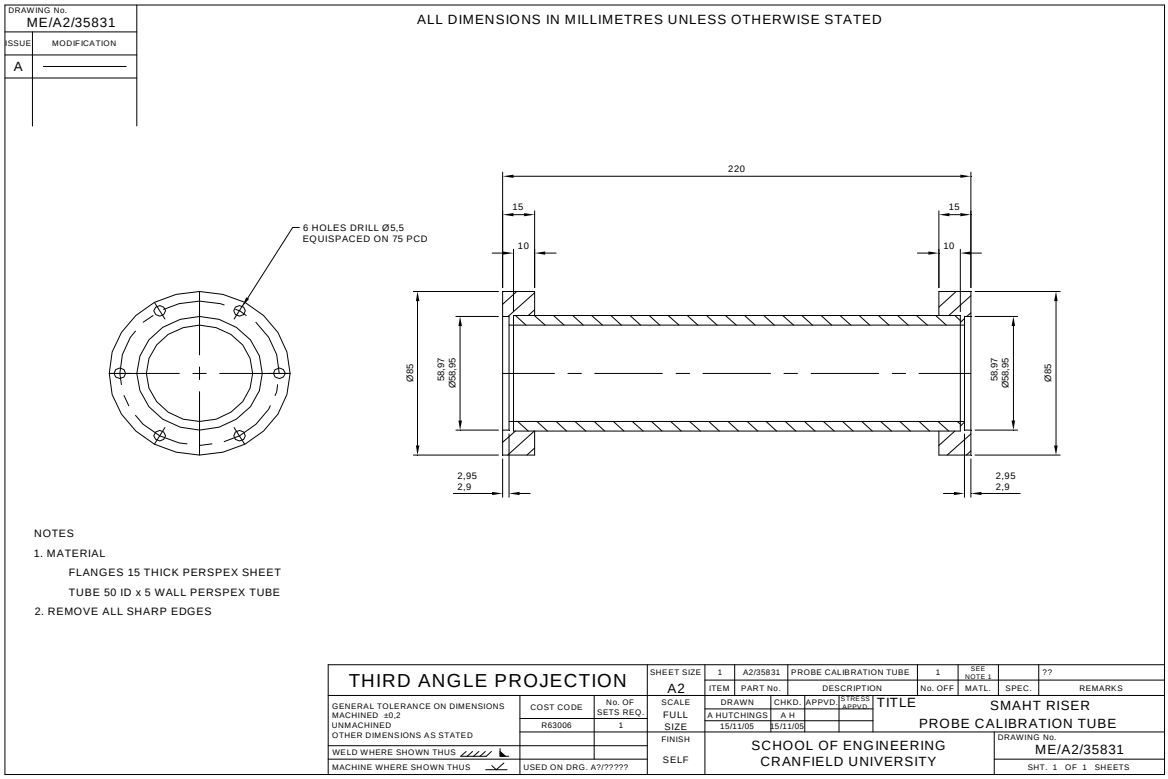

Appendix D9